University of Southampton

FACULTY OF ENGINEERING AND PHYSICAL SCIENCES
School of Physics and Astronomy

Theories of flavour from the Planck scale to the electroweak scale

by

Mario Fernández Navarro
ORCiD: 0000-0002-8796-0172

A thesis for the degree of
Doctor of Philosophy

March 2024

University of Southampton

Abstract

FACULTY OF ENGINEERING AND PHYSICAL SCIENCES
School of Physics and Astronomy

Doctor of Philosophy

Theories of flavour from the Planck scale to the electroweak scale

by Mario Fernández Navarro

The flavour puzzle remains as one of the most intriguing enigmas of particle physics. *A priori*, there is no apparent reason for the existence of three identical families of fundamental fermions in Nature. Moreover, the high number of free parameters in the flavour sector, along with their particular hierarchical patterns, suggest the existence of new physics that provide a dynamical explanation for the flavour structure of the Standard Model: such a theory describing the complicated flavour sector in terms of simple and natural principles is called a *theory of flavour*.

In this thesis, we propose and study theories of flavour which generically hint to a multi-scale origin of flavour. First we explore the idea of fermiophobic models, where the fermion mass hierarchies and the smallness of quark mixing are explained via the mechanism of messenger dominance. The general idea is that the chiral fermions of the Standard Model are uncharged under (part of) an extended gauge symmetry, which also forbids the presence of Yukawa couplings for chiral fermions. These are generated effectively due to the presence of hierarchically heavy messengers, including vector-like fermions and/or heavy Higgs doublets. The heavy messengers may also induce effective couplings for the chiral fermions to TeV-scale gauge bosons associated to the spontaneous breaking of the extended symmetry, leading to a predictive phenomenology connected to the origin of flavour hierarchies.

First we apply this idea to an extension of the Standard Model by a $U(1)'$ local abelian factor, where we seek to provide a significant contribution to the anomalous magnetic moment of the muon via exchange of a heavy $Z' \sim (\mathbf{1}, \mathbf{1}, 0)$ boson, and we find an interesting correlation with a suppression of the Higgs decay to two photons. Then we apply the same idea to a twin Pati-Salam symmetry which provides a TeV-scale vector leptoquark $U_1 \sim (\mathbf{3}, \mathbf{1}, 2/3)$ that can explain the so-called B-physics anomalies. We find that this model can be tested due to the correlated enhancement of key low-energy observables, and also via direct production of the new heavy degrees of freedom at the LHC.

Secondly, we leave behind the ideas of messenger dominance and fermiophobic models to study the possibility that the Standard Model originates from a non-universal gauge theory in the ultraviolet. We argue that one of the most simple ways to achieve this is by assigning a separate gauge hypercharge to each fermion family at high energies, spontaneously broken down to the usual weak hypercharge which is the diagonal subgroup. This simple framework denoted as "tri-hypercharge" avoids the family replication of the Standard Model, and could be the first step towards a deep non-universal gauge structure in the ultraviolet. If the Higgs doublet(s) only carries third family hypercharge, then only third family renormalisable Yukawa couplings are allowed by the gauge symmetry. However, non-renormalisable Yukawa couplings for the light families may be induced by the high scale scalar fields which break the three hypercharges down to the usual weak hypercharge, providing an explanation for fermion mass hierarchies and the smallness of quark mixing. Interestingly, in order to explain neutrino mixing, it is useful to introduce right-handed neutrinos which carry non-zero hypercharges (although their sum must vanish), which then turn out to get Majorana masses at the lowest scale of symmetry breaking, that could be as low as a few TeV. In fact, we find that the model has a rich phenomenology via Z' bosons if the new physics scales are relatively low: from flavour-violating observables to LHC physics and electroweak precision observables.

Finally, we propose a gauge unified origin for gauge non-universal frameworks such as the aforementioned tri-hypercharge theory. The model consists on assigning a separate $SU(5)$ group to each fermion family. However, assuming that the three $SU(5)$ groups are related by a cyclic permutation symmetry $\mathbb{Z}_3$, then the model is described by a single gauge coupling in the ultraviolet, despite $SU(5)^3$ being a non-simple group. First, we show a general $SU(5)^3$ "tri-unification" framework where gauge non-universal theories of flavour may be embedded, and secondly we construct a minimal tri-hypercharge example which can account for all the quark and lepton (including neutrino) masses and mixing parameters, with the five gauge couplings of the tri-hypercharge group unifying at the GUT scale into a single gauge coupling associated to the cyclic $SU(5)^3$ group, and we study the implications for the stability of the proton in such a setup.

To those who, despite all the sacrifices, never lost the joy of learning more about physics

We owe all progress to them

Contents

Acknowledgements

"Yes, I began my journey alone, and I ended it alone.
But that does not mean that I walked alone."

- Brandon Sanderson, *Oathbringer*

This is most likely the most difficult part to write of the whole thesis. Ever since I started doing "research", back in late 2018 during the final year of my physics degree, several PhD thesis have passed through my hands, shared with me by colleagues and supervisors as useful introductory texts into specific topics. I cannot help but say that the first thing I would always read were the Acknowledgements: here, for a few lines of text, you can connect with the emotions of a young researcher who struggled to push a PhD thesis forward for several years, and finally made it to this section. Writing these lines is a task that I have been putting off and, for various reasons, I know it will be impossible to write it without getting emotional. Well, this is finally my turn: here we go.

First and foremost, I have to start by expressing my most sincere (and endless) gratitude to my supervisor, guide, mentor, boss and also colleague, Steve King. I believe that I always carried inside myself the joy of learning more about physics, the enthusiasm for discovering the unknown and the optimism of the model builder, but I know that Steve is the one who was able to enlighten all this latent feelings inside me. I lost the hope once, on all of this, but Steve was able to drive me back into the right way, and I will never forget that conversation. Your time has been invaluable to me, and I will always be thankful for all the fruitful discussions and for the exciting work we did together. And of course, thanks for giving me the opportunity to work with you back in 2020 when I was a student who knew nothing, and thanks for putting me forward to give a plenary talk at Moriond (where I learnt how to ski). I have become the physicist I am today thanks to Steve.

My heart-felt gratitude also goes to all my collaborators for their unwavering support and for their endless patience: Marzia, Valerie, Avelino and Miguel.

From Marzia I learnt many things, including how important it is to do precise calculations (otherwise we are no better than model builders) and to understand the Standard Model in order to discuss possible new physics. I really appreciate your time and advice when I was in the difficult period of postdoc applications (and offers). I feel that Marzia is a person who always remembers, protects and fights for her friends and collaborators, and I feel blessed to find myself in this select group.

I thank Valerie for welcoming me at CERN-TH and for introducing me into the amazing environment of CERN-Cosmo. I feel that I am in the company of a world-class leading expert in the field of early Universe cosmology, where I think we may learn a lot about fundamental physics in the coming future. She always had good advice when I needed it and the answer to many of my fundamental, out-of-context questions. Valerie is also the creator of the 4π factor theorem in scientific writing ("always multiply your intended deadline for paper submission by a 4π factor"). I express my most sincere gratitude to her, for the time spent at CERN, for offering me to collaborate with her and for giving me a reference letter when I most needed it.

I also owe many thanks to Avelino. He was my first contact into the world of model building, which I really wanted to join. Avelino made a lot of work in order to prepare an excellent FPU application back in 2020, so that I could join the group at IFIC and start a PhD with him, work which in the end was unpaid because I couldn't join the group. I have been looking forward to collaborate with you since then, and I am happy that the opportunity finally came to us recently!

And of course I cannot forget about Miguel. I still remember your kind smile at Invisibles22 when you first approached to my poster, a poster about flavour physics and anomalies nonetheless, and we ended up talking about neutrinos, cosmology, research and life. This was the beginning of a friendship that I hope will last forever. Thank you as well for your kind welcome at CERN and for showing me the most beautiful, hidden places of Geneva. I couldn't have made my postdoc applications without all your help, guidance and support during the most uncertain times. You always had time for me when I needed it, including that warm phone call from Naples when I was deciding between my postdoc offers (this I will never forget). I hope that eventually I can learn from you how to be such a good, organised physicist, so that I can have a proper work-life balance and stop working during the weekends!

Obviously I cannot escape these lines without dedicating a paragraph to Xavi (and honestly I could write a full chapter). Everyday I am thankful that I was assigned the secondment in Padova so that we could met. I sincerely admit that I couldn't have finished this PhD without you. You appeared like a gift fallen from heaven when I needed help with Madgraph and package-X on the more technical side, and on the more personal side I needed someone around who would listen to the ramblings about my research. I hope one day to know half the physics that you know. Beyond all of this, I am happy for every conversation we had about the open "problems" and "puzzles" in physics, and about life in general. You were also there when the difficulties of the academic life hit me the hardest (I will always remember that call from Glasgow when I was lost in flat-hunting), and I admit that all the uncertainties and all the problems were easier to handle because you were always there. I know our friendship goes beyond physics and our PhDs, and I hope I have here a friend for life. The future right now is uncertain, but I hope you will eventually find in yourself the enthusiasm for discovering new physics that I found while doing this PhD, which is as yours as it is mine.

I also want to dedicate a few lines to Nikolai, who was sharing the office with me at Southampton for the last two years. I am happy for every conversation we had and for every time you gave me some chat to disconnect from work. I remember those nights when we stayed working in the office beyond 10 pm and 11 pm, which would have been much more difficult if you had not been around. Even though we work in very different topics, you were always kind to listen to my maunderings about the problems in my research, and you were there to help me the best you could. Having you around was also great to learn more about lattice QCD, although I admit that sometimes I didn't understand everything you say, but this is only because I have the small mind of a phenomenologist! Even though now we part ways to start new postdocs in different places, I hope more opportunities to meet and catch up will arise in the future.

Even if it may seem that the life of a researcher, and by extension the life of a PhD student, can be a lonely enterprise, I must admit fortunately it was not. I was lucky to share the journey with many fellow students and researchers who made the whole task of doing a PhD much easier. Among them I count all my fellow students at Southampton: Alessandro, Arran, Ben, Mauricio, Giorgio, Michele, Rajnandini, Dalius, Vlad, Jacan, Jack, Bowen, Giovanna, Shubhani... I had the best time as well during my two months at CERN thanks to Stefan, Pepe, Salva and Virgile, who shared all the lunches and ping pong sessions with me, plus I also thank all the nice, more senior members of CERN-TH who contributed to a very welcoming and friendly environment to discuss about physics, including Nick, Fabrizio, Andreas, Tobias... and thanks to Alba as well for the nice party tours at night around Geneva.

Before CERN, I found a second home in Padova that I will always miss, within the very warm group of local PhD students who became my italian family: Federico, Sofia, Clemens, Gabriele Levati, Gabriele Perna, Federica, Fabio, Anna, Giulio, Leonardo, Sara, Alfredo, Pietro... and of course, last but not least, *il grandissimo* Stefano Di Noi. Thank you guys for the amazing months that we spent together in Padova. I also thank Stefano Rigolin for the nice welcome to Padova and Luca Di Luzio for his time, patience and feedback back from when I was working on 4321 models.

I am thankful as well to all the nice people of the HIDDeN family. In particular, thanks to Jaime, Joao, Arturo, María, Salva, Virgile, Francesco, Patrick, Gioacchino, Federica, Valentina, Giacomo and Luca, for making the best time possible at any school or conference. I keep all the adventures in my heart. Thanks also to Silvia, Olga, Joerg, Rebeca and Enrico for keeping everything under control, and more generally thanks to HIDDeN for the excellent conditions of my PhD and for the amazing secondments in Padova and CERN, which made me grow both as a physicist and as a person.

The people of the AHEP group in Valencia also deserve my most sincere gratitude: they have always remembered me and supported me even though we parted ways three years ago in 2020. I am especially thankful to Sergio for always trusting me, for always remembering me and for doing the effort of keeping in touch. I am thankful to Pablo Martínez as well, who was there when I needed him the most.

I don't have words to express how thankful I am to José Ignacio Illana, who lead my first steps into research back in 2018 and 2019 when I was finishing my physics degree in Granada: I would not be the physicist I am today without you, thanks José.

I am also thankful to the people of the Glasgow PPT group, which will be my new home for the next few years. In particular, thanks Sophie and Christoph for trusting me for working with you, and thanks as well for the support with housing and flat-hunting and for the nice conversations about physics and life in academia that we had already (hopefully the first of many!). I express my gratitude to Ben Allanach and Stefano Moretti as well, for being my reviewers despite the significant extension of this manuscript, I am sure we will have nice discussions during the viva!

I met many nice people in conferences and schools as well, among them I am the most thankful to Daniel Naredo, Nico Gubernari, Simone, Jonathan, Renato, Miguel Levy, Jorge Terol and Javier Lizana for the nice sessions of beers after the talks, and for the great discussions about physics and life that came with them.

We are now getting close to the end, where I want to express my gratitude to my family. Despite all the complications and sacrifices of the last three years, I thank my parents, Rosa and Miguel, for always supporting my decisions, even though some of them were difficult. The life of a physicist may not be what they were expecting for me, but they have always been there when I needed someone to hold my back, and all of this would be impossible without them. I am also thankful to my aunts, uncles and cousins who, despite having a growing family to take care of, always remember that cousin who travelled far away in order to pursue his dream of being a physicists. I don't forget my best friends from Málaga, Álvaro, Andrés and Nacho, who have been there since I have memory. Each day with you guys is a blessing, and even though I have travelled far away and visited many countries, the best place I have ever been to is in Málaga with you, having a beer and talking about anything.

Finally, I am lovingly indebted to Sonalee, who joined my life when I started this thesis three years ago. Thank you for so many wonderful moments and for making me smile. Thank you, for always having time to listen to me, for your patience and support in my darkest moments. I am sorry that the circumstances may have not been the best, and I am sorry for having to work on the weekends, for having to travel so much and for having to move to a different city, away from you. I am sorry that physics takes so much from me that I have little left to give, but I am thankful to you for sharing this path, difficult as it is, with me.

While working on this thesis I found that the Universe and its fundamental laws are an exciting study, which goes beyond our small role as tiny humans living finite lives. I discovered something that is worth doing for a living, something that will make me feel happier the day I die. This is why I do what I do: because I want to be there when something new about Nature is revealed to us. And I hope I can continue sharing this journey with all of you who make it possible. From the deepest of my heart, thank you for not letting me walk alone.

Declaration of Authorship

I declare that this thesis and the work presented in it is my own and has been generated by me as the result of my own original research.

I confirm that:

1. This work was done wholly or mainly while in candidature for a research degree at this University;
2. Where any part of this thesis has previously been submitted for a degree or any other qualification at this University or any other institution, this has been clearly stated;
3. Where I have consulted the published work of others, this is always clearly attributed;
4. Where I have quoted from the work of others, the source is always given. With the exception of such quotations, this thesis is entirely my own work;
5. I have acknowledged all main sources of help;
6. Where the thesis is based on work done by myself jointly with others, I have made clear exactly what was done by others and what I have contributed myself;
7. Parts of this work have been published as: [1], [2], [3] and [4] in peer-reviewed journals, [5] as preprint under review, [6] and [7] as conference proceedings.

Signed:..... Date:.....

List of Figures

List of Tables

Acronyms and Abbreviations

2HDM	Two Higgs Doublet Model
BP	Benchmark Point
BSM	Beyond the Standard Model
CKM	Cabibbo–Kobayashi–Maskawa
CL	Confidence Level
CLFV	Charged Lepton Flavour Violation
CP	Charge conjugation Parity
DM	Dark Matter
EDM	Electric Dipole Moment
EFT	Effective Field Theory
Eq.	Equation
EW	Electroweak
EWPOs	Electroweak Precision Observables
FCC	Future Circular Collider
FCCCs	Flavour Changing Charged Currents
FCNCs	Flavour Changing Neutral Currents
Fig.	Figure
FN	Froggatt-Nielsen
GR	General Relativity
GIM	Glashow–Iliopoulos–Maiani
GUT	Grand Unified Theory
HL-LHC	High-Luminosity Large Hadron Collider
IR	Infrared
LEFT	Low-energy Effective Field Theory
LEP	Large Electron-Positron collider
LFU	Lepton Flavour Universality
LFUV	Lepton Flavour Universality Violation
LFV	Lepton Flavour Violation
LH	Left-handed
LHC	Large Hadron Collider
MFV	Minimal Flavour Violation
$\overline{\text{MS}}$	Modified Minimal Subtraction (a renormalisation scheme)

MSSM	Minimal Supersymmetric Standard Model
NLO	Next-to-Leading-Order
NNLO	Next-to-Next-to-Leading-Order
NP	New Physics
PMNS	Pontecorvo–Maki–Nakagawa–Sakata
PS	Pati-Salam
QCD	Quantum Chromodynamics
QED	Quantum Electrodynamics
QFT	Quantum Field Theory
Ref.	Reference
RGE	Renormalisation Group Evolution
RH	Right-handed
SM	Standard Model
SMEFT	Standard Model Effective Field Theory
SSB	Spontaneous Symmetry Breaking
SUSY	Supersymmetry
TH	Tri-hypercharge
UFO	Universal FeynRules Output
UV	Ultraviolet
VEV	Vacuum Expectation Value
VL	Vector-like
WC	Wilson Coefficient
WIMPs	Weakly Interacting Massive Particles

Preface

> "The purpose of a storyteller is not to tell you how to think, but to give you questions to think upon."
>
> – Brandon Sanderson, *The Way of Kings*

Physics thrives on crisis[1]. This is probably the most important lesson that one can extract from the history of (particle) physics. During the last few hundred years, we have witnessed how every apparent failure of the contemporaneous theories has led to abrupt developments in our understanding of Nature. The Standard Model of particle physics is no exception: in spite of its remarkable success, it leaves several open problems and puzzles that very likely hint to a path towards a more fundamental understanding of Nature. Despite my own experience forces me to be humble, this is the reason for writing this thesis: the honest hope that I will be able to learn something about Nature that has not yet been revealed to us.

Among the various open questions of the Standard Model (SM), the flavour puzzle may be one of the most perverse. In contrast to other shortcomings of the SM, the flavour puzzle does not point to any particular energy scale for the new dynamics that might be behind the origin of flavour. Most of the proposed theories rely on *a priori* undetermined flavour scales, which may be *anywhere from the Planck scale to the electroweak scale*, giving its name to this thesis.

However, this is no reason to be negative: the origin of flavour may still be around the corner, waiting to be discovered in particle physics experiments that test the origin of flavour *from the bottom-up*. In fact, one of the findings of this thesis is that flavour might originate from several new physics scales that may cover several orders of magnitude from the Planck scale to the electroweak scale, suggesting a possible multi-scale origin of flavour. If the lower layer of new physics is low enough, we might be seeing its first signals in the form of anomalies in low-energy flavour observables that hint to new flavour-specific interactions, or that suggest the breaking of accidental flavour symmetries of the SM such as lepton flavour universality. This thesis is therefore motivated by the spirit of model building, in the sense that I humbly believe that I can provide something new and significant to the already vast set of theories that try to explain the unknown. Moreover, I remain optimistic that my theories may be tested in the current

[1] Quoting the great sentence by Steven Weinberg in [8].

or upcoming generation of particle physics experiments, and this motivates the lengthy phenomenological analyses that you will find along the following chapters.

In Chapter 1 I will perform a somewhat lengthy introduction to the Standard Model, focusing on its open questions and on the particular role of flavour. Among other topics, I will discuss the full set of free parameters of the SM, I will introduce the type I seesaw mechanism as a possible origin of neutrino masses and I will discuss the approximate flavour symmetries of the SM, which are of great importance for flavour model building. I will also motivate here the need for a theory of flavour, and I will introduce the *a priori* undetermined flavour scales of a theory of flavour in the illustrative example of Froggatt-Nielsen models.

In Chapter 2 I will introduce the LEFT and the SMEFT, which are very useful effective field theories for phenomenological analyses of heavy new physics. I will discuss key flavour observables which show experimental anomalies, hinting to a consistent departure from the SM emerging from an underlying theory of flavour. I will highlight the significance of these anomalies and the emerging puzzles regarding theory prediction or experimental determination that put the BSM interpretation of these observables under question. I will also introduce a significant set of observables which are so far not anomalous, but are correlated to the anomalous observables in well-motivated BSM scenarios, hence being important for testing the proposed models. Regarding the so-called B-physics anomalies, I will highlight an emerging BSM scenario that is preferred by current data, which will be later on realised by the explicit theory of flavour discussed in Chapter 4.

In Chapter 3 I will study a class of local $U(1)'$ extensions of the SM, where chiral fermions are uncharged under the $U(1)'$ but an exotic family of vector-like fermions is not, providing effective Z' couplings for chiral fermions via mixing. This feature gives the name *fermiophobic* to this class of models. I will show how a simplified fermiophobic framework can explain the $(g-2)_\mu$ anomaly via the basic idea of chiral enhancement, correlating the enhancement of $(g-2)_\mu$ with a suppression of Higgs diphoton decay. Afterwards, I will study a theory of flavour with fermiophobic Z' that can explain the origin of the SM flavour structure via the mechanism of messenger dominance. This theory connects the origin of Yukawa couplings in the SM with the origin of effective Z' couplings for chiral fermions, hence connecting the origin of flavour hierarchies in the SM with the low-energy phenomenology of the model. We conclude that ultimately the $(g-2)_\mu$ anomaly cannot be explained in the context of this theory of flavour due to a correlated enhancement of $\mathcal{B}(\tau \to \mu\gamma)$. Nevertheless, we find that the flavour structure of the model allows for the Z' boson to be as light as 1 TeV, within the reach of current particle physics experiments.

In Chapter 4 I will study a twin Pati-Salam theory of flavour which contains a TeV scale vector leptoquark $U_1 \sim (\mathbf{3}, \mathbf{1}, 2/3)$. The model features a fermiophobic framework as well, where both the effective Yukawa couplings for chiral fermions and their effective

U_1 couplings originate again from mixing with heavy vector-like fermions. The mechanism of messenger dominance plays a fundamental role here to simultaneously explain the fermion mass hierarchies and deliver the flavour structure required to explain the B-physics anomalies. I will show that one vector-like fermion family is not enough to achieve such flavour structure, but indeed three vector-like fermion families are required. In this case, the model predicts a plethora of low-energy signals in flavour observables, several of them fundamentally related to the origin of fermion mass hierarchies and mixing. The model can also be tested via direct searches of the new heavy degrees of freedom at the LHC, including the vector-like fermions, the U_1 leptoquark, and a coloron $g' \sim (\mathbf{8}, \mathbf{1}, 0)$ and Z' gauge bosons.

In Chapter 5 I will study the possibility that the Standard Model originates from a non-universal gauge theory in the ultraviolet. I will argue that one of the most simple ways to achieve this is by assigning a separate gauge hypercharge to each fermion family at high energies, broken down to the usual weak hypercharge which is the diagonal subgroup. This simple framework avoids the family replication of the SM, and could be the first step towards a deep non-universal gauge structure in the UV. If the Higgs doublet(s) only carry third family hypercharge, then only third family renormalisable Yukawa couplings are allowed by the gauge symmetry. However, non-renormalisable Yukawa couplings for the light families may be induced by the high scale scalar fields which break the three hypercharges down to the SM hypercharge, providing an explanation for fermion mass hierarchies and the smallness of CKM quark mixing. I will show that in order to explain neutrino mixing, it is useful to introduce right-handed neutrinos which carry non-zero hypercharges (although their sum must vanish), which then turn out to get Majorana masses at the lowest scale of symmetry breaking, that could be as low as a few TeV. Indeed, I will motivate that the model has a rich phenomenology via Z' bosons if the flavour scales are relatively low: from flavour-violating observables to LHC physics and electroweak precision observables.

In Chapter 6 I will propose a gauge unified origin for gauge non-universal frameworks such as the aforementioned tri-hypercharge theory. The model consists on assigning a separate $SU(5)$ group to each fermion family. However, assuming that the three $SU(5)$ groups are related by a cyclic permutation symmetry $\mathbb{Z}_3$, then the model is described by a single gauge coupling in the UV, despite $SU(5)^3$ being a non-simple group. In this manner, $SU(5)^3$ "tri-unification" reconciles the idea of gauge non-universality with the idea of gauge coupling unification, opening the possibility to build consistent non-universal descriptions of Nature that are valid all the way up to the GUT scale. First, I will show a general $SU(5)^3$ tri-unification framework where gauge non-universal theories of flavour may be embedded, and secondly I will construct a minimal tri-hypercharge example which can account for all the quark and lepton (including neutrino) masses and mixing parameters, with the five gauge couplings of the tri-hypercharge group unifying at the GUT scale into a single gauge coupling associated to the cyclic $SU(5)^3$ group. I will study the implications for the stability of the proton in such a setup.

Finally, in Chapter 7 I will summarise my own findings and the main results extracted from each chapter. I will also motivate next possible steps in my research and give my own view about the future ahead of us in particle physics. I hope the reader finds interesting the particular approaches to the flavour puzzle discussed here, along with all the related phenomenology and discovery prospects. And on top of everything, I hope the reader enjoys as much as I did when learning and thinking about the work included in this thesis.

Chapter 1

Flavour in the Standard Model and beyond

> "The standard theory may survive as a part of the ultimate theory, or it may turn out to be fundamentally wrong. In either case, it will have been an important way-station, and the next theory will have to be better."
>
> – Sheldon L. Glashow

In this chapter we provide an introduction to the Standard Model (SM) of particle physics, with special attention to the flavour sector and its particular properties (for a more complete review see e.g. [9–12]). The SM is a mathematical model of Nature built upon fundamental principles. It provides a simple framework in which the different fundamental components of matter and their interactions can be understood. At the end of the chapter, we will show that despite its remarkable success in describing the vast majority of experimental data, the SM cannot be the ultimate theory of Nature: it leaves several experimental and theoretical questions unanswered, motivating us to go beyond.

1.1 The basics of the Standard Model: Fundamental Principles and particle content

The SM was built to understand the strong, weak and electromagnetic interactions observed in Nature, along with the fundamental matter components which experience such interactions at the quantum level. As such, the SM is a quantum field theory based on the principles of locality, causality and renormalisability. In the SM, the concept of symmetry plays a central role. The SM postulates that Nature is invariant under the spacetime (Poincaré) symmetries and under the so-called SM gauge (local) symmetry group

$$SU(3)_c \times SU(2)_L \times U(1)_Y \,. \tag{1.1}$$

Field	$SU(3)_c$	$SU(2)_L$	$U(1)_Y$
$Q_{L1} = \begin{pmatrix} u_{L1} \\ d_{L1} \end{pmatrix}$	**3**	**2**	1/6
u_{R1}	**3**	**1**	2/3
d_{R1}	**3**	**1**	$-1/3$
$L_{L1} = \begin{pmatrix} \nu_{L1} \\ e_{L1} \end{pmatrix}$	**1**	**2**	$-1/2$
e_{R1}	**1**	**1**	-1
$Q_{L2} = \begin{pmatrix} u_{L2} \\ d_{L2} \end{pmatrix}$	**3**	**2**	1/6
u_{R2}	**3**	**1**	2/3
d_{R2}	**3**	**1**	$-1/3$
$L_{L2} = \begin{pmatrix} \nu_{L2} \\ e_{L2} \end{pmatrix}$	**1**	**2**	$-1/2$
e_{R2}	**1**	**1**	-1
$Q_{L3} = \begin{pmatrix} u_{L3} \\ d_{L3} \end{pmatrix}$	**3**	**2**	1/6
u_{R3}	**3**	**1**	2/3
d_{R3}	**3**	**1**	$-1/3$
$L_{L3} = \begin{pmatrix} \nu_{L3} \\ e_{L3} \end{pmatrix}$	**1**	**2**	$-1/2$
e_{R3}	**1**	**1**	-1

TABLE 1.1: The fundamental fermions of the SM and their transformation properties under the SM gauge group. We show explicitly the two components of the $SU(2)_L$ doublets, while colour indices are implicit.

Each of the components of the SM gauge group is associated with a quantum number to be preserved in Nature. $SU(3)_c$ is associated to the so-called color, while $U(1)_Y$ is associated to the so-called hypercharge. Remarkably, $SU(2)_L$ acts over fermions as the left-handed chirality of the Lorentz group[1] (subgroup of the full Poincaré spacetime symmetry). This will have important implications for the fermion content of the theory. Electric charge $U(1)_Q$ is contained within the so-called *electroweak* symmetry group $SU(2)_L \times U(1)_Y$.

The SM further postulates the existence of fundamental spin-1/2 fermions, understood as Dirac four-component spinor fields $\psi(x) = \psi(x)_L \oplus \psi(x)_R$ containing both the left-handed and right-handed[2] chiralities of the Lorentz group, which are related via the parity symmetry. The left-handed and right-handed components of a Dirac four-spinor can be extracted as two-component Weyl spinors via the chiral projectors

$$\psi_L \equiv P_L\psi = \frac{1-\gamma_5}{2}\psi\,, \qquad \psi_R \equiv P_R\psi = \frac{1+\gamma_5}{2}\psi\,, \tag{1.2}$$

[1] However, the $SU(2)_L$ gauge symmetry of the SM should not be confused with the $SU(2)_L$ symmetry of the Lorentz group, as they are fundamentally different. An example of this is the Higgs doublet, which transforms as a doublet under the SM $SU(2)_L$ but is a spin-0 scalar under the Lorentz symmetry.

[2] With the exception of the right-handed chirality of neutrinos, as discussed later in this section.

where $\gamma_5 \equiv i\gamma^0\gamma^1\gamma^2\gamma^3$ and γ^μ are the gamma matrices (also called Dirac matrices), with $\mu = 0, 1, 2, 3$ being a Lorentz index.

The fundamental fermions undergo particular transformation properties under the SM gauge group, as given in Table 1.1. Each fundamental fermion comes in three copies, with identical transformation rules under the SM gauge group. Remarkably, the left-handed components of fundamental fermions transform as doublets under $SU(2)_L$, while the right-handed components transform as singlets,

$$Q^a_{Li} = \begin{pmatrix} u^a_{Li} \\ d^a_{Li} \end{pmatrix}, \quad u^a_{Ri}, \quad d^a_{Ri}, \tag{1.3}$$
$$L_{Li} = \begin{pmatrix} \nu_{Li} \\ e_{Li} \end{pmatrix}, \quad e_{Ri}.$$

In this manner, parity is explicitly violated within the SM, and we say that the SM is a chiral theory[3]. As anticipated before, fundamental fermions come in three identical copies that we denote as flavours, such that $i = 1, 2, 3$. The fermions in the first line of Eq. (1.3) all carry colour $a = r, g, b$ (red, green, blue), in such a way that they can be arranged as a triplet under $SU(3)_c$,

$$q = \begin{pmatrix} q^r \\ q^g \\ q^b \end{pmatrix}, \tag{1.4}$$

where $q = u_{Li}\,, d_{Li}\,, u_{Ri}\,, d_{Ri}$ since $SU(3)_c$ does not discriminate by chirality nor flavour. These "colourful" fermions are denoted as *quarks*. In this manner, the quark content of the SM consists of three *up-type* quarks $u^a_{L,Ri}$ and three *down-type* quarks $d^a_{L,Ri}$, all carrying colour but discriminated by their different hypercharge, plus their left-handed components are arranged in $SU(2)_L$ doublets as per the first line in Eq. (1.3). The remaining fermions are called *leptons*, and they transform as singlets under $SU(3)_c$, hence carrying no color. We discriminate between *charged leptons* $e_{L,Ri}$ and *neutrinos* ν_{Li}. The latter will be shown to carry zero electric charge, in contrast with the former. In this manner, we have identified the different *charged sectors* of the SM fermions, each of them including three identical flavours. Remarkably, we have chosen not to introduce the right-handed counterpart of the neutrino fields: it would transform as a complete singlet under the SM, $\nu_R \sim (\mathbf{1}, \mathbf{1}, 0)$, therefore it would not experience any gauge interaction and would be an unphysical field so far. We will come back to the discussion of right-handed neutrinos when we introduce the origin of fermion masses in the SM.

Having discussed the transformation properties of fundamental fermions under the

[3]The fundamental reason for the SM to be a chiral theory is a mystery, related to the question of why Nature has chosen the particular symmetry group in Eq. (1.1) and not any other.

SM gauge group, we proceed to explicitly include for completeness the gauge transformations of a generic fermion $\psi(x)$ under each component of the SM gauge group,

$$U(1)_Y : \quad \psi(x) \to \exp\left[-iY_\psi \theta_Y(x)\right] \psi(x)\,, \tag{1.5}$$

$$SU(2)_L : \quad \psi(x) \to \exp\left[-iT^a \theta_L^a(x)\right] \psi(x)\,, \tag{1.6}$$

$$SU(3)_c : \quad \psi(x) \to \exp\left[-it^\alpha \theta_c^\alpha(x)\right] \psi(x)\,, \tag{1.7}$$

where repeated indices are always taken as summed. Y is the generator of the hypercharge $U(1)_Y$ group, such that Y_ψ is the hypercharge of the ψ fermion. T^a with $a = 1, 2, 3$ are the generators of $SU(2)_L$, while t^α with $\alpha = 1, ..., 8$ are the generators of $SU(3)_c$. When acting upon a doublet representation of $SU(2)_L$, $T^a = \sigma^a/2$ where σ^a are the Pauli matrices, while when acting upon singlets $T^a = 0$. This way, the two different components of a $SU(2)_L$ doublet can be discriminated by their third component of weak isospin T_3: by convention, up-quarks and neutrinos carry $T_3 = 1/2$, while down-quarks and charged leptons carry $T_3 = -1/2$. For the case of $SU(3)_c$, the triplet representations transform with $t^\alpha = \lambda^\alpha/2$, where λ^α are the Gell-Mann matrices, while singlet representations transform as $t^\alpha = 0$.

The particular choice of fermion transformation properties and hypercharge assignments under the SM gauge group is not arbitrary. We will see that the transformation properties of the SM fermions are motivated by experimental evidence (such as the fact that only quarks experience the strong interaction), plus the requirement to cancel gauge anomalies, which is crucial for any consistent quantum field theory. Any other choice would be incompatible with experimental data, or require the addition of extra, unseen fermions, being again incompatible with experimental evidence. Nevertheless, there is no fundamental reason to have three copies for each fermion (flavours), since gauge anomaly cancellation occurs in the SM for each individual family. The most simple choice would be to have only one family formed by one up-quark, down-quark, charged lepton and neutrino. However, the experimental data tell us that three families do exist, with identical transformation properties under the SM gauge group.

Postulating the existence of a gauge symmetry naturally predicts the existence of the so-called gauge bosons: physical, fundamental and massless particles with spin-1, transforming as four-vectors V_μ ($\mu = 0, 1, 2, 3$) under the Lorentz group. Gauge bosons act as mediators of interactions among spin-1/2 fermions. The gauge bosons are ultimately associated to the generators of the gauge group and live in the adjoint representation, as we shall see. Therefore, in the SM we have 8 massless gluons $G_\mu^\alpha \sim (\mathbf{8}, \mathbf{1}, 0)$ which mediate the strong interactions, with $\alpha = 1, ..., 8$, associated to $SU(3)_c$. We also have three gauge bosons $W_\mu^a \sim (\mathbf{1}, \mathbf{3}, 0)$ with $a = 1, 2, 3$ associated to $SU(2)_L$, and one gauge boson $B_\mu \sim (\mathbf{1}, \mathbf{1}, 0)$ associated to $U(1)_Y$.

1.2 The gauge sector

Having introduced the gauge symmetry of the SM, the fundamental fermions and their transformation rules, now we are led to write a Lagrangian in order to study the dynamics of this system. We require our Lagrangian to preserve the Poincaré symmetry of spacetime plus the gauge symmetry of the SM. Following common practice, we start by introducing kinetic terms for all fermion fields and gauge fields, so they can propagate through spacetime. The resulting Lagrangian is

$$\mathcal{L}_{\text{gauge}} = -\frac{1}{4}G^{\alpha}_{\mu\nu}G^{\mu\nu\alpha} - \frac{1}{4}W^{a}_{\mu\nu}W^{\mu\nu a} - \frac{1}{4}B_{\mu\nu}B^{\mu\nu} + i\sum_{f}\overline{\psi}_{f}\gamma^{\mu}\partial_{\mu}\psi_{f}\,, \tag{1.8}$$

where $\overline{\psi} \equiv \psi^{\dagger}\gamma^{0}$ is the adjoint Dirac spinor. The sum over fermions runs for all the different fields in Table 1.1. The so-called strength tensors are given by

$$G^{\alpha}_{\mu\nu} = \partial_{\mu}G^{\alpha}_{\nu} - \partial_{\nu}G^{\alpha}_{\mu} + g_{s}f_{\alpha\beta\rho}G^{\beta}_{\mu}G^{\rho}_{\nu}\,, \tag{1.9}$$

$$W^{a}_{\mu\nu} = \partial_{\mu}W^{a}_{\nu} - \partial_{\nu}W^{a}_{\mu} + g_{L}\epsilon_{abc}W^{b}_{\mu}W^{c}_{\nu}\,, \tag{1.10}$$

$$B_{\mu\nu} = \partial_{\mu}B_{\nu} - \partial_{\nu}B_{\mu}\,, \tag{1.11}$$

where g_s and g_L are the coupling constants of $SU(3)_c$ and $SU(2)_L$, respectively. The commutator between generators of a Lie group provides the structure constants[4]. For $SU(3)_c$, $[t^{\alpha}, t^{\beta}] = if_{\alpha\beta\rho}t^{\rho}$ provides the antisymmetric structure constants $f_{\alpha\beta\rho}$. For $SU(2)_L$, $[T^{a}, T^{b}] = i\epsilon_{abc}T^{c}$ where ϵ_{abc} is the completely antisymmetric three-index tensor.

One can check that the strength tensor of the abelian factor is gauge invariant. In contrast, the strength tensors of the non-abelian factors are not gauge invariant, in this case only the product of two strength tensors contracted over all indices is gauge invariant[5]. This ensures that the kinetic gauge terms preserve the SM gauge symmetry. However, one can check that the fermion kinetic terms introduced in Eq. (1.8) are not gauge invariant by simply applying the transformations in Eqs. (1.5-1.7). We can obtain gauge invariant fermion kinetic terms by replacing the derivative in Eq. (1.8) by a covariant derivative,

$$D_{\mu} = \partial_{\mu} - ig_{s}t^{\alpha}G^{\alpha}_{\mu} - ig_{L}T^{a}W^{a}_{\mu} - ig_{Y}YB_{\mu}\,. \tag{1.12}$$

The covariant derivative transforms as an adjoint of the complete gauge group, and therefore the gauge boson fields live in the adjoint representation.

[4] We remind the reader that the vector space of generators of a Lie group, with the commutator between generators as inner product, provides the so-called Lie algebra of the given group.

[5] Remember the infinitesimal gauge transformations of gauge boson fields $V^{a}_{\mu} \to V^{a}_{\mu} - \frac{1}{g}\partial_{\mu}\alpha^{a}(x) - f_{abc}V^{c}_{\mu}\alpha^{b}(x)$ for $SU(N)$ gauge bosons and $V_{\mu} \to V_{\mu} - \frac{1}{g}\partial_{\mu}\alpha(x)$ for $U(1)$ gauge bosons, where $\alpha^{(a)}(x) \ll 1$ are arbitrary functions of spacetime.

One can check that the resulting Lagrangian,

$$\mathcal{L}_{\text{gauge}} = -\frac{1}{4}G^{\alpha}_{\mu\nu}G^{\mu\nu\alpha} - \frac{1}{4}W^{a}_{\mu\nu}W^{\mu\nu a} - \frac{1}{4}B_{\mu\nu}B^{\mu\nu} + i\sum_{f}\overline{\psi}_{f}\gamma^{\mu}D_{\mu}\psi_{f}\,, \tag{1.13}$$

is invariant under the SM gauge group. As a consequence of imposing gauge invariance, the Lagrangian now contains interaction terms coupling fermions with gauge bosons. For example, after expanding the covariant derivative, one can find a term $g_Y\overline{\psi}\gamma^{\mu}B_{\mu}\psi$ in the Lagrangian, coupling fermions to the hypercharge gauge boson. This is the beauty of the gauge principle: just by imposing gauge symmetry arguments, we can reproduce complicated interactions between fermions and gauge bosons observed in Nature. Since all the SM families have the same gauge symmetry transformations, the interactions among the SM fermions and gauge bosons are *universal in flavour*. In other words, all the fermion flavours have exactly the same interactions with the gauge bosons. This fact translates into the appearance of a global flavour symmetry (exact in the gauge sector at the classical level) as

$$U(3)^5 = U(3)_Q \times U(3)_L \times U(3)_u \times U(3)_d \times U(3)_e\,. \tag{1.14}$$

This flavour symmetry of the SM is denoted as *accidental*, because it is not imposed nor postulated, but simply arises as a consequence of having three identical families of fermions.

Due to the non-abelian nature of the $SU(3)_c$ and the $SU(2)_L$ symmetries, the kinetic terms for the corresponding gauge fields also generate self-interactions. These terms play a crucial role in the explanation of several key features of the strong interactions, such as confinement and asymptotic freedom [13–17]. The strong interactions mediated by gluons lead to composite subatomic particles made by quarks, that we denote as hadrons. Hadrons consist of baryons, made of three quarks, and mesons, made of a quark-antiquark pair. Some remarkable examples of baryons are the proton and neutron, which interact as well via the strong force in order to build the atomic nuclei. A dedicated review of the strong interactions is beyond the scope of this thesis, but we refer the interested reader to Ref. [18].

The Lagrangian included so far would be enough to describe a classical theory. The quantisation of gauge fields involves a number of subtleties, related to the fact that the quanta (gauge bosons) are massless spin-1 particles with just two degrees of freedom embedded in a vector field that has four. The usual solution consists in modifying the Lagrangian by adding a gauge-fixing term, $\mathcal{L} = \mathcal{L}_{\text{gauge}} + \mathcal{L}_{\text{GF}}$, in order to get rid of the extra degrees of freedom that would lead to an inconsistent quantum field theory. The quantisation of non-abelian gauge theories, like $SU(3)_c$ and $SU(2)_L$, also requires the addition of auxiliary anticommuting spin-0 fields, usually denoted as *ghost* fields. However, these fields are unphysical, as they never appear as external fields but only in internal lines of Feynman diagrams, and are just required for consistency of the quantum field theory [19]. It can be shown that a quantum field theory with these ingredients

is renormalisable (see e.g. [20]). This means that the ultraviolet divergences appearing from quantum corrections (*loops*) can be absorbed by an appropriate redefinition of the parameters and fields in the classical Lagrangian. In this manner, all physical observables can be reliably calculated.

All things considered, so far we have constructed a consistent and renormalisable gauge theory described by the following Lagrangian

$$\mathcal{L}_{\rm SM} = \mathcal{L}_{\rm gauge} + \mathcal{L}_{\rm GF} + \mathcal{L}_{\rm ghosts}\,, \tag{1.15}$$

where massless gauge bosons interact with massless fermions. Notice that the fact that the SM is a chiral theory, i.e. that left-handed and right-handed fermions transform differently under the gauge group, implies that conventional Dirac mass terms violate gauge invariance. Therefore, all fermions should indeed be massless. In a similar manner, all gauge bosons associated to unbroken gauge symmetries are massless. This description of the SM introduced so far, based only on fundamental principles, gauge symmetry and fundamental fermions, is however not realised in Nature. Quarks need to become massive in order to provide the observed spectrum of hadrons, plus charged lepton masses have been measured to be non-zero with good precision [21]. Moreover, data suggest that the electroweak part of the SM, $SU(2)_L \times U(1)_Y$, is somehow broken down to electric charge $U(1)_Q$, and as a consequence of such a process, linear combinations of the W^a_μ and B_μ bosons become massive, leading to the mediators of the weak force $W^\pm_\mu$ and Z_μ. The massless photon is recovered as the linear combination of W^3_μ and B_μ associated to the unbroken $U(1)_Q$. In the next two sections, we introduce the mechanism responsible for breaking the electroweak symmetry, leading to the weak and electromagnetic interactions, along with the masses of (most) fundamental fermions. This will involve the addition of extra terms to the renormalisable Lagrangian, leading to

$$\mathcal{L}_{\rm SM} = \mathcal{L}_{\rm gauge} + \mathcal{L}_{\rm GF} + \mathcal{L}_{\rm ghosts} + \mathcal{L}_{\rm scalar} - \mathcal{L}_{\rm Yukawa}\,. \tag{1.16}$$

1.3 Scalar sector and electroweak symmetry breaking

In the previous sections, we have built a consistent and renormalisable quantum field theory based on the SM gauge symmetry. However, such a theory only contains massless gauge bosons, making it impossible to explain the weak interactions observed in Nature. Nevertheless, in 1964, Peter Higgs, François Englert and Robert Brout proposed a mechanism that allows to *spontaneously* break a gauge symmetry, giving mass to the gauge bosons associated to the broken generators [22, 23]. This mechanism was later applied by Weinberg and Salam [24–26] to the electroweak part of the SM originally proposed by Glashow [27], leading to its spontaneous symmetry breaking down to $U(1)_Q$. The idea consists in constructing a theory with a fully symmetric Lagrangian, but whose vacuum is not invariant under the symmetry. This can be achieved in a rather minimal way by introducing in the theory a complex spin-0 field, transforming as a scalar under

the Lorentz group. This so-called Higgs field will develop a vacuum expectation value (VEV) that will trigger the spontaneous breaking of the electroweak symmetry.

Since we need to break $SU(2)_L$, the Higgs should transform non-trivially under it. The most simple choice is to postulate that the Higgs field transforms as a doublet under $SU(2)_L$. In a similar manner, we want to break $U(1)_Y$, so the Higgs field must carry non-zero hypercharge. Finally, it should carry no color in order to preserve $SU(3)_c$, which describes the strong interaction. With these considerations, a particularly appealing choice is $H \sim (\mathbf{1}, \mathbf{2}, 1/2)$. We can parameterise such a Higgs doublet as

$$H = \begin{pmatrix} \sigma \\ \phi \end{pmatrix} . \tag{1.17}$$

Interestingly, the component ϕ of the doublet carries $T_3 = -1/2$ (and $Y = 1/2$), meaning that if such component develops a VEV, then the electroweak symmetry is spontaneously broken but a gauge $U(1)$ associated to the linear combination $T_3 + Y$ remains unbroken. Indeed, such a gauge $U(1)$ can be associated to the electromagnetic interactions or quantum electrodynamics (QED), giving rise to the massless photon. The most general renormalisable Lagrangian for the Higgs doublet can be written as

$$\mathcal{L}_{\text{scalar}} = (D_\mu H)^\dagger (D^\mu H) - V(H) , \tag{1.18}$$

where the first term is the Higgs kinetic term. Just like in the fermion sector, the covariant derivative has been introduced to render the kinetic term gauge invariant. When applied to the Higgs doublet, the covariant derivative reads

$$D_\mu H = \left(\partial_\mu - i g_L \frac{\sigma^a}{2} W_\mu^a - i g_Y \frac{1}{2} B_\mu \right) . \tag{1.19}$$

On the other hand, gauge invariance and renormalisability also allow the inclusion of a scalar potential with the form

$$V(H) = m_H^2 H^\dagger H + \lambda \left(H^\dagger H \right)^2 , \tag{1.20}$$

containing a mass term for the Higgs doublet and a self-interaction term.

The vacuum state of the theory can be obtained by minimising the scalar potential

$$\left. \frac{\partial V}{\partial H} \right|_{H=\langle H \rangle} = m_H^2 \frac{v_{\text{SM}}}{\sqrt{2}} + \lambda \frac{v_{\text{SM}}^3}{\sqrt{2}} = 0 , \tag{1.21}$$

where

$$\langle H \rangle = \frac{1}{\sqrt{2}} \begin{pmatrix} 0 \\ v_{\text{SM}} \end{pmatrix} \tag{1.22}$$

is the VEV of the Higgs doublet, and we can take v_{SM} to be real and positive without loss of generality. It is straightforward to check that for $m_H^2 > 0$, the condition in Eq. (1.21) provides just one real minimum at $v_{\text{SM}} = 0$. However, for $m_H^2 < 0$, the

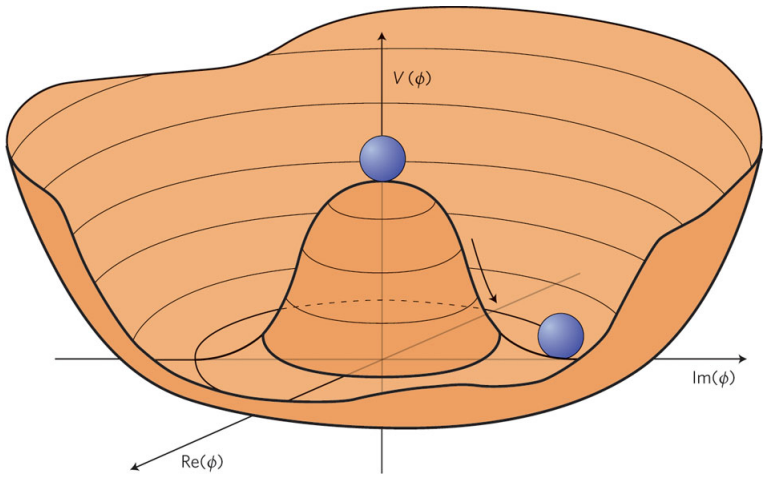

FIGURE 1.1: Higgs scalar potential for the case $m_H^2 < 0$ in terms of the neutral component of the Higgs doublet, ϕ. Figure taken from [28].

potential has two real and positive extrema

$$v_{\rm SM} = 0\,, \qquad v_{\rm SM} = \sqrt{-\frac{m_H^2}{\lambda}}\,. \tag{1.23}$$

If $\lambda < 0$, the potential is not bounded from below, making it impossible to define the ground state. Instead, if we impose $\lambda > 0$, then $v_{\rm SM} = 0$ corresponds to a local maximum while $v_{\rm SM} = \sqrt{-m_H^2/\lambda} > 0$ corresponds to the global minimum of the scalar potential, that we identify with the ground state. As depicted in Fig. 1.1, there is an infinite set of degenerate configurations for the neutral component ϕ that lead to the same vacua. Choosing one of those vacua triggers the spontaneous breaking of the electroweak gauge symmetry,

$$SU(2)_L \times U(1)_Y \to U(1)_Q\,, \tag{1.24}$$

where, as anticipated before, the unbroken $U(1)$ is associated to the electromagnetic force, in such a way that only electrically charged fermions carry non-zero charges under $U(1)_Q$. We can study which generators of the subgroup $SU(2)_L \times U(1)_Y$ are left unbroken by applying the generators to the vacuum $\langle H \rangle$ and verifying whether it is left invariant or not. The vacuum is left invariant by a generator G if

$$e^{i\alpha G}\langle H \rangle = \langle H \rangle\,, \tag{1.25}$$

which, for an infinitesimal transformation ($\alpha \ll 1$) leads to

$$e^{i\alpha G}\langle H \rangle \simeq (1 + i\alpha G)\,\langle H \rangle\,, \tag{1.26}$$

Field	u_i	d_i	ν_i	e_i
$U(1)_Q$	$2/3$	$-1/3$	0	-1

TABLE 1.2: Electric charges of fundamental fermions, related to weak isospin and hypercharge via Eq. (1.32). $i = 1, 2, 3$ is the flavour index.

which implies $G\langle H\rangle = 0$. In this case, we say that "G annihilates the vacuum". We can now apply all four generators of the electroweak gauge group to the vacuum. We find

$$T_1\langle H\rangle = \frac{\sigma_1}{2}\langle H\rangle = \frac{1}{2}\begin{pmatrix} 0 & 1 \\ 1 & 0 \end{pmatrix}\begin{pmatrix} 0 \\ \frac{v_{\rm SM}}{\sqrt{2}} \end{pmatrix} = \frac{1}{2}\begin{pmatrix} \frac{v_{\rm SM}}{\sqrt{2}} \\ 0 \end{pmatrix} \neq \begin{pmatrix} 0 \\ 0 \end{pmatrix} \text{ Broken}\,, \quad (1.27)$$

$$T_2\langle H\rangle = \frac{\sigma_2}{2}\langle H\rangle = \frac{1}{2}\begin{pmatrix} 0 & -i \\ i & 0 \end{pmatrix}\begin{pmatrix} 0 \\ \frac{v_{\rm SM}}{\sqrt{2}} \end{pmatrix} = -\frac{i}{2}\begin{pmatrix} \frac{v_{\rm SM}}{\sqrt{2}} \\ 0 \end{pmatrix} \neq \begin{pmatrix} 0 \\ 0 \end{pmatrix} \text{ Broken}\,, \quad (1.28)$$

$$T_3\langle H\rangle = \frac{\sigma_3}{2}\langle H\rangle = \frac{1}{2}\begin{pmatrix} 1 & 0 \\ 0 & -1 \end{pmatrix}\begin{pmatrix} 0 \\ \frac{v_{\rm SM}}{\sqrt{2}} \end{pmatrix} = -\frac{1}{2}\begin{pmatrix} 0 \\ \frac{v_{\rm SM}}{\sqrt{2}} \end{pmatrix} \neq \begin{pmatrix} 0 \\ 0 \end{pmatrix} \text{ Broken}\,, \quad (1.29)$$

$$Y\langle H\rangle = Y_H\langle H\rangle = \frac{1}{2}\langle H\rangle = \frac{1}{2}\begin{pmatrix} 0 \\ \frac{v_{\rm SM}}{\sqrt{2}} \end{pmatrix} \neq \begin{pmatrix} 0 \\ 0 \end{pmatrix} \text{ Broken}\,. \quad (1.30)$$

In this manner, we confirm that the electric charge operator Q is associated to the combination of generators of $SU(2)_L \times U(1)_Y$ that leaves the vacuum invariant,

$$Q\langle H\rangle = (T_3 + Y)\langle H\rangle = \left(\frac{\sigma_3}{2} + Y_H\right)\langle H\rangle = \frac{1}{2}\begin{pmatrix} 1 & 0 \\ 0 & 0 \end{pmatrix}\begin{pmatrix} 0 \\ \frac{v_{\rm SM}}{\sqrt{2}} \end{pmatrix} = \begin{pmatrix} 0 \\ 0 \end{pmatrix} \text{ Unbroken}\,. \quad (1.31)$$

Therefore, as anticipated before, the electric charge operator generating $U(1)_Q$ is given by

$$Q = T_3 + Y\,, \quad (1.32)$$

which immediately allows to extract the electric charges of fundamental fermions as per Table 1.2.

We find that electric charge is indeed unbroken after SSB. This is a consequence of choosing the neutral component of the Higgs doublet as the one that develops the VEV.

In the following, we will show how gauge bosons associated to (combinations of) the broken generators of $SU(2)_L \times U(1)_Y$ get a mass. When expanding the covariant derivative applied to the vacuum of the Higgs doublet, we obtain

$$\begin{aligned} D_\mu\langle H\rangle &= \left(\partial_\mu - i\frac{g_L}{2}\begin{bmatrix} W_\mu^3 & \sqrt{2}W_\mu \\ \sqrt{2}W_\mu^\dagger & -W_\mu^3 \end{bmatrix} - i\frac{g_Y}{2}B_\mu\right)\begin{pmatrix} 0 \\ v_{\rm SM}/\sqrt{2} \end{pmatrix} \quad (1.33) \\ &= \frac{v_{\rm SM}}{\sqrt{2}}\begin{pmatrix} -i\frac{g_L}{2}\sqrt{2}W_\mu \\ i\frac{g_L}{2}W_\mu^3 - i\frac{g_Y}{2}B_\mu \end{pmatrix}\,, \end{aligned}$$

where we have defined $W_\mu = (W_\mu^1 - iW_\mu^2)/\sqrt{2}$. With this, we can expand the kinetic term of the Higgs doublet in Eq. (1.18), obtaining

$$(D_\mu\langle H\rangle)^\dagger D^\mu\langle H\rangle = \frac{g_L^2 v_{\rm SM}^2}{4} W_\mu W^\mu + \frac{v_{\rm SM}^2}{2}\frac{1}{4}\begin{pmatrix} B_\mu & W_\mu^3 \end{pmatrix}\begin{pmatrix} g_Y^2 & -g_Y g_L \\ -g_Y g_L & g_L^2 \end{pmatrix}\begin{pmatrix} B^\mu \\ W^{3\mu} \end{pmatrix}. \tag{1.34}$$

It directly follows that the gauge bosons W_μ and $W_\mu^\dagger$, which we associate with the charged bosons W_μ^+ and W_μ^-, get a mass term after SSB. The gauge bosons B_μ and W_μ^3 also get mass terms, indicating a mass mixing. In order to obtain the mass eigenstates we need to diagonalise the off-diagonal matrix above, obtaining

$$(D_\mu\langle H\rangle)^\dagger D^\mu\langle H\rangle = \frac{g_L^2 v_{\rm SM}^2}{4} W_\mu^\dagger W^\mu + \frac{v_{\rm SM}^2}{2}\frac{1}{4}\begin{pmatrix} A_\mu & Z_\mu \end{pmatrix}\begin{pmatrix} 0 & 0 \\ 0 & (g_L^2+g_Y^2) \end{pmatrix}\begin{pmatrix} A^\mu \\ Z^\mu \end{pmatrix}, \tag{1.35}$$

where

$$\begin{pmatrix} A_\mu \\ Z_\mu \end{pmatrix} = \begin{pmatrix} \cos\theta_W & \sin\theta_W \\ -\sin\theta_W & \cos\theta_W \end{pmatrix}\begin{pmatrix} B_\mu \\ W_\mu^3 \end{pmatrix} = \begin{pmatrix} \cos\theta_W B_\mu + \sin\theta_W W_\mu^3 \\ -\sin\theta_W B_\mu + \cos\theta_W W_\mu^3 \end{pmatrix}, \tag{1.36}$$

where the mixing angle is commonly denoted as the "weak mixing angle" or the "Weinberg[6] angle", and is given by

$$\sin\theta_W = \frac{g_Y}{\sqrt{g_Y^2 + g_L^2}}. \tag{1.37}$$

In conclusion, expanding the kinetic term of the Higgs doublet reveals that the $W_\mu^\pm$ bosons and the Z_μ boson, given as linear combinations of the original gauge bosons of the massless theory, become massive gauge bosons after SSB. Their mass can be readily extracted from Eq. (1.35) as

$$M_W = \frac{1}{2} g_L v_{\rm SM}, \qquad M_Z = \frac{v_{\rm SM}}{2}\sqrt{g_L^2+g_Y^2} = \frac{1}{2\cos\theta_W} g_L v_{\rm SM}. \tag{1.38}$$

Instead, the A_μ boson (also known as the photon) remains massless, associated to the unbroken generator of $U(1)_Q$ with gauge coupling

$$e = \frac{g_L g_Y}{\sqrt{g_L^2 + g_Y^2}}, \tag{1.39}$$

which is commonly expressed as $\alpha_{\rm EM} = e^2/(4\pi)$ and denoted as the *fine-structure constant*. We can see that the masses of the $W_\mu^\pm$ and the Z_μ bosons are not independent but instead they follow the tree-level relation

$$\rho \equiv \frac{M_W^2}{M_Z^2\cos^2\theta_W} = 1. \tag{1.40}$$

[6] Although it appeared for the first time in the 1961 paper by Glashow [27].

The tree-level relation in Eq. (1.40) is a consequence of the so-called *custodial symmetry*. The Higgs potential $V(H)$ is invariant not only under the SM symmetry, but it is also accidentally invariant under a global $SO(4) \cong SU(2)_L \times SU(2)_R$ transformation. This can be easily seen by parameterising the Higgs doublet in terms of a four-dimensional vector of real scalar fields, $\vec{H} = (H_1, H_2, H_3, H_4)$, and noting that one has for the terms in the potential

$$(H^\dagger H) = \vec{H} \cdot \vec{H} \,, \tag{1.41}$$

which is invariant under four-dimensional rotations. After SSB, the accidental symmetry $SU(2)_L \times SU(2)_R$ gets spontaneously broken down to the diagonal subgroup. This symmetry is the reason for the tree-level relation among the gauge boson masses given in Eq. (1.40). However, the custodial symmetry is not a true accidental symmetry of the full Lagrangian, and gets explicitly broken by the gauging of the $U(1)_Y$ symmetry (and also by the different Yukawa couplings of up-quarks and down-quarks, to be introduced in Sections 1.4 and 1.6.1). Thanks to the smallness of the hypercharge gauge coupling and the smallness of most Yukawa couplings, these breaking effects are small and custodial symmetry remains as a good approximate symmetry. A consequence of this is the fact that the $W_\mu^\pm$ and Z_μ bosons have similar masses. Another consequence is that one obtains just small departures from $\rho = 1$ at higher orders in perturbation theory. Since these corrections are small, extensions of the SM that explicitly break the custodial symmetry, altering the tree-level relation in Eq. (1.40), typically receive very strong bounds from the experimental measurements of the ρ parameter, which has been tested to be in good agreement with the SM prediction [21].

A careful reader might have noticed that after SSB, our physical system seems to have more degrees of freedom than before SSB. Indeed, massless gauge bosons carry two degrees of freedom, while massive gauge bosons carry three. What is the origin of these extra degrees of freedom, associated to the now massive $W_\mu^\pm$ and Z_μ bosons? The Goldstone theorem [29] states that the spontaneous breaking of a symmetry leads to the appearance of a set of massless bosons, one for each of the broken generators. These are the so-called Goldstone bosons. Interestingly, when the broken symmetry is a gauge symmetry, the Goldstone bosons "get eaten" by the gauge fields and become their longitudinal components, providing enough degrees of freedom for a massive gauge boson. This can be easily seen if we parameterise the Higgs doublet in the following way

$$H = e^{i\frac{\varphi^a \sigma^a}{2v_{\rm SM}}} \begin{pmatrix} 0 \\ \frac{1}{\sqrt{2}}(v_{\rm SM} + h) \end{pmatrix} . \tag{1.42}$$

where the Goldstone bosons, φ^a $(a = 1, 2, 3)$, related to excitations along the minima of the scalar potential, are isolated in the exponential factor. It is clear that the Goldstone bosons are no longer physical: we can use the local $SU(2)_L$ gauge invariance to rotate away the Goldstone bosons, which effectively consists in setting $\varphi^a = 0$ in Eq. (1.42). This rotation corresponds to the choice of a specific gauge that receives the name of

unitary gauge. In this gauge, the Higgs doublet then reads

$$H = \frac{1}{\sqrt{2}} \begin{pmatrix} 0 \\ v_{\rm SM} + h \end{pmatrix} . \tag{1.43}$$

In this manner, the unphysical Goldstone bosons had been rotated away, their three physical degrees of freedom absorbed by the now massive $W_\mu^\pm$ and Z_μ gauge bosons. Nevertheless, we notice the existence of a physical scalar field associated to the radial excitation of the Higgs doublet, h. If we expand the kinetic term in Eq. (1.18) with the Higgs doublet in the unitary gauge, then we find that the field h couples at tree-level to the massive gauge bosons $W_\mu^\pm$ and Z_μ, with couplings proportional to their squared masses, but it does not couple to the massless photon. Indeed, the neutral scalar h is a key prediction of the model: the *Higgs boson*.

Finally, if we write the scalar potential of Eq. (1.20) in terms of the Higgs boson via Eq. (1.43), we obtain

$$V(h) = \frac{1}{2} m_h^2 h^2 + \frac{m_h^2}{2v_{\rm SM}} h^3 + \frac{m_h^2}{8v_{\rm SM}^2} h^4 - \frac{m_h^2 v_{\rm SM}^2}{8} , \tag{1.44}$$

which reveals that the Higgs boson acquires a mass proportional to its VEV, $m_h^2 = 2\lambda v_{\rm SM}^2$, as well as cubic and quartic self-interactions that are proportional to its mass. The Higgs boson predicted by the SM was discovered at the LHC in 2012 [30, 31], and its mass is now a well known quantity $m_h = 125.25 \pm 0.17\,\text{GeV}$ [21]. In this manner, the Higgs self-couplings are completely fixed in the SM at tree-level in terms of its mass. However, testing this key prediction of the SM is difficult: The HL-LHC will only probe order one departures from the SM prediction [32], and pushing the energy frontier further will be required in order to gain one order of magnitude in precision [33]. Finally, the constant term in Eq. (1.44) contributes to the energy of the vacuum, so it becomes a contribution to the cosmological constant of the Universe. However, this contribution turns out to be 56 orders of magnitude larger (and with the opposite sign) than the observed value of the cosmological constant, which is required to be introduced in the equations of General Relativity in order to explain the accelerated expansion of our Universe. This implies that there should be an incredibly fine-tuned cancellation between $-m_h^2 v_{\rm SM}^2/8$ and a bare vacuum energy parameter that can be introduced in the Lagrangian, leading to the worst fine-tuning problem of the SM [8, 34, 35].

1.4 Yukawa sector

We have now built the Standard Model as a consistent QFT based on gauge symmetry, where the electroweak part of the SM group is spontaneously broken via the Higgs mechanism down to QED, and the $W_\mu^\pm$ and Z_μ bosons become massive and mediate the weak interactions. In this section, we shall explain how most of the fundamental fermions of the SM also become massive via the Higgs mechanism (except for neutrinos

that will remain massless). The particular representations of fundamental fermions and the Higgs doublet under the SM gauge group allow to introduce the following terms in the SM Lagrangian,

$$\mathcal{L}_{\text{Yukawa}} = y^u_{ij}\overline{Q}_{Li}\tilde{H}u_{Rj} + y^d_{ij}\overline{Q}_{Li}Hd_{Rj} + y^e_{ij}\overline{L}_{Li}He_{Rj} + \text{h.c.}\,, \tag{1.45}$$

where $\tilde{H} = i\sigma^2 H^*$ is the conjugate of H with well-defined transformations (doublet of $SU(2)_L$ with $Y = -1/2$), $i, j = 1, 2, 3$ are flavour indices and $y^{u,d,e}_{ij}$ are completely generic 3×3 complex matrices. The interaction terms above, and usually also the matrices $y^{u,d,e}_{ij}$ containing the coupling constants, are denoted as the *Yukawa couplings* of the SM. After the Higgs doublet develops a VEV, the Yukawa couplings above provide mass terms for charged fermions along with couplings to the Higgs boson. Working in the unitary gauge as introduced in Eq. (1.43), we obtain

$$\mathcal{L}_{\text{Yukawa}} = \frac{1}{\sqrt{2}}(v_{\text{SM}} + h)\left[y^u_{ij}\bar{u}_{Li}u_{Rj} + y^d_{ij}\frac{1}{\sqrt{2}}\bar{d}_{Li}d_{Rj} + y^e_{ij}\frac{1}{\sqrt{2}}\bar{e}_{Li}e_{Rj}\right] + \text{h.c.} \tag{1.46}$$

Remarkably, neutrinos do not obtain mass terms nor couplings to the Higgs boson, so they remain massless: this is a consequence of the absent of right-handed neutrinos in the SM. On the other hand, it is definitely remarkable that the same mechanism that gives masses to the gauge bosons (SSB), also gives masses to the charged fermions. Now, in general the three Yukawa matrices are not diagonal, but rather completely generic 3×3 complex matrices. In order to obtain mass eigenstates and eigenvalues, the Yukawa matrices in Eq. (1.46) must be brought to diagonal form. Since all mass terms in $\mathcal{L}_{\text{Yukawa}}$ are of Dirac type, this must be done by means of biunitary transformations: Given a general complex matrix $\mathcal{M}$, there exist two unitary matrices V and V' (verifying $VV^\dagger = V^\dagger V = \mathbb{I}$ and $V'V'^\dagger = V'^\dagger V' = \mathbb{I}$) such that

$$V\mathcal{M}V'^\dagger = \tilde{\mathcal{M}}\,, \tag{1.47}$$

where $\tilde{\mathcal{M}}$ is diagonal. This general result can be applied to the Yukawa matrices of Eq. (1.46). From a physical point of view, independent transformations rotate the left-handed and right-handed spinors from the interaction basis to the mass basis, obtaining

$$\begin{aligned}\mathcal{L}_{\text{Yukawa}} = \frac{1}{\sqrt{2}}(v_{\text{SM}} + h)\Big[&\bar{u}_L V^\dagger_{u_L} V_{u_L} y^u V^\dagger_{u_R} V_{u_R} u_{Rj} + \bar{d}_L V^\dagger_{d_L} V_{d_L} y^d V^\dagger_{d_R} V_{d_R} d_{Rj} \\ &+\bar{e}_L V^\dagger_{e_L} V_{e_L} y^e V^\dagger_{e_R} V_{e_R} e_{Rj}\Big] + \text{h.c.}\,,\end{aligned} \tag{1.48}$$

where rather than including a large number of flavour indices, we have defined three-component fermion vectors containing the three flavours as $f_L = (f_{L1}, f_{L2}, f_{L3})^{\text{T}}$ and $f_R = (f_{R1}, f_{R2}, f_{R3})^{\text{T}}$, where $f = u, d, e$. Thanks to the unitary property of the rotation matrices, one can check that $\mathcal{L}_{\text{Yukawa}}$ remains invariant, but written in the form of

Eq. (1.48) one can identify the diagonal Yukawa matrices as

$$V_{u_L} y^u V_{u_R}^\dagger = \mathrm{diag}(y_u, y_c, y_t)\,, \tag{1.49}$$

$$V_{d_L} y^d V_{d_R}^\dagger = \mathrm{diag}(y_d, y_s, y_b)\,, \tag{1.50}$$

$$V_{e_L} y^e V_{e_R}^\dagger = \mathrm{diag}(y_e, y_\mu, y_\tau)\,, \tag{1.51}$$

along with the mass eigenstates

$$\begin{pmatrix} u_L \\ c_L \\ t_L \end{pmatrix} = V_{u_L} \begin{pmatrix} u_{L1} \\ u_{L2} \\ u_{L3} \end{pmatrix}, \qquad \begin{pmatrix} u_R \\ c_R \\ t_R \end{pmatrix} = V_{u_R} \begin{pmatrix} u_{R1} \\ u_{R2} \\ u_{R3} \end{pmatrix}, \tag{1.52}$$

$$\begin{pmatrix} d_L \\ s_L \\ b_L \end{pmatrix} = V_{d_L} \begin{pmatrix} d_{L1} \\ d_{L2} \\ d_{L3} \end{pmatrix}, \qquad \begin{pmatrix} d_R \\ s_R \\ b_R \end{pmatrix} = V_{d_R} \begin{pmatrix} d_{R1} \\ d_{R2} \\ d_{R3} \end{pmatrix}, \tag{1.53}$$

$$\begin{pmatrix} e_L \\ \mu_L \\ \tau_L \end{pmatrix} = V_{e_L} \begin{pmatrix} e_{L1} \\ e_{L2} \\ e_{L3} \end{pmatrix}, \qquad \begin{pmatrix} e_R \\ \mu_R \\ \tau_R \end{pmatrix} = V_{e_R} \begin{pmatrix} e_{R1} \\ e_{R2} \\ e_{R3} \end{pmatrix}. \tag{1.54}$$

One can notice that the different flavours of mass eigenstates enjoy a dedicated notation, as they receive particular names by convention. The first family of charged fermions is formed by the up-quark, the down-quark and the electron. The second family is formed by the charm-quark, the strange-quark and the muon. Finally, the third family is formed by the top-quark, the bottom-quark and the tau. The three flavours of neutrinos, massless in the SM, remain aligned with the original interaction eigenstates and are given names associated to the flavours of charged leptons: electron neutrino, muon neutrino and tau neutrino.

After diagonalising the Yukawa matrices, the mass eigenstates of charged fermions obtain a well-defined mass given by

$$m_\alpha = y_\alpha \frac{v_{\mathrm{SM}}}{\sqrt{2}}\,. \tag{1.55}$$

The masses of charged leptons can be measured in the experiment, while the masses of quarks can be estimated by QCD methods from the masses of hadrons. The Higgs VEV v_{SM} can also be extracted from the experiment such that the physical Yukawa couplings y_α can be univocally determined. The interactions of the Higgs boson with charged fermions are proportional to the physical Yukawa couplings y_α, which are generally different for each fermion. Given that the gauge sector is flavour universal, the Yukawa couplings are the only source of *flavour physics* in the SM. This is translated to the fact that the Yukawa couplings break the accidental $U(3)^5$ flavour symmetry of the SM introduced in Eq. (1.14). More about this will be discussed in Section 1.9.

Particle physics experiments are sensitive to the physical mass eigenstates of fermions, therefore it is important to write the SM gauge interactions in the mass basis. For the particular case of the weak interactions mediated by the $W_\mu^\pm$ bosons, we will see that fermion mixing originated from the Yukawa couplings plays a fundamental role.

1.5 Weak interactions and CKM mixing: flavour violation

Having completed the SM with the scalar and Yukawa sectors, now we are ready to write the weak interactions for fundamental fermions as the final step of our description of the SM. We are interested on the terms of the covariant derivative related to the physical bosons $W_\mu^\pm$, Z_μ and A_μ,

$$\mathcal{L}_{\text{gauge}} \supset \left(\frac{g_L}{\sqrt{2}} J_\mu^+ W^{\mu+} + \text{h.c.}\right) + \left(g_L \cos\theta_W J_\mu^3 - g_Y \sin\theta_W J_\mu^Y\right) Z^\mu + e J_\mu^{\text{em}} A^\mu \,, \quad (1.56)$$

where

$$J_\mu^+ = \bar{u}_L \gamma_\mu d_L + \bar{\nu}_L \gamma_\mu e_L \,, \quad (1.57)$$

$$J_\mu^3 = \frac{1}{2}\bar{u}_L \gamma_\mu u_L - \frac{1}{2}\bar{d}_L \gamma_\mu d_L + \frac{1}{2}\bar{\nu}_L \gamma_\mu \nu_L - \frac{1}{2}\bar{e}_L \gamma_\mu e_L \,, \quad (1.58)$$

$$J_\mu^Y = \frac{1}{6}\bar{u}_L \gamma_\mu u_L + \frac{1}{6}\bar{d}_L \gamma_\mu d_L - \frac{1}{2}\bar{\nu}_L \gamma_\mu \nu_L - \frac{1}{2}\bar{e}_L \gamma_\mu e_L + \frac{2}{3}\bar{u}_R \gamma_\mu u_R - \frac{1}{3}\bar{d}_R \gamma_\mu d_R - \bar{e}_R \gamma_\mu e_R \,, \quad (1.59)$$

$$J_\mu^{\text{em}} = \frac{2}{3}\left(\bar{u}_L \gamma_\mu u_L + \bar{u}_R \gamma_\mu u_R\right) - \frac{1}{3}\left(\bar{d}_L \gamma_\mu d_L + \bar{d}_R \gamma_\mu d_R\right) - \left(\bar{e}_L \gamma_\mu e_L + \bar{e}_R \gamma_\mu e_R\right) . \quad (1.60)$$

and $e = g_L \sin\theta_W = g_Y \cos\theta_W$ is the gauge coupling of QED, univocally determined by g_L and g_Y via Eq. (1.39). The equations above are written in terms of interaction eigenstates, defined as three-component vectors containing the three flavours as $f_L = (f_{L1}, f_{L2}, f_{L3})^{\text{T}}$ and $f_R = (f_{R1}, f_{R2}, f_{R3})^{\text{T}}$, where $f = u, d, \nu, e$. We can notice already that QED interactions and the neutral currents mediated by Z_μ are flavour universal: the rotations V_{f_L} and V_{f_R} cancel by unitarity for every term in the Lagrangian. The fundamental reason for Z_μ interactions being flavour universal is that all mass eigenstates of a given electric charge originate from the same $SU(2)_L \times U(1)_Y$ representations, otherwise Z_μ would mediate flavour transitions at tree-level. For QED (and QCD), the fundamental reason is the flavour universality of the kinetic terms in the canonical basis, which imposes the universality of the interactions related to the unbroken symmetries. Remarkably, the SM was not proposed as a minimal theory to explain the observed phenomena, but rather as a non-minimal model that predicted the neutral currents mediated by the Z_μ boson as a smoking-gun signal. Weak neutral currents were discovered in 1973 at the Gargamelle experiment of CERN [36].

We now focus on the charged currents mediated by $W_\mu^\pm$, and we rotate fermion states from the interaction basis to the mass basis

$$\begin{aligned}\mathcal{L}_{\text{cc}} &= \frac{g_L}{\sqrt{2}} \left(\bar{u}_L \gamma_\mu d_L + \bar{\nu}_L \gamma_\mu e_L\right) W^{\mu+} + \text{h.c.} \\ &= \frac{g_L}{\sqrt{2}} \left(\hat{\bar{u}}_L V_{u_L}^\dagger V_{d_L} \gamma_\mu \hat{d}_L + \bar{\nu}_L V_{e_L} \gamma_\mu \hat{e}_L\right) W^{\mu+} + \text{h.c.}\,,\end{aligned} \tag{1.61}$$

where $\hat{f}$ denotes mass eigenstates. We notice that the charged currents are sensitive to the product of left-handed quark mixing matrices, that is denoted as the *Cabbibo-Kobayashi-Maskawa (CKM) matrix* [37, 38],

$$V_{\text{CKM}} = V_{u_L}^\dagger V_{d_L}\,. \tag{1.62}$$

On the other hand, since neutrinos are massless in the SM, the rotation matrix V_{e_L} is unphysical in the SM, as it can be absorbed by redefining the neutrino states.

In contrast, the neutral currents mediated by Z_μ, along with the QED and QCD interactions, all couple fermions with their conjugate counterparts, such that the rotation matrices cancel by unitarity. Therefore, the right-handed rotation matrices V_{u_R,d_R,e_R}, along with V_{e_L}, are all unphysical in the SM: no interaction is sensitive to them. As a consequence, these interactions are flavour universal and do not mediate flavour transitions at tree-level. In the lepton sector, this is denoted as lepton flavour universality (LFU) in the SM: gauge interactions do not discriminate between the different lepton flavours, up to small corrections given by the different masses of charged leptons.

The rotation matrices V_{u_L} and V_{d_L} are not physical themselves, but rather their product V_{CKM} as per Eq. (1.62) is physical. This way, the charged currents provide tree-level flavour transitions proportional to the off-diagonal elements of the CKM matrix, leading to flavour physics. Remarkably, in the absence of Yukawa couplings, fermion mixing would vanish and the charged currents would not mediate family transitions. As anticipated, Yukawa couplings in the SM are the only source of flavour physics. Moreover, we shall see that the CKM matrix contains one physical complex phase, meaning that weak interactions break the so-called CP symmetry that relates particles and antiparticles.

As a final remark, when one goes beyond the SM, it is possible that the new interactions are sensitive to each of the individual rotation matrices that connect the interaction and mass basis, such that they become physical. This can happen even in an effective field theory framework such as the SMEFT [39].

1.6 The flavour puzzle

1.6.1 Parameters of the SM: mass hierarchies and quark mixing

The Higgs VEV v_{SM} can be extracted from the Fermi constant $G_F = 1.1663788(6) \times 10^{-5}$ GeV^{-2} [21], which has been accurately measured from the process of muon decay

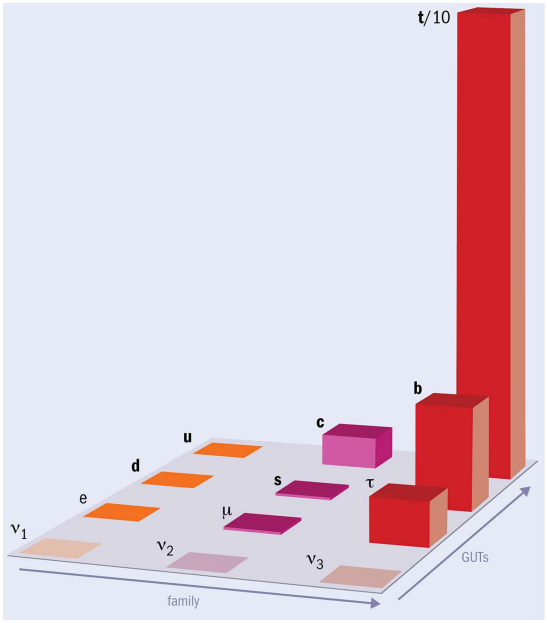

FIGURE 1.2: Fermion mass hierarchies between the different families and charge sectors.

into an electron and two neutrinos. The resulting value is

$$v_{\rm SM} = \left(\sqrt{2}G_F\right)^{-1/2} = 246.21964(6)\ \text{GeV}\,, \tag{1.63}$$

which sets the energy scale for the spontaneous breaking of the electroweak symmetry. The Yukawa interactions of the Higgs doublet with charged fermions introduce most of the free parameters of the SM: 3 charged lepton masses, 6 quark masses, 3 mixing angles for the CKM matrix and the CP-violating phase. The masses of charged leptons can be directly measured in the experiment, while the masses of quarks can be estimated by QCD methods from the masses of hadrons (which can be measured in the experiment as well). The determination of these parameters provides a hierarchical spectrum of fermion masses. At low energies, the masses of charged fermions can be approximately described in terms of the Wolfenstein parameter $\lambda \simeq 0.225$ as [21]

$$m_t \sim \frac{v_{\rm SM}}{\sqrt{2}}\,, \qquad m_c \sim \lambda^{3.3}\frac{v_{\rm SM}}{\sqrt{2}}\,, \qquad m_u \sim \lambda^{7.5}\frac{v_{\rm SM}}{\sqrt{2}}\,, \tag{1.64}$$

$$m_b \sim \lambda^{2.5}\frac{v_{\rm SM}}{\sqrt{2}}\,, \qquad m_s \sim \lambda^{5.0}\frac{v_{\rm SM}}{\sqrt{2}}\,, \qquad m_d \sim \lambda^{7.0}\frac{v_{\rm SM}}{\sqrt{2}}\,, \tag{1.65}$$

$$m_\tau \sim \lambda^{3.0}\frac{v_{\rm SM}}{\sqrt{2}}\,, \qquad m_\mu \sim \lambda^{4.9}\frac{v_{\rm SM}}{\sqrt{2}}\,, \qquad m_e \sim \lambda^{8.4}\frac{v_{\rm SM}}{\sqrt{2}}\,. \tag{1.66}$$

Although the specific values of fermion masses depend on the energy scale, as they experience RGE running, the mass ratios of fermions from different families but in the same charged sector are constant. For example, $m_c/m_t \sim \lambda^{3.3}$ is RGE-independent, and similar ratios can be constructed for each charged sector. It is clear this way that the third family is the heaviest, while the first and second families are hierarchically lighter,

up-quarks		down-quarks		charged leptons	
m_t	172.69 ± 0.30 GeV	m_b	$4.18^{+0.03}_{-0.02}$ GeV	m_τ	1.77686 ± 0.12 GeV
m_c	1.27 ± 0.02 GeV	m_s	$93.4^{+8.6}_{-3.4}$ MeV	m_μ	105.6583755(23) MeV
m_u	$2.16^{+0.49}_{-0.26}$ MeV	m_d	$4.67^{+0.48}_{-0.17}$ MeV	m_e	0.51099895000(15) MeV

TABLE 1.3: Numerical values for charged fermion masses in the SM [21]. The u-, d-, and s-quark masses are the $\overline{\text{MS}}$ masses at the scale $\mu = 2$ GeV. The c- and b-quark masses are the $\overline{\text{MS}}$ masses renormalised at their $\overline{\text{MS}}$ mass scale, i.e. $\mu = m_c\,, m_b$ respectively. The t-quark mass is extracted from event kinematics. Charged lepton masses are measured in low-energy experiments.

with the first family being lighter than the second, as highlighted in Fig. 1.2. These hierarchies are difficult to understand due to the fact that the three fermion families are identical objects under the gauge symmetry. There also exist hierarchies between charged sectors, i.e. among fermions that transform differently under the gauge group:

- In the third family, top is heavier than bottom and tau, while bottom and tau have a mass of a similar order of magnitude.
- In the second family, charm is heavier than strange and muon, while strange and muon have a mass of a similar order of magnitude.
- In contrast, in the first family the down-quark is the heaviest, while the up-quark is heavier than the electron.

The hierarchies between charged sectors are, however, affected by RGE running. We introduce the specific numerical values of low-energy fermion masses in Table 1.3.

Quark mixing is accounted by the CKM matrix, which is a 3×3 complex and unitary matrix. In all generality, such a matrix would contain 3 moduli and 6 phases, however 5 of them can be reabsorbed by quark field redefinitions,

$$u_L^i \to e^{i\alpha_i} u_L^i\,, \qquad d_L^j \to e^{i\beta_j} d_L^j\,, \qquad V_{\text{CKM}}^{ij} \to V_{\text{CKM}}^{ij} e^{i(\alpha_i - \beta_j)}\,, \tag{1.67}$$

such that only one phase remains physical. In this manner, the CKM matrix can be parameterised by three moduli associated to mixing angles, and one CP-violating phase. Of the many possible conventions, a standard choice has become [40]

$$\begin{aligned} V_{\text{CKM}} &= \begin{pmatrix} 1 & 0 & 0 \\ 0 & c_{23} & s_{23} \\ 0 & -s_{23} & c_{23} \end{pmatrix} \begin{pmatrix} c_{13} & 0 & s_{13} e^{-i\delta_{\text{CKM}}} \\ 0 & 1 & 0 \\ -s_{13} e^{i\delta_{\text{CKM}}} & 0 & c_{13} \end{pmatrix} \begin{pmatrix} c_{12} & s_{12} & 0 \\ -s_{12} & c_{12} & 0 \\ 0 & 0 & 1 \end{pmatrix} \\ &= \begin{pmatrix} c_{12}c_{13} & s_{12}c_{13} & s_{13} e^{-i\delta_{\text{CKM}}} \\ -s_{12}c_{13} - c_{12}s_{23}s_{13} e^{i\delta_{\text{CKM}}} & c_{12}c_{23} - s_{12}s_{23}s_{13} e^{i\delta_{\text{CKM}}} & s_{23}c_{13} \\ s_{12}s_{23} - c_{12}c_{23}s_{13} e^{i\delta_{\text{CKM}}} & -c_{12}s_{23} - s_{12}c_{23}s_{13} e^{i\delta_{\text{CKM}}} & c_{23}c_{13} \end{pmatrix}, \end{aligned} \tag{1.68}$$

where $s_{ij} \equiv \sin\theta_{ij}$, $c_{ij} \equiv \cos\theta_{ij}$ and $\delta_{\rm CKM}$ is the phase responsible for all CP-violating phenomena in flavour-changing processes in the SM. The violation of the CP symmetry in the charged currents leads to different interactions for particles and antiparticles. CP violation was experimentally discovered in neutral kaon decays in 1964 [41], and observed in recent years in B meson decays [42] and in the charm sector [43].

The angles θ_{ij} can be chosen to lie in the first quadrant, so that $s_{ij}, c_{ij} \geq 0$. A global fit to the mixing angles and CP-violating phase in Eq. (1.68) reveals [21]

$$\sin\theta_{12} = 0.22500 \pm 0.00067\,, \qquad \sin\theta_{13} = 0.00369 \pm 0.00011\,, \tag{1.69}$$

$$\sin\theta_{23} = 0.04182^{+0.00085}_{-0.00074}\,, \qquad \delta_{\rm CKM} = 1.144 \pm 0.027\,. \tag{1.70}$$

It follows that the CKM matrix is hierarchical, described by $s_{13} \ll s_{23} \ll s_{12} \ll 1$ where the largest angle θ_{12} is traditionally known as the *Cabibbo angle* [37], and the CP-violating phase is of $\mathcal{O}(1)$. To exhibit more clearly the hierarchy of the CKM matrix, it is convenient to adopt the Wolfenstein parameterisation, where we define [21]

$$s_{12} \equiv \lambda\,, \qquad s_{23} \equiv A\lambda^2\,, \qquad s_{13}e^{i\delta_{\rm CKM}} \equiv A\lambda^3(\rho + i\eta)\,, \tag{1.71}$$

where the Wolfenstein parameter $\lambda = s_{12} \simeq 0.225$ is associated to the Cabibbo angle, and is also used to parameterise charged fermion masses as per Eqs. (1.64-1.66). We now write the CKM matrix in the Wolfenstein parameterisation up to $\mathcal{O}(\lambda^4)$, obtaining

$$V_{\rm CKM} = \begin{pmatrix} 1-\lambda^2/2 & \lambda & A\lambda^3(\rho - i\eta) \\ -\lambda & 1-\lambda^2/2 & A\lambda^2 \\ A\lambda^3(1-\rho-i\eta) & -A\lambda^2 & 1 \end{pmatrix} + \mathcal{O}(\lambda^4)\,. \tag{1.72}$$

A global fit of recent data to the Wolfenstein parameters (assuming the unitarity constraints of a three generation CKM matrix) reveals [21]

$$\lambda = 0.22500 \pm 0.00067\,, \qquad A = 0.826^{+0.018}_{-0.015}\,, \tag{1.73}$$

$$\rho = 0.159 \pm 0.010\,, \qquad \eta = 0.348 \pm 0.010\,.$$

Finally, it is also common to denote the different elements of the CKM matrix by the quark transitions associated to them in the charged currents,

$$V_{\rm CKM} = \begin{pmatrix} V_{ud} & V_{us} & V_{ub} \\ V_{cd} & V_{cs} & V_{cb} \\ V_{td} & V_{ts} & V_{tb} \end{pmatrix}\,. \tag{1.74}$$

We also introduce the Jarlskog invariant [21, 44]

$$\begin{aligned} J &= {\rm Im}(V_{us}V_{cb}V_{ub}^*V_{cs}^*) = c_{12}c_{13}^2c_{23}s_{12}s_{13}s_{23}\sin\delta_{\rm CKM} \\ &= (3.08^{+0.15}_{-0.13}) \times 10^{-5}\,, \end{aligned} \tag{1.75}$$

which is a quantitative measure of CP violation in weak interactions independent of conventions. In the parameterisation of Eq. (1.74), we highlight key off-diagonal elements associated to the mixing angles, and their scaling with λ as

$$V_{us} \sim s_{12} \sim \lambda\,, \qquad V_{cb} \sim s_{23} \sim \lambda^2\,, \qquad V_{ub} \sim s_{13} \sim \lambda^3\,. \tag{1.76}$$

The specific numerical values for the magnitude of each CKM element $|V_{\alpha\beta}|$ are [21]

$$|V_{\rm CKM}| = \begin{pmatrix} 0.97373(31) & 0.2243(8) & 0.00382(20) \\ 0.221(4) & 0.975(6) & 0.0408(14) \\ 0.0086(2) & 0.0415(9) & 1.014(29) \end{pmatrix}, \tag{1.77}$$

where for V_{cb} and V_{ub} we show the results obtained from exclusive meson decays[7]. We note here that the CKM elements are commonly used as input in flavour physics calculations. However, if NP afflict the observables used in the experimental determination of the CKM elements, then this NP infection would be translated to flavour physics computations, making the results unreliable. Alternative approaches to circumvent this issue have been proposed in the literature [45].

Finally, the remaining parameters of the SM include the gauge couplings g_s, g_L and g_Y. g_s can be extracted via QCD methods as long as a confinement scale is provided [46], which is usually given via the pion decay constant $f_\pi = 130.19(89)$ MeV or the Ω^- baryon mass, $m_{\Omega^-} = 1672.45(29)$ MeV, [21, 46]. The couplings g_L and g_Y are commonly extracted from the mass of the Z boson, $M_Z = 91.1876(21)$ GeV, and from the fine-structure constant, $\alpha^{-1}_{\rm EM}(M_Z) = 127.916 \pm 0.015$ [21], obtaining (using tree-level expressions)

$$g_s(M_Z) = 1.217(5)\,, \qquad g_L(M_Z) = 0.64842(3)\,, \qquad g_Y(M_Z) = 0.35804(3)\,. \tag{1.78}$$

For a more precise calculation, see the values computed at NNLO in Ref. [47]. The smallness of the gauge couplings g_L and g_Y allows to perform reliable perturbative calculations in quantum field theory for QED and weak interactions at low energies. This is not the case for g_s, which is larger and grows via RGE at low energies due to asymptotic freedom. It is also common to express the gauge couplings as $\alpha_i = g_i^2/4\pi$, such that [21]

$$\alpha_s(M_Z) = 0.1179(9)\,, \qquad \alpha_L(M_Z) = 0.033458(3)\,, \qquad \alpha_Y(M_Z) = 0.0102012(17)\,. \tag{1.79}$$

In principle, one may add a gauge invariant topological term for each of $SU(3)_c$, $SU(2)_L$ and $U(1)_Y$ to the Lagrangian of the gauge sector (1.13), leading to three extra parameters. The so-called $\theta_{\rm QCD}$ and $\theta_{SU(2)_L}$ may be observable due to non-perturbative instanton effects, while $\theta_{U(1)_Y}$ is unphysical [48, 49]. Given that $SU(2)_L$ acts chirally

[7] We note that there exists tension between the inclusive and exclusive determinations of V_{cb} and V_{ub}, and also a small deficit in first row unitarity of the CKM matrix. This is briefly discussed in Section 1.7.

on SM fermions, it is possible to absorb $\theta_{SU(2)_L}$ via a chiral rotation associated to an anomalous (but classically conserved) $U(1)$ (say e.g. $U(1)_{B+L}$), meaning it is unphysical as well[8]. In contrast, since QCD acts vector-like over SM quarks, $\theta_{\rm QCD}$ cannot be rotated away and is responsible for CP violation in QCD interactions. However, from experimental constraints on the neutron EDM one derives[9] $|\overline{\theta}_{\rm QCD}| < 10^{-10}$ [51]. We denote such apparent (and unexplained) absence of CP violation in the QCD sector as the *strong CP puzzle*, which will be briefly introduced in Section 1.7.

The last parameter of the SM is the mass of the Higgs boson $m_h = 125.25 \pm 0.17\,\text{GeV}$ [21]. All things considered, the SM contains 19 parameters: the three gauge couplings and $\overline{\theta}_{\rm QCD}$, nine fermion masses and four quark mixing parameters, the Higgs VEV and the mass of the Higgs boson. This is already a rather large set of parameters for a fundamental theory. Going beyond the SM, the parameter counting is enlarged when massive neutrinos are considered.

1.6.2 The origin of neutrino masses and mixing

In the decade of the 1990s, a series of neutrino experiments showed conspicous discrepancies with the neutrino flux predictions of the SM. In 1998, the Super-Kamiokande collaboration discovered evidence that neutrinos do oscillate in flavour [52–54], explaining the discrepancies in the observed fluxes of atmospheric neutrinos. In 2002, the SNO collaboration further confirmed the evidence for neutrino oscillations, reporting that solar neutrinos do also oscillate in flavour [55]. The neutrino flavour oscillations can only be realised in Nature if there exists neutrino mixing, which can only happen if at least two neutrinos are massive. Neutrino oscillations have become a confirmed discrepancy between the experiment and the SM, which cannot account for the existence of massive neutrinos without being extended.

Going beyond the SM, the most simple way to obtain a mass term for neutrinos is to introduce right-handed neutrinos that transform as complete singlets under the SM, $N_{Rj} \sim (\mathbf{1}, \mathbf{1}, 0)$. Given that for all the other fermions both chiralities are present in Nature, it seems natural to think that right-handed neutrinos do also exists. With this addition, one can write Yukawa couplings between neutrinos and the Higgs doublet in a similar manner as for charged fermions. As a toy example, let us consider that only one left-handed neutrino flavour ν_L exists in Nature, transforming as a doublet under $SU(2)_L$ along with his left-handed charged lepton partner $L_L = (\nu_L, e_L)^{\rm T}$. Now let us introduce one right-handed neutrino $N_R \sim (\mathbf{1}, \mathbf{1}, 0)$. We are now free to write the

[8] Although $\theta_{SU(2)_L}$ becomes observable (but its effects are generally very suppressed) in specific BSM scenarios where both baryon and lepton number are broken [50]. An example of this are gauge unified frameworks such as $SU(5)$ spontaneously broken to the SM, where all group factors get the same θ parameter and $\theta_{SU(2)_L}$ becomes observable via $\Delta B = \Delta L = \pm 1$ processes (further suppressed by the scale of grand unification) [49].

[9] Formally speaking, only the linear combination $\overline{\theta}_{\rm QCD} = \theta_{\rm QCD} + \text{Arg}[\text{Det}(Y_u Y_d)]$ is invariant under quark chiral rotations, and hence physically observable.

following gauge invariant coupling in our Lagrangian,

$$\mathcal{L}_\nu \supset y^\nu \bar{L}_L \widetilde{H} N_R + \text{h.c.} \tag{1.80}$$

However, the fact that N_R is a complete singlet under the SM allows to introduce a bare mass term in the Lagrangian that preserves gauge invariance,

$$\mathcal{L}_\nu = y^\nu \bar{L}_L \widetilde{H} N_R + \frac{1}{2} M_R \bar{N}_R^C N_R + \text{h.c.}\,, \tag{1.81}$$

where $N_R^C = C\bar{N}_R^{\mathrm{T}}$, with $C = i\gamma^0\gamma^2$ denoting the charge conjugation operator. This new term is called a Majorana mass: it violates all $U(1)$ charges by two units, including lepton number. In this manner, only SM singlet fermions can receive a Majorana mass, and are denoted Majorana fermions. In principle, M_R is not subject to any symmetry and could take any value. One possible choice is to take $M_R = 0$. In this case, the neutrino becomes massive via a Dirac mass term once the Higgs doublet gets a VEV, in the usual way. However, in order to obtain a very tiny neutrino mass $m_\nu \sim \mathcal{O}(0.05\,\text{eV})$, as suggested by data, one would need a very small Yukawa coupling as $y^\nu \sim 10^{-12}$. This process can be generalised to three neutrino generations, and having complete freedom over the Yukawa couplings y^ν_{ij}, one could fit all neutrino oscillations data with Dirac neutrinos. However, this mechanism does not seem very natural: the flavour sector of the SM becomes even more puzzling with incredibly tiny Yukawa couplings and Majorana masses set to zero by hand (or by imposing the conservation of lepton number). A more appealing solution is to consider that M_R is non-zero and then extract the physical masses of neutrinos. One can write all the couplings in Eq. (1.81) in matrix form as

$$\mathcal{L}_\nu = \frac{1}{2} \begin{pmatrix} \bar{\nu}_L & \bar{N}_R^C \end{pmatrix} \begin{pmatrix} 0 & m_D \\ m_D & M_R \end{pmatrix} \begin{pmatrix} \nu_L^C \\ N_R \end{pmatrix} + \text{h.c.} \tag{1.82}$$

where we have exchanged the Higgs doublet by its VEV and expanded the product of $SU(2)_L$ doublets, such that $m_D = y^\nu v_{\mathrm{SM}}/\sqrt{2}$. Since the right-handed neutrino is an electroweak singlet, the Majorana mass of the right-handed neutrino M_R may be orders of magnitude above the electroweak scale. It follows that $m_D \ll M_R$, and in this case we can extract in all generality the smaller eigenvalue of the mass matrix above as

$$m_\nu \simeq \frac{m_D^2}{M_R}\,. \tag{1.83}$$

Assuming that y^ν is of $\mathcal{O}(1)$, which is the natural expectation, we find that $M_R \approx \mathcal{O}(10^{15}\,\text{GeV})$ is required in order to obtain $m_\nu \sim \mathcal{O}(0.05\,\text{eV})$. This is known as the *seesaw mechanism*: the left-handed neutrino is very light because its right-handed counterpart is very heavy. More exactly, the left-handed neutrino gets a tiny effective Majorana mass through mixing with the heavy Majorana neutrino, propitiated via the Higgs Yukawa coupling. Since Majorana particles are their own antiparticle, active neutrinos being Majorana particles leads to key phenomenological predictions such as neutrinoless double

beta decay [56], which are currently being tested. It is also intriguing the fact that the mass scale of right-handed neutrinos is close to the scale of Grand Unification Theories, where the gauge couplings of the SM may unify into a single gauge coupling (see a longer discussion in Section 1.7). So far we have only discussed a simplified example of the so-called *type I seesaw mechanism*, firstly introduced in 1977 by Peter Minkowsky [57], although many more versions had been proposed since then, including low scale variations (see e.g. [58]) where the right-handed neutrinos may be much lighter. Many more seesaw models beyond type I are available in the literature, containing different types of BSM particle content, most notably the type II seesaw containing a scalar triplet [59] and the type III seesaw containing a fermion triplet [60]. Given that the right-handed neutrinos of the traditional type I seesaw mechanism are much heavier than the electroweak scale, we may integrate them out to parameterise their low-energy effect in terms of an effective, non-renormalisable operator with energy dimension 5,

$$\frac{c}{\Lambda}(\bar{L}_L^C \widetilde{H})(L_L \widetilde{H}) + \text{h.c.}\,, \tag{1.84}$$

denoted as the Weinberg operator [61], which violates lepton number explicitly in two units. The heavy cut-off scale is associated with M_R, while $c = (y^\nu)^2$. A similar operator arises from other neutrino mass models in the literature that generate Majorana masses for the active neutrinos, just with different matching conditions for Λ and c. This way, such an operator can be incorporated into the SM in order to account for Majorana neutrino masses, while remaining agnostic to the details of the neutrino mass mechanism in the UV.

The type I seesaw mechanism can be easily generalised to three generations of neutrinos. If we introduce two right-handed neutrinos, then two neutrinos will become massive and one will remain massless, which is compatible with current data. The new Lagrangian is given by

$$\mathcal{L}_\nu = y^\nu_{ij} \bar{L}_{Li} \widetilde{H} N_{Rj} + \frac{1}{2} M_{Rjk} \bar{N}^C_{Rj} N_{Rk} + \text{h.c.}\,, \tag{1.85}$$

where $i = 1, 2, 3$, $j, k = 1, 2$. Note that since N_{R1} and N_{R2} share the same quantum numbers, they are related by a global $U(2)$ symmetry. We can take advantage of this symmetry to rotate away the mixing term M_{R12} without loss of generality (the consequence is simply an unphysical redefinition of the couplings y^ν_{ij} and M_{Rjj} with respect to the original basis). Then we can write the Lagrangian in matrix form as

$$\mathcal{L}_\nu = \frac{1}{2} \begin{pmatrix} \bar{\nu}_L & \bar{N}_R^C \end{pmatrix} \begin{pmatrix} 0 & m_D \\ m_D^{\mathrm{T}} & M_R \end{pmatrix} \begin{pmatrix} \nu_L^C \\ N_R \end{pmatrix} + \text{h.c.}\,, \tag{1.86}$$

where now $\nu_L \equiv (\nu_{L1}, \nu_{L2}, \nu_{L3})^{\mathrm{T}}$ contains the three left-handed neutrino interaction eigenstates, $N_R \equiv (N_{R1}, N_{R2})^{\mathrm{T}}$ contains the two right-handed neutrinos, and we have

defined the following matrices in flavour space

$$m_D = y^\nu_{ij} \frac{v_{\rm SM}}{\sqrt{2}} \,, \tag{1.87}$$

$$M_R = \begin{pmatrix} M_{R11} & 0 \\ 0 & M_{R22} \end{pmatrix} . \tag{1.88}$$

Provided that $m_D \ll M_R$, the seesaw formula in Eq. (1.83) can be generalised to a matrix product

$$m_\nu \simeq m_D M_R^{-1} m_D^{\rm T} \,. \tag{1.89}$$

After applying the seesaw formula above, we obtain m_ν as a non-trivial and symmetric 3×3 matrix full of y^ν_{ij} couplings of $\mathcal{O}(1)$ that we can use to fit neutrino oscillations data. The precise values of the neutrino masses are still unknown, however their squared mass splittings, $\Delta m^2_{ij} = m^2_i - m^2_j$, can be extracted from oscillations data. The mass ordering of neutrino masses is unknown as well: it could be normal with $\Delta m^2_{31} > 0$, or inverted with $\Delta m^2_{31} < 0$, although the former is currently preferred by data. Indeed, if one neutrino is massless, then normal ordering reveals that the mass of the heaviest neutrino is $m_3 = \sqrt{\Delta m^2_{31}} \approx 0.05$ eV, as anticipated before.

In analogy with the CKM matrix in Eq. (1.62), one can define a mixing matrix $U_{\rm PMNS}$ describing lepton mixing in terms of left-handed rotations as,

$$U_{\rm PMNS} = V^\dagger_{\nu_L} V_{e_L} \,, \tag{1.90}$$

where V_{ν_L} is obtained from diagonalising m_ν in Eq. (1.89), while V_{e_L} is obtained from diagonalising the charged lepton Yukawa couplings. In analogy with the quark sector, due to PMNS mixing charged currents mediate tree-level flavour-changing transitions in the lepton sector, that would violate lepton flavour universality. However, such transitions only exist because neutrinos are massive, being very suppressed due to the very tiny neutrino masses. Notice that a non-trivial $U_{\rm PMNS}$ can be obtained via both neutrino mixing or charged lepton mixing: only the product $U_{\rm PMNS} = V^\dagger_{\nu_L} V_{e_L}$ is physical with the known interactions.

However, it can be shown that due to their large mass splittings, charged leptons in weak interactions are always produced as states with well-defined mass, since any admixture of e, μ and τ mass eigenstates is always produced incoherently or cannot maintain coherence over macroscopic distances [63] (except at extremely high energies, not accessible to current experiments). In this manner, from the observational point of view, the PMNS matrix is carried over to the neutrino state, which is produced as a coherent admixture of neutrino mass eigenstates $|\nu_i\rangle$ (where $i = 1, 2, 3$), such that the produced neutrino is $|\nu_\alpha\rangle = U^{*,\alpha i}_{\rm PMNS} |\nu_i\rangle$. The states $|\nu_\alpha\rangle$ are denoted by convention as "interaction eigenstates"[10], associated to the mass eigenstates of the charged leptons, that we can detect in the experiment (such that $\alpha = e, \mu, \tau$). By solving the Schrödinger

[10] Sometimes also denoted as "flavour eigenstates".

	Normal Ordering	Inverted Ordering
$\sin\theta_{12}$	0.550 ± 0.011	0.550 ± 0.011
$\sin\theta_{23}$	0.672 ± 0.014	0.754 ± 0.014
$\sin\theta_{13}$	0.1492 ± 0.0020	0.1491 ± 0.0019
δ_{PMNS}/π	$1.29^{+0.19}_{-0.16}$	$1.53^{+0.12}_{-0.16}$
$\dfrac{\Delta m^2_{21}}{10^{-5}\text{eV}^2}$	$7.41^{+0.21}_{-0.20}$	$7.41^{+0.21}_{-0.20}$
$\dfrac{\Delta m^2_{31}}{10^{-3}\text{eV}^2}$	$+2.507^{+0.026}_{-0.027}$	$-2.486^{+0.025}_{-0.028}$

TABLE 1.4: Numerical values for neutrino oscillation parameters taken from the global fit [62]. Uncertainties in the mixing angles have been symmetrised and assumed to be Gaussian distributed.

equation, one can check that the produced neutrino evolves into an admixture of interaction eigenstates. Finally, at the detection point, the wave function collapses into a well-defined interaction eigenstate and the associated charged lepton is detected. Therefore, the interaction state at the detection point can be different from the interaction state originally produced. This is the phenomenon of neutrino oscillations[11].

Just like the CKM matrix, U_{PMNS} is described by three mixing angles and six CP-violating phases. If neutrinos are Dirac particles, then only one CP phase δ_{PMNS} is physical, which has not yet been measured with enough precision. Instead, if neutrinos are Majorana, one has less freedom to absorb complex phases via field redefinitions, such that U_{PMNS} contains three physical CP-violating phases. Therefore, the flavour sector now contains 26 parameters if neutrinos are Dirac, or 28 if they are Majorana. Neutrino mixing angles can be parameterised as [62, 65]

$$\tan\theta_{23} \sim 1\,, \qquad \tan\theta_{12} \sim \frac{1}{\sqrt{2}}\,, \qquad \theta_{13} \sim \frac{\lambda}{\sqrt{2}}\,, \tag{1.91}$$

while the exact numerical values are given in Table 1.4, which shows also the measured values of the mass splittings $\Delta m^2_{ij} = m^2_i - m^2_j$.

Oscillation experiments with atmospheric neutrinos are particularly sensitive to the angle θ_{23}, which is commonly denoted as the *atmospheric* angle. In a similar manner, θ_{12} is denoted as the *solar* angle and θ_{13} is denoted as the *reactor* angle. In contrast with quark mixing angles, neutrino mixing angles are large and seemingly anarchic, with the smaller angle θ_{13} being of the same order as the Cabibbo angle. The reason of why neutrino mixing is so different from quark mixing is unknown, maybe suggesting a deeper understanding of both in a UV theory that goes beyond the simplified seesaw mechanism introduced here. Such a theory could explain the very complicated flavour sector of the SM+neutrinos in terms of simple and natural principles: this is called *a theory of flavour*.

[11] For a review of neutrino oscillations as a quantum mechanical phenomenon, see e.g. [64].

1.7 Other open questions in the SM

Beyond the flavour puzzle, there are several hints for an extended framework beyond the SM from both the theoretical and the experimental side:

- **Quantum gravity:** The SM, being a quantum field theory, explains all the fundamental interactions observed in Nature except for gravity. General Relativity is a successful theory of gravity at the classical level, but the SM *must* be extended in order to include a theory of quantum gravity, which would be crucial to understand physical phenomena like the singularity of black holes or the (possible) singularity at the beginning of our Universe. However, attempts to quantise gravity via the traditional methods of quantum field theory have failed so far. Since quantum gravity effects are only expected to become manifest around the Planck scale $M_{\text{Planck}} \sim 10^{19}$ GeV, the SM can be understood as an effective field theory of Nature that provides a good description of low energy physics, well below the Planck scale.

- **Dark Matter**: According to cosmological observations (described in the framework of General Relativity), the SM only accounts for 25% of matter in our Universe, where we understand matter as massive particles experiencing the gravity force. The remaining 75% of matter could correspond to BSM particles, new colorless matter that does not interact electromagnetically, the so-called *Dark Matter*. A well-motivated candidate for Dark Matter were WIMPs, particles with masses around the EW scale interacting via SM-weak-like interactions, although they have not been detected so far. Axions are a well-motivated candidate as well, also connected with the strong CP puzzle. However, notice that Dark Matter is a problem related to our understanding of gravity in the Universe: since we believe that a further theory of gravity beyond GR exists, at least to account for quantum gravity, it is possible that such a theory can properly describe the observed Universe without the need of DM. In this case, DM would be an artifact of GR being not the final theory of gravity in Nature. It is also possible that Dark Matter is made by BSM particles which however do not interact with the SM particles at all, hence making it difficult to test their properties.

- **Accelerated expansion of the Universe**: An Universe consisting of SM matter and cold Dark Matter is expected to experience a decelerated expansion. However, cosmological observations show that the Universe is experiencing an accelerated expansion. This can only be accounted for within the equations of General Relativity by adding a cosmological constant term, which is associated to the energy of vacuum itself. The SM does provide a contribution to the vacuum energy (see the end of Section 1.3), however this contribution turns out to be 56 orders of magnitude larger (and with the opposite sign) than the observed value of the cosmological constant. This implies that there should be an incredibly *fine-tuned*

cancellation between the SM contribution and a bare vacuum energy parameter that can be introduced in the Lagrangian, leading to the largest fine-tuning problem of the SM [8, 34, 35]. In the absence of an explanation for the accelerated expansion of the Universe, the cosmological constant is associated with an unknown *Dark Energy* component that constitutes roughly 70% of the energy density in our Universe.

- **Horizon and flatness problems of the standard cosmology:** Cosmology aims to describe the history of the Universe in terms of the known theories of physics. General Relativity describes the evolution of the Universe and their different components (SM matter, Dark Matter, radiation and Dark Energy), while the SM describes the interactions among particles that are crucial to understand the early Universe, when all particles were interacting in a thermal plasma. The so-called ΛCDM model provides an overall successful description of most cosmological observations. However, it fails to provide a proper explanation for the observed isotropy and homogeneity of the CMB [66]. For example, photons from the last scattering surface coming from different directions were not in casual contact in the past, yet they show the same temperature today. This is known as the *horizon problem*. Cosmological observations also suggest that the Universe is geometrically flat [66] (the metric of the spatial sections is close to that of the euclidian plane $\mathbb{R}^3$). However, General Relativity predicts that if the Universe is flat now, it should have been incredibly flatter in the very early Universe, implying a large fine-tuning of the energy density of the Universe during the very first instants of time. This is known as the *flatness problem*. Both problems cannot be understood within the ΛCDM framework based on the SM. A well-motivated explanation is the *inflationary model*, which requires the addition of a new scalar, the *inflaton* field, which couples to SM particles. However, the inflationary model has not yet been experimentally confirmed.

- **Matter-antimatter asymmetry:** The SM interactions are CP invariant, meaning that matter and antimatter experience the same interactions, with the exception of the CP-violating phase in the CKM matrix that breaks CP in the charged currents mediated by $W_\mu^\pm$. However, this amount of CP violation is not enough to explain that our observed Universe is mostly made of matter. Assuming that in the early Universe matter and antimatter were initially produced in a similar amount (as inflationary models generally suggest [67]), then in order to explain the matter-antimatter asymmetry of our Universe the SM has to be extended. It is possible however that the starting conditions of our Universe as a dynamic system included more matter than antimatter, or that the matter-antimatter asymmetry is generated at the end of inflation through the decay of the inflaton: this only deepends into our lack of understanding about the origin of the Universe and the origin of matter, calling for a more fundamental theory that can describe the very

first instants of time (when quantum gravity effects were non-negligible), in order to shed light over the initial conditions of the Universe.

- **Hierarchy puzzle of the Higgs mass:** The Higgs field responsible for electroweak symmetry breaking in the SM is quadratically sensitive to NP scales. Notice that this is not the case for fermions, whose masses are protected by chiral symmetry [68, 69], or the $W^{\pm}$ and Z bosons, whose masses are protected by electroweak symmetry. In the presence of NP, the Higgs mass would receive radiative corrections proportional to the new energy scale, i.e. $m_h^2 \to m_h^2 + \delta m_h^2$ where

$$\delta m_h^2 \sim \frac{\Lambda_{\rm NP}^2}{16\pi^2}\,, \tag{1.92}$$

if the NP couple to the Higgs (otherwise the corrections are still quadratically divergent but they carry further loop suppression). We have introduced $\Lambda_{\rm NP}$ as the NP scale where new degrees of freedom become manifest. Given that we expect new degrees of freedom to account for neutrino masses, one could consider $\Lambda_{\rm NP} \sim M_{\rm seesaw} \sim 10^{15}$ GeV. In this manner, one would expect the Higgs to be very heavy due to the large corrections provided by $M_{\rm seesaw}$ [70, 71]. In order to preserve its mass at the electroweak scale, one should introduce a large cancellation between the bare mass m_h^2 and the large correction δm_h^2. This is called *fine-tuning*. The situation is even worse if one considers NP degrees of freedom at the Planck scale $M_{\rm Planck} \sim 10^{19}$ GeV, where quantum gravity becomes manifest, and an even larger fine-tuning is needed. In other words, the Higgs hierarchy puzzle is also the question of why the electroweak scale and the Planck scale are so far from each other: a puzzle of hierarchies. The Higgs hierarchy puzzle could be solved by invoking new physics that screen the Higgs mass from heavier NP scales. Examples of this are Supersymmetry [72, 73] (a symmetry imposing that each fermion has a boson partner and viceversa) and composite Higgs models [74] (the Higgs boson is not an elementary particle, but a bound state of some more fundamental, strongly-interacting fermions). Ideally, these NP should be manifest close to the electroweak scale in order to ameliorate the fine-tuning of the Higgs mass. Given that flavour observables are sensitive to NP far above the TeV scale, it is remarkable that no signals of NP addressing the hierarchy puzzle have been found so far. Is there any suppression mechanism of FCNCs in the UV that prevents NP from showing up? This is known as the *NP flavour puzzle*, and motivates that NP might approximately preserve some flavour symmetry in order to suppress FCNCs (see Section 1.9).

- **Strong CP puzzle:** In principle, QCD could violate CP invariance. The QCD Lagrangian allows for the addition of a topological gauge invariant term accounting for CP violation, parameterised via the free parameter $\overline{\theta}_{\rm QCD}$. However, from non-observation of the neutron EDM, we know that $|\overline{\theta}_{\rm QCD}| < 10^{-10}$ [51], meaning that either CP is conserved by the strong force or its violation is extremely small.

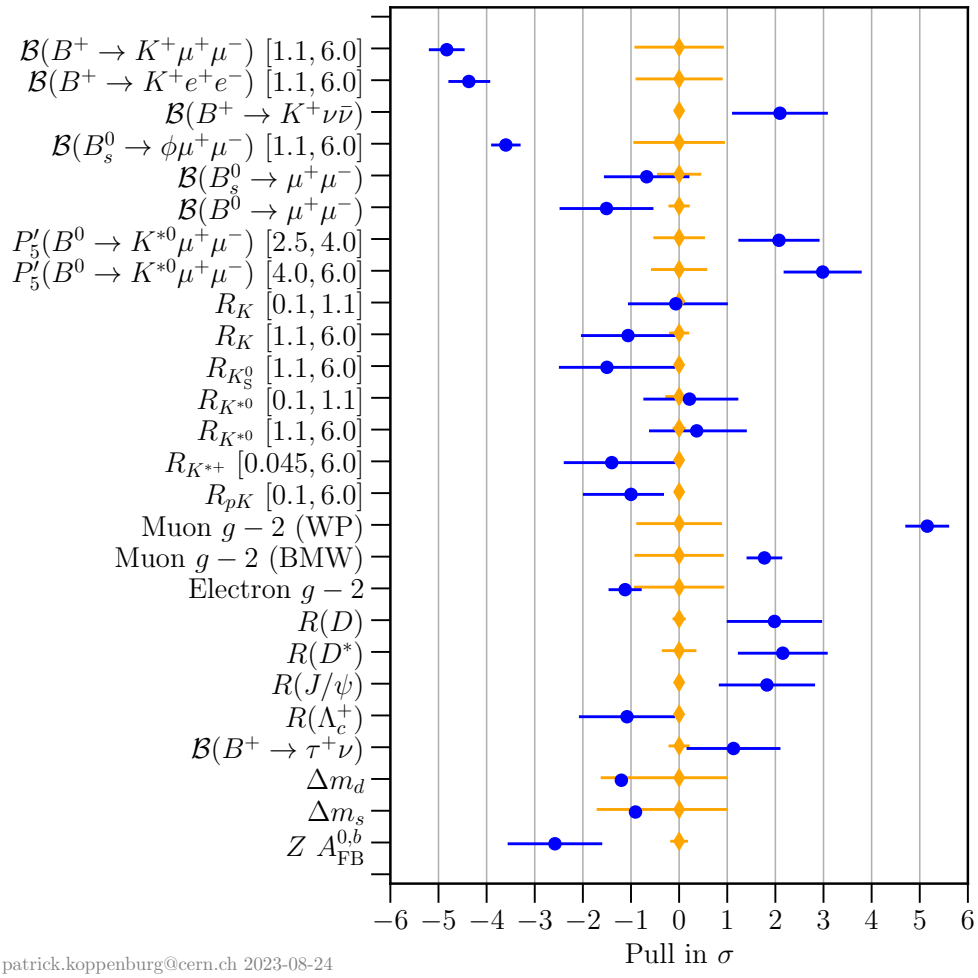

FIGURE 1.3: Compilation of experimental anomalies in low-energy observables and their pull in standard deviations. Experimental measurements are shown in blue, the SM predictions are shown in orange. Figure available in the website of Patrick Koppenburg: https://www.nikhef.nl/ pkoppenb/anomalies.html.

Given that CP is largely violated in the quark sector by the weak interaction, explaining the non-observation of strong CP violation in QCD is challenging. Ultimately, the puzzle is related to why θ_{QCD} is so small when the other source of CP violation in the SM, δ_{CKM}, is of $\mathcal{O}(1)$: another puzzle of hierarchies. A well-motivated solution is the existence of an axion field, as a pseudo-Goldstone boson from a spontaneously broken Peccei-Quinn global symmetry. Such a particle would naturally ensure $\overline{\theta}_{\mathrm{QCD}} = 0$ [75], and it could also behave as Dark Matter in our Universe [76].

- **Experimental anomalies:** Despite the remarkable success of the SM in explaining the vast majority of particle physics data, some observables remain in tension with the SM predictions. An illustrative compilation of selected experimental anomalies can be found in Fig. 1.3, for a review see e.g. [77]. However, no single

tension is significant enough to claim the discovery of NP. We discuss the flavour-related anomalies in detail in Chapter 2. For the moment, we just highlight the anomalous magnetic moment of the muon $(g-2)_\mu$, which is in 5.1σ tension[12] with the SM [78,79]. The $R_{D^{(*)}}$ ratios are in 3.3σ tension with the SM [80], suggesting the breaking of lepton flavour universality in B-meson decays. The recent data in $\mathcal{B}(B^+ \to K^+\nu\bar{\nu})$ obtained by Belle II is in 2.8σ discrepancy with the SM as well [81]. There is also a substantial tension in $b \to s\mu\mu$ data, although these observables are afflicted by large QCD uncertainties [82]. The CDF collaboration reported a very anomalous measurement of the $W^\pm_\mu$ boson mass [83], although this measurement is in tension with current and previous data by LHC, LEP and Tevatron. The Cabibbo angle anomaly [84] is related to a deficit of unitarity in the first row of the CKM matrix, and the determinations of V_{ub} and V_{cb} via exclusive and inclusive meson decays do not agree with each other [21]. There are several hints for new resonances at the LHC, mainly in di-photon channels at 95 GeV [85,86] (this one is supported by mild excesses in both ATLAS and CMS data, plus an old excess at LEP), 151 GeV [87] and 670 GeV [88]. Finally, there are mild deviations in electroweak precision observables (EWPOs) that worsen the global fit of the SM to electroweak data, for example the 2σ tensions in the forward-backward asymmetry of $Z \to \bar{b}b$ and the asymmetry observable in $Z \to e^+e^-$ [89].

- **Hubble tension:** Beyond the above anomalies in particle physics experiments, there exists a long-lasting discrepancy in the different cosmological determinations of the Hubble constant, H_0, which measures the current expansion rate of our Universe [90,91]. More accurately, the early time determinations (e.g. from the CMB) are in roughly 5σ tension with the late time determinations obtained from observing stars such as superonovae and cepheids. This hints to a possible failure of the cosmological model ΛCDM, which nevertheless provides a very successful description of many other observables. Given that ΛCDM is supported on SM physics, it is possible that the solution to the long-lasting Hubble tension may be due to the presence of BSM physics.

1.8 Gauge unification and flavour

Beyond the aforementioned open questions of the SM, charge quantisation, namely why the proton and the electron have equal but opposite electric charges despite being apparently very different in nature, has been a mystery since the early days of quantum mechanics. With the advent of the SM, this question has escalated to explain the particular quantum numbers and transformation properties of known elementary particles under the SM gauge group, and the relative strength of their interactions.

[12] We discuss $(g-2)_\mu$ in detail in Section 2.3.3. However, we note already that different SM predictions for the hadronic vacuum polarisation, that enters into the determination of $(g-2)_\mu$, are in tension. Namely, the predictions from lattice QCD do not agree with the data driven predictions obtained from $e^+e^- \to$ hadrons data.

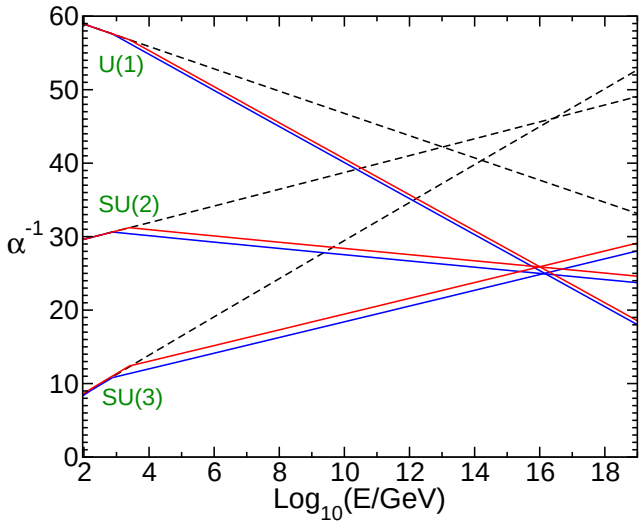

FIGURE 1.4: Two-loop RGE of the inverse gauge couplings $\alpha_a^{-1} = 4\pi/g_a^2$ in the SM (dashed lines) and the MSSM (solid lines). In the MSSM case, the sparticle masses are treated as a common threshold varied between 750 GeV and 2.5 TeV, and $\alpha_3(M_Z)$ is varied between 0.117 and 0.120. Figure taken from [72].

With great elegance and simplicity, a Grand Unified Theory (GUT) postulates that the plethora of different charges and interactions of the SM is just a low-energy manifestation of a deeper underlying unity. Therefore, in the ultraviolet, the separate parts of the SM gauge group are merged into an unique gauge symmetry, and SM fermions are unified into representations under the GUT gauge group. GUTs rely on the assumption that SM gauge couplings evolve in the UV and join each other, via RGE running. In the SM they approach but do not quite unify, although they unify in the Minimal Supersymmetric SM (MSSM) at the very high scale $M_{\rm GUT} \sim 10^{16}$ GeV [92], see Fig. 1.4. This scale is suspiciously close to the heavy scale $M_{\rm seesaw} \sim 10^{15}$ GeV of right-handed neutrinos in the type I seesaw mechanism.

The minimal[13] gauge group where the SM forces may unify is $SU(5)$ [93], which we introduce here as it will be greatly discussed in Chapter 6 of this thesis. One can check that $SU(5)$ contains the generators of $SU(3)$ and $SU(2)$ as

$$t^\alpha = \left(\begin{array}{c|c} \frac{1}{2}\lambda^\alpha & 0 \\ \hline 0 & 0 \end{array}\right), \qquad T^a = \left(\begin{array}{c|c} 0 & 0 \\ \hline 0 & \frac{1}{2}\sigma^a \end{array}\right), \tag{1.93}$$

where $\alpha = 1, ..., 8$ and $a = 1, 2, 3$, with λ^α and σ^a being the Gell-Mann and Pauli matrices, respectively. The only remaining generator of $SU(5)$ commuting with t^α and T^a is

$$\mathcal{T}_Y = \mathcal{N}\,\mathrm{diag}(-1/3, -1/3, -1/3, 1/2, 1/2) \equiv \mathcal{N} Y\,, \tag{1.94}$$

which we associate to SM hypercharge up to a normalisation factor. The normalisation factor is chosen by convention so that all $SU(5)$ generators satisfy $\mathrm{Tr}(\mathcal{T}_A \mathcal{T}_B) = \frac{1}{2}\delta_{AB}$,

[13] The other simple rank 4 algebras beyond $SU(5)$ do not work since they do not have complex representations.

where $A, B = 1, ..., 24$. Therefore, one can check that $\mathrm{Tr}(\mathcal{T}_Y \mathcal{T}_Y) = \frac{1}{2}$ if $\mathcal{N} = \sqrt{\frac{3}{5}}$. This normalisation factor is commonly absorbed in a redefinition of the coupling strength g_Y.

The adjoint representation of $SU(5)$ may be decomposed under the SM as

$$\mathbf{24} = (\mathbf{8},\mathbf{1})_0 \oplus (\mathbf{1},\mathbf{3})_0 \oplus (\mathbf{1},\mathbf{1})_0 \oplus (\mathbf{3},\mathbf{2})_{-5/6} \oplus (\overline{\mathbf{3}},\overline{\mathbf{2}})_{5/6}\,. \tag{1.95}$$

Beyond gluons and the electroweak gauge bosons, we also find 12 exotic gauge bosons commonly denoted as $X \sim (\mathbf{3},\mathbf{2})_{-5/6}$ and $X^* \sim (\overline{\mathbf{3}},\overline{\mathbf{2}})_{5/6}$[14], which are associated to the remaining generators of $SU(5)$. The $X^{(*)}$ gauge bosons become massive after spontaneous breaking of the $SU(5)$ group down to the SM, which usually proceeds via a fundamental scalar in the adjoint representation getting a VEV in the SM singlet component.

The chiral fermions of the SM do also unify into representations of $SU(5)$. For a given family of SM chiral fermions described by two-component Weyl spinors, the lepton doublet and the CP-conjugate down-quark singlet are combined into a $\overline{\mathbf{5}}$, and the quark doublet is combined with the CP-conjugate up-quark and lepton singlets into a $\mathbf{10}$[15],

$$\overline{\mathbf{5}}_i = \begin{pmatrix} d_r^c \\ d_g^c \\ d_b^c \\ \nu \\ e \end{pmatrix}_i , \qquad \mathbf{10}_i = \frac{1}{\sqrt{2}} \begin{pmatrix} 0 & u_b^c & -u_g^c & u_r & d_r \\ -u_b^c & 0 & u_r^c & u_g & d_g \\ u_g^c & -u_r^c & 0 & u_b & d_b \\ -u_r & -u_g & -u_b & 0 & e^c \\ -d_r & -d_g & -d_b & -e^c & 0 \end{pmatrix}_i , \tag{1.96}$$

where $i = 1, 2, 3$ denote the three fermion families of the SM. It is clear then than in the $SU(5)$ grand unified model, the three fermion families remain as three identical copies under the gauge symmetry. Remarkably, the hypercharges of chiral fermions are no longer seemingly arbitrary values (constrained by the cancellation of gauge anomalies), but are rather associated to a discretely valued and traceless generator of $SU(5)$ as given in Eq. (1.94). As a consequence, the generator of the residual group $U(1)_Q$ is given as a linear combination of generators of $SU(5)$, namely $Q = T_3 + \mathcal{T}_Y$, therefore being discretely valued and traceless as well. Given the fermion representations in Eq. (1.96), this enforces the charge of the down quark to be 1/3 of the charge of the electron, and the charge of the up quark to be 2/3 the charge of the positron, explaining the observed quantisation of electric charge.

The Higgs doublet of the SM is embedded into a $\mathbf{5}$ representation that allows to write Yukawa couplings as

$$\mathcal{L}_{\text{Yukawa}} = Y^u_{ij} \mathbf{10}_i \mathbf{10}_j \mathbf{5}_H + Y^{de}_{ij} \mathbf{10}_i \overline{\mathbf{5}}_j \overline{\mathbf{5}}_H + \text{h.c.} \tag{1.97}$$

[14] We note that $\overline{\mathbf{2}} = \mathbf{2}$ because the fundamental representation of $SU(2)$ is pseudo-real, but commonly we will still show the bar in $\overline{\mathbf{2}}$ for the sake of clarity.

[15] For this reason, this convention where all fermions are described by two-component left-handed Weyl spinors (CP-conjugate right-handed fermions are actually left-handed) is very convenient for model building studies, in contrast with the convention of four-component left-right Dirac spinors which is more common for phenomenological studies. Both conventions are described in Appendix A.

Important consequences are that the up-quark Yukawa matrix is symmetric, while the down-quark and charged lepton Yukawa couplings both emerge from Y_{ij}^{de} and verify $Y^d = (Y^e)^\dagger$. This means that down quarks and charged leptons are predicted to have the same mass at $M_{\rm GUT} \sim 10^{16}$ GeV where $SU(5)$ is spontaneously broken. However, this unification of Yukawa couplings is so far inconsistent with experimental data and further model building needs to be done [94], plus Yukawa couplings remain hierarchical for the different families as in the SM, leaving the flavour puzzle unanswered or even worsened. Moreover, note that the $SU(5)$ theory says nothing about neutrino masses, since right-handed neutrinos remain singlets as in the SM.

The fact that some quarks and leptons are unified in the same representations means that the $X^{(*)}$ gauge bosons can transform quarks into leptons and viceversa, giving them the name of *leptoquarks*. In particular, this leads to the striking prediction of proton decay, which is in tension with current data unless the GUT symmetry is spontaneously broken at very high scales, compatible with $M_{\rm GUT} \sim 10^{16}$ GeV [95] (see a more complete treatment of gauge boson-mediated proton decay in Section 2.3.11). Notice that colour-triplet Higgs scalars contained in $\mathbf{5}_H$ commonly mediate proton decay as well, requiring their masses to be very heavy. This is in conflict with the fact that the SM Higgs doublet contained in $\mathbf{5}_H$ lives at the electroweak scale, since one would naturally expect fields within the same multiplet to have masses at the same scale. This inconsistency is denoted as the doublet-triplet splitting problem.

Beyond $SU(5)$, the next simple unification framework is based on the gauge group $SO(10)$[16] [96, 97], which is rank 5. Here all 15 chiral fermions of a given family[17] are unified into a single **16**-dimensional spinor representation, including one SM singlet that is associated to a right-handed neutrino. The SM Higgs doublet is then embedded into a **10** representation, which allows to write a common Yukawa coupling for all fermions within the same family. This is phenomenologically unsuccessful and requires the addition of further Higgs bosons and model building. The $SO(10)$ group may be broken down to the SM in various steps, which include $SU(5)$ and the Pati-Salam gauge group $SU(4)_c \times SU(2)_L \times SU(2)_R$ [100]. Despite not being a grand unified theory, the latter predicts the quantisation of hypercharge as well via $Y = (B-L)/2 + T_{3R}$[18], the restoration of parity and the unification of quarks and leptons within the same representations,

[16] Notice that the Lie group with **16**-dimensional spinor representations is formally Spin(10), and by $SO(10)$ we refer to its Lie algebra.

[17] Indeed even in $SO(10)$ one still needs three fermion representations, one for each SM fermion family. Naively, all SM+3ν_R fermions (48 Weyl spinors) can be unified into the fundamental representation of $SU(48)$ without introducing exotic fermions (beware of gauge anomalies) [98, 99]. However, with increasingly big unification groups the possibilities for embedding the SM in them grow in a seemingly exponential way [98]. For this reason, one might argue that models based on very large gauge groups are not as attractive as those based on smaller ones: they contain many subgroups, therefore a significant tuning of the scalar sector parameters would likely be needed in order to have the correct symmetry breaking.

[18] Note that baryon number minus lepton number $B - L$ is associated to a discretely valued and traceless generator of $SU(4)_c$ (up to a 1/2 normalisation factor).

with leptons being the "fourth colour" (including right-handed neutrinos),

$$\psi_i(\mathbf{4},\mathbf{2},\mathbf{1}) = \begin{pmatrix} u_r & u_g & u_b & \nu \\ d_r & d_g & d_b & e \end{pmatrix}_i \equiv (Q_i, L_i)\ , \tag{1.98}$$

$$\psi^c_j(\overline{\mathbf{4}},\mathbf{1},\overline{\mathbf{2}}) = \begin{pmatrix} u^c_r & u^c_g & u^c_b & \nu^c \\ d^c_r & d^c_g & d^c_b & e^c \end{pmatrix}_j \equiv \left(u^c_j, d^c_j, \nu^c_j, e^c_j\right)\ , \tag{1.99}$$

where $i,j = 1,2,3$ are flavour indices. The SM Higgs doublet is embedded as $H \sim (\mathbf{1},\mathbf{2},\mathbf{2})$ which again provides a common Yukawa coupling for all fermions within the same family as in $SO(10)$. As shown, the correct description of fermion masses and mixings is usually a challenge for the GUT program and for many BSM theories. In Chapters 4 and 6 we will propose models based on modifications of Pati-Salam and $SU(5)$ respectively, that are able to describe fermion masses and mixings successfully along with explaining their hierarchical patterns.

1.9 Flavour symmetries of the SM and beyond

Flavour dynamics in the SM are encoded as processes or parameters that break the flavour symmetry $U(3)^5$. The flavour symmetry may be of great importance in order to understand the precise structure of the Yukawa couplings, which in the SM are just free parameters, and might provide some insights about possible underlying flavour dynamics, which may be connected to the origin of flavour in the SM. Therefore, understanding $U(3)^5$ and its possible breaking by NP is fundamental for flavour model building.

1.9.1 $U(3)^5$: the accidental symmetries of the SM

We have built the SM as a theory where each fundamental fermion comes in three flavours that transform in the same way under the gauge group, the only difference between fermion flavours being their masses. As mentioned in Section 1.2, this fact translates into the appearance of an approximate, global flavour symmetry

$$U(3)^5 = U(3)_Q \times U(3)_L \times U(3)_u \times U(3)_d \times U(3)_e\,. \tag{1.100}$$

Given that $U(3)^5 \cong SU(3)^5 \times U(1)^5$, we can replace the flavour symmetry by

$$U(3)^5 \cong SU(3)^3_q \times SU(3)^2_\ell \times U(1)^5\,, \tag{1.101}$$

where

$$SU(3)^3_q = SU(3)_Q \times SU(3)_u \times SU(3)_d\,, \tag{1.102}$$

$$SU(3)^2_\ell = SU(3)_L \times SU(3)_e\,, \tag{1.103}$$

$$U(1)^5 = U(1)_B \times U(1)_L \times U(1)_Y \times U(1)_{\rm PQ} \times U(1)_{e_R}\,. \tag{1.104}$$

Out of the five $U(1)$ charges, we identify baryon number (B), total lepton number (L), SM hypercharge (which is gauged), the Peccei-Quinn (PQ) symmetry whereby the Higgs doublet and the d_{Ri}, e_{Ri} fields have opposite charges, and finally $U(1)_{e_R}$ corresponds to a global phase of e_{Ri} only.

The Yukawa couplings of the SM break the flavour symmetry in Eq. (1.100). However, one can always rephase all quark fields by the same phase, which is associated to a global $U(1)$ in the quark sector that remains unbroken by the Yukawa couplings. This is the abelian symmetry associated to baryon number. The fact that there are no right-handed neutrinos in the SM implies that the three charged lepton masses are the only physical parameters of the lepton sector, associated to the diagonal entries of the lepton Yukawa matrix. We are always free to rephase the three diagonal charged lepton bilinears by three independent phases, associated to the three global abelian symmetries of the three lepton family numbers. Therefore, we conclude that the global flavour symmetry of the SM is broken by the Yukawa couplings down to (not displaying the gauged hypercharge which of course remains unbroken)

$$U(3)^5 \to U(1)_B \times U(1)_{L_e} \times U(1)_{L_\mu} \times U(1)_{L_\tau} \,, \tag{1.105}$$

where the lepton family numbers, L_e, L_μ and L_τ, contain the total lepton number L as the diagonal subgroup. These accidental symmetries have fundamental consequences: the proton is stable in the SM, and lepton flavour violating processes such as $\mu \to e\gamma$ are forbidden. However, given that these symmetries are accidental, nothing forbids us to write operators with energy dimension higher than four (non-renormalisable) which break these symmetries. Two examples are the following,

$$\frac{c_{ij}}{\Lambda}(\bar{L}^C_{Li}\widetilde{H})(L_{Lj}\widetilde{H}) + \text{h.c.}\,, \tag{1.106}$$

$$\frac{c_{ijkl}}{\Lambda^2}(\bar{Q}^C_{Li}Q_{Lj})(\bar{Q}^C_{Lk}L_l)\,. \tag{1.107}$$

The careful reader may have noticed the Weinberg operator already introduced in Eq. (1.84) (generalised to three generations in Eq. (1.106)), that generates Majorana neutrino masses and violates lepton number in two units. The operator in Eq. (1.107) violates both baryon number and lepton number in one unit, and can mediate proton decay for particular flavour indices. B-violating operators such that (1.107) are predicted by GUTs, as mentioned in Section 1.8. Indeed, the proton has been observed to be extremely stable [95], setting strong bounds on the cut-off scale of the operators (1.107).

The global symmetries in Eq. (1.105) are anomalous, meaning that they are only preserved at the classical level. In fact, they are explicitly broken by non-perturbative quantum effects such as the sphaleron process [101]. Even though this symmetry breaking effects are negligible at low energies (or equivalently at low temperatures), they may play an important role in the early Universe when temperatures where very high. For

example, they could play a role in the origin of the matter-antimatter asymmetry (see a brief discussion in Section 1.7), or when one aims for the construction of an extended gauge sector. Out of the four remaining $U(1)$ factors, only the subgroup corresponding to one of the combinations of lepton family numbers $U(1)_{L_\alpha - L_\beta}$ ($\alpha, \beta = e, \mu, \tau$ with $\alpha \neq \beta$) remains anomaly-free in the SM [102]. Interestingly, if one includes three right-handed neutrinos, singlets under the SM gauge group (which could account for neutrino masses as described in Section 1.6.2), the global accidental anomaly-free symmetry of the theory is extended to [103]

$$U(1)_{B-L} \times U(1)_{L_e - L_\mu} \times U(1)_{L_\mu - L_\tau} \,. \tag{1.108}$$

These accidental, anomaly-free symmetries will get either partially or totally broken once we include all the details from the neutrino sector. For instance, we know from the measured values of the PMNS matrix that the $U(1)_{L_e - L_\mu} \times U(1)_{L_\mu - L_\tau}$ symmetry is broken. On the other hand, the $U(1)_{B-L}$ symmetry would be broken if neutrinos are Majorana particles.

Even though the Yukawa couplings indeed break the flavour symmetry as per Eq. (1.105), the smallness of the Yukawa couplings in the SM leads to a small breaking of the flavour symmetry. Notice that if the Yukawa couplings were absent, the flavour symmetry would remain unbroken and the SM would be a flavour conserving theory. This has important consequences for flavour physics in the SM: flavour-changing charged currents (FCCCs) are suppressed by the smallness of the CKM mixing, and flavour-changing neutral currents (FCNCs) only appear at loop-level and are suppressed as well by small CKM elements. Another extra suppression enters in FCNCs: notice that if all quarks in a given sector (up or down) were degenerate, the flavour-changing $W^\pm$-couplings in Eq. (1.61) would vanish. A consequence of this is the fact that FCNCs in the down (up) sector are proportional to mass-squared differences between the quarks of the up (down) sector. For FCNCs that involve only quarks of the first two generations, this leads to a strong suppression factor related to the light quark masses, and known as *Glashow-Iliopoulos-Maiani (GIM) suppression* [104]. This extra suppression factor allowed Glashow, Iliopoulos and Maiani to explain kaon mixing and predict the existence of the charm quark, giving an upper bound for its mass.

Instead, going beyond the SM, FCNCs can occur at tree-level, with negligible suppression. However, the large suppression of FCNCs predicted by the SM turns out to be very well realised in Nature: rare decays of mesons and meson-antimeson mixing have been tested to agree well with the SM. Given that there are good reasons to expect new physics beyond the SM near the TeV scale (see Section 1.7). Why do we see no deviations in flavour physics observables, which are sensitive to very high NP scales?

In the following we provide a few examples of flavour symmetries proposed to dictate the flavour structure of NP in order to make it compatible with current bounds from flavour observables.

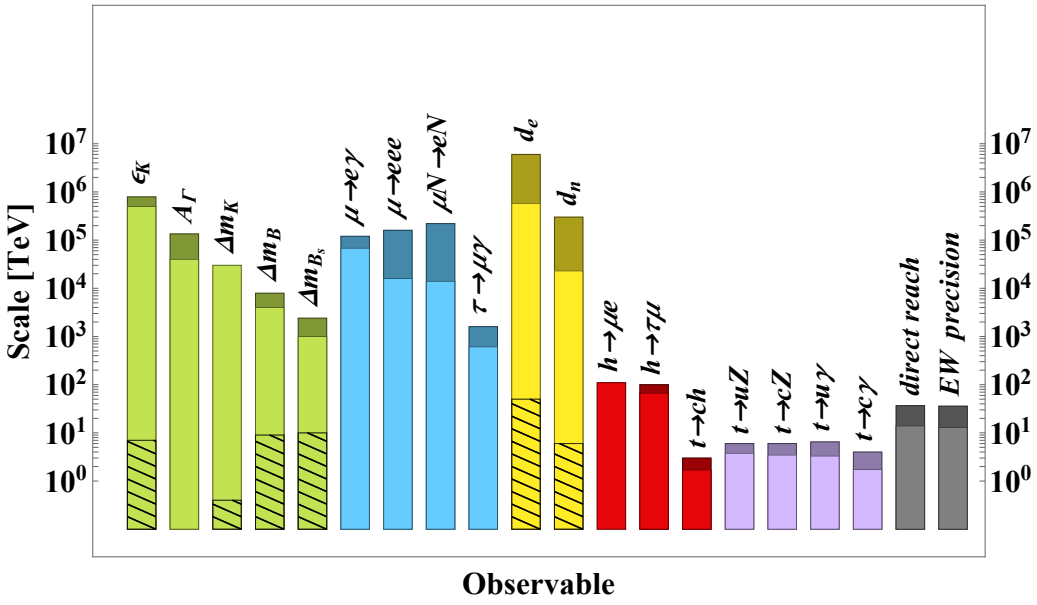

FIGURE 1.5: Reach in new physics scale of present and future facilities, from generic dimension-six operators. The colour coding of observables is: green for mesons, blue for leptons, yellow for EDMs, red for Higgs flavoured couplings and purple for the top quark. The grey columns illustrate the reach of direct flavour-blind searches and EW precision measurements. The operator coefficients are taken to be either ~ 1 (plain coloured columns) or suppressed by MFV factors (hatch filled surfaces). Light (dark) colours correspond to present data (mid-term prospects, including HL-LHC, Belle II, MEG II, Mu3e, Mu2e, COMET, ACME, PIK and SNS). Figure taken from [106].

1.9.2 Minimal Flavour Violation

A possibility to accommodate relatively light NP with flavour physics observables arises from the understanding of $U(3)^5$ and its breaking in the SM: if the SM Yukawa couplings remain as the only breaking source of $U(3)^5$, this guarantees that low-energy flavour changing processes deviate only very little from the SM predictions. In this scenario, denoted as *Minimal Flavour Violation* (MFV) [105], flavour transitions mediated by NP enjoy a similar suppression as they do in the SM. This ameliorates the strong flavour bounds over the scale of NP, as shown in Fig. 1.5, allowing the possibility of TeV-scale NP as suggested by the Higgs hierarchy puzzle.

Let us now formulate this principle in a formal way. Given that in the SM the flavour symmetry $U(3)^5$ is only broken by the Yukawa couplings, we can formally recover flavour invariance by promoting the Yukawa matrices to dimensionless auxiliary fields, *spurions*, transforming under $SU(3)_q^3 \times SU(3)_\ell^2$ as

$$Y_u \sim (\mathbf{3}, \overline{\mathbf{3}}, \mathbf{1})_{SU(3)_q^3}\,, \qquad Y_d \sim (\mathbf{3}, \mathbf{1}, \overline{\mathbf{3}})_{SU(3)_q^3}\,, \qquad Y_e \sim (\mathbf{3}, \mathbf{1})_{SU(3)_\ell^2}\,. \tag{1.109}$$

In this manner, the Yukawa interactions

$$\mathcal{L}_{\text{Yukawa}} = Y_u \overline{Q}_L \tilde{H} u_R + Y_d \overline{Q}_L H d_R + Y_e \overline{L}_L H e_R \tag{1.110}$$

now preserve the flavour symmetry, with quarks and charged leptons transforming as triplets under their corresponding $SU(3)$ factors. Having the freedom of the $SU(3)_q^3 \times SU(3)_\ell^2$ symmetry, we can use unitary transformations to rotate to the particular basis

$$Y_u = V_{\rm CKM}^\dagger \lambda_u \,, \qquad Y_d = \lambda_d \,, \qquad Y_e = \lambda_e \,, \tag{1.111}$$

where $\lambda_{u,d,e}$ are diagonal matrices,

$$\lambda_u = {\rm diag}(y_u, y_c, y_t) \,, \qquad \lambda_d = {\rm diag}(y_d, y_s, y_b) \,, \qquad \lambda_e = {\rm diag}(y_e, y_\mu, y_\tau) \,. \tag{1.112}$$

As an example, we may apply the MFV hypothesis to effective operators describing NP effects in an EFT framework. We define that our effective field theory satisfies the criterion of MFV if all higher-dimensional operators, constructed from SM and Yukawa spurions, are invariant under CP and (formally) under the flavour group $U(3)^5$. In other words, MFV requires that the dynamics of flavour violation are completely determined by the structure of the ordinary Yukawa couplings. This requirement translates into the fact that all relevant flavour non-diagonal operators in the EFT are proportional to powers of $Y_u Y_u^\dagger$. Since the SM Yukawa couplings are small for all fermions except for the top quark, one obtains $(Y_u Y_u^\dagger)_{ij} \approx y_t^2 V_{\rm CKM}^{ti*} V_{\rm CKM}^{tj}$. For example, for a four-quark operator violating fermion number by two units ($\Delta F = 2$), like the operators which contribute to meson-antimeson mixing processes, one obtains

$$\mathcal{O}_{ijkl} = \left(\overline{Q}_{Li} (\lambda_{\rm FC})_{ij} \gamma_\mu Q_{Lj}\right) \left(\overline{Q}_{Lk} (\lambda_{\rm FC})_{kl} \gamma^\mu Q_{Ll}\right) \,, \tag{1.113}$$

where we have defined

$$(\lambda_{\rm FC})_{ij} = \begin{cases} (Y_u Y_u^\dagger)_{ij} \approx y_t^2 V_{\rm CKM}^{ti*} V_{\rm CKM}^{tj} & i \neq j \,, \\ 0 & i = j \,. \end{cases} \tag{1.114}$$

It is clear now that the factor $(\lambda_{\rm FC})_{ij}$ provides CKM suppression for the flavour-violating operators as in the SM. This would explain the absence of NP signals in the flavour observables of the quark sector, allowing relatively light NP as long as their flavour structure is SM-like. The MFV hypothesis can also be extended to the lepton sector. However, since the mechanism responsible for neutrino masses is unknown at present, there is no unique way to introduce the MFV principle in the lepton sector. For the realisation of MFV in a scenario inspired in the type I seesaw mechanism, see e.g. [107].

The MFV prescription imposes that the flavour structure of NP is SM-like. From the point of view of a theory of flavour, this means that the new flavour dynamics addressing the flavour puzzle are very heavy, leaving as a low-energy remnant the flavour structure of the SM and relatively light MFV NP. In this sense, the MFV hypothesis suggests that the *a priori* unknown scales of the theory of flavour (Λ_F and $\langle \phi_F \rangle$) are very heavy, possibly close to the seesaw scale $M_{\rm seesaw} \approx 10^{15}$ GeV or to the GUT scale $M_{\rm GUT} \approx 10^{16}$ GeV, where we definitely expect BSM physics to manifest. This is an

interesting idea: NP following the flavour structure of the SM may manifest at relatively low energies, as required in order to solve the Higgs hierarchy puzzle and other open questions of the SM. In contrast, the new flavour dynamics from the theory of flavour, that would break explicitly $U(3)^5$, would manifest at much higher scales.

1.9.3 $U(2)^5$ and a multi-scale origin of flavour

Although the MFV hypothesis is successful in suppressing flavour-violating NP effects, it also predicts large flavour-universal NP effects. Notice that the Higgs boson has its largest fermion coupling with the top-quark, and NP addressing the Higgs hierarchy puzzle are usually coupled to both. If we would introduce TeV-scale NP coupled to the top-quark and the Higgs boson, the MFV prescription would also impose couplings to the light quark generations. However, TeV-scale NP coupled to light quark generations are strongly constrained by direct searches at the LHC, see e.g. the direct reach band in Fig. 1.5 or the CMS summary plots in Ref. [108]. This usually pushes the scale of MFV NP above 10 TeV, worsening the fine-tuning of the Higgs mass.

In contrast with the MFV prescription, one may consider NP that dominantly couple to the third family. This is interesting from the point of view of a theory of flavour: just like the third family Yukawa couplings are the largest, flavour dynamics connected to the origin of flavour might be dominantly coupled to the third family. Remarkably, direct LHC bounds over NP that predominantly couple to the third family are much weaker than those over flavour-universal NP.

We can formally establish this hypothesis by imposing that in the theory of flavour, only third family Yukawa couplings are allowed at renormalisable level,

$$\mathcal{L}_{\text{Yukawa}} = y_t \overline{Q}_{L3} \tilde{H} u_{R3} + y_b \overline{Q}_{L3} H d_{R3} + y_\tau \overline{L}_{L3} H e_{R3} \,. \tag{1.115}$$

The Yukawa couplings above break the usual $U(3)^5$ flavour symmetry of the SM down to [109–112]

$$U(2)^5 = U(2)_Q \times U(2)_L \times U(2)_u \times U(2)_d \times U(2)_e \,. \tag{1.116}$$

Given that the Yukawa couplings of first and second family fermions are very small compared to the third family, the SM with massless first and second family fermions is a good first order description of the SM fermion spectrum. In that case, the $U(2)^5$ symmetry would be exactly preserved at the classical level. In reality, the small Yukawa couplings of first and second family fermions provide small breaking effects of $U(2)^5$ that we can parameterise via the spurion formalism. In the Yukawa matrices of the quark sector, we introduce a spurion transforming as $V_Q \sim (\mathbf{2}, \mathbf{1}, \mathbf{1})$ under $U(2)_Q \times U(2)_u \times U(2)_d$. Similarly, we introduce $\Delta Y_u \sim (\mathbf{2}, \overline{\mathbf{2}}, \mathbf{1})$ and $\Delta Y_d \sim (\mathbf{2}, \mathbf{1}, \overline{\mathbf{2}})$, obtaining

$$\mathcal{L}^q_{\text{Yukawa}} = \begin{pmatrix} \Delta Y_u & V_Q \\ 0 & y_t \end{pmatrix} \overline{Q}_L \tilde{H} u_R + \begin{pmatrix} \Delta Y_d & V_Q \\ 0 & y_b \end{pmatrix} \overline{Q}_L H d_R \,. \tag{1.117}$$

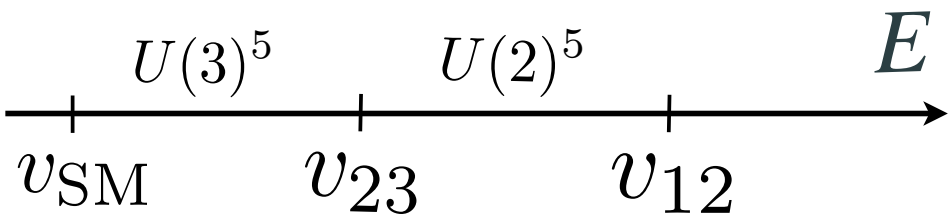

FIGURE 1.6: Multi-scale picture for a theory of flavour: v_{23} denotes the low scale where $U(2)^5$ is approximately preserved, and the hierarchy m_2/m_3 is explained. v_{12} denotes the higher scale where $U(2)^5$ is explicitly broken and the hierarchy m_1/m_2 is explained.

The spurion V_Q parameterises the small breaking of $U(2)^5$ that provides V_{cb} and V_{ub}. The $U(2)^5$ hypothesis cannot distinguish between them, but this is not a bad approximation given that $V_{cb} \approx \lambda^2$ and $V_{ub} \approx \lambda^3$. In a similar manner, the $U(2)^5$ hypothesis cannot distinguish between first and second family masses: further dynamics in the UV must provide the splitting of the spurions ΔY_u, ΔY_d and V_Q into first and second family contributions. This is an interesting idea: light NP at the TeV-scale may approximately preserve $U(2)^5$ and explain the smallness of V_{cb} and V_{ub}, along with the mass hierarchies between light families and the third family, i.e. m_2/m_3, while m_1/m_2, the difference (and alignment) between V_{cb} and V_{ub} and the Cabibbo angle are explained in the UV via heavier dynamics that explicitly break $U(2)^5$. This naturally leads to the idea of a multi-scale picture behind the origin of flavour: the theory of flavour could be a non-universal theory broken in (at least) two hierarchical steps down to the SM [113], as in Fig. 1.6. The approximate $U(2)^5$ flavour symmetry may arise accidentally if the theory of flavour is based on a non-universal gauge group [3, 5, 113–127].

However, we notice that the $U(2)^5$ hypothesis does not give any information about the flavour hierarchies between different charged sectors, e.g. m_b/m_t, which are left to be reproduced via small dimensionless coefficients. This is unsatisfactory given that some hierarchies like m_b/m_t are significant, suggesting the need to incorporate a dynamical mechanism to generate these hierarchies in theories of flavour based on $U(2)^5$. In a similar manner, the $U(2)^5$ hypothesis does not give any predictions about the alignment of the CKM matrix.

From a phenomenological point of view, the $U(2)^5$ hypothesis dictates that NP may couple non-universally to the third family but universally to the lighter generations. In particular, couplings to light generations can be absent in the interaction basis, only generated via fermion mixing. This latter case provides an efficient suppression of the production of NP degrees of freedom at colliders, relaxing bounds from LHC, while large NP in the third family (that could address the Higgs hierarchy puzzle) are allowed. If NP couplings to light generations are present, $U(2)^5$ protects from the appearance of the most dangerous FCNCs at tree-level, since they involve flavour transitions between

the first and second families[19]. Flavour transitions between the (left-handed) third family and light families are allowed, but they carry the CKM suppression of V_{cb} and V_{ub}. Flavour transitions between right-handed fermions, if mediated by NP approximately preserving $U(2)^5$, are naturally suppressed with respect to left-handed flavour transitions. This is a very desirable feature, given the tight bounds over FCNCs involving right-handed fermions (see Section 2.3.4).

Finally, we remark that in a realistic framework, the spurions in Eq. (1.117) would be promoted to physical scalars that provide non-renormalisable operators of the form

$$\mathcal{L}^{q,d=5}_{\text{Yukawa}} = c^u_{i3}\frac{V_Q}{\Lambda_Q}\overline{Q}_{Li}\tilde{H}u_{R3} + c^u_{ij}\frac{\Delta Y_u}{\Lambda_u}\overline{Q}_{Li}\tilde{H}u_{Rj} + c^d_{i3}\frac{V_Q}{\Lambda_Q}\overline{Q}_{Li}Hd_{R3} + c^d_{ij}\frac{\Delta Y_d}{\Lambda_d}\overline{Q}_{Li}Hd_{Rj}\,, \tag{1.118}$$

such that

$$\mathcal{L}^{q}_{\text{Yukawa}} = \begin{pmatrix} c^u_{ij}\dfrac{\Delta Y_u}{\Lambda_u} & c^u_{i3}\dfrac{V_Q}{\Lambda_Q} \\ 0 & y_t \end{pmatrix}\overline{Q}_L\tilde{H}u_R + \begin{pmatrix} c^d_{ij}\dfrac{\Delta Y_d}{\Lambda_d} & c^d_{i3}\dfrac{V_Q}{\Lambda_Q} \\ 0 & y_b \end{pmatrix}\overline{Q}_L H d_R\,, \tag{1.119}$$

where $i,j = 1,2$. If the physical scalars V_Q, ΔY_u and ΔY_d develop a VEV spontaneously (minimally) breaking the global $U(2)^5$ symmetry, then the effective Yukawa couplings involving light families are naturally suppressed by the heavy scales $\Lambda_{Q,u,d}$. The coefficients $c^{u,d}_{23}$, $c^{u,d}_{22}$ and $c^{u,d}_{12}$ could naturally be $\mathcal{O}(1)$, while y_b and $c^{u,d}_{11}$ need to be small in order to reproduce the remaining flavour hierarchies that $U(2)^5$ cannot explain.

A similar formalism can be applied to the charged lepton sector. However, the $U(2)^5$ hypothesis, if extended to the neutrino sector, would naively predict a third family neutrino much heavier than the others, with small mixing. This is at odds with neutrino oscillation data that suggests large and seemingly anarchic neutrino mixing, therefore requiring to introduce an extra mechanism in the theory of flavour in order to account for a proper description of neutrino masses and mixing.

1.10 Towards a theory of flavour: from the Planck scale to the electroweak scale

The complicated flavour sector of the SM leaves several questions unanswered:

- **Why three families of fermions, transforming as identical copies under the SM gauge group?** One may argue that we need at least three quark families to have CP-violating phases in the CKM matrix [38], and we need less than nine quark families to preserve the asymptotic freedom of QCD [13]. But this is equivalent to arguing that all experimental data suggests the existence of three families of fermions, see e.g. the invisible decay width of the Z boson [21]. It is

[19] In the complete theory of flavour, heavier NP would eventually break explicitly $U(2)^5$ to explain the origin of the flavour structure that involves first and second family fermions. Such NP may potentially mediate the most dangerous 1-2 FCNCs, however they would be heavier in a multi-scale picture of flavour, allowing to pass the stringent bounds from flavour observables.

clear that these *a posteriori* explanations are unsatisfactory as they do not provide any fundamental principle to understand why Nature has chosen the number three.

- **Why the three identical families of fermions interact so differently with the Higgs, leading to a hierarchical pattern of charged fermion masses and CKM mixing?**
- **What is the origin of the very tiny neutrino masses and lepton mixing?**
- **Why quark mixing and lepton mixing are so different, namely why the CKM matrix is almost diagonal while the PMNS matrix is seemingly anarchic?**

We highlight that the gauge couplings of the SM in Eq. (1.78) are not far from $\mathcal{O}(1)$. Even the tree-level mass of the Higgs boson is $\mathcal{O}(v_{\rm SM})$, such that the quartic coupling λ of the scalar potential (remember $m_h = \sqrt{2\lambda} v_{\rm SM}$) is not much smaller than $\mathcal{O}(1)$. This is what one would expect from a fundamental theory based on *naturalness* arguments: the free parameters take arbitrary values of the same order of magnitude, and any hierarchy or cancellation is explained in terms of dynamical mechanisms. There is no apparent reason for the parameters of a fundamental theory to greatly differ from each other, since they all appear in a similar way as free parameters of the renormalisable Lagrangian. Nevertheless, the flavour sector apparently is not guided by naturalness principles: rather than being of the same order, both the charged fermion masses and the CKM mixing angles follow hierarchical patterns. The high number of free parameters in the flavour sector, maybe too many for a fundamental theory of Nature, along with their particular hierarchical patterns, may be hinting at the existence of new physics that provide a dynamical explanation for the flavour structure of the SM: such a theory describing the complicated flavour sector of the SM in terms of simple and natural principles is called a *theory of flavour*.

The lack of understanding of the flavour sector of the SM has classically being denoted as the *flavour puzzle*. We stress here that this is not a *problem* of the SM, which works perfectly well with the input of the flavour parameters, but rather a puzzle of Nature for us to identify the dynamical mechanism behind these parameters in terms of our mathematical models. After the discovery of neutrino masses, the flavour sector is enlarged with extra flavour parameters accounting for neutrino masses and mixing, which now do become a problem of the SM: the inability of the SM to account for the observed physical phenomenon of neutrino oscillations, making the flavour puzzle difficult to ignore.

This thesis is devoted to the flavour puzzle: the development and study of new models to understand the origin of flavour in the SM, along with their phenomenology and discovery prospects. Flavour physics phenomenology will also play a central role, as it would not be unreasonable that a theory of flavour beyond the SM leads to new flavour specific interactions connected to the dynamical mechanisms behind the origin of flavour.

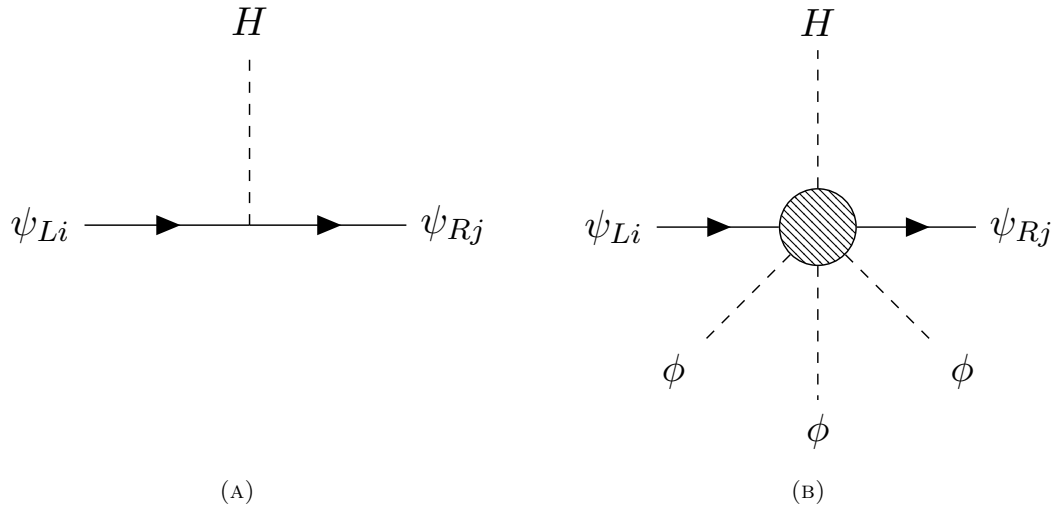

FIGURE 1.7: ***Left:*** Renormalisable Yukawa couplings in the SM. ***Right:*** Effective Yukawa couplings arising from non-renormalisable operators containing insertions of flavon fields ϕ.

Given that most of the Yukawa couplings are much smaller than $\mathcal{O}(1)$, a good starting point to model them in a more natural way would be to assume that Yukawa couplings in the SM are effective remnants of a UV theory. In this manner, they would carry the natural suppression of non-renormalisable operators. For example, let us consider that a symmetry beyond the SM forbids the SM Yukawa couplings at renormalisable level[20]. One example would be the global $U(1)_{\rm FN}$ flavour symmetry[21] of Froggatt-Nielsen (FN) models [133], which is spontaneously broken by the VEV of a SM scalar singlet ϕ_F, that we denote as the *flavon* field. For the moment, we shall remain agnostic to the particular UV theory, but we will assume that the flavon field ϕ_F transforms in the appropriate way under the BSM symmetry, allowing to write dimension-5 operators as

$$\mathcal{L}^{d=5}_{\rm Yukawa} = \frac{c}{\Lambda_F}\phi_F \overline{\Psi}_L \overset{(\sim)}{H} \psi_R + \text{h.c.}\,, \tag{1.120}$$

where Ψ_L denotes a generic $SU(2)_L$ fermion doublet of the SM, ψ_R denotes the accompanying $SU(2)_L$ fermion singlet, and H couples to down-quarks and charged leptons while $\widetilde{H}$ couples to up-quarks. The heavy scale Λ_F is the cut-off of the EFT, associated to new degrees of freedom present in the UV theory. When the flavon field ϕ_F develops a VEV spontaneously breaking the BSM symmetry, the operator in Eq. (1.120) provides an *effective Yukawa coupling* as

$$\mathcal{L}_{\rm Yukawa} = c\frac{\langle\phi_F\rangle}{\Lambda_F} \overline{\Psi}_L \overset{(\sim)}{H} \psi_R + \text{h.c.} \tag{1.121}$$

[20] We note that the flavour puzzle can be addressed without invoking new symmetries, e.g. in extra dimensional frameworks (see e.g. [128, 129]), however we will not consider this approach in this thesis. For a review about different approaches to the flavour puzzle, see e.g. [130].

[21] Note that spontaneously broken discrete flavour symmetries are also possible, for a review of mass matrices in such a framework see [131, 132].

In contrast with the SM, now the Yukawa couplings are obtained from non-renormalisable operators built with the insertion of the flavon field, as in Fig. 1.7. Assuming $\langle\phi_F\rangle \ll \Lambda_F$, the effective Yukawa coupling in Eq. (1.121) is naturally suppressed from unity, with the dimensionless coefficient c being naturally of $\mathcal{O}(1)$. At the level of our EFT framework, we have the freedom to assign a numerical value to the ratio $\langle\phi_F\rangle/\Lambda_F$. A convenient choice is

$$\frac{\langle\phi_F\rangle}{\Lambda_F} \simeq \lambda\,, \tag{1.122}$$

where $\lambda \simeq 0.225$ is the Wolfenstein parameter already introduced in Section 1.6.1. In the Froggatt-Nielsen framework, all SM fermions and ϕ_F may carry charge assignments under the global $U(1)_{\rm FN}$ symmetry. By convention, we assign -1 FN charge to ϕ_F without loss of generality. In this manner, the effective Yukawa couplings of SM fermions may be given by

$$\mathcal{L}_{\rm Yukawa} = c^u_{ij}\left(\frac{\langle\phi_F\rangle}{\Lambda_F}\right)^{\left|q_{\rm FN}(\overline{Q}_{Li})+q_{\rm FN}(u_{Rj})+q_{\rm FN}(\tilde{H})\right|}\overline{Q}_{Li}\widetilde{H}u_{Rj} \tag{1.123}$$

$$+\,c^d_{ij}\left(\frac{\langle\phi_F\rangle}{\Lambda_F}\right)^{\left|q_{\rm FN}(\overline{Q}_{Li})+q_{\rm FN}(d_{Rj})+q_{\rm FN}(H)\right|}\overline{Q}_{Li}Hd_{Rj} \tag{1.124}$$

$$+\,c^e_{ij}\left(\frac{\langle\phi_F\rangle}{\Lambda_F}\right)^{\left|q_{\rm FN}(\overline{L}_{Li})+q_{\rm FN}(e_{Rj})+q_{\rm FN}(H)\right|}\overline{L}_{Li}He_{Rj} + \text{h.c.}\,, \tag{1.125}$$

where $i,j = 1,2,3$. With the assignment of Eq. (1.122), each entry in the effective Yukawa matrices carries an individual suppression via powers of the Wolfenstein parameter, λ^α, where α is determined in terms of the FN charge assignments of SM fermions and the Higgs doublet. As a concrete example, we take the following set of charges:

$$q_{\rm FN}(\overline{Q}_{Li}) = (3,2,0)\,, \qquad q_{\rm FN}(u_{Ri}) = (4,1,0)\,, \tag{1.126}$$

$$q_{\rm FN}(d_{Ri}) = (4,3,2)\,, \qquad q_{\rm FN}(\overline{L}_{Li}) = (5,3,0)\,, \tag{1.127}$$

$$q_{\rm FN}(e_{Ri}) = (3,2,2)\,, \qquad q_{\rm FN}(H) = 0\,. \tag{1.128}$$

This choice leads to the following parametric suppression of the Yukawa couplings:

$$\mathcal{L}_{\rm Yukawa} = \begin{pmatrix}\overline{Q}_{L1} & \overline{Q}_{L2} & \overline{Q}_{L3}\end{pmatrix}\begin{pmatrix}\lambda^7 & \lambda^4 & \lambda^3\\ \lambda^6 & \lambda^3 & \lambda^2\\ \lambda^4 & \lambda & 1\end{pmatrix}\begin{pmatrix}u_{R1}\\ u_{R2}\\ u_{R3}\end{pmatrix}\widetilde{H} \tag{1.129}$$

$$+\begin{pmatrix}\overline{Q}_{L1} & \overline{Q}_{L2} & \overline{Q}_{L3}\end{pmatrix}\begin{pmatrix}\lambda^7 & \lambda^6 & \lambda^5\\ \lambda^6 & \lambda^5 & \lambda^4\\ \lambda^4 & \lambda^3 & \lambda^2\end{pmatrix}\begin{pmatrix}d_{R1}\\ d_{R2}\\ d_{R3}\end{pmatrix}H \tag{1.130}$$

$$+\begin{pmatrix}\overline{L}_{L1} & \overline{L}_{L2} & \overline{L}_{L3}\end{pmatrix}\begin{pmatrix}\lambda^8 & \lambda^7 & \lambda^7\\ \lambda^6 & \lambda^5 & \lambda^5\\ \lambda^3 & \lambda^2 & \lambda^2\end{pmatrix}\begin{pmatrix}e_{R1}\\ e_{R2}\\ e_{R3}\end{pmatrix}H + \text{h.c.}\,, \tag{1.131}$$

where we have omitted the dimensionless coefficients $c^{u,d,e}_{ij}$, naturally expected to be of

$\mathcal{O}(1)$. The Yukawa matrices above are hierarchical and approximately diagonal (the off-diagonal entries are small), therefore, in good approximation, the physical Yukawa couplings obtained after the diagonalisation will scale with powers of λ as the diagonal entries above. In this manner, one can check that our simplified FN model performs a good description of charged fermion masses.

Fermion mixing is approximately given by the ratios of off-diagonal over diagonal entries, upper off-diagonal entries for left-handed mixing and lower off-diagonal entries for right-handed mixing. In this manner, we obtain $V_{cb} \sim \lambda^2$, $V_{ub} \sim \lambda^3$ and $V_{us} \approx \lambda^4/\lambda^3 \sim \lambda$ for the CKM mixing. Remarkably, our toy FN model predicts non-vanishing charged lepton mixing, although too small to account for PMNS mixing, that must therefore come dominantly from the neutrino sector. The model also predicts significant right-handed fermion mixing, such as $s_{23}^{u_R} \sim \lambda$. In this manner, the Yukawa matrices in Eqs. (1.129-1.131) are an example of Yukawa *textures* broadly compatible with current data. Other examples include texture zeros, where one or more of the entries in the effective mass matrices may be filled with zeros. For a systematic study of possible textures for the charged fermion and neutrino mass matrices, we refer the reader to Refs. [134–136].

We notice that the description of the flavour sector does not point to any particular scale for $\langle \phi_F \rangle$ and Λ_F: the explanation of the SM flavour structure is successful as long as the ratio $\langle \phi_F \rangle / \Lambda_F$ is held fixed, but the independent scales of flavour $\langle \phi_F \rangle$ and Λ_F may be anywhere *from the Planck scale to the electroweak scale*.

This is not just a feature of the FN mechanism, but common to most theories of flavour based on BSM symmetries where Yukawa couplings are explained via effective operators. In particular, this applies to all the theories of flavour that will be explored in this thesis.

In the FN setup, the tree-level exchange of a radial mode of ϕ_F provides NP contributions to meson mixing observables that are compatible with current data only if the mass of ϕ_F is above $\sim 10^5$ TeV [137, 138] (note that this is the approximate bound that recent studies of successful FN models reveal, despite the obvious dependence on the charge assignments of fermions under the FN symmetry), thus setting the NP scales of the model far above our current reach for direct detection. Going beyond the FN setup, one may find different arguments to fix the *a priori* undetermined flavour scales:

- Motivated by gauge coupling unification, one may suggest that the very heavy scale where the gauge sector gets simplified and described by a single gauge coupling is also the scale where the new dynamics that explain and simplify the flavour sector become manifest [139–147]. This hypothesis is also supported by the heavy scale for the origin of neutrino masses suggested by the seesaw mechanism, and in good agreement with the prescription of Minimal Flavour Violation [142]. In particular, in recent years it has been noted the possibility that modular forms, motivated by string theory, could play an important role to explain the flavour

sector [148–153]. Modular symmetries can be incorporated to GUTs in order to build elegant theories of flavour at very high energy scales [154–158].

- New flavour dynamics addressing the flavour puzzle may leave its imprints in flavour observables, which are sensitive to scales far above the TeV. In this direction, experimental anomalies in observables that suggest new flavour-specific interactions [78, 79], or the breaking of lepton flavour universality [159], could be indirect signals of a theory of flavour. This suggests that the NP flavour scales may be closer to the electroweak scale, within the range for detection in current experiments. In particular, TeV-scale leptoquarks or Z' bosons would mediate new interactions to explain the flavour anomalies, with the flavour structure of their couplings to fermions dictated by the theory of flavour and connected to the origin of Yukawa couplings in the SM [1, 2, 160–169].

- Another interesting possibility is that the theory of flavour consists of multiple NP scales, that may cover a wide range of energy *from the Planck scale to the electroweak scale*. This is realised in multi-scale theories of flavour [2, 3, 5, 113–127, 163, 169], where a first layer of NP explains the flavour hierarchies m_2/m_3 and the smallness of CKM mixing, while a second layer explains the flavour hierarchy m_1/m_2 and the Cabibbo angle. The lower layer of NP also offers the opportunity to connect the theory with the flavour anomalies [2, 115, 119, 120, 169, 170], while the higher layer may provide a gauge unified framework [5]. The explanation of neutrino masses and PMNS mixing could be incorporated at low energies via a low scale seesaw mechanism [3, 5, 117], or at very high energies as a new step in the multi-scale picture [169]. Some examples of multi-scale theories of flavour predict an approximate $U(2)^5$ flavour symmetry [3, 5, 113–126], but their exist other alternatives such as [2, 163, 169] based on the idea of messenger dominance [171]. Remarkably, the various steps of symmetry breaking may offer the opportunity to connect the theory with other subjects like quark-lepton unification, the origin of matter-antimatter asymmetry [172] or the unification of electroweak and flavour symmetry [120, 121], and might be tested via cosmological observations of the different phase transitions in the early Universe associated to the several steps of symmetry breaking [173].

In this thesis, we propose and explore theories of flavour of the last kind, which may be connected to other open problems of the SM via the different layers of the multi-scale picture. Moreover, these theories enjoy a rich phenomenology and have the potential to be discovered in the current or next generation of particle physics experiments. In Chapter 3 we discuss a class of fermiophobic $U(1)'$ extensions of the SM, where the flavour structure of the SM is explained via the mechanism of messenger dominance [171], and we seek for an enhancement of the anomalous magnetic moment of the muon. In Chapter 4, we explore a twin Pati-Salam theory of flavour also based on messenger dominance, where the origin of flavour hierarchies is connected to the effective couplings

of a TeV-scale vector leptoquark $U_1 \sim (\mathbf{3}, \mathbf{1}, 2/3)$ that explains the so-called B-physics anomalies. In Chapter 5 we propose a gauge non-universal embedding of the SM in which a separate weak hypercharge is assigned to each fermion family. If the Higgs doublet(s) only carries third family hypercharge, then the third family is naturally heavier and flavour hierarchies arise naturally after the spontaneous breaking of the tri-hypercharge group. Finally, in Chapter 6 we show how gauge non-universal frameworks like the tri-hypercharge theory, among others, may emerge from a gauge unified group containing one separate $SU(5)$ for each family, where the three $SU(5)$ groups are related by a cyclic permutation symmetry that ensures a single gauge coupling at the GUT scale and the unification of all SM fermions into a single representation.

Chapter 2

Testing a theory of flavour: EFT formalism and flavour observables

> "Soon I knew the craft of experimental physics was beyond me - it was the sublime quality of patience - patience in accumulating data, patience with recalcitrant equipment - which I sadly lacked."
>
> – Abdus Salam

In order to test a new physics model, such as a theory of flavour, it is usually convenient to integrate out the new heavy degrees of freedom to obtain the low energy Effective Field Theory (EFT) of the model. In this context, we will introduce the Standard Model Effective Field Theory (SMEFT) that extends the SM via non-renormalisable operators which capture the NP effects originated by heavy physics above the electroweak scale. We will also introduce the Low Energy Effective Field Theory (LEFT) that contains the effective Lagrangian below the electroweak scale, and is useful to study NP contributions to low-energy observables. Finally, we will introduce and discuss particular flavour observables that suggest the presence of NP, and are well motivated from the point of view of a theory of flavour.

2.1 The Standard Model Effective Field Theory

The SMEFT is the effective field theory that contains the SM Lagrangian (1.16) plus all possible higher dimensional operators invariant under the SM gauge symmetry (1.1). In this thesis, we will only consider operators in the SMEFT up to dimension six. In fact, a few SMEFT operators have already been introduced in Chapter 1. One example is the dimension five Weinberg operator (1.84) that violates lepton number explicitly in two units, and provides Majorana masses for active neutrinos. Remarkably, the Weinberg operator is the only dimension five operator that one can write with SM fields. Another example is the dimension six operator in Eq. (1.107), which breaks both lepton number and baryon number in one unit and can mediate the decay of nucleons.

We introduce the SMEFT Lagrangian as

$$\mathcal{L}^{d\leq 6}_{\text{SMEFT}} = \mathcal{L}^{d\leq 4}_{\text{SM}} + \mathcal{L}^{d=5}_{\text{Weinberg}} - \sum_i \frac{1}{\Lambda_i^2} C_i(\mu) Q_i \,, \tag{2.1}$$

Although in Eq. (2.1) we have included one high cut-off scale for every operator, in principle each operator can contain different contributions from different UV models associated to different NP scales. Notice also that the SMEFT Wilson coefficients $C_i(\mu)$ depend on the energy scale μ, and hence experience renormalisation group evolution (RGE) effects. We will take the latter into account by using dedicated software such as `DsixTools 2.1` [174].

In Appendix D.1, Table D.3 [39], we list all dimension six SMEFT operators conserving baryon and lepton number, while the dimension six operators that violate baryon and lepton number are listed in Table D.2. We highlight Higgs-bifermion operators (class-3) and purely Higgs operators (class-7), which are useful to study contributions to electroweak precision observables, while the baryon number violating operators in Table D.2 are useful to study nucleon decay. Finally, we also highlight the set of baryon number conserving four-fermion operators (class-8), which are relevant for the study of flavour observables.

When referring to effective operators through this chapter, we denote lepton flavour indices as $\alpha = e, \mu, \tau$, and quark flavour indices as $i = 1, 2, 3$, in such a way that greek indices denote lepton flavours while latin indices denote quark flavours.

Finally, we comment that a more general EFT than the SMEFT do exists, the so-called Higgs Effective Field Theory (HEFT). SMEFT contains one Higgs doublet field as prescripted in the SM, however scenarios where the observed Higgs boson does not belong to an elementary exact $SU(2)_L$ doublet are still allowed within the current experimental accuracy. Those may be described by the HEFT where the Higgs boson is treated as a gauge singlet and the Goldstone bosons are treated separately. However, in this thesis all the UV models proposed contain at least one exact Higgs doublet performing EW symmetry breaking, with the canonical SM being a low scale limit in all cases, therefore all the NP effects will be well captured by the SMEFT framework.

2.2 The Low Energy Effective Field Theory

The LEFT is the effective field theory that describes low energy scales $\mu \ll M_Z$, at which the electroweak gauge invariance is broken and the remaining gauge symmetry is $SU(3)_c \times U(1)_Q$. The effective Lagrangian containing operators up to dimension six is given by

$$\mathcal{L}^{d\leq 6}_{\text{LEFT}} = \mathcal{L}_{\text{QED}} + \mathcal{L}_{\text{QCD}} - \frac{4G_F}{\sqrt{2}} \sum_i C_i(\mu) \mathcal{O}_i \,, \tag{2.2}$$

where $-4G_F/\sqrt{2}$ is a conventional normalisation factor that allows to easily compare the strength of the NP effect with that of the weak interactions, both generally contributing

to the Wilson coefficients $C_i(\mu)$. Throughout this thesis, we will commonly consider $\mu = m_b$ as our low-energy scale, since we will consider several observables related to B-meson physics.

In Appendix D.2, Table D.4 [175], we list baryon and lepton number conserving operators up to dimension six, while in Table D.5 we list baryon and/or lepton number violating operators up to dimension six. We highlight the four-fermion operators in Table D.4, distinguished by their different chiralities, which will play an important role for the study of flavour observables.

We provide tree-level matching conditions between the operators in the SMEFT and the LEFT [175] in Appendix D.3. Notice that particular operators in the LEFT do not get any contributions from the SMEFT at tree-level, therefore they can only get suppressed contributions (e.g. via RGE) from dimension six NP operators preserving $SU(2)_L \times U(1)_Y$.

2.3 Flavour observables

In the following, we discuss key flavour observables that are in tension with the SM and might be connected to a possible theory of flavour. We denote these observables as *anomalies*. We also discuss several observables that get modified as well in NP scenarios that explain the anomalies. These observables offer the possibility to test and discriminate between the different NP explanations.

2.3.1 $R_{K^{(*)}}$ and $b \to s\mu\mu$

Lepton flavour universality (LFU) is a key prediction of the SM: all lepton flavours experience gauge interactions in the same way, up to corrections related to the different masses of charged leptons[1]. After the discovery of neutrino oscillations, we know that LFU is not an exact symmetry of Nature. However, the breaking effects of LFU via lepton mixing are suppressed by the very tiny neutrino masses, being generally unobservable with current experimental precision. In this manner, the observation of LFU breaking in low-energy processes would be a clear indication of new physics.

Although purely leptonic observables so far show no significant hints of violation of LFU (see e.g. LFU in τ decays in Section 2.3.10), semileptonic observables are also sensitive to the breaking of LFU. In contrast with purely leptonic modes, they can be afflicted by substantial QCD uncertainties, however it is possible to build very clean observables in terms of ratios of semileptonic processes. In this direction, the $R_{K^{(*)}}$ ratios were proposed

$$R_{K^{(*)}} = \frac{\mathcal{B}(B \to K^{(*)}\mu^+\mu^-)}{\mathcal{B}(B \to K^{(*)}e^+e^-)} \,. \tag{2.3}$$

Within the SM, lepton universality predicts $R_{K^{(*)}} = 1$ for $q^2\,\epsilon\,[1.1, 6]$ GeV^2, where q^2 denotes the dilepton invariant-mass squared, up to corrections of order 1% [176] due to

[1] These corrections are most relevant for processes involving τ charged leptons, which are heavier.

the different masses of muons and electrons. Notice that the $b \to s\mu\mu$ transition is a FCNC in the SM, therefore being generally loop suppressed, GIM suppressed and CKM suppressed. This strong suppression makes these processes particularly sensitive to new physics.

It turns out that the experimental measurements of the $R_{K^{(*)}}$ ratios showed deviations from the SM for almost eight years. In particular, the R_K ratio alone reached a 3.1σ tension with the SM in the LHCb update of 2021 [177], and several deviations sitting at the 2σ level showed up in R_{K^*} [178] and other LFU ratios involving kaons. These measurements suggested the presence of NP contributions interfering with the SM contribution and mainly coupled to muons, leading to $R_{K^{(*)}} < 1$.

This pattern was supported by other semileptonic observables, including $\mathcal{B}(B \to K^{(*)}\mu^+\mu^-)$, $\mathcal{B}(B_s \to \phi\mu^+\mu^-)$ and the angular observable P_5', all of them afflicted however by significant hadronic uncertainties [179]. Remarkably, the very clean leptonic decay $\mathcal{B}(B_s \to \mu^+\mu^-)$ was also in good agreement with the muon deficit observed in $R_{K^{(*)}}$ [180]. This consistent set of anomalies was easy to accommodate in the context of a theory of flavour: new dynamics connected to the origin of the Yukawa couplings $y_e \ll y_\mu$ might as well couple preferentially to muons. In this direction, we proposed a simplified phenomenological model based on a fermiophobic Z' boson [1] where effective couplings to SM fermions were obtained via mixing with a fourth family of vector-like fermions. This simplified model could not only explain $R_{K^{(*)}}$ but also $(g-2)_\mu$ simultaneously, and was motivated by a theory of flavour with fermiophobic Z' [163] already proposed in the literature to explain $R_{K^{(*)}}$. Later on, we considered a complete theory of flavour based on a twin Pati-Salam gauge group that contains a TeV scale $U_1 \sim (\mathbf{3}, \mathbf{1}, 2/3)$ vector leptoquark [169]. This theory could potentially explain $R_{K^{(*)}}$ via U_1 exchange, along with the $R_{D^{(*)}}$ anomalies which also suggest a consistent breaking of LFU (see Section 2.3.2). We concluded that such a theory could not explain the anomalies in its minimal version, but with extra model building efforts we showed that the theory was able to simultaneously explain both $R_{K^{(*)}}$ and $R_{D^{(*)}}$ while remaining compatible with all experimental data [2]. The anomalous measurements of $R_{K^{(*)}}$ that motivated these efforts were [177, 178]

$$R_K^{[1.1,6]} = \frac{\mathcal{B}\left(B \to K\mu^+\mu^-\right)}{\mathcal{B}\left(B \to Ke^+e^-\right)} = 0.846^{+0.044}_{-0.041}\,, \qquad (2.4)$$
$$R_{K^*}^{[1.1,6]} = \frac{\mathcal{B}\left(B \to K^*\mu^+\mu^-\right)}{\mathcal{B}\left(B \to K^*e^+e^-\right)} = 0.69^{+0.16}_{-0.12}\,,$$

where $q^2\,\epsilon\,[1.1, 6]$ GeV^2 denotes the dilepton invariant-mass squared. As of 2021, the global average of the theoretically clean observable $\mathcal{B}(B_s \to \mu^+\mu^-)$ was (see e.g. [181])

$$\mathcal{B}(B_s \to \mu^+\mu^-) = (2.8 \pm 0.3) \times 10^{-9}\,, \qquad (2.5)$$

to be compared with the SM prediction $\mathcal{B}(B_s \to \mu^+\mu^-)_{\rm SM} = (3.67 \pm 0.15) \times 10^{-9}$ [182]. In order to describe these measurements at the level of the LEFT, it is convenient to

define a new basis of LEFT operators beyond the San Diego basis [175] that discriminates operators by the chirality of quarks and by the vector-like or vector-axial components of muons, leading to the following effective Lagrangian:

$$\mathcal{L}_{b\to s\mu\mu} = \frac{4G_F}{\sqrt{2}} V_{tb}V_{ts}^* \frac{\alpha_{\rm EM}}{4\pi} \left[(C_9^{\rm SM} + C_9^{\mu\mu})\mathcal{O}_9^{\mu\mu} + (C_{10}^{\rm SM} + C_{10}^{\mu\mu})\mathcal{O}_{10}^{\mu\mu} + \text{h.c.} \right] \quad , \tag{2.6}$$

where

$$\mathcal{O}_9^{\mu\mu} = (\bar{s}\gamma_\mu P_L b)\,(\bar{\mu}\gamma^\mu \mu) \ , \tag{2.7}$$

$$\mathcal{O}_{10}^{\mu\mu} = (\bar{s}\gamma_\mu P_L b)\,(\bar{\mu}\gamma^\mu \gamma_5 \mu) \ . \tag{2.8}$$

We have omitted semileptonic scalar and tensor operators from Eq. (2.6). The former provide a chiral enhancement of $\mathcal{B}(B_s \to \mu^+\mu^-)$ which is at odds with current data, and the latter are not generated at tree-level from dimension six SMEFT operators. Similarly, primed operators $\mathcal{O}_9'^{\mu\mu}$ and $\mathcal{O}_{10}'^{\mu\mu}$ are obtained by exchanging P_L by P_R in Eqs. (2.7) and (2.8), however these operators involving right-handed quarks are as well disfavoured by current data. Notice also the different normalisation factor of Eq. (2.6) with respect to Eq. (2.2), highlighting the CKM suppression of the $b \to s\mu\mu$ transition. For simplicity, in Eq. (2.6) we suppressed the scale dependence of the Wilson coefficients, that have to be evaluated at $\mu = m_b$.

The Wilson coefficients $C_9^{\rm SM} = 4.27$ and $C_{10}^{\rm SM} = -4.17$ [183] encode the SM contributions, while $C_9^{\mu\mu}$ and $C_{10}^{\mu\mu}$ are associated to NP. Performing a combined χ^2 fit of the observables $R_{K^{(*)}}$ and $\mathcal{B}(B_s \to \mu^+\mu^-)$ one obtains the parameter space of $C_9^{\mu\mu}$ and $C_{10}^{\mu\mu}$ preferred by NP, as can be seen in Fig. 2.1a. As of 2021, scenarios involving only $C_9^{\mu\mu}$ or $C_{10}^{\mu\mu}$ could describe the experimental data up to 2σ precision, while left-handed NP $C_9^{\mu\mu} = -C_{10}^{\mu\mu}$ were in excellent agreement with experimental data and preferred over the SM hypothesis by more than 4σ.

In late 2022, a reanalysis of the $R_{K^{(*)}}$ ratios by LHCb revealed that backgrounds in the electron channel had been misidentified in all previous analyses. After this systematic effect was taken into account, the collaboration updated the $R_{K^{(*)}}$ ratios as [185]

$$\begin{aligned} R_K^{[1.1,6]} &= \frac{\mathcal{B}\left(B \to K\mu^+\mu^-\right)}{\mathcal{B}\left(B \to Ke^+e^-\right)} = 0.949^{+0.047}_{-0.046} \, , \\ R_{K^*}^{[1.1,6]} &= \frac{\mathcal{B}\left(B \to K^*\mu^+\mu^-\right)}{\mathcal{B}\left(B \to K^*e^+e^-\right)} = 1.027^{+0.077}_{-0.073} \, , \end{aligned} \tag{2.9}$$

with correlation factor $\rho = -0.017$. This way, the $R_{K^{(*)}}$ ratios are now in good agreement with SM lepton universality, although some space for NP is still left. The CMS collaboration presented a precise new measurement of $\mathcal{B}(B_s \to \mu^+\mu^-)$ in 2022 as well [186], which is in good agreement with the SM. When combined with the existing measurements by LHCb and ATLAS, the global average now reads (see e.g. [187, 188])

$$\mathcal{B}(B_s \to \mu^+\mu^-) = (3.28 \pm 0.26) \times 10^{-9} \, , \tag{2.10}$$

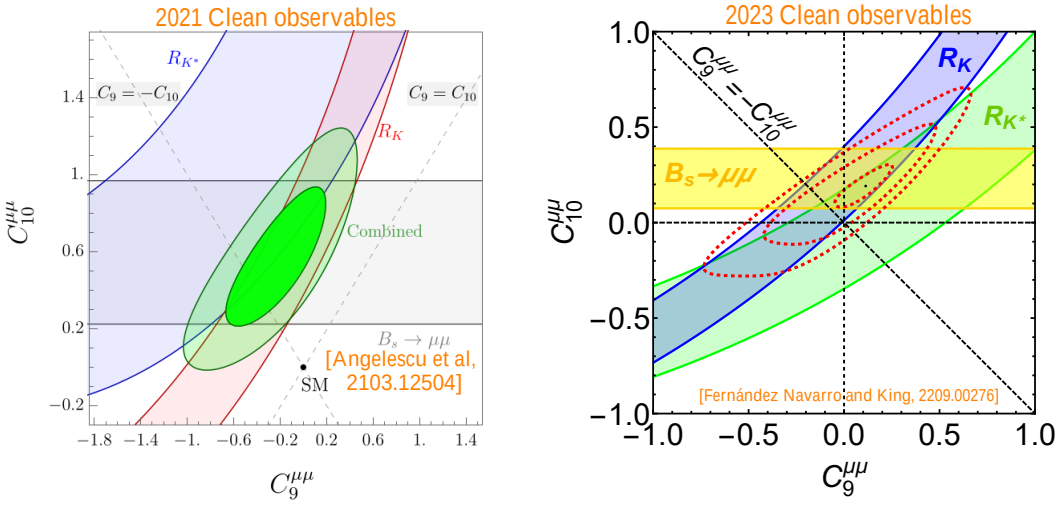

(A) (B)

FIGURE 2.1: Allowed regions in the plane $C_9^{\mu\mu}$ vs $C_{10}^{\mu\mu}$ to 1σ accuracy derived by using 2021 (left) and 2023 (right) data on R_K, R_{K^*} and $\mathcal{B}(B_s \to \mu^+\mu^-)$. The green (left) and red (right) contours denote the 1σ, 2σ and 3σ regions of the χ^2 fit. The left plot is taken from [184]. The right plot is our own work (originally presented in [2]), and the black dot denotes the best fit point with $\Delta\chi^2/\text{dof} \approx 0.56$.

which is in good agreement with the SM prediction $\mathcal{B}\left(B_s \to \mu^+\mu^-\right)_{\text{SM}} = (3.67 \pm 0.15) \times 10^{-9}$, albeit leaving some space for NP. The expressions for the observables of interest $R_K^{[1.1,6]}$, $R_{K^*}^{[1.1,6]}$ and $\mathcal{B}(B_s \to \mu^+\mu^-)$ in terms of the Wilson coefficients $C_9^{\mu\mu}$ and $C_{10}^{\mu\mu}$ are [189] (we do not include expressions for the lower q^2 interval for $R_{K^{(*)}}$ where NP contributions are suppressed)

$$R_K^{[1.1,6]} = R_{K,\text{SM}}^{[1.1,6]} \frac{1 + 0.24\text{Re}(C_9^{\mu\mu}) - 0.26\text{Re}(C_{10}^{\mu\mu}) + 0.03(|C_9^{\mu\mu}|^2 + |C_{10}^{\mu\mu}|^2)}{1 + 0.24\text{Re}(C_9^{ee}) - 0.26\text{Re}(C_{10}^{ee}) + 0.03(|C_9^{ee}|^2 + |C_{10}^{ee}|^2)}\,, \tag{2.11}$$

$$R_{K^*}^{[1.1,6]} = R_{K^*,\text{SM}}^{[1.1,6]} \frac{1 + 0.18\text{Re}(C_9^{\mu\mu}) - 0.29\text{Re}(C_{10}^{\mu\mu}) + 0.03(|C_9^{\mu\mu}|^2 + |C_{10}^{\mu\mu}|^2)}{1 + 0.18\text{Re}(C_9^{ee}) - 0.29\text{Re}(C_{10}^{ee}) + 0.03(|C_9^{ee}|^2 + |C_{10}^{ee}|^2)}\,, \tag{2.12}$$

$$\mathcal{B}\left(B_s \to \mu^+\mu^-\right) = \mathcal{B}\left(B_s \to \mu^+\mu^-\right)_{\text{SM}} \left|1 + \frac{C_{10}^{\mu\mu}}{C_{10}^{\text{SM}}}\right|^2 . \tag{2.13}$$

In Fig. 2.1b we show the parameter space in the plane $(C_9^{\mu\mu}, C_{10}^{\mu\mu})$ preferred by the 2023 $R_{K^{(*)}}$ ratios and the 2023 average of $\mathcal{B}(B_s \to \mu^+\mu^-)$. We also display the result of a combined χ^2 fit to the three observables as the red ellipses, denoting 1σ, 2σ and 3σ intervals. Our results show that a small but non-zero value of $C_{10}^{\mu\mu}$ is still preferred by $\mathcal{B}(B_s \to \mu^+\mu^-)$. On the other hand, $C_9^{\mu\mu}$ is compatible with zero, but small positive and negative values are still allowed by the new $R_{K^{(*)}}$ ratios at 1σ.

In particular, we highlight that left-handed NP $C_9^{\mu\mu} = -C_{10}^{\mu\mu}$ are not far away from the 1σ region, and our 1-dimensional fit reveals

$$C_9^{\mu\mu} = -C_{10}^{\mu\mu} = [-0.0111, -0.1425] \quad (1\sigma)\,, \tag{2.14}$$

with a best fit value of $C_9^{\mu\mu} = -C_{10}^{\mu\mu} = -0.0725$ with $\Delta\chi^2/\text{dof} \approx 0.58$. Although left-handed NP are still allowed by the new data, the WCs are much smaller than those preferred by 2021 data (see Fig. 2.1a).

Finally, we highlight that although the anomalies in $R_{K^{(*)}}$ have disappeared, strong hints for NP still remain in $b \to s\mu\mu$ observables such as $\mathcal{B}(B \to K^{(*)}\mu^+\mu^-)$, $\mathcal{B}(B_s \to \phi\mu^+\mu^-)$ and the angular observable P_5'. However, the significance of these anomalies depends on assumptions about the unknown QCD uncertainties that affect these observables. Although some analyses suggest that the tension in $\mathcal{B}(B \to K^{(*)}\mu^+\mu^-)$ can reach the 4σ level (see e.g. [179]), these claims should be taken with care. The remaining anomalies in $b \to s\mu\mu$ data could be explained by a lepton universal contribution to the operator C_9, provided that the NP effect is $C_9 \approx 1$ [82] (roughly one fourth of the SM C_9). We denote such contribution as C_9^U. It could be generated via a Z' boson with flavour universal couplings to leptons, or it could also be generated via RGE effects provided by leptoquarks that couple preferentially to third family fermions, such as those proposed to address $R_{D^{(*)}}$ (see Section 2.3.2). Remarkably, the scenario most preferred by current data involves a large C_9^U plus a small LFU-violating left-handed contribution $C_9^{\mu\mu} = -C_{10}^{\mu\mu}$ [82],

$$C_9^U = -1.10^{+0.17}_{-0.19} \quad (\text{LFU})\,, \qquad C_9^{\mu\mu} = -C_{10}^{\mu\mu} = -0.08^{+0.07}_{-0.06} \quad (\text{LFUV})\,. \tag{2.15}$$

We will see that this scenario is very well motivated from the point of view of a theory of flavour, as it could arise from leptoquarks with hierarchical couplings to charged leptons, following the pattern of SM Yukawa couplings $y_e \ll y_\mu \ll y_\tau$.

2.3.2 $R_{D^{(*)}}$ anomalies and their interpretation in a theory of flavour

Even though the $R_{K^{(*)}}$ ratios are now in good agreement with the SM, strong hints for the breaking of LFU are still present in $b \to c\ell\nu$ transitions. Here one can construct relatively clean LFU ratios of B mesons decaying to $D^{(*)}$ mesons and a lepton-neutrino pair. Particularly interesting are the $R_{D^{(*)}}$ ratios,

$$R_{D^{(*)}} = \left.\frac{\mathcal{B}(B \to D^{(*)}\tau\bar{\nu})}{\mathcal{B}(B \to D^{(*)}\ell\bar{\nu})}\right|_{\ell=e,\,\mu}\,, \tag{2.16}$$

which test the universality of the decays into taus with respect to the decays into light charged leptons. In the following, we display the arithmetic average of existing SM predictions given in [80],

$$R_D^{\text{SM}} = 0.298 \pm 0.004\,, \qquad R_{D^*}^{\text{SM}} = 0.254 \pm 0.005\,. \tag{2.17}$$

In contrast with the $R_{K^{(*)}}$ ratios, the SM prediction of $R_{D^{(*)}}$ is smaller than unity due to the large mass of tau with respect to the light charged leptons. The uncertainties sit at the level of a few per cent (slightly larger than those of the $R_{K^{(*)}}$ ratios), due to

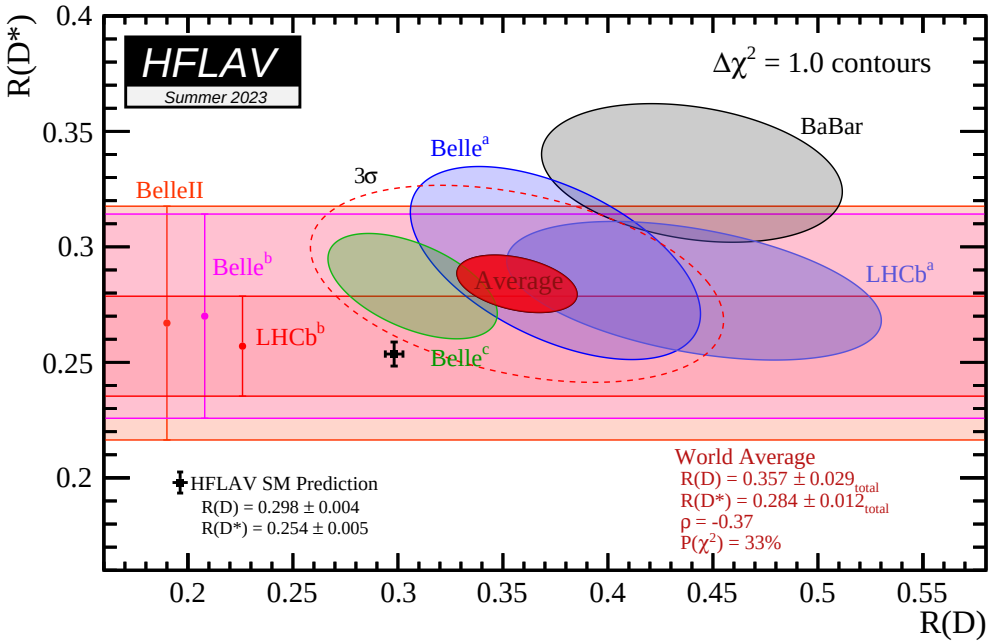

FIGURE 2.2: Experimental picture of the $R_{D^{(*)}}$ anomalies as of Summer 2023, along with the HFLAV average SM prediction. The horizontal bands are 1σ (68% CL) bands, whereas the solid ellipses correspond to $\Delta\chi^2 = 1$ (61% CL) contours. In particular, the solid red ellipse corresponds to the $\Delta\chi^2 = 1$ (61% CL) contour for the global average, while the dashed red ellipse corresponds to the 3σ contour for the global average. Figure taken from the website of HFLAV.

uncertainties in the lattice QCD determinations of hadronic form factors [190–192]. It is important to mention that, despite the recent progress, the lattice QCD results for the $B \to D^*$ form factors show tensions among each other and with experimental data, hence requiring further investigation.

The $R_{D^{(*)}}$ ratios were firstly measured by the BaBar collaboration in 2012 [159,193], who presented experimental values of R_D and R_{D^*} larger than the SM prediction by about 2-3σ. Since then, new measurements by the Belle collaboration [194–197] and by the LHCb collaboration [198,199] have shown small deviations from the SM, consistent with the BaBar measurements, but no singular measurement has been significant enough to claim evidence for new physics. Nevertheless, the global picture shows a consistent pattern of deviations where R_D and R_{D^*} are both larger than the SM predictions. As of Summer 2023, the global average by HFLAV of all official measurements of the $R_{D^{(*)}}$ ratios reads [80]

$$R_D^{\text{HFLAV}} = 0.357 \pm 0.029\,, \qquad R_{D^*}^{\text{HFLAV}} = 0.284 \pm 0.013\,. \tag{2.18}$$

These values exceed the SM predictions given before by 2σ and 2.2σ, respectively. Considering the R_D-R_{D^*} correlation of $\rho = -0.37$, the resulting combined deviation from the SM is at the level of 3.3σ, as shown in Fig. 2.2. We note that in the near future,

we expect experimental input from the Belle II[2] collaboration to confirm or exclude the existing pattern of deviations.

Other $b \to c\ell\nu$ observables beyond $R_{D^{(*)}}$ have been measured, namely $R_{J/\psi}$ [200] and R_{Λ_b} [201], which are affected by larger experimental uncertainties. They are consistent with the current deviations in $R_{D^{(*)}}$, but they are not yet precise enough to shed light on the $b \to c\ell\nu$ LFU puzzle.

In order to describe the $b \to c\tau\bar{\nu}$ transition at the level of the LEFT, we introduce the following effective operators,

$$\begin{aligned}\mathcal{L}_{b\to c\tau\nu} = -\frac{4G_F}{\sqrt{2}}V_{cb}\Bigg[&\left(1+\left[C^{V,LL}_{\nu edu}\right]^{\tau\tau 32*}\right)\left[\mathcal{O}^{V,LL}_{\nu edu}\right]^{\tau\tau 32\dagger} \\ &+\left[C^{S,RL}_{\nu edu}\right]^{\tau\tau 32*}\left[\mathcal{O}^{S,RL}_{\nu edu}\right]^{\tau\tau 32\dagger}+\text{h.c.}\Bigg]\,,\end{aligned} \tag{2.19}$$

where the Wilson coefficients are at the m_b scale. In the effective Lagrangian of Eq. (2.19), we have omitted operators which will not be relevant for the NP models presented in this thesis. The $R_{D^{(*)}}$ ratios are described in terms of the NP Wilson coefficients as,

$$\begin{aligned}R_D = R_D^{\text{SM}}\Bigg[&\left|1+\left[C^{V,LL}_{\nu edu}\right]^{\tau\tau 32*}\right|^2+1.5\text{Re}\left\{\left(1+\left[C^{V,LL}_{\nu edu}\right]^{\tau\tau 32*}\right)\left[C^{S,RL}_{\nu edu}\right]^{\tau\tau 32*}\right\} \\ &+1.03\left|\left[C^{S,RL}_{\nu edu}\right]^{\tau\tau 32*}\right|^2\Bigg]\,,\end{aligned} \tag{2.20}$$

$$\begin{aligned}R_{D^*} = R_{D^*}^{\text{SM}}\Bigg[&\left|1+\left[C^{V,LL}_{\nu edu}\right]^{\tau\tau 32*}\right|^2+0.12\text{Re}\left\{\left(1+\left[C^{V,LL}_{\nu edu}\right]^{\tau\tau 32*}\right)\left[C^{S,RL}_{\nu edu}\right]^{\tau\tau 32*}\right\} \\ &+0.04\left|\left[C^{S,RL}_{\nu edu}\right]^{\tau\tau 32*}\right|^2\Bigg]\,,\end{aligned} \tag{2.21}$$

where the numerical coefficients are obtained from integrating over the full kinematical distributions for the $B \to D^{(*)}$ semileptonic decay [202, 203]. Notice that the vector operator $\left[\mathcal{O}^{V,LL}_{\nu edu}\right]^{\tau\tau 32\dagger}$ predicts that both R_D and R_{D^*} are similarly modified by NP, such that their deviations from the SM follow $\Delta R_D = \Delta R_{D^*}$, where a fit to $b \to c\tau\bar{\nu}$ data prefers $\left[C^{V,LL}_{\nu edu}\right]^{\tau\tau 32*} = 0.08 \pm 0.02$ [204]. Instead, the scalar operator $\left[\mathcal{O}^{S,RL}_{\nu edu}\right]^{\tau\tau 32\dagger}$ predicts a larger enhancement of R_D with respect to R_{D^*}, such that $\Delta R_D > \Delta R_{D^*}$, where a fit to $b \to c\tau\bar{\nu}$ data prefers $\left[C^{S,RL}_{\nu edu}\right]^{\tau\tau 32*} = 0.17 \pm 0.05$ [204]. The preferred NP candidates to generate these operators and explain the $R_{D^{(*)}}$ anomalies are vector and/or scalar leptoquarks, which generally avoid tree-level contributions to the most dangerous $\Delta F = 2$ processes.

If confirmed, the $R_{D^{(*)}}$ anomalies suggest the existence of NP dominantly interacting with taus rather than with light charged leptons, leading to a 10-20% enhancement over

[2]We note here that the Belle II collaboration presented their first preliminary measurement of R_{D^*} simultaneously at the Lepton-Photon 2023 and SUSY 2023 conferences, being compatible with the existing pattern of deviations, although this measurement is not significant enough to extract any further conclusions.

the SM prediction in the tau channel. Notice that the $b \to c\ell\nu$ transition is a tree-level charged current in the SM. Therefore, relevant NP contributions to the $R_{D^{(*)}}$ ratios very likely have to be tree-level and associated to the TeV scale, otherwise the NP effect would be completely screened by the SM contribution. This is in contrast with the $R_{K^{(*)}}$ ratios, which are sensitive to heavier NP scales due to loop, GIM and CKM suppressions.

The $R_{D^{(*)}}$ ratios and the still anomalous $b \to s\mu\mu$ data are commonly denoted as the "B-anomalies". During the time when the $R_{K^{(*)}}$ ratios showed tensions with the SM, deviations in both LFU ratios $R_{D^{(*)}}$ and $R_{K^{(*)}}$ were consistently understood in the framework of a theory of flavour. New dynamics connected to the origin of the SM flavour structure might very well couple hierarchically to SM fermions, following the behaviour of SM Yukawa couplings. Given that in the SM $y_e \ll y_\mu \ll y_\tau$, then if the new dynamics follow the same hierarchical pattern, it would be natural to see a large effect in the $R_{D^{(*)}}$ ratio, followed by a hierarchically smaller effect that modifies the $R_{K^{(*)}}$ ratios. From the point of view of a theory of flavour, the fact that the $R_{K^{(*)}}$ ratios are now consistent with the SM only means that the new dynamics coupling to muons are smaller than we expected. In other words, if the theory of flavour predicts generic NP couplings $\beta_\mu \ll \beta_\tau$, then the new data on $R_{K^{(*)}}$ only means that β_μ is smaller than we expected, but still completely consistent with the expected hierarchical pattern. However, if β_μ is indeed connected to the origin of y_μ, then eventually a deviation in $R_{K^{(*)}}$ from the SM prediction should be seen with further precision. Model building in this direction will be considered in Chapter 4 via a theory of flavour containing a $U_1 \sim (\mathbf{3}, \mathbf{1}, 2/3)$ vector leptoquark.

2.3.3 $(g-2)_\mu$ anomaly

Independent of the anomalies in B-physics data, there also exists a possible discrepancy with the SM prediction in the experimentally measured anomalous magnetic moment $a = (g-2)/2$ of the muon. The long-lasting non-compliance of a_μ with the SM was first observed by the Brookhaven E821 experiment at BNL [205]. More recently, this discrepancy has been confirmed by the FNAL experiment [78, 79],

$$\Delta a_\mu^{\mathrm{R}} = a_\mu^{\mathrm{exp}} - a_\mu^{\mathrm{SM,R}} = (249 \pm 48) \times 10^{-11}\,, \tag{2.22}$$

a result 5.1σ larger than the SM prediction obtained by the muon g-2 theory initiative [206]. However, this SM prediction is based on data from $e^+e^- \to$ hadrons [207–209], and does not include the lattice QCD results by the BMW collaboration for the hadronic vacuum polarisation [210], which reduce the tension to the 1.8σ level,

$$\Delta a_\mu^{\mathrm{BMW}} = a_\mu^{\mathrm{exp}} - a_\mu^{\mathrm{SM,BMW}} = (105 \pm 59) \times 10^{-11}\,. \tag{2.23}$$

Note that the results of BMW have been confirmed by other lattice collaborations [211–213], but only in the so-called "intermediate window" [214], which represents only a third of the total contribution to the hadronic vacuum polarisation. Apparently, the hadronic

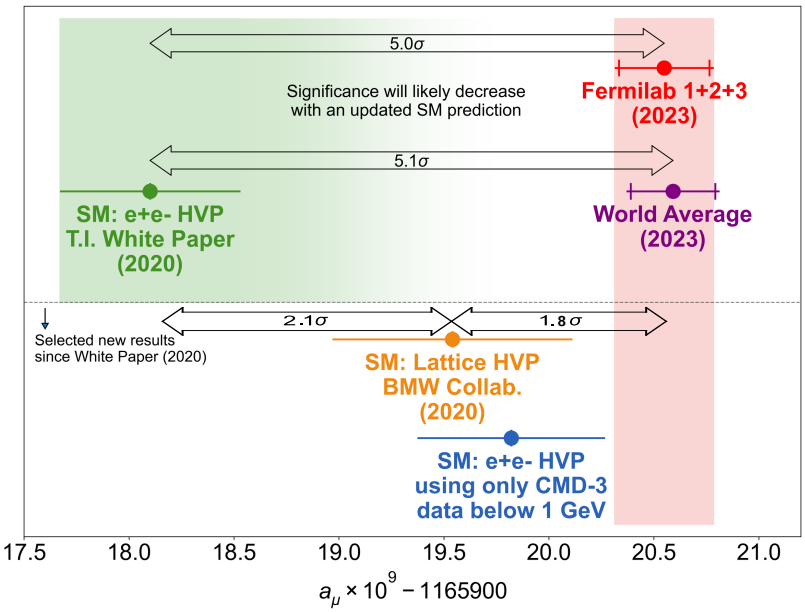

FIGURE 2.3: Current picture of $a_\mu \equiv (g-2)_\mu/2$ data, including the data driven SM prediction (White Paper), the data driven prediction considering only the recent CMD-3 data, the BMW lattice prediction, and the experimental measurements including FNAL and the current world average (see more in the main text). Figure taken from the slides of Graziano Venanzoni for the EPS-HEP2023 conference.

vacuum polarisation predicted by BMW also worsens the SM fit to EWPOs [215]. The situation becomes even more puzzling if we consider the most recent measurement of $e^+e^- \to$ hadrons by the CMD-3 collaboration [216], which would render the data driven prediction closer to the measurement, however the recent results obtained by CMD-3 are in conflict with more than 20 years of data from e^+e^- experiments. This complicated situation regarding the theory prediction of $(g-2)_\mu$ is illustrated in Fig. 2.3.

While we wait for new data and theory improvement to establish a clear picture, it is interesting to study the BSM interpretation of the result in Eq. (2.22). Moreover, although the BMW prediction is still in rough agreement with the experimental value, with the increasing precision in the experimental measurement is possible that a small tension at the 2σ level emerges in the near future.

Any BSM contribution to $(g-2)_\mu$ involves both left-handed and right-handed muons, hence relying on a chirality flip, which can be provided by the muon Yukawa coupling in the SM. Given the smallness of y_μ in the SM, only light NP such as a sub-GeV Z' [217] can explain the anomaly in this manner. However, such NP are difficult to connect to a theory of flavour, plus the parameter space is becoming very constrained (see e.g. Ref. [218] for a review of new physics in $(g-2)_\mu$). Because the deviation from the SM prediction is as large as its electroweak contribution, heavy NP at or above the TeV scale must possess an enhancement factor. This can be provided via the mechanism of chiral enhancement, meaning that the chirality flip does not originate from the small muon Yukawa coupling but rather from a larger coupling of other particles to the SM Higgs. Models of this kind include the MSSM, where chiral enhancement is connected

to tanβ [219], models with generic new scalars and fermions [220–225], and also models with the scalar leptoquarks $S_1 \sim (\overline{\mathbf{3}}, \mathbf{1}, 1/3)$ and/or $R_2 \sim (\mathbf{3}, \mathbf{2}, 7/6)$ [226–230] which provide a m_t/m_μ chiral enhancement.

Another interesting class of models involves the addition of extra vector-like fermions charged under a new $U(1)'$ gauge group. The SM fermions remain uncharged under $U(1)'$, such that the massive Z' boson does not couple directly to SM fermions, only through possible mixing between vector-like fermions and SM fermions. This feature gives the name of "fermiophobic" to this class of models [1, 162, 231–236], which were able to connect $(g-2)_\mu$ with $R_{K^{(*)}}$ in the past [1], and will be further discussed in Chapter 3. We will see that such models can be connected as well with the origin of Yukawa couplings in the SM [163], providing a connection between the $(g-2)_\mu$ anomaly and the origin of the flavour structure of the SM.

2.3.4 Meson mixing

In the SM, charged current weak interactions provide meson-antimeson transitions for neutral mesons, which are commonly denoted as $\Delta F = 2$ processes because they change fermion flavour in two units[3]. This mixing provides a misalignment between meson flavour and mass eigenstates, that was firstly observed throught the oscillations of neutral kaons [237]. The meson mixing process is highly loop, CKM and GIM suppressed in the SM, being sensitive to very high NP scales. Given that no significant deviation from the SM has been found so far in meson mixing observables, they set very strong bounds over the scale of NP contributions. The effective Lagrangian to describe meson-antimeson mixing contains the following 4-quark operators

$$\mathcal{L}_{\Delta F=2} = \sum_{i=1}^{5} C_i^{qq'} \mathcal{Q}_i^{qq'} + \sum_{i=1}^{5} \tilde{C}_i^{qq'} \tilde{\mathcal{Q}}_i^{qq'} \,, \tag{2.24}$$

where

$$\mathcal{Q}_1^{qq'} = (\bar{q}_L^\alpha \gamma_\mu q_L'^\alpha)(\bar{q}_L \gamma^\mu q_L'^\beta) \,, \tag{2.25}$$
$$\mathcal{Q}_2^{qq'} = (\bar{q}_R^\alpha q_L'^\alpha)(\bar{q}_R^\beta q_L'^\beta) \,, \tag{2.26}$$
$$\mathcal{Q}_3^{qq'} = (\bar{q}_R^\alpha q_L'^\beta)(\bar{q}_R^\beta q_L'^\alpha) \,, \tag{2.27}$$
$$\mathcal{Q}_4^{qq'} = (\bar{q}_R^\alpha q_L'^\alpha)(\bar{q}_L^\beta q_R'^\beta) \,, \tag{2.28}$$
$$\mathcal{Q}_5^{qq'} = (\bar{q}_R^\alpha q_L'^\beta)(\bar{q}_L^\beta q_R'^\alpha) \,, \tag{2.29}$$

where α and β are colour indices, q and q' refer to the two different quark flavours in the neutral mesonic system, and the tilde operators are obtained by replacing $L \longleftrightarrow R$ everywhere. Note that some of the operators in the basis above are not included in the San Diego basis of the LEFT, however they match into operators of the San Diego basis via Fierz rearrangements. In Fig. 2.4, we show the very strong bounds from meson

[3] This is in contrast with semileptonic processes, which change flavour in one unit $\Delta F = 1$.

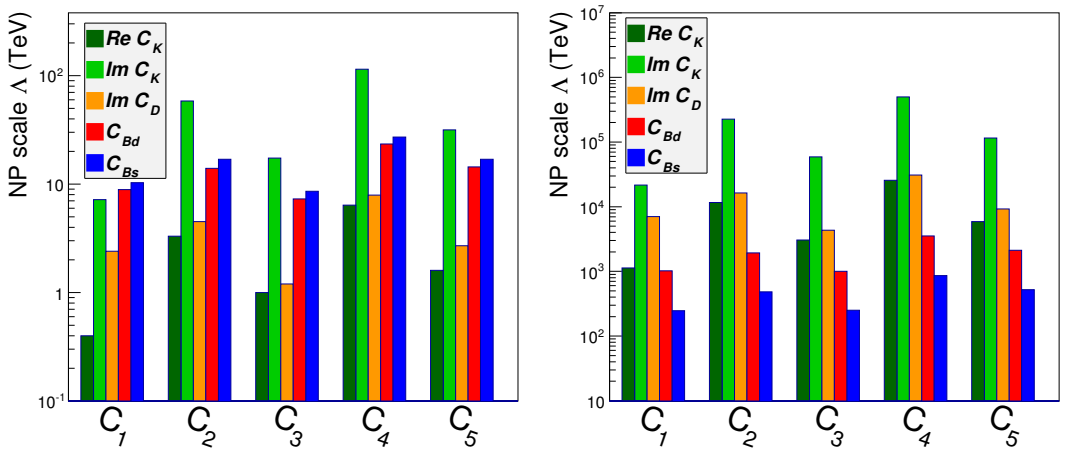

FIGURE 2.4: Summary of the 95% CL lower bound on the NP scale Λ for strongly-interacting NP in the $U(2)^5$ scenario (left) and in the flavour anarchic NP scenario (right). Results from all the neutral meson systems are shown. Figure taken from [240].

mixing observables over the Wilson coefficients in Eq. (2.24), under the assumption of anarchic flavour structure (right panel) and $U(2)^5$ flavour structure (left panel) for the NP contributions (see Section 1.9.3). The figures highlight the high reach of flavour observables over NP scales, but the fact that such reach is significantly reduced in flavour symmetry frameworks, such as MFV and $U(2)^5$, gives hints about the possible flavour structure of NP. In contrast, in the case of anarchic flavour structure, the bounds can reach scales as high as 10^6 TeV for the imaginary part of the Wilson coefficients of scalar operators. Remarkably, the largest bounds come from $K-\bar{K}$ mixing observables, followed by $D-\bar{D}$, $B_d-\bar{B}_d$ and $B_s-\bar{B}_s$ in decreasing order [238, 239].

$B_s-\bar{B}_s$ mixing

For the NP models presented in this thesis, $B_s-\bar{B}_s$ is particularly interesting because is sensitive to models featuring 2-3 flavour transitions. The most relevant observable is the mass difference ΔM_s, which controls the frequency of the $B_s-\bar{B}_s$ oscillations. The experimental value is known very precisely, see for example the most recent HFLAV average [80], which is dominated by the updated measurement by LHCb [241]. However, the SM prediction historically suffered from larger uncertainties, and we need a precise knowledge of the SM contribution in order to quantify the impact of possible contributions from new physics. The theoretical determination of ΔM_s is limited by our understanding of non-perturbative matrix elements of dimension six operators. The matrix elements can be determined with lattice simulations or sum rules. As discussed in Ref. [242], the 2019 FLAG average [243] is dominated by the lattice results [244–246], and suffers from an uncertainty just below 10% with the central value being 1.8σ above the experiment,

$$\Delta M_s^{\text{FLAG'19}} = \left(1.13^{+0.07}_{-0.09}\right) \Delta M_s^{\text{exp}} \,. \tag{2.30}$$

If one considers the value above as the SM prediction for ΔM_s, then NP models with positive contributions to ΔM_s (which is the common case for Z' and leptoquark models suggested to explain the B-anomalies), have very small room to be compatible with the experimental value at the 2σ level. Instead,

$$\Delta M_s^{\text{Average}'19} = \left(1.04^{+0.04}_{-0.07}\right) \Delta M_s^{\text{exp}} \,, \tag{2.31}$$

was computed in [242] as a weighted average of both the FLAG'19 average [243] and sum rule results [247–249]. The weighted average shows better agreement with experiment, and a reduction of the total uncertainty (see the further discussion in [242]). The Average'19 result for ΔM_s leaves some room for positive NP contributions at the 2σ level. We extract an upper bound over the NP contribution by considering the lower limit of the 2σ range, $\Delta M_s^{\text{SM}} \approx 0.9 \Delta M_s^{\text{exp}}$, hence

$$\frac{\Delta M_s^{\text{SM}} + \Delta M_s^{\text{NP}}}{\Delta M_s^{\text{exp}}} \approx 0.9 \frac{\Delta M_s^{\text{SM}} + \Delta M_s^{\text{NP}}}{\Delta M_s^{\text{SM}}} \approx 1 \Rightarrow \Delta M_s^{\text{NP}} \lesssim 0.11 \Delta M_s^{\text{SM}} \,. \tag{2.32}$$

In other words, $\Delta M_s^{\text{Average}'19}$ allows for roughly a 10% positive NP correction over the SM value. This is in line with the 10% criteria commonly considered in the literature, which are possibly motivated by $\Delta M_s^{\text{Average}'19}$ as well. As a specific NP example, the bound in Eq. (2.32) translates directly over the Wilson coefficient $C_1^{bs}\big|_{\text{NP}}$. Let us normalise the effective operator as

$$\mathcal{L}_{bs} = -\frac{C_1^{bs}}{2} \mathcal{Q}_1^{bs} \tag{2.33}$$

The bound over $\delta(\Delta M_s)$ then translates to a bound over $C_1^{bs}\big|_{\text{NP}}$ as

$$\delta(\Delta M_s) \equiv \frac{\Delta M_s - \Delta M_s^{\text{SM}}}{\Delta M_s^{\text{SM}}} = \left| 1 + \frac{C_1^{bs}\big|_{\text{NP}}}{C_1^{bs}\big|_{\text{SM}}} \right| - 1 = \frac{C_1^{bs}\big|_{\text{NP}}}{C_1^{bs}\big|_{\text{SM}}} \lesssim 0.11 \,, \tag{2.34}$$

where in the second step we have assumed real and positive Wilson coefficients. The SM contribution to the Wilson coefficient reads

$$C_1^{bs}\big|_{\text{SM}} = \frac{G_F^2 m_W^2}{2\pi^2} \left(V_{tb}^* V_{ts}\right)^2 S_0(x_t) \,, \tag{2.35}$$

with $S_0(x_t) = 2.37$ [250]. This way, we obtain the numerical bound

$$C_1^{bs}\big|_{\text{NP}} \lesssim \frac{1}{(225\,\text{TeV})^2} \,, \tag{2.36}$$

which is in good agreement with the $(220\,\text{TeV})^{-2}$ bound obtained in [242] from $\Delta M_s^{\text{Average}'19}$. Instead, if we consider $\Delta M_s^{\text{FLAG}'19}$ as the SM prediction, the resulting bound is

$$\Delta M_s^{\text{NP}} \lesssim 0.0526\, \Delta M_s^{\text{SM}} \Rightarrow C_1^{bs}\big|_{\text{NP}} \lesssim \frac{1}{(330\,\text{TeV})^2} \,, \tag{2.37}$$

which is again in good agreement with the bound presented in [242].

We finally note that NP mediators proposed to address the B-anomalies usually receive strong constraints from ΔM_s. In particular, Z' bosons and other neutral mediators like colour octets usually contribute at tree-level to ΔM_s, and particular suppression mechanisms are sometimes implemented in order to ameliorate the bounds. On the other hand, leptoquark mediators contribute to ΔM_s at 1-loop, enjoying a natural suppression. Because of this, leptoquarks are the preferred NP explanation of the $R_{D^{(*)}}$ anomalies, where a NP scale not far above the TeV is required.

2.3.5 $b \to s\tau\tau$

We treat the $b \to s\tau\tau$ transition separately from the muon and electron channels discussed in Section 2.3.1, because the tau channel remains much more unexplored and allows for larger NP contributions. We introduce the effective Lagrangian

$$\begin{aligned}\mathcal{L}_{b\to s\tau\tau} = \frac{4G_F}{\sqrt{2}} V_{tb}V_{ts}^* \frac{\alpha_{\rm EM}}{4\pi}\Big[&(C_9^{\rm SM} + C_9^{\tau\tau})\mathcal{O}_9^{\tau\tau} + (C_{10}^{\rm SM} + C_{10}^{\tau\tau})\mathcal{O}_{10}^{\tau\tau} \\ &+ C_S^{\tau\tau}\mathcal{O}_S^{\tau\tau} + C_P^{\tau\tau}\mathcal{O}_P^{\tau\tau}\Big] + \text{h.c.}\,,\end{aligned} \tag{2.38}$$

where

$$\mathcal{O}_9^{\tau\tau} = (\bar{s}\gamma_\mu P_L b)\,(\bar{\tau}\gamma^\mu \tau)\,, \qquad \mathcal{O}_S^{\tau\tau} = (\bar{s}P_R b)\,(\bar{\tau}\tau)\,, \tag{2.39}$$

$$\mathcal{O}_{10}^{\tau\tau} = (\bar{s}\gamma_\mu P_L b)\,(\bar{\tau}\gamma^\mu\gamma_5 \tau)\,, \qquad \mathcal{O}_P^{\tau\tau} = (\bar{s}P_R b)\,(\bar{\tau}\gamma_5\tau)\,, \tag{2.40}$$

where for simplicity we suppressed the scale dependence of the Wilson coefficients, which are at the scale $\mu = m_b$. With these definitions, the expressions for the observables of interest in the $b \to s\tau\tau$ transition read [189]

$$\begin{aligned}\mathcal{B}(B_s \to \tau\tau) = \mathcal{B}(B_s \to \tau\tau)_{\rm SM}\Bigg\{&\left|1 + \frac{C_{10}^{\tau\tau}}{C_{10}^{\rm SM}} + \frac{C_P^{\tau\tau}}{C_{10}^{\rm SM}}\frac{M_{B_s}^2}{2m_\tau\,(m_b+m_s)}\right|^2 \\ &+ \left(1 - \frac{4m_\tau^2}{M_{B_s}^2}\right)\left|\frac{C_S^{\tau\tau}}{C_{10}^{\rm SM}}\frac{M_{B_s}^2}{2m_\tau\,(m_b+m_s)}\right|^2\Bigg\}\end{aligned} \tag{2.41}$$

$$\begin{aligned}\mathcal{B}(B^+ \to K^+\tau\tau) = 10^{-9}\Big(&2.2\left|C_9^{\tau\tau} + C_9^{\rm SM}\right|^2 + 6.0\left|C_{10}^{\tau\tau} + C_{10}^{\rm SM}\right|^2 + 8.3\,|C_S^{\tau\tau}|^2 \\ &+ 8.9\,|C_P^{\tau\tau}|^2 + 4.8\text{Re}[C_S^{\tau\tau}(C_9^{\tau\tau} + C_9^{\rm SM})^*] + 5.9\text{Re}[C_P^{\tau\tau}(C_{10}^{\tau\tau} + C_{10}^{\rm SM})^*]\Big)\,,\end{aligned} \tag{2.42}$$

where we use $\mathcal{B}(B_s \to \tau\tau)_{\rm SM} = (7.73 \pm 0.49) \times 10^{-7}$ [182]. The numerical values for the NP contributions to $B^+ \to K^+\tau\tau$ decays are taken from [251].

It is interesting to introduce the matching between the operators in the basis of Eq. (2.38) and the San Diego LEFT basis. In particular, the operators $C_9^{\tau\tau}$ and $C_{10}^{\tau\tau}$ are

$\mathcal{B}(B_s \to \tau\tau)$	LHCb ($36\,\text{fb}^{-1}$) (current)	$< 6.8 \times 10^{-3}$ (95% CL) [252]
	LHCb ($50\ \text{fb}^{-1}$)	$< 1.3 \times 10^{-3}$ (95% CL) [253]
	LHCb ($300\ \text{fb}^{-1}$)	$< 5 \times 10^{-4}$ (95% CL) [253]
$\mathcal{B}(B^+ \to K^+\tau\tau)$	BaBar ($424\ \text{fb}^{-1}$) (current)	$< 2.25 \times 10^{-3}$ (90% CL) [254]
	Belle II ($5\ \text{ab}^{-1}$)	$< 6.5 \times 10^{-5}$ (95% CL) [255]
	Belle II ($50\ \text{ab}^{-1}$)	$< 2.0 \times 10^{-5}$ (95% CL) [255]

TABLE 2.1: Current and projected bounds for $\mathcal{B}(B_s \to \tau\tau)$ and $\mathcal{B}(B^+ \to K^+\tau\tau)$ as given by the experimental collaborations.

related to $[C_{ed}^{V,LL}]^{\tau\tau 23}$ and $[C_{de}^{V,LR}]^{23\tau\tau}$ via

$$C_9^{\tau\tau} = \frac{2\pi}{\alpha_{\text{EM}} V_{ts}^* V_{tb}} \left([C_{ed}^{V,LL}]^{\tau\tau 23} + [C_{de}^{V,LR}]^{23\tau\tau} \right) , \tag{2.43}$$
$$C_{10}^{\tau\tau} = \frac{2\pi}{\alpha_{\text{EM}} V_{ts}^* V_{tb}} \left([C_{de}^{V,LR}]^{23\tau\tau} - [C_{ed}^{V,LL}]^{\tau\tau 23} \right) ,$$

while the operators $[C_{ed}^{S,LL}]^{\tau\tau 23}$ and $[C_{ed}^{S,LR}]^{\tau\tau 23}$ are related to $C_S^{\tau\tau}$ and $C_P^{\tau\tau}$ via

$$C_S^{\tau\tau} = \frac{2\pi}{\alpha_{\text{EM}} V_{ts}^* V_{tb}} \left([C_{ed}^{S,RR}]^{\tau\tau 23} - [C_{ed}^{S,LR}]^{\tau\tau 23} \right) , \tag{2.44}$$
$$C_P^{\tau\tau} = \frac{2\pi}{\alpha_{\text{EM}} V_{ts}^* V_{tb}} \left([C_{ed}^{S,RR}]^{\tau\tau 23} + [C_{ed}^{S,LR}]^{\tau\tau 23} \right) .$$

Even though the current experimental bounds over $\mathcal{B}(B_s \to \tau\tau)$ and $\mathcal{B}(B \to K\tau\tau)$ are weak, specific NP models that address the $R_{D^{(*)}}$ anomalies predict a large enhancement of these processes that might be testable in the near future. The enhancement is larger in models featuring scalar operators, in particular for $\mathcal{B}(B_s \to \tau\tau)$, since these provide a significant chiral enhancement. Current bounds and future projections given by the experimental collaborations are given in Table 2.1.

Beyond the direct bounds obtained by the experimental collaborations, in [4] we studied alternative flavour observables that have the potential to provide indirect bounds over $b \to s\tau\tau$. We present these results in the following section, along with their application to the well motivated example of the vector leptoquark $U_1 \sim (\mathbf{3}, \mathbf{1}, 2/3)$.

2.3.6 τ_{B_s}/τ_{B_d}: the $U_1 \sim (\mathbf{3}, \mathbf{1}, 2/3)$ vector leptoquark example

Beyond the direct bounds obtained by the experimental collaborations over $b \to s\tau\tau$ observables, in [4] we studied alternative flavour observables that have the potential to provide indirect bounds over $b \to s\tau\tau$. Our study highlights that NP effects in $b \to s\tau\tau$ operators also affect the lifetime ratio of B_s and B_d mesons. If we assume no NP effects in the B_d lifetime, we have

$$\frac{\tau_{B_s}}{\tau_{B_d}} = \left(\frac{\tau_{B_s}}{\tau_{B_d}} \right)_{\text{SM}} \left(1 + \frac{\Gamma(B_s \to \tau\tau)_{\text{NP}}}{\Gamma(B_s)_{\text{SM}}} \right)^{-1} , \tag{2.45}$$

where we define $\Gamma(B_s \to \tau\tau)_{\rm NP} = \Gamma(B_s \to \tau\tau)_{\rm total} - \Gamma(B_s \to \tau\tau)_{\rm SM}$, which encodes the NP contribution to the partial decay width. The expression for $\Gamma(B_s \to \tau\tau)_{\rm total}$ can be extracted from Eq. (2.41). The SM prediction for the lifetime ratio can be found in Ref. [256], and it depends on non-perturbative parameters in the Heavy Quark Expansion as well as on the size of $SU(3)_f$ breaking between the B_s and the B_d system. We employ the central values and errors for the expectation values of the next-to-leading power matrix element in the B_d field from [257]. Concerning the size of $SU(3)_f$ breaking, estimates using Heavy-Quark Effective Theory relations [256,258] and preliminary lattice QCD estimations [259,260] are affected by large errors. To be very conservative, we use the central values from [258] and assign 100% errors. With this, we obtain:

$$\left(\frac{\tau_{B_s}}{\tau_{B_d}}\right)_{\rm SM} = 1.02 \pm 0.02\,, \qquad \Gamma(B_s)_{\rm SM} = 0.597^{+0.106}_{-0.069}\,{\rm ps}^{-1}\,, \tag{2.46}$$

that has to be compared with the current experimental HFLAV average [80],

$$\left(\frac{\tau_{B_s}}{\tau_{B_d}}\right)_{\rm HFLAV\,2022} = 1.001 \pm 0.004\,. \tag{2.47}$$

At the current status, we find good agreement between the SM predictions and the lifetime average, albeit with large uncertainties due to the unknown $SU(3)_f$ breaking.

We note that in the literature, it has been discussed the impact of using the values from a different set of non-perturbative parameters in the lifetime ratio [256,261], which yield to a large shift. However, it has to be noticed that the values for these parameters change a lot depending on whether higher dimensional operators are considered or not, hinting at non-trivial correlations. This is not observed in [257], that we adopt as our reference. We can now extract an indirect limit over NP contributions to $\mathcal{B}(B_s \to \tau\tau)$ from the lifetime ratio. Using Eq. (2.45), we obtain

$$\mathcal{B}(B_s \to \tau\tau)_{\rm NP} < 5.5 \times 10^{-2}\,, \tag{2.48}$$

at the 95% CL, which has to be compared with the direct bound from LHCb [252], namely $\mathcal{B}(B_s \to \tau\tau)_{\rm NP} < 6.8 \times 10^{-3}$. Currently, the direct bound over $\mathcal{B}(B_s \to \tau\tau)_{\rm NP}$ obtained by the LHCb collaboration is 40% better than the indirect bound obtained from the lifetime ratio.

We then repeat this comparison with the projected sensitivities. The results are shown in Table 2.2. For the experimental measurement, we explore the possibility that the error will reduce to 1 per mille. For the SM prediction, we explore two hypotheses corresponding to either no change in the central value or a substantial reduction of it, towards a strong indication of small $SU(3)_f$ breaking. In hypothesis H1, we assume that the $SU(3)_f$ breaking parameters could be measured to a 10% precision, as possible in the foreseeable future using lattice QCD, but retaining the current central values, while in H2 we impose no $SU(3)_f$ breaking up to the per mill level. The LHCb collaboration

		$\mathcal{B}(B_s \to \tau\tau)_{\rm NP}$		
Assumptions	Input	τ_{B_s}/τ_{B_d}	LHCb ($50\,\text{fb}^{-1}$)	LHCb ($300\ \text{fb}^{-1}$)
H1	$\left(\frac{\tau_{B_s}}{\tau_{B_d}}\right)_{\rm SM} = 1.020(5)$	$1.7(6)\cdot 10^{-2}$	$< 1.3\cdot 10^{-3}$	$< 5\cdot 10^{-4}$
	$\left(\frac{\tau_{B_s}}{\tau_{B_d}}\right)_{\rm exp} = 1.001(1)$			
H2	$\left(\frac{\tau_{B_s}}{\tau_{B_d}}\right)_{\rm SM} = 1.001(1)$	$< 2.6\cdot 10^{-3}$		
	$\left(\frac{\tau_{B_s}}{\tau_{B_d}}\right)_{\rm exp} = 1.001(1)$			

TABLE 2.2: Projected bounds at 95% CL for $\mathcal{B}(B_s \to \tau\tau)_{\rm NP}$ obtained from the lifetime ratio τ_{B_s}/τ_{B_d} are confronted against the projected bounds from LHCb [253]. For the projections in the lifetime ratio, we assume that the uncertainties will reduce to 1 per mille in the experiment. We display different results under two different hypothesis for the SM prediction: that the central value will remain as the current one and the $SU(3)_F$ breaking parameters could be measured to a 10% precision (H1), and that the central value will shift to match the experiment and there is no $SU(3)_F$ breaking up to the per mille level (H2).

provides two expected upper bounds for $\mathcal{B}(B_s \to \tau\tau)$: a first projection is based on a luminosity of 50 fb^{-1}, which in contrast to the expectations in [253] will be reached only after 2032. The second upper bound from the LHCb collaboration is based on an expected luminosity of 300 fb^{-1}, which with respect to the expectations in [253], will be reached only after 2041. This shows that improved measurements and predictions of the lifetime ratios have the potential of improving the current bound on $\mathcal{B}(B_s \to \tau\tau)$, while waiting for LHCb to collect the necessary statistics to obtain even more stringent bounds. This motivates extra efforts from both the theoretical and experimental communities to investigate τ_{B_s}/τ_{B_d} as a potential channel to constrain NP effects.

Application to the vector leptoquark $U_1 \sim (\mathbf{3}, \mathbf{1}, 2/3)$

The $U_1 \sim (\mathbf{3}, \mathbf{1}, 2/3)$ vector leptoquark is a well motivated mediator to explain the R_D and R_{D^*} anomalies [262–269]. A gauge U_1 leptoquark is predicted by the Pati-Salam group [100], that provides a natural connection with quark-lepton unification. Moreover, explanations of the $R_{D^{(*)}}$ anomalies via exchange of the U_1 vector leptoquark had been shown to be naturally connected with the origin of flavour hierarchies and the flavour structure of the SM [2, 115–117, 119, 120, 169, 170]. In this direction, we will provide in Chapter 4 of this thesis a theory of flavour containing a TeV scale U_1 leptoquark that can explain the B-anomalies [2]. Remarkably, the contributions of the U_1 vector leptoquark to $R_{D^{(*)}}$ are correlated to an enhancement of $b \to s\tau\tau$, hence potentially undergoing the constraints from τ_{B_s}/τ_{B_d} described before.

At an effective scale Λ higher than the electroweak scale, the U_1 interactions are well described in the context of the SMEFT as:

$$\mathcal{L}^{U_1}_{\rm SMEFT} \supset -\frac{1}{\Lambda^2}\left[\frac{C^{\alpha\beta ij}_{LL}}{2}\left(Q^{(1)}_{\ell q} + Q^{(3)}_{\ell q}\right)^{\alpha\beta ij} - \left(2C^{\alpha\beta ij}_{LR}\left(Q^{\dagger}_{\ell e d q}\right)^{\alpha\beta ij} + \text{h.c.}\right)\right]. \quad (2.49)$$

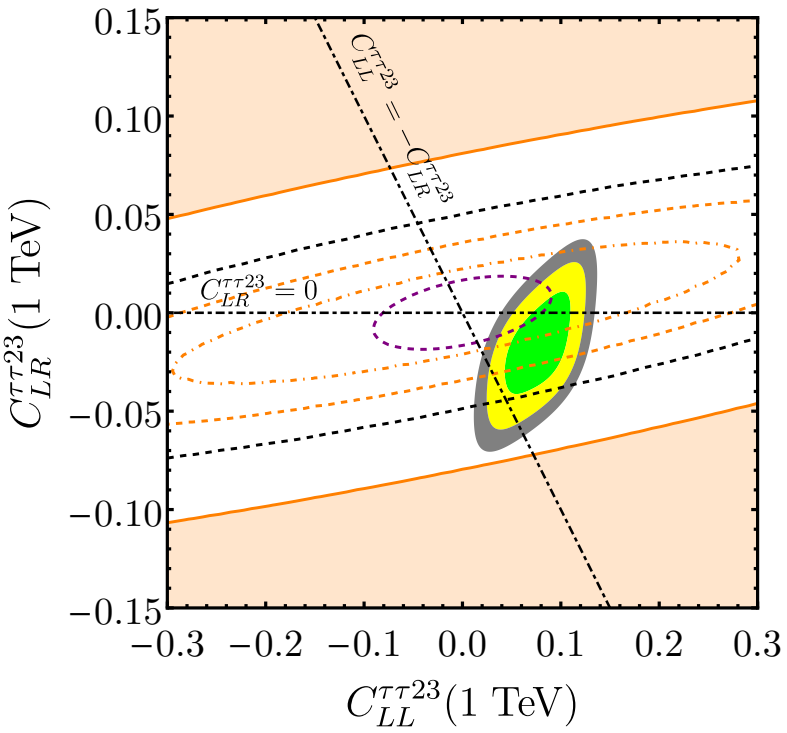

FIGURE 2.5: Parameter space of Wilson coefficients motivated by the U_1 vector leptoquark explanation of $R_{D^{(*)}}$ (see main text). The green, yellow and grey regions represent the 1σ, 2σ and 3σ regions preferred by $R_{D^{(*)}}$, respectively. Orange contours represent the direct bounds from $\mathcal{B}(B_s \to \tau\tau)$, while the black contour represents the indirect bound obtained from τ_{B_s}/τ_{B_d} and the purple contour represents the direct bounds from $\mathcal{B}(B^+ \to K^+\tau\tau)$. Solid (dashed) contours denote current (projected) 95% CL exclusions, except for the two projections for $\mathcal{B}(B_s \to \tau\tau)$ by LHCb: 50 fb^{-1} (orange dashed) and 300 fb^{-1} (orange dash-dotted). Dash-dotted black lines represent two interesting benchmark scenarios motivated in the main text.

The matching between the relevant LEFT and SMEFT Wilson coefficients reads:

$$\left[C_{\nu edu}^{V,LL}\right]^{\tau\tau 32*}(m_b) = \eta_V^{\tau\nu} C_{LL}^{\tau\tau 23}(\Lambda)\frac{v^2}{2V_{cb}\Lambda^2}\,, \tag{2.50}$$

$$\left[C_{\nu edu}^{S,RL}\right]^{\tau\tau 32*}(m_b) = -\eta_S^{\tau\nu} 2C_{LR}^{\tau\tau 23}(\Lambda)\frac{v^2}{2V_{cb}\Lambda^2}\,,$$

$$\left[C_{ed}^{V,LL}\right]^{\tau\tau 23}(m_b) = \eta_V^{\tau\tau} C_{LL}^{\tau\tau 23}(\Lambda)\frac{v^2}{2\Lambda^2}\,, \tag{2.51}$$

$$\left[C_{ed}^{S,LR}\right]^{\tau\tau 23}(m_b) = -\eta_S^{\tau\tau} 2C_{LR}^{\tau\tau 23}(\Lambda)\frac{v^2}{2\Lambda^2}\,,$$

where the factors $\eta_i^{\tau\tau}$ and $\eta_i^{\tau\nu}$ encode the running from the high scale $\Lambda = 1$ TeV and are evaluated with `DsixTools 2.1` [174], obtaining $\eta_V^{\tau\tau} \simeq 0.96$, $\eta_S^{\tau\tau} \simeq 1.57$ $\eta_V^{\tau\nu} \simeq 1.03$ and $\eta_S^{\tau\nu} \simeq 1.64$. The operators in Eq. (2.51) match into $C_9^{\tau\tau} = -C_{10}^{\tau\tau}$ and $C_S^{\tau\tau} = -C_P^{\tau\tau}$ via Eq. (2.43) and Eq. (2.44), respectively. The presence of the scalar operator $\left[C_{ed}^{S,LR}\right]^{\tau\tau 23}$, which ultimately provides $C_S^{\tau\tau} = -C_P^{\tau\tau}$, delivers a chirally enhanced contribution to $\mathcal{B}(B_s \to \tau\tau)$ connected to the size of $C_{LR}^{\tau\tau 23}$. If $C_{LR}^{\tau\tau 23} = 0$, then $\mathcal{B}(B_s \to \tau\tau)$ is still substantially enhanced by the presence of $C_9^{\tau\tau} = -C_{10}^{\tau\tau}$, but chiral enhancement is lost.

In Fig. 2.5 we explore the parameter space of SMEFT Wilson coefficients in the model, highlighting two particularly motivated benchmark scenarios. The case $C_{LL}^{\tau\tau 23} = -C_{LR}^{\tau\tau 23}$ is a good benchmark for 4321 models featuring TeV scale third family quark-lepton unification [115–117,119,120,262–264], while the case $C_{LR}^{\tau\tau 23} = 0$ is a good benchmark for the flavour universal (fermiophobic) 4321 model [2,169,267,268], including the twin Pati-Salam theory of flavour [2] introduced in Chapter 4 of this thesis.

Given that U_1 is a vector leptoquark, the leading contribution to ΔM_s arising at 1-loop depends on the specific UV completion. For the well-motivated case of 4321 models, the contribution to ΔM_s is dominated by a vector-like lepton running in the loop, and the most stringent constraints can be avoided as long as the mass of the vector-like lepton is around or below the TeV scale [2,263,268]. Similarly, the U_1 leptoquark also avoids tree-level contributions to $b \to s\nu\nu$ transitions. In this manner, the model is able to address $R_{D^{(*)}}$ and the enhancement of $\mathcal{B}(B_s \to \tau\tau)$ becomes a key prediction.

Due to chiral enhancement, $\mathcal{B}(B_s \to \tau\tau)$ is particularly sensitive to scenarios with large $|C_{LR}^{\tau\tau 23}|$, but current direct bounds from LHCb cannot yet test the preferred region by the benchmark case $C_{LL}^{\tau\tau 23} = -C_{LR}^{\tau\tau 23}$. Remarkably, in the near future we expect the indirect bound from the lifetime ratio τ_{B_s}/τ_{B_d} [4] to constrain a significant region of the parameter space preferred by $C_{LL}^{\tau\tau 23} = -C_{LR}^{\tau\tau 23}$, while the parameter space preferred by $C_{LR}^{\tau\tau 23} = 0$ is expected to remain unconstrained. In the longer term, projected direct measurements of $\mathcal{B}(B_s \to \tau\tau)$ and $\mathcal{B}(B^+ \to K^+\tau\tau)$ have the potential to test most of the parameter space preferred by R_D and R_{D^*}.

In conclusion, the lifetime ratio τ_{B_s}/τ_{B_d} could be able to discriminate between different U_1 models explaining $R_{D^{(*)}}$ in the near future, setting strong constraints over models featuring TeV scale quark-lepton unification [115–117, 119, 120, 262–264], while the twin Pati-Salam model [2] is expected to remain as the only viable theory of flavour containing a U_1 leptoquark that explains the $R_{D^{(*)}}$ anomalies.

2.3.7 $b \to s\nu\nu$

The process $b \to s\nu\nu$ is correlated to the enhancement of $b \to c\tau\nu$ in particular NP scenarios via $SU(2)_L$ invariance. Given the significant bounds over $b \to s\nu\nu$ enhancement, this transition allows to discriminate between different NP models proposed to address the $R_{D^{(*)}}$ anomalies. We define the relevant Lagrangian to describe $b \to s\nu\nu$ transitions as

$$\mathcal{L}_{b\to s\nu\nu} = \frac{4G_F}{\sqrt{2}} V_{tb}V_{ts}^* \left(C_{\nu,\mathrm{NP}}^{\alpha\beta} + C_{\nu,\mathrm{SM}}\right) (\bar{s}_L\gamma_\mu b_L) \left(\bar{\nu}_L^\alpha \gamma^\mu \nu_L^\beta\right) + \text{h.c.}\,, \tag{2.52}$$

plus the primed operators that involve the exchange $L \to R$ in the quark fields, however these operators are highly constrained by data so we do not consider them. The universal SM contribution reads

$$C_{\nu,\mathrm{SM}} = -\frac{\alpha_L}{2\pi} X_t\,, \tag{2.53}$$

where $X_t = 1.48 \pm 0.01$ [270], and $\alpha_L = g_L^2/(4\pi)$ as defined in Eq. (1.79). In the context of models explaining $R_{D^{(*)}}$, we expect the NP to couple mostly to the third family (this

structure is also well motivated from the point of view of a theory of flavour, as we shall see), therefore we will assume that all $C^{\alpha\beta}_{\nu,\mathrm{NP}}$ are negligible except for $C^{\tau\tau}_{\nu,\mathrm{NP}}$. It is interesting to study the deviation from the SM due to the NP effects. In this direction, we define

$$\delta\mathcal{B}(B\to K^{(*)}\nu\bar{\nu}) = \frac{\mathcal{B}(B\to K^{(*)}\nu\bar{\nu})}{\mathcal{B}(B\to K^{(*)}\nu\bar{\nu})_{\mathrm{SM}}} - 1 \approx \frac{1}{3}\left|\frac{C^{\tau\tau}_{\nu,\mathrm{NP}} + C^{\mathrm{SM}}_{\nu\nu}}{C^{\mathrm{SM}}_{\nu\nu}}\right|^2 - \frac{1}{3}\,, \tag{2.54}$$

where current data sets the following bounds [271, 272]

$$\delta\mathcal{B}(B\to K^{(*)}\nu\bar{\nu}) < 2.6\ (1.7)\ (90\%\ \mathrm{CL})\,. \tag{2.55}$$

We note however that in Summer 2023 the Belle II collaboration presented the following measurement [81]

$$\delta\mathcal{B}(B^+\to K^+\nu\bar{\nu}) = 3.8\pm 1.5\,, \tag{2.56}$$

which shows a 2.8σ tension with the SM prediction. When combined with the previous measurements by Belle and BaBar [271,272] the significance is reduced to the 2.2σ level. In any case, current data implies that $b\to s\nu\nu$ cannot be enhanced much above the SM prediction, while in the previous sections we have shown that $b\to s\tau\tau$ is enhanced several orders of magnitude above the SM prediction in models that explain $R_{D^{(*)}}$. Therefore, $b\to s\nu\nu$ sets important constraints to NP models where $b\to s\nu\nu$ and $b\to c\tau\nu$ are strongly correlated. This is the case for the $S_3\sim(\overline{\mathbf{3}},\mathbf{3},1/3)$ scalar leptoquark[4]. Instead, the $U_1\sim(\mathbf{3},\mathbf{1},2/3)$ model avoids tree-level contributions to $b\to s\nu\nu$, but contributions at 1-loop can be relevant (although they depend on the specific UV completion, see e.g. Section 4.6.6).

Remarkably, the Belle II collaboration is expected to measure $\mathcal{B}(B\to K^{(*)}\nu\bar{\nu})$ up to 10% of the SM value [255], hence confirming the anomaly hinted in [81] and testing most of the remaining NP models which contribute to $b\to s\nu\nu$ either at tree-level or 1-loop.

2.3.8 Purely leptonic CLFV processes

Processes involving violation of family lepton number via charged lepton transitions are strongly constrained by data. In order to study CLFV decays of the type $e^-_\beta\to e^-_\alpha\gamma$ and $e^-_\beta\to e^-_\alpha e^+_\alpha e^-_\alpha$, where $\alpha\neq\beta$, we define the following effective Lagrangian built from operators in the San Diego basis of the LEFT,

$$\begin{aligned}\mathcal{L}_{\text{leptonic LFV}} = &-\frac{4G_F}{\sqrt{2}}\Big[m_\beta\,[C_{e\gamma}]^{\alpha\beta}\,\bar{e}^\alpha_L\sigma^{\mu\nu}e^\beta_R F_{\mu\nu} + m_\beta\,[C_{e\gamma}]^{\beta\alpha}\,\bar{e}^\beta_L\sigma^{\mu\nu}e^\alpha_R F_{\mu\nu} \\ &+ \Big[C^{V,LL}_{ee}\Big]^{\alpha\beta\alpha\alpha}(\bar{e}^\alpha_L\gamma_\mu e^\beta_L)(\bar{e}^\alpha_L\gamma^\mu e^\alpha_L) + \Big[C^{V,LR}_{ee}\Big]^{\alpha\beta\alpha\alpha}(\bar{e}^\alpha_L\gamma_\mu e^\beta_L)(\bar{e}^\alpha_R\gamma^\mu e^\alpha_R)\end{aligned} \tag{2.57}$$

[4]Notice that in the $S_1\sim(\overline{\mathbf{3}},\mathbf{1},1/3)$ leptoquark model, the explanation of $R_{D^{(*)}}$ via $\left[C^{V,LL}_{\nu edu}\right]^{\tau\tau 32*}$ receives constraints from $b\to s\nu\nu$ as well, but these constraints can be avoided if $R_{D^{(*)}}$ are explained via scalar and tensor operators (which involve right-handed couplings) [184].

$$+\left[C_{ee}^{V,LR}\right]^{\alpha\alpha\alpha\beta}(\bar{e}_L^\alpha\gamma_\mu e_L^\alpha)(\bar{e}_R^\alpha\gamma^\mu e_R^\beta)+\left[C_{ee}^{V,RR}\right]^{\alpha\beta\alpha\alpha}(\bar{e}_R^\alpha\gamma_\mu e_R^\beta)(\bar{e}_R^\alpha\gamma^\mu e_R^\alpha)$$
$$+\left[C_{ee}^{S,RR}\right]^{\alpha\beta\alpha\alpha}(\bar{e}_L^\alpha e_R^\beta)(\bar{e}_L^\alpha e_R^\alpha)+\left[C_{ee}^{S,RR}\right]^{\beta\alpha\alpha\alpha}(\bar{e}_L^\beta e_R^\alpha)(\bar{e}_L^\alpha e_R^\alpha)\Big]+\text{h.c.}\,,$$

where all Wilson coefficients are dimensionless, including those of the dipole operators. In terms of this basis of effective operators, the branching fraction of the $e_\beta^- \to e_\alpha^-\gamma$ decay is given by (neglecting small corrections proportional to the lightest lepton mass) [273]

$$\mathcal{B}(e_\beta^- \to e_\alpha^-\gamma)=\left(\frac{4G_F}{\sqrt{2}}\right)^2\alpha_{\rm EM}m_\beta^5\tau_\beta\left(\left|[C_{e\gamma}]^{\alpha\beta}\right|^2+\left|[C_{e\gamma}]^{\beta\alpha}\right|^2\right), \tag{2.58}$$

where τ_β is the lifetime of the $\beta = e, \mu, \tau$ charged lepton. All the processes of the form $e_\beta \to e_\alpha\gamma$, namely $\mu \to e\gamma$, $\tau \to \mu\gamma$ and $\tau \to e\gamma$ are predicted by well motivated BSM models, and this has motivated an intensive search by the experimental collaborations. In the absence of any NP signal so far, strong bounds are set over the various branching fractions. The bound over the $\mu \to e\gamma$ process is particularly strong as [21]

$$\mathcal{B}(\mu^- \to e^-\gamma) < 3.1\times10^{-13}\ (90\%\ \text{CL})\,, \tag{2.59}$$

having the largest reach in NP scale out of all LFV processes, and having a NP reach comparable to that of $K-\bar{K}$ mixing observables, as shown in Fig. 1.5. The processes involving tau lepton decays remain so far less constrained as [21]

$$\mathcal{B}(\tau^- \to \mu^-\gamma) < 4.2\times10^{-8}\ (90\%\ \text{CL})\,, \tag{2.60}$$

$$\mathcal{B}(\tau^- \to e^-\gamma) < 3.3\times10^{-8}\ (90\%\ \text{CL})\,. \tag{2.61}$$

These processes are interesting because they test scenarios with NP mostly coupled to the third family that predict 2-3 and 1-3 charged lepton mixing. A well motivated example are theories of flavour based on the $U(2)^5$ flavour symmetry (see e.g. [3]).

In order to describe the $e_\beta^- \to e_\alpha^- e_\alpha^+ e_\alpha^-$ branching fractions, it is useful to introduce auxiliary variables,

$$C_1=\frac{\left|\left[C_{ee}^{S,RR}\right]^{\alpha\beta\alpha\alpha}\right|^2}{16}+\left|\left[C_{ee}^{V,RR}\right]^{\alpha\beta\alpha\alpha}\right|^2, \tag{2.62}$$

$$C_2=\frac{\left|\left[C_{ee}^{S,RR}\right]^{\beta\alpha\alpha\alpha}\right|^2}{16}+\left|\left[C_{ee}^{V,LL}\right]^{\alpha\beta\alpha\alpha}\right|^2, \tag{2.63}$$

$$C_3=\left|\left[C_{ee}^{V,LR}\right]^{\alpha\alpha\alpha\beta}\right|^2, \tag{2.64}$$

$$C_4=\left|\left[C_{ee}^{V,LR}\right]^{\alpha\beta\alpha\alpha}\right|^2, \tag{2.65}$$

$$C_5=\left|e\,[C_{e\gamma}]^{\alpha\beta}\right|^2, \tag{2.66}$$

$$C_6=\left|e\,[C_{e\gamma}]^{\beta\alpha}\right|^2, \tag{2.67}$$

$$C_7 = \text{Re}\left[e\,[C_{e\gamma}]^{\alpha\beta}\left(\left[C_{ee}^{V,LL}\right]^{\alpha\beta\alpha\alpha}\right)^*\right], \tag{2.68}$$

$$C_8 = \text{Re}\left[e\,[C_{e\gamma}]^{\beta\alpha}\left(\left[C_{ee}^{V,RR}\right]^{\alpha\beta\alpha\alpha}\right)^*\right], \tag{2.69}$$

$$C_9 = \text{Re}\left[e\,[C_{e\gamma}]^{\alpha\beta}\left(\left[C_{ee}^{V,LR}\right]^{\alpha\beta\alpha\alpha}\right)^*\right], \tag{2.70}$$

$$C_{10} = \text{Re}\left[e\,[C_{e\gamma}]^{\beta\alpha}\left(\left[C_{ee}^{V,LR}\right]^{\alpha\alpha\alpha\beta}\right)^*\right], \tag{2.71}$$

where $e = \sqrt{4\pi\alpha_{\text{EM}}}$ is the QED gauge coupling (also associated to the elementary electric charge). Having defined these auxiliary variables, the branching fraction of the $e_\beta^- \to e_\alpha^- e_\alpha^+ e_\alpha^-$ process is given by (neglecting small corrections proportional to the lightest lepton mass) [273]

$$\begin{aligned}\mathcal{B}(e_\beta^- \to e_\alpha^- e_\alpha^+ e_\alpha^-) =& 2(C_1 + C_2) + (C_3 + C_4) + 32\left[\log\left(\frac{m_\beta^2}{m_\alpha^2}\right) - \frac{11}{4}\right](C_5 + C_6) \\ &+ 16(C_7 + C_8) + 8(C_9 + C_{10})\,.\end{aligned} \tag{2.72}$$

Notice the significant enhancement factor $\log(m_\beta^2/m_\alpha^2)$ that enters the branching fraction when the dipole operators are present (although it becomes negligible if dipoles are generated at 1-loop level). The various processes $e_\beta^- \to e_\alpha^- e_\alpha^+ e_\alpha^-$, namely $\mu \to 3e$, $\tau \to 3\mu$ and $\tau \to 3e$ are also well motivated by BSM models, and have been searched by the experimental collaborations with no positive signal so far. The bounds read [21],

$$\mathcal{B}(\mu^- \to e^- e^+ e^-) < 1.0 \times 10^{-12} \qquad (90\%\ \text{CL})\,, \tag{2.73}$$

$$\mathcal{B}(\tau^- \to \mu^- \mu^+ \mu^-) < 2.1 \times 10^{-8} \qquad (90\%\ \text{CL})\,, \tag{2.74}$$

$$\mathcal{B}(\tau^- \to e^- e^+ e^-) < 2.7 \times 10^{-8} \qquad (90\%\ \text{CL})\,. \tag{2.75}$$

Again the bound over the muon decay process is the strongest, just below $\mathcal{B}(\mu^- \to e^-\gamma)$, while the bounds over the tau decay processes are weaker. Before concluding, we notice that current experiments are seeking to improve the current bounds over the CLFV processes outlined in this section. We first highlight the future bounds over $\mu \to e\gamma$ and $\mu \to 3e$ projected by the MEG II and Mu3e collaborations (highlighting the impressive bound projected by Mu3e) [274, 275]

$$\mathcal{B}(\mu^- \to e^-\gamma) < 6 \times 10^{-14} \qquad (90\%\ \text{CL})\,, \tag{2.76}$$

$$\mathcal{B}(\mu^- \to e^- e^+ e^-) < 10^{-16} \qquad (90\%\ \text{CL})\,. \tag{2.77}$$

Bounds over the processes involving tau decays are expected to be improved by the Belle II collaboration, which provides the following projections [255]

$$\mathcal{B}(\tau^- \to \mu^-\gamma) < 4 \times 10^{-10} \qquad (90\%\ \text{CL})\,, \tag{2.78}$$

$$\mathcal{B}(\tau^- \to \mu^- \mu^+ \mu^-) < 3 \times 10^{-10} \qquad (90\%\ \text{CL})\,, \tag{2.79}$$

$$\mathcal{B}(\tau^- \to e^-\gamma) < 10^{-9} \qquad (90\%\ \text{CL})\,, \tag{2.80}$$

$$\mathcal{B}(\tau^- \to e^-e^+e^-) < 5\times 10^{-10} \qquad (90\%\ \text{CL})\,. \tag{2.81}$$

The impressive efforts by the experimental collaborations will allow to test very well motivated BSM scenarios, including specific theories of flavour presented in this thesis.

2.3.9 Semileptonic CLFV processes

Violation of family lepton number via charged lepton transitions is also possible in semileptonic processes. We are particularly interested in $b \to s e_\alpha e_\beta$ processes, where $\alpha \neq \beta$, which are predicted in several NP scenarios addressing the anomalies in $R_{D^{(*)}}$ and/or $b \to s\mu\mu$ data. We define the effective Lagrangian as

$$\begin{aligned}\mathcal{L}_{b\to s e_\alpha e_\beta} = \frac{4G_F}{\sqrt{2}} V_{tb}V_{ts}^* \frac{\alpha_{\rm EM}}{4\pi}\Big[& C_9^{\alpha\beta}\mathcal{O}_9^{\alpha\beta} + C_{10}^{\alpha\beta}\mathcal{O}_{10}^{\alpha\beta} \\ & + C_S^{\alpha\beta}\mathcal{O}_S^{\alpha\beta} + C_P^{\alpha\beta}\mathcal{O}_P^{\alpha\beta}\Big] + \text{h.c.}\,,\end{aligned} \tag{2.82}$$

where

$$\mathcal{O}_9^{\alpha\beta} = (\bar{s}\gamma_\mu P_L b)\left(\bar{e}^\alpha\gamma^\mu e^\beta\right)\,, \qquad \mathcal{O}_S^{\alpha\beta} = (\bar{s}P_R b)\left(\bar{e}^\alpha e^\beta\right)\,, \tag{2.83}$$

$$\mathcal{O}_{10}^{\alpha\beta} = (\bar{s}\gamma_\mu P_L b)\left(\bar{e}^\alpha\gamma^\mu\gamma_5 e^\beta\right)\,, \qquad \mathcal{O}_P^{\alpha\beta} = (\bar{s}P_R b)\left(\bar{e}^\alpha\gamma_5 e^\beta\right)\,, \tag{2.84}$$

plus primed operators which are obtained by exchanging $L \longleftrightarrow R$ in the quark bilineals. Having defined the relevant set of effective operators, the branching fraction of the process $B_s \to e_\alpha e_\beta$ is given by [189]

$$\begin{aligned}\mathcal{B}(B_s \to e_\alpha e_\beta) = {} & \frac{\tau_{B_s}}{64\pi^3}\frac{\alpha_{\rm EM}^2 G_F^2}{m_{B_s}^3} f_{B_s}^2 |V_{tb}V_{ts}^*|^2 \sqrt{f(m_{B_s},m_\alpha,m_\beta)} \\ & \times\Bigg\{[m_{B_s}^2 - (m_\alpha+m_\beta)^2]\cdot\left|(C_9^{\alpha\beta}-C_9^{\prime\alpha\beta})(m_\alpha-m_\beta) + (C_S^{\alpha\beta}-C_S^{\prime\alpha\beta})\frac{m_{B_s}^2}{m_b+m_s}\right|^2 \\ & + [m_{B_s}^2 - (m_\alpha-m_\beta)^2]\cdot\left|(C_{10}^{\alpha\beta}-C_{10}^{\prime\alpha\beta})(m_\alpha+m_\beta) + (C_P^{\alpha\beta}-C_P^{\prime\alpha\beta})\frac{m_{B_s}^2}{m_b+m_s}\right|^2\Bigg\}\end{aligned} \tag{2.85}$$

where $f(a,b,c) = [a^2-(b-c)^2][a^2-(b+c)^2]$, and we use $f_{B_s} = 230.3 \pm 1.3$ MeV [276], $\tau_{B_s} = 1.515 \pm 0.005$ ps [21] and $M_{B_s} = 5366.92 \pm 0.10$ MeV [21] as input values.

Assuming only vector operators, the branching fraction of the processes $B \to K^{(*)} e_\alpha e_\beta$ are given by [189]

$$\begin{aligned}\mathcal{B}\left(B \to K^{(*)} e_\alpha e_\beta\right) = 10^{-9}\Big(& a_{K^{(*)}}^{\alpha\beta}\left|C_9^{\alpha\beta}+C_9^{\prime\alpha\beta}\right|^2 + b_{K^{(*)}}^{\alpha\beta}\left|C_{10}^{\alpha\beta}+C_{10}^{\prime\alpha\beta}\right|^2 \\ & + c_{K^{(*)}}^{\alpha\beta}\left|C_9^{\alpha\beta}-C_9^{\prime\alpha\beta}\right|^2 + d_{K^{(*)}}^{\alpha\beta}\left|C_{10}^{\alpha\beta}-C_{10}^{\prime\alpha\beta}\right|^2\Big)\,,\end{aligned} \tag{2.86}$$

$\alpha\beta$	$a_{K^*}^{\alpha\beta}$	$b_{K^*}^{\alpha\beta}$	$c_{K^*}^{\alpha\beta}$	$d_{K^*}^{\alpha\beta}$	$a_K^{\alpha\beta}$	$b_K^{\alpha\beta}$	$c_K^{\alpha\beta}$	$d_K^{\alpha\beta}$
$e\mu$	7.8(9)	7.8(9)	34(6)	34(6)	20(2)	20(2)	0	0
$e\tau$	3.8(4)	3.9(4)	18(2)	18(2)	12.7(9)	12.7(9)	0	0
$\mu\tau$	4.1(5)	3.6(4)	18(2)	17(2)	12.5(1.0)	12.9(9)	0	0

(A)

$\alpha\beta$	$e_{K^*}^{\alpha\beta}$	$f_{K^*}^{\alpha\beta}$	$g_{K^*}^{\alpha\beta}$	$h_{K^*}^{\alpha\beta}$	$e_K^{\alpha\beta}$	$f_K^{\alpha\beta}$	$g_K^{\alpha\beta}$	$h_K^{\alpha\beta}$
$e\mu$	0	0	12(1)	12(1)	26.2(4)	26.2(4)	0	0
$e\tau$	0	0	5.5(6)	5.5(6)	15.0(2)	15.0(2)	0	0
$\mu\tau$	0	0	5.2(6)	5.8(7)	14.4(2)	15.5(2)	0	0

(B)

TABLE 2.3: Values for the multiplicative factors defined in Eqs. (2.86) and (2.87). The quoted uncertainties are at the 1σ level. Table taken from [189].

while if we assume only scalar operators, the expression for the branching fractions is given by [189]

$$\mathcal{B}\left(B \to K^{(*)} e_\alpha e_\beta\right) = 10^{-9}\left(e_{K^{(*)}}^{\alpha\beta}\left|C_S^{\alpha\beta} + C_S^{\prime\alpha\beta}\right|^2 + f_{K^{(*)}}^{\alpha\beta}\left|C_P^{\alpha\beta} + C_P^{\prime\alpha\beta}\right|^2 + g_{K^{(*)}}^{\alpha\beta}\left|C_S^{\alpha\beta} - C_S^{\prime\alpha\beta}\right|^2 + h_{K^{(*)}}^{\alpha\beta}\left|C_P^{\alpha\beta} - C_P^{\prime\alpha\beta}\right|^2\right). \tag{2.87}$$

The numerical values for the factors $a_{K^{(*)}}^{\alpha\beta} - h_{K^{(*)}}^{\alpha\beta}$ are given in Table 2.3 for the various processes. We will not consider the scenario with both vector and scalar Wilson coefficients because it is not predicted by any of the NP models proposed in this thesis, but we refer the interested reader to [189].

Out of the different $b \to s e_\alpha e_\beta$ transitions, processes of the form $b \to s\tau\mu$ are very interesting because they receive contributions in particular theories of flavour proposed in this thesis, see more in Chapter 4. Current bounds over these processes exclude branching fractions larger than 10^{-5} [277, 278],

$$\mathcal{B}\left(B_s \to \tau^\pm \mu^\mp\right) < 3.4 \times 10^{-5}\ (90\%\ \text{CL})\,, \tag{2.88}$$

$$\mathcal{B}\left(B^+ \to K^+ \tau^\pm \mu^\mp\right) < 2.25 \times 10^{-5}\ (90\%\ \text{CL})\,. \tag{2.89}$$

Remarkably, the LHCb collaboration is expected to improve the bounds over the processes above by one order of magnitude after Upgrade II [253]

$$\mathcal{B}\left(B_s \to \tau^\pm \mu^\mp\right) < 3 \times 10^{-6}\ (90\%\ \text{CL})\,, \tag{2.90}$$

$$\mathcal{B}\left(B^+ \to K^+ \tau^\pm \mu^\mp\right) < 10^{-6}\ (90\%\ \text{CL})\,. \tag{2.91}$$

The hadronic tau decay $\tau^\pm \to \mu^\pm \phi$ can be modified as well in models addressing

the B-anomalies. We include its branching fraction in the presence of left-handed NP currents [279],

$$\mathcal{B}\left(\tau^{\pm}\to\mu^{\pm}\phi\right)=\frac{\tau_\tau G_F^2 f_\phi^2 m_\tau^3}{16\pi}\left(1-\frac{m_\phi^2}{m_\tau^2}\right)^2\left(1+2\frac{m_\phi^2}{m_\tau^2}\right)\left|\left[C_{ed}^{V,LL}\right]^{\mu\tau 22}\right|^2, \tag{2.92}$$

where $\tau_\tau=(290.3\pm0.5)\times10^{-15}\ s$, $f_\phi\simeq225\,\text{MeV}$ and $m_\phi^2/m_\tau^2\approx0.33$ [21]. The current bound is $\mathcal{B}\left(\tau\to\mu\phi\right)<8.4\times10^{-8}$ (90% CL) [280], which is expected to be improved by the Belle II collaboration to $\mathcal{B}\left(\tau\to\mu\phi\right)<2\times10^{-9}$ (90% CL) [255].

Before concluding, we highlight the process $K_L\to\mu e$ that provides strong constraints over the vector leptoquark $U_1\sim(\mathbf{3},\mathbf{1},2/3)$ of the Pati-Salam model [100]. We introduce the effective Lagrangian

$$\mathcal{L}_{s\to d\mu e}=-\frac{G_F}{\sqrt{2}}V_{ud}V_{us}^*\left[C_{7V}^{\mu e}\left(\bar{s}\gamma_\mu P_L d\right)\left(\bar{\mu}\gamma^\mu e\right)+C_{7A}^{\mu e}\left(\bar{s}\gamma_\mu P_L d\right)\left(\bar{\mu}\gamma^\mu\gamma_5 e\right)\right], \tag{2.93}$$

where the Wilson coefficients $C_{7V}^{\mu e}$ and $C_{7A}^{\mu e}$, equivalent to the B-physics coefficients $C_9^{\alpha\beta}$ and $C_{10}^{\alpha\beta}$ but for the kaon system, are related to operators from the San Diego basis via

$$C_{7V}^{\mu e}=\frac{2}{V_{ub}V_{us}^*}\left([C_{ed}^{V,LL}]^{\mu e21}+[C_{de}^{V,LR}]^{21\mu e}\right),\quad C_{7A}^{\mu e}=\frac{2}{V_{ub}V_{us}^*}\left([C_{de}^{V,LR}]^{21\mu e}-[C_{ed}^{V,LL}]^{\mu e21}\right). \tag{2.94}$$

The branching fraction of the $K_L\to\mu e$ process is given by [281]

$$\mathcal{B}\left(K_L\to\mu^{\pm}e^{\mp}\right)=\frac{\tau_{K_L}f_K^2m_\mu^2m_{K^0}}{64\pi}G_F^2\left|V_{ub}V_{us}^*\right|^2\left(1-\frac{m_\mu^2}{m_K^2}\right)^2\left(|C_{7V}^{\mu e}|^2+|C_{7A}^{\mu e}|^2\right), \tag{2.95}$$

where $m_{K^0}=497.611\pm0.013$ MeV, $f_K=155.7\pm0.3$ MeV, and $\tau_{K_L}=(5.116\pm0.021)\times10^{-8}\ s$ [21]. The very strong bound over $\mathcal{B}\left(K_L\to\mu^{\pm}e^{\mp}\right)$ was obtained by the BNL collaboration [282]

$$\mathcal{B}\left(K_L\to\mu^{\pm}e^{\mp}\right)<4.7\times10^{-12}\ (90\%\ \text{CL}). \tag{2.96}$$

which naively pushes the breaking scale of the traditional Pati-Salam group [100] above the PeV [283]. In this manner, realistic model building based on low-scale implementations of the Pati-Salam gauge group faces the challenge of ameliorating this constraint, which can be achieved e.g. if the $U_1\sim(\mathbf{3},\mathbf{1},2/3)$ vector leptoquark is mostly coupled to the third family.

2.3.10 Universality in τ decays

As discussed in Section 2.3.2, the $R_{D^{(*)}}$ anomalies suggest the breaking of LFU in semileptonic $b\to c\ell\nu$ processes, hinting at NP interactions that discriminate between the tau and light charged leptons. In this direction, it seems sensible to ask whether the decays of taus into light charged leptons are sensitive to this kind of NP.

By comparing the measured decay widths of leptonic or hadronic tau decays which only differ by the flavour of the final charged lepton, one can test experimentally that the $W^\pm$ interaction is indeed universal to good approximation, i.e. that $g_e = g_\mu = g_e$, where g_α denotes the couplings of leptons to the $W^\pm$ boson. In this manner, tau decay rates provide a powerful test of lepton flavor universality via the ratios [279]

$$\left(\frac{g_\tau}{g_{\mu(e)}}\right)_\ell = \left[\frac{\mathcal{B}(\tau \to e(\mu)\nu\bar{\nu})/\mathcal{B}(\tau \to e(\mu)\nu\bar{\nu})_{\rm SM}}{\mathcal{B}(\mu \to e\nu\bar{\nu})/\mathcal{B}(\mu \to e\nu\bar{\nu})_{\rm SM}}\right]^{\frac{1}{2}} . \tag{2.97}$$

One can build similar ratios to test LFU in tau decays to light mesons and one neutrino,

$$\left(\frac{g_\tau}{g_\mu}\right)_\pi = \left[\frac{\mathcal{B}(\tau \to \pi\nu)/\mathcal{B}(\tau \to \pi\nu)_{\rm SM}}{\mathcal{B}(\pi \to \mu\bar{\nu})/\mathcal{B}(\pi \to \mu\bar{\nu})_{\rm SM}}\right]^{\frac{1}{2}} , \tag{2.98}$$

$$\left(\frac{g_\tau}{g_\mu}\right)_K = \left[\frac{\mathcal{B}(\tau \to K\nu)/\mathcal{B}(\tau \to K\nu)_{\rm SM}}{\mathcal{B}(K \to \mu\bar{\nu})/\mathcal{B}(K \to \mu\bar{\nu})_{\rm SM}}\right]^{\frac{1}{2}} , \tag{2.99}$$

where we have not included the hadronic (g_τ/g_e) ratios because the meson decays to electrons are strongly helicity suppressed, leading to less precise experimental measurements. NP contributions to the three ratios above can be described via the following effective Lagrangian (containing operators from the San Diego basis)

$$\begin{aligned}\mathcal{L}_{\tau,\,\rm LFU} = -\frac{4G_F}{\sqrt{2}}\Bigg[&\left[C_{\nu e}^{V,LL}\right]^{\alpha\beta\rho\lambda}(\bar{\nu}_L^\alpha\gamma_\mu\nu_L^\beta)(\bar{e}_L^\rho\gamma^\mu e_L^\lambda) \\ &+\sum_\alpha\left(\delta_{\alpha 3}V_{ud}^* + \left[C_{\nu edu}^{V,LL}\right]^{\alpha\beta 11}\right)(\bar{\nu}_L^\alpha\gamma_\mu e_L^\beta)(\bar{d}_L\gamma^\mu u_L) \\ &+\sum_\alpha\left(\delta_{\alpha 3}V_{us}^* + \left[C_{\nu edu}^{V,LL}\right]^{\alpha\beta 21}\right)(\bar{\nu}_L^\alpha\gamma_\mu e_L^\beta)(\bar{s}_L\gamma^\mu u_L)\Bigg] + \text{h.c.}\,,\end{aligned} \tag{2.100}$$

where we have neglected operators containing right-handed fields, plus scalar and tensor Lorentz structures, as they are all strongly constrained by current data. We have also included the SM contributions for the semileptonic Wilson coefficients. We find the following theoretical predictions for the LFU ratios in terms of the Wilson coefficients above,

$$\left(\frac{g_\tau}{g_{\mu(e)}}\right)_\ell = \left[\frac{\sum_{\alpha\beta}\left(\delta_{\alpha\tau}\delta_{\beta e(\mu)} + \left|\left[C_{\nu e}^{V,LL}\right]^{\alpha\beta e(\mu)\tau}\right|^2\right)}{\sum_{\alpha\beta}\left(\delta_{\alpha\mu}\delta_{\beta e} + \left|\left[C_{\nu e}^{V,LL}\right]^{\alpha\beta e\mu}\right|^2\right)}\right]^{\frac{1}{2}} , \tag{2.101}$$

$$\left(\frac{g_\tau}{g_\mu}\right)_\pi = \left[\frac{\sum_{\alpha}\left(\delta_{\alpha\tau}V_{ud}^* + \left|\left[C_{\nu edu}^{V,LL}\right]^{\alpha\tau 11}\right|^2\right)}{\sum_{\alpha}\left(\delta_{\alpha\mu}V_{ud} + \left|\left[C_{\nu edu}^{V,LL}\right]^{\alpha\mu 11}\right|^2\right)}\right]^{\frac{1}{2}} , \tag{2.102}$$

$$\left(\frac{g_\tau}{g_\mu}\right)_K = \left[\frac{\sum_\alpha \left(\delta_{\alpha\tau} V_{us}^* + \left|\left[C_{\nu edu}^{V,LL}\right]^{\alpha\tau 21}\right|^2\right)}{\sum_\alpha \left(\delta_{\alpha\mu} V_{us} + \left|\left[C_{\nu edu}^{V,LL}\right]^{\alpha\mu 21}\right|^2\right)}\right]^{\frac{1}{2}} . \tag{2.103}$$

Current data over the various LFU ratios in tau decays is in good agreement with the SM. By averaging the three (g_τ/g_μ) ratios, the observed bound is [80]

$$\left(\frac{g_\tau}{g_\mu}\right)_{\ell+\pi+K} = 1.0003 \pm 0.0014\,. \tag{2.104}$$

Therefore, given the $R_{D^{(*)}}$ anomalies suggesting NP that discriminate between taus and light charged leptons, one could ask why the $(g_\tau/g_{\mu(e)})$ ratios show no deviations so far. Regarding the hadronic ratios, the NP invoked to address the anomalies usually have very small couplings to light quarks, therefore suppressing the contributions to $(g_\tau/g_\mu)_{\pi+K}$. Regarding the purely leptonic ratios, the point is that the NP proposed to address $R_{D^{(*)}}$, such as leptoquark mediators, provide semileptonic operators at tree-level but purely leptonic operators only arise at 1-loop, therefore suppressing the contributions to $(g_\tau/g_\mu)_\ell$. It is also worth mentioning that the operator $\left[\mathcal{O}_{\nu edu}^{V,LL}\right]^{\tau\tau 33\dagger}$ that is well motivated in models that address $R_{D^{(*)}}$ mixes via RGE running into $\left[C_{\nu e}^{V,LL}\right]^{\tau\tau e(\mu)\tau}$. Therefore, the ratios $(g_\tau/g_\mu)_{\ell+\pi+K}$ can still provide significant bounds over models addressing $R_{D^{(*)}}$, and very likely some deviation in $(g_\tau/g_{\mu(e)})$ should be seen in the future with more experimental precision, if indeed the $R_{D^{(*)}}$ anomalies are due to NP.

2.3.11 Proton decay

Proton decay is a crucial prediction of Grand Unified Theories, which we will explore in Chapter 6 of this thesis by using the tools outlined here. We will focus on the golden channel $p \to e^+\pi^0$ which drives the phenomenology in many well-motivated GUTs. We focus as well in the contributions mediated by the superheavy gauge bosons arising after spontaneous breaking of the GUT group. When the heavy leptoquarks are integrated out, we obtain dimensions six operators violating both baryon and lepton number in one unit, but preserving $B - L$. SMEFT operators of this type are listed in Table D.2 for the Warsaw basis, although here we shall choose to work in a different basis more common in proton decay studies[5],

$$\mathcal{O}_I^{d=6} = \Lambda_1^2 \epsilon^{\alpha\beta\lambda}\epsilon^{ab}(\overline{u_{\alpha i}^C}\gamma^\mu Q_{\beta ai})(\overline{e_j^C}\gamma_\mu Q_{\lambda bj})\,, \qquad \mathcal{O}_{II}^{d=6} = \Lambda_1^2 \epsilon^{\alpha\beta\lambda}\epsilon^{ab}(\overline{u_{\alpha i}^C}\gamma^\mu Q_{\beta ai})(\overline{d_{\lambda j}^C}\gamma_\mu L_{bj})\,, \tag{2.105}$$

$$\mathcal{O}_{III}^{d=6} = \Lambda_2^2 \epsilon^{\alpha\beta\lambda}\epsilon^{ab}(\overline{d_{\alpha i}^C}\gamma^\mu Q_{\beta bi})(\overline{u_{\lambda j}^C}\gamma_\mu L_{aj})\,, \qquad \mathcal{O}_{IV}^{d=6} = \Lambda_2^2 \epsilon^{\alpha\beta\lambda}\epsilon^{ab}(\overline{d_{\alpha i}^C}\gamma^\mu Q_{\beta bi})(\overline{\nu_j^C}\gamma_\mu Q_{\lambda aj})\,, \tag{2.106}$$

[5]Note that here we are actually working with 4-component Dirac spinors but removing the chiral left-right notation, and C denotes charge conjugation.

where $\alpha, \beta, \lambda = 1, 2, 3$ are colour indices, $a, b = 1, 2$ are $SU(2)_L$ indices and $i, j = 1, 2, 3$ are flavour indices. The effective operators $\mathcal{O}_I^{d=6}$ and $\mathcal{O}_{II}^{d=6}$ are generated when we integrate out the $X \sim (\mathbf{3}, \mathbf{2})_{-5/6}$ leptoquarks. This is the case of theories based on the gauge group $SU(5)$. In contrast, the effective operators $\mathcal{O}_{III}^{d=6}$ and $\mathcal{O}_{IV}^{d=6}$ are generated when we integrate out the $X' \sim (\mathbf{3}, \mathbf{2})_{1/6}$ leptoquarks. This is the case of flipped $SU(5)$ theories [284, 285], while in $SO(10)$ models both X and X' are present. In this manner, $\Lambda_1 = g_{\rm GUT}/(\sqrt{2}M_X)$ and $\Lambda_2 = g_{\rm GUT}/(\sqrt{2}M_{X'})$, where $M_X, M_{X'} \sim M_{\rm GUT}$ are the masses of the superheavy gauge bosons and $g_{\rm GUT}$ is the single gauge coupling of the theory at the GUT scale.

The operators in Eqs. (2.105) and (2.106) are written in the interaction basis. In the mass basis, the relevant effective operators leading to the $p \to e^+\pi^0$ decay are expressed as [48]

$$\mathcal{O}_L^{d=6} = C_L \epsilon^{\alpha\beta\lambda} (\overline{u_\alpha^C} \gamma^\mu u_\beta)(\overline{e^C} \gamma_\mu d_\lambda)\,, \tag{2.107}$$

$$\mathcal{O}_R^{d=6} = C_R \epsilon^{\alpha\beta\lambda} (\overline{u_\alpha^C} \gamma^\mu u_\beta)(\overline{d_\lambda^C} \gamma_\mu e)\,, \tag{2.108}$$

where the Wilson coefficients are given by

$$C_L = \Lambda_1^2 \left[(V_{u^c}^\dagger V_u)^{11} (V_{e^c}^\dagger V_d)^{11} + (V_{u^c}^\dagger V_u V_{\rm CKM})^{11} (V_{e^c}^\dagger V_d V_{\rm CKM}^\dagger)^{11} \right], \tag{2.109}$$

$$C_R = \Lambda_1^2 (V_{u^c}^\dagger V_u)^{11} (V_{d^c}^\dagger V_e)^{11} + \Lambda_2^2 (V_{d^c}^\dagger V_d V_{\rm CKM}^\dagger)^{11} (V_{u^c}^\dagger V_u V_{\rm CKM} V_{d^c} V_d^\dagger V_{d^c}^\dagger V_e)^{11}\,, \tag{2.110}$$

where the $V_{\psi^{(c)}}$ matrices refer to fermion mixing in the $\psi^{(c)}$ sector. The partial decay width of the $p \to e^+\pi^0$ process is then given by [286, 287]

$$\begin{aligned} \Gamma(p \to e^+\pi^0) = & \frac{m_p}{8}\pi \left(1 - \frac{m_{\pi^0}^2}{m_p^2}\right)^2 A_L^2 \frac{\alpha_{\rm GUT}^2}{M_{\rm GUT}^4} \times \Big[A_{SL}^2 |C_L|^2 \left| \langle \pi^0 | (ud)_L u_L | p \rangle \right|^2 \\ & + A_{SR}^2 |C_R|^2 \left| \langle \pi^0 | (ud)_R u_L | p \rangle \right|^2 \Big]\,, \end{aligned} \tag{2.111}$$

where $\alpha_{\rm GUT} = g_{\rm GUT}^2/4\pi$, $A_L \approx 1.247$ accounts for the QCD RGE from the M_Z scale to m_p [286], and $A_{SL(R)}$ accounts for the short-distance RGE from the GUT scale to M_Z, given by

$$A_{SL(R)} = \prod_A^{M_Z \le M_A \le M_{\rm GUT}} \prod_i \left[\frac{\alpha_i(M_{A+1})}{\alpha_i(M_A)} \right]^{\frac{\gamma_{iL(R)}}{b_i}}\,, \tag{2.112}$$

where b_i and $\gamma_{iL(R)}$ denote the β-function coefficients and the anomalous dimensions respectively, computed for the various intermediate scales M_A that may contain the given model. The $\gamma_{iL(R)}$ are computed as loop corrections to the effective operators $\mathcal{O}_L^{d=6}$ and $\mathcal{O}_R^{d=6}$ (vertex corrections and the self-energy corrections), which can be done by following the algorithm in Appendix A of Ref. [287]. Therefore, most model dependence is carried by the $A_{SL(R)}$ factors and by the C_L and C_R coefficients.

The following form factors [288]

$$\langle \pi^0 | (ud)_L u_L | p \rangle = 0.134(5)(16)\,{\rm GeV}^2\,, \tag{2.113}$$

$$\langle \pi^0 | (ud)_R u_L | p \rangle = -0.131(4)(13)\,\text{GeV}^2\,, \tag{2.114}$$

correspond to the $\mathcal{O}_L^{d=6}$ and $\mathcal{O}_R^{d=6}$ operators, respectively, and the errors (shown in the parenthesis) denote statistical and systematic uncertainties. The lifetime of the proton is finally computed as $\tau_p \simeq 1/\Gamma(p \to e^+\pi^0)$. In many cases, the following estimation

$$\tau_p \approx \frac{M_{\text{GUT}}^4}{\alpha_{\text{GUT}}^2 m_p^5}\,, \tag{2.115}$$

provides a very good approximation to the more accurate results obtained via Eq. (2.111), as the technicalities of the full calculation usually lead to just $\mathcal{O}(1)$ variations.

2.3.12 Connection between $R_{D^{(*)}}$ and $b \to s\ell\ell$

In Section 2.3.2 we have sketched the connection between $R_{D^{(*)}}$ and $R_{K^{(*)}}$ that becomes manifest in a theory of flavour. However, the connection between the $R_{D^{(*)}}$ anomalies and $b \to s\ell\ell$ goes beyond $R_{K^{(*)}}$ [289]. Let us assume that the $R_{D^{(*)}}$ anomalies are dominantly explained via the NP operator $\left[\mathcal{O}_{\nu edu}^{V,LL}\right]^{\tau\tau 32\dagger}$ in Eq. (2.19), which involves only left-handed fermions. At the level of the SMEFT, semileptonic decays involving only left-handed quarks and leptons are described by the two $SU(2)_L$ invariant operators $[Q_{\ell q}^{(1)}]^{\tau\tau 23}$ and $[Q_{\ell q}^{(3)}]^{\tau\tau 23}$. At low energies, these operators provide $\left[\mathcal{O}_{\nu edu}^{V,LL}\right]^{\tau\tau 32\dagger}$ plus $\left[\mathcal{O}_{ed}^{V,LL}\right]^{\tau\tau 23}$ and $\left[\mathcal{O}_{\nu d}^{V,LL}\right]^{\tau\tau 23}$. The latter leads to dangerous contributions to $b \to s\nu\nu$, unless $[C_{\ell q}^{(1)}]^{\tau\tau 23} = [C_{\ell q}^{(3)}]^{\tau\tau 23}$. This is a prominent SMEFT scenario which predicts $\left[C_{\nu edu}^{V,LL}\right]^{\tau\tau 32*} \approx \left[C_{ed}^{V,LL}\right]^{\tau\tau 23}$, that then matches into a large contribution to $C_9^{\tau\tau} = -C_{10}^{\tau\tau}$ correlated to $\left[C_{\nu edu}^{V,LL}\right]^{\tau\tau 32*}$. In other words, this scenario correlates an enhancement of the $R_{D^{(*)}}$ ratios to a significant enhancement of $b \to s\tau\tau$.

Due to RGE effects, the large Wilson coefficients $C_9^{\tau\tau} = -C_{10}^{\tau\tau}$ then mix into a universal contribution to $\mathcal{O}_9^{\ell\ell}$, with the leading diagram being an off-shell photon penguin involving the insertion of $\left[\mathcal{O}_{ed}^{V,LL}\right]^{\tau\tau 23}$ (or equivalently $\mathcal{O}_9^{\tau\tau}$ and $\mathcal{O}_{10}^{\tau\tau}$ with the relation $C_9^{\tau\tau} = -C_{10}^{\tau\tau}$), see Fig. 2.6a. This provides a sizable C_9^U, which is known to provide an excellent fit to the anomalies in $b \to s\mu\mu$ data without entering in conflict with the SM-like $R_{K^{(*)}}$ ratios. Therefore, this scenario provides a correlation between an enhancement of the $R_{D^{(*)}}$ ratios and $b \to s\ell\ell$, which greatly improves the global fit to the latter [82, 290]. The scenario $[C_{\ell q}^{(1)}]^{\tau\tau 23} = [C_{\ell q}^{(3)}]^{\tau\tau 23}$ can be obtained by integrating out a heavy singlet vector leptoquark $U_1 \sim (\mathbf{3}, \mathbf{1}, 2/3)$ [291], or alternatively several copies of scalar leptoquarks $R_2 \sim (\mathbf{3}, \mathbf{2}, 7/6)$ [292] or $S_1 + S_3$ [293, 294].

In Fig. 2.6b it can be seen that the region of parameter space where $R_{D^{(*)}}$ is enhanced to explain the experimental values agrees nicely with the region preferred by $b \to s\mu\mu$ data. Remarkably, the inclusion of a small LFUV contribution $C_9^{\mu\mu} = -C_{10}^{\mu\mu}$, which contributes to $R_{K^{(*)}}$ without being in conflict with the recent update by LHCb, further improves the global fit to all existing data.

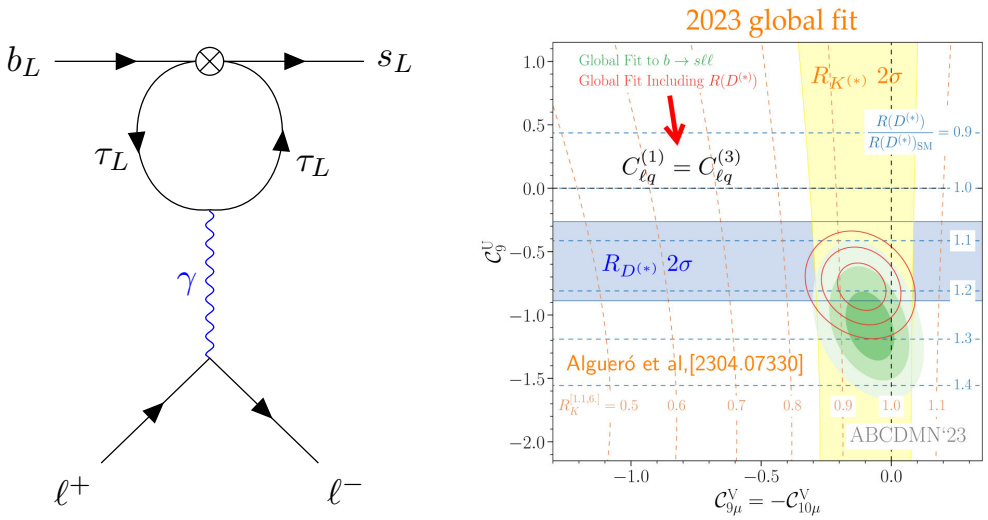

(A) (B)

FIGURE 2.6: ***Left:*** Off-shell photon penguin diagram mixing $\left[\mathcal{O}_{ed}^{V,LL}\right]^{\tau\tau 32}$ into a lepton universal contribution to $\mathcal{O}_9^{\ell\ell}$. The crossed dot indicates the insertion of a 4-fermion operator. ***Right:*** Parameter space of C_9^U and LFUV $C_9^{\mu\mu} = -C_{10}^{\mu\mu}$ in the particular SMEFT scenario $[C^{(1)}_{\ell q}]^{\tau\tau 23} = [C^{(3)}_{\ell q}]^{\tau\tau 23}$ that correlates $R_{D^{(*)}}$ with $b \to s\ell\ell$ (see main text). The blue region is preferred by $R_{D^{(*)}}$ at 2σ, while the yellow region is preferred by the updated, SM-like $R_{K^{(*)}}$ ratios at 2σ. The green region is preferred by the global fit of $b \to s\mu\mu$ (contours denote 1σ, 2σ, 3σ respectively), and the contours get modified to the red ellipses if $R_{D^{(*)}}$ are included in the global fit. Plot taken from [82].

In conclusion, low-energy data on semileptonic B-decays suggests the existence of a large contribution to $\left[\mathcal{O}_{\nu edu}^{V,LL}\right]^{\tau\tau 32\dagger}$ which simultaneously explains $R_{D^{(*)}}$ and the anomalous $b \to s\mu\mu$ data, plus a small LFUV contribution $C_9^{\mu\mu} = -C_{10}^{\mu\mu}$ that slightly diminish $R_{K^{(*)}}$ without being in conflict with current data. In Chapter 4, we will show that this scenario arises naturally from a theory of flavour involving two copies of the Pati-Salam gauge group [2].

Chapter 3

Fermiophobic Z' models

> "The most important step a man can take. It's not the first one, is it? It's the next one. Always the next step, Dalinar."
>
> – Brandon Sanderson, *Oathbringer*

In this chapter we discuss a class of well-motivated extensions of the SM that contain a Z' boson which does not couple directly to SM fermions, only through mixing via heavy vector-like fermions. This mixing controls the size of the Z' couplings to SM fermions, which can then be large or very small in a natural way. Such a setup provides a framework where flavour anomalies can be explained with Z' masses ranging from a few GeV to a few TeV, and it can be connected to a natural origin of the SM Yukawa couplings and the flavour hierarchies.

3.1 Introduction

The 2021 updates of R_K [177] (see Section 2.3.1) and $(g-2)_\mu$ [78] (see Section 2.3.3) by LHCb and FNAL, respectively, increased the mounting evidence for new physics preferentially coupled to muons, suggesting the breaking of lepton flavour universality. This motivated model building efforts to understand the so-called *flavour anomalies* in terms of extensions of the SM. Beyond the well-motivated case of the $U_1 \sim (\mathbf{3},\mathbf{1},2/3)$ vector leptoquark (see Chapter 4), scalar leptoquarks or $Z' \sim (\mathbf{1},\mathbf{1},0)$ bosons were promising candidates for the explanation of the $R_{K^{(*)}}$ anomalies, see e.g. the dedicated study of Ref. [187].

Scalar leptoquarks could just be added by hand to the SM Lagrangian, providing a renormalisable theory. This setup, however, is not very predictive: a large number of possible leptoquark couplings are allowed in the renormalisable Lagrangian, not restricted by any principle, but rather the model builder usually assumes that only the minimal set of couplings required for the flavour anomalies are non-zero. Moreover, such a scalar leptoquark apparently does not give any hints about the possible solution to long-standing puzzles in fundamental physics, but actually it does the opposite: the

flavour sector is enlarged by an extra number of leptoquark couplings with arbitrary values motivated by phenomenology, worsening the flavour puzzle, and the hierarchy puzzle is enlarged with the mass of another relatively light fundamental scalar that is quadratically sensitive to NP corrections.

In contrast to scalar leptoquarks, Z' bosons cannot be added by hand to the SM Lagrangian if one seeks for a renormalisable theory. Instead, massive Z' bosons generally arise from extra $U(1)$ gauge groups, spontaneously broken by the VEV of a scalar(s) singlet ϕ, such that $M_{Z'} \sim g' \langle\phi\rangle$. Moreover, the couplings of the Z' to chiral fermions are given by their charges under the extra $U(1)$, constrained by the requirement of cancelling gauge anomalies. This provides a more predictive framework than that of scalar leptoquarks, featuring an extension of the SM gauge group that might be connected to more fundamental questions like the origin of flavour.

However, Z' bosons explaining the $R_{K^{(*)}}$ anomalies contribute at tree-level to $B_s - \bar{B}_s$ meson mixing, requiring the bsZ' coupling to be rather small, while the $\mu\mu Z'$ coupling then need to be rather large to explain $R_{K^{(*)}}$. Beyond opening some questions about the naturalness of the framework, these conditions might be difficult to achieve within the stringent constraints from gauge anomaly cancellation [295–303]. All these concerns are solved if the SM fermions are not charged under the extra $U(1)$, but only vector-like fermions are charged, which then mix with the SM fermions via Yukawa couplings provided by the new scalar singlet ϕ. This is called a *fermiophobic* Z' model [162, 233]. The setup is naturally anomaly-free and allows effective couplings to SM fermions that are controlled by the mixing angles, connected to ratios of the form $\langle\phi\rangle / M_i$ where M_i generically denotes the masses of the vector-like fermions. The case $\langle\phi\rangle \ll M_i$ provides naturally small mixing angles, hence the effective Z' couplings are naturally small as well, while the case $\langle\phi\rangle / M_i \sim 1$ provides mixing angles and Z' couplings not much smaller than $\mathcal{O}(1)$.

The situation of the $(g-2)_\mu$ anomaly is not very different: both scalar leptoquarks and Z' bosons can explain the anomaly (see also models with just new scalar content and/or vector-like fermions [223–225, 304]). The Z' models can largely be classified depending on the origin of the chirality flip that occurs in the loop. The traditional Z' model involves a chirality flip on the muon line, requiring the Z' boson to be light, below the GeV range [217]. Another option involves Z' models that include $\tau\mu Z'$ couplings, such that a chirally enhanced contribution to $(g-2)_\mu$ is obtained via the ratio m_τ/m_μ [305]. However, a much larger chiral enhancement is required for heavy Z' explanations of $(g-2)_\mu$. Fermiophobic Z' models provide a very efficient solution: a heavy vector-like lepton of the fermiophobic model gets a Yukawa coupling to the SM Higgs doublet. This coupling provides a chiral enhancement of $(g-2)_\mu$ via the ratio M_4^C/m_μ, with the "chiral mass" of the vector-like lepton M_4^C naturally of the order of the top mass. The vector-like lepton mixes with muons, such that the Z' boson mediates the new chirally enhanced contribution to $(g-2)_\mu$ [231, 232, 234–236, 306–308].

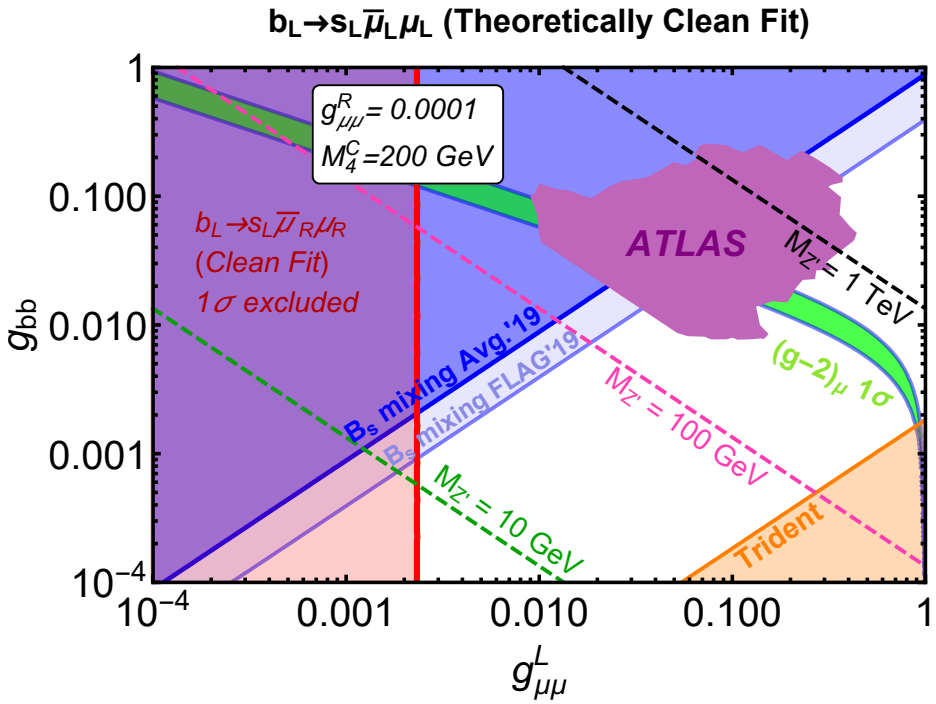

FIGURE 3.1: Legacy plot with simultaneous explanation of the 2021 $R_{K^{(*)}}$ and $(g-2)_\mu$ anomalies in the fermiophobic Z' model of Ref. [1]. All points in the plot are made compatible with the central values of the 2021 $R_{K^{(*)}}$ anomalies via a varying $M_{Z'}$ mass. Shaded regions are excluded except for the green region, which is preferred by the $(g-2)_\mu$ anomaly at 1σ.

This way, the class of fermiophobic Z' models provided a well-motivated solution to the $R_{K^{(*)}}$ and $(g-2)_\mu$ anomalies separately. In Ref. [1] we presented a novel study showing that both anomalies could be addressed simultaneously in a fermiophobic Z' framework with a minimal number of couplings, as shown in Fig 3.1. Moreover, fermiophobic Z' models can also be naturally connected to the origin of Yukawa couplings in the SM [163]. The basic idea is replacing the SM Higgs doublet by a pair of Higgs doublets charged under the new $U(1)$, while SM fermions remain uncharged, in such a way that SM Yukawa couplings for SM fermions are forbidden but generated effectively through the presence of heavy messengers, including the vector-like fermions. The same mechanism generates effective Z' couplings for SM fermions, hence connecting the origin of Yukawa couplings and flavour hierarchies with the origin of the low-energy flavour anomalies. In this manner, the flavour anomalies fix the usually undetermined NP scales of the theory of flavour to the TeV, within the reach of current experiments. Notice that this is not the case for similar constructions based on scalar leptoquarks [164,167], where the mass of the leptoquark needs to be at the TeV scale but the scales of the theory of flavour may be anywhere *from the Planck scale to the electroweak scale*. We shall see that both the origin of flavour hierarchies and hierarchical Z' couplings are explained via the hierarchical masses of heavy messengers, known as the mechanism of *messenger dominance* [171]. Despite the elegance of the theory of flavour with fermiophobic Z', it was never shown whether this model could actually account simultaneously for fermion

masses and for both flavour anomalies $R_{K^{(*)}}$ and $(g-2)_\mu$ while remaining compatible with all known data.

In spite of the vanishing of the $R_{K^{(*)}}$ anomalies that motivated our previous work [1], $(g-2)_\mu$ remains as a possible hint for new physics. As shown in Section 2.3.3, even in the case that the BMW computation is capturing well the SM prediction, a small tension of almost 2σ with the increasingly precise experimental measurement may arise. Therefore, in Section 3.2 of this chapter we will present a minimal version of the fermiophobic Z' model that can explain the $(g-2)_\mu$ anomaly. In Section 3.3 we will present a theory of flavour based on the fermiophobic Z' model, and study whether the $(g-2)_\mu$ anomaly can be explained in this framework while being compatible with all constraints. Finally, we will assess the experimental constraints over the theory of flavour independently of the $(g-2)_\mu$ anomaly, to extract lower bounds over the undetermined NP scales of the flavour model.

3.2 Fermiophobic Z' model for the $(g-2)_\mu$ anomaly

3.2.1 The model

The fermiophobic model features a $U(1)'$ gauge group under which the chiral fermions of the SM are uncharged, as shown in Table 3.1. The model includes a SM singlet scalar ϕ that gets a VEV to spontaneously break the $U(1)'$ symmetry, leading to a Z' boson with mass $M_{Z'} \sim g' \langle\phi\rangle$, where g' is the gauge coupling of the $U(1)'$ group. The model also includes a so-called "4th family" of vector-like leptons, including doublets L_{L4}, $\widetilde{L}_{R4}$ and singlets e_{L4}, $\widetilde{e}_{R4}$ with the same charge under $U(1)'$. The mass terms for the various fermions are then given by the following renormalisable Lagrangian

$$\begin{aligned}\mathcal{L}^{\text{ren}} &= y^u_{ij}\overline{Q}_{Li}\widetilde{H}u_{Rj} + y^d_{ij}\overline{Q}_{Li}Hd_{Rj} + y^e_{ij}\overline{L}_{Li}He_{Rj} \\ &+ y^e_4\overline{L}_{L4}He_{R4} + \widetilde{y}^e_4\overline{\widetilde{e}}_{L4}H^\dagger\widetilde{L}_{R4} \\ &+ x^L_i\phi\overline{L}_{Li}\widetilde{L}_{R4} + x^e_i\phi\overline{\widetilde{e}}_{L4}e_{Ri} \\ &+ M^L_4\overline{L}_{L4}\widetilde{L}_{R4} + M^e_4\overline{\widetilde{e}}_{L4}e_{R4} + \text{h.c.}\,,\end{aligned} \tag{3.1}$$

where $\widetilde{H} = i\sigma_2 H^\dagger$ and $i = 1,2,3$. Out of the various terms in the Lagrangian above, those in the first line provide Yukawa couplings for chiral fermions in the usual way, leading to the known masses of chiral fermions after the Higgs doublet gets a VEV. In contrast, the vector-like leptons get mass from two different sources:

- Firstly, from the arbitrary vector-like masses M^L_4 and M^e_4.
- Secondly, from Yukawa terms involving the SM Higgs doublet, i.e. $y^e_4\overline{L}_{L4}He_{R4}$ and $\widetilde{y}^e_4\overline{\widetilde{e}}_{L4}\widetilde{H}\widetilde{L}_{R4}$, which get promoted to fourth family mass terms M^C_4 and $\widetilde{M}^C_4$ relating the vector-like doublet and singlet once the Higgs doublet acquires a VEV,

$$M^C_4 = y^e_4\frac{v_{\text{SM}}}{\sqrt{2}}\,, \tag{3.2}$$

Field	$SU(3)_c$	$SU(2)_L$	$U(1)_Y$	$U(1)'$
Q_{Li}	**3**	**2**	1/6	0
u_{Ri}	**3**	**1**	2/3	0
d_{Ri}	**3**	**1**	-1/3	0
L_{Li}	**1**	**2**	-1/2	0
e_{Ri}	**1**	**1**	-1	0
$L_{L4}, \widetilde{L}_{R4}$	**1**	**2**	-1/2	1
$\tilde{e}_{L4}, e_{R4}$	**1**	**1**	-1	1
ϕ	**1**	**1**	0	-1
H	**1**	**2**	1/2	0

TABLE 3.1: Particle assignments under the $SU(3)_c \times SU(2)_L \times U(1)_Y \times U(1)'$ gauge symmetry, with $i = 1, 2, 3$.

$$\widetilde{M}_4^C = \widetilde{y}_4^e \frac{v_{\rm SM}}{\sqrt{2}} \,. \tag{3.3}$$

We shall denote these mass terms as "chiral masses" to make a distinction with the arbitrary vector-like mass terms. Perturbation theory naively requires $y \lesssim \sqrt{4\pi} \approx 3.5$ for generic Yukawa couplings in the renormalisable Lagrangian, therefore the chiral masses above naturally live at the electroweak scale, setting an effective bound $M_4^C \lesssim 600$ GeV in order to preserve the perturbativity of the model.

Bounds over vector-like leptons generally require their physical masses to be larger than 200 GeV [309], therefore without loss of generality we work in the regime $m_\mu \ll M_{E_1}, M_{E_2}$, where M_{E_1} and M_{E_2} are the physical masses of the fourth family (vector-like) leptons. In this regime, the physical masses M_{E_1} and M_{E_2} are obtained by diagonalising the following mass matrix,

$$\begin{pmatrix} & \widetilde{L}_{R4} & e_{R4} \\ \hline \overline{L}_{L4} & M_4^L & M_4^C \\ \overline{\tilde{e}}_{L4} & \widetilde{M}_4^C & M_4^e \end{pmatrix} , \tag{3.4}$$

via two unitary rotations that we generally parameterise by the mixing angles $\sin\theta_L^E \equiv s_L^E$ and $\sin\theta_R^E \equiv s_R^E$. We shall see that the presence of the chiral masses, especially M_4^C, is of fundamental importance to explain the $(g-2)_\mu$ anomaly. We anticipate that the terms in the third line of Eq. (3.1) mix chiral lepton doublets L_{Li} with the partner doublet L_{L4} and the chiral lepton singlets e_{Ri} with the partner singlet e_{R4}, leading to effective Z' couplings for the SM chiral leptons as discussed in the next subsection. The presence of chiral masses for the fourth family leptons in the Lagrangian also leads to mixing between the conjugate (tilde) leptons $\widetilde{L}_{R4}$ and $\widetilde{e}_{L4}$ and the chiral leptons of the

SM, however in the regime $v_{\rm SM} \ll M_4^{L,e}$ where we shall (mostly) work, this mixing will be suppressed by the small angles s_L^E and s_R^E, such that it can be neglected.

3.2.2 Fermion mixing and effective Z' couplings

For the sake of simplicity, we assume a minimal mixing framework which provides the minimal set of couplings needed to address the $(g-2)_\mu$ anomaly[1]. This requires that the vector-like leptons only mix with L_{L2} and with e_{R2}. Such a minimal mixing framework could be enforced for example by a Z_2 discrete symmetry under which only vector-like leptons and L_{L2}, e_{R2} are not even. We also assume $v_{\rm SM} \ll M_4^{L,e}$ such that the physical masses of vector-like leptons are well approximated by $M_{E_1} \approx M_4^L$ and $M_{E_2} \approx M_4^e$. In this regime, for the purpose of extracting the effective Z' couplings we can neglect the mixing angles s_L^E and s_R^E introduced in the previous subsection. We shall see that this approximation holds for all the parameter space relevant for $(g-2)_\mu$.

In the mass insertion approximation where $\langle\phi\rangle \ll M_4^L, M_4^e$, the mixing angles are well approximated by $s_{24}^L \sim x_2^L \langle\phi\rangle / M_4^L$ and $s_{24}^e \sim x_2^L \langle\phi\rangle / M_4^e$, see also the diagrams in Fig. 3.2. However, it might be necessary to go beyond the mass insertion approximation, where $s_{24}^L, s_{24}^e \ll 1$, since the explanation of the $(g-2)_\mu$ anomaly might require larger mixing angles, which are naturally obtained in the regime $\langle\phi\rangle / M_4^{L,e} \sim 1$. In this case, the mass insertion approximation breaks and we need to work in a large mixing angle formalism (see Appendix B). We always work in the regime where $m_\mu \ll \langle\phi\rangle$, i.e. we do not consider Z' masses lighter[2] than 1 GeV. In this regime, the mixing induced by the couplings in the third line of Eq. (3.1) is well captured by the following mixing angles

$$s_{24}^L = \frac{x_2^L \langle\phi\rangle}{\sqrt{\left(x_2^L \langle\phi\rangle\right)^2 + \left(M_4^L\right)^2}}, \qquad c_{24}^L = \frac{M_4^L}{\sqrt{\left(x_2^L \langle\phi\rangle\right)^2 + \left(M_4^L\right)^2}}, \tag{3.5}$$

$$s_{24}^e = \frac{x_2^e \langle\phi\rangle}{\sqrt{\left(x_2^e \langle\phi\rangle\right)^2 + \left(M_4^e\right)^2}}, \qquad c_{24}^e = \frac{M_4^e}{\sqrt{\left(x_2^e \langle\phi\rangle\right)^2 + \left(M_4^e\right)^2}}, \tag{3.6}$$

where $s_{24}^{L,e} \equiv \sin\theta_{24}^{L,e}$, $c_{24}^{L,e} \equiv \cos\theta_{24}^{L,e}$. Assuming that we have freedom over the various parameters $\langle\phi\rangle$, $x_2^{L,e}$ and $M_4^{L,e}$, we have complete freedom over the numerical values of the mixing angles $s_{24}^{L,e}$. Notice that this mixing modifies the expression for the muon mass as $m_\mu \approx y_\mu c_{24}^L c_{24}^e v_{\rm SM}/\sqrt{2}$. However, due to the smallness of the muon Yukawa coupling in the SM, it is possible to recover the experimental value of the muon mass as long as $c_{24}^L c_{24}^e \gtrsim 0.0006$, which only excludes extremely large mixing angles with sine close to unity.

Before any mixing, the Z' boson only couples to the vector-like leptons as

$$\mathcal{L}_{Z'} \supset g' \left(\overline{L}_{L4} \gamma^\mu L_{L4} + \overline{e}_{R4} \gamma^\mu e_{R4} + \overline{\widetilde{L}}_{R4} \gamma^\mu \widetilde{L}_{R4} + \overline{\widetilde{e}}_{L4} \gamma^\mu \widetilde{e}_{L4} \right) Z'_\mu \,. \tag{3.7}$$

[1] For a complete framework also connected with the origin of the SM flavour structure see the theory of flavour with fermiophobic Z' in Section 3.3.

[2] We shall see that this choice is also motivated by the strong bounds on kinetic mixing for light Z' bosons with masses below 1 GeV.

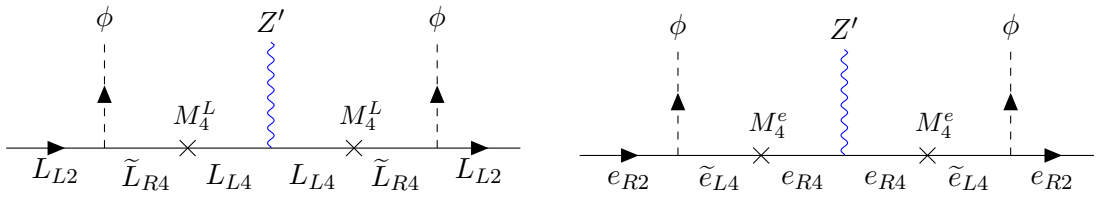

(A) (B)

FIGURE 3.2: Diagrams in the model which lead to the effective Z' couplings in the mass insertion approximation.

We then define the following matrices in lepton flavour space

$$D_{L,e} = \mathrm{diag}(0,0,0,1)\,, \tag{3.8}$$

such that

$$\mathcal{L}_{Z'} = g'\left(\overline{L}_L\gamma^\mu D_L L_L + \overline{e}_R\gamma^\mu D_e e_R + \overline{\widetilde{L}}_{R4}\gamma^\mu\widetilde{L}_{R4} + \overline{\widetilde{e}}_{L4}\gamma^\mu\widetilde{e}_{L4}\right)Z'_\mu\,, \tag{3.9}$$

where we have defined L_L and e_R as 4-component vectors containing the leptonic interaction eigenstates.

Now we define the mixing transformations

$$V_{24}^{L,e} = \begin{pmatrix} 1 & 0 & 0 & 0 \\ 0 & c_{24}^{L,e} & 0 & s_{24}^{L,e} \\ 0 & 0 & 1 & 0 \\ 0 & -s_{24}^{L,e} & 0 & c_{24}^{L,e} \end{pmatrix}. \tag{3.10}$$

Therefore, after the mixing, the Z' couplings read

$$\mathcal{L}_{Z'} = g'\left(\overline{L'}_L\gamma^\mu D'_L L'_{L4} + \overline{e'}_R\gamma^\mu D'_e e'_R + \overline{\widetilde{L}}_{R4}\gamma^\mu\widetilde{L}_{R4} + \overline{\widetilde{e}}_{L4}\gamma^\mu\widetilde{e}_{L4}\right)Z'_\mu\,, \tag{3.11}$$

where

$$D'_{L,e} = \left(V_{24}^{L,e}\right)^\dagger D_{L,e} V_{24}^{L,e} = \begin{pmatrix} 1 & 0 & 0 & 0 \\ 0 & \left(s_{24}^{L,e}\right)^2 & 0 & -s_{24}^{L,e}c_{24}^{L,e} \\ 0 & 0 & 1 & 0 \\ 0 & -s_{24}^{L,e}c_{24}^{L,e} & 0 & \left(c_{24}^{L,e}\right)^2 \end{pmatrix}. \tag{3.12}$$

where L'_L and e'_R are the 4-component vectors containing the leptonic mass eigenstates defined as

$$L'_L = V_{24}^{L,e}L_L\,, \qquad e'_R = V_{24}^{L,e}e_R\,. \tag{3.13}$$

From Eq. (3.11), it is clear that the Z' boson now has effective couplings to muon pairs,

$$\begin{aligned}\mathcal{L}_{Z'} \supset \Big[&g^L_{\mu\mu}\overline{L'}_{L2}\gamma^\mu L'_{L2} + g^R_{\mu\mu}\overline{\mu}_R\gamma^\mu\mu_R + g^L_{EE}\overline{L'}_{L4}\gamma^\mu L'_{L4} + g^R_{EE}\overline{e'}_{R4}\gamma^\mu e'_{R4} \\ &+ \left(g^L_{\mu E}\overline{L'}_{L2}\gamma^\mu L'_{L4} + g^R_{\mu E}\overline{\mu}_R\gamma^\mu e'_{R4} + \text{h.c.}\right)\Big]Z'_\mu\end{aligned} \tag{3.14}$$

where

$$g_{\mu\mu}^{L,R} = g' \left(s_{24}^{L,e}\right)^2 , \qquad g_{EE}^{L,R} = g' \left(c_{24}^{L,e}\right)^2 , \tag{3.15}$$

$$g_{\mu E}^{L,R} = -g' s_{24}^{L,e} c_{24}^{L,e} . \tag{3.16}$$

As we shall see, the effective couplings $g_{\mu E}^{L,R}$ are of crucial importance for the explanation of the $(g-2)_\mu$ anomaly. Notice that the tilde leptons $\widetilde{L}_{R4}$ and $\widetilde{e}_{L4}$ do not mix with SM leptons in the regime $v_{\rm SM} \ll M_4^{L,e}$ where we can neglect the mixing angles s_L^E and s_R^E.

3.2.3 Higgs diphoton decay

After electroweak symmetry breaking, the Yukawa terms in Eq. (3.1) involving the SM Higgs field and the vector-like leptons give rise to the chiral masses M_4^C and $\widetilde{M}_4^C$, which will be crucial for accommodating $(g-2)_\mu$ with the experimental measurements. On the other hand, the chiral masses are also expected to give an extra contribution to the decay of the SM Higgs to two photons, a key process that played a major role in the discovery of the Higgs boson at the LHC. In the following, we check whether the current data on Higgs diphoton decay can set any constraints over the chiral masses.

Firstly, within the SM, chiral fermions (Fig. 3.3a) and $W^\pm$ bosons (Figs. 3.3c, 3.3d) contribute to the decay channel $h^0 \to \gamma\gamma$ [310]

$$\Gamma(h^0 \to \gamma\gamma)_{\rm SM} = \frac{\alpha_{\rm EM}^2 m_h^3}{256\pi^3 v_{\rm SM}^2} \left| F_1(\tau_W) + \sum_{f\,\epsilon\,{\rm SM}} N_{cf} Q_f^2 F_{1/2}(\tau_f) \right|^2 , \tag{3.17}$$

where $N_{cf} = 1$ (leptons), 3 (quarks) and Q_f is the electromagnetic charge of the fermion f, with the loop functions defined as

$$F_1(\tau) = 2 + 3\tau + 3\tau\,(2-\tau)\,f(\tau) , \tag{3.18}$$

$$F_{1/2}(\tau) = -2\tau\,[1 + (1-\tau)\,f(\tau)] , \tag{3.19}$$

where

$$\tau_i = 4m_i^2/m_h^2 \tag{3.20}$$

and

$$f(\tau) = \begin{cases} \left[\arcsin\left(1/\sqrt{\tau}\right)\right]^2 , & \text{if} \quad \tau \geq 1 , \\ -\dfrac{1}{4}\left[\ln\left(\dfrac{1+\sqrt{1-\tau}}{1-\sqrt{1-\tau}}\right) - i\pi\right]^2 , & \text{if} \quad \tau < 1 . \end{cases} \tag{3.21}$$

Note here that for large τ, $F_{1/2} \to -4/3$. The dominant contribution to $\Gamma(h^0 \to \gamma\gamma)_{\rm SM}$ is the contribution of the $W^\pm$ bosons,

$$F_1(\tau_W) \approx 8.33 , \tag{3.22}$$

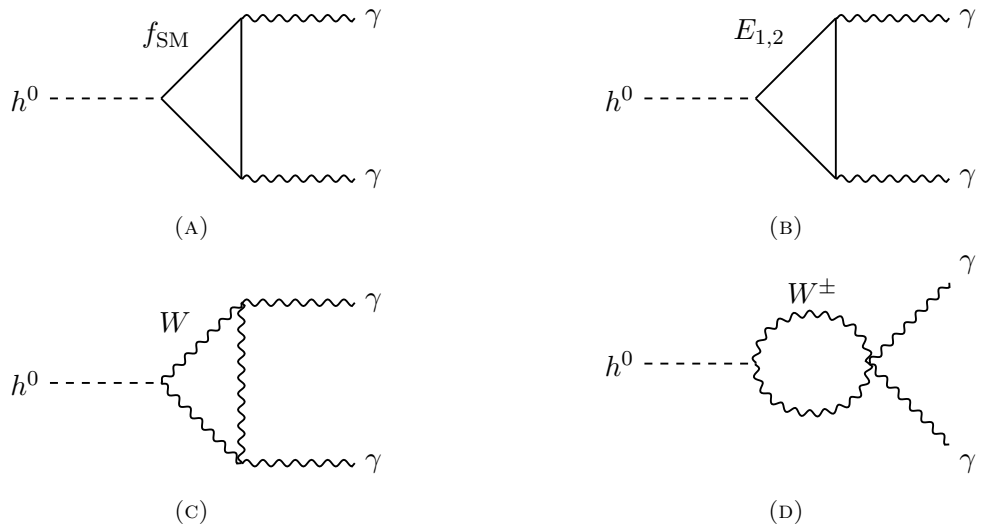

FIGURE 3.3: Diagrams contributing to the Higgs diphoton decay, $h^0 \to \gamma\gamma$, where $f_{\rm SM} = u_i, d_i, e_i$, $i = 1, 2, 3$ and $E_{1,2}$ denotes the "4th family" (vector-like) leptons.

and it interferes destructively with the top-quark loop that dominates the contribution from SM chiral fermions,

$$N_{ct} Q_t^2 F_{1/2}(\tau_t) \approx -1.84\,. \tag{3.23}$$

Now we add the contributions of the vector-like leptons (Fig. 3.3b) with physical masses M_{E_1} and M_{E_2}. The couplings of the physical fourth family leptons to the SM Higgs boson are obtained by rotating the Yukawa couplings in the second line of Eq. (3.1) by the same transformations that diagonalise the matrix in Eq. (3.4), parameterised by the mixing angles $s^E_{L,R}$. We obtain [311–313],

$$\begin{aligned}\Gamma(h^0 \to \gamma\gamma) =& \frac{\alpha_{\rm EM}^2 m_h^3}{256\pi^3 v_{\rm SM}^2} \Bigg| F_1(\tau_W) + \sum_{f\,\epsilon\,{\rm SM}} N_{cf} Q_f^2 F_{1/2}(\tau_f) \\ &+ \frac{M_4^C c_L^E c_R^E + \widetilde{M}_4^C s_L^E s_R^E}{M_{E_1}} F_{1/2}\left(\tau_{E_1}\right) + \frac{M_4^C s_L^E s_R^E + \widetilde{M}_4^C c_L^E c_R^E}{M_{E_2}} F_{1/2}\left(\tau_{E_2}\right) \Bigg|^2 .\end{aligned} \tag{3.24}$$

We can see that the new contributions proportional to the chiral masses are suppressed by the physical masses of the fourth family (vector-like) leptons $M_{E_{1,2}}$. In the regime $v_{\rm SM} \ll M_4^{L,e}$, we obtain $M_{E_1} \approx M_4^L$ and $M_{E_2} \approx M_4^e$, along with $s^E_{L,R} \ll 1$, such that $\Gamma(h^0 \to \gamma\gamma)$ is given by the more simple form

$$\begin{aligned}\Gamma(h^0 \to \gamma\gamma) \approx& \frac{\alpha_{\rm EM}^2 m_h^3}{256\pi^3 v_{\rm SM}^2} \Bigg| F_1(\tau_W) + \sum_{f\,\epsilon\,{\rm SM}} N_{cf} Q_f^2 F_{1/2}(\tau_f) \\ &+ \frac{M_4^C}{M_4^L} F_{1/2}\left(\tau_{L_4}\right) + \frac{\widetilde{M}_4^C}{M_4^e} F_{1/2}\left(\tau_{e_4}\right) \Bigg|^2 .\end{aligned} \tag{3.25}$$

Although in the phenomenological analysis we work with the exact expression in Eq. (3.24), we find that all the parameter space motivated by the $(g-2)_\mu$ anomaly is within the

regime $v_{\rm SM} \ll M_4^{L,e}$, well described by the equation above. Therefore, the new contributions to $h^0 \to \gamma\gamma$ mediated by the fourth family leptons are suppressed by the heavy vector-like masses $M_4^{L,e}$. Moreover, these new contributions generally interfere destructively with the most sizable contribution of the $W^\pm$ bosons, decreasing $\Gamma(h^0 \to \gamma\gamma)$. Let us now compare with the experimental results for the h^0 signal strength in the $h^0 \to \gamma\gamma$ channel,

$$R_{\gamma\gamma} = \frac{\Gamma(h^0 \to \gamma\gamma)}{\Gamma(h^0 \to \gamma\gamma)_{\rm SM}}\,, \tag{3.26}$$

where current data reveals $R_{\gamma\gamma}^{\rm PDG,\,2023} = 1.10 \pm 0.07$ [21], and future projections show that ATLAS and CMS could reduce the uncertainties down to the per cent level after the high luminosity phase of the LHC [314, 315].

Finally, we comment that the vector-like leptons do not only contribute at 1-loop level to the $h^0 \to \gamma\gamma$ decay, but they also modify the $h^0 \to Z\gamma$ mode which has been recently observed at the LHC [316]. However, in our scenario where we consider vector-like leptons with similar quantum numbers as the SM leptons, notice that the Z couplings are suppressed with respect to electromagnetic couplings (roughly by $1 - s^2_{\theta_W} \simeq 0.08$). Moreover, it has been shown that the doublet and the singlet fermions have opposite trends in terms of the interference pattern with the SM amplitudes [317]. Therefore, the two effects tend to cancel each other and $h^0 \to Z\gamma$ remains SM-like to an excellent approximation. We note however that this strong suppression does not arise in models where the vector-like leptons carry exotic hypercharges [318].

3.2.4 $(g-2)_\mu$ anomaly

As discussed in Section 2.3.3, the current picture of $(g-2)_\mu$ is very puzzling. The SM prediction based on data from $e^+e^- \to$ hadrons [206] is in 5.1σ tension with the most recent experimental measurement by FNAL [79]. Numerically, we obtain (see Section 2.3.3)

$$\Delta a_\mu^{\rm R} = a_\mu^{\rm exp} - a_\mu^{\rm SM,R} = (249 \pm 48) \times 10^{-11}\,, \tag{3.27}$$

where $a = (g-2)/2$. In contrast, the SM prediction by the BMW lattice collaboration is in agreement with the experiment at the 1.8σ level,

$$\Delta a_\mu^{\rm BMW} = a_\mu^{\rm exp} - a_\mu^{\rm SM,BMW} = (105 \pm 59) \times 10^{-11}\,. \tag{3.28}$$

While we wait for new data and theory improvement to establish a clear picture, it is interesting to study the BSM interpretation of the results above. Although the BMW prediction is still in rough agreement with the experimental value, with the increasing precision in the experimental measurement is possible that a small tension at the 2σ level is established in the near future.

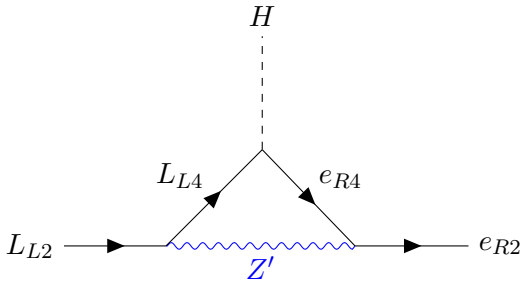

FIGURE 3.4: Dominant and chirally enhanced contribution to $(g-2)_\mu$ in the fermiophobic Z' model. The Higgs insertion provides a chiral mass M_4^C for the fourth family (vector-like) lepton after electroweak symmetry breaking, such that the low-energy process involves the emission of a photon (not shown).

In our model, in the regime $v_{\rm SM} \ll M_4^{L,e}$ where we can neglect the $s_{L,R}^E$ mixing, the NP contribution to $(g-2)_\mu$ is given as [319, 320]

$$\Delta a_\mu = -\frac{m_\mu^2}{8\pi^2 M_{Z'}^2}\left[\left(\left|g_{\mu\mu}^L\right|^2+\left|g_{\mu\mu}^R\right|^2\right)F(m_\mu^2/M_{Z'}^2)+\left(\left|g_{\mu E}^L\right|^2+\left|g_{\mu E}^R\right|^2\right)F(M_{E_1}^2/M_{Z'}^2)\right.$$
$$\left.+\mathrm{Re}\left[g_{\mu\mu}^L\left(g_{\mu\mu}^R\right)^*\right]G(m_\mu^2/M_{Z'}^2)+\mathrm{Re}\left[g_{\mu E}^L\left(g_{\mu E}^R\right)^*\right]\frac{M_4^C}{m_\mu}G(M_{E_1}^2/M_{Z'}^2)\right], \tag{3.29}$$

where $M_{E_1} \approx M_4^L$ is the physical mass of the vector-like lepton mostly aligned with the fourth family doublets. The loop functions are given by

$$F(x) = \frac{5x^4-14x^3+39x^2-38x-18x^2\log x+8}{12(1-x)^4}, \tag{3.30}$$

$$G(x) = \frac{x^3+3x-6x\log x-4}{2(1-x)^3}. \tag{3.31}$$

Since the loop functions satisfy $G(x)<0$ and $F(x)>0$, the contributions proportional to $G(x)$ and $F(x)$ in Eq. (3.29) interfere negatively. However, for a chiral mass M_4^C of $\mathcal{O}(v_{\rm SM})$, as naturally expected, the term proportional to M_4^C in Eq. (3.29) is dominant and positive due to $G(x)<0$, matching the required sign to explain the deviations in Eqs. (3.27) and (3.28). This dominant contribution arises from the diagram in Fig. 3.4, and given that naturally $M_4^C \gg m_\mu$, we can approximate Δa_μ as

$$\Delta a_\mu \simeq -\frac{m_\mu^2}{8\pi^2 M_{Z'}^2}\mathrm{Re}\left[g_{\mu E}^L\left(g_{\mu E}^R\right)^*\right]\frac{M_4^C}{m_\mu}G\left((M_4^L/M_{Z'})^2\right). \tag{3.32}$$

We see that the relevant couplings to address the $(g-2)_\mu$ anomaly are $g_{\mu E}^{L,R}$, which are connected to the mixing angles of the model via Eq. (3.16). For the parameter space relevant for $(g-2)_\mu$ we find $M_4^L \gtrsim M_{Z'}$. In this case, we have $|G(x)| \approx \mathcal{O}(1)$, and we can neglect the order 1 factor of the loop function in order to extract $M_{Z'}$ as a function

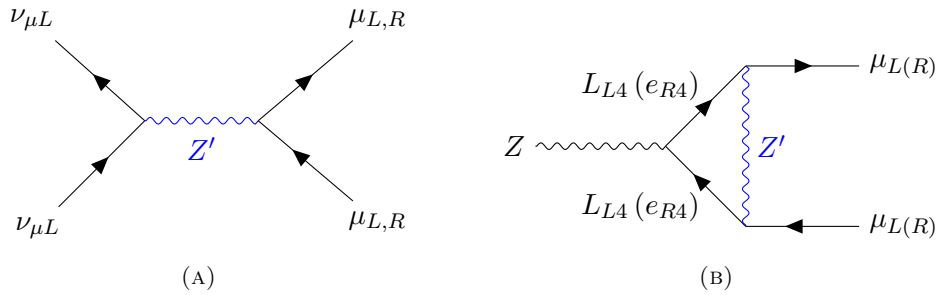

(A) (B)

FIGURE 3.5: Z' exchange diagrams contributing to neutrino trident production (left) and 1-loop contribution to $Z \to \mu\mu$ involving the Z' and the heavy vector-like leptons (right).

of the relevant parameters of the model and Δa_μ, obtaining

$$M_{Z'}^2 \simeq \frac{m_\mu^2}{8\pi^2 \Delta a_\mu} (g')^2 \left(s_{34}^L\right)^2 (s_{34}^e)^2 \frac{M_4^C}{m_\mu} \,. \tag{3.33}$$

In Fig. 3.6 we study the parameter space of s_{34}^L and s_{34}^e while fixing $M_{Z'}$ via the relation (3.33) above, where we take the central value of $\Delta a_\mu^{\rm R}$. We also take $g' \sim 1$ for simplicity, as a natural benchmark value. In this manner, all the points in Fig. 3.6 address the central value of the 5σ $(g-2)_\mu$ anomaly with respect to $e^+e^- \to$ hadrons data. We also highlight the parameter space excluded by the neutrino[3] trident production $\nu_\mu \gamma^* \to \nu_\mu \mu^+ \mu^-$ [321–324] (see also Fig. 3.5),

$$\frac{\sigma_{\rm SM+NP}}{\sigma_{\rm SM}} = 1 + 8 \frac{g_{\mu\mu}^L}{g_L^2} \frac{M_W^2}{M_{Z'}^2} \frac{(1+4s_W^2)(g_{\mu\mu}^L + g_{\mu\mu}^R) + (g_{\mu\mu}^L - g_{\mu\mu}^R)}{(1+4s_W^2)^2 + 1} \lesssim 0.83 \pm 0.18 \,. \tag{3.34}$$

We notice another constraint arising from LHC measurements of the Z decays to four muons, with the second muon pair produced in the SM via a virtual photon [325, 326] and in our model via the Z', $pp \to Z \to 4\mu$. This process sets constraints in the region $5\,{\rm GeV} \lesssim M_{Z'} \lesssim 70\,{\rm GeV}$, however we note that these constraints mostly overlap with neutrino trident production [233, 324, 327, 328], and hence we neglect it. We further notice a 1-loop contribution to the precisely measured $Z \to \mu\mu$ decay with the Z' and the vector-like leptons running in the loop, as shown in Fig. 3.5. We find the following modifications of the Z couplings due to the Z' loop:

$$\frac{g_{\mu_L\mu_L}^Z}{g_{e_Le_L}^Z} \simeq 1 + \frac{(g_{\mu E}^L)^2}{16\pi^2} \mathcal{K}(M_Z^2/M_{Z'}^2) \,, \tag{3.35}$$

plus a similar modification of the right-handed coupling obtained by setting $L \to R$ everywhere. The loop function $\mathcal{K}$ is given by [329]

$$\mathcal{K}(x) = -\frac{4+7x}{2x} + \frac{2+3x}{x} \log x - \frac{2(1+x)^2}{x^2} \left[\log x \log(1+x) + {\rm Li}_2(-x)\right] \,, \tag{3.36}$$

[3] Note that muon neutrinos also get effective Z' couplings in our model, along with muons.

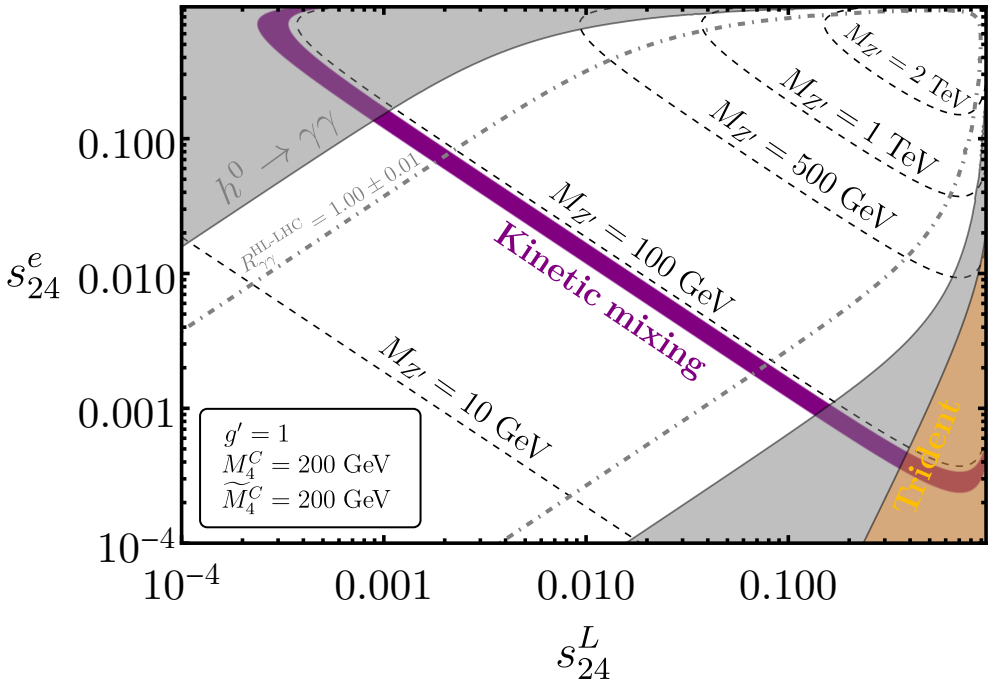

FIGURE 3.6: All the parameter space shown in the plot is compatible with the central value of Δa_μ^{R} . $M_{Z'}$ varies through the parameter space because it is related to the mixing angles and to Δa_μ^{R} via Eq. (3.33). Shaded regions are excluded at 95% CL, while the dot-dashed line shows the projection for $R_{\gamma\gamma}$ that might be reached by ATLAS and CMS after HL-LHC [314, 315].

where $\text{Li}_2(x) = -\int_0^x dt \log(1-t)$ is the di-logarithm. In Eq. (3.35) we use the electron Z couplings as a convenient normalisation, as they are not affected by NP. We find that LEP measurements [89] allow for per mille deviations from unity in the ratios of Eq. (3.35), however in our model the Z' loop is suppressed by small mixing angles and/or by a heavy Z' mass, leading to no constraints at 95% CL over the relevant parameter space shown in Fig. 3.6.

Another relevant constraint originates from kinetic mixing between the abelian groups $U(1)_Y$ and $U(1)'$. The vector-like leptons in the model are charged under both $U(1)$s, generating kinetic mixing at 1-loop as $\epsilon \sim 3 g_Y g' \log(M_E/\mu)(32\pi^2)$, where μ is a renormalisation scale. Typically this provides $\epsilon \sim 0.01$. Kinetic mixing of this size is bounded in the sub-GeV region of $M_{Z'}$ [330], which we hence neglect in our analysis, and also around the Z-pole mass, which we exhibit as the purple region excluded in Fig. 3.6.

As shown in Fig. 3.6, Higgs diphoton decay constrains large mixing angles when the Z' boson is relatively light. The reason is that large mixing angles require $\langle\phi\rangle / M_4^{L,e} \sim 1$ (remember $M_{Z'} \sim \langle\phi\rangle$), such that if $M_{Z'}$ is light then $M_4^{L,e}$ are also light and the NP contributions to $h^0 \to \gamma\gamma$ in Eq. (3.25) are no longer suppressed. In contrast, if $M_{Z'}$ is heavy then $\langle\phi\rangle / M_4^{L,e} \sim 1$ can be achieved with $M_4^{L,e} \gg v_{\text{SM}}$ and the NP contributions to Higgs diphoton decay remain suppressed. Notice that for all the parameter space in Fig. 3.6 at least one of the mixing angles is small, except for the region of heavy

Z'. This implies that at least one of the vector-like masses M_4^L and M_4^e (or both) is heavy, such that at least one of the angles $s_{L,R}^E$ that diagonalise Eq. (3.4) is small. This allows us to neglect the presence of the conjugate (tilde) fermions $\widetilde{L}_{R4}$ and $\widetilde{e}_{L4}$ in the phenomenological analysis, as anticipated at the beginning of this section, because their Z' couplings to SM fermions are further suppressed by the small mixing angles $s_{L,R}^E$.

All in all, we show in Fig. 3.6 that our model can address the $\Delta a_\mu^{\rm R}$ anomaly for Z' masses ranging from the GeV scale to the few TeV range. The nature of the sine and cosine functions does not allow effective Z' couplings larger than 1, which requires $M_{Z'} \lesssim 3.6$ TeV in order to fit the central values of $\Delta a_\mu^{\rm R}$, but one can always take g' larger than 1 or increase M_4^C above its natural values $M_4^C \approx 200$ GeV up to the perturbative limit $M_4^C \approx 600\,\text{GeV}$ if one seeks to explain $\Delta a_\mu^{\rm R}$ with even heavier Z' masses. In this case, the bounds from Higgs diphoton decay should remain similar because even though we increase M_4^C, a heavier Z' is needed as well and therefore heavier $M_4^{L,e}$ are also required to obtain large mixing angles. Of course if we consider the BMW prediction, $\Delta a_\mu^{\rm BMW}$, we can further improve the agreement with the experiment and we have even more freedom in the parameter space due to the smaller shift required with respect to $\Delta a_\mu^{\rm R}$. The HL-LHC projections by ATLAS and CMS over Higgs diphoton decay show that the uncertainties in $R_{\gamma\gamma}$ could be reduced down to the per cent level [314, 315], testing a significant region of parameter space in the model as shown by the dot-dashed line in Fig. 3.6 (assuming that the central values match the SM prediction). We find that the whole parameter space of the model that can explain the central value of $\Delta a_\mu^{\rm R}$ can be tested if $h^0 \to \gamma\gamma$ is measured to the few per mille precision.

3.3 Theory of flavour with fermiophobic Z' boson

In the previous section we introduced a simplified fermiophobic Z' model that can address the $(g-2)_\mu$ anomaly. In the following we will show how this simple construction may emerge from a complete theory of flavour, where the same mixing that generates the effective Z' couplings will generate effective Yukawa couplings for the SM fermions, connecting the origin of the flavour hierarchies with the origin of flavour anomalies.

3.3.1 The renormalisable Lagrangian for charged fermions

In contrast with the simplified model introduced in the previous section, here we consider a complete "fourth" family of vector-like fermions (including a vector-like neutrino) charged under $U(1)'$, while chiral fermions remain uncharged. Notice that $SU(2)_L$ doublet and singlet fermions now carry opposite charges under $U(1)'$, as shown in Table 3.2. We preserve the SM singlet scalar ϕ that gets a VEV to spontaneously break the $U(1)'$ symmetry, leading to a Z' boson with mass $M_{Z'} \sim g' \langle\phi\rangle$, where g' is the gauge coupling of the $U(1)'$ group. However, we exchange the SM-like Higgs of the simplified model by a pair of Higgs doublets equally charged under $U(1)'$. The fact that the Higgs doublets are charged under $U(1)'$ while the chiral fermions are not forbids SM-like Yukawa

Field	$SU(3)_c$	$SU(2)_L$	$U(1)_Y$	$U(1)'$
Q_{Li}	**3**	**2**	1/6	0
u_{Ri}	**3**	**1**	2/3	0
d_{Ri}	**3**	**1**	-1/3	0
L_{Li}	**1**	**2**	-1/2	0
e_{Ri}	**1**	**1**	-1	0
$Q_{L4}, \widetilde{Q}_{R4}$	**3**	**2**	1/6	1
$\tilde{u}_{L4}, u_{R4}$	**3**	**1**	2/3	-1
$\tilde{d}_{L4}, d_{R4}$	**3**	**1**	-1/3	-1
$L_{L4}, \widetilde{L}_{R4}$	**1**	**2**	-1/2	1
$\tilde{e}_{L4}, e_{R4}$	**1**	**1**	-1	-1
$\tilde{\nu}_{L4}, \nu_{R4}$	**1**	**1**	0	-1
ϕ	**1**	**1**	0	-1
H_u	**1**	**2**	-1/2	1
H_d	**1**	**2**	1/2	1

TABLE 3.2: Particle assignments under the $SU(3)_c \times SU(2)_L \times U(1)_Y \times U(1)'$ gauge symmetry in the theory of flavour with fermiophobic Z' , where $i = 1, 2, 3$.

couplings, in contrast with the simplified model presented in the previous section. The renormalisable mass terms involving charged fermions are then given by

$$\begin{aligned}\mathcal{L}_{\rm cf}^{\rm ren} &= y^u_{i4} H_u \overline{Q}_{Li} u_{R4} + y^d_{i4} H_d \overline{Q}_{Li} d_{R4} + y^e_{i4} H_d \overline{L}_{Li} e_{R4} \\ &+ y^u_{4i} H_u \overline{Q}_{L4} u_{Ri} + y^d_{4i} H_d \overline{Q}_{L4} d_{Ri} + y^e_{4i} H_d \overline{L}_{L4} e_{Ri} \\ &+ x^Q_i \phi \overline{Q}_{Li} \widetilde{Q}_{R4} + x^L_i \phi \overline{L}_{Li} \widetilde{L}_{R4} + x^u_i \phi \overline{\widetilde{u}}_{L4} u_{Ri} + x^d_i \phi \overline{\widetilde{d}}_{L4} d_{Ri} + x^e_i \phi \overline{\widetilde{e}}_{L4} e_{Ri} \\ &+ M^Q_4 \overline{Q}_{L4} \widetilde{Q}_{R4} + M^L_4 \overline{L}_{L4} \widetilde{L}_{R4} + M^u_4 \overline{\widetilde{u}}_{L4} u_{R4} + M^d_4 \overline{\widetilde{d}}_{L4} d_{R4} + M^e_4 \overline{\widetilde{e}}_{L4} e_{R4} + \text{h.c.}\,,\end{aligned} \tag{3.37}$$

where $i = 1, 2, 3$. Notice that the fact that both Higgs doublets are equally charged under $U(1)'$ while carrying opposite hypercharges not only forbids the SM-like Yukawa couplings, but also enforces a natural type II two Higgs doublet model (2HDM) that forbids tree-level FCNCs mediated by the Higgs doublets. The terms in the fourth line of the Lagrangian above are the arbitrary vector-like masses of the fourth family fermions. The terms in the third line provide mixing between chiral and vector-like fermions mediated by the singlet scalar ϕ when it acquires a VEV. Once chiral and vector-like fermions mix, the terms in the first and second lines provide effective Yukawa couplings for chiral fermions as $y \sim \langle\phi\rangle / M$, which are able to explain the origin of naturally small Yukawa couplings in the SM. As usual for a theory of flavour, the NP scales $\langle\phi\rangle$ and M may be anywhere *from the Planck scale to the electroweak scale*, as long as the ratios $\langle\phi\rangle / M$ are held fixed. However, flavour anomalies like $(g-2)_\mu$ might suggest that these NP scales are actually close to the TeV, as we shall consider here. In fact, the Z' boson only couples originally to vector-like fermions, but obtains effective couplings to chiral fermions via the same mixing that provides the effective Yukawa couplings, leading to a predictive phenomenology as we shall see.

3.3.2 Neutrino masses and the type Ib seesaw mechanism

The renormalisable Lagrangian for neutrinos includes the mass terms

$$\mathcal{L}_\nu^{\rm ren} = y^\nu_{i4} H_u \overline{L}_{Li} \nu_{R4} + \widetilde{y}^\nu_{i4} \widetilde{H}_d \overline{L}_{Li} \widetilde{\nu}^C_{L4} + M^\nu_4 \overline{\widetilde{\nu}}_{L4} \nu_{R4} + \text{h.c.} \tag{3.38}$$

where C denotes charge conjugation. Notice the unusual Yukawa coupling as the second term above, breaking lepton number and involving the second Higgs H_d, hinting that this is a different version of the usual type I seesaw mechanism. Indeed, one may have noticed that the choice of two Higgs doublets with opposite hypercharge but equal charges under $U(1)'$ forbids the usual Weinberg operator $(\overline{L}^C_L H)(L_L H)$, but allows for an alternative Weinberg operator involving the two Higgs doublets

$$\mathcal{L}_{\rm Weinberg} = c^\nu_{ij} (\overline{L}^C_{Li} H_u)(L_{Lj} \widetilde{H}_d) + \text{h.c.} \tag{3.39}$$

By simply assuming $M^\nu_4 \gg \langle H_{u,d} \rangle$ and integrating out the vector-like neutrino, one obtains the operator above and the coefficients c^ν_{ij} as

$$c^\nu_{ij} = \frac{1}{M^\nu_4} \left(y^\nu_{i4} \widetilde{y}^\nu_{j4} + \widetilde{y}^\nu_{i4} y^\nu_{j4} \right) . \tag{3.40}$$

After the Higgs doublets develop VEVs $\langle H_{u,d} \rangle = v_{u,d}/\sqrt{2}$, the Weinberg operator provides an effective mass matrix for active neutrinos as

$$m_\nu = \frac{v_u v_d}{2 M^\nu_4} \left(y^\nu_{i4} \widetilde{y}^\nu_{j4} + \widetilde{y}^\nu_{i4} y^\nu_{j4} \right) . \tag{3.41}$$

The Yukawa couplings above provide enough freedom to fit the observed PMNS mixing and neutrino mass splittings [62, 65], for both normal and inverted orderings. Of course if we arrange the various mass terms of Eq. (3.38) in matrix formalism as

$$\mathcal{L}_\nu^{\rm ren} = \frac{1}{2} \begin{pmatrix} \overline{L}_{Li} & \overline{\nu}^C_{R4} & \overline{\widetilde{\nu}}_{L4} \end{pmatrix} M^\nu \begin{pmatrix} L^C_{Li} \\ \nu_{R4} \\ \widetilde{\nu}^C_{L4} \end{pmatrix} + \text{h.c.} \,, \tag{3.42}$$

where

$$M^\nu = \begin{pmatrix} & L^C_{L1} & L^C_{L2} & L^C_{L3} & \nu_{R4} & \widetilde{\nu}^C_{L4} \\ \hline \overline{L}_{L1} & 0 & 0 & 0 & y^\nu_{14} H_u & \widetilde{y}^\nu_{14} \widetilde{H}_d \\ \overline{L}_{L2} & 0 & 0 & 0 & y^\nu_{24} H_u & \widetilde{y}^\nu_{24} \widetilde{H}_d \\ \overline{L}_{L3} & 0 & 0 & 0 & y^\nu_{34} H_u & \widetilde{y}^\nu_{34} \widetilde{H}_d \\ \overline{\nu}^C_{R4} & y^\nu_{14} H_u & y^\nu_{24} H_u & y^\nu_{34} H_u & 0 & M^\nu_4 \\ \overline{\widetilde{\nu}}_{L4} & \widetilde{y}^\nu_{14} \widetilde{H}_d & \widetilde{y}^\nu_{24} \widetilde{H}_d & \widetilde{y}^\nu_{34} \widetilde{H}_d & M^\nu_4 & 0 \end{pmatrix} \equiv \begin{pmatrix} 0_{3\times3} & m_{D\,3\times2} \\ m^{\rm T}_{D\,2\times3} & M_{N\,2\times2} \end{pmatrix} , \tag{3.43}$$

and now we apply the seesaw formula assuming $M_4^\nu \gg \langle H_{u,d}\rangle$, then we obtain the same result as

$$m_\nu \simeq m_D M_N^{-1} m_D^{\mathrm{T}} = \frac{v_u v_d}{2M_4^\nu}\left(y_{i4}^\nu \widetilde{y}_{j4}^\nu + \widetilde{y}_{i4}^\nu y_{j4}^\nu\right) . \tag{3.44}$$

This mechanism is denoted as *type Ib* seesaw mechanism [331]. Note that in Ref. [331] it was considered the possibility that the couplings $\widetilde{y}_{i4}^\nu$ are small, as they originate from an operator breaking lepton number. This scenario leads to a low scale seesaw with potentially large violations of unitarity of the leptonic mixing matrix. However, in this chapter we refrain to discuss further the neutrino sector, and instead we focus in the following on the origin of charged fermion masses and the associated Z' phenomenology.

3.3.3 Effective quark Yukawa couplings and messenger dominance

We may arrange the plethora of quark mass terms in Eq. (3.37) into a more convenient matrix formalism as

$$\mathcal{L}_q^{\mathrm{ren}} = \begin{pmatrix} \overline{Q}_{Li} & \overline{Q}_{L4} & \overline{\widetilde{u}}_{L4} \end{pmatrix} M^u \begin{pmatrix} u_{Ri} \\ u_{R4} \\ \widetilde{Q}_{R4} \end{pmatrix} + \begin{pmatrix} \overline{Q}_{Li} & \overline{Q}_{L4} & \overline{\widetilde{d}}_{L4} \end{pmatrix} M^d \begin{pmatrix} d_{Ri} \\ d_{R4} \\ \widetilde{Q}_{R4} \end{pmatrix} + \text{h.c.} \tag{3.45}$$

where $i = 1, 2, 3$ and

$$M^u = \left(\begin{array}{c|ccccc} & u_{R1} & u_{R2} & u_{R3} & u_{R4} & \widetilde{Q}_{R4} \\ \hline \overline{Q}_{L1} & 0 & 0 & 0 & y_{14}^u H_u & x_1^Q \phi \\ \overline{Q}_{L2} & 0 & 0 & 0 & y_{24}^u H_u & x_2^Q \phi \\ \overline{Q}_{L3} & 0 & 0 & 0 & y_{34}^u H_u & x_3^Q \phi \\ \overline{Q}_{L4} & y_{41}^u H_u & y_{42}^u H_u & y_{43}^u H_u & 0 & M_4^Q \\ \overline{\widetilde{u}}_{L4} & x_1^u \phi & x_2^u \phi & x_3^u \phi & M_4^u & 0 \end{array}\right) , \tag{3.46}$$

with M^d given by replacing $u \to d$ everywhere in the matrix above. Notice that since the upper 3×3 block of Eq. (3.46) contains zeros, the rotations of the first three families are so far unphysical. As a consequence, the Z' couplings to the first three families remain zero under such rotations. Therefore, we are free to rotate the first three families as we wish, in other words we are free to choose a convenient basis to start the diagonalisation process. For example, we are allowed to rotate Q_{L1} and Q_{L3} to set x_{14}^Q to zero and then rotate Q_{L2} and Q_{L3} to set x_{24}^Q to zero. We can apply similar rotations to u_{R1} and u_{R2} to set y_{41}^u to zero, and then we rotate u_{R2} and u_{R3} to set y_{42}^u to zero. We can repeat these rotations in the down sector to set y_{41}^d and y_{42}^d to zero. We can rotate as well Q_{L1} and Q_{L2} to set y_{14}^u to zero (note that in general $y_{14}^d \neq 0$ since the quark doublet rotations have all already been used up), and a similar rotation goes also for u_{R1} and

u_{R2} to switch off x^u_{41}. Finally, we rotate d_{R1} and d_{R2} to switch off x^d_{41}. In this basis, the matrices M^u and M^d become respectively

$$M^u = \begin{array}{c|ccccc} & u_{R1} & u_{R2} & u_{R3} & u_{R4} & \widetilde{Q}_{R4} \\ \hline \overline{Q}_{L1} & 0 & 0 & 0 & 0 & 0 \\ \overline{Q}_{L2} & 0 & 0 & 0 & y^u_{24}H_u & 0 \\ \overline{Q}_{L3} & 0 & 0 & 0 & y^u_{34}H_u & x^Q_3\phi \\ \overline{Q}_{L4} & 0 & 0 & y^u_{43}H_u & 0 & M^Q_4 \\ \overline{\widetilde{u}}_{L4} & 0 & x^u_2\phi & x^u_3\phi & M^u_4 & 0 \end{array} , \tag{3.47}$$

$$M^d = \begin{array}{c|ccccc} & d_{R1} & d_{R2} & d_{R3} & d_{R4} & \widetilde{Q}_{R4} \\ \hline \overline{Q}_{L1} & 0 & 0 & 0 & y^d_{14}H_d & 0 \\ \overline{Q}_{L2} & 0 & 0 & 0 & y^d_{24}H_d & 0 \\ \overline{Q}_{L3} & 0 & 0 & 0 & y^d_{34}H_d & x^Q_3\phi \\ \overline{Q}_{L4} & 0 & 0 & y^d_{43}H_d & 0 & M^Q_4 \\ \overline{\widetilde{d}}_{L4} & 0 & x^d_2\phi & x^d_3\phi & M^d_4 & 0 \end{array} . \tag{3.48}$$

There are several distinct mass scales in the mass matrices above: the VEVs of the Higgs doublets $\langle H_{u,d}\rangle$, the VEV of the scalar singlet $\langle\phi\rangle$ and the vector-like fourth family mass terms $M^{Q,u,d}_4$. Assuming the latter are much heavier than all the VEVs, we may integrate out the fourth family to generate effective Yukawa couplings for chiral quarks, as in the diagrams of Fig. 3.7. This is denoted as the *mass insertion approximation*, which provides the following effective Yukawa couplings for chiral quarks (see Appendix B)

$$m^u_{\text{eff}} \simeq y^u_{ij}\langle H_u\rangle = \begin{pmatrix} 0 & 0 & 0 \\ 0 & 0 & 0 \\ 0 & 0 & x^Q_3 y^u_{43} \end{pmatrix} \frac{\langle\phi\rangle}{M^Q_4}\langle H_u\rangle + \begin{pmatrix} 0 & 0 & 0 \\ 0 & y^u_{24}x^u_2 & y^u_{24}x^u_3 \\ 0 & y^u_{34}x^u_2 & y^u_{34}x^u_3 \end{pmatrix} \frac{\langle\phi\rangle}{M^u_4}\langle H_u\rangle , \tag{3.49}$$

$$m^d_{\text{eff}} \simeq y^d_{ij}\langle H_d\rangle = \begin{pmatrix} 0 & 0 & 0 \\ 0 & 0 & 0 \\ 0 & 0 & x^Q_3 y^d_{43} \end{pmatrix} \frac{\langle\phi\rangle}{M^Q_4}\langle H_d\rangle + \begin{pmatrix} 0 & y^d_{14}x^d_2 & y^d_{14}x^d_3 \\ 0 & y^d_{24}x^d_2 & y^d_{24}x^d_3 \\ 0 & y^d_{34}x^d_2 & y^d_{34}x^d_3 \end{pmatrix} \frac{\langle\phi\rangle}{M^d_4}\langle H_d\rangle . \tag{3.50}$$

By imposing the *dominance* of the doublet messenger fermions over the singlet messenger fermions [171], i.e.

$$M^Q_4 \ll M^{u,d}_4 , \tag{3.51}$$

then the first matrices in Eqs. (3.49) and (3.50) will dominate over the second ones, explaining the heaviness of third family quarks and the smallness of the CKM elements

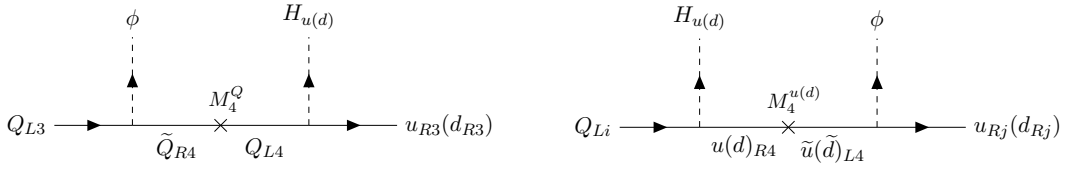

(A) (B)

FIGURE 3.7: Diagrams in the model which lead to the effective Yukawa couplings for second and third family fermions ($i, j = 2, 3$) in the mass insertion approximation.

V_{cb} and V_{ub}. In contrast, the Cabibbo angle is naturally larger and connected to the ratio y^d_{14}/y^d_{24}. Notice that in order to reproduce the smaller mass hierarchy in the down sector, we expect $M^u_4 < M^d_4$ such that V_{cb} and V_{ub} originate mostly from down-quark mixing. In addition, notice that the effective Yukawa matrices in Eqs. (3.49) and (3.50) consist of the sum of two rank 1 matrices, so the first family quarks are massless so far. Indeed, first family quark masses are protected by an accidental $U(1)^3$ flavour symmetry, that could be minimally broken in the UV to generate the tiny masses of the up-quark and down-quark, suggesting a multi-scale origin of flavour as discussed in Section 1.10. A simple way to achieve this is to introduce a heavy Higgs messenger uncharged under $U(1)'$ as $h(\mathbf{1}, \mathbf{2}, 1/2, 0)$, which does not get a VEV. The addition of such field allows to write new terms in the Lagrangian as

$$\begin{aligned}\mathcal{L}_h \supset\ & Y^u_{ij}\overline{Q}_{Li}\widetilde{h}u_{Rj} + Y^d_{ij}\overline{Q}_{Li}hd_{Rj} + Y^e_{ij}\overline{L}_{Li}he_{Rj} \\ & + \frac{1}{2}M_h^2 hh^\dagger + f^u h\phi H_u + f^d h^\dagger \phi H_d + \text{h.c.}\,,\end{aligned} \tag{3.52}$$

where the couplings $f^{u,d}$ carry mass dimensions, and we generally assume $f^{u,d} \sim M_h$. Assuming $\langle H_{u,d}\rangle \ll \langle\phi\rangle \ll M_h$, we are able to obtain effective Yukawa couplings for chiral quarks in the mass insertion approximation via the diagrams in Fig. 3.8,

$$Y'^u_{ij} = Y^u_{ij} f^u \frac{\langle\phi\rangle}{M_h^2}\,, \tag{3.53}$$

$$Y'^d_{ij} = Y^d_{ij} f^d \frac{\langle\phi\rangle}{M_h^2}\,, \tag{3.54}$$

which need to be added to the effective mass matrices in Eqs. (3.49) and (3.50). The new Higgs needs to be much heavier than the vector-like quarks in order to explain the smallness of first family quark masses, i.e. the *messenger dominance* of Eq. (3.51) is extended to

$$M^Q_4 \ll M^u_4 < M^d_4 \ll M_h\,. \tag{3.55}$$

Although Eqs. (3.53) and (3.54) generate 3×3 effective Yukawa matrices, the messenger dominance above implies that the matrices in Eqs. (3.49) and (3.50) dominate, explaining not only second and third family quark masses but also CKM mixing originated mostly from the down sector. The matrices in Eqs. (3.53) and (3.54) suppressed by the smaller

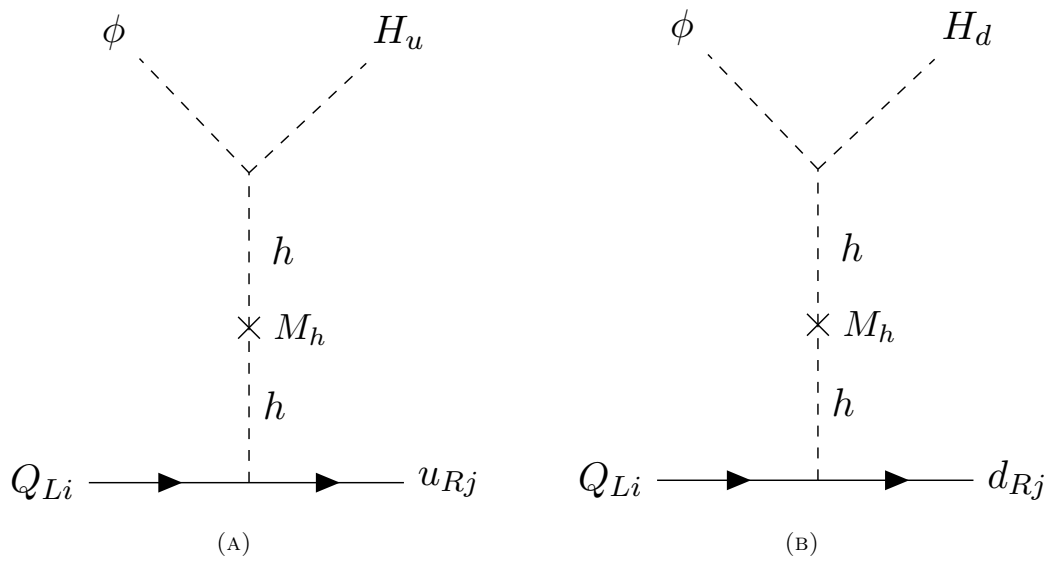

FIGURE 3.8: Diagrams in the model which lead to the masses of the up-quark and down-quark in the mass insertion approximation.

ratio $\langle\phi\rangle / M_h$ provide masses for the up-quark and down-quark, along with tiny 1-2 and 1-3 right-handed mixing in both the up and down sectors. Tiny 1-2 and 1-3 left-handed mixing in the up sector is negligible with respect to the larger down-quark mixing, giving a negligible contribution to the CKM matrix. Given that the masses of the up-quark and down-quark are very similar, the Yukawa couplings Y^u_{11} and Y^d_{11} can fit both masses with $\mathcal{O}(1)$ values.

Finally, notice that since the new Higgs is not charged under $U(1)'$, no effective Z' couplings for first family quarks are generated, hence the first family can be ignored for phenomenological purposes.

3.3.4 Effective quark Yukawa couplings beyond the mass insertion approximation

The mass insertion approximation discussed in the previous subsection works generally very well due to the smallness of Yukawa couplings in the SM, and is very useful for illustrative purposes. However, the mass insertion approximation breaks for the top Yukawa coupling which requires $\langle\phi\rangle / M_4^Q \sim 1$. Therefore, for the top-quark we need to go beyond and work in a large mixing angle formalism, as described in Appendix B. Assuming $\langle H_{u,d}\rangle \ll \langle\phi\rangle, M_4^{Q,u,d}$ we can block-diagonalise the matrices in Eqs. (3.47-3.48) via the transformations

$$V_{34}^{Q,u,d} = \begin{pmatrix} 1 & 0 & 0 & 0 \\ 0 & 1 & 0 & 0 \\ 0 & 0 & c_{34}^{Q,u,d} & s_{34}^{Q,u,d} \\ 0 & 0 & -s_{34}^{Qu,d} & c_{34}^{Q,u,d} \end{pmatrix}, \quad V_{24}^{u,d} = \begin{pmatrix} 1 & 0 & 0 & 0 \\ 0 & c_{24}^{u,d} & 0 & s_{24}^{u,d} \\ 0 & 0 & 1 & 0 \\ 0 & -s_{24}^{u,d} & 0 & c_{24}^{u,d} \end{pmatrix}, \tag{3.56}$$

where

$$s_{34}^{Q} = \frac{x_3^Q \langle\phi\rangle}{\sqrt{\left(x_3^Q \langle\phi\rangle\right)^2 + \left(M_4^Q\right)^2}}\,, \qquad s_{24}^{u,d} = \frac{x_2^{u,d} \langle\phi\rangle}{\sqrt{\left(x_2^{u,d} \langle\phi\rangle\right)^2 + \left(M_4^{u,d}\right)^2}}\,, \tag{3.57}$$

$$s_{34}^{u,d} = \frac{x_3^{u,d} \langle\phi\rangle}{\sqrt{\left(x_2^{u,d} \langle\phi\rangle\right)^2 + \left(x_3^{u,d} \langle\phi\rangle\right)^2 + \left(M_4^{u,d}\right)^2}}\,.$$

The 3-4 and 2-4 rotations above introduce zeros in the fifth rows and columns of Eqs. (3.47-3.48), by absorbing the $x_i^{Q,u,d} \langle\phi\rangle$ factors into a redefinition of the vector-like masses as

$$\hat{M}_4^Q = \sqrt{\left(x_3^Q \langle\phi\rangle\right)^2 + \left(M_4^Q\right)^2}\,, \tag{3.58}$$

$$\hat{M}_4^{u,d} = \sqrt{\left(x_2^{u,d} \langle\phi\rangle\right)^2 + \left(x_3^{u,d} \langle\phi\rangle\right)^2 + \left(M_4^{u,d}\right)^2}\,, \tag{3.59}$$

which are indeed the physical masses of the vector-like fermions valid for arbitrary $\langle\phi\rangle$ and $M_4^{Q,u,d}$ (as long as $\langle H_{u,d}\rangle \ll \langle\phi\rangle\,, M_4^{Q,u,d}$). Therefore, in the basis (primed) obtained after applying the rotations in Eq. (3.56) the fourth family is effectively decoupled, and the total mass matrices are

$$M^u = \begin{pmatrix} & u'_{R1} & u'_{R2} & u'_{R3} & u'_{R4} & \widetilde{Q'}_{R4} \\ \hline \overline{Q'}_{L1} & & & & & 0 \\ \overline{Q'}_{L2} & & & & & 0 \\ \overline{Q'}_{L3} & & & y'^u_{\alpha\beta} H_u & & 0 \\ \overline{Q'}_{L4} & & & & & \hat{M}_4^Q \\ \overline{\widetilde{u'}}_{L4} & 0 & 0 & 0 & \hat{M}_4^u & 0 \end{pmatrix}\,, \tag{3.60}$$

with M^d given by replacing $u \to d$ everywhere in the matrix above. The effective Yukawa couplings $y'^{u,d}_{\alpha\beta}$ are given by

$$y'^u_{\alpha\beta} = \left(V_{34}^Q\right)^\dagger \begin{pmatrix} 0 & 0 & 0 & 0 \\ 0 & 0 & 0 & y_{24}^u H_u \\ 0 & 0 & 0 & y_{34}^u H_u \\ 0 & 0 & y_{43}^u H_u & 0 \end{pmatrix} V_{24}^u V_{34}^u\,, \tag{3.61}$$

$$y'^{d}_{\alpha\beta} = \left(V^{Q}_{34}\right)^{\dagger} \begin{pmatrix} 0 & 0 & 0 & y^{d}_{14}H_d \\ 0 & 0 & 0 & y^{d}_{24}H_d \\ 0 & 0 & 0 & y^{d}_{34}H_d \\ 0 & 0 & y^{d}_{43}H_d & 0 \end{pmatrix} V^{d}_{24}V^{d}_{34}\,. \tag{3.62}$$

After performing the algebra we obtain,

$$m^{u}_{\text{eff}} = y'^{u}_{ij}\langle H_u\rangle = \begin{pmatrix} 0 & 0 & 0 \\ 0 & 0 & 0 \\ 0 & 0 & y^{u}_{43}c^{u}_{34}s^{Q}_{34} \end{pmatrix}\langle H_u\rangle + \begin{pmatrix} 0 & 0 & 0 \\ 0 & y^{u}_{24}s^{u}_{24} & y^{u}_{24}c^{u}_{24}s^{u}_{34} \\ 0 & y^{u}_{34}c^{Q}_{34}s^{u}_{24} & y^{u}_{34}c^{Q}_{34}c^{u}_{24}s^{u}_{34} \end{pmatrix}\langle H_u\rangle\,, \tag{3.63}$$

$$m^{d}_{\text{eff}} = y'^{d}_{ij}\langle H_d\rangle = \begin{pmatrix} 0 & 0 & 0 \\ 0 & 0 & 0 \\ 0 & 0 & y^{d}_{43}c^{d}_{34}s^{Q}_{34} \end{pmatrix}\langle H_d\rangle + \begin{pmatrix} 0 & y^{d}_{14}s^{d}_{24} & y^{d}_{14}c^{d}_{24}s^{d}_{34} \\ 0 & y^{d}_{24}s^{d}_{24} & y^{d}_{24}c^{d}_{24}s^{d}_{34} \\ 0 & y^{d}_{34}c^{Q}_{34}s^{d}_{24} & y^{d}_{34}c^{Q}_{34}c^{d}_{24}s^{d}_{34} \end{pmatrix}\langle H_d\rangle\,, \tag{3.64}$$

where, if we take the limit $\langle\phi\rangle \ll M_4^{Q,u,d}$ in Eq. (3.57) to obtain $s_{i4}^{Q,u,d} \approx x_i^{Q,u,d}\langle\phi\rangle/M_4^{Q,u,d}$, then the results in the mass insertion approximation as shown in the previous subsection are recovered. However, we shall continue working in the large mixing angle formalism to account for $\langle\phi\rangle/M_4^{Q} \sim 1$ as required to address the large top Yukawa coupling.

Since the angles $s_{34}^{u,d}$ need to be small in order to explain the smallness of V_{cb}, we are left with s_{34}^{Q}, the Higgs VEVs $\langle H_{u,d}\rangle$ and the couplings $y_{43}^{u,d}$ to fit the top and bottom masses. The hierarchy m_b/m_t could be explained either by having an unnaturally small $y_{43}^{d} \sim 0.01$ coupling, or by assuming that the ratio of Higgs VEVs $\tan\beta = v_u/v_d$ is large. We follow this second path, taking a large 3-4 mixing $s_{34}^{Q} \sim 1/\sqrt{2}$ in order to explain the large top Yukawa. By taking $\tan\beta = v_u/v_d \approx 30$ we have $y_{43}^{d} \approx 1$ and $y_{43}^{u} \approx \sqrt{2} \approx 1.4$, which are reasonable values. Notice that $s_{34}^{Q} \sim 1/\sqrt{2}$ requires $M_4^{Q} \sim \langle\phi\rangle$, hinting to the existence of a relatively light vector-like quark, within the reach of the LHC.

The smallness of m_c and m_s can be naturally explained by taking small mixing angles $s_{24}^{u,d}$. In particular, we find $s_{24}^{u} \sim 0.01$ and $s_{24}^{d} \sim 0.02$ to deliver a good fit of m_c and m_s. In this manner, we expect $s_{34}^{u,d}$ of similar order because they live at the same scale. Therefore, given that only s_{34}^{Q} is large while all the other angles are small, we can apply the limit $\langle\phi\rangle \ll M_4^{u,d}$ to recover the expressions in the mass insertion approximation as

$$m^{u}_{\text{eff}} = y'^{u}_{ij}\langle H_u\rangle = \begin{pmatrix} 0 & 0 & 0 \\ 0 & 0 & 0 \\ 0 & 0 & y^{u}_{43}c^{u}_{34}s^{Q}_{34} \end{pmatrix}\langle H_u\rangle + \begin{pmatrix} 0 & 0 & 0 \\ 0 & y^{u}_{24}x^{u}_{2} & y^{u}_{24}x^{u}_{3} \\ 0 & y^{u}_{34}c^{Q}_{34}x^{u}_{2} & y^{u}_{34}c^{Q}_{34}x^{u}_{3} \end{pmatrix}\frac{\langle\phi\rangle}{M^{d}_{4}}\langle H_u\rangle \tag{3.65}$$

$$+\begin{pmatrix} Y^u_{11} & Y^u_{12} & Y^u_{13} \\ Y^u_{21} & Y^u_{22} & Y^u_{23} \\ Y^u_{31}c^Q_{34} & Y^u_{32}c^Q_{34} & Y^u_{33}c^Q_{34} \end{pmatrix} f^u \frac{\langle\phi\rangle}{M_h^2}\langle H_u\rangle \ ,$$

$$m^d_{\text{eff}} = y'^d_{ij}\langle H_d\rangle = \begin{pmatrix} 0 & 0 & 0 \\ 0 & 0 & 0 \\ 0 & 0 & y^d_{43}c^d_{34}s^Q_{34} \end{pmatrix}\langle H_d\rangle + \begin{pmatrix} 0 & y^d_{14}x^d_2 & y^d_{14}x^d_3 \\ 0 & y^d_{24}x^d_2 & y^d_{24}x^d_3 \\ 0 & y^d_{34}c^Q_{34}x^d_2 & y^d_{34}c^Q_{34}x^d_3 \end{pmatrix}\frac{\langle\phi\rangle}{M_4^d}\langle H_d\rangle \tag{3.66}$$

$$+\begin{pmatrix} Y^d_{11} & Y^d_{12} & Y^d_{13} \\ Y^d_{21} & Y^d_{22} & Y^d_{23} \\ Y^d_{31}c^Q_{34} & Y^d_{32}c^Q_{34} & Y^d_{33}c^Q_{34} \end{pmatrix} f^d \frac{\langle\phi\rangle}{M_h^2}\langle H_d\rangle \ ,$$

where we have also included the contributions from the heavy Higgs messengers that provide the mass of the up-quark and down-quark, plus negligible up-quark mixing and right-handed down-quark mixing.

3.3.5 Effective charged lepton Yukawa couplings

Having discussed in detail the origin of quark mass hierarchies and mixing, we now build the charged lepton sector in a similar way. We construct the full charged lepton mass matrix as

$$\mathcal{L}^{\text{ren}}_q = \begin{pmatrix} \overline{L}_{Li} & \overline{L}_{L4} & \overline{\widetilde{e}}_{L4} \end{pmatrix} M^e \begin{pmatrix} e_{Ri} \\ e_{R4} \\ \widetilde{L}_{R4} \end{pmatrix} + \text{h.c.}\,, \tag{3.67}$$

where

$$M^e = \begin{pmatrix} & e_{R1} & e_{R2} & e_{R3} & e_{R4} & \widetilde{L}_{R4} \\ \hline \overline{L}_{L1} & 0 & 0 & 0 & 0 & 0 \\ \overline{L}_{L2} & 0 & 0 & 0 & y^e_{24}H_d & 0 \\ \overline{L}_{L3} & 0 & 0 & 0 & y^e_{34}H_d & x^L_3\phi \\ \overline{L}_{L4} & 0 & 0 & y^e_{43}H_d & 0 & M^L_4 \\ \overline{\widetilde{e}}_{L4} & 0 & x^e_2\phi & x^e_3\phi & M^e_4 & 0 \end{pmatrix} \tag{3.68}$$

where we have already taking advantage of the upper 3×3 zeros to perform suitable rotations of the first family fields that introduce extra zeros in the full mass matrix without loss generality, as we did in the quark sector (see Eqs. (3.47-3.48) and the discussion therein). Here we work directly in the large mixing angle formalism as in

Section 3.3.4, because we are seeking for large mixing angles in the charged lepton sector that will contribute to large Z' couplings for $(g-2)_\mu$. Assuming $\langle H_d\rangle \ll \langle\phi\rangle, M_4^{L,e}$ we can block-diagonalise the matrix in Eq. (3.68) via the transformations

$$V_{34}^{L,e} = \begin{pmatrix} 1 & 0 & 0 & 0 \\ 0 & 1 & 0 & 0 \\ 0 & 0 & c_{34}^{L,e} & s_{34}^{L,e} \\ 0 & 0 & -s_{34}^{L,e} & c_{34}^{L,e} \end{pmatrix}, \qquad V_{24}^{e} = \begin{pmatrix} 1 & 0 & 0 & 0 \\ 0 & c_{24}^{e} & 0 & s_{24}^{e} \\ 0 & 0 & 1 & 0 \\ 0 & -s_{24}^{e} & 0 & c_{24}^{e} \end{pmatrix}, \tag{3.69}$$

where

$$s_{34}^{L} = \frac{x_3^L \langle\phi\rangle}{\sqrt{\left(x_3^L \langle\phi\rangle\right)^2 + \left(M_4^L\right)^2}}, \qquad s_{24}^{e} = \frac{x_2^e \langle\phi\rangle}{\sqrt{\left(x_2^e \langle\phi\rangle\right)^2 + \left(M_4^e\right)^2}}, \tag{3.70}$$
$$s_{34}^{e} = \frac{x_3^e \langle\phi\rangle}{\sqrt{\left(x_2^e \langle\phi\rangle\right)^2 + \left(x_3^e \langle\phi\rangle\right)^2 + \left(M_4^e\right)^2}}.$$

The 3-4 and 2-4 rotations above introduce zeros in the fifth row and column of Eq. (3.68), by absorbing the $x_i^{L,e}\langle\phi\rangle$ factors into a redefinition of the vector-like masses as

$$\hat{M}_4^L = \sqrt{\left(x_3^L \langle\phi\rangle\right)^2 + \left(M_4^L\right)^2}, \tag{3.71}$$
$$\hat{M}_4^e = \sqrt{\left(x_2^e \langle\phi\rangle\right)^2 + \left(x_3^e \langle\phi\rangle\right)^2 + \left(M_4^e\right)^2}, \tag{3.72}$$

in complete analogy with the situation in the quark sector. Therefore, in the basis (primed) obtained after applying the rotations in Eq. (3.69) the fourth family is effectively decoupled, and the total mass matrix is similar to the up-quark mass matrix in Eq. (3.60). The effective Yukawa couplings can then be readily extracted as

$$m_{\text{eff}}^e = y_{ij}'^e \langle H_d\rangle = \begin{pmatrix} 0 & 0 & 0 \\ 0 & 0 & 0 \\ 0 & 0 & y_{43}^e c_{34}^e s_{34}^L \end{pmatrix} \langle H_d\rangle + \begin{pmatrix} 0 & 0 & 0 \\ 0 & y_{24}^e s_{24}^e & y_{24}^e c_{24}^e s_{34}^e \\ 0 & y_{34}^e c_{34}^L s_{24}^e & y_{34}^e c_{34}^L c_{24}^e s_{34}^e \end{pmatrix} \langle H_d\rangle . \tag{3.73}$$

Notice that the electron remains massless so far, however it can get a mass at the scale of the up-quark and down-quark masses via the heavy Higgs h, in complete analogy with the quark sector as discussed in Eqs. (3.53-3.54) and paragraphs therein. However, in order to explain the smallness of the electron mass with respect to the masses of first family quarks, we would need a small dimensionless coupling at the 10% level. This could be avoided by adding another Higgs h' a bit heavier than h which generates the smaller mass of the electron, without generating any effective couplings to the Z' boson, such that the related phenomenology is dominated by the 2-3 sector. Therefore, in the following we ignore the first family and proceed with our discussion of the 2-3 sector.

Given that we have enforced $\tan\beta = v_u/v_d \approx 30$ in our discussion of the quark sector, we need $s^L_{34} \approx 0.3$ to explain the tau mass, and $s^e_{24} \approx 0.02$ to explain the muon mass. Therefore, the charged fermion mass hierarchies are explained by the messenger dominance $M^L_4 \ll M^e_4$, which then predicts that s^e_{34} is of a similar order than s^e_{24}. By taking $s^e_{34} \approx 0.02$ and assuming $y^e_{43} \approx y^e_{24} \approx 1$, we obtain a significant 2-3 left-handed charged lepton mixing as $s^{e_L}_{23} \approx s^e_{34}/s^L_{34} \approx 0.07$. Similarly, by taking $y^e_{34} \approx 1$ we obtain significant 2-3 right-handed charged lepton mixing as $s^{e_R}_{23} \approx s^e_{24}/s^L_{34} \approx 0.07$. This non-vanishing 2-3 mixing will be very relevant for the low-energy phenomenology. On the one hand, it will generate effective couplings to left-handed muons necessary to give a contribution to $(g-2)_\mu$, which would otherwise vanish, and on the other hand it will induce lepton flavour-violating transitions such as $\tau \to \mu\gamma$.

3.3.6 Effective Z' couplings

Since all chiral fermions are uncharged under $U(1)'$, in the interaction basis the massive Z' boson only couples to the fourth family vector-like fermions,

$$\mathcal{L}_{Z'} \supset g' \left(\overline{Q}_L D_Q \gamma^\mu Q_L + \overline{u}_R D_u \gamma^\mu u_R + \overline{d}_R D_d \gamma^\mu d_R + \overline{L}_L D_L \gamma^\mu L_L + \overline{\ell}_R D_\ell \gamma^\mu \ell_R \right) Z'_\mu \,, \tag{3.74}$$

where we are ignoring couplings to the conjugate (tilde) fermions, because so far they do not mix with chiral fermions and so are not relevant for the low-energy phenomenology. We are also ignoring couplings to vector-like neutrinos, assuming that they are very heavy and decoupled from low-energy phenomenology, as suggested by the type Ib seesaw mechanism implemented in Section 3.3.2. We have defined 4-component vectors including the four families (3 chiral families plus the fourth vector-like), and the D_ψ matrices are defined as

$$D_Q = D_L = \mathrm{diag}(0,0,0,1)\,, \tag{3.75}$$

$$D_u = D_d = D_e = \mathrm{diag}(0,0,0,-1)\,. \tag{3.76}$$

The same rotations that diagonalise the full mass matrices in Sections 3.3.4 and 3.3.5 need to be applied now in order to go to the basis of mass eigenstates. For illustrative purposes, one can see the diagrams in Fig. 3.2 that provided effective Z' couplings in the mass insertion approximation for the simplified model. In contrast, here we shall work in the more general large mixing angle formalism, even though most of the mixing angles turn out to be small. Up to the effects of chiral fermion mixing, we obtain

$$(V^{Q,L}_{34})^\dagger D_{Q,L} V^{Q,L}_{34} = \begin{pmatrix} 0 & 0 & 0 & 0 \\ 0 & 0 & 0 & 0 \\ 0 & 0 & (s^{Q,L}_{34})^2 & -c^{Q,L}_{34} s^{Q,L}_{34} \\ 0 & 0 & -c^L_{34} s^{Q,L}_{34} & (c^{Q,L}_{34})^2 \end{pmatrix}, \tag{3.77}$$

$$(V_{24}^{u,d,e}V_{34}^{u,d,e})^\dagger D_{u,d,e}V_{24}^{u,d,e}V_{34}^{u,d,e} = -\begin{pmatrix} 0 & 0 & 0 & 0 \\ 0 & (s_{24}^{e_R})^2 & s_{24}^{e_R}s_{34}^{e_R} & c_{34}^{e_R}c_{24}^{e_R}s_{24}^{e_R} \\ 0 & s_{24}^{e_R}s_{34}^{e_R} & (c_{24}^{e_R}s_{34}^{e_R})^2 & -c_{34}^{e_R}(c_{24}^{e_R})^2 s_{34}^{e_R} \\ 0 & c_{34}^{e_R}c_{24}^{e_R}s_{24}^{e_R} & -c_{34}^{e_R}(c_{24}^{e_R})^2 s_{34}^{e_R} & (c_{24}^{e_R}c_{34}^{e_R})^2 \end{pmatrix}. \tag{3.78}$$

Notice that the same mixing that provides the effective Yukawa couplings also leads to effective Z' couplings for chiral fermions. In the left-handed sector only the third family (and fourth) couples to the Z' so far, but effective couplings to the second family are introduced when 2-3 chiral fermion mixing is considered, splitting the $SU(2)_L$ doublets and leading to

$$\begin{aligned} &(V_{34}^{Q}V_{23}^{u_L,d_L})^\dagger D_{u_L,d_L}V_{34}^{Q}V_{23}^{u_L,d_L} \\ &= \begin{pmatrix} 0 & 0 & 0 & 0 \\ 0 & (s_{34}^{Q}s_{23}^{u_L,d_L})^2 & -(s_{34}^{Q})^2 c_{23}^{u_L,d_L}s_{23}^{u_L,d_L} & c_{34}^{Q}s_{34}^{Q}s_{23}^{u_L,d_L} \\ 0 & -(s_{34}^{Q})^2 c_{23}^{u_L,d_L}s_{23}^{u_L,d_L} & (s_{34}^{Q}c_{23}^{u_L,d_L})^2 & -c_{34}^{Q}s_{34}^{Q}c_{23}^{u_L,d_L} \\ 0 & c_{34}^{Q}s_{34}^{Q}s_{23}^{u_L,d_L} & -c_{34}^{Q}s_{34}^{Q}c_{23}^{u_L,d_L} & (c_{34}^{Q})^2 \end{pmatrix}, \end{aligned} \tag{3.79}$$

$$\begin{aligned} &(V_{34}^{L}V_{23}^{e_L})^\dagger D_{e_L}V_{34}^{L}V_{23}^{e_L} \\ &= \begin{pmatrix} 0 & 0 & 0 & 0 \\ 0 & (s_{34}^{L}s_{23}^{e_L})^2 & -(s_{34}^{L})^2 c_{23}^{e_L}s_{23}^{e_L} & c_{34}^{L}s_{34}^{L}s_{23}^{e_L} \\ 0 & -(s_{34}^{L})^2 c_{23}^{e_L}s_{23}^{e_L} & (s_{34}^{L}c_{23}^{e_L})^2 & -c_{34}^{L}s_{34}^{L}c_{23}^{e_L} \\ 0 & c_{34}^{L}s_{34}^{L}s_{23}^{e_L} & -c_{34}^{L}s_{34}^{L}c_{23}^{e_L} & (c_{34}^{L})^2 \end{pmatrix}. \end{aligned} \tag{3.80}$$

The origin of first family masses is connected to the much heavier Higgs messengers that are uncharged under $U(1)'$, providing no effective Z' couplings to first family fermions. These would arise via chiral fermion mixing, but will be further suppressed by powers of small mixing angles so that we can safely neglect them. When we include 2-3 chiral fermion mixing for right-handed chiral fermions, the expressions for the D_{u_R,d_R,e_R} matrices become very lengthy. Since only the charged lepton sector is relevant for $(g-2)_\mu$, we shall include below the explicit Z' couplings for charged leptons as

$$g_{\mu\mu}^R = -g'(s_{24}^{e_R}c_{23}^{e_R} - c_{24}^{e_R}s_{34}^{e_R}s_{23}^{e_R})^2\,, \tag{3.81}$$

$$g_{\tau\tau}^R = -g'(s_{24}^{e_R}s_{23}^{e_R} + c_{24}^{e_R}s_{34}^{e_R}c_{23}^{e_R})^2\,, \tag{3.82}$$

$$g_{\mu\tau}^R = g'(s_{24}^{e_R}c_{23}^{e_R} - c_{24}^{e_R}s_{34}^{e_R}s_{23}^{e_R})(s_{24}^{e_R}s_{23}^{e_R} + c_{24}^{e_R}s_{34}^{e_R}c_{23}^{e_R})\,, \tag{3.83}$$

$$g_{\mu E}^R = g'c_{34}^{e_R}c_{24}^{e_R}(c_{23}^{e_R}s_{24}^{e_R} - c_{24}^{e_R}s_{34}^{e_R}s_{23}^{e_R})\,, \tag{3.84}$$

$$g_{\tau E}^R = g'c_{34}^{e_R}c_{24}^{e_R}(s_{24}^{e_R}s_{23}^{e_R} + c_{24}^{e_R}c_{23}^{e_R}s_{34}^{e_R})\,, \tag{3.85}$$

$$g_{EE}^{R} = -g'(c_{24}^{e_R} c_{34}^{e_R})^2 \,, \tag{3.86}$$

defined as in the Lagrangian of Eq. (3.14). In the next section we shall study the phenomenology of the model, with particular attention to the lepton sector and $(g-2)_\mu$.

3.4 Phenomenology of the flavour model

3.4.1 $B_s - \bar{B}_s$ mixing

The effective Z' couplings of the flavour model in the previous section naturally contribute to flavour-violating 2-3 transitions. Assuming that the CKM mixing originates from the down sector as discussed in Section 3.3.3, and neglecting the small Z' couplings to right-handed quarks which are suppressed by the heavier messengers, then the model predicts a significant tree-level contribution to the operator $\mathcal{Q}_1^{bs}$ contributing to $B_s - \bar{B}_s$ meson mixing (see Section 2.3.4). We obtain the bound

$$C_1^{bs} = \frac{\left(g_{bs}^{L}\right)^2}{M_{Z'}^2} \simeq \frac{\left(g'(s_{34}^{Q})^2 V_{cb}\right)^2}{M_{Z'}^2} \lesssim \frac{1}{(225\,\text{TeV})^2} \,. \tag{3.87}$$

The mixing angle s_{34}^{Q} needs to be large in order to explain the heaviness of the top mass. In particular, perturbativity of the Yukawa coupling $y_{43}^{u} \lesssim \sqrt{4\pi}$ imposes $s_{34}^{Q} \gtrsim 0.285$, which translates to the lower 95% CL bound $M_{Z'}/g' \gtrsim 750\,\text{GeV}$ via $B_s - \bar{B}_s$ meson mixing. In contrast, if we take $y_{43}^{u} \approx \sqrt{2}$ then we require $s_{34}^{Q} \approx 1/\sqrt{2}$ as discussed in Section 3.3.4, which translates into a bound $M_{Z'}/g' \gtrsim 4.5\,\text{TeV}$.

3.4.2 B-physics: $R_{K^{(*)}}$ and $B_s \to \mu\mu$

In our model, the effective Z' couplings are connected to the origin of flavour hierarchies in the SM. Therefore, the effective Z' couplings break lepton flavour universality in a similar manner as the usual Yukawa couplings do in the SM. Our Z' is mostly coupled to third family left-handed fermions, while couplings to light fermions are induced via small chiral fermion mixing in the left-handed sector, or via small mixing angles connected to the origin of second family masses in the right-handed sector. The smallest Z' couplings are then found for first family fermions, suppressed by powers of small mixing angles.

This explicit breaking of lepton flavour universality was suggested as a possible explanation of the $R_{K^{(*)}}$ anomalies [163], but it was soon concluded that providing a significant contribution to the $R_{K^{(*)}}$ ratios was either in conflict with the combined bounds from $B_s - \bar{B}_s$ meson mixing and $\tau \to 3\mu$ [332], or required the vector-like leptons to mix predominantly with muons rather than taus, disposing of the natural explanation of charged lepton mass hierarchies [163].

After the recent update by LHCb [185], the $R_{K^{(*)}}$ ratios are now in agreement with the SM but leaving some space for NP contributions. In our model, we can safely neglect very small contributions to $\mathcal{O}_9^{ee}$ and $\mathcal{O}_{10}^{ee}$, and consider only the contributions

to the operators $\mathcal{O}_9^{\mu\mu}$ and $\mathcal{O}_{10}^{\mu\mu}$ obtained as (see Section 2.3.1 for the definition of the operators)

$$C_9^{\mu\mu} = -\frac{2\pi}{\alpha_{\rm EM}(V_{tb}V_{ts})^*}\frac{\sqrt{2}}{4G_F}\frac{\left(g_{bs}^L g_{\mu\mu}^L + g_{bs}^L g_{\mu\mu}^R\right)}{M_{Z'}^2}\,, \tag{3.88}$$

$$C_{10}^{\mu\mu} = -\frac{2\pi}{\alpha_{\rm EM}(V_{tb}V_{ts})^*}\frac{\sqrt{2}}{4G_F}\frac{\left(-g_{bs}^L g_{\mu\mu}^L + g_{bs}^L g_{\mu\mu}^R\right)}{M_{Z'}^2}\,. \tag{3.89}$$

The $R_{K^{(*)}}$ ratios are then computed via Eqs. (2.11-2.12). The effective Z' couplings above involving second family fermions are generally suppressed by small mixing angles, in such a way that for the typical configurations of mixing angles in the model (see Sections 3.3.4 and 3.3.5) we obtain at 95% CL $M_{Z'}/g' \gtrsim 350$ GeV. The Wilson coefficient $C_{10}^{\mu\mu}$ also contributes to $\mathcal{B}(B_s \to \mu\mu)$, however we find the obtained bounds to be generally smaller than those from $R_{K^{(*)}}$, obtaining for the typical benchmark of the model $M_{Z'}/g' \gtrsim 270$ GeV at 95% CL. Going beyond the benchmark discussed in Sections 3.3.4 and 3.3.5, as it might be required by the $(g-2)_\mu$ anomaly, these bounds could become more significant if we consider larger mixing angles in the charged lepton sector. In this manner, we do not expect that our model can provide significant contributions to $b \to s\mu\mu$ without entering in conflict with the $R_{K^{(*)}}$ ratios.

Given that the Z' boson is mostly coupled to third family fermions, we have studied the enhancement of $b \to s\tau\tau$ and $b \to s\nu\nu$. However, in both cases we find that any significant enhancement is in tension with bounds from $B_s - \bar{B}_s$ mixing over the $\bar{s}bZ'$ coupling. For example, we find that $\mathcal{B}(B \to K^{(*)}\nu\bar{\nu})$ can be enhanced just by a 10% factor over the SM prediction (similar to the conclucion of [333]), making impossible to provide a significant contribution that ameliorates the 2.8σ tension in the recent measurement by Belle II [81].

3.4.3 Collider searches

The Z' boson is produced at the LHC mainly via the partonic process $b\bar{b} \to Z'$, because couplings to light quarks are heavily suppressed by powers of small mixing angles. Then it decays mostly to third families fermions, and to a lesser extent to second family fermions. Other modes such as $Z' \to W^+W^-$ and $Z' \to Zh$ arise from $Z - Z'$ mixing. Assuming kinetic mixing is not generated at tree-level (e.g. if $U(1)_Y$ and $U(1)'$ originate from different semi-simple groups), then $Z - Z'$ mixing may still be generated at 1-loop mediated by $H_{u,d}$ and the VL fermions which are charged under both $U(1)$s (as discussed in Section 3.2.4), or via the VEVs of $H_{u,d}$ but carrying a suppression of $\sim M_Z^2/M_{Z'}^2$. In either case, we find the modes $Z' \to WW$ and $Z' \to Zh$ to be sufficiently suppressed and the bounds extracted from the experimental searches [334, 335] are not competitive with those obtained from the Drell-Yan modes.

We have prepared the UFO file of the model using `FeynRules` [336], and then we have computed the Z' production cross section from 13 TeV pp collisions using `Madgraph5` [337] with the default PDF `NNPDF23LO`. We estimated analytically the decay

width to fermion modes as

$$\Gamma(Z' \to f_\alpha \overline{f}_\beta) = \frac{N_c}{24\pi} M_{Z'} \left((g^L_{f_\alpha f_\beta})^2 + (g^R_{f_\alpha f_\beta})^2 \right) , \tag{3.90}$$

where $N_c = 3$ (quarks), 1 (leptons). We assume that decays into vector-like fermions are kinematically forbidden or suppressed, and we treat the top-quark separately due to its larger mass,

$$\Gamma(Z' \to t\bar{t}) = \frac{1}{8\pi} M_{Z'} \left((g^L_{tt})^2 + (g^R_{tt})^2 \right) \left(1 - \frac{m_t^2}{M_{Z'}^2} \right) \sqrt{\left(1 - \frac{4m_t^2}{M_{Z'}^2} \right)} , \tag{3.91}$$

and finally the branching fraction is estimated as $\mathcal{B}(Z' \to f_\alpha \overline{f}_\beta) = \Gamma(Z' \to f_\alpha \overline{f}_\beta)/\Gamma(Z' \to$ all). In the natural benchmark for the flavour model we find the total decay width to be narrow $\Gamma_{Z'}/M_{Z'} \sim \mathcal{O}(1\%)$, as the Z' couplings to light families are generally suppressed and decays to VL fermions are kinematically forbidden. In the next section we will tune $s_{24}^{e_R}$ to be large in order to get a larger coupling to muons, in this case we find $\Gamma_{Z'}/M_{Z'} \sim 5\%$.

We compute the total cross section by applying the narrow width approximation $\sigma(pp \to Z' \to f_\alpha \overline{f}_\beta) \approx \sigma(pp \to Z')\mathcal{B}(Z' \to f_\alpha \overline{f}_\beta)$. We confront our results with the limits from the most recent light dilepton resonance searches by ATLAS [338] and CMS [339] in order to obtain 95% CL exclusion bounds. However, given that the Z' is mostly coupled to third family fermions, the bounds from ditau [340] and ditop [341] searches generally dominate over the light dilepton searches. For the benchmark values motivated in Sections 3.3.4 and 3.3.5 to explain the origin of flavour hierarchies, we obtain that the most stringent bounds come from ditau searches (despite the lesser integrated luminosity of this analysis), leading to $M_{Z'} \gtrsim 1.1$ TeV for $g' \approx 1$ at 95% CL. However, as we shall see in the next subsection, if we increase the mixing angles of the lepton sector in our seek for explaining $(g-2)_\mu$, the light dilepton searches become more constraining than ditau and ditop searches.

Finally we comment on vector-like fermion searches. In order to explain fermion mass hierarchies, we expect most of the vector-like fermions to be much heavier than the Z' boson, and only Q_4 and L_4 may live at the TeV scale. Current bounds on vector-like quark masses lie around 1 TeV, however the strongest bounds are usually model dependent (see e.g. [342]). Therefore, while L_4 most likely escapes detection, Q_4 is produced at the LHC via gluon fusion and may be observable through its decays to third family quarks.

3.4.4 $(g-2)_\mu$ and $\mathcal{B}(\tau \to \mu\gamma)$

As discussed in the simplified model, if we want to provide a significant contribution to $(g-2)_\mu$ mediated by a relatively heavy Z' boson, then we need vector-like leptons to couple to the SM Higgs in order to provide a chiral enhancement. This was achieved in the simplified model via a coupling of the form $\overline{L}_{L4} H e_{R4}$, which is forbidden in the

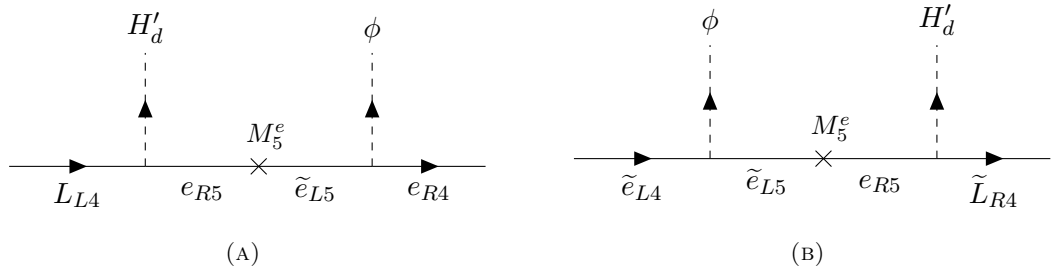

(A) (B)

FIGURE 3.9: Effective Higgs Yukawa couplings for the fourth family vector-like leptons in the theory of flavour with fermiophobic Z'.

Field	$SU(3)_c$	$SU(2)_L$	$U(1)_Y$	$U(1)'$	Z_2
$\tilde{e}_{L5}, e_{R5}$	**1**	**1**	-1	0	(-)
H'_d	**1**	**2**	-1/2	1	(-)

TABLE 3.3: New fields required to obtain a significant chiral mass for fourth family vector-like leptons in the theory of flavour. The rest of fields in the model (shown in Table 3.2) are even under Z_2.

theory of flavour due to the non-zero $U(1)'$ charges of the Higgs doublets. Nevertheless, we can obtain effective couplings to H_d via non-renormalisable operators of the form $\phi\overline{L}_{L4}H_d e_{R4}$. Such operators may be provided by adding an extra vector-like lepton singlet uncharged under $U(1)'$, i.e. $\widetilde{e}_{L5}$ and e_{R5} with vector-like mass M_5^e. After ϕ develops a VEV, we obtain effective couplings in the mass insertion approximation as shown in Fig. 3.9. Going beyond the mass insertion approximation but preserving the assumption $\langle H_d\rangle \ll \langle\phi\rangle$, one of the effective couplings is explicitly given by

$$y_5^e \frac{x_5^e \langle\phi\rangle}{\sqrt{(x_5^e \langle\phi\rangle)^2 + (M_5^e)^2}} \overline{L}_{L4} H_d e_{R4}\,. \tag{3.92}$$

However, given that we are working in the large $\tan\beta$ regime in order to explain the m_b/m_t hierarchy, we expect $\langle H_d\rangle \approx \mathcal{O}(\text{GeV})$, too small to provide a significant chiral enhancement. A cheap solution consists in adding another Higgs doublet $H'_d \sim (\mathbf{1}, \mathbf{2}, 1/2, 1)$, along with a Z_2 discrete symmetry that only discriminates $\widetilde{e}_{L5}$, e_{R5} and the new Higgs H'_d, such that these new particles only play the role of providing the effective couplings in Fig. 3.9 (see also Table 3.3). We assume that the new Higgs gets a VEV $\langle H'_d\rangle \approx \mathcal{O}(100\,\text{GeV})$. Then if $\langle\phi\rangle \sim M_5^e$, the effective coupling in Eq. (3.92) is well approximated by y_5^e, and we assume the usual perturbativity constraint $y_5^e \lesssim \sqrt{4\pi}$. Of course, with three Higgs doublets we have $v_{\text{SM}}^2 = v_u^2 + v_d^2 + v_d'^2$, where in our case $v_d \ll v_u, v'_d$. Notice that we remain protected from FCNCs in the Higgs sector thanks to the $U(1)'$ charge assignments and the Z_2 discrete symmetry.

After the Higgs doublet H'_d gets a VEV, the effective coupling $\overline{L}_{L4}H'_d e_{R4}$ in Eq. (3.92) provides a chiral mass M_4^C for the fourth family (vector-like) leptons. A similar coupling

for the conjugate fermions $\overline{\widetilde{e}}_{L4} H'_d \widetilde{L}_{R4}$ provides a chiral mass $\widetilde{M}_4^C$, reproducing the framework of the simplified model in Section 3.2. As in the simplified model, the presence of chiral masses for fourth family (vector-like) leptons leads to mixing between the conjugate leptons $\widetilde{L}_{R4}$ and $\widetilde{e}_{L4}$ and the chiral leptons of the SM. The dominant contributions to $(g-2)_\mu$ are indeed proportional to the chiral masses as (see also the top panels of Fig. 3.10)

$$\begin{aligned}\Delta a_\mu \simeq -\frac{m_\mu^2}{8\pi^2 M_{Z'}^2}\Bigg[&\mathrm{Re}\left[g^L_{\mu E_1}\left(g^R_{\mu E_1}\right)^*\right] G(M_{E_1}^2/M_{Z'}^2)\frac{M_4^C c_L^E c_R^E + \widetilde{M}_4^C s_L^E s_R^E}{m_\mu} \\ &+\mathrm{Re}\left[g^L_{\mu E_2}\left(g^R_{\mu E_2}\right)^*\right] G(M_{E_2}^2/M_{Z'}^2)\frac{M_4^C s_L^E s_R^E + \widetilde{M}_4^C c_L^E c_R^E}{m_\mu}\Bigg] .\end{aligned} \tag{3.93}$$

Notice that the couplings $g^{L,R}_{\mu E_2}$ are proportional to the mixing angles $s^E_{L,R}$ obtained after diagonalising Eq. (3.4). For the simplified model discussed in Section 3.2, these mixing angles where suppressed since all the relevant parameter space was fulfilling $v_{\rm SM} \ll M_4^{L,e}$ for at least one of the vector-like masses. However, notice that in the flavour model the Z' dominantly couples to third family left-handed fermions, and couplings to right-handed fermions or second family left-handed fermions are generally suppressed. This implies that in order to provide a significant contribution to $(g-2)_\mu$, we will need to work in a regime of large mixing angles where both $M_4^{L,e} \sim \langle\phi\rangle$ with $\langle\phi\rangle \sim 1$ TeV. Notice that smaller $\langle\phi\rangle$ would be in tension with $B_s - \bar{B}_s$ meson mixing, while larger $\langle\phi\rangle$ would suppress the contribution to $(g-2)_\mu$. We need as well both M_4^C and $\widetilde{M}_4^C$ close to perturbativity limits in order to obtain the largest contribution to $(g-2)_\mu$. In this regime, we find that both M_4^L and M_4^e may be not much larger than M_4^C and $\widetilde{M}_4^C$, such that the mixing angles $s^E_{L,R}$ may be large and the effective couplings $g^{L,R}_{\mu E_2}$ cannot be neglected, contrary to the case of the simplified model.

In contrast with the simplified model, due to the presence of Z' couplings for both third and second family fermions, in the flavour model a significant contribution to $\mathcal{B}(\tau \to \mu\gamma)$ arises, connected to the contribution to $(g-2)_\mu$ and to the chiral masses M_4^C and $\widetilde{M}_4^C$, namely (see also central and bottom panels in Fig. 3.10)

$$\begin{aligned}\mathcal{B}(\tau \to \mu\gamma) \simeq \frac{\alpha_{\rm EM}}{1024\pi^4}\frac{m_\tau^5}{\Gamma_\tau M_{Z'}^4}\Bigg[&\left|g^L_{\mu E_1}\left(g^R_{\tau E_1}\right)^* G(M_{E_1}^2/M_{Z'}^2)\frac{M_4^C c_L^E c_R^E + \widetilde{M}_4^C s_L^E s_R^E}{m_\mu}\right. \\ &\left.+g^L_{\mu E_2}\left(g^R_{\tau E_2}\right)^* G(M_{E_2}^2/M_{Z'}^2)\frac{M_4^C s_L^E s_R^E + \widetilde{M}_4^C c_L^E c_R^E}{m_\mu}\right|^2 \\ &+\left|g^R_{\mu E_1}\left(g^L_{\tau E_1}\right)^* G(M_{E_1}^2/M_{Z'}^2)\frac{M_4^C c_L^E c_R^E + \widetilde{M}_4^C s_L^E s_R^E}{m_\mu}\right. \\ &\left.+g^R_{\mu E_2}\left(g^L_{\tau E_2}\right)^* G(M_{E_2}^2/M_{Z'}^2)\frac{M_4^C s_L^E s_R^E + \widetilde{M}_4^C c_L^E c_R^E}{m_\mu}\right|^2\Bigg] .\end{aligned} \tag{3.94}$$

Contributions to related LFV processes such as $\tau \to 3\mu$ also arise, however we find $\tau \to \mu\gamma$ to provide the leading constraints in the regime of large chiral masses M_4^C and

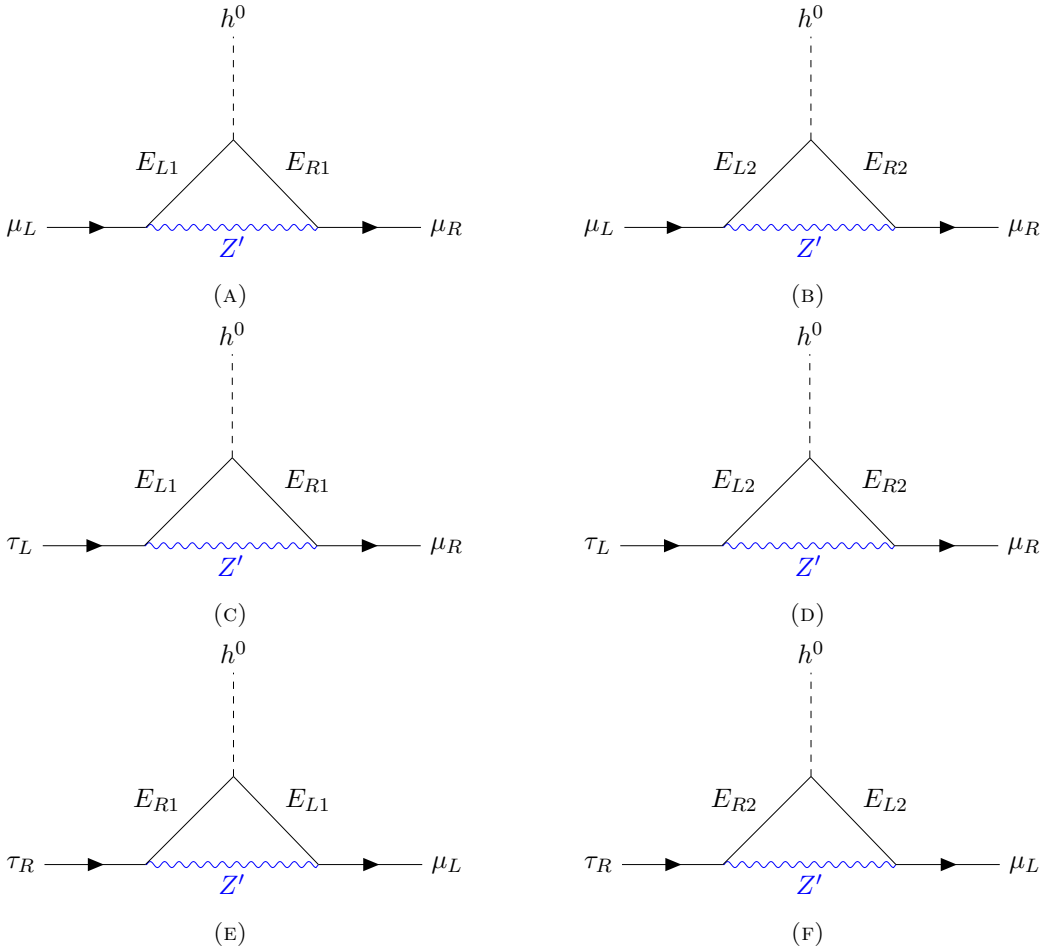

FIGURE 3.10: Leading contributions to $(g-2)_\mu$ and $\mathcal{B}(\tau \to \mu\gamma)$ in the theory of flavour with fermiophobic Z'. The effective couplings of the vector-like fermions $E_{1,2}$ to the SM Higgs boson lead to a chiral enhancement of both $(g-2)_\mu$ and $\mathcal{B}(\tau \to \mu\gamma)$, and a photon is emitted (not shown).

$\widetilde{M}_4^C$ where we shall work.

As shown in Fig. 3.11, the large contribution to $\tau \to \mu\gamma$ is the dominant constraint over the parameter space, ruling out the possibility of having a significant contribution to $(g-2)_\mu$ in the theory of flavour with fermiophobic Z'. Higgs diphoton decay also constrains the region of parameter space preferred by $\Delta a_\mu^{\rm R}$ (the 5σ deviation with respect to $e^+e^- \to$ hadrons data). Notice that reducing M_4^C and $\widetilde{M}_4^C$ ameliorates the bounds from $\tau \to \mu\gamma$ but also reduces the contribution to $(g-2)_\mu$. Note that in the parameter space motivated by $(g-2)_\mu$, the leading LHC constraint is the dimuon Drell-Yan channel due to the large $s_{24}^{e_R} \approx 0.5$ required, while for its natural value $s_{24}^{e_R} \approx V_{cb}$ the ditau Drell-Yan channel is more competitive as mentioned.

The crucial difference with respect to the simplified model is the presence of flavour-violating $\mu\tau$ couplings to the Z' boson. The $(g-2)_\mu$ anomaly could be addressed if the vector-like leptons mix dominantly with muons, but this is not possible in the theory of flavour since we need at least one of the vector-like leptons to mix with taus in order to obtain their effective Yukawa coupling. Nevertheless, it is possible that with

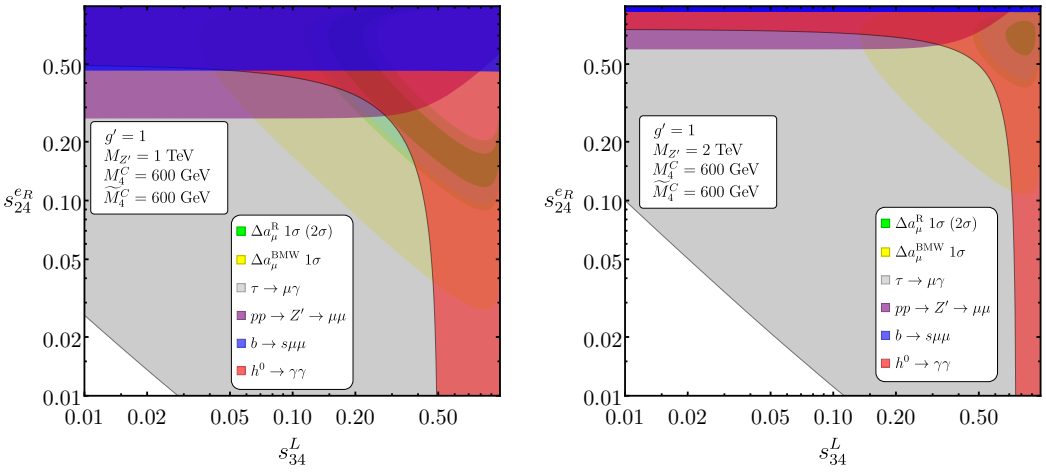

(A) (B)

FIGURE 3.11: Parameter space s_{34}^L vs $s_{24}^{e_R}$ for $M_{Z'} = 1$ TeV (left) and $M_{Z'} = 2$ TeV (right) with chiral masses close to the perturbativity limit as shown in the panels. The green (lighter green) region is preferred at 1σ (2σ) by $\Delta a_\mu^{\rm R}$ ($e^+e^- \to$ hadrons) while the yellow region is preferred at 1σ by $\Delta a_\mu^{\rm BMW}$. The rest of the shaded regions are excluded at 95% CL, with the leading constraint given by $\mathcal{B}(\tau \to \mu\gamma)$ as shown by the grey-shaded region.

further model building one could achieve a cancellation in $\tau \to \mu\gamma$ while preserving the enhancement of $(g-2)_\mu$, however this probably involves the addition of more fields and symmetries, enlarging the number of free parameters, making the model less predictive and disconnecting the explanation of $(g-2)_\mu$ from the origin of flavour hierarchies, going against the spirit of the model.

3.4.5 Parameter space in the flavour model

For the first time, we have considered the possibility of addressing the $(g-2)_\mu$ anomaly within the framework of a complete theory of flavour with a fermiophobic Z' boson. Although our analysis reveals that a significant contribution to $(g-2)_\mu$ is in tension with $\mathcal{B}(\tau \to \mu\gamma)$, the dangerous contributions to LFV processes are much reduced if we neglect the chiral masses of vector-like fermions M_4^C and $\widetilde{M}_4^C$, which anyway required an extension of the original flavour model. The model as presented in Section 3.3 remains a well-motivated possibility to explain the origin of the SM flavour structure, and it is interesting to study the allowed parameters and the experimental bounds over the NP scales of the model.

As motivated in Section 3.4.1, the stronger bounds from $B_s - \bar{B}_s$ meson mixing are very sensitive to the value of the mixing angle s_{34}^Q. As presented in Section 3.3.4, if we assume $y_{43}^u \approx \sqrt{2}$, then we expect $s_{34}^Q \approx 1/\sqrt{2}$. In this case, $B_s - \bar{B}_s$ meson mixing leads to the most stringent bounds over $M_{Z'}/g'$ as shown in Fig. 3.11a, such that for natural values of g' we would expect to find $M_{Z'}$ above 4 TeV. We find $pp \to Z' \to \tau\tau$ to be the leading LHC constraint over the parameter space, and $\tau \to \mu\gamma$ to be the leading signal

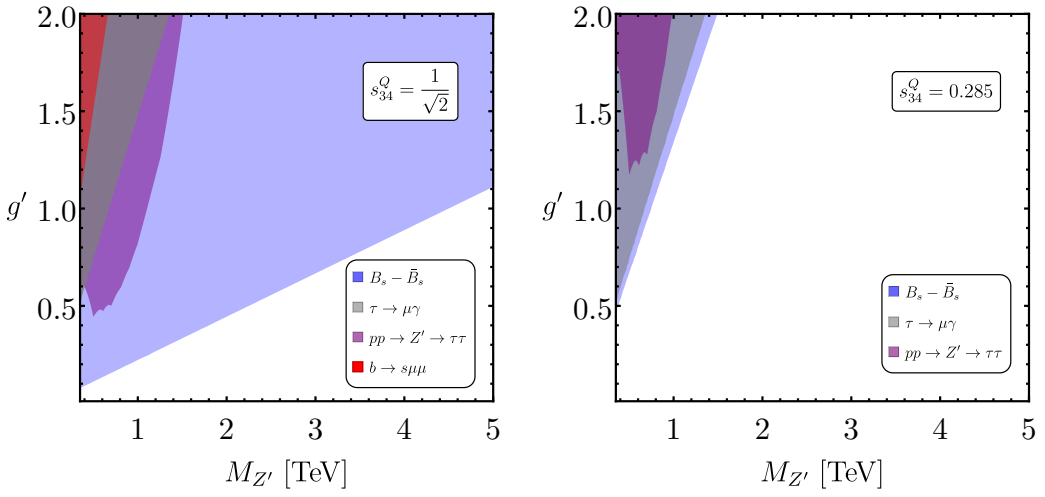

FIGURE 3.12: Parameter space $M_{Z'}$ vs g' for $s_{34}^Q = 1/\sqrt{2}$ (left) and $s_{34}^Q = 0.285$ (right). The shaded regions are excluded at 95% CL.

in LFV processes. $pp \to Z' \to \mu\mu$, $b \to s\mu\mu$ and $\tau \to 3\mu$ are further suppressed due to the small right-handed mixing angles or small 2-3 mixing.

If we push y_{43}^u close to perturbativity bounds (i.e. $y_{43}^u \approx \sqrt{4\pi}$), then we can fit the top mass via $s_{34}^Q \approx 0.285$ and reduce the bounds from $B_s - \bar{B}_s$ mixing. As shown in Fig. 3.11b, in this case the bounds from $pp \to Z' \to \tau\tau$ and $b \to s\mu\mu$ are also suppressed due to the smaller Z' couplings to bottom quarks, while the bounds from $\tau \to \mu\gamma$ remain the same. In this case, for natural values of g' we could have $M_{Z'}$ as low as 1 TeV.

We conclude that in any case, the flavour structure of the fermiophobic Z' flavour model allows for relatively low Z' masses, within the reach of current and upcoming experiments.

3.5 Conclusions

In this chapter we have studied fermiophobic Z' models, which were a well-motivated class of SM extensions to address flavour anomalies in $R_{K^{(*)}}$ and $(g-2)_\mu$ [1]. We have shown that a simplified fermiophobic Z' model is still able to explain large deviations in $(g-2)_\mu$ with Z' masses ranging from the GeV to the few TeV. The main idea is that the Z' boson only couples originally to vector-like fermions, which then mix with chiral fermions providing effective Z' couplings that can be controlled by the size of the mixing angles. The vector-like leptons obtain chiral masses at the electroweak scale via couplings to the SM Higgs (although their physical mass is dominated by the vector-like mass terms), which provide a chiral enhancement of $(g-2)_\mu$. Interestingly, this enhancement is correlated to a suppression of the Higgs decay to two photons, where further experimental precision could test the full parameter space of the model.

Afterwards, we went beyond the simplified framework to propose a complete theory of flavour containing a fermiophobic Z' boson. The flavour structure of the SM is

explained via messenger dominance [171], such that third family fermion masses are obtained from mixing with TeV scale vector-like fermion doublets while second family fermion masses and small CKM mixing are obtained from mixing with heavier vector-like fermion singlets. This mixing also provides effective couplings for chiral fermions to the Z' boson, leading to a predictive phenomenology at low energies connected to the origin of flavour hierarchies. First family fermion masses are explained via a heavy Higgs doublet that gets an small effective VEV via mixing with the much lighter Higgs doublets that perform electroweak symmetry breaking. The heavier Higgs does not couple to the Z' boson and therefore does not introduce effective Z' couplings for first family fermions, protecting the model from the appearance of the most dangerous FCNCs. Finally, the origin of tiny neutrino masses and PMNS mixing is addressed via the type Ib seesaw mechanism [331].

Obtaining an effective chiral mass for vector-like leptons in the flavour model requires the addition of an extra vector-like lepton and a Z_2 discrete symmetry. However, we have found that in the flavour model, the enhancement of $(g-2)_\mu$ is correlated as well with a chiral enhancement of $\mathcal{B}(\tau \to \mu\gamma)$, which renders impossible to obtain large contributions to $(g-2)_\mu$. It is remarkable that the simplified model works fine for $(g-2)_\mu$ while the full flavour model fails, questioning the BSM interpretation of $(g-2)_\mu$ within a theory of flavour.

Finally, we have dropped the extra dynamics introduced to obtain chiral masses for the vector-like leptons, in order to study the parameter space of the flavour model without addressing $(g-2)_\mu$. We have found that the leading constraint is generally $B_s - \bar{B}_s$ meson mixing, followed by ditau searches at the LHC and $\mathcal{B}(\tau \to \mu\gamma)$. We conclude that the flavour structure in the model allows for Z' masses as low as 1 TeV for natural values of the gauge coupling, within the reach of current and upcoming experiments.

Chapter 4

Twin Pati-Salam theory of flavour

"Make everything as simple as possible, but not simpler."

– Albert Einstein

In this chapter, based on Refs. [2,6,7], we introduce a theory of flavour consisting of two copies of the Pati-Salam gauge group, broken in two steps down to the SM. The last step of the symmetry breaking can be as low as the TeV scale, giving rise to a $U_1 \sim (\mathbf{3}, \mathbf{1}, 2/3)$ vector leptoquark which explains the B-anomalies. This model will connect the origin of Yukawa couplings and flavour hierarchies of the SM with the effective couplings of the vector leptoquark that explain the B-anomalies.

4.1 Introduction

The picture of anomalies in B-meson decays, including the discrepancy in the $R_{K^{(*)}}$ ratios that lasted until late 2022 (see Section 2.3.1), led to important model building efforts by the community during the last eight years, in order to interpret these anomalies as a low-energy signal of a consistent BSM model. Leptoquarks were identified as excellent NP candidates for the B-anomalies, because unlike other mediators they avoid dangerous contributions to $B_s - \bar{B}_s$ meson mixing observables at tree-level. Different scalar leptoquarks were proposed to address either $R_{K^{(*)}}$ or $R_{D^{(*)}}$ separately (see e.g. [164, 184, 292–294, 343, 344]). Interestingly, the vector leptoquark $U_1 \sim (\mathbf{3}, \mathbf{1}, 2/3)$ was identified as the only single mediator capable of addressing both the $R_{K^{(*)}}$ and $R_{D^{(*)}}$ anomalies simultaneously [184]. Given that both anomalies suggested the departure from lepton flavour universality, it was soon realised that the U_1 explanation of the B-anomalies could be connected to the origin of the flavour structure of the SM (see Section 2.3.2).

However, the gauge nature of U_1 requires to specify a UV completion that explains its origin. The original ideas by Pati and Salam (PS) [100], led to tensions with unobserved processes such as $K_L \to \mu e$ (see Section 2.3.9). Instead, an interesting proposal was firstly laid out in the Appendix of [345], and more formally later in [267], following the idea introduced in [346] that colour could appear as a diagonal subgroup of a larger

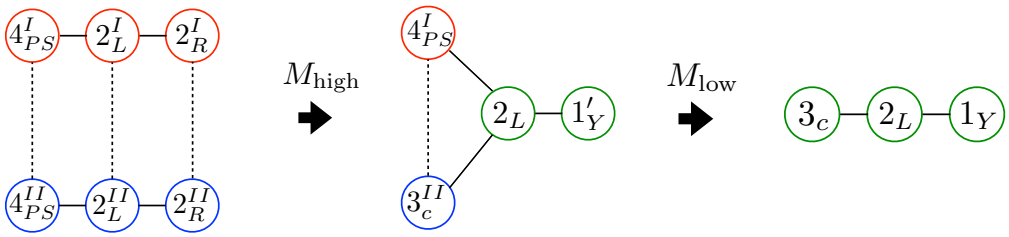

FIGURE 4.1: The model is based on two copies of the Pati-Salam gauge group $SU(4)_{PS} \times SU(2)_L \times SU(2)_R$. The circles represent the gauge groups with the indicated symmetry breaking. The twin Pati-Salam symmetry is broken down to the 4321 symmetry at high energies $M_{\text{High}} \gtrsim 1\,\text{PeV}$, then the 4321 group is further broken to the SM at the TeV scale $M_{\text{low}} \sim \mathcal{O}(\text{TeV})$.

$SU(3+N) \times SU(3)'$ local symmetry restored at high energies. The particular choice $N = 1$ leads to the so-called "4321" gauge symmetry,

$$G_{4321} \equiv SU(4) \times SU(3)'_c \times SU(2)_L \times U(1)_{Y'}\,, \tag{4.1}$$

which can be broken at the TeV scale while satisfying the experimental bounds [262,263, 267,268], provided that at least the first and second families of SM fermions are singlets under $SU(4)$. This breaking leads to a rich gauge boson spectrum at the TeV scale, containing the vector leptoquark U_1 along with a massive colour octet $g' \sim (\mathbf{8},\mathbf{1},0)$ and a massive $Z' \sim (\mathbf{1},\mathbf{1},0)$ with suppressed couplings to light SM fermions. Vector-like fermions need to be introduced in order to obtain effective couplings for (at least) second family fermions to U_1. The model, though it is not minimal, is very predictive and leads to a rich phenomenology in both low-energy and high-p_T searches. However, the flavour structure of the model was rather ad-hoc, and it was hinted that the 4321 gauge group could be the TeV scale effective field theory of a complete model addressing more open questions of the SM. Given that both the $R_{K^{(*)}}$ and $R_{D^{(*)}}$ anomalies suggested a departure from LFU consistent with the idea of a theory of flavour (see Section 2.3.2), it was soon realised that the U_1 explanation of the B-anomalies, and in particular the 4321 model, could originate from a theory of flavour.

The very first theories of flavour containing a TeV-scale U_1 to explain the B-anomalies [115,117,119,120] were based on the flavour deconstruction of the SM gauge group, predicting an accidental $U(2)^5$ flavour symmetry (see Section 1.9.3). Instead, the twin Pati-Salam theory [169] was proposed from a completely different perspective. Unlike the alternative models in the market, the twin PS model treats all three fermion families in the same way, and does not require to perform a very aggressive family decomposition of the SM (avoiding dangerous contributions to electroweak precision observables). The basic idea is that all three families of SM chiral fermions transform under one PS group, while families of vector-like fermions, which are required in any implementation of the 4321 model, transform under the other one. The first PS group, broken at a high scale, provides Pati-Salam unification of all SM quarks and leptons, while a fourth family of vector-like fermions transforms under a second PS group, broken at the

TeV scale to the SM, as shown in Fig. 4.1. The full twin Pati-Salam symmetry, together with the absence of a standard Higgs doublet, forbids the usual Yukawa couplings for the SM fermions. Instead, effective Yukawa couplings arise through the mixing between SM fermions and vector-like partners. The same mixing leads to U_1 couplings for SM fermions which could address the B-anomalies. This way, B-anomalies and the flavour puzzle are dynamically and parametrically connected. In this manner, the twin Pati-Salam model features a *fermiophobic* framework where both B-anomalies and flavour hierarchies are explained via the mechanism of *messenger dominance* [171], as in the Z' model of Chapter 3.

The origin of second and third family masses and mixing is connected with the TeV scale dynamics and first PS breaking that address the B-anomalies, while the origin of first family masses and mixing is connected to the heavier scale of second PS breaking. In this manner, the twin Pati-Salam model is an example of a multi-scale origin of flavour as introduced in Section 1.10, however without the need to family decompose the SM as all the alternative theories do. Furthermore, the twin PS model predicts dominantly left-handed U_1 currents as preferred by the current picture of B-anomalies [82,269], while the alternative proposals [115–117, 119, 120] predict large couplings for right-handed third family fermions, which lead to tight constraints from high-p_T searches [269].

In this chapter we study the phenomenology of the simplified twin PS model proposed in [169] to address the B-anomalies, which turns out to be incompatible with low-energy data. Afterwards, we perform further model building and present an extended version of the model that can explain the most updated picture of B-anomalies and address charged fermion masses and mixings, while being compatible with all existing data. The model [2, 6, 7] was initially built to connect both $R_{K^{(*)}}$ and $R_{D^{(*)}}$, however we will show that the model is also compatible with the 2022 updates of $R_{K^{(*)}}$ by LHCb, which are consistent with the SM. Nevertheless, the connection is not lost: eventually some deviations in $R_{K^{(*)}}$ should be seen with more precision if our model is indeed realised in Nature at the TeV scale to explain the $R_{D^{(*)}}$ anomalies.

The layout of the remainder of the chapter is as follows. In Section 4.2 we introduce the simplified twin Pati-Salam model as presented in [169], featuring only one vector-like family coupled to U_1, and we show the origin of fermion masses and mixing in this model. In Section 4.3 we show the tree-level SMEFT matching of 4-fermion operators in the model, relevant for phenomenological analyses. Then in Section 4.4 we show that the simplified model is unable to explain $R_{D^{(*)}}$ while being compatible with the stringent constraints from $B_s - \bar{B}_s$ mixing. Instead, in Section 4.5 we present a new, extended version of the twin Pati-Salam model including three vector-like families and a discrete flavour symmetry, which is successful to address the B-anomalies while being compatible with all the experimental constraints. The phenomenological analysis and the discussion of the results are shown in Section 4.6, highlighting promising signals to test the model in low-energy observables and high-p_T searches, along with a study of

the perturbativity of the model. Section 4.7 includes a comparison of our predictions with alternative models in the market. Finally, we conclude the chapter in Section 4.8.

4.2 Simplified twin Pati-Salam theory of flavour

4.2.1 The High Energy Model

In the traditional Pati-Salam theory [100], the chiral quarks and leptons are unified into $SU(4)_{PS}$ multiplets with leptons as the fourth colour (red, green, blue, lepton),

$$\psi_i(\mathbf{4},\mathbf{2},\mathbf{1}) = \begin{pmatrix} u_r & u_g & u_b & \nu \\ d_r & d_g & d_b & e \end{pmatrix}_i \equiv (Q_i, L_i)\ , \tag{4.2}$$

$$\psi^c_j(\overline{\mathbf{4}},\mathbf{1},\overline{\mathbf{2}}) = \begin{pmatrix} u^c_r & u^c_g & u^c_b & \nu^c \\ d^c_r & d^c_g & d^c_b & e^c \end{pmatrix}_j \equiv \left(u^c_j, d^c_j, \nu^c_j, e^c_j\right)\ , \tag{4.3}$$

where ψ_i contains the left-handed quarks and leptons while ψ^c_j contains the CP-conjugated right-handed quarks and leptons (so that they become left-handed[1]), and $i,j = 1,2,3$ are family indices. We consider here two copies of the Pati-Salam symmetry [169],

$$G^I_{422} \times G^{II}_{422} = \left(SU(4)^I_{PS} \times SU(2)^I_L \times SU(2)^I_R\right) \times \left(SU(4)^{II}_{PS} \times SU(2)^{II}_L \times SU(2)^{II}_R\right)\ . \tag{4.4}$$

The matter content and the quantum numbers of each field are displayed in Table 4.1. The usual three families of chiral fermions originate from the second PS group G^{II}_{422}, broken at a high scale, and transform under Eq. (4.4) as

$$\psi_{1,2,3}(\mathbf{1},\mathbf{1},\mathbf{1};\mathbf{4},\mathbf{2},\mathbf{1})\,, \quad \psi^c_{1,2,3}(\mathbf{1},\mathbf{1},\mathbf{1};\overline{\mathbf{4}},\mathbf{1},\overline{\mathbf{2}})\,. \tag{4.5}$$

This simplified version of the theory includes only one vector-like family of fermions originating from the first PS group, whose $SU(4)^I_{PS}$ is broken at the TeV scale, and transforms under Eq. (4.4) as

$$\psi_4(\mathbf{4},\mathbf{2},\mathbf{1};\mathbf{1},\mathbf{1},\mathbf{1})\,, \quad \overline{\psi_4}(\overline{\mathbf{4}},\overline{\mathbf{2}},\mathbf{1};\mathbf{1},\mathbf{1},\mathbf{1})\,, \quad \psi^c_4(\overline{\mathbf{4}},\mathbf{1},\overline{\mathbf{2}};\mathbf{1},\mathbf{1},\mathbf{1})\,, \quad \overline{\psi^c_4}(\mathbf{4},\mathbf{1},\mathbf{2};\mathbf{1},\mathbf{1},\mathbf{1})\,. \tag{4.6}$$

On the other hand, according to the matter content in Table 4.1, there are no standard Higgs fields which transform as $(\mathbf{1},\overline{\mathbf{2}},\mathbf{2})$ under G^{II}_{422}, hence the standard Yukawa couplings involving the chiral fermions are forbidden by the twin PS symmetry. This is what we call a *fermiophobic model*, in complete analogy with the fermiophobic Z' model discussed in Chapter 3. For the third and second families, these will be generated effectively via mixing with the fourth family of vector-like fermions, which only have

[1] The reader who is not familiar with this notation based on left-handed 2-component Weyl spinors can find the connection with the traditional 4-component, left-right notation in Appendix A.

Field	$SU(4)^I_{PS}$	$SU(2)^I_L$	$SU(2)^I_R$	$SU(4)^{II}_{PS}$	$SU(2)^{II}_L$	$SU(2)^{II}_R$
$\psi_{1,2,3}$	**1**	**1**	**1**	**4**	**2**	**1**
$\psi^c_{1,2,3}$	**1**	**1**	**1**	$\overline{\mathbf{4}}$	**1**	$\overline{\mathbf{2}}$
ψ_4	**4**	**2**	**1**	**1**	**1**	**1**
$\overline{\psi_4}$	$\overline{\mathbf{4}}$	$\overline{\mathbf{2}}$	**1**	**1**	**1**	**1**
ψ^c_4	$\overline{\mathbf{4}}$	**1**	$\overline{\mathbf{2}}$	**1**	**1**	**1**
$\overline{\psi^c_4}$	**4**	**1**	**2**	**1**	**1**	**1**
ϕ	**4**	**2**	**1**	$\overline{\mathbf{4}}$	$\overline{\mathbf{2}}$	**1**
$\overline{\phi}$	$\overline{\mathbf{4}}$	**1**	$\overline{\mathbf{2}}$	**4**	**1**	**2**
H	$\overline{\mathbf{4}}$	$\overline{\mathbf{2}}$	**1**	**4**	**1**	**2**
$\overline{H}$	**4**	**1**	**2**	$\overline{\mathbf{4}}$	$\overline{\mathbf{2}}$	**1**
H'	**1**	**1**	**1**	**4**	**1**	**2**
Φ	**1**	**2**	**1**	**1**	$\overline{\mathbf{2}}$	**1**
$\overline{\Phi}$	**1**	**1**	$\overline{\mathbf{2}}$	**1**	**1**	**2**

TABLE 4.1: The field content under $G^I_{422} \times G^{II}_{422}$, see the main text for details. We do not include here extra content related to the origin of first family fermion masses and mixing, to be discussed in Section 4.2.4.

quantum numbers under the first PS group, G^I_{422}. This mixing is facilitated by the non-standard Higgs scalar doublets contained in ϕ, $\overline{\phi}$, H, $\overline{H}$ in Table 4.1, via the couplings,

$$\mathcal{L}^{ren}_{\text{mass}} = y^{\psi}_{i4}\overline{H}\psi_i\psi^c_4 + y^{\psi}_{4i}H\psi_4\psi^c_i + x^{\psi}_{i4}\phi\psi_i\overline{\psi_4} + x^{\psi^c}_{4i}\overline{\psi^c_4}\overline{\phi}\psi^c_i + M^{\psi}_4\psi_4\overline{\psi_4} + M^{\psi^c}_4\psi^c_4\overline{\psi^c_4} \quad (4.7)$$

plus h.c., where $i = 1, 2, 3$; x, y are dimensionless coupling constants and M^{ψ,ψ^c}_4 are the vector-like mass terms. These couplings mix the chiral fermions with the vector-like fermions, and will be responsible for generating effective Yukawa couplings for the second and third families (the origin of first family Yukawa couplings is discussed in Section 4.2.4 and involves the second PS group). Moreover, the same mixing leads to effective couplings to TeV scale $SU(4)^I_{PS}$ gauge bosons which violate lepton universality between the second and third families, as we shall see.

4.2.2 High scale symmetry breaking

The twin Pati-Salam symmetry displayed in Eq. (4.4) is spontaneously broken to the 4321 symmetry at the high scale $M_{\text{High}} \gtrsim 1\,\text{PeV}$ (the latter bound due to the non-observation of $K_L \to \mu e$ [282, 283]),

$$G^I_{422} \times G^{II}_{422} \to G_{4321} \equiv SU(4)^I_{PS} \times SU(3)^{II}_c \times SU(2)^{I+II}_L \times U(1)_{Y'}\,. \quad (4.8)$$

We can think of this as a two part symmetry breaking:
(i) The two pairs of left-right groups break down to their diagonal left-right subgroup, via the VEVs $\langle\Phi\rangle \sim v_\Phi$ and $\langle\overline{\Phi}\rangle \sim v_{\overline{\Phi}}$, leading to the symmetry breaking,

$$SU(2)^I_L \times SU(2)^{II}_L \to SU(2)^{I+II}_L\,, \qquad SU(2)^I_R \times SU(2)^{II}_R \to SU(2)^{I+II}_R\,. \tag{4.9}$$

Since the two $SU(4)_{PS}$ groups remain intact, the above symmetry breaking corresponds to[2]

$$G^I_{422} \times G^{II}_{422} \to G_{4422} \equiv SU(4)^I_{PS} \times SU(4)^{II}_{PS} \times SU(2)^{I+II}_L \times SU(2)^{I+II}_R\,. \tag{4.10}$$

(ii) Then we assume that the second PS group is broken at a high scale via the Higgs H' in Table 4.1, which under G_{4422} transforms as

$$H'(\mathbf{1},\mathbf{4},\mathbf{1},\mathbf{2}) = \begin{pmatrix} u^r_{H'} & u^b_{H'} & u^g_{H'} & \nu_{H'} \\ d^r_{H'} & d^b_{H'} & d^g_{H'} & e_{H'} \end{pmatrix}, \tag{4.11}$$

and develops a VEV in its right-handed neutrino (neutral) component, $\langle\nu_{H'}\rangle \gtrsim 1\,\text{PeV}$, leading to the symmetry breaking

$$G_{4422} \to G_{4321} \equiv SU(4)^I_{PS} \times SU(3)^{II}_c \times SU(2)^{I+II}_L \times U(1)_{Y'}\,, \tag{4.12}$$

where $SU(4)^{II}_{PS}$ is broken to $SU(3)^{II}_c \times U(1)^{II}_{B-L}$ (at the level of fermion representations, chiral quarks and leptons are split $\mathbf{4}^{II} \to (\mathbf{3},1/6)^{II} \oplus (\mathbf{1},-1/2)^{II}$), while $SU(2)^{I+II}_R$ is broken to $U(1)^{I+II}_{T_{3R}}$ and the abelian generators are broken to $U(1)_{Y'}$, where $Y' = T^{II}_{B-L} + T^{I+II}_{3R}$. The broken generators of $SU(4)^{II}_{PS}$ are associated with PeV-scale gauge bosons that will mediate processes at acceptable rates, beyond the sensitivity of current experiments and colliders. Instead, the further symmetry breaking of G_{4321} will lead to a rich phenomenology at the TeV scale, as we shall see. We anticipate that $SU(2)^{I+II}_L$ is already the $SU(2)_L$ of the SM gauge group, while SM color and hypercharge are embedded in $SU(4)^I_{PS} \times SU(3)^{II}_c \times U(1)_{Y'}$.

On the other hand, the Yukon scalars ϕ and $\overline{\phi}$ in Table 4.1, responsible for mixing chiral and vector-like fermions, decompose under $G^I_{422} \times G^{II}_{422} \to G_{4422} \to G_{4321}$ as

$$\begin{aligned} &\phi(\mathbf{4},\mathbf{2},\mathbf{1};\overline{\mathbf{4}},\overline{\mathbf{2}},\mathbf{1}) \to \phi(\mathbf{4},\overline{\mathbf{4}},\mathbf{1}\oplus\mathbf{3},\mathbf{1}) \to \phi_3(\mathbf{4},\overline{\mathbf{3}},\mathbf{1}\oplus\mathbf{3},-1/6) \oplus \phi_1(\mathbf{4},\mathbf{1},\mathbf{1}\oplus\mathbf{3},1/2)\,, \\ &\overline{\phi}(\overline{\mathbf{4}},\mathbf{1},\overline{\mathbf{2}};\mathbf{4},\mathbf{1},\mathbf{2}) \to \overline{\phi}(\overline{\mathbf{4}},\mathbf{4},\mathbf{1},\mathbf{1}\oplus\mathbf{3}) \to \overline{\phi_3}(\overline{\mathbf{4}},\mathbf{3},\mathbf{1},1/6) \oplus \overline{\phi_1}(\overline{\mathbf{4}},\mathbf{1},\mathbf{1},-1/2)\,, \end{aligned} \tag{4.13}$$

[2]We note that the mechanism for generating first family masses discussed in Section 4.2.4 suggests that the scale of $SU(2)^I_L \times SU(2)^{II}_L \to SU(2)^{I+II}_L$ breaking may be below the scale of $SU(4)^{II}_{PS}$ breaking. However, this has no implications for the conclusions of this chapter.

plus extra $\overline{\phi_3}$ and $\overline{\phi_1}$ with different values of Y' associated to the breaking of the $SU(2)_R^{I+II}$ triplet, that we ignore because they do not couple to fermions. The decomposition above is of phenomenological interest, as the Yukons ϕ_3, $\overline{\phi_3}$ will couple to quarks while ϕ_1, $\overline{\phi_1}$ will couple to leptons, allowing non-trivial mixing between SM fermions and vector-like fermions. They will also lead to a non-trivial breaking of G_{4321} down to the SM.

The Higgs scalars H and $\overline{H}$ in Table 4.1 decompose under $G_{422}^I \times G_{422}^{II} \to G_{4321}$ as (we skip the G_{4422} decomposition here for simplicity)

$$H(\overline{\mathbf{4}},\overline{\mathbf{2}},\mathbf{1};\mathbf{4},\mathbf{1},\mathbf{2}) \to H_t(\overline{\mathbf{4}},\mathbf{3},\overline{\mathbf{2}},2/3),\ H_b(\overline{\mathbf{4}},\mathbf{3},\overline{\mathbf{2}},-1/3),\ H_\tau(\overline{\mathbf{4}},\mathbf{1},\overline{\mathbf{2}},-1),\ H_{\nu_\tau}(\overline{\mathbf{4}},\mathbf{1},\overline{\mathbf{2}},0)\,, \tag{4.14}$$

$$\overline{H}(\mathbf{4},\mathbf{1},\mathbf{2};\overline{\mathbf{4}},\overline{\mathbf{2}},\mathbf{1}) \to H_c(\mathbf{4},\overline{\mathbf{3}},\overline{\mathbf{2}},1/3),\ H_s(\mathbf{4},\overline{\mathbf{3}},\overline{\mathbf{2}},-2/3),\ H_\mu(\overline{\mathbf{4}},\mathbf{1},\overline{\mathbf{2}},0),\ H_{\nu_\mu}(\overline{\mathbf{4}},\mathbf{1},\overline{\mathbf{2}},1)\,, \tag{4.15}$$

where the notation anticipates that a separate personal Higgs doublet contributes to each of the second and third family quark and lepton masses, as we shall see. Models with multiple light Higgs doublets face the phenomenological challenge of FCNCs arising from tree-level exchange of the scalar doublets in the Higgs basis. Therefore we assume that only one pair of Higgs doublets H_u and H_d are light, given by linear combinations of the personal Higgs,

$$H_u = \widetilde{\alpha}_u H_t + \widetilde{\beta}_u H_c + \widetilde{\gamma}_u H_{\nu_\tau} + \widetilde{\delta}_u H_{\nu_\mu}\,, \quad H_d = \widetilde{\alpha}_d H_b + \widetilde{\beta}_d H_s + \widetilde{\gamma}_d H_\tau + \widetilde{\delta}_d H_\mu\,, \tag{4.16}$$

where $\widetilde{\alpha}_{u,d}$, $\widetilde{\beta}_{u,d}$, $\widetilde{\gamma}_{u,d}$, $\widetilde{\delta}_{u,d}$ are complex elements of two unitary Higgs mixing matrices. The orthogonal linear combinations are assumed to be very heavy, well above the TeV scale in order to sufficiently suppress the FCNCs. We will further assume that only the light Higgs doublets H_u and H_d get VEVs in order to perform EW symmetry breaking,

$$\langle H_u \rangle = v_u, \quad \langle H_d \rangle = v_d, \tag{4.17}$$

while the heavy linear combinations do not, i.e. we assume that in the Higgs basis the linear combinations which do not get VEVs are very heavy. The discussion of such Higgs potential is beyond the scope of this work, for the interested reader a deeper discussion was made in Section 3.4 of [169]. We shall just anticipate that the situation is familiar from $SO(10)$ models [347], where there are six Higgs doublets arising from the **10**, **120** and $\overline{\mathbf{126}}$ representations, denoted as $H_{\mathbf{10}}$, $H_{\mathbf{120}}$ and $H_{\overline{\mathbf{126}}}$, two from each, but below the $SO(10)$ breaking scale only two Higgs doublets are assumed to be light, similar to H_u and H_d above in our case. Another example is the PS^3 theory of flavour [115], also proposed to address the B-anomalies, where the Higgs $(\mathbf{15},\mathbf{1},\mathbf{1})_3$ and $(\mathbf{1},\mathbf{2},\mathbf{2})_3$ are assumed to give rise to a specific set of light doublets. In any case, we shall invert the unitary transformations in Eq. (4.16) to express each of the personal Higgs doublets in

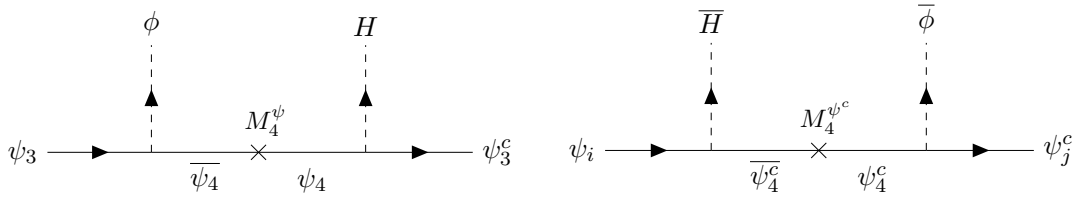

(A) (B)

FIGURE 4.2: Diagrams in the model which lead to the effective Yukawa couplings in the mass insertion approximation, $i, j = 2, 3$.

terms of the light doublets H_u, H_d,

$$H_t = \alpha_u H_u + \dots, \quad H_b = \alpha_d H_d + \dots, \quad H_\tau = \gamma_d H_d + \dots, \quad H_{\nu_\tau} = \gamma_u H_u + \dots,$$

$$H_c = \beta_u H_u + \dots, \quad H_s = \beta_d H_d + \dots, \quad H_\mu = \delta_d H_d + \dots, \quad H_{\nu_\mu} = \delta_u H_u + \dots, \tag{4.18}$$

ignoring the heavy states indicated by dots. When the light Higgs H_u and H_d gain their VEVs in Eq. (4.17), the personal Higgs in the original basis can be thought of as gaining effective VEVs $\langle H_t \rangle = \alpha_u v_u$, etc... This approach will be used in the next subsection when constructing the low energy quark and lepton mass matrices.

4.2.3 Effective Yukawa couplings and fermion masses for the second and third family

We have already remarked that the usual Yukawa couplings involving purely chiral fermions are absent in the twin PS model. In this subsection, we show how they may be generated effectively via mixing with the vector-like fermions.

We may write the mass terms and couplings in Eq. (4.7) as a 5×5 matrix in flavour space (we also define 5-dimensional vectors as ψ_α^{T} and ψ_β^c),

$$\mathcal{L}_{\mathrm{mass}}^{ren} = \psi_\alpha^{\mathrm{T}} M^\psi \psi_\beta^c + \mathrm{h.c.}\,, \tag{4.19}$$

$$\psi_\alpha^{\mathrm{T}} \equiv \begin{pmatrix} \psi_1 & \psi_2 & \psi_3 & \psi_4 & \overline{\psi_4^c} \end{pmatrix}, \qquad \psi_\beta^c \equiv \begin{pmatrix} \psi_1^c & \psi_2^c & \psi_3^c & \psi_4^c & \overline{\psi_4} \end{pmatrix}^{\mathrm{T}}, \tag{4.20}$$

$$M^\psi = \begin{pmatrix} & \psi_1^c & \psi_2^c & \psi_3^c & \psi_4^c & \overline{\psi_4} \\ \hline \psi_1 | & 0 & 0 & 0 & 0 & 0 \\ \psi_2 | & 0 & 0 & 0 & y_{24}^\psi \overline{H} & 0 \\ \psi_3 | & 0 & 0 & 0 & y_{34}^\psi \overline{H} & x_{34}^\psi \phi \\ \psi_4 | & 0 & 0 & y_{43}^\psi H & 0 & M_4^\psi \\ \overline{\psi_4^c} | & 0 & x_{42}^{\psi^c} \overline{\phi} & x_{43}^{\psi^c} \overline{\phi} & M_4^{\psi^c} & 0 \end{pmatrix}. \tag{4.21}$$

where the extra zeros have been achieved via suitable rotations of ψ_i, ψ_j^c $(i,j=1,2,3)$, that leave unchanged the upper 3×3 block (for further details see Section 3.3.3 and the discussion therein). There are several distinct mass scales in this matrix: the Higgs VEVs $\langle H\rangle$ and $\langle\overline{H}\rangle$, the Yukon VEVs $\langle\phi\rangle$ and $\langle\overline{\phi}\rangle$ and the vector-like fourth family masses M_4^{ψ}, $M_4^{\psi^c}$. Assuming the latter are heavier than all the VEVs, we may integrate out the fourth family to generate effective Yukawa couplings for chiral quarks and leptons, as in the diagrams of Fig. 4.2. This is denoted as the mass insertion approximation (see Appendix B).

However, from the diagrams in Fig. 4.2 one can anticipate that the heavy top mass requires $\langle\phi\rangle/M_4^{\psi}\sim 1$, and thus it is necessary to go beyond the mass insertion approximation and work in the large mixing angle formalism (see Appendix B). We shall block-diagonalise the mass matrix in Eq. (4.21) in order to obtain the effective Yukawa couplings for the chiral families,

$$M^{\psi'}=\begin{array}{c}\\ \psi_1'|\\ \psi_2'|\\ \psi_3'|\\ \psi_4'|\\ \overline{\psi_4'^c}|\end{array}\begin{array}{c}\begin{array}{ccccc}\psi_1'^c & \psi_2'^c & \psi_3'^c & \psi_4'^c & \overline{\psi_4'}\end{array}\\ \left(\begin{array}{ccccc} & & & & 0\\ & & & & 0\\ & & \widetilde{y}_{\alpha\beta}^{\psi'} & & 0\\ & & & & \hat{M}_4^{\psi}\\ 0 & 0 & 0 & \hat{M}_4^{\psi^c} & 0\end{array}\right)\end{array}, \tag{4.22}$$

where $\widetilde{y}_{\alpha\beta}^{\psi'}$ is the upper 4×4 block of the mass matrix in this basis. The key feature of Eq. (4.22) are the zeros in the fifth row and column which are achieved by rotating the four families by the unitary 4×4 transformations,

$$V_{\psi}=V_{34}^{\psi}=\begin{pmatrix}1&0&0&0\\0&1&0&0\\0&0&c_{34}^{\psi}&s_{34}^{\psi}\\0&0&-s_{34}^{\psi}&c_{34}^{\psi}\end{pmatrix}, \tag{4.23}$$

$$V_{\psi^c}=V_{34}^{\psi^c}V_{24}^{\psi^c}=\begin{pmatrix}1&0&0&0\\0&1&0&0\\0&0&c_{34}^{\psi^c}&s_{34}^{\psi^c}\\0&0&-s_{34}^{\psi^c}&c_{34}^{\psi^c}\end{pmatrix}\begin{pmatrix}1&0&0&0\\0&c_{24}^{\psi^c}&0&s_{24}^{\psi^c}\\0&0&1&0\\0&-s_{24}^{\psi^c}&0&c_{24}^{\psi^c}\end{pmatrix},$$

where we have defined $s_{i4}^{\psi^{(c)}} \equiv \sin\theta_{i4}^{\psi^{(c)}}$, $c_{i4}^{\psi^{(c)}} \equiv \cos\theta_{i4}^{\psi^{(c)}}$, with the mixing angles and the physical masses of the vector-like fermions given by

$$s_{34}^{\psi} = \frac{x_{34}^{\psi}\langle\phi\rangle}{\sqrt{\left(x_{34}^{\psi}\langle\phi\rangle\right)^2 + \left(M_4^{\psi}\right)^2}}\,, \qquad s_{24}^{\psi^c} = \frac{x_{42}^{\psi^c}\langle\overline{\phi}\rangle}{\sqrt{\left(x_{42}^{\psi^c}\langle\overline{\phi}\rangle\right)^2 + \left(M_4^{\psi^c}\right)^2}}\,, \tag{4.24}$$

$$s_{34}^{\psi^c} = \frac{x_{43}^{\psi^c}\langle\overline{\phi}\rangle}{\sqrt{\left(x_{42}^{\psi^c}\langle\overline{\phi}\rangle\right)^2 + \left(x_{43}^{\psi^c}\langle\overline{\phi}\rangle\right)^2 + \left(M_4^{\psi^c}\right)^2}}\,, \qquad \hat{M}_4^{\psi} = \sqrt{\left(x_{34}^{\psi}\langle\phi\rangle\right)^2 + \left(M_4^{\psi}\right)^2}\,, \tag{4.25}$$

$$\hat{M}_4^{\psi^c} = \sqrt{\left(x_{42}^{\psi^c}\langle\overline{\phi}\rangle\right)^2 + \left(x_{43}^{\psi^c}\langle\overline{\phi}\rangle\right)^2 + \left(M_4^{\psi^c}\right)^2}\,, \tag{4.26}$$

Notice that we recover the expressions in the mass insertion approximation when $\langle\phi\rangle \ll M$, and in this case the mixing angles above are given by the usual NP scales ratios of a theory of flavour, $\langle\phi\rangle/M$ (see Section 1.10). As long as these ratios are held fixed to explain the SM Yukawa couplings, the independent scales $\langle\phi\rangle$ and M may be anywhere *from the Planck scale to the electroweak scale.* In our model, however, we shall see that some of these scales will be fixed to the TeV via the connection with the B-anomalies, leading to a testable theory of flavour with significant low-energy implications.

Now we apply the transformations in Eq. (4.23) to the upper 4×4 block of (4.21), obtaining effective Yukawa couplings for the chiral fermions as the upper 3×3 block of the mass matrix in the new basis,

$$\mathcal{L}_{eff}^{Yuk3\times3} = \psi'^{\mathrm{T}}_i V_\psi y^{\psi}_{\alpha\beta} V^{\dagger}_{\psi^c} \psi'^{c}_j + \text{h.c.}\,, \tag{4.27}$$

$$\psi'^{\mathrm{T}}_\alpha = \psi^{\mathrm{T}}_\alpha V^{\dagger}_\psi\,, \qquad \psi'^{c}_\alpha = V_{\psi^c}\psi^c_\alpha\,, \tag{4.28}$$

where $i,j=1,2,3$. We obtain

$$\mathcal{L}_{eff}^{Yuk,3\times3} = \begin{pmatrix} & \psi'^c_1 & \psi'^c_2 & \psi'^c_3 \\ \hline \psi'_1| & 0 & 0 & 0 \\ \psi'_2| & 0 & 0 & 0 \\ \psi'_3| & 0 & 0 & c_{34}^{\psi^c} s_{34}^{\psi} y_{43}^{\psi} \end{pmatrix} H + \begin{pmatrix} & \psi'^c_1 & \psi'^c_2 & \psi'^c_3 \\ \hline \psi'_1| & 0 & 0 & 0 \\ \psi'_2| & 0 & s_{24}^{\psi^c} y_{24}^{\psi} & c_{24}^{\psi^c} s_{34}^{\psi^c} y_{24}^{\psi} \\ \psi'_3| & 0 & c_{34}^{\psi} s_{24}^{\psi^c} y_{34}^{\psi} & c_{34}^{\psi} c_{24}^{\psi^c} s_{34}^{\psi^c} y_{34}^{\psi} \end{pmatrix} \overline{H} \tag{4.29}$$

plus hermitian conjugate. Until the breaking of the twin PS symmetry, the matrix above is Pati-Salam universal, so all fermions of the same family share the same effective Yukawa couplings. If we impose the dominance of the doublet messenger fermions over the singlet messenger fermions, as we did in Chapter 3,

$$M_4^{\psi} \ll M_4^{\psi^c}\,, \tag{4.30}$$

then the first matrix in Eq. (4.29) generates larger effective third family Yukawa couplings, while the second matrix generates suppressed second family Yukawa couplings

and mixings. This way, the hierarchy of quark and lepton masses in the SM is re-expressed as the hierarchy of scales in Eq. (4.30). Remarkably, the hierarchical relation in Eq. (4.30) will lead to small couplings of ψ^c chiral fermions (eventually SM $SU(2)_L$ singlets) to $SU(4)^I_{PS}$ gauge bosons, hence obtaining dominantly left-handed U_1 couplings. The couplings of the ψ^c fermions will be suppressed, connected to the origin of second family fermion masses, and this way the tight high-p_T constraints that afflict other U_1 models can be relaxed (see more in Section 4.6.8).

On the other hand, since the sum of the two matrices in Eq. (4.29) has rank 1, the first family will be massless, which is a good first order approximation. Indeed, the masses of first family fermions are protected by an accidental $U(1)$ symmetry that will be broken at much higher energies via new dynamics connected the second PS group, providing the small masses of first family fermions as discussed in the next subsection.

After the symmetry breaking of the twin PS group to G_{4321}, the Yukawa couplings x^{ψ}_{34}, $x^{\psi^c}_{42,43}$ and vector-like masses M^{ψ}_4, $M^{\psi^c}_4$ remain universal up to small RGE effects, however the Yukons decompose in a different way for lepton and quarks as per Eq. (4.13). Due to this decomposition, the mixing angles in Eq. (4.29) are now different for quarks and leptons. The VEVs of the Yukons break the remaining $SU(4)$ symmetry relating quarks and leptons, but the Yukawa couplings still exhibit an accidental $SU(2)_R$ symmetry relating u^c and d^c quarks. Hence, the mixing angles $s^{u^c}_{i4}$ and $s^{d^c}_{i4}$ are the same for up and down quarks, and we define $q^c = u^c, d^c$. On the other hand, the Higgs fields H and $\overline{H}$ decompose as personal Higgs doublets for the second and third fermions as per Eqs. (4.14) and (4.15). The personal Higgs are introduced in order to break the accidental symmetry $SU(2)_R$ in the Yukawa couplings, otherwise the mass matrices in the up and down sector would remain identical at tree-level. A similar discussion applies to charged leptons and neutrinos, and personal Higgses apply in the same way. Mass terms for second and third family fermions will be obtained after the personal Higgs develop VEVs $\langle H_\alpha \rangle \ll \langle \phi \rangle$, which also play the role of breaking EW symmetry in the SM, see Section 4.2.2. This way, Eq. (4.29) decomposes for each charged sector as the following effective mass matrices,

$$M^u_{\text{eff}} = \begin{pmatrix} & u'^c_1 & u'^c_2 & u'^c_3 \\ \hline Q'_1 & 0 & 0 & 0 \\ Q'_2 & 0 & 0 & 0 \\ Q'_3 & 0 & 0 & s^{Q}_{34} y^{\psi}_{43} \end{pmatrix} \langle H_t \rangle + \begin{pmatrix} & u'^c_1 & u'^c_2 & u'^c_3 \\ \hline Q'_1 & 0 & 0 & 0 \\ Q'_2 & 0 & s^{q^c}_{24} y^{\psi}_{24} & s^{q^c}_{34} y^{\psi}_{24} \\ Q'_3 & 0 & c^{Q}_{34} s^{q^c}_{24} y^{\psi}_{34} & c^{Q}_{34} s^{q^c}_{34} y^{\psi}_{34} \end{pmatrix} \langle H_c \rangle + \text{h.c.}\,, \tag{4.31}$$

$$M^d_{\text{eff}} = \begin{pmatrix} & d'^c_1 & d'^c_2 & d'^c_3 \\ \hline Q'_1 & 0 & 0 & 0 \\ Q'_2 & 0 & 0 & 0 \\ Q'_3 & 0 & 0 & s^{Q}_{34} y^{\psi}_{43} \end{pmatrix} \langle H_b \rangle + \begin{pmatrix} & d'^c_1 & d'^c_2 & d'^c_3 \\ \hline Q'_1 & 0 & 0 & 0 \\ Q'_2 & 0 & s^{q^c}_{24} y^{\psi}_{24} & s^{q^c}_{34} y^{\psi}_{24} \\ Q'_3 & 0 & c^{Q}_{34} s^{q^c}_{24} y^{\psi}_{34} & c^{Q}_{34} s^{q^c}_{34} y^{\psi}_{34} \end{pmatrix} \langle H_s \rangle + \text{h.c.}\,, \tag{4.32}$$

$$M^e_{\rm eff} = \begin{pmatrix} & e'^c_1 & e'^c_2 & e'^c_3 \\ L'_1| & 0 & 0 & 0 \\ L'_2| & 0 & 0 & 0 \\ L'_3| & 0 & 0 & s^L_{34} y^\psi_{43} \end{pmatrix} \langle H_\tau \rangle + \begin{pmatrix} & e'^c_1 & e'^c_2 & e'^c_3 \\ L'_1| & 0 & 0 & 0 \\ L'_2| & 0 & s^{e^c}_{24} y^\psi_{24} & s^{e^c}_{34} y^\psi_{24} \\ L'_3| & 0 & c^L_{34} s^{e^c}_{24} y^\psi_{34} & c^L_{34} s^{e^c}_{34} y^\psi_{34} \end{pmatrix} \langle H_\mu \rangle + \text{h.c.}\,, \tag{4.33}$$

where the Yukawas y^ψ_{43} and $y^\psi_{24,34}$ are Pati-Salam universal, and we have approximated all cosines related to ψ^c fields to be 1 due to the hierarchy of vector-like masses in Eq. (4.30). We obtain a similar Dirac mass matrix for neutrinos, to be discussed in the next subsection.

Due to the fact that vector-like fermions are much heavier than SM fermions, the fourth row and column, that we have intentionally ignored when writing Eqs. (4.31), (4.32) and (4.33), can be decoupled from the 3×3 upper blocks, which we can diagonalise via independent 2-3 transformations for each charged sector V^u_{23}, V^d_{23} and V^e_{23}. Similar transformations apply for $SU(2)_L$ singlet fermions u^c, d^c, e^c, in such a way that the mass matrices in Eqs. (4.31), (4.32), (4.33) are diagonalised as

$$V^u_{23} M^u_{\rm eff} V^{u^c\dagger}_{23} = \text{diag}(0, m_c, m_t)\,, \tag{4.34}$$

$$V^d_{23} M^d_{\rm eff} V^{d^c\dagger}_{23} = \text{diag}(0, m_s, m_b)\,, \tag{4.35}$$

$$V^e_{23} M^e_{\rm eff} V^{e^c\dagger}_{23} = \text{diag}(0, m_\mu, m_\tau)\,. \tag{4.36}$$

The CKM matrix is then given by

$$V_{\rm CKM} = V^u_{23} V^{d\dagger}_{23} = \begin{pmatrix} 1 & 0 & 0 \\ 0 & c^u_{23}c^d_{23} + s^u_{23}s^d_{23} & c^d_{23}s^u_{23} - c^u_{23}s^d_{23} \\ 0 & -\left(c^d_{23}s^u_{23} - c^u_{23}s^d_{23}\right) & c^u_{23}c^d_{23} + s^u_{23}s^d_{23} \end{pmatrix} \approx \begin{pmatrix} 1 & 0 & 0 \\ 0 & V_{cs} & V_{cb} \\ 0 & V_{ts} & V_{tb} \end{pmatrix}. \tag{4.37}$$

We do not address the mixing involving the first family nor the CP-violating phase since so far first family fermions remain massless, as previously discussed. We are however required to preserve V_{cb} as [21]

$$V_{cb} = (40.8 \pm 1.4) \times 10^{-3} \approx s^u_{23} - s^d_{23}\,, \tag{4.38}$$

where in the last step we have approximated the cosines to be 1. We will not fit V_{ts}, V_{tb} and V_{cs} up to the experimental precision, as corrections related to the first family mixing (and CP-violating phase) are required.

In the following we explore the parameters in the mass matrices of Eqs. (4.31), (4.32), (4.33), and their impact over the diagonalisation of the mass matrices:

- In very good approximation, the mass of the top quark is given by the (3,3) entry in the first matrix of Eq. (4.31), i.e.

$$m_t \approx s^Q_{34} y^\psi_{43} \langle H_t \rangle = s^Q_{34} y^\psi_{43} \alpha_u \frac{1}{\sqrt{1+\tan^{-2}\beta}} \frac{v_{\rm SM}}{\sqrt{2}}\,, \tag{4.39}$$

where we have applied $\langle H_t \rangle = \alpha_u v_u$ as per Eq. (4.18), with

$$v_u = \sin\beta \frac{v_{\rm SM}}{\sqrt{2}} = \frac{1}{\sqrt{1+\tan^{-2}\beta}} \frac{v_{\rm SM}}{\sqrt{2}}\,, \tag{4.40}$$

as in usual 2HDM. If we consider $\tan\beta \approx 10$ and $\alpha_u \sim \mathcal{O}(1)$, then we obtain

$$m_t \approx s_{34}^Q y_{43}^\psi \frac{v_{\rm SM}}{\sqrt{2}} \equiv y_t \frac{v_{\rm SM}}{\sqrt{2}}\,. \tag{4.41}$$

From the expression above, it is clear that very large mixing $s_{34}^Q \approx 1$ is required in order to preserve a natural y_{43}^ψ, and to avoid perturbativity issues in the top Yukawa. Moreover, we will see that maximal values for s_{34}^Q are also well motivated by the $R_{D^{(*)}}$ anomaly, leading to a clear connection between B-physics and the flavour puzzle only present in this model.

- In the bullet point above, the effective top Yukawa coupling in the Higgs basis has been estimated as $y_t \approx 1$. By following the same procedure, we can see that all fermion masses can be accommodated with natural parameters. Remarkably, we obtain that all the effective Yukawa couplings are SM-like in the Higgs basis, explaining the observed pattern of SM Yukawa couplings at low energies.

- The mixing between left-handed quark fields arise mainly from the off-diagonal (2,3) entry in the quark mass matrices, which is controlled by $s_{34}^{q^c}$. This mixing can be estimated for each sector by the ratio of the (2,3) entry over the (3,3) entry, i.e.

$$\theta_{23}^u \approx \frac{s_{34}^{q^c} y_{24}^\psi \langle H_c \rangle}{s_{34}^Q y_{43}^\psi \langle H_t \rangle} \approx \frac{m_c}{m_t} \simeq \mathcal{O}(0.1 V_{cb})\,, \qquad \theta_{23}^d \approx \frac{s_{34}^{q^c} y_{24}^\psi \langle H_s \rangle}{s_{34}^Q y_{43}^\psi \langle H_b \rangle} \approx \frac{m_s}{m_b} \simeq \mathcal{O}(V_{cb})\,, \tag{4.42}$$

obtained under the assumption $s_{34}^{q^c} \approx s_{24}^{q^c}$, which is reasonable given that both are suppressed by the same scale $M_4^{\psi^c}$. Therefore, the model predicts that V_{cb} originates mainly from the down sector, while the mixing in the up sector is small, suppressed by the larger mass hierarchy of the up sector. The specific values of the mixing angles can be different if we relax $s_{24}^{q^c} \approx s_{34}^{q^c}$, but the CKM remains down-dominated in any case.

- The charged lepton sector follows a similar discussion as that of the quark sector. If $s_{34}^Q \approx 1$, then s_{34}^L is expected to be large as well and we obtain $\langle H_\tau \rangle \approx m_\tau$. Under the assumption $s_{24}^{e^c} \approx s_{34}^{e^c}$, the charged lepton mixing is predicted as

$$\theta_{23}^e \approx \frac{s_{34}^{e^c} y_{24}^\psi \langle H_\mu \rangle}{s_{34}^L y_{43}^\psi \langle H_\tau \rangle} \approx \frac{m_\mu}{m_\tau} \simeq \mathcal{O}(V_{cb})\,. \tag{4.43}$$

A particularly interesting situation arises when $s_{34}^{e^c} > s_{24}^{e^c}$, where a larger θ_{23}^e contributing to large atmospheric neutrino mixing is obtained. In this scenario,

Field	$SU(4)^I_{PS}$	$SU(2)^I_L$	$SU(2)^I_R$	$SU(4)^{II}_{PS}$	$SU(2)^{II}_L$	$SU(2)^{II}_R$	$\mathbb{Z}_2$
$\psi_{1,2,3}$	$\mathbf{1}$	$\mathbf{1}$	$\mathbf{1}$	$\mathbf{4}$	$\mathbf{2}$	$\mathbf{1}$	(-), (+), (+)
$\psi^c_{1,2,3}$	$\mathbf{1}$	$\mathbf{1}$	$\mathbf{1}$	$\overline{\mathbf{4}}$	$\mathbf{1}$	$\overline{\mathbf{2}}$	(-), (+), (+)
ψ_5	$\mathbf{1}$	$\mathbf{2}$	$\mathbf{1}$	$\mathbf{4}$	$\mathbf{1}$	$\mathbf{1}$	(+)
$\overline{\psi_5}$	$\mathbf{1}$	$\overline{\mathbf{2}}$	$\mathbf{1}$	$\overline{\mathbf{4}}$	$\mathbf{1}$	$\mathbf{1}$	(+)
ψ^c_5	$\mathbf{1}$	$\mathbf{2}$	$\mathbf{1}$	$\overline{\mathbf{4}}$	$\overline{\mathbf{2}}$	$\overline{\mathbf{2}}$	(+)
$\overline{\psi^c_5}$	$\mathbf{1}$	$\overline{\mathbf{2}}$	$\mathbf{1}$	$\mathbf{4}$	$\mathbf{2}$	$\mathbf{2}$	(+)
h	$\mathbf{1}$	$\overline{\mathbf{2}}$	$\mathbf{1}$	$\mathbf{1}$	$\mathbf{1}$	$\mathbf{2}$	(-)
Φ	$\mathbf{1}$	$\mathbf{2}$	$\mathbf{1}$	$\mathbf{1}$	$\overline{\mathbf{2}}$	$\mathbf{1}$	(+)
$\overline{\Phi}$	$\mathbf{1}$	$\mathbf{1}$	$\overline{\mathbf{2}}$	$\mathbf{1}$	$\mathbf{1}$	$\mathbf{2}$	(+)
ξ_{15}	$\mathbf{1}$	$\mathbf{1}$	$\mathbf{1}$	$\mathbf{15}$	$\mathbf{1}$	$\mathbf{1}$	(+)

TABLE 4.2: Fields participating in the origin of first family fermion masses and mixing.

interesting signals in CLFV processes such as $\tau \to 3\mu$ or $\tau \to \mu\gamma$ arise, mediated at tree-level by $SU(4)^I_{PS}$ gauge bosons. This is obtained if $x^{\psi^c}_{43} > x^{\psi^c}_{42}$, without the need of any tuning.

- Unlike private Higgs models [348–351], the personal Higgs VEVs are not hierarchical, all of order 1-10 GeV, with the exception of the top one whose VEV is approximately that of the SM Higgs doublet, as discussed above. The reason is that the fermion mass hierarchies arise from the hierarchies $s^{\psi}_{34} \gg s^{\psi^c}_{24}, s^{\psi^c}_{34}$, which find their natural origin in the messenger dominance $M^{\psi}_4 \ll M^{\psi^c}_4$ of Eq. (4.30). The latter simultaneously leads to dominantly left-handed leptoquark currents, which is an interesting connection only present in our model.

4.2.4 First family fermion masses and comments about neutrino masses

So far we have shown how the masses and mixing of second and third family fermions arise in the twin PS model, via dynamics connected to the $SU(4)^I_{PS}$ group broken at the TeV scale. The first family remains massless so far, protected by an accidental $U(1)$ symmetry. In this section we introduce small breaking of such symmetry via dynamics connected to the second PS group $SU(4)^{II}_{PS}$, broken at a much higher scale $M_{\text{High}} \gtrsim 1$ PeV. In this sense, our model is a multi-scale theory of flavour where the different flavour hierarchies are explained by hierarchical NP scales, in the spirit of other theories of flavour such as [3, 114–121], which are commonly connected with the B-anomalies as well. However, all those alternative theories require the family decomposition of the SM group to obtain an approximate $U(2)^5$ flavour symmetry (see Section 1.9.3). In contrast, our model achieves the same goals without the need of family decomposing the SM nor claiming $U(2)^5$, but rather via mixing between SM and vector-like fermions controlled by the mechanism of messenger dominance [171], this way providing an alternative and novel approach to connect the B-anomalies with the origin of the flavour structure of the SM.

In order to explain first family masses, we add an extra family of vector-like fermions that we call the "fifth" family, transforming in the fundamental of $SU(4)^{II}_{PS}$ but being a singlet under $SU(4)^{I}_{PS}$. We also introduce a non-standard Higgs field, as shown in Table 4.2. This choice ensures that the new vector-like family will mix with chiral fermions, including the first family, without providing couplings of the first family to the TeV scale $SU(4)^{I}_{PS}$ gauge bosons that are relevant for B-physics.

We also introduce a discrete symmetry $\mathbb{Z}_2$ to distinguish the first family and the new Higgs h, in order to achieve a texture zero in the (1,1) entry of the effective Yukawa matrices. Such a texture has been suggested to explain the empirical relation $V_{us} \sim \sqrt{m_d/m_s}$ [352], delivering a Cabibbo angle that mostly originates from mixing in the down sector. The new terms in the renormalisable Lagrangian are

$$\mathcal{L}_5^{ren} = y^{\psi}_{15} h \psi_1 \psi^c_5 + y^{\psi}_{51} h \psi_5 \psi^c_1 + x^{\psi}_{i5} \Phi \psi_i \overline{\psi_5} + x^{\psi^c}_{5i} \overline{\psi^c_5} \Phi \psi^c_i + M^{\psi}_5 \psi_5 \overline{\psi_5} + M^{\psi^c}_5 \psi^c_5 \overline{\psi^c_5}\,, \quad (4.44)$$

plus h.c., where $i = 2, 3$. Note that Φ gets a VEV spontaneously breaking $SU(2)^I_L$ and $SU(2)^{II}_L$ down to their diagonal subgroup at very high energies. We can arrange these couplings in matrix form along with those of Eq. (4.21), obtaining

$$M^{\psi} = \begin{pmatrix} & \psi^c_1 & \psi^c_2 & \psi^c_3 & \psi^c_4 & \overline{\psi_4} & \psi^c_5 & \overline{\psi_5} \\ \hline \psi_1 | & 0 & 0 & 0 & 0 & 0 & y^{\psi}_{15} h & 0 \\ \psi_2 | & 0 & 0 & 0 & y^{\psi}_{24} \overline{H} & 0 & 0 & x^{\psi}_{25} \Phi \\ \psi_3 | & 0 & 0 & 0 & y^{\psi}_{34} \overline{H} & x^{\psi}_{34} \phi & 0 & x^{\psi}_{35} \Phi \\ \psi_4 | & 0 & 0 & y^{\psi}_{43} H & 0 & M^{\psi}_4 & 0 & 0 \\ \overline{\psi^c_4} | & 0 & x^{\psi^c}_{42} \overline{\phi} & x^{\psi^c}_{43} \overline{\phi} & M^{\psi^c}_4 & 0 & 0 & 0 \\ \psi_5 | & y^{\psi}_{51} h & 0 & 0 & 0 & 0 & 0 & M^{\psi}_5 \\ \overline{\psi^c_5} | & 0 & x^{\psi^c}_{52} \Phi & x^{\psi^c}_{53} \Phi & 0 & 0 & M^{\psi^c}_5 & 0 \end{pmatrix} . \quad (4.45)$$

Assuming $\langle h \rangle, \langle \Phi \rangle \ll M^{\psi,\psi^c}_5$, effective Yukawa couplings for the first family can be extracted in the mass insertion approximation as

$$\mathcal{L}^{Yuk,3\times3}_{eff} = \begin{pmatrix} & \psi^c_1 & \psi^c_2 & \psi^c_3 \\ \hline \psi_1 | & 0 & 0 & 0 \\ \psi_2 | & x^{\psi}_{25} y^{\psi}_{51} & 0 & 0 \\ \psi_3 | & x^{\psi}_{35} y^{\psi}_{51} & 0 & 0 \end{pmatrix} \frac{\langle \Phi \rangle}{M^{\psi}_5} h + \begin{pmatrix} & \psi^c_1 & \psi^c_2 & \psi^c_3 \\ \hline \psi_1 | & 0 & y^{\psi}_{15} x^{\psi^c}_{52} & y^{\psi}_{15} x^{\psi^c}_{53} \\ \psi_2 | & 0 & 0 & 0 \\ \psi_3 | & 0 & 0 & 0 \end{pmatrix} \frac{\langle \Phi \rangle}{M^{\psi^c}_5} h + \text{h.c.}\,, \quad (4.46)$$

which needs to be added to the matrix in Eq. (4.29) in order to obtain the full set of effective Yukawa couplings. One can see that such effective Yukawa couplings provide masses for the first family, and their hierarchical smallness with respect to the second and third family fermions can be explained if we extend the messenger dominance in

Eq. (4.30) to include the fifth family,

$$\frac{\langle\Phi\rangle}{M_5^{\psi}}, \frac{\langle\Phi\rangle}{M_5^{\psi^c}} \ll \frac{\langle\overline{\phi}\rangle}{M_4^{\psi^c}} \ll \frac{\langle\phi\rangle}{M_4^{\psi}} \lesssim 1\,. \tag{4.47}$$

In this manner, the hierarchies of quark and charged lepton masses in the SM Yukawa couplings are re-expressed as the hierarchy of scales in Eq. (4.47). This is not just a reparameterisation of the hierarchies, since it involves extra dynamics and testable experimental predictions, such as the vector-like fermion spectrum with $M_4^{\psi} \sim 1$ TeV as motivated to explain the $R_{D^{(*)}}$ anomalies.

The Higgs h decomposes at low energies as a type II 2HDM, where $h_u \sim (\mathbf{1}, \overline{\mathbf{2}}, -1/2)$ and $h_d \sim (\mathbf{1}, \overline{\mathbf{2}}, 1/2)$ get effective VEVs like the personal Higgs as $\langle h_u\rangle = \epsilon_u\langle H_u\rangle$ and $\langle h_d\rangle = \epsilon_d\langle H_d\rangle$. These VEVs split the up-quark and down-quark masses, which would otherwise be degenerate due to the twin PS symmetry. However, the down-quark mass and the electron mass remain degenerate so far. They can be split simply by introducing a Higgs transforming in the adjoint representation of $SU(4)^{II}_{PS}$, $\xi_{15} \sim (\mathbf{15}, \mathbf{1}, \mathbf{1})_{II}$, that gets a VEV to split the masses of the fifth family fermions. This allows to write the couplings

$$\mathcal{L}_5^{ren} \supset \lambda^{\psi}\psi_5\overline{\psi_5}\xi_{15} + \lambda^{\psi^c}\psi_5^c\overline{\psi_5^c}\xi_{15} + \text{h.c.} \tag{4.48}$$

These couplings result in quark-lepton mass splittings proportional to the generator $T^{II}_{15} = \text{diag}(1,1,1,-3)/(2\sqrt{6})$ leading to different contributions to the fifth family quark and lepton masses,

$$M_5^Q \equiv M_5^{\psi} + \frac{\lambda^{\psi}\langle\xi_{15}\rangle}{2\sqrt{6}}\,, \quad M_5^L \equiv M_5^{\psi} - 3\frac{\lambda^{\psi}\langle\xi_{15}\rangle}{2\sqrt{6}}\,, \tag{4.49}$$

$$M_5^{q^c} \equiv M_5^{\psi^c} + \frac{\lambda^{\psi^c}\langle\xi_{15}\rangle}{2\sqrt{6}}\,, \quad M_5^{e^c} \equiv M_5^{\psi^c} - 3\frac{\lambda^{\psi^c}\langle\xi_{15}\rangle}{2\sqrt{6}}\,. \tag{4.50}$$

If the mass terms proportional to $\langle\xi_{15}\rangle$ dominate over the original mass terms, then they can be responsible for the smallness of the electron mass compared to the down-quark mass. Notice that the VEV $\langle\xi_{15}\rangle$ breaks $SU(4)^{II}_{PS}$ at very high scales, providing a natural suppression for the first family masses. We also mention that an alternative mechanism was presented in [169], where the mass of the fifth family is split via a non-renormalisable operator containing the Higgs H' and $\overline{H}'$, which then combine into an adjoint of $SU(4)^{II}_{PS}$ as discussed in [353] to give the desired splitting proportional to T^{II}_{15}.

Finally we comment on the origin of neutrino masses in our model. In principle, neutrinos get a Dirac mass matrix similar to that of up-type quarks, hence predicting $m_{\nu_\tau} = m_t$ as usual in Pati-Salam models, along with a hierarchical pattern of neutrino masses with small mixing. However, the singlet neutrinos ν^c can get a further Majorana mass matrix via non-renormalisable operators containing the Higgs H' and $\overline{H}'$ that break $SU(4)^{II}_{PS}$. By means of adding a $\mathbb{Z}_6$ family symmetry broken by a Majoron scalar, it was

shown in [169] that the tiny masses of active neutrinos can be obtained via a type I seesaw mechanism featuring single right-handed neutrino dominance [354, 355]. One right-handed neutrino is much heavier than the others, getting a mass at the heavy scale $\langle H' \rangle$ which has to be close to the GUT scale in order to explain the tiny neutrino masses. The hierarchies of Majorana masses for right-handed neutrinos then cancel the hierarchies of the Dirac neutrino matrix, allowing to reproduce the PMNS mixing matrix with large mixing angles. Note that this type of mechanism are common in Pati-Salam models. However, we will see later that the explanation of the B-anomalies pushes the twin PS model close to the boundary of the perturbative domain, requiring that $SU(4)^{II}_{PS}$ is broken not far above 1 PeV. This seems in tension with $\langle H' \rangle \approx 10^{16}$ GeV as in the seesaw mechanism of [169], suggesting the implementation of a low scale seesaw mechanism. Given that in our model the origin of neutrino masses is independent of the low-energy phenomenology explaining the B-anomalies, we leave a further discussion about the origin of neutrino masses for the future. In a similar manner, given that the origin of first family masses is related to dynamics at the very heavy scale of $SU(4)^{II}_{PS}$ breaking, with negligible impact for low-energy phenomenology, in the rest of this chapter we will neglect first family fermion masses and focus on B-physics phenomenology.

4.2.5 The low energy theory G_{4321}

In this section we shall discuss the G_{4321} theory that breaks down to the SM symmetry group at low energies $G_{4321} \to G_{\rm SM}$, achieved via the scalars $\phi_3(\mathbf{4}, \overline{\mathbf{3}}, \mathbf{1} \oplus \mathbf{3}, -1/6)$ and $\phi_1(\mathbf{4}, \mathbf{1}, \mathbf{1} \oplus \mathbf{3}, 1/2)$ developing the VEVs

$$\langle \phi_3 \rangle = \begin{pmatrix} \frac{v_3}{\sqrt{2}} & 0 & 0 \\ 0 & \frac{v_3}{\sqrt{2}} & 0 \\ 0 & 0 & \frac{v_3}{\sqrt{2}} \\ 0 & 0 & 0 \end{pmatrix}, \quad \langle \phi_1 \rangle = \begin{pmatrix} 0 \\ 0 \\ 0 \\ \frac{v_1}{\sqrt{2}} \end{pmatrix}, \tag{4.51}$$

where v_1, $v_3 \lesssim 1\,\text{TeV}$, and analogously for $\overline{\phi_3}$ and $\overline{\phi_1}$ developing VEVs $\overline{v}_3$ and $\overline{v}_1$, leading to the symmetry breaking of G_{4321} down to the SM gauge group,

$$SU(4)^I_{PS} \times SU(3)^{II}_c \times SU(2)^{I+II}_L \times U(1)_{Y'} \to SU(3)_c \times SU(2)_L \times U(1)_Y\,. \tag{4.52}$$

Here $SU(4)^I_{PS}$ is broken to $SU(3)^I_c \times U(1)^I_{B-L}$(at the level of fermion representations, vector-like quarks and leptons are split $\mathbf{4}^I \to (\mathbf{3}, 1/6)^I \oplus (\mathbf{1}, -1/2)^I$), with $SU(3)^I_c \times SU(3)^{II}_c$ further broken to the diagonal subgroup $SU(3)^{I+II}_c$, identified as SM QCD. On the other hand, $SU(2)^{I+II}_L$ remains as the SM $SU(2)_L$. The abelian generators are broken to SM hypercharge $U(1)_Y$ given by $Y = T^I_{B-L} + Y' = T^I_{B-L} + T^{II}_{B-L} + T^{I+II}_{3R}$. The physical massive scalar spectrum includes a real colour octet, three SM singlets and a complex scalar transforming as $(\mathbf{3}, \mathbf{1}, 2/3)$. The heavy gauge boson spectrum includes a vector leptoquark $U^\mu_1 \sim (\mathbf{3}, \mathbf{1}, 2/3)$, a colour octet $g'_\mu \sim (\mathbf{8}, \mathbf{1}, 0)$ also identified as coloron, and a $Z'_\mu \sim (\mathbf{1}, \mathbf{1}, 0)$. The heavy gauge bosons arise from the different steps of

the symmetry breaking,

$$SU(4)^I_{PS} \to SU(3)^I_c \times U(1)^I_{B-L} \quad \Rightarrow U_1^\mu(\mathbf{3},\mathbf{1},2/3)\,, \tag{4.53}$$
$$SU(3)^I_c \times SU(3)^{II}_c \to SU(3)^{I+II}_c \quad \Rightarrow g'^\mu(\mathbf{8},\mathbf{1},0)\,, \tag{4.54}$$
$$U(1)^I_{B-L} \times U(1)_{Y'} \to U(1)_Y \quad \Rightarrow Z'^\mu(\mathbf{1},\mathbf{1},0)\,. \tag{4.55}$$

The gauge boson masses resulting from the symmetry breaking in Eq. (4.30) are a generalisation of the results in [267, 345],

$$\begin{aligned} M_{U_1} &= \frac{1}{\sqrt{2}} g_4 \sqrt{v_1^2 + v_3^2}\,, \\ M_{g'} &= \sqrt{g_4^2 + g_3^2}\, v_3\,, \\ M_{Z'} &= \frac{\sqrt{3}}{2}\sqrt{g_4^2 + \frac{2}{3}g_1^2}\sqrt{v_1^2 + \frac{1}{3}v_3^2}\,, \end{aligned} \tag{4.56}$$

where we have assumed $\overline{v}_3 \approx v_3$ and $\overline{v}_1 \approx v_1$ for simplicity. The mass of the coloron depends only on v_3, and the scenario $v_3 \gg v_1$ leads to the approximate relation $M_{g'} \approx \sqrt{2} M_{U_1}$. This way the coloron, which suffers from stronger high-p_T constraints, can be slightly heavier than the vector leptoquark, as the latter is the only one required to be light in order to explain the R_{D^*} anomalies.

In the original interaction basis, the heavy gauge bosons couple to left-handed fermions (including VL left-handed fermions) via the interactions[3]

$$\frac{g_4}{\sqrt{2}} \left(Q_4^\dagger \bar{\sigma}^\mu L_4 + \text{h.c.} \right) U_{1\mu} + \text{h.c.}\,, \tag{4.57}$$

$$\frac{g_4 g_s}{g_3} \left(Q_4^\dagger \bar{\sigma}^\mu T^a Q_4 - \frac{g_3^2}{g_4^2} Q_i^\dagger \bar{\sigma}^\mu T^a Q_i \right) g'^a_\mu\,, \tag{4.58}$$

$$\frac{\sqrt{3}}{\sqrt{2}} \frac{g_4 g_Y}{g_1} \left(\frac{1}{6} Q_4^\dagger \bar{\sigma}^\mu Q_4 - \frac{1}{2} L_4^\dagger \bar{\sigma}^\mu L_4 - \frac{g_1^2}{9 g_4^2} Q_i^\dagger \bar{\sigma}^\mu Q_i + \frac{g_1^2}{3 g_4^2} L_i^\dagger \bar{\sigma}^\mu L_i \right) Z'_\mu\,. \tag{4.59}$$

Similar couplings are obtained for right-handed fermions, although the small mixing between right-handed fermions and VL fermions heavily suppresses the couplings of U_1 to right-handed fermions. This is not a trivial result, as these mixing angles are small because they are connected to the origin of second family fermion masses (see Section 4.2.3). Therefore, the couplings of U_1 to right-handed fermions can be safely neglected. This way, the U_1 couplings will be dominantly left-handed, which can alleviate the stringent bounds from high-p_T searches, in contrast to the alternative models in the literature based on the family decomposition of the SM [115–117, 119, 120]. Similar couplings are obtained for the VL partners in the conjugate representations, however those couplings are irrelevant for the phenomenology since the conjugate partners do not mix with the SM fermions. The couplings of the coloron and Z' to chiral fermions remain

[3] Notice that we continue working in the 2-component notation introduced in Appendix A

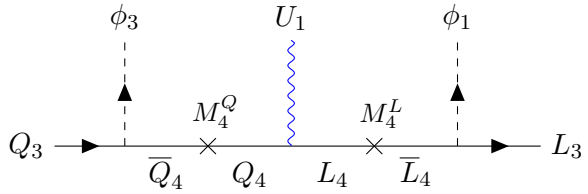

FIGURE 4.3: Diagram in the model which leads to the effective U_1 couplings in the mass insertion approximation.

flavour universal, in contrast to the left-handed sector, hence providing no meaningful phenomenology for flavour processes[4].

The gauge couplings of $SU(3)_c$ and $U(1)_Y$ are given by

$$g_s = \frac{g_4 g_3}{\sqrt{g_4^2 + g_3^2}}\,, \qquad g_Y = \frac{g_4 g_1}{\sqrt{g_4^2 + \frac{2}{3} g_1^2}}\,, \tag{4.60}$$

where $g_{4,3,2,1}$ are the gauge couplings of G_{4321}. The scenario $g_4 \gg g_{3,2,1}$ is well motivated from the phenomenological point of view, since here the flavour universal couplings of light fermions to the heavy Z' and g' are suppressed by the ratios g_1/g_4 and g_3/g_4, which will inhibit the direct production of these states at the LHC. In this scenario, the relations above yield the simple expressions $g_s \approx g_3$ and $g_Y \approx g_1$ for the SM gauge couplings.

A key feature of the gauge boson couplings in Eqs. (4.57-4.59) is that, while the coloron g'_μ and the Z'_μ couple to all chiral and vector-like quarks and leptons, the vector leptoquark U_1^μ only couples to the fourth family vector-like fermions. However, the couplings in Eqs. (4.57-4.59) are written in the original interaction basis. We shall perform the transformation to the decoupling basis (primed) as per Eq. (4.23),

$$\mathcal{L}_{U_1}^{\text{gauge}} = \frac{g_4}{\sqrt{2}} Q'^\dagger_\alpha V_{34}^Q \bar{\sigma}^\mu \text{diag}\,(0,0,0,1)\, V_{34}^{L\dagger} L'_\beta U_{1\mu} + \text{h.c.}\,, \tag{4.61}$$

where $\alpha, \beta = 1, .., 4$ and the indices of the matrices are implicit. We obtain an effective coupling for the third family due to mixing with the fourth family,

$$\mathcal{L}_{U_1}^{\text{gauge}} = \frac{g_4}{\sqrt{2}} Q'^\dagger_i \bar{\sigma}^\mu \text{diag}(0,0,s_{34}^Q s_{34}^L) L'_j U_{1\mu} + \text{h.c.}\,, \tag{4.62}$$

where we have omitted the fourth column and row for simplicity. The diagrams in Fig. 4.3 are illustrative, however it must be remembered that the mass insertion approximation is not accurate here due to the heavy top mass, instead we have to work in the large mixing angle formalism as presented in Section 4.2.3. In principle, the couplings in Eq. (4.62) can simultaneously contribute to both LFU ratios $R_{K^{(*)}}$ and $R_{D^{(*)}}$ once the further 2-3 transformations required to diagonalise the quark and lepton mass matrices are taken into account. At low energies, these transformations provide different effective

[4] Although these couplings can be relevant for direct production at high-p_T of the coloron and Z'.

U_1 couplings for the different components of the $SU(2)_L$ doublets[5],

$$\mathcal{L}^{\text{gauge}}_{U_1} = \frac{g_4}{\sqrt{2}}\hat{u}^\dagger_i\bar{\sigma}^\mu \begin{pmatrix} 0 & 0 & 0 \\ 0 & 0 & s^Q_{34}s^L_{34}s^u_{23} \\ 0 & 0 & s^Q_{34}s^L_{34}c^u_{23} \end{pmatrix} \hat{\nu}_j U_{1\mu} + \frac{g_4}{\sqrt{2}}\hat{d}^\dagger_i\bar{\sigma}^\mu \begin{pmatrix} 0 & 0 & 0 \\ 0 & s^Q_{34}s^L_{34}s^d_{23}s^e_{23} & s^Q_{34}s^L_{34}s^d_{23}c^e_{23} \\ 0 & s^Q_{34}s^L_{34}c^d_{23}s^e_{23} & s^Q_{34}s^L_{34}c^d_{23}c^e_{23} \end{pmatrix} \hat{e}_j U_{1\mu} + \text{h.c.} \tag{4.63}$$

It is clear now that the effective leptoquark couplings that contribute to LFU ratios arise due to the same mixing effects which diagonalise the mass matrices of the model, yielding mass terms for the SM fermions. Therefore, the flavour puzzle and the B-physics anomalies are dynamically and parametrically connected in this model, leading to a predictive framework.

Following the same methodology, we obtain the coloron and Z' couplings in the basis of mass eigenstates,

$$\mathcal{L}^{\text{gauge}}_{g'} = \frac{g_4 g_s}{g_3}\hat{d}^\dagger_i\bar{\sigma}^\mu T^a \times \begin{pmatrix} -\frac{g_3^2}{g_4^2} & 0 & 0 \\ 0 & -\left(c^d_{23}\right)^2\frac{g_3^2}{g_4^2} + \left(s^Q_{34}s^d_{23}\right)^2 & \left(s^Q_{34}\right)^2 s^d_{23}c^d_{23} \\ 0 & \left(s^Q_{34}\right)^2 s^d_{23}c^d_{23} & \left(s^Q_{34}c^d_{23}\right)^2 - \left(c^Q_{34}c^d_{23}\right)^2\frac{g_3^2}{g_4^2} \end{pmatrix} \hat{d}_j g^{a'}_\mu + (d \to u)\ , \tag{4.64}$$

$$\mathcal{L}^{\text{gauge}}_{Z',q} = \frac{\sqrt{3}}{\sqrt{2}}\frac{g_4 g_Y}{g_1}\hat{d}^\dagger_i\bar{\sigma}^\mu \times \begin{pmatrix} -\frac{g_1^2}{9g_4^2} & 0 & 0 \\ 0 & -\left(c^d_{23}\right)^2\frac{g_1^2}{9g_4^2} + \frac{1}{6}\left(s^Q_{34}s^d_{23}\right)^2 & \frac{1}{6}\left(s^Q_{34}\right)^2 s^d_{23}c^d_{23} \\ 0 & \frac{1}{6}\left(s^Q_{34}\right)^2 s^d_{23}c^d_{23} & \frac{1}{6}\left(s^Q_{34}c^d_{23}\right)^2 - \left(c^Q_{34}c^d_{23}\right)^2\frac{g_1^2}{9g_4^2} \end{pmatrix} \hat{d}_j Z'_\mu + (d \to u)\ , \tag{4.65}$$

$$\mathcal{L}^{\text{gauge}}_{Z',e} = \frac{\sqrt{3}}{\sqrt{2}}\frac{g_4 g_Y}{g_1}\hat{e}^\dagger_i\bar{\sigma}^\mu \times \begin{pmatrix} \frac{g_1^2}{3g_4^2} & 0 & 0 \\ 0 & \left(c^e_{23}\right)^2\frac{g_1^2}{3g_4^2} - \frac{1}{2}\left(s^L_{34}s^e_{23}\right)^2 & -\frac{1}{2}\left(s^L_{34}\right)^2 s^e_{23}c^e_{23} \\ 0 & -\frac{1}{2}\left(s^L_{34}\right)^2 s^e_{23}c^e_{23} & -\frac{1}{2}\left(s^L_{34}c^e_{23}\right)^2 + \left(c^L_{34}c^e_{23}\right)^2\frac{g_1^2}{3g_4^2} \end{pmatrix} \hat{e}_j Z'_\mu + (e \to \nu)\ . \tag{4.66}$$

The flavour-violating couplings of U_1 in Eq. (4.63) are all proportional to mixing between chiral fermions. In principle, such mixing is of order V_{cb} in the down sector, and of order $0.1V_{cb}$ in the up sector (see the discussion in Section 4.2.3). The small mixing

[5]Notice that first family fermions get couplings to U_1 as well via powers of small CKM-like mixing angles, such that they are suppressed enough to be neglected for the phenomenology.

in the up sector leads to a small U_1 2-3 coupling, possibly too small for $R_{D^{(*)}}$, however a deeper analysis is required as we shall see in the next few sections. Moreover, flavour-violating couplings involving the coloron and Z' could be sizable in the 2-3 down sector, since the CKM mostly originates from the down sector in this model. We shall study whether this is compatible or not with the stringent constraints coming from $B_s - \bar{B}_s$ meson mixing observables.

4.3 Matching the twin Pati-Salam model to the SMEFT

In order to systematically study the low-energy phenomenology of the twin Pati-Salam model, here we include the set of 4-fermion operators obtained at tree-level after integrating out the heavy U_1, Z' and g',

$$\begin{aligned}\mathcal{L}_{\text{4-fermion}} = -\frac{2}{v_{\text{SM}}^2}\Big[&\Big[C_{lq}^{(1)}\Big]^{\alpha\beta ij}\Big[Q_{lq}^{(1)}\Big]^{\alpha\beta ij} + \Big[C_{lq}^{(3)}\Big]^{\alpha\beta ij}\Big[Q_{lq}^{(3)}\Big]^{\alpha\beta ij} \\ &+ \Big[C_{qq}^{(1)}\Big]^{ijkl}\Big[Q_{qq}^{(1)}\Big]^{ijkl} + \Big[C_{qq}^{(3)}\Big]^{ijkl}\Big[Q_{qq}^{(3)}\Big]^{ijkl} + [C_{ll}]^{\alpha\beta\delta\lambda}[Q_{ll}]^{\alpha\beta\delta\lambda}\Big]\,, \end{aligned} \tag{4.67}$$

where we have chosen latin indices for quark flavours and greek indices for lepton flavours. The SMEFT operators above can be matched to the LEFT via the formalism introduced in Appendix D, and then they enter directly in the expressions for low-energy observables introduced in Chapter 2. In our model, the Wilson coefficients are given by

$$\Big[C_{lq}^{(1)}\Big]^{\alpha\beta ij} = \frac{1}{2}C_U\beta_{i\alpha}\beta^*_{j\beta} - 2C_{Z'}\xi_{ij}\xi_{\alpha\beta}\,, \qquad \Big[C_{lq}^{(3)}\Big]^{\alpha\beta ij} = \frac{1}{2}C_U\beta_{i\alpha}\beta^*_{j\beta}\,, \tag{4.68}$$

$$\Big[C_{qq}^{(1)}\Big]^{ijkl} = \frac{1}{4}C_{g'}\kappa_{il}\kappa_{jk} - \frac{1}{6}C_{g'}\kappa_{ij}\kappa_{kl} + C_{Z'}\xi_{ij}\xi_{kl}\,, \quad \Big[C_{qq}^{(3)}\Big]^{ijkl} = \frac{1}{4}C_{g'}\kappa_{il}\kappa_{jk}\,, \tag{4.69}$$

$$[C_{ll}]^{\alpha\beta\delta\lambda} = C_{Z'}\xi_{\alpha\beta}\xi_{\delta\lambda}\,, \tag{4.70}$$

where we have defined

$$C_U = \frac{g_4^2 v_{\text{SM}}^2}{4M_{U_1}^2}\,, \qquad C_{g'} = \frac{g_4^2 g_s^2}{2g_3^2}\frac{v_{\text{SM}}^2}{M_{g'}^2}\,, \qquad C_{Z'} = \frac{3g_4^2 g_Y^2}{4g_1^2}\frac{v_{\text{SM}}^2}{M_{Z'}^2}\,. \tag{4.71}$$

We consider all the fields in (4.67) to be mass eigenstates, as the effects of fermion mixing are encoded into the U_1 ($\beta_{i\alpha}$), g' (κ_{ij}) and Z' ($\xi_{ij}, \xi_{\alpha\beta}$) couplings given in Eqs. (4.63-4.66) for the simplified model. For the extended model of Section 4.5, the same set of SMEFT operators applies, just changing the expressions for the couplings by those of Eqs. (4.110), (4.112), (4.116-4.118).

4.4 Phenomenology of the simplified model

4.4.1 $R_{K^{(*)}}$ and $R_{D^{(*)}}$

New contributions to the $R_{D^{(*)}}$ and $R_{K^{(*)}}$ ratios arise in our model via tree-level contributions mediated by the U_1 vector leptoquark as in Fig. 4.4, see also the SMEFT

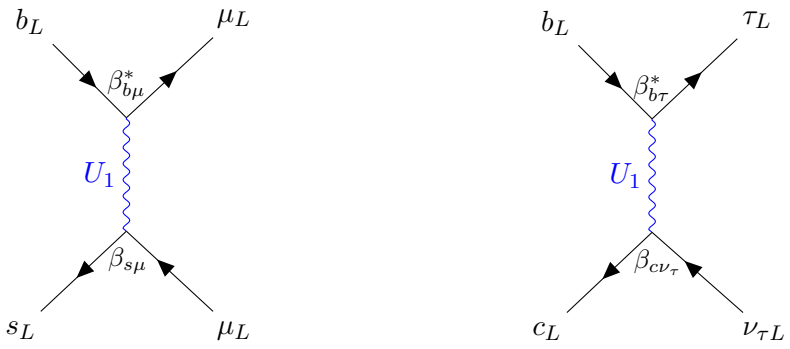

(A) (B)

FIGURE 4.4: U_1-mediated tree-level diagrams contributing to $b \to s\mu\mu$ (left panel) and $b \to c\tau\nu$ (right panel).

matching of the model in the previous section, along with the expressions for $R_{D^{(*)}}$ and $R_{K^{(*)}}$ given in Chapter 2. After integrating out U_1, we observe the following scaling in terms of mixing angles of the model,

$$|\Delta R_{D^{(*)}}| \propto \left(s^L_{34} s^Q_{34}\right)^2 s^u_{23} c^u_{23}\,, \tag{4.72}$$

$$|\Delta R_{K^{(*)}}| \propto \left(s^L_{34} s^Q_{34}\right)^2 \left(s^e_{23}\right)^2 s^d_{23} c^d_{23}\,. \tag{4.73}$$

From Eq. (4.72) it can be seen that our contribution to $R_{D^{(*)}}$ is proportional to the mixing angle θ^u_{23}. Such angle is naturally small in our model, roughly $\mathcal{O}(0.1V_{cb})$ as per Eq. (4.42), due to the fact that the CKM originates mostly from the down sector. As a consequence, the contribution to $R_{D^{(*)}}$ is suppressed. On the other hand, the contribution of U_1 to $R_{K^{(*)}}$ is further suppressed by the $\mathcal{O}(V_{cb})$ mixing angles θ^d_{23} and θ^e_{23}, for a total expected suppression of $\mathcal{O}(V^3_{cb})$.

4.4.2 $B_s - \bar{B}_s$ mixing

Flavour-violating couplings involving the coloron and Z' could be sizable in the 2-3 down sector, since the CKM originates mostly from the down sector in this model. The general description of $B_s - \bar{B}_s$ mixing in terms of effective operators is included in Section 2.3.4. Given that the flavour-violating couplings in our model are dominantly left-handed, after integrating out the heavy gauge bosons we obtain effective contributions to C^{bs}_1 only.

The bounds are highly constraining over this model because both the coloron and Z' mediate tree-level contributions to ΔM_s, which interfere positively with the SM prediction, while the latter is already larger than the experimental result. We estimate that, in order to satisfy the bound $\Delta M^{\rm NP}_s / \Delta M^{\rm SM}_s < 0.11$ (95% CL), the 2-3 down-quark mixing needs to satisfy $\left|s^d_{23}\right| \lesssim 0.1 V_{cb}$ if the 3-4 mixing is maximal $s^Q_{34} \approx 1$.

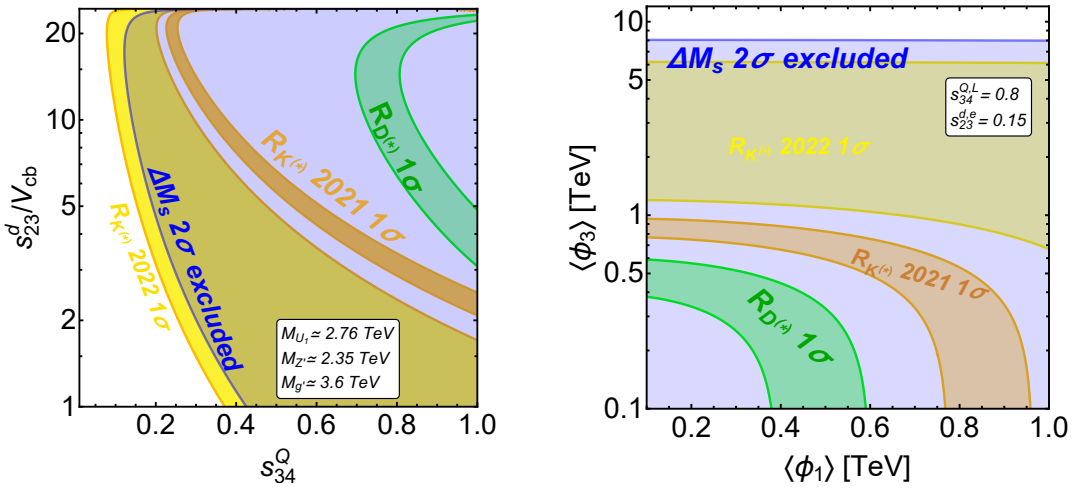

(A) (B)

FIGURE 4.5: ***Left:*** Regions compatible with $R_{D^{(*)}}$ and $R_{K^{(*)}}$ (2022 and 2021 data) in the plane (s^Q_{34}, s^d_{23}), the heavy gauge boson masses are fixed as depicted in the panel. ***Right:*** Regions compatible with $R_{D^{(*)}}$ and $R_{K^{(*)}}$ (2022 and 2021 data) in the plane $(\langle\phi_1\rangle,\langle\phi_3\rangle)$, which allows to explore the spectrum of heavy gauge boson masses. The mixing angles are fixed as depicted in the plot. In both panels the blue regions are excluded by the ΔM_s bound, see Eq. (2.36).

4.4.3 Parameter space of the simplified model

As anticipated in the previous sections, the contribution of the vector leptoquark to the $R_{D^{(*)}}$ anomalies is strongly suppressed by a naturally small mixing angle $\theta^u_{23} \approx m_c/m_t$, leading to a suppression of $\mathcal{O}(0.1V_{cb})$. In Fig. 4.5a it can be seen that for a typical benchmark mass $M_{U_1} = 3\,\text{TeV}$, a large $s^u_{23} \gtrsim 4V_{cb}$ is needed in order to give a significant contribution to the $R_{D^{(*)}}$ anomaly, provided that the 3-4 mixing is maximal.

The contribution to $R_{K^{(*)}}$ also suffers from an overall suppression of $\mathcal{O}(V^3_{cb})$. We can go beyond the natural value of θ^u_{23} by increasing the mixing angle $s^{q_c}_{34}$ (i.e. increasing the fundamental Yukawa $x^{\psi^c}_{34}$, or reducing the VL mass $M^{\psi^c}_4$), which controls the overall size of the off-diagonal (2,3) entry in the effective mass matrices of Eqs. (4.31) and (4.32). This way, we can explore the parameter space of larger 2-3 mixing angles, provided that the experimental value of V_{cb} is preserved through Eq. (4.38), which relates both quark mixings θ^u_{23} and θ^d_{23}. We further assume $s^Q_{34} = s^L_{34}$ and $s^d_{23} = s^e_{23}$ for simplicity, both assumptions are well motivated due to the underlying twin Pati-Salam symmetry.

Our results are depicted in Fig. 4.5a for a spectrum of heavy gauge boson masses compatible with high-p_T searches (see Section 4.6.8). We find that for the given benchmark, a small region of the parameter space is compatible with the 2022 data of $R_{K^{(*)}}$, however the 1σ region of $R_{D^{(*)}}$ is not compatible with ΔM_s. This version of the model was already unable to explain the 2021 data of both LFU anomalies due to the large constraints from tree-level Z' and coloron contributions to ΔM_s.

In Fig. 4.5b we have varied the VEVs of ϕ_3 and ϕ_1, effectively exploring the parameter space of gauge boson masses, in line with Eq. (4.56). However, we find that

the stringent constraints from ΔM_s are only alleviated when $\langle \phi_3 \rangle \gtrsim 8\,\text{TeV}$, which corresponds to a coloron with mass $M_{g'} \gtrsim 50\,\text{TeV}$ and a vector leptoquark with mass $M_{U_1} \gtrsim 34\,\text{TeV}$, too heavy to address $R_{D^{(*)}}$.

We conclude that the model in this simplified version is over-constrained by large tree-level contributions to ΔM_s mediated by the coloron and Z'. Such FCNCs arise due to the 2-3 CKM mixing having its origin in the down sector. Moreover, the same small 2-3 mixing angles suppress the contribution of the model to $R_{D^{(*)}}$. However, we shall show that the proper flavour structure to be compatible with all data is achieved in the extended version of the model presented in Section 4.5, which is successful to address the B-anomalies.

4.5 Extending the simplified twin Pati-Salam theory of flavour

In this section we present an extended version of the simplified twin Pati-Salam model, featuring extra matter content and a discrete flavour symmetry. This new version can achieve the proper flavour structure required to be compatible with all data, solving the problems of the simplified twin Pati-Salam model discussed in Section 4.2. Firstly, we will introduce the extended version of the model. Secondly, we will revisit the diagonalisation of the mass matrix, leading to the fermion masses and to the new couplings with the heavy gauge bosons. Finally, we will study the phenomenology, showing that the model is compatible with all data while predicting promising signals in flavour-violating observables, rare B-decays and high-p_T searches.

4.5.1 New matter content and discrete flavour symmetry

As firstly identified in [268], when one considers a 4321 model with all chiral fermions transforming as $SU(4)$ singlets (fermiophobic framework), three vector-like fermion families can achieve the proper flavour structure to explain the B-anomalies. Such flavour structure can provide a GIM-like suppression of FCNCs, along with large leptoquark couplings that can contribute to the LFU ratios. Hence, as depicted in Table 4.3, we extend now the simplified model by two extra vector-like families, to a total of three vector-like families charged under $SU(4)^I_{PS}$,

$$\begin{aligned} &\psi_{4,5,6}(\mathbf{4},\mathbf{2},\mathbf{1};\mathbf{1},\mathbf{1},\mathbf{1})_{(1,1,\alpha)}\,,\,\overline{\psi}_{4,5,6}(\overline{\mathbf{4}},\overline{\mathbf{2}},\mathbf{1};\mathbf{1},\mathbf{1},\mathbf{1})_{(1,1,\alpha^3)}\,,\\ &\psi^c_{4,5,6}(\overline{\mathbf{4}},\mathbf{1},\overline{\mathbf{2}};\mathbf{1},\mathbf{1},\mathbf{1})_{(1,1,\alpha)}\,,\,\overline{\psi^c}_{4,5,6}(\mathbf{4},\mathbf{1},\mathbf{2};\mathbf{1},\mathbf{1},\mathbf{1})_{(1,1,\alpha^3)}\,, \end{aligned} \tag{4.74}$$

Field	$SU(4)^I_{PS}$	$SU(2)^I_L$	$SU(2)^I_R$	$SU(4)^{II}_{PS}$	$SU(2)^{II}_L$	$SU(2)^{II}_R$	$\mathbb{Z}_4$
$\psi_{1,2,3}$	$\mathbf{1}$	$\mathbf{1}$	$\mathbf{1}$	$\mathbf{4}$	$\mathbf{2}$	$\mathbf{1}$	α, 1, 1
$\psi^c_{1,2,3}$	$\mathbf{1}$	$\mathbf{1}$	$\mathbf{1}$	$\overline{\mathbf{4}}$	$\mathbf{1}$	$\overline{\mathbf{2}}$	α, α^2, 1
$\psi_{4,5,6}$	$\mathbf{4}$	$\mathbf{2}$	$\mathbf{1}$	$\mathbf{1}$	$\mathbf{1}$	$\mathbf{1}$	1, 1, α
$\overline{\psi}_{4,5,6}$	$\overline{\mathbf{4}}$	$\overline{\mathbf{2}}$	$\mathbf{1}$	$\mathbf{1}$	$\mathbf{1}$	$\mathbf{1}$	1, 1, α^3
$\psi^c_{4,5,6}$	$\overline{\mathbf{4}}$	$\mathbf{1}$	$\overline{\mathbf{2}}$	$\mathbf{1}$	$\mathbf{1}$	$\mathbf{1}$	1, 1, α
$\overline{\psi^c}_{4,5,6}$	$\mathbf{4}$	$\mathbf{1}$	$\mathbf{2}$	$\mathbf{1}$	$\mathbf{1}$	$\mathbf{1}$	1, 1, α^3
ϕ	$\mathbf{4}$	$\mathbf{2}$	$\mathbf{1}$	$\overline{\mathbf{4}}$	$\overline{\mathbf{2}}$	$\mathbf{1}$	1
$\overline{\phi}, \overline{\phi'}$	$\overline{\mathbf{4}}$	$\mathbf{1}$	$\overline{\mathbf{2}}$	$\mathbf{4}$	$\mathbf{1}$	$\mathbf{2}$	1, α^2
H	$\overline{\mathbf{4}}$	$\overline{\mathbf{2}}$	$\mathbf{1}$	$\mathbf{4}$	$\mathbf{1}$	$\mathbf{2}$	1
$\overline{H}$	$\mathbf{4}$	$\mathbf{1}$	$\mathbf{2}$	$\overline{\mathbf{4}}$	$\overline{\mathbf{2}}$	$\mathbf{1}$	1
H'	$\mathbf{1}$	$\mathbf{1}$	$\mathbf{1}$	$\mathbf{4}$	$\mathbf{1}$	$\mathbf{2}$	1
$\overline{H}'$	$\mathbf{1}$	$\mathbf{1}$	$\mathbf{1}$	$\overline{\mathbf{4}}$	$\mathbf{1}$	$\overline{\mathbf{2}}$	1
Φ	$\mathbf{1}$	$\mathbf{2}$	$\mathbf{1}$	$\mathbf{1}$	$\overline{\mathbf{2}}$	$\mathbf{1}$	1
$\overline{\Phi}$	$\mathbf{1}$	$\mathbf{1}$	$\overline{\mathbf{2}}$	$\mathbf{1}$	$\mathbf{1}$	$\mathbf{2}$	1
Ω_{15}	$\mathbf{15}$	$\mathbf{1}$	$\mathbf{1}$	$\mathbf{1}$	$\mathbf{1}$	$\mathbf{1}$	1

TABLE 4.3: The field content under $G^I_{422} \times G^{II}_{422} \times \mathbb{Z}_4$, see the main text for details. Fields transform under $\mathbb{Z}_4$ via powers of $\alpha = e^{i\pi/2}$. We do not include here extra content related to the origin of first family fermion masses and mixing, which is discussed in Section 4.2.4.

where it can be seen that the so-called fourth, fifth[6] and sixth VL families originate from the first Pati-Salam group, being singlets under the second. They are indistinguishable under the twin Pati-Salam symmetry in Eq. (4.4), however a newly introduced $\mathbb{Z}_4$ flavour symmetry discriminates the sixth family from the fourth and fifth, via different powers of the $\mathbb{Z}_4$ charge $\alpha = e^{i\pi/2}$. This way, the total symmetry group of the high energy model is extended to

$$G^I_{422} \times G^{II}_{422} \times \mathbb{Z}_4 \,. \tag{4.75}$$

The new $\mathbb{Z}_4$ discrete symmetry is introduced for phenomenological purposes, as it will prevent fine-tuning, reduce the total number of parameters of the model and protect from FCNCs involving the first family of SM-like chiral fermions. Moreover, $\mathbb{Z}_4$ will simplify the diagonalisation of the full mass matrices and preserve the success of the effective Yukawa couplings for SM fermions given in Section 4.2.3, with specific modifications. The origin of the chiral fermion families is still the second Pati-Salam group, however now they transform in a non-trivial way under $\mathbb{Z}_4$,

$$\psi_{1,2,3}(\mathbf{1},\mathbf{1},\mathbf{1};\mathbf{4},\mathbf{2},\mathbf{1})_{(\alpha,1,1)} \,, \quad \psi^c_{1,2,3}(\mathbf{1},\mathbf{1},\mathbf{1};\overline{\mathbf{4}},\mathbf{1},\overline{\mathbf{2}})_{(\alpha,\alpha^2,1)} \,. \tag{4.76}$$

[6]Note that we have relabeled the fifth VL family in this section with respect to the fifth family of the simplified model that provides first family fermion masses and mixing, which should then be relabeled to a different notation in the extended model. However, since the presence of this family does not induce any couplings to $SU(4)^I_{PS}$ gauge bosons, it has no low-energy phenomenological implications and we shall omit it throughout this section.

Finally, the scalar content is extended by an additional scalar Ω_{15} which transforms in the adjoint representation of $SU(4)^I_{PS}$, whose VEV $\langle\Omega_{15}\rangle = T^I_{15} v_{15}$ splits the vector-like masses of quarks and leptons, where $T^I_{15} = \mathrm{diag}(1,1,1,-3)/(2\sqrt{6})$.

We also include an additional copy of the Yukon $\overline{\phi}$, denoted as $\overline{\phi'}$, featuring α^2 charge under $\mathbb{Z}_4$. The simplified Lagrangian in Eq. (4.7) is extended by the new matter content to

$$\begin{aligned}\mathcal{L}^{ren}_{\text{mass}} = {} & y^{\psi}_{ia}\overline{H}\psi_i\psi^c_a + y^{\psi}_{a3}H\psi_a\psi^c_3 + x^{\psi}_{ia}\phi\psi_i\overline{\psi}_a + x^{\psi^c}_{a2}\overline{\psi^c_a\phi'}\psi^c_2 + x^{\psi^c}_{a3}\overline{\psi^c_a\phi}\psi^c_3 \\ & + x^{\psi}_{16}\phi\psi_1\overline{\psi}_6 + x^{\psi^c}_{61}\overline{\psi^c_6\phi}\psi^c_1 + M^{\psi}_{ab}\psi_a\overline{\psi_b} + M^{\psi^c}_{ab}\psi^c_a\overline{\psi^c_b} + M^{\psi}_{66}\psi_6\overline{\psi_6} + M^{\psi^c}_{66}\psi^c_6\overline{\psi^c_6} \\ & + \lambda^{aa}_{15}\Omega_{15}\psi_a\overline{\psi_a} + \lambda^{66}_{15}\Omega_{15}\psi_6\overline{\psi_6} + \bar{\lambda}^{aa}_{15}\Omega_{15}\psi^c_a\overline{\psi^c_a} + \bar{\lambda}^{66}_{15}\Omega_{15}\psi^c_6\overline{\psi^c_6} + \text{h.c.}\,,\end{aligned} \tag{4.77}$$

where $i = 2,3$ and $a,b = 4,5$ (terms $i = 1$ and $a,b = 6$ forbidden by $\mathbb{Z}_4$). The symmetry breaking and the decomposition of the various fields proceeds just like in the simplified model, see Section 4.2.2, however the VEVs of the additional scalars $\overline{\phi'}$ and Ω_{15} play a role in the spontaneous breaking of the 4321 symmetry, and the corresponding gauge boson masses become (assuming $v_{1,3} \approx \overline{v}_{1,3} \approx \overline{v'}_{1,3}$ for simplicity)

$$\begin{aligned} M_{U_1} &= \frac{1}{2}g_4\sqrt{3v_1^2 + 3v_3^2 + \frac{4}{3}v_{15}^2}\,, \\ M_{g'} &= \frac{\sqrt{3}}{\sqrt{2}}\sqrt{g_4^2 + g_3^2}v_3\,, \\ M_{Z'} &= \frac{1}{2}\sqrt{\frac{3}{2}}\sqrt{g_4^2 + \frac{2}{3}g_1^2}\sqrt{3v_1^2 + v_3^2}\,. \end{aligned} \tag{4.78}$$

4.5.2 Effective Yukawa couplings in the extended model

In this section, we diagonalise the full mass matrix of the extended model, following the same procedure as in Section 4.2.3, but including the extra matter content of the extended model. We may write the mass terms and couplings in Eq. (4.77) as a 9×9 matrix in flavour space (we also define 9-dimensional vectors as ψ_α and ψ^c_β below),

$$\mathcal{L}^{ren}_{4,5,6} = \psi^{\mathrm{T}}_\alpha M^{\psi}\psi^c_\beta + \text{h.c.}\,, \tag{4.79}$$

$$\psi_\alpha = \begin{pmatrix} \psi_1 & \psi_2 & \psi_3 & \psi_4 & \psi_5 & \psi_6 & \overline{\psi^c_4} & \overline{\psi^c_5} & \overline{\psi^c_6} \end{pmatrix}^{\mathrm{T}}\,, \tag{4.80}$$

$$\psi^c_\beta = \begin{pmatrix} \psi^c_1 & \psi^c_2 & \psi^c_3 & \psi^c_4 & \psi^c_5 & \psi^c_6 & \overline{\psi_4} & \overline{\psi_5} & \overline{\psi_6} \end{pmatrix}^{\mathrm{T}}\,, \tag{4.81}$$

$$M^{\psi} = \left(\begin{array}{c|cccccccc} & \psi_1^c & \psi_2^c & \psi_3^c & \psi_4^c & \psi_5^c & \psi_6^c & \overline{\psi_4} & \overline{\psi_5} & \overline{\psi_6} \\ \hline \psi_1 & 0 & 0 & 0 & 0 & 0 & 0 & 0 & 0 & x_{16}^{\psi}\phi \\ \psi_2 & 0 & 0 & 0 & y_{24}^{\psi}\overline{H} & y_{25}^{\psi}\overline{H} & 0 & 0 & x_{25}^{\psi}\phi & 0 \\ \psi_3 & 0 & 0 & 0 & y_{34}^{\psi}\overline{H} & y_{35}^{\psi}\overline{H} & 0 & x_{34}^{\psi}\phi & x_{35}^{\psi}\phi & 0 \\ \psi_4 & 0 & 0 & y_{43}^{\psi}H & 0 & 0 & 0 & M_{44}^{Q,L} & M_{45}^{\psi} & 0 \\ \psi_5 & 0 & 0 & y_{53}^{\psi}H & 0 & 0 & 0 & M_{54}^{\psi} & M_{55}^{Q,L} & 0 \\ \psi_6 & 0 & 0 & 0 & 0 & 0 & 0 & 0 & 0 & M_{66}^{Q,L} \\ \overline{\psi_4^c} & 0 & x_{42}^{\psi^c}\overline{\phi'} & x_{43}^{\psi^c}\overline{\phi} & M_{44}^{\psi^c} & M_{45}^{\psi^c} & 0 & 0 & 0 & 0 \\ \overline{\psi_5^c} & 0 & x_{52}^{\psi^c}\overline{\phi'} & x_{53}^{\psi^c}\overline{\phi} & M_{54}^{\psi^c} & M_{55}^{\psi^c} & 0 & 0 & 0 & 0 \\ \overline{\psi_6^c} & x_{61}^{\psi^c}\overline{\phi} & 0 & 0 & 0 & 0 & M_{66}^{\psi^c} & 0 & 0 & 0 \end{array}\right), \tag{4.82}$$

where the diagonal mass parameters $M^{Q,L}_{44,55,66}$ are split for quarks and leptons due to the VEV of Ω_{15},

$$M^Q_{aa} \equiv M^{\psi}_{aa} + \frac{\lambda^{aa}_{15}\langle\Omega_{15}\rangle}{2\sqrt{6}}\,, \qquad M^L_{aa} \equiv M^{\psi}_{aa} - 3\frac{\lambda^{aa}_{15}\langle\Omega_{15}\rangle}{2\sqrt{6}}\,, \tag{4.83}$$

where $a = 4, 5, 6$. Similar equations are obtained for the ψ^c sector, however in the ψ^c sector the mass splitting is minimal due to $\langle\Omega_{15}\rangle$ being of order a few hundreds GeV while $M^{\psi^c}_{aa}$ are much heavier due to a generalisation of the messenger dominance in Eq. (4.97). The zeros in Eq. (4.82) are enforced by the $\mathbb{Z}_4$ symmetry, except for the zero in the (2,7) entry which is obtained by rotating ψ_2 and ψ_3, without loss of generality thanks to the zeros in the upper 3×3 block (see Section 3.3.3 and the discussion therein).

The matrix in Eq. (4.82) features three different mass scales, the Higgs VEVs $\langle H\rangle$ and $\langle\overline{H}\rangle$, the Yukon VEVs $\langle\phi\rangle$, $\langle\overline{\phi}\rangle$, $\langle\overline{\phi'}\rangle$ and the vector-like mass terms M^{ψ}_{ab} and $M^{\psi^c}_{ab}$. We can block diagonalise the matrix above by taking advantage of the different mass scales. Firstly, we diagonalise the 2×2 sub-blocks containing the heavy masses M^{ψ}_{ab} and $M^{\psi^c}_{ab}$,

$$\begin{aligned} \begin{pmatrix} M_4^Q & 0 \\ 0 & M_5^Q \end{pmatrix} &= V_{45}^{Q} \begin{pmatrix} M_{44}^Q & M_{45}^{\psi} \\ M_{54}^{\psi} & M_{55}^Q \end{pmatrix} V_{45}^{\overline{Q}\dagger}\,, \\ \begin{pmatrix} M_4^L & 0 \\ 0 & M_5^L \end{pmatrix} &= V_{45}^{L} \begin{pmatrix} M_{44}^L & M_{45}^{\psi} \\ M_{54}^{\psi} & M_{55}^L \end{pmatrix} V_{45}^{\overline{L}\dagger}\,, \end{aligned} \tag{4.84}$$

and similarly in the ψ^c sector. The 4-5 rotations above just redefine the elements in the 4th, 5th, 7th and 8th rows and columns of the full mass matrix, leaving the upper 3×3 blocks unchanged (plus we are allowed to introduce now the zero in the (2,7) entry by performing the rotation of ψ_2 and ψ_3). Then we perform a further sequence

of rotations to go to the decoupling basis, where no large elements appear apart from the diagonal heavy masses (i.e. those terms in the seventh, eighth and ninth rows and columns involving the fields ϕ and $\overline{\phi}$ are all absorbed into a redefinition of the heavy masses), and we obtain a block-diagonal matrix similar to that of Eq. (4.22) but enlarged with the fifth and sixth vector-like families. The total set of unitary transformations is given by

$$V_\psi = V_{16}^{\psi} V_{35}^{\psi} V_{25}^{\psi} V_{34}^{\psi} V_{45}^{\psi} V_{45}^{\overline{\psi^c}} \,, \tag{4.85}$$

$$V_{\psi^c} = V_{16}^{\psi^c} V_{35}^{\psi^c} V_{25}^{\psi^c} V_{34}^{\psi^c} V_{24}^{\psi^c} V_{45}^{\psi^c} V_{45}^{\overline{\psi}} \approx V_{34}^{\psi^c} V_{24}^{\psi^c} \,. \tag{4.86}$$

The mixing angles controlling the unitary transformations can be obtained in the large mixing angle formalism (see Section 4.2.3) as

$$s_{34}^{Q} = \frac{x_{34}^{\psi} \langle \phi_3 \rangle}{\sqrt{\left(x_{34}^{\psi} \langle \phi_3 \rangle\right)^2 + \left(M_4^Q\right)^2}} \,, \qquad s_{34}^{L} = \frac{x_{34}^{\psi} \langle \phi_1 \rangle}{\sqrt{\left(x_{34}^{\psi} \langle \phi_1 \rangle\right)^2 + \left(M_4^L\right)^2}} \,, \tag{4.87}$$

$$s_{25}^{Q} = \frac{x_{25}^{\psi} \langle \phi_3 \rangle}{\sqrt{\left(x_{25}^{\psi} \langle \phi_3 \rangle\right)^2 + \left(M_5^Q\right)^2}} \,, \qquad s_{25}^{L} = \frac{x_{25}^{\psi} \langle \phi_1 \rangle}{\sqrt{\left(x_{25}^{\psi} \langle \phi_1 \rangle\right)^2 + \left(M_5^L\right)^2}} \,, \tag{4.88}$$

$$s_{35}^{Q} = \frac{c_{34}^{Q} x_{35}^{\psi} \langle \phi_3 \rangle}{\sqrt{\left(c_{34}^{Q} x_{35}^{\psi} \langle \phi_3 \rangle\right)^2 + \left(x_{25}^{\psi} \langle \phi_3 \rangle\right)^2 + \left(M_5^Q\right)^2}} \,, \qquad s_{35}^{L} = \frac{c_{34}^{L} x_{35}^{\psi} \langle \phi_1 \rangle}{\sqrt{\left(c_{34}^{L} x_{35}^{\psi} \langle \phi_1 \rangle\right)^2 + \left(x_{25}^{\psi} \langle \phi_1 \rangle\right)^2 + \left(M_5^L\right)^2}} \,, \tag{4.89}$$

$$s_{16}^{Q} = \frac{x_{16}^{\psi} \langle \phi_3 \rangle}{\sqrt{\left(x_{16}^{\psi} \langle \phi_3 \rangle\right)^2 + \left(M_6^Q\right)^2}} \,, \qquad s_{16}^{L} = \frac{x_{16}^{\psi} \langle \phi_1 \rangle}{\sqrt{\left(x_{16}^{\psi} \langle \phi_1 \rangle\right)^2 + \left(M_6^L\right)^2}} \,, \tag{4.90}$$

$$s_{24}^{q^c} = \frac{x_{42}^{\psi^c} \langle \overline{\phi_3} \rangle}{\sqrt{\left(x_{42}^{\psi^c} \langle \overline{\phi_3} \rangle\right)^2 + \left(M_4^{\psi^c}\right)^2}} \,, \qquad s_{24}^{e^c} = \frac{x_{42}^{\psi^c} \langle \overline{\phi_1} \rangle}{\sqrt{\left(x_{42}^{\psi^c} \langle \overline{\phi_1} \rangle\right)^2 + \left(M_4^{\psi^c}\right)^2}} \,, \tag{4.91}$$

$$s_{34}^{q^c} = \frac{x_{43}^{\psi^c} \langle \overline{\phi_3} \rangle}{\sqrt{\left(x_{42}^{\psi^c} \langle \overline{\phi_3} \rangle\right)^2 + \left(x_{43}^{\psi^c} \langle \overline{\phi_3} \rangle\right)^2 + \left(M_4^{\psi^c}\right)^2}} \,, \qquad s_{34}^{e^c} = \frac{x_{43}^{\psi^c} \langle \overline{\phi_1} \rangle}{\sqrt{\left(x_{42}^{\psi^c} \langle \overline{\phi_1} \rangle\right)^2 + \left(x_{43}^{\psi^c} \langle \overline{\phi_1} \rangle\right)^2 + \left(M_4^{\psi^c}\right)^2}} \,, \tag{4.92}$$

$$\hat{M}_4^Q = \sqrt{\left(x_{34}^{\psi} \langle \phi_3 \rangle\right)^2 + \left(M_4^Q\right)^2} \,, \qquad \hat{M}_4^L = \sqrt{\left(x_{34}^{\psi} \langle \phi_1 \rangle\right)^2 + \left(M_4^L\right)^2} \,, \tag{4.93}$$

$$\hat{M}_5^Q = \sqrt{\left(x_{25}^{\psi} \langle \phi_3 \rangle\right)^2 + \left(x_{35}^{\psi} \langle \phi_3 \rangle\right)^2 + \left(M_5^Q\right)^2} \,, \qquad \hat{M}_5^L = \sqrt{\left(x_{25}^{\psi} \langle \phi_1 \rangle\right)^2 + \left(x_{35}^{\psi} \langle \phi_1 \rangle\right)^2 + \left(M_5^L\right)^2} \,, \tag{4.94}$$

$$\hat{M}_6^Q = \sqrt{\left(x_{16}^{\psi} \langle \phi_3 \rangle\right)^2 + \left(M_6^Q\right)^2} \,, \qquad \hat{M}_6^L = \sqrt{\left(x_{16}^{\psi} \langle \phi_1 \rangle\right)^2 + \left(M_6^L\right)^2} \,, \tag{4.95}$$

$$\hat{M}_4^{q^c} = \sqrt{\left(x_{42}^{\psi^c} \langle \overline{\phi_3} \rangle\right)^2 + \left(x_{43}^{\psi^c} \langle \overline{\phi_3} \rangle\right)^2 + \left(M_4^{\psi^c}\right)^2} \,, \qquad \hat{M}_4^{e^c} = \sqrt{\left(x_{42}^{\psi^c} \langle \overline{\phi_1} \rangle\right)^2 + \left(x_{43}^{\psi^c} \langle \overline{\phi_1} \rangle\right)^2 + \left(M_4^{\psi^c}\right)^2} \,. \tag{4.96}$$

The transformations in the ψ^c sector shown in Eq. (4.86) can be described by $V_{34}^{\psi^c} V_{24}^{\psi^c}$ in good approximation, whose mixing angles are given above. This approximation is accurate as far as the mixing involving the 5th and 6th ψ^c fields is further suppressed by a generalisation of the messenger dominance in Eq. (4.30) to three vector-like families, namely

$$M_{44}^{Q,L} \ll M_{55}^{Q,L} \sim M_{66}^{Q,L} \ll M_{44}^{\psi^c} \ll M_{55}^{\psi^c}, M_{66}^{\psi^c} \,. \tag{4.97}$$

The hierarchy above will preserve most features of the simplified model, including large third family Yukawa couplings arising from mixing with ψ_4 fermions, and small second

family Yukawa couplings arising from mixing with ψ_4^c fermions. The couplings of U_1 to chiral fermions will remain dominantly left-handed, since the couplings to ψ^c chiral fermions (or equivalently right-handed fermions) will remain suppressed by small mixing angles. On the other hand, the hierarchy $M_{44}^{Q,L} \ll M_{55}^{Q,L}$ will provide hierarchical couplings of U_1 to third family and second family fermions, so we anticipate a small contribution to $R_{K^{(*)}}$ and a large contribution to $R_{D^{(*)}}$.

We obtain the effective Yukawa couplings for SM fermions by applying the set of unitary transformations in Eqs. (4.85) and (4.86) to the upper 6×6 block of Eq. (4.82), in the same way as in Eq. (4.27). In this basis (primed), the mass matrix for each charged sector reads (assuming a small x_{35}^{ψ}, see Section 4.6.3 for the motivation, and approximating cosines in the ψ^c sector to be 1),

$$M^u_{\text{eff}} = \begin{pmatrix} & u'^c_1 & u'^c_2 & u'^c_3 \\ Q'_1| & 0 & 0 & 0 \\ Q'_2| & 0 & 0 & s^Q_{25} y^{\psi}_{53} \\ Q'_3| & 0 & 0 & s^Q_{34} y^{\psi}_{43} \end{pmatrix} \langle H_t \rangle + \begin{pmatrix} & u'^c_1 & u'^c_2 & u'^c_3 \\ Q'_1| & 0 & 0 & 0 \\ Q'_2| & 0 & c^Q_{25} s^{q^c}_{24} y^{\psi}_{24} & c^Q_{25} s^{q^c}_{34} y^{\psi}_{24} \\ Q'_3| & 0 & c^Q_{34} s^{q^c}_{24} y^{\psi}_{34} & c^Q_{34} s^{q^c}_{34} y^{\psi}_{34} \end{pmatrix} \langle H_c \rangle + \text{h.c.}\,, \tag{4.98}$$

$$M^d_{\text{eff}} = \begin{pmatrix} & d'^c_1 & d'^c_2 & d'^c_3 \\ Q'_1| & 0 & 0 & 0 \\ Q'_2| & 0 & 0 & s^Q_{25} y^{\psi}_{53} \\ Q'_3| & 0 & 0 & s^Q_{34} y^{\psi}_{43} \end{pmatrix} \langle H_b \rangle + \begin{pmatrix} & d'^c_1 & d'^c_2 & d'^c_3 \\ Q'_1| & 0 & 0 & 0 \\ Q'_2| & 0 & c^Q_{25} s^{q^c}_{24} y^{\psi}_{24} & c^Q_{25} s^{q^c}_{34} y^{\psi}_{24} \\ Q'_3| & 0 & c^Q_{34} s^{q^c}_{24} y^{\psi}_{34} & c^Q_{34} s^{q^c}_{34} y^{\psi}_{34} \end{pmatrix} \langle H_s \rangle + \text{h.c.}\,, \tag{4.99}$$

$$M^e_{\text{eff}} = \begin{pmatrix} & e'^c_1 & e'^c_2 & e'^c_3 \\ L'_1| & 0 & 0 & 0 \\ L'_2| & 0 & 0 & s^L_{25} y^{\psi}_{53} \\ L'_3| & 0 & 0 & s^L_{34} y^{\psi}_{43} \end{pmatrix} \langle H_\tau \rangle + \begin{pmatrix} & e'^c_1 & e'^c_2 & e'^c_3 \\ L'_1| & 0 & 0 & 0 \\ L'_2| & 0 & c^L_{25} s^{e^c}_{24} y^{\psi}_{24} & c^L_{25} s^{e^c}_{34} y^{\psi}_{24} \\ L'_3| & 0 & c^L_{34} s^{e^c}_{24} y^{\psi}_{34} & c^L_{34} s^{e^c}_{34} y^{\psi}_{34} \end{pmatrix} \langle H_\mu \rangle + \text{h.c.}\,, \tag{4.100}$$

which are diagonalised by 2-3 rotations, and the CKM matrix is obtained via Eq. (4.37). The first family masses and mixings can be obtained by adding a heavier family of vector-like fermions that originates from the second PS group, as shown in Section 4.2.4, however this has no implications for low-energy phenomenology. The mass matrices above are of similar form to Eqs. (4.31), (4.32), (4.33), just featuring an extra off-diagonal component in the (2,3) entry of the first matrix in each sector, arising from mixing with the 5th family. This new term can be used to partially cancel the down-quark 2-3 mixing while simultaneously enhancing the up-quark mixing to preserve the CKM, involving a mild tuning:

- Let us impose that the total (2,3) entry in the down-quark mass matrix is small, i.e.

$$-s^Q_{25} \left| y^{\psi}_{53} \right| \langle H_b \rangle + c^Q_{25} s^{q^c}_{34} y^{\psi}_{24} \langle H_s \rangle \approx 0\,. \tag{4.101}$$

  Following the discussion of Section 4.2.3, a natural benchmark is $\langle H_b \rangle \approx m_b$ and $s^{q^c}_{34} y^{\psi}_{24} \langle H_s \rangle \approx m_s$, hence

$$-s^Q_{25} \left| y^{\psi}_{53} \right| m_b + m_s \approx 0 \Rightarrow \left| y^{\psi}_{53} \right| = \frac{m_s}{s^Q_{25} m_b}\,. \tag{4.102}$$

On the other hand, the mixing angle s^Q_{25} is very relevant for the B-decays and related phenomenology, and we obtain the typical value $s^Q_{25} \approx 0.2$ in Section 4.6, featuring another connection between the flavour puzzle and B-physics in our model. With this input, we obtain

$$\left|y^\psi_{53}\right| \approx \mathcal{O}(0.1). \tag{4.103}$$

In particular, the benchmark in Table 4.5 suppresses the down mixing with the choice $y^\psi_{53} = -0.3$, obtaining $s^d_{23} \approx \mathcal{O}(10^{-3})$ which is enough to control the stringent constraints from $B_s - \bar{B}_s$ meson mixing (see Section 4.4.2).

- At the same time that y^ψ_{53} partially cancels the down mixing, it leads to large up mixing which preserves the CKM. Let us now estimate the 2-3 mixing in the up sector as the ratio of the (2,3) entry over the (3,3) entry in the up-quark mass matrix,

$$\frac{-s^Q_{25}\left|y^\psi_{53}\right|\langle H_t\rangle + c^Q_{25}s^{q^c}_{34}y^\psi_{24}\langle H_c\rangle}{s^Q_{34}y^\psi_{43}\langle H_t\rangle} \approx \frac{s^Q_{25}\left|y^\psi_{53}\right|\langle H_t\rangle + m_c}{m_t} \approx s^Q_{25}\left|y^\psi_{53}\right| \approx \mathcal{O}(V_{cb})\,, \tag{4.104}$$

where we have considered $y^\psi_{43} = 1$, $s^Q_{34} \approx 1$, as required to explain the top mass (see the discussion in the first bullet point in Section 4.2.3) and we have neglected the m_c/m_t small factor. This way, we have taken advantage of the new contribution via the 5th family (and of the different hierarchies m_c/m_t and m_s/m_b) to cancel the dangerous down-quark mixing while preserving the CKM via up-quark mixing.

- The situation in the lepton sector is similar due to Pati-Salam universality of the parameters, i.e.

$$\frac{-s^L_{25}\left|y^\psi_{53}\right|\langle H_\tau\rangle + c^L_{25}s^{e^c}_{34}y^\psi_{24}\langle H_\mu\rangle}{s^L_{34}y^\psi_{43}\langle H_\tau\rangle} \approx \frac{-s^L_{25}\left|y^\psi_{53}\right|\langle H_\tau\rangle + m_\mu}{m_\tau} \approx s^L_{25}\left|y^\psi_{53}\right| \approx \mathcal{O}(V_{cb})\,. \tag{4.105}$$

However, the leptonic mixing angles $s^{e^c}_{24}$ and $s^{e^c}_{34}$ are smaller than the quark ones if we assume the phenomenological relation $\langle\phi_3\rangle \gg \langle\phi_1\rangle$. This leads to $\langle H_\mu\rangle$ being above the scale of the muon mass, which predicts a quick growth of lepton mixing in the scenario $s^{e^c}_{34} > s^{e^c}_{24}$. This can be easily achieved in natural benchmarks. In this scenario, interesting signals arise in LFV processes such as $\tau \to 3\mu$ or $\tau \to \mu\gamma$, mediated at tree-level by the Z' boson, see Section 4.6.4.

Other than the bullet points above, the mass matrices in Eqs. (4.98), (4.99), (4.100) lead to similar predictions as those of the simplified model in Section 4.2.3.

4.5.3 Vector-fermion interactions in the extended model

In this section we shall compute the vector-fermion couplings involving the heavy gauge bosons U_1, g', Z' for the extended twin Pati-Salam model. We omit the couplings of the

vector-like partners in the conjugate representations $\overline{\psi}_\alpha$ and $\overline{\psi^c_\alpha}$, since they do not mix with SM fermions.

U_1 couplings

In the original interaction basis, the vector leptoquark couples to the heavy $SU(2)_L$ doublets via the left-handed interactions[7],

$$\mathcal{L}^{\text{gauge}}_{U_1} = \frac{g_4}{\sqrt{2}}\left(Q_4^\dagger \bar{\sigma}_\mu L_4 + Q_5^\dagger \bar{\sigma}_\mu L_5 + Q_6^\dagger \bar{\sigma}_\mu L_6 + \text{h.c.}\right) U_1^\mu \,, \tag{4.106}$$

where similar couplings to the heavy $SU(2)_L$ singlets ψ^c are also present, however they lead to suppressed couplings to SM fermions due to the messenger dominance in Eq. (4.97). This way, we obtain dominantly left-handed U_1 couplings in good approximation. Now we shall apply the unitary transformations in Eq. (4.85) to rotate the fields from the original interaction basis to the decoupling basis (primed),

$$\mathcal{L}^{\text{gauge}}_{U_1} = \frac{g_4}{\sqrt{2}} Q'^\dagger_\alpha V_Q \bar{\sigma}_\mu \text{diag}(0,0,0,1,1,1) V_L^\dagger L'_\beta U_1^\mu + \text{h.c.}\,, \tag{4.107}$$

where

$$V_Q = V_{16}^Q V_{35}^Q V_{25}^Q V_{34}^Q V_{45}^Q \,, \qquad V_L = V_{16}^L V_{35}^L V_{25}^L V_{34}^L V_{45}^L \,. \tag{4.108}$$

The 4-5 rotations are different for quarks and leptons due to $\langle \Omega_{15} \rangle$ splitting the mass terms of the vector-like fermions. They lead to a non-trivial CKM-like matrix for the U_1 couplings,

$$W_{LQ} = V_{45}^Q V_{45}^{L\dagger} = \begin{pmatrix} c_{\theta_{LQ}} & -s_{\theta_{LQ}} & 0 \\ s_{\theta_{LQ}} & c_{\theta_{LQ}} & 0 \\ 0 & 0 & 1 \end{pmatrix} , \tag{4.109}$$

where $s_{\theta_{LQ}}$ depends on the angles s_{45}^Q and s_{45}^L, obtained from the diagonalisation in Eq. (4.84). The unitary matrix W_{LQ} can be regarded as a generalisation of the CKM matrix to $SU(4)^I_{PS}$ or quark-lepton flavour space. Similarly to the CKM case, the W_{LQ} matrix is the only source of flavour-changing transitions among $SU(4)^I_{PS}$ states, and it appears only in interactions mediated by U_1. In this sense, the vector leptoquark U_1 is analogous to the SM $W^\pm$ bosons. Similarly, the Z' and g' are analogous to the SM Z boson, and we will show that their interactions are $SU(4)^I_{PS}$ flavour-conserving at tree-level. In analogy to the SM, we will denote U_1 transitions as charged currents and Z', g' transitions as neutral currents. As in the SM, FCNCs proportional to the W_{LQ} matrix are generated at loop level. This mechanism was firstly identified in [268] for a similar 4321 framework.

The same mixing that leads to the SM fermion masses and mixings, see Eq. (4.108), also leads to effective U_1 couplings to SM fermions which can contribute to the LFU

[7] Notice that we continue working in the 2-component notation introduced in Appendix A.

ratios,

$$\mathcal{L}_{U_1}^{\text{gauge}} = \frac{g_4}{\sqrt{2}} Q'^{\dagger}_i \bar{\sigma}_\mu \begin{pmatrix} s^Q_{16} s^L_{16} \epsilon & 0 & 0 \\ 0 & c_{\theta_{LQ}} s^Q_{25} s^L_{25} & s_{\theta_{LQ}} s^Q_{25} s^L_{34} \\ 0 & -s_{\theta_{LQ}} s^Q_{34} s^L_{25} & c_{\theta_{LQ}} s^Q_{34} s^L_{34} \end{pmatrix} L'_j U_1^\mu + \text{h.c.}\,, \tag{4.110}$$

where we have considered that $s^{Q,L}_{35}$ are small, see Sections 4.5.2 and 4.6.3. The first family coupling can be diluted via mixing with vector-like fermions, which is parameterised via the effective parameter ϵ (see Section 4.6.4 for more details). The couplings above receive small corrections due to 2-3 fermion mixing arising after diagonalising the effective mass matrices in Eqs. (4.98), (4.99), (4.100). It can be seen from Eq. (4.110) that a large (2,3) coupling $\beta_{c\nu_\tau}$ arises now, proportional to the large sines $s_{\theta_{LQ}}$, s^L_{34} and s^Q_{25}. This solves one important issue of the simplified model, where the flavour-violating couplings $\beta_{c\nu_\tau}$ and $\beta_{b\mu}$ where connected to small 2-3 mixing angles, suppressing the contributions of U_1 to the LFU ratios. In any case, the leptoquark couplings that contribute to B-decays arise due to the same mixing effects which diagonalise the mass matrices of the model, yielding mass terms for the SM fermions. This way, the flavour puzzle and the B-anomalies are dynamically and parametrically connected in this model, leading to a predictive framework. Notice that thanks to the connection with the flavour puzzle, our U_1 couplings are dominantly left-handed, in contrast with the alternative theories in the market [115–117, 119, 120].

Coloron couplings and GIM-like mechanism

In the original interaction basis, the coloron couplings are flavour-diagonal, featuring the following couplings to $SU(2)_L$ doublets,

$$\mathcal{L}_{g'}^{\text{gauge}} = \frac{g_4 g_s}{g_3} \left(Q_4^\dagger \bar{\sigma}^\mu T^a Q_4 + Q_5^\dagger \bar{\sigma}^\mu T^a Q_5 + Q_6^\dagger \bar{\sigma}^\mu T^a Q_6 - \frac{g_3^2}{g_4^2} Q_i^\dagger \bar{\sigma}^\mu T^a Q_i \right) g'^a_\mu\,, \tag{4.111}$$

where $i = 1, 2, 3$. Now we rotate to the decoupling basis by applying the transformations in Eq. (4.108), (assuming small x^ψ_{35} as discussed in Section 4.6.3) obtaining

$$\begin{aligned} \mathcal{L}_{g'}^{\text{gauge}} &= \frac{g_4 g_s}{g_3} Q'^{\dagger}_i \bar{\sigma}^\mu T^a \\ &\times \begin{pmatrix} \left(s^Q_{16}\right)^2 - \left(c^Q_{16}\right)^2 \frac{g_3^2}{g_4^2} & 0 & 0 \\ 0 & \left(s^Q_{25}\right)^2 - \left(c^Q_{25}\right)^2 \frac{g_3^2}{g_4^2} & 0 \\ 0 & 0 & \left(s^Q_{34}\right)^2 - \left(c^Q_{34}\right)^2 \frac{g_3^2}{g_4^2} \end{pmatrix} Q'_j g'^a_\mu\,, \end{aligned} \tag{4.112}$$

Here V^Q_{45} cancels due to unitarity and due to the coloron couplings between vector-like quarks being flavour universal in the original basis of Eq. (4.111). Therefore, as anticipated, the CKM-like matrix W_{LQ} does not affect the neutral currents mediated by g' (and similarly for the Z' boson). The coloron couplings in Eq. (4.112) receive small corrections due to 2-3 mixing arising after diagonalising the effective mass matrices in

Eqs. (4.98), (4.99), (4.100), predominantly in the up sector due to the down-aligned flavour structure achieved in Section 4.5.2. We obtain similar couplings for $SU(2)_L$ singlets, however their mixing angles are suppressed by the messenger dominance in Eq. (4.97), and so they remain as in the original interaction basis to good approximation.

The coloron couplings of Eq. (4.112) are family universal if

$$s^Q_{34} = s^Q_{25} = s^Q_{16}\,, \tag{4.113}$$

leading to a GIM-like protection from tree-level FCNCs mediated by the coloron. The condition above was already identified in [268], denoted as *full alignment limit*. However, we have seen that maximal $s^Q_{34} \approx 1$ is well motivated in our model to protect the perturbativity of the top Yukawa, by the fit of the $R_{D^{(*)}}$ anomaly, and furthermore it naturally suppresses s^Q_{35} via a small c^Q_{34}. The caveat is that if the condition in Eq. (4.113) is implemented, then s^Q_{16} and s^Q_{25} would also be maximal, leading to large couplings to valence quarks which would blow up the production of the coloron at the LHC. This fact was already identified in [268], where large s^Q_{34} was also suggested by the B-anomalies, and this motivated a partial alignment limit,

$$s^Q_{25} = s^Q_{16}\,, \tag{4.114}$$

which suppresses FCNCs between the first and second quark families, proportional to the largest off-diagonal elements of the CKM matrix. FCNCs between the second and third families still arise, however we are protected from the stringent constraints of $B_s - \bar{B}_s$ meson mixing due to the down-aligned flavour structure achieved in Section 4.5.2. Finally, FCNCs between the first and third families are also under control, as they are proportional to the smaller elements of the CKM matrix.

The GIM-like condition of Eq. (4.114) translates, in terms of fundamental parameters of our model, into

$$\frac{x^\psi_{25}\langle\phi_3\rangle}{\sqrt{\left(x^\psi_{25}\langle\phi_3\rangle\right)^2 + \left(M^Q_5\right)^2}} = \frac{x^\psi_{16}\langle\phi_3\rangle}{\sqrt{\left(x^\psi_{16}\langle\phi_3\rangle\right)^2 + \left(M^Q_6\right)^2}}\,, \tag{4.115}$$

which could be naively achieved with natural couplings and M^Q_5, M^Q_6 being of the same order, as allowed by the messenger dominance in Eq. (4.97). The couplings and vector-like mass terms can also be chosen differently, as far as Eq. (4.115) is preserved. At the moment, the GIM-like mechanism is accidental. However, Eq. (4.115) suggests that the sixth and fifth family, and also the first and second families, might transform as doublets under a global $SU(2)$ symmetry, enforcing the parametric relations of Eq. (4.115).

Z' couplings

We can follow the same procedure to extract the couplings of the Z' boson to chiral fermions,

$$\mathcal{L}^{\text{gauge}}_{Z',q} = \frac{\sqrt{3}}{\sqrt{2}}\frac{g_4 g_Y}{g_1} Q'^{\dagger}_i \bar{\sigma}^\mu \times \begin{pmatrix} \frac{1}{6}\left(s^Q_{16}\right)^2 - \left(c^Q_{16}\right)^2 \frac{g_1^2}{9g_4^2} & 0 & 0 \\ 0 & \frac{1}{6}\left(s^Q_{25}\right)^2 - \left(c^Q_{25}\right)^2 \frac{g_1^2}{9g_4^2} & 0 \\ 0 & 0 & \frac{1}{6}\left(s^Q_{34}\right)^2 - \left(c^Q_{34}\right)^2 \frac{g_1^2}{9g_4^2} \end{pmatrix} Q'_j Z'_\mu \,, \tag{4.116}$$

$$\mathcal{L}^{\text{gauge}}_{Z',\ell} = -\frac{\sqrt{3}}{\sqrt{2}}\frac{g_4 g_Y}{g_1} L'^{\dagger}_i \bar{\sigma}^\mu \times \begin{pmatrix} \frac{1}{2}\left(s^L_{16}\right)^2 - \left(c^L_{16}\right)^2 \frac{g_1^2}{3g_4^2} & 0 & 0 \\ 0 & \frac{1}{2}\left(s^L_{25}\right)^2 - \left(c^L_{25}\right)^2 \frac{g_1^2}{3g_4^2} & 0 \\ 0 & 0 & \frac{1}{2}\left(s^L_{34}\right)^2 - \left(c^L_{34}\right)^2 \frac{g_1^2}{3g_4^2} \end{pmatrix} L'_j Z'_\mu \,, \tag{4.117}$$

where the up-quark couplings above receive small corrections due to 2-3 mixing arising after diagonalising the effective mass matrices in Eqs. (4.98), (4.99). However, larger 2-3 charged lepton mixing is possible (see Section 4.5.2), obtaining for charged leptons:

$$\mathcal{L}^{\text{gauge}}_{Z',e} \approx -\frac{\sqrt{3}}{\sqrt{2}}\frac{g_4 g_Y}{g_1} \hat{e}^{\dagger}_i \bar{\sigma}^\mu \times \begin{pmatrix} \frac{1}{2}\left(s^L_{16}\right)^2 - \left(c^L_{16}\right)^2 \frac{g_1^2}{3g_4^2} & 0 & 0 \\ 0 & \frac{1}{2}\left(s^L_{25}\right)^2 - \left(c^L_{25}\right)^2 \frac{g_1^2}{3g_4^2} & \frac{1}{2}\left[\left(s^L_{34}\right)^2 - \left(s^L_{25}\right)^2\right] s^e_{23} \\ 0 & \frac{1}{2}\left[\left(s^L_{34}\right)^2 - \left(s^L_{25}\right)^2\right] s^e_{23} & \frac{1}{2}\left(s^L_{34}\right)^2 - \left(c^L_{34}\right)^2 \frac{g_1^2}{3g_4^2} \end{pmatrix} \hat{e}_j Z'_\mu \,, \tag{4.118}$$

at first order in s^e_{23} and taking $c^e_{23} \approx 1$. The flavour-violating couplings above can lead to interesting signals in LFV processes such as $\tau \to 3\mu$ and $\tau \to \mu\gamma$, see more in Section 4.6.4.

In order to suppress LFV between the first and second lepton families, a similar condition similar to Eq. (4.114) but for leptons can be implemented,

$$s^L_{25} = s^L_{16} \,. \tag{4.119}$$

Remarkably, if the condition of Eq. (4.114) is fulfilled, then Eq. (4.119) would also be fulfilled in good approximation thanks to the underlying twin Pati-Salam symmetry, the small breaking effects given by the splitting of vector-like masses via $\langle \Omega_{15} \rangle$.

Observable	Experiment/constraint	Th. expr.
$[C^*_{\nu edu}]^{\tau\tau 32}$ $(R_{D^{(*)}})$	0.08 ± 0.02 (68% CL) [184]	(4.120)
$C_9^{\mu\mu} = -C_{10}^{\mu\mu}$ $(R^{2021}_{K^{(*)}})$	$[-0.31, -0.48]$ (68% CL) [181]	(4.121)
$C_9^{\mu\mu} = -C_{10}^{\mu\mu}$ $(R^{2022}_{K^{(*)}})$	$[-0.01, -0.14]$ (68% CL)(2.14)	(4.121)
$\delta(\Delta M_s)$	$\lesssim 0.11$ (95% CL) [242]	(2.34)
$\mathcal{B}(\tau \to 3\mu)$	$< 2.1 \times 10^{-8}$ (90% CL) [357]	(2.73)
$\mathcal{B}(\tau \to \mu\gamma)$	$< 5.0 \times 10^{-8}$ (90% CL) [358]	(2.58)
$\mathcal{B}(B_s \to \tau^{\pm}\mu^{\mp})$	$< 3.4 \times 10^{-5}$ (90% CL) [277]	(2.85)
$\mathcal{B}(B^+ \to K^+\tau^{\pm}\mu^{\mp})$	$< 2.8 \times 10^{-5}$ (90% CL) [278]	(2.86)
$\mathcal{B}(\tau \to \mu\phi)$	$< 8.4 \times 10^{-8}$ (90% CL) [280]	(2.92)
$\mathcal{B}(K_L \to \mu^{\pm}e^{\mp})$	$< 4.7 \times 10^{-12}$ (90% CL) [282]	(2.95)
$(g_\tau/g_{e,\mu})_{\ell+\pi+K}$	1.0003 ± 0.0014 [80]	(4.147)
$\mathcal{B}(B_s \to \tau^+\tau^-)$	$< 5.2 \times 10^{-3}$ (90% CL) [252]	(2.41)
$\mathcal{B}(B \to K\tau^+\tau^-)$	$< 2.25 \times 10^{-3}$ (90% CL) [254]	(2.42)
$\mathcal{B}(B^+ \to K^+\nu\bar{\nu})/\mathcal{B}(B^+ \to K^+\nu\bar{\nu})_{\rm SM}$	2.8 ± 0.8 (68% CL) [81]	(2.54)
$\mathcal{B}(B \to K^*\nu\bar{\nu})/\mathcal{B}(B \to K^*\nu\bar{\nu})_{\rm SM}$	< 2.7 (90% CL) [271, 272]	(2.54)

TABLE 4.4: Set of observables explored in the phenomenological analysis, including current experimental constraints.

4.6 Phenomenology of the extended model

The twin Pati-Salam model features a fermiophobic low-energy 4321 theory with a rich phenomenology. Although extensive analyses of general 4321 models have been performed during the last few years, the vast majority of them have been performed in the framework of non-fermiophobic 4321 models [115, 170, 262, 263, 356]. Instead, the twin Pati-Salam model offers a fermiophobic scenario with a different phenomenology. Being a theory of flavour, extra constraints and correlations arise via the generation of the SM Yukawa couplings and the prediction of fermion masses and mixing, including striking signals in LFV processes. Moreover, the underlying twin Pati-Salam symmetry introduces universality (and perturbativity) constraints over several parameters, which are not present in alternative models. These features motivate a dedicated analysis. We will highlight key observables for which the intrinsic nature of the model can be disentangled from all alternative proposals. All low-energy observables considered are listed in Table 4.4, with references to current experimental bounds and links to theory expressions.

The benchmark points BP1 and BP2 in Table 4.5 address the $R_{D^{(*)}}$ anomalies and are compatible with the 2021 and 2022 data on $R_{K^{(*)}}$, respectively, plus all the considered low-energy observables and high-p_T searches. They provide a good starting point to study the relevant phenomenology, featuring typical configurations of the model, and allow us to confront the 2021 picture of the model versus the new situation with

Benchmark				Output			
g_4	3.5	λ_{15}^{44}	-0.5	s_{34}^{Q}	0.978	$M_{g'}$	3782.9 GeV
$g_{3,2,1}$	1, 0.65, 0.36	λ_{15}^{55}, λ_{15}^{66}	2.5, 1.1	s_{34}^{L}	0.977	$M_{Z'}$	2414.3 GeV
x_{34}^{ψ}	2	$x_{42}^{\psi^c}$	0.4	$s_{25}^{Q} = s_{16}^{Q}$	0.20*, 0.17**	s_{23}^{u}	0.042556
$x_{25}^{\psi} = x_{16}^{\psi}$	0.41* , 0.35**	$x_{43}^{\psi^c}$	1	$s_{25}^{L} = s_{16}^{L}$	0.1455	s_{23}^{d}	0.001497
M_{44}^{ψ}	320 GeV	$M_{44}^{\psi^c}$	5 TeV	$s_{\theta_{LQ}}$	0.7097	s_{23}^{e}	-0.111
M_{55}^{ψ}	780 GeV	$y_{53,43,34,24}^{\psi}$	-0.3, 1, 1, 1	$\hat{M}_4^Q$	1226.8 GeV	V_{cb}	0.04106
M_{66}^{ψ}	1120 GeV	$\langle H_t \rangle$	177.2 GeV	$\hat{M}_5^Q$	1238.7 GeV	m_t	172.91 GeV
M_{45}^{ψ}	-700 GeV	$\langle H_c \rangle$	26.8 GeV	$\hat{M}_4^L$	614.04 GeV	m_c	1.270 GeV
M_{54}^{ψ}	50 GeV	$\langle H_b \rangle$	4.25 GeV	$\hat{M}_5^L$	845.26 GeV	m_b	4.180 GeV
$\langle \phi_3 \rangle$	0.6 TeV	$\langle H_s \rangle$	2.1 GeV	$\hat{M}_6^Q$	1234.6 GeV	m_s	0.0987 GeV
$\langle \phi_1 \rangle$	0.3 TeV	$\langle H_\tau \rangle$	1.75 GeV	$\hat{M}_6^L$	859.4 GeV	m_τ	1.7765 GeV
$\langle \Omega_{15} \rangle$	0.4 TeV	$\langle H_\mu \rangle$	4.58 GeV	M_{U_1}	2987.1 GeV	m_μ	105.65 MeV

TABLE 4.5: Input and output parameters for the benchmark points BP1 and BP2, * indicates BP1 while ** indicates BP2, otherwise both benchmarks share the same parameters. BP1 is compatible with 2021 data on $R_{K^{(*)}}$, while BP2 is compatible with the 2022 updates by LHCb.

LFU preserved in μ/e ratios. Moreover, they fit second and third family charged fermion masses and mixings, featuring a down-aligned flavour structure with $\mathcal{O}(0.1)$ $\mu-\tau$ lepton mixing. The latter is more benchmark dependent, with the common range being $s_{23}^{e} = [V_{cb}, 5V_{cb}]$. The case $s_{23}^{e} \approx 0.1$ is interesting because it leads to intriguing signals in LFV processes, as we shall see. BP1 and BP2 also feature $x_{25}^{\psi} \approx x_{16}^{\psi}$ and $M_5^{Q,L} \approx M_6^{Q,L}$, providing a GIM-like suppression of 1-2 FCNCs.

In the forthcoming sections we will assume the couplings of the fundamental Lagrangian to be universal, such as x_{34}^{ψ} and x_{25}^{ψ}, however their universality is broken by small RGE effects which we estimate in Section 4.6.7 to be below 8%. We neglect the small RGE effects and preserve universal parameters for the phenomenological analysis, in order to simplify the exploration of the parameter space and highlight the underlying twin Pati-Salam symmetry.

4.6.1 $R_{D^{(*)}}$ and $R_{K^{(*)}}$

In our model, the left-handed WCs $[C^*_{\nu edu}]^{\tau\tau 32}$ and $C_9^{\mu\mu} = -C_{10}^{\mu\mu}$ are obtained at tree-level after integrating out the heavy gauge bosons, with the overall contribution being dominated by U_1 tree-level exchange as in Fig. 4.4,

$$[C^*_{\nu edu}]^{\tau\tau 32}(m_b) = \frac{2\eta_V^{\nu\tau}}{V_{cb}} \left[C_{lq}^{(3)}\right]^{\tau\tau 23}(\Lambda)\,, \tag{4.120}$$

$$C_9^{\mu\mu}(m_b) = -C_{10}^{\mu\mu}(m_b) = -\frac{2\pi}{\alpha_{\rm EM} V_{tb}V_{ts}^*}\eta_V^{\ell\ell}\left(\left[C_{lq}^{(3)}\right]^{\mu\mu 23}(\Lambda) + \left[C_{lq}^{(1)}\right]^{\mu\mu 23}(\Lambda)\right)\,, \tag{4.121}$$

where the negligible RGE effect is encoded as $\eta_V^{\nu\tau} \approx 1.00144$, $\eta_V^{\ell\ell} \approx 0.974$ and has been computed with `DsixTools 2.1` [174] for $\Lambda = 1\,\text{TeV}$. Notice also the tree-level matching of the twin Pati-Salam model to the SMEFT in Section 4.3. In order to be compatible with the SM-like $R_{K^{(*)}}$ ratios, constraints over $C_9^{\mu\mu} = -C_{10}^{\mu\mu}$ are shown in Table 4.4. Similarly, in order to explain the $R_{D^{(*)}}$ anomalies there is a preferred region for the $[C^*_{\nu edu}]^{\tau\tau 32}$ coefficient, as shown in Table 4.4. The full EFT description of these observables (including the definition of the Wilson coefficients) plus a discussion of current experimental data can be found in Sections 2.3.1 and 2.3.2.

In terms of fundamental parameters of the model, the deviations from the SM in the LFU ratios scale as follows,

$$|\Delta R_{D^{(*)}}| \propto \left| \left(x_{34}^{\psi}\right)^3 x_{25}^{\psi} \right| , \tag{4.122}$$

$$|\Delta R_{K^{(*)}}| \propto \left| x_{34}^{\psi} \left(x_{25}^{\psi}\right)^3 \right| , \tag{4.123}$$

where we have fixed the vector-like masses and the 4321-breaking VEVs to the values of our benchmark in Table 4.5. This way, the Yukawa couplings above control the contributions to most of the relevant phenomenology, including the LFU ratios. The Pati-Salam universality of x_{34}^{ψ} and x_{25}^{ψ} provides here a welcome constraint, not present in other 4321 models. In particular, one can see that both $R_{D^{(*)}}$ and $R_{K^{(*)}}$ are connected via the same parameters and deviations in both are expected, while in general 4321 models (such as the fermiophobic model of Refs. [267, 268]) the analog of a single $x_{i\alpha}^{\psi}$ decomposes into several parameters for quarks and leptons, which decouple $R_{K^{(*)}}$ from $R_{D^{(*)}}$.

Following from Eqs. (4.122) and (4.123), the cubic dependence of $R_{K^{(*)}}$ on x_{25}^{ψ} anticipates that we can suppress the contribution to $R_{K^{(*)}}$, while preserving a large contribution to $R_{D^{(*)}}$ thanks to its linear dependence on x_{25}^{ψ}. As a consequence, the yellow band of parameter space preferred by 2022 $R_{K^{(*)}}$ is just shifted below the orange band of 2021 $R_{K^{(*)}}$ in Fig. 4.8b. The 2022 $R_{K^{(*)}}$ band is compatible with $R_{D^{(*)}}$ at 1σ only in a narrow region of the parameter space. This is encouraging, given the fact that the model was built to address the 2021 tensions in both LFU ratios. However, in order to explain $R_{D^{(*)}}$, small deviations from the SM in the $R_{K^{(*)}}$ ratios are unavoidable, to be tested in the future via more precise measurements of LFU by the LHCb collaboration. Moreover, lower central values for $R_{D^{(*)}}$ are also expected.

Remarkably, the fact that the twin Pati-Salam model only generates the effective operator $(\bar{c}_L \gamma_\mu b_L)\,(\bar{\tau}_L \gamma^\mu \nu_{\tau L})$ implies that both R_D and R_{D^*} are corrected in the same direction and with the same size, i.e. $\Delta R_D = \Delta R_{D^*}$. Instead, non-fermiophobic 4321 models also predict the scalar operator $(\bar{c}_L b_R)(\bar{\tau}_R \nu_{\tau L})$, which leads to a larger correction for R_D than that of R_{D^*} (about 5/2 larger for the PS^3 model, see Eq. (27) in [115]). Current data is equally compatible with both according to recent global fits [269].

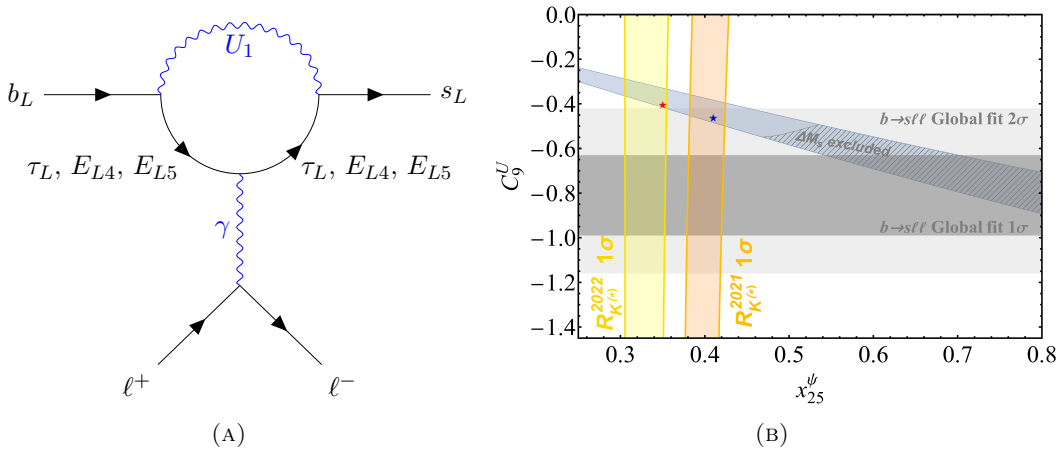

(A) (B)

FIGURE 4.6: ***Left:*** Off-shell photon penguin with tau leptons in the loop that generates C_9^U, a contribution to the lepton universal operator $\mathcal{O}_9^{23\ell\ell}$ that participates in $b \to s\ell\ell$ transitions. ***Right:*** C_9^U as a function of x_{25}^ψ via Eq. (4.124), with x_{34}^ψ varied in the range [1, 3.5] as preferred by $R_{D^{(*)}}$ (blue region), with the rest of parameters fixed as in Table 4.5. The grey (light grey) region denotes the 1σ (2σ) contour of C_9^U as preferred by a global fit to $b \to s\ell\ell$ data taken from [359]. The yellow (orange) band denotes the 1σ region preferred by $R_{K^{(*)}}^{2022}$ ($R_{K^{(*)}}^{2021}$). The blue and red stars denote BP1 and BP2 respectively.

4.6.2 Off-shell photon penguin with tau leptons

As discussed in Section 2.3.12, the SMEFT scenario $\left[C_{lq}^{(1)}\right]^{\tau\tau 23} = \left[C_{lq}^{(3)}\right]^{\tau\tau 23}$ correlates $R_{D^{(*)}}$ with a large contribution to $C_9^{\tau\tau} = -C_{10}^{\tau\tau}$, which then mixes into a lepton universal contribution to the operator C_9 via RGE effects. The U_1 model is an specific example of this scenario, where the same leptoquark couplings that explain $R_{D^{(*)}}$ are correlated to those in $b \to s\tau\tau$ due to $SU(2)_L$ invariance. The specific contributions to $b \to s\tau\tau$ will be explored in Section 4.6.6, but in this section we explore the impact of the universal contribution to $\mathcal{O}_9^{\ell\ell}$, denoted as C_9^U, over the anomalous $b \to s\mu\mu$ transition. The contribution of U_1 to C_9^U originates from a 1-loop off-shell photon penguin diagram with tau leptons running in the loop, shown in Fig. 4.6a. Notice that this diagram is similar to that of Fig. 2.6a but exchanging the insertion of the 4-fermion operator by the insertion of the U_1 leptoquark in the loop, plus adding new contributions provided by the vector-like leptons of our model running in the loop. We finally obtain

$$C_9^U = -\frac{v_{\rm SM}^2 g_4^2}{6 V_{tb} V_{ts}^* M_{U_1}^2}\left(\log\left[\frac{2m_b^2}{g_4^2 M_{U_1}^2}\right]\beta_{s\tau}\beta_{b\tau}^* + \log\left[\frac{2m_{E_5}^2}{g_4^2 M_{U_1}^2}\right]\beta_{sE_5}\beta_{bE_5}^* + \log\left[\frac{2m_{E_4}^2}{g_4^2 M_{U_1}^2}\right]\beta_{sE_4}\beta_{bE_4}^*\right), \tag{4.124}$$

which is explicitly correlated to $b \to s\tau\tau$, as well as to $R_{D^{(*)}}$ since $SU(2)_L$ invariance implies $\beta_{s\tau} \approx \beta_{c\nu_\tau}$ for the U_1 couplings. Therefore, the scaling is $|C_9^U| \propto (x_{34}^\psi)^3 x_{25}^\psi$, just like $R_{D^{(*)}}$. Notice that the contribution of our model to C_9^U differs from those of alternative models in the literature [291] due to the vector-like leptons $E_{4,5}$ running in the loop. Unfortunately, due to the flavour structure of our model, the contributions via

vector-like leptons interfere negatively with the leading contribution via the tau loop, and hence our overall contribution to C_9^U is generally smaller than in the alternative models. The contribution from E_4 is negligible, but the contribution from E_5 reduces C_9^U by a 20% factor of the tau loop contribution.

In our model, $R_{D^{(*)}}$ and $R_{K^{(*)}}$ are correlated, as can be seen from Eqs. (4.122) and (4.123). Therefore, C_9^U is not only correlated with $R_{D^{(*)}}$ but also with $R_{K^{(*)}}$. Given that deviations from 1 in $R_{K^{(*)}}$ are now constrained by the new LHCb measurements, our final contribution to C_9^U is constrained to be $C_9^U \approx -0.4$, as can be seen in Fig. 4.6b. However, global fits of $b \to s\ell\ell$ data (see e.g. [82,188,359]), mostly driven by anomalies in $\text{Br}(B \to K\mu\mu)$, $\text{Br}(B_s \to \phi\mu\mu)$ and $P_5'(B \to K^*\mu\mu)$ (see the discussion in Section 2.3.1), prefer a larger value $C_9^U \approx -0.8$. Therefore, we conclude that our model is not able to fully address the anomalies in $b \to s\ell\ell$ via the off-shell photon penguin, although our contribution to C_9^U ameliorates the tensions. Performing a more ambitious analysis would require to make assumptions about the hadronic uncertainties afflicting $\text{Br}(B \to K\mu\mu)$, $\text{Br}(B_s \to \phi\mu\mu)$ and $P_5'(B \to K^*\mu\mu)$, which is beyond the scope of this work.

However, we notice that in principle our model has the ideal structure to the address all the anomalies in B-physics, i.e. we reproduce the preferred scenario presented in [82] (see also Section 2.3.12) where a large contribution to $[C^*_{\nu edu}]^{\tau\tau 32}$ addresses $R_{D^{(*)}}$ and ameliorates tensions in $b \to s\mu\mu$ data, while a small contribution to $C_9^{\mu\mu} = -C_{10}^{\mu\mu}$ further improves the overall fit. Even though our contribution to C_9^U does not reach the preferred values by the global fits, it improves the overall description of $b \to s\mu\mu$ data with respect to the SM.

4.6.3 $B_s - \bar{B}_s$ mixing

In the extended twin Pati-Salam model, tree-level contributions to $B_s - \bar{B}_s$ mixing via 2-3 quark mixing are suppressed due to the down-aligned flavour structure achieved in Section 4.5.2. A further 1-loop contribution mediated by U_1 has been studied in the literature [263, 268, 360] for other 4321 models, and vector-like charged leptons are known to play a crucial role. In Ref. [268], a framework with three vector-like charged leptons was considered, however the loop function was generalised from the SM $W^\pm$ box diagram, so the bounds were expected to be slightly overestimated. Instead, in [360] the proper loop function was derived, but a framework with only one vector-like charged lepton was considered. For this work, we have generalised the loop function of [360] to the case of three vector-like leptons. The 1-loop contribution to the effective Wilson coefficient C_1^{bs} (see Section 2.3.4) mediated by U_1 reads,

$$C_1^{bs}\Big|_{\text{NP}}^{\text{loop}} = \frac{g_4^4}{(8\pi M_{U_1})^2} \sum_{\alpha,\beta} (\beta^*_{s\alpha}\beta_{b\alpha}) \left(\beta^*_{s\beta}\beta_{b\beta}\right) F(x_\alpha, x_\beta)\,, \tag{4.125}$$

where $\alpha, \beta = \mu, \tau, E_4, E_5$ run for all charged leptons, including the vector-like partners (except for electrons and the sixth charged lepton which do not couple to the second or third generation), and $x_\alpha = (m_\alpha/M_{U_1})^2$. The contribution corresponds to the box

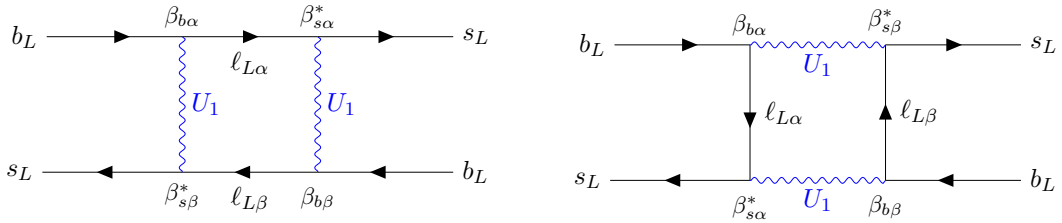

FIGURE 4.7: U_1-mediated 1-loop diagrams contributing to $B_s - \bar{B}_s$ mixing. The indices α, β run for all charged leptons including vector-like, i.e. $\ell_{L\alpha} = (\mu_L, \tau_L, E_{L4}, E_{L5})$.

diagrams in Fig. 4.7. The product of couplings $\beta^*_{s\alpha}\beta_{b\alpha}$ has the fundamental property

$$\sum_\alpha \beta^*_{s\alpha}\beta_{b\alpha} = 0\,, \tag{4.126}$$

which arises from unitarity of the transformations in Eq. (4.108). This property, similarly to the GIM mechanism in the SM, is essential to render the loop finite. However, the property holds as long as the 2-3 down mixing and s^Q_{35} are small. In particular, s^Q_{35} is naturally small in the scenario $s^Q_{34} \approx 1$, as it is suppressed by the small cosine c^Q_{34}, see the definition of s^Q_{35} in Eq. (4.89). Ultimately, the mixing angle s^Q_{35} is controlled by the fundamental parameter x^ψ_{35}, and we obtained that $x^\psi_{35} \lesssim 0.09$ is required to pass the ΔM_s bound.

The loop function reads

$$F(x_\alpha, x_\beta) = \left(1 + \frac{x_\alpha x_\beta}{4}\right) B(x_\alpha, x_\beta)\,, \tag{4.127}$$

where

$$B(x_\alpha, x_\beta) = \frac{1}{(1-x_\alpha)(1-x_\beta)} + \frac{x^2_\alpha \log x_\alpha}{(x_\beta - x_\alpha)(1-x^2_\alpha)} + \frac{x^2_\beta \log x_\beta}{(x_\alpha - x_\beta)\left(1-x^2_\beta\right)}\,. \tag{4.128}$$

In this manner, the loop function is dominated by the vector-like partners because they are much heavier than chiral charged leptons. In particular, in the motivated scenario with maximal s^L_{34}, the couplings with the fourth family $\beta^*_{sE_4}\beta_{bE_4}$ are suppressed by the small cosine c^L_{34}. This way, the loop is dominated by E_5 in good approximation. We obtain the effective loop function in this scenario by removing all constants in $x_{\alpha,\beta}$, which vanish due to the property (4.126),

$$\tilde{F}(x) \approx F(x,x) - 2F(x,0) + F(0,0) = \frac{x\,(x+4)\,(-1+x^2-2x\log x)}{4\,(x-1)^3}\,, \tag{4.129}$$

and in this approximation the contribution to C^{bs}_1 reads

$$C^{bs}_1\Big|^{\rm loop}_{\rm NP} = \frac{g^4_4}{(8\pi M_{U_1})^2}\left(\beta^*_{sE_5}\beta_{bE_5}\right)^2 \tilde{F}(x_{E_5})\,. \tag{4.130}$$

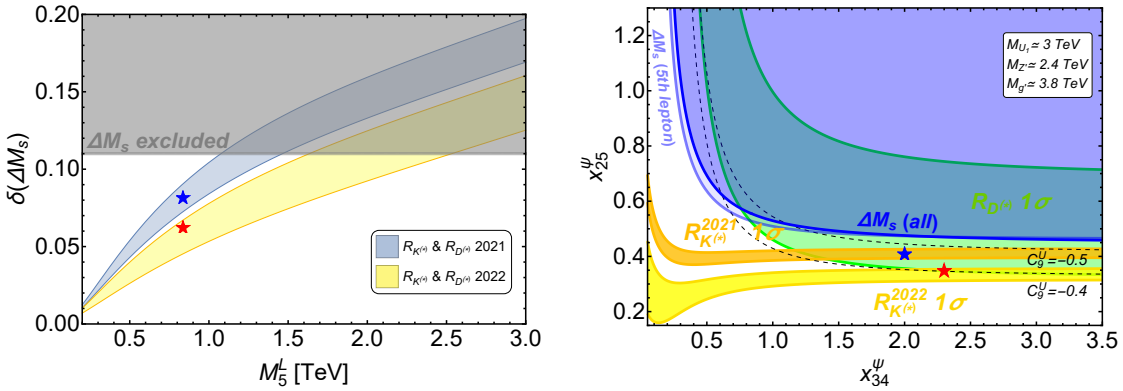

(A) (B)

FIGURE 4.8: ***Left:*** $\delta(\Delta M_s)$ (Eq. (2.34)) as a function of the 5th vector-like mass term. x^{ψ}_{25} is varied in the range $x^{\psi}_{25} = [0.3, 0.35]$ ($[0.4, 0.45]$) preferred by $R^{2022}_{K^{(*)}}$ ($R^{2021}_{K^{(*)}}$), obtaining the yellow (blue) band. The grey region is excluded by the ΔM_s bound, see Eq. (2.32). ***Right:*** Parameter space in the plane $(x^{\psi}_{34}, x^{\psi}_{25})$ compatible with $R_{D^{(*)}}$ and $R_{K^{(*)}}$ at 1σ. The remaining parameters are fixed as in Table 4.5 for both panels. The dashed lines show contours of constant C^U_9. The blue region is excluded by the ΔM_s bound, the region excluded only due to the contribution via the 5th lepton is also shown in lighter blue for comparison. The blue and red stars denote BP1 and BP2 respectively.

The loop function grows with x_{E_5}. However, in the limit of large bare mass term M^L_5 the effective coupling $\beta^*_{sE_5} \propto s^Q_{25}$ vanishes (since large M^L_5 also implies large M^Q_5 due to the Pati-Salam symmetry), hence both the contribution to C^{bs}_1 and $R_{D^{(*)}}$ go away. In Fig. 4.8a we plot $\delta(\Delta M_s)$ defined in Eq. (2.34) in terms of M^L_5, and we vary x^{ψ}_{25} in the ranges compatible with $R_{D^{(*)}}$ and $R^{2022}_{K^{(*)}}$ ($R^{2021}_{K^{(*)}}$). We can see that the ΔM_s bound requires a vector-like lepton around 1.5-2 TeV in the 2022 case, while 2021 data was pointing to a vector-like lepton with a mass around 1 TeV.

In Fig. 4.8b we show that Eq. (4.130) is indeed a good approximation, up to small interference effects between the 4th and 5th family contributions in the small x^{ψ}_{34} region, where the fourth lepton is lighter. We also show the parameter space compatible with ΔM_s and the LFU ratios in our benchmark scenario. In particular, ΔM_s turns out to be the strongest constraint over the parameter space other than $R^{2022}_{K^{(*)}}$.

4.6.4 LFV processes

$\tau \to 3\mu$

The partial alignment condition of Eq. (4.119) allows for Z'-mediated FCNCs in $\tau\mu$ processes, due to the fact that the model predicts significant mixing between the muon and tau charged leptons. This is a crucial prediction of the twin Pati-Salam theory of flavour, not present in general 4321 models. Of particular interest is the process $\tau \to 3\mu$, which receives a tree-level Z'-mediated contribution that grows with the $\tau\mu$ mixing angle

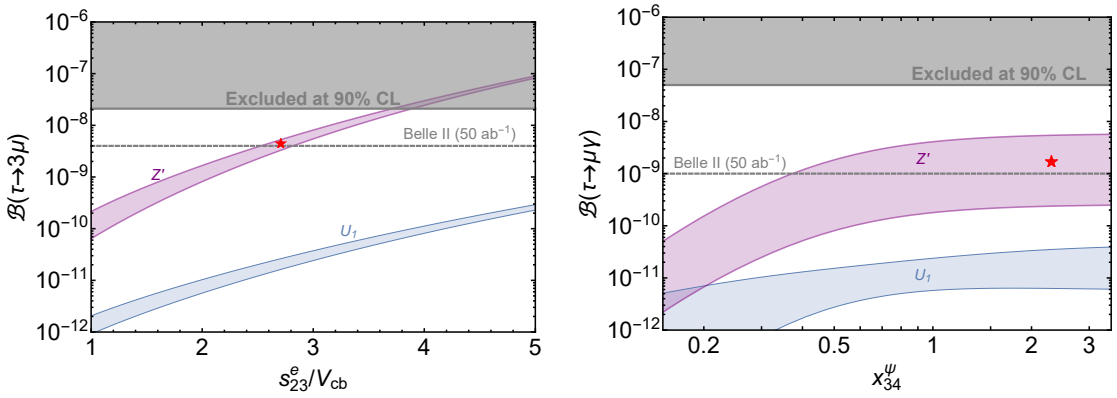

(A) (B)

FIGURE 4.9: ***Left:*** $\mathcal{B}(\tau \to 3\mu)$ as a function of the 2-3 charged lepton mixing sine s^e_{23}. The purple region denotes the Z' contribution while the blue region denotes the U_1 contribution, for both we have varied $x^\psi_{25} = [0.3, 0.35]$ which is compatible with $R^{2022}_{K^{(*)}}$. ***Right:*** $\mathcal{B}(\tau \to \mu\gamma)$ as a function of x^ψ_{34}. The purple region denotes the Z' contribution for which we have varied $s^e_{23} = [V_{cb}, 5V_{cb}]$. The blue region denotes the U_1 contribution, for which we have varied $x^\psi_{25} = [0.1, 1]$. The grey regions are excluded by the experiment, the dashed lines show the projected future bound. The red star shows BP2.

s^e_{23}. Beyond the latter, $\tau \to 3\mu$ also receives a U_1-mediated 1-loop contribution

$$\left[C^{V,LL}_{ee}\right]^{\mu\tau\mu\mu}\Big|^{\text{loop}}_{U_1} = \frac{3g_4^4}{128\pi^2 M^2_{U_1}} \beta^*_{D_5\mu}\beta_{D_5\tau}\left(\beta_{D_5\mu}\right)^2 \tilde{F}(x_{D_5})\,. \tag{4.131}$$

The effective coupling $\beta_{D_5\mu}$ is proportional to $s^L_{25} \approx 0.1$, which provides a further suppression of $\mathcal{O}((s^L_{25})^3)$ that renders the loop negligible against the much larger tree-level Z'-mediated contribution $\left[C^{V,LL}_{ee}\right]^{\mu\tau\mu\mu}\Big|_{Z'}$, that is obtained from the tree-level matching to the SMEFT in Section 4.3. The typical benchmark $s^L_{25} \approx 0.1$ naturally suppresses the $\mu\mu Z'$ coupling, keeping the Z' contribution to $\tau \to 3\mu$ under control, and simultaneously protects from $Z' \to \mu\mu$ dilepton searches at the LHC (see Section 4.6.8).

As depicted in Fig. 4.9a, the Z' contribution dominates over the U_1 contribution, and the regions of the parameter space with very large s^e_{23} are already excluded by the experiment. We have chosen to plot the results of the 2022 case only, since this observable depends mostly on s^e_{23} and there is little variation with 2021 data. The Belle II collaboration will test a further region of the parameter space [255], setting the bound $s^e_{23} < 2.8V_{cb}$ if no signal is detected. In general 4321 models (such as [262, 263, 267, 268]) the $\mu - \tau$ mixing is unspecified, so only the small U_1 signal is predicted. Therefore, the large Z' signal offers the opportunity to disentangle the twin Pati-Salam model from alternative 4321 proposals.

As depicted in Fig. 4.11b, $\tau \to 3\mu$ is the most constraining signal over the parameter space out of all the LFV processes, provided that the 2-3 charged lepton mixing is $\mathcal{O}(0.1)$.

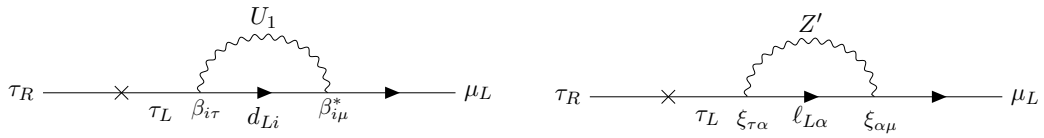

(A) (B)

FIGURE 4.10: U_1 (left panel) and Z' (right panel) 1-loop contributions to $\tau \to \mu\gamma$. Photon lines are implicit. The index i runs for all down-quarks including vector-like, i.e $d_{Li} = (s_L, b_L, D_{L4}, D_{L5})$, while α runs for all charged leptons including vector-like, i.e. $\ell_{L\alpha} = (\mu_L, \tau_L, E_{L4}, E_{L5})$.

$\tau \to \mu\gamma$

The dipole operator $[\mathcal{O}_{e\gamma}]^{\mu\tau}$ receives 1-loop contributions in our model via both U_1 and Z',

$$[C_{e\gamma}]^{\mu\tau} = [C_{e\gamma}]^{\mu\tau}|_{U_1} + [C_{e\gamma}]^{\mu\tau}|_{Z'} \,, \tag{4.132}$$

where

$$[C_{e\gamma}]^{\mu\tau}|_{U_1}(\Lambda) = -\frac{C_U}{32\pi^2}\sum_i \beta^*_{i\mu}\beta_{i\tau}\left[G_1(x_i) - 2G_2(x_i)\right] \,, \tag{4.133}$$

$$[C_{e\gamma}]^{\mu\tau}|_{Z'}(\Lambda) = -\frac{C_{Z'}}{32\pi^2}\sum_\alpha \xi_{\tau\alpha}\xi_{\alpha\mu}\widetilde{G}(x_\alpha) \,, \tag{4.134}$$

where $i = s, b, D_4, D_5$ and $\alpha = \mu, \tau, E_4, E_5$. The loop functions are given by [234,263,360]

$$G_1(x) = x\left[\frac{2-5x}{2(x-1)^4}\log x - \frac{4-13x+3x^2}{4(x-1)^3}\right] \,, \tag{4.135}$$

$$G_2(x) = x\left[\frac{4x-1}{2(x-1)^4}x\log x - \frac{2-5x-3x^2}{4(x-1)^3}\right] \,, \tag{4.136}$$

$$\widetilde{G}(x) = \frac{5x^4 - 14x^3 + 39x^2 - 38x - 18x^2\log x + 8}{12(1-x)^4} \,. \tag{4.137}$$

The running of the dipole operator from $\Lambda = 2$ TeV to the scale $\mu \sim m_\tau$ is given by $[C_{e\gamma}]^{\mu\tau}(m_\tau) \approx 0.92[C_{e\gamma}]^{\mu\tau}(\Lambda)$, as estimated with `DsixTools 2.1` [174]. Neglecting the muon mass, the branching ratio $\mathcal{B}(\tau \to \mu\gamma)$ is given by Eq. (2.58).

Provided that the 3-4 mixing is maximal, the U_1 loop is dominated by the 5th vector-like quark, and in this situation the couplings $\beta^*_{D_5\mu}\beta_{D_5\tau}$ are controlled by x^ψ_{25}. The Z' loop is dominated by chiral leptons, in particular by the τ lepton, since the coupling $\xi_{\tau\tau}$ is maximal while $\xi_{\mu\mu}$ is suppressed. In this scenario, the overall Z' contribution is controlled by $\xi_{\tau\mu}$ which grows with the $\mu-\tau$ mixing angle s^e_{23}, and the variation via x^ψ_{25} is minimal.

In Fig. 4.9b we can see that the Z' contribution dominates the branching fraction in the range of large x^ψ_{34} motivated by $R_{D^{(*)}}$, leading to the predictions for $\mathcal{B}(\tau \to \mu\gamma)$ being one/three orders of magnitude below the current experimental limit depending on the value of s^e_{23}. We have also included the bound projected by Belle II [255], which will partially test the parameter space. In the 4321 models of [267, 268] the $\mu - \tau$ mixing

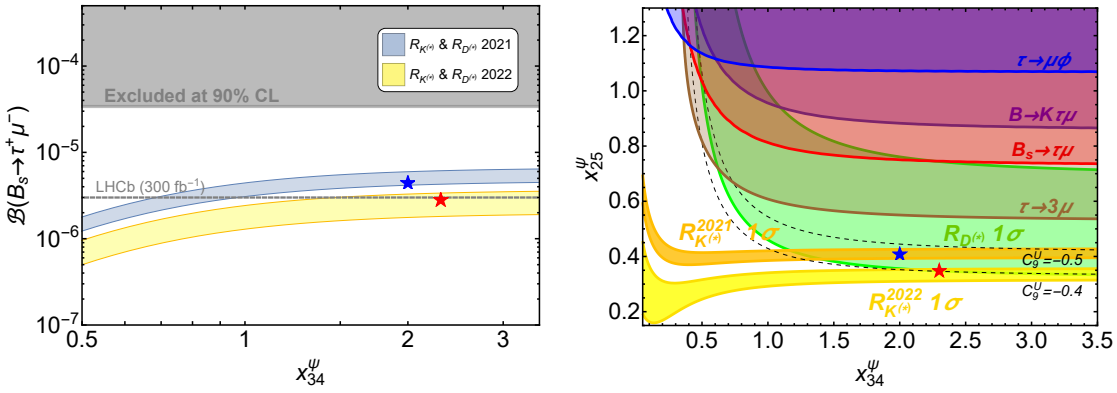

(A) (B)

FIGURE 4.11: ***Left:*** $\mathcal{B}(B_s \to \tau^+\mu^-)$ as a function of x_{34}^{ψ}. The yellow (blue) band is obtained by varying x_{25}^{ψ} in the range $x_{25}^{\psi} = [0.3, 0.35]([0.4, 0.45])$ preferred by $R_{K^{(*)}}^{2022}$ ($R_{K^{(*)}}^{2021}$). The grey region is excluded by the experiment, the dashed line shows the projected future bound. ***Right:*** Parameter space in the plane (x_{34}^{ψ}, x_{25}^{ψ}) compatible with $R_{D^{(*)}}$ and $R_{K^{(*)}}$ at 1σ. The remaining parameters are fixed as in Table 4.5. The dashed lines show contours of constant C_9^U. The regions excluded by LFV violating processes are displayed. The blue (red) star shows BP1 (BP2).

is unspecified, so only the blue U_1 signal is predicted. For non-fermiophobic models, this signal is largely enhanced via a chirality flip involving the bottom quark in the loop [262, 263, 356, 360, 361], predicting a larger signal $\mathcal{B}(\tau \to \mu\gamma) \approx 10^{-8}$. Instead, our Z' signal lies below, offering the opportunity to disentangle the twin Pati-Salam model from all alternative proposals.

$B_s \to \tau\mu$, $B \to K\tau\mu$ and $\tau \to \mu\phi$

The vector leptoquark U_1 mediates tree-level contributions to flavour-violating (semi) leptonic B-decays to (kaons), taus and muons. The experimental bound for $B_s \to \tau\mu$ was obtained by LHCb [277], while for $B \to K\tau\mu$ experimental bounds are only available for the decays $B^+ \to K^+\tau\mu$ [278]. The process $\tau \to \mu\phi$ receives tree-level contributions from both U_1 and Z'. However, $\tau \to \mu\phi$ turns out to be suppressed by the small effective couplings $\beta_{s\mu} \propto s_{25}^Q s_{25}^L$ and $\xi_{ss} \propto \left(s_{25}^Q\right)^2$, so that we find $\mathcal{B}(\tau \to \mu\phi) \approx 10^{-9}$, roughly two orders of magnitude below the current experimental bounds, and just below the future sensitivity of Belle II [255].

As can be seen in Fig. 4.11b, $B_s \to \tau^+\mu^-$ implies the strongest constraint over the parameter space out of all semileptonic LFV processes involving τ leptons, followed by $B^+ \to K^+\tau^+\mu^-$ and $\tau \to \mu\phi$. The present experimental bounds lead to mild constraints over the parameter space compatible with $R_{D^{(*)}}$. As depicted in Fig. 4.11a, the 2021 region for $B_s \to \tau^+\mu^-$ was partially within LHCb projected sensitivity, but the 2022 region will mostly remain untested.

field	$\mathbb{Z}_2$
$\overline{\psi}_6$, ψ_6	1
$\overline{\psi'}_6$, ψ'_6	-1
χ	-1

Input		Output	
M^{ψ}_{66}	900 GeV	$\hat{M}^{Q}_{66}$	1211 GeV
$M^{\psi}_{66'}$	1100 GeV	$\hat{M}^{L}_{66}$	834 GeV
$x_{66}\langle\chi\rangle$	-700	s^{Q}_{66}	0.298
$x'_{66}\langle\chi\rangle$	680	s^{L}_{66}	0.967
λ^{66}_{15}, $\lambda^{66'}_{15}$	1.5, 2.5	$\cos\theta_6$	0.045

TABLE 4.6: ***Left:*** Charge assignments under $\mathbb{Z}_2$ that allow the desired mixing. ***Right:*** Benchmark parameters which lead to a dilution $\epsilon < 0.1$.

$K_L \to \mu e$

The LFV process $K_L \to \mu e$ sets a strong bound over all models featuring a vector leptoquark U_1 coupled to the first and second families. In our model, the contribution is proportional to the couplings $\left|\beta_{de}\beta^*_{s\mu}\right|^2$ (see the tree-level matching to the SMEFT in Section 4.3 and the EFT description of $K_L \to \mu e$ in Section 2.3.9). The first family coupling β_{de} can be diluted via mixing with vector-like fermions, which we parameterised via the effective parameter ϵ in Eq. (4.110), so that $\beta_{se} \approx s^{Q}_{16}s^{L}_{16}\epsilon$.

This can be done by adding an extra sixth-primed vector-like family transforming in the same way as the sixth family under the twin Pati-Salam symmetry, but discriminated by a flavour symmetry which we assume as $\mathbb{Z}_2$ for simplicity (we could use the $\mathbb{Z}_4$ symmetry of the model as well), which forbids mixing between the sixth-primed family and any chiral family. Instead, mixing between the sixth and sixth-primed fermion families is allowed via a twin Pati-Salam singlet charged under the new $\mathbb{Z}_2$, i.e.

$$\mathcal{L}_{\text{mix}} = x_{66}\chi\psi'_6\overline{\psi}_6 + x'_{66}\chi^*\psi_6\overline{\psi}'_6 + \text{h.c.} \tag{4.138}$$

The mass terms of the sixth and sixth-primed fields are split via Ω_{15} in the usual way,

$$\mathcal{L}_{\text{mass}} = (M^{\psi}_{66} + \lambda^{66}_{15}T_{15}\Omega_{15})\psi_6\overline{\psi}_6 + (M^{\psi}_{66'} + \lambda^{66'}_{15}T_{15}\Omega_{15})\psi'_6\overline{\psi}'_6 + \text{h.c.} \tag{4.139}$$

After Ω_{15} and the singlet χ develop VEVs, we obtain the following mass matrices for quarks and leptons

$$\mathcal{L}_{\text{mass}} + \mathcal{L}_{\text{mix}} = \left(\begin{array}{c|cc} & Q_6 & Q'_6 \\ \hline \overline{Q}_6 & M^{Q}_{66} & x_{66}\langle\chi\rangle \\ \overline{Q}'_6 & x'_{66}\langle\chi\rangle & M^{Q}_{66'} \end{array}\right) + \left(\begin{array}{c|cc} & L_6 & L'_6 \\ \hline \overline{L}_6 & M^{L}_{66} & x_{66}\langle\chi\rangle \\ \overline{L}'_6 & x'_{66}\langle\chi\rangle & M^{L}_{66'} \end{array}\right) + \text{h.c.}\,, \tag{4.140}$$

where we have defined

$$M^{Q}_{66} = M^{\psi}_{66} + \frac{\lambda^{66}_{15}}{2\sqrt{6}}\langle\Omega_{15}\rangle\ , \quad M^{L}_{66} = M^{\psi}_{66} - 3\frac{\lambda^{66}_{15}}{2\sqrt{6}}\langle\Omega_{15}\rangle\ , \tag{4.141}$$

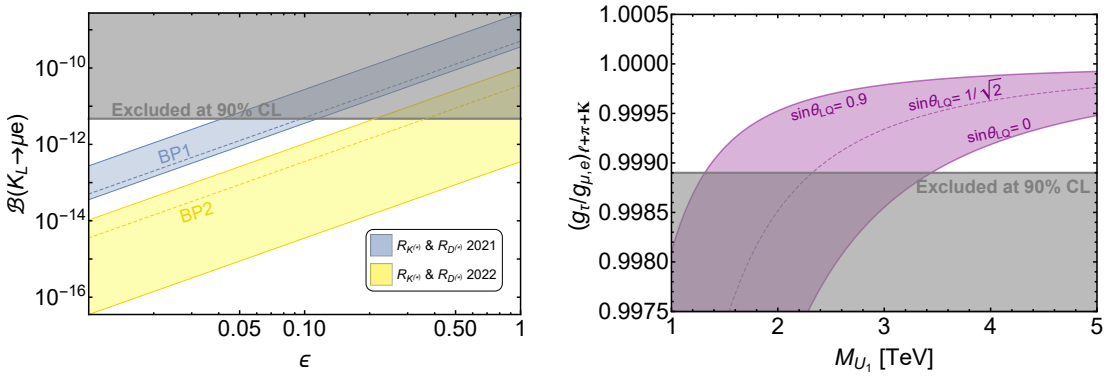

(A) (B)

FIGURE 4.12: ***Left:*** $\mathcal{B}(K_L \to \mu^\pm e^\mp)$ (Eq. (2.95)) as a function of ϵ (see main text for details). x_{25}^ψ is varied in the range $x_{25}^\psi = [0.3, 0.35]$ ($[0.4, 0.45]$) preferred by $R_{K^{(*)}}^{2022}$ ($R_{K^{(*)}}^{2021}$), obtaining the yellow (blue) band. ***Right:*** LFU ratios originated from τ decays (Eq. (4.147)) as a function of the mass of the vector leptoquark M_{U_1}, $\sin\theta_{LQ}$ is varied in the range $\sin\theta_{LQ} = [0, 0.9]$ and $g_4 = 3.5$. The remaining parameters are fixed as in Table 4.5 for both panels, and current exclusion limits are shown.

$$M_{66'}^Q = M_{66'}^\psi + \frac{\lambda_{15}^{66'}}{2\sqrt{6}}\langle\Omega_{15}\rangle\ , \quad M_{66'}^L = M_{66'}^\psi - 3\frac{\lambda_{15}^{66'}}{2\sqrt{6}}\langle\Omega_{15}\rangle\ . \tag{4.142}$$

The mass matrices in Eq. (4.140) are diagonalised by different unitary transformations in the quark and lepton sector, $V_{66'}^Q$ and $V_{66'}^L$, in such a way that the U_1 couplings are given by

$$\mathcal{L}_{U_1} = \frac{g_4}{\sqrt{2}}\begin{pmatrix} Q_6^\dagger & Q_6^{\dagger\prime}\end{pmatrix}\gamma_\mu V_{66'}^Q \mathrm{diag}(1,1) V_{66'}^{L\dagger}\begin{pmatrix} L_6 \\ L_6'\end{pmatrix} U_1^\mu + \text{h.c.} \tag{4.143}$$

If we define

$$V_{66'}^Q V_{66'}^{L\dagger} \equiv \begin{pmatrix} \cos\theta_6 & \sin\theta_6 \\ -\sin\theta_6 & \cos\theta_6\end{pmatrix}\ , \tag{4.144}$$

then the first family U_1 coupling receives a suppression via $\cos\theta_6$ as

$$\beta_{de} = s_{16}^Q s_{16}^L \cos\theta_6\ . \tag{4.145}$$

which is identified with the suppression parameter ϵ in Eq. (4.110),

$$\epsilon \equiv \cos\theta_6. \tag{4.146}$$

We can achieve values of $\cos\theta_6$ smaller than 0.1 without any aggressive tuning of the parameters, obtaining the mild suppression desired for $K_L \to \mu e$ as per Fig. 4.12a. A suitable benchmark can be found in Table 4.6. Interestingly, this mechanism does not affect the Z' and g' interactions, as the unitary matrices $V_{66'}^Q$ and $V_{66'}^L$ cancel in neutral currents. This allows the GIM-like protection from 1-2 FCNCs to remain in place for both the quark and lepton sectors via $s_{16}^Q = s_{25}^Q$ and $s_{16}^L = s_{25}^L$, without entering in conflict with $K_L \to \mu e$ nor with B-physics.

In Fig. 4.12a we can see that for the 2022 case, some region of the parameter space

is compatible with $K_L \to \mu e$ without the need of diluting the coupling. Instead, for the benchmark values BP1 and BP2, a mild suppression is required. This signal is a direct consequence of the underlying twin Pati-Salam symmetry and the GIM-like mechanism, which lead to quasi-degenerate mixing angles $s_{16}^Q \approx s_{16}^L$ that are equal to their 25 counterparts, and as a consequence $\beta_{de} \neq 0$. Therefore, it is not present in other 4321 models [262, 263, 267, 268, 356].

4.6.5 Tests of universality in leptonic tau decays

NP contributions to $R_{D^{(*)}}$ commonly involve large couplings to tau leptons, which can have an important effect over LFU ratios originated from tau decays. Such tests are constructed by performing ratios of the partial widths of the tau lepton decaying to lighter leptons and/or hadrons. We find all ratios in our model to be well approximated by (see the tree-level matching to the SMEFT in Section 4.3 and the EFT description of τ LFU ratios in Section 2.3.10),

$$\left(\frac{g_\tau}{g_{\mu,e}}\right)_{\ell+\pi+K} \approx 1 - 0.079 C_U \left|\beta_{b\tau}\right|^2 , \tag{4.147}$$

where $\beta_{b\tau} \approx \cos\theta_{LQ}$ assuming maximal 3-4 mixing. Therefore, it can be seen as a constraint over the $\beta_{b\tau}$ coupling, and hence is not directly related to $R_{K^{(*)}}$ so we do not plot two bands here. The high-precision measurements of these effective ratios only allow for per mil modifications, see the HFLAV average [80] in Table 4.4. As depicted in Fig. 4.12b, this constraint sets the lower bound $M_{U_1} \gtrsim 2.2\,\text{TeV}$ for $\sin\theta_{LQ} = 1/\sqrt{2}$ and $g_4 = 3.5$. This bound becomes more restrictive for $\cos\theta_{LQ} \approx 1$, or equivalently $\beta_{b\tau} \approx 1$, for which we find $M_{U_1} \gtrsim 3.3\,\text{TeV}$ if $g_4 = 3.5$ and $M_{U_1} \gtrsim 2.9\,\text{TeV}$ if $g_4 = 3$. The latter case, more constrained by data, is predicted by non-fermiophobic 4321 models such as PS^3 and variants [115, 170, 262, 263, 356].

4.6.6 Signals in rare B-decays

$B_s \to \tau\tau$ and $B \to K\tau\tau$

As anticipated in Section 4.6.2, the enhancement of $R_{D^{(*)}}$ via the U_1 leptoquark is correlated to an enhancement of $b \to s\tau\tau$ via $SU(2)_L$ invariance of the U_1 couplings to fermions. The respective branching fractions are of order 10^{-7} in the SM and mild upper bounds have been obtained by LHCb [252] and BaBar [254], respectively. See Section 2.3.5 for a further discussion of these observables.

In Fig. 4.13, we plot the branching fractions as a function of x_{34}^ψ, while x_{25}^ψ is varied in the ranges compatible with 2021 and 2022 $R_{K^{(*)}}$, respectively. We find that the predictions are far below the current bounds, however they lie closer to the expected future bounds from LHCb and Belle II data [253, 255]. This prediction is different in non-fermiophobic 4321 models [262, 263, 356], where these contributions are chirally enhanced

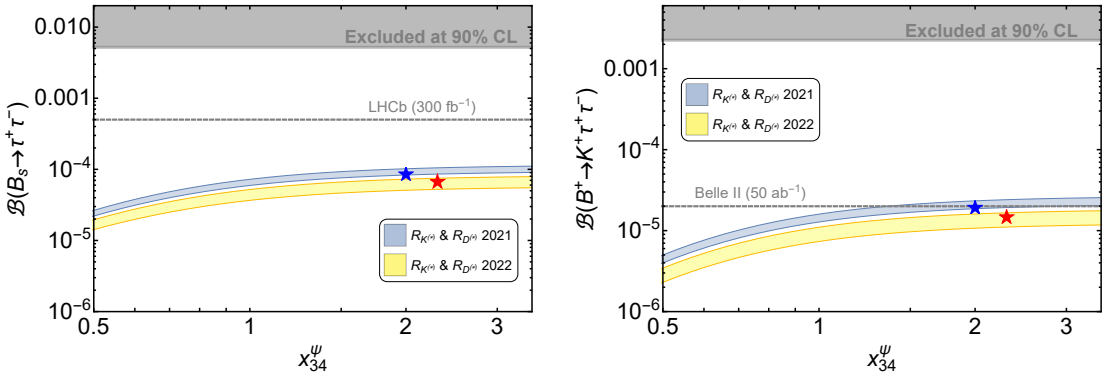

(A) (B)

FIGURE 4.13: The branching fractions $\mathcal{B}(B_s \to \tau^+\tau^-)$ (left) and $\mathcal{B}(B^+ \to K^+\tau^+\tau^-)$ (right) as a function of x_{34}^{ψ}, with x_{25}^{ψ} varied in the range $x_{25}^{\psi} = [0.3, 0.35]$ ([0.4, 0.45]) preferred by $R_{K^{(*)}}^{2022}$ ($R_{K^{(*)}}^{2021}$), obtaining the yellow (blue) band. The rest of the parameters are fixed as in Table 4.5. Current exclusion limits are displayed, along with their future projections. The blue (red) star shows BP1 (BP2).

due to the presence of scalar operators, and all the parameter space is expected to be tested in the $B^+ \to K^+\tau^+\tau^-$ process by Belle II, see the full discussion in Section 2.3.6.

The lifetime ratio τ_{B_s}/τ_{B_d} introduced in Section 2.3.6 can potentially provide significant direct bounds over $\mathcal{B}(B_s \to \tau^+\tau^-)$ in the future [4], which can discriminate as well between the twin Pati-Salam model and non-fermiophobic 4321 models, see Fig. 2.5.

$B \to K\nu\nu$

The U_1 leptoquark does not contribute at tree-level to $b \to s\nu\nu$ transitions, and the tree-level exchange of the Z' is suppressed due to the down-aligned flavour structure of the model. However, loop-level corrections can lead to an important enhancement of the channel $B \to K\nu_\tau\bar{\nu}_\tau$ [263]. We parameterise corrections to the SM branching fraction as in Eq. (2.54), where the EFT and the Wilson coefficients are defined in Section 2.3.7.

We only obtain sizable contributions in the $\tau\tau$ channel due to the flavour structure of the model, and we split the NP effects into Z' and U_1 contributions as follows,

$$C_{\nu,\mathrm{NP}}^{\tau\tau} = -\frac{1}{V_{tb}V_{ts}^*}\frac{\sqrt{2}}{4G_F}\left(C_{\nu,Z'}^{\tau\tau} + C_{\nu,U_1}^{\tau\tau}\right). \tag{4.148}$$

The U_1 contribution at NLO accuracy reads [360]

$$C_{\nu,U_1}^{\tau\tau} \approx C_{\nu,U_1}^{\mathrm{RGE}} + \frac{g_4^4}{32\pi^2 M_{U_1}^2}\sum_{\alpha,j}\left(\beta_{s\alpha}^*\beta_{b\alpha}\right)\left(\beta_{j\nu_\tau}\right)^2 F(x_\alpha, x_j), \tag{4.149}$$

where the second term arises from the semileptonic box diagram in Fig. 4.14a, and the first term encodes the RGE-induced contribution from the tree-level leptoquark-mediated operator $[C_{ed}^{V,LL}]^{\tau\tau 23}$, computed with `DsixTools 2.1` [174] as

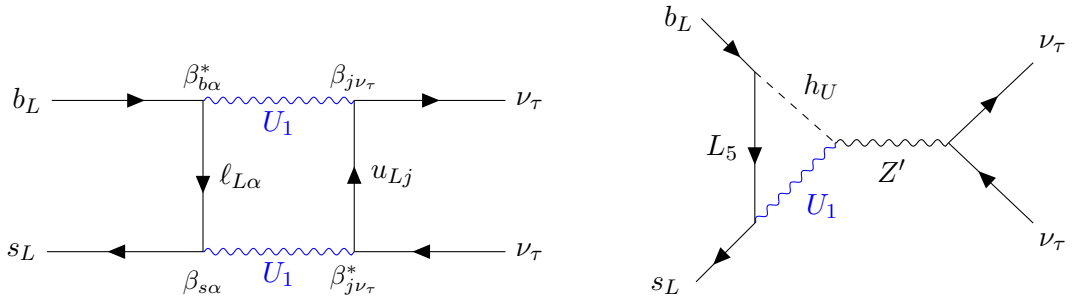

FIGURE 4.14: Box and penguin diagrams contributing to $B \to K\nu\nu$. The index α runs for all charged leptons including vector-like, i.e. $\ell_{L\alpha} = (\mu_L, \tau_L, E_{L4}, E_{L5})$, and the index j runs for all up-type quarks, including vector-like $u_{Lj} = (c_L, t_L, U_{L4}, U_{L5})$. See more details in the main text.

$$C^{\rm RGE}_{\nu,U_1} = 0.047 \frac{g_4^2}{2M_{U_1}^2} \beta_{b\tau}\beta_{s\tau}\,. \tag{4.150}$$

The Z' contribution to NLO accuracy reads

$$C^{\tau\tau}_{\nu,Z'} \approx \frac{3g_4^2}{2M_{Z'}^2}\left[\xi_{bs}\xi_{\nu_\tau\nu_\tau}\left(1+\frac{3}{2}\frac{g_4^2}{16\pi^2}\xi^2_{\nu_\tau\nu_\tau}\right)\right. \\ \left. \frac{g_4^2}{16\pi^2}\beta^*_{sE_5}\beta_{bE_5}\xi_{\nu_\tau\nu_\tau} G_{\Delta Q=1}(x_{E_5}, x_{Z'}, x_R)\right]\,, \tag{4.151}$$

where $x_{E_5} \equiv (M_5^L/M_{U_1})^2$, $x_{Z'} \equiv M^2_{Z'}/M^2_{U_1}$ and $x_R \equiv M_R^2/M^2_{U_1}$ with M_R being a scale associated to the radial mode $h_U(\mathbf{3},\mathbf{1},2/3)$ arising from $\phi_{3,1}$. The first term in Eq. (4.151) corresponds to the tree-level contribution plus a 1-loop Z' correction to the leptonic vertex. The coupling ξ_{bs} is suppressed by the small down mixing angle $\theta^d_{23} \approx 0.001$, leading to per cent corrections to $\mathcal{B}(B \to K^{(*)}\nu\bar{\nu})$. The second term in Eq. (4.151) corresponds to a 1-loop correction to the flavour-violating Z' vertex, with U_1, the fifth vector-like lepton E_5 and h_U running in the loop, see Fig. 4.14b. The loop function is given by [263, 360]

$$G_{\Delta Q=1}(x_1,x_2,x_3) \approx \frac{5}{4}x_1 + \frac{x_1}{2}\left(x_2-\frac{3}{2}\right)\left(\ln x_3 - \frac{5}{2}\right)\,. \tag{4.152}$$

In the twin Pati-Salam framework, we expect extra radial modes associated to $\overline{\phi}_{3,1}$ and $\overline{\phi'}_{3,1}$, however they only couple to right-handed chiral fermions and hence they cannot contribute to $C^{\tau\tau}_{\nu,\rm NP}$ which involves only left-handed chiral fermions.

Both 1-loop contributions are dominated by the fifth vector-like charged lepton and grow with its bare mass, M_5^L. This way, the overall contribution to $B \to K\nu\nu$ can be sizable, yielding up to $\mathcal{O}(1)$ corrections with respect to the SM value, as depicted in Fig. 4.15.

For low M_5^L, the enhancement of $\delta\mathcal{B}(B \to K^{(*)}\nu\bar{\nu})$ corresponds mostly to $C^{\rm RGE}_{\nu,U}$. For large M_5^L, however, we have seen that stringent constraints from $B_s - \bar{B}_s$ meson mixing

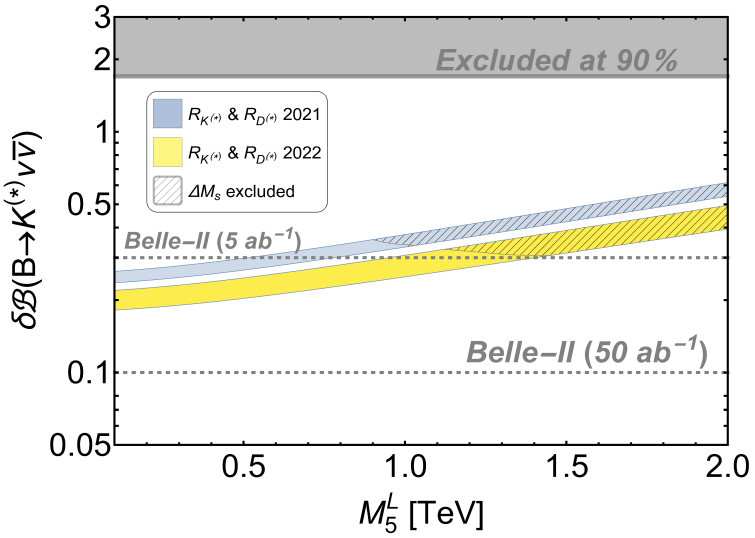

FIGURE 4.15: $\delta\mathcal{B}(B \to K^{(*)}\nu\bar{\nu})$ (Eq. (2.54)) as a function of the 5th family vector-like mass term. x_{25}^{ψ} is varied in the range $x_{25}^{\psi} = [0.3, 0.35]$ ($[0.4, 0.45]$) preferred by $R_{K^{(*)}}^{2022}$ ($R_{K^{(*)}}^{2021}$), obtaining the yellow (blue) band. The hatched region is excluded by the ΔM_s bound, see Eq. (2.32). The grey region is excluded by current experimental measurements, the dashed line indicates the projected future bound.

play an important role, see Section 4.6.3. This constraint is depicted as the hatched region in Fig. 4.15, correlating $B \to K\nu\nu$ and ΔM_s, a feature which has not been highlighted in previous analyses. In particular, ΔM_s rules out the region where $\delta\mathcal{B}(B \to K^{(*)}\nu\bar{\nu})$ can reach values close to current experimental limits, making impossible to address the 2.8σ anomaly in $\mathcal{B}(B^+ \to K^+\nu\bar{\nu})$ suggested by the recent Belle II data [81]. Nevertheless, the Belle II collaboration is expected to measure $\mathcal{B}(B \to K^{(*)}\nu\bar{\nu})$ up to 10% of the SM value [255], hence testing all the parameter space of our model.

Our signal of $B \to K^{(*)}\nu\bar{\nu}$ also offers a great opportunity to disentangle our twin Pati-Salam framework from non-fermiophobic 4321 models and from the PS^3 model [115, 262, 263, 356], as they predict a much smaller signal (see Fig. 4.4 of [263] and compare their purple region with our Fig. 4.15).

4.6.7 Perturbativity

The explanation of the $R_{D^{(*)}}$ anomaly requires large mixing angles s_{34}^{Q} and s_{34}^{L}, which translate into a sizeable Yukawa coupling x_{34}^{ψ}, thus pushing the model close to the boundary of the perturbative domain. Perturbativity is a serious constraint over our model, since we need the low-energy 4321 theory to remain perturbative until the high scale of the twin Pati-Salam symmetry. When assessing the issue of perturbativity, two conditions must be satisfied:

- Firstly, the low-energy observables must be calculable in perturbation theory. For Yukawa couplings, we consider the bound $x_{34}^{\psi} < \sqrt{4\pi}$. Regarding the gauge coupling g_4, standard perturbativity criteria imposes the beta function criterion [362] $|\beta_{g_4}/g_4| < 1$, which yields $g_4 < 4\pi\sqrt{3}/\sqrt{28} \approx 4.11$.

- Secondly, the couplings must remain perturbative up to the energy scale of the UV completion, i.e. we have to check that the couplings of the model do not face a Landau pole below the energy scale of the second PS breaking, namely $\mu \approx 1\,\text{PeV}$.

The phenomenologically convenient choice of large g_4 is not a problem for the extrapolation in the UV, thanks to the asymptotic freedom of the $SU(4)$ gauge factor (see Fig. 4.16). To investigate the running of the most problematic Yukawa x^{ψ}_{34}, we use the 1-loop renormalisation group equations of the 4321 model. For the gauge coupling beta functions $\beta_{g_i} = (dg_i/d\mu)/\mu$ we have [268]

$$(4\pi)^2\,\beta_{g_1} = \frac{131}{18}g_1^3\,, \quad (4\pi)^2\,\beta_{g_2} = \left(-\frac{19}{6} + \frac{8n_\Psi}{3}\right)g_2^3\,, \tag{4.153}$$

$$(4\pi)^2\,\beta_{g_3} = -\frac{19}{3}g_3^3\,, \quad (4\pi)^2\,\beta_{g_4} = \left(-\frac{40}{3} + \frac{4n_\Psi}{3}\right)g_4^3\,, \tag{4.154}$$

where $n_\Psi = 3$ is the number of vector-like fermion families. The Pati-Salam universality of the Yukawas $x^{\psi}_{i\alpha}$ is broken by RGE effects which we quantify through the equations

$$\begin{aligned}(4\pi)^2\,\beta_{x_Q} = {}& \frac{7}{2}x_Q x_Q^\dagger x_Q + \frac{1}{2}x_Q x_L^\dagger x_L + \frac{15}{8}x_Q\lambda_{15}\lambda_{15}^\dagger + 2\text{Tr}\left(x_Q x_Q^\dagger\right)x_Q \\ & - \frac{1}{12}g_1^2 x_Q - \frac{9}{2}g_2^2 x_Q - 4g_3^2 x_Q - \frac{45}{8}g_4^2 x_Q\,,\end{aligned} \tag{4.155}$$

$$\begin{aligned}(4\pi)^2\,\beta_{x_L} = {}& \frac{5}{2}x_L x_L^\dagger x_L + \frac{3}{2}x_L x_Q^\dagger x_Q + \frac{15}{8}x_L\lambda_{15}\lambda_{15}^\dagger + 2\text{Tr}\left(x_L x_L^\dagger\right)x_L \\ & - \frac{3}{4}g_1^2 x_L - \frac{9}{2}g_2^2 x_L - \frac{45}{8}g_4^2 x_L\,,\end{aligned} \tag{4.156}$$

$$\begin{aligned}(4\pi)^2\,\beta_{\lambda_{15}} = {}& \frac{21}{4}\lambda_{15}\lambda_{15}\lambda_{15}^\dagger + \frac{3}{2}\lambda_{15}x_Q^\dagger x_Q + \frac{1}{2}\lambda_{15}x_L^\dagger x_L + 4\text{Tr}\left(\lambda_{15}\lambda_{15}^\dagger\right)\lambda_{15} \\ & - \frac{9}{2}g_2^2\lambda_{15} - \frac{45}{4}g_4^2\lambda_{15}\,,\end{aligned} \tag{4.157}$$

where any contributions from the Yukawas of the personal Higgs, $y^{\psi}_{i\alpha}$, are negligible as they are all 1 or smaller.

The running of the effective Yukawa couplings is protected, as the top Yukawa is order 1 and all of the others are smaller, SM-like (see the discussion in Section 4.5.2). This feature is different from [268] which was not a theory of flavour, causing the top mass to be accidentally suppressed by the equivalent of c^Q_{34} in our model, hence requiring a large, non-perturbative top Yukawa to preserve the top mass. Instead, in our model the effective top Yukawa arises proportional to the maximal angle s^Q_{34}, rendering the top Yukawa natural and perturbative. The matrices of couplings $x_{Q,L}$ and λ_{15} are defined

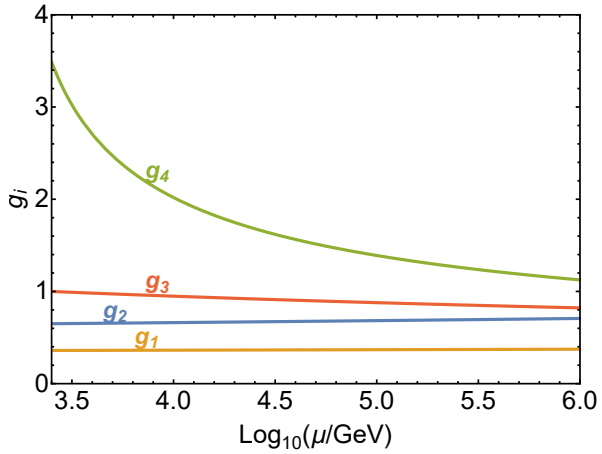

FIGURE 4.16: RGE of the gauge couplings in our benchmark scenario from the TeV scale to the scale of the twin Pati-Salam symmetry $\mu \sim 1\,\mathrm{PeV}$.

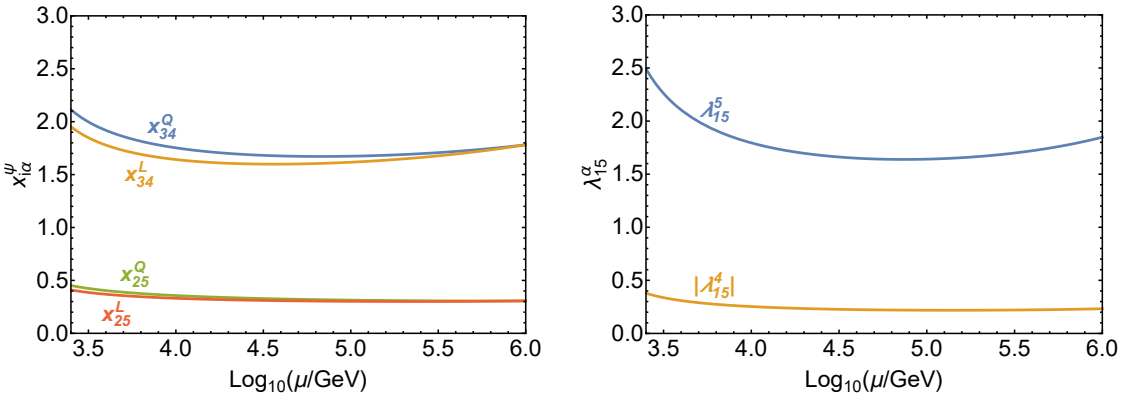

(A) (B)

FIGURE 4.17: RGE of the fundamental Yukawa couplings in our benchmark scenario (Table 4.5) from the TeV scale to the scale of the twin Pati-Salam symmetry $\mu \sim 1\,\mathrm{PeV}$. The left panel shows the $x^{\psi}_{i\alpha}$ Yukawas which lead to the mixing between SM fermions and vector-like partners. The right panel shows the λ_{15} Yukawas which split the vector-like masses of quarks and leptons.

as (assuming small x^{ψ}_{35} as discussed in Section 4.6.3)

$$x_\psi = \begin{pmatrix} x^{\psi}_{16} & 0 & 0 \\ 0 & x^{\psi}_{25} & 0 \\ 0 & 0 & x^{\psi}_{34} \end{pmatrix}, \quad \lambda_{15} = \begin{pmatrix} \lambda^{6}_{15} & 0 & 0 \\ 0 & \lambda^{5}_{15} & 0 \\ 0 & 0 & \lambda^{4}_{15} \end{pmatrix}, \quad \psi = Q,\, L\,. \tag{4.158}$$

The Yukawas x^{ψ}_{25} and x^{ψ}_{16} are not dangerous as they are order 1 of smaller. The problematic Yukawa is x^{ψ}_{34}, which is required to be large in order to address $R_{D^{(*)}}$, and it is also connected with the physical mass of the fourth family lepton as per Eq. (4.93). Large λ^{5}_{15} is also required to obtain a large splitting of vector-like masses, which provides a large θ_{LQ} as required by $R_{D^{(*)}}$.

Fig. 4.17 shows that the Yukawas of our benchmark scenario remain perturbative up to the high energy scale $\mu \approx 1\,\mathrm{PeV}$, thanks to the choice of a large $g_4 = 3.5$. However,

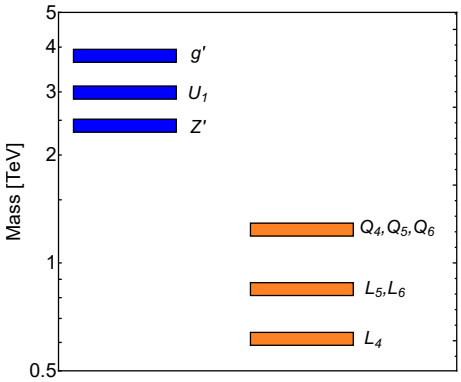

(A)

Particle	Decay mode	$\mathcal{B}$(BP)	Γ/M
U_1	$Q_3L_5 + Q_5L_3$	~ 0.47	0.32
	Q_3L_3	~ 0.22	
	Q_5L_5	~ 0.24	
	$Q_iL_a + Q_aL_i$	~ 0.07	
g'	Q_3Q_3	~ 0.3	0.5
	Q_5Q_5	~ 0.3	
	Q_6Q_6	~ 0.3	
	Q_1Q_6+$Q_2Q_5 + Q_3Q_4$	~ 0.1	
Z'	L_5L_5	~ 0.29	0.24
	L_6L_6	~ 0.29	
	L_3L_3	~ 0.27	
	Q_3Q_3+$Q_5Q_5 + Q_6Q_6$	~ 0.09	
	$L_1L_6 + L_2L_5 + L_3L_4$	~ 0.06	

(B)

FIGURE 4.18: ***Left:*** Spectrum of new vector bosons and fermions in our benchmark scenario (BP, Table 4.5) around the TeV scale. ***Right:*** Main decay channels of the new vectors U_1, g' and Z' in BP. Addition (+) implies that the depicted channels have been summed when computing the branching fraction $\mathcal{B}$(BP). $i = 1, 2$ and $a = 5, 6$.

we have checked that the Landau pole is hit when $x_{34}^{\psi} > 2.5$, hence this region should be considered as disfavoured by the perturbativity criteria.

The small RGE effects that break the Pati-Salam universality of the Yukawa couplings are below 8% in any case, hence the universality of the couplings is preserved at the TeV scale to good approximation.

4.6.8 High-p_T signatures

General 4321 models predict a plethora of high-p_T signatures involving the heavy gauge bosons and at least one family of vector-like fermions, requiring dedicated analyses such as those in [263, 268, 363]. In particular, our model predicts a similar high-p_T phenomenology as that of [268], which also considers effective U_1 couplings via mixing with three families of vector-like fermions. However, the bounds obtained in the high-p_T analysis of [268] are mostly outdated. Moreover, certain differences arise due to the underlying twin Pati-Salam symmetry in our model, plus the different implementation of the scalar sector and VEV structure. In contrast, the most recent high-p_T studies of the 4321 model assume a non-fermiophobic framework [263,363], where the heavy gauge bosons have large couplings to right-handed third family fermions. In this manner, some of the bounds in [263,363] are overestimated for our model. This motivates a dedicated high-p_T analysis of the twin Pati-Salam model.

We have included the particle spectrum of our benchmark scenario in Fig. 4.18a, as a typical configuration for the masses of the new vectors and fermions. Table 4.18b shows the main decay channels of the new vector bosons, which feature large decay widths Γ/M due to all the available decay channels to vector-like fermions, plus the choice of large $g_4 = 3.5$ close to the boundary of the perturbative regime.

In this section, we revisit some of the most simple collider signals, including coloron dijet searches and Z' dilepton searches. We will also comment on U_1 searches, coloron

ditop searches and vector-like fermion searches. We will point out the differences between our framework and general 4321 models, motivating a further dedicated high-p_T analysis of the twin Pati-Salam model.

Coloron signals

The heavy colour octet has a large impact over collider searches for 4321 models, and its production usually sets the lower bound on the scale of the model. In our case, the heavy coloron has a gauge origin, hence the coloron couplings to two gluons are absent at tree-level, reducing the coloron production at the LHC. Moreover, in the motivated scenario $\langle\phi_3\rangle \gg \langle\phi_1\rangle$, the coloron is slightly heavier than the vector leptoquark at roughly $M_{g'} \approx \sqrt{2}M_{U_1}$, helping to suppress the impact of the coloron over collider searches while preserving a slightly lighter U_1 to explain the B-anomalies. In the scenario $g_4 \gg g_{3,1}$, the coupling strength of the coloron is roughly g_4, which receives NLO corrections via the K-factor [364, 365]

$$K_{\rm NLO} \approx \left(1 + 2.65\frac{g_4^2}{16\pi^2} + 8.92\frac{g_s^2}{16\pi^2}\right)^{-1/2}, \quad g_{g'} \approx K_{\rm NLO} g_4\,. \tag{4.159}$$

We have computed the coloron production cross section from 13 TeV pp collisions with `Madgraph5` [337] using the default `NNPDF23LO` PDF set and the coloron UFO model, publicly available in the `FeynRules` [336] model database[8]. We verify in Fig. 4.19a that coloron production is dominated by valence quarks, even though the coupling to left-handed bottoms is maximal while the coupling to valence quarks is suppressed. The coloron couples to light left-handed quarks (see Eq. (4.112)) via the mixing $s_{25}^Q \approx s_{16}^Q$ of $\mathcal{O}(0.1)$, which interferes destructively with the flavour universal term, allowing for a certain cancellation of the left-handed couplings to light quarks. However, this partial cancellation is not possible for the flavour–universal couplings to right-handed quarks.

We estimate analytically the branching fraction to all SM quarks excluding tops, and then we compute the total cross section via the narrow width approximation. Finally, we confront our results with the limits for a $q\bar{q}$-initiated spin-1 resonance provided by CMS in Fig. 10 of [366] (with acceptance $A \approx 0.5$). The results are displayed in Fig. 4.20a, where we have varied the coupling to light left-handed quarks κ_{qq} and fixed the rest of parameters as in Table 4.5. We find bounds ranging from $M_{g'} \gtrsim 2.5\,\text{TeV}$ when $\kappa_{qq} \approx 0$ and $M_{g'} \gtrsim 3\,\text{TeV}$ when $\kappa_{qq} \approx g_s^2/g_4^2$. These bounds are slightly milder than those obtained in [263], the reason being that in [263] right-handed bottom quarks are assumed to couple maximally to the coloron, while in our model this coupling is suppressed.

We expect to find more stringent bounds in resonant coloron production with $t\bar{t}$ final states, due to the maximal couplings of the coloron to the third generation $SU(2)_L$ quark doublet. According to the recent analysis in [263], our benchmark scenario would

[8] `https://feynrules.irmp.ucl.ac.be/wiki/LeptoQuark`

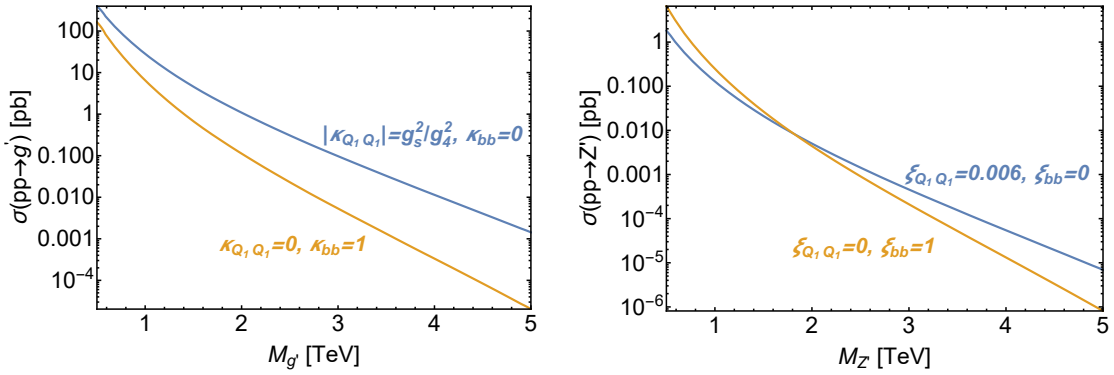

(A) (B)

FIGURE 4.19: Production cross sections via 13 TeV pp collisions for the coloron (left) and Z' (right), via their typical couplings to valence quarks (blue) and bottoms (orange). The choice of $\xi_{Q_1Q_1} = 0.006$ corresponds to a mixing angle $s_{16}^Q \approx 0.2$.

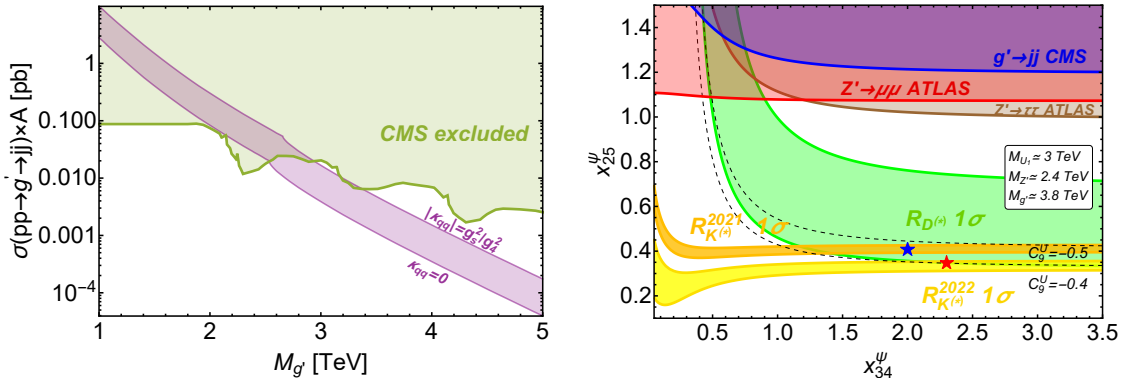

(A) (B)

FIGURE 4.20: ***Left:*** Total cross section for the coloron dijet channel in the narrow width approximation, with $|\kappa_{qq}|$ varied in the range $|\kappa_{qq}| = [0, g_s^2/g_4^2]$, where $q = Q_1, Q_2$. The remaining parameters are fixed as in Table 4.5 for both panels. The exclusion bound from CMS is shown in green. ***Right:*** Parameter space in the plane $(x_{34}^\psi,\, x_{25}^\psi)$ compatible with the LFU ratios. The dashed lines show contours of constant C_9^U. The regions excluded by the collider searches considered are included. The blue (red) star shows BP1 (BP2).

lie below current bounds, due to the large decay width $\Gamma_{g'}/M_{g'} \approx 0.5$ provided by extra decay channels to TeV scale vector-like quarks. The limit over the coloron mass is roughly 3.5 TeV, however this bound might be overestimated again for our model due to the different couplings of the coloron to right-handed third family quarks. Reconstructing the $t\bar{t}$ channel requires a dedicated analysis and a different methodology, which is beyond the scope of this work.

Z' signals

For the Z' boson, the flavour universal couplings to valence quarks are more heavily suppressed than those of the coloron, via the small ratio g_Y^2/g_4^2. Therefore, cancellation between the term proportional to $s_{25}^Q \approx s_{16}^Q$ and the flavour universal one is not possible here. In contrast with the coloron, the large left-handed couplings to bottoms can play

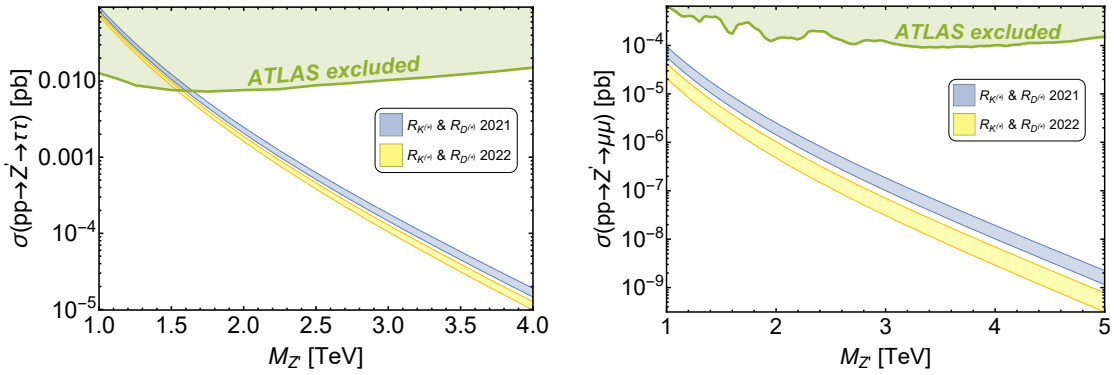

(A) (B)

FIGURE 4.21: Total cross section for ditau (left) and dimuon (right) production via a heavy Z' in the narrow width approximation, with x^{ψ}_{25} varied in the range $x^{\psi}_{25} = [0.3, 0.35]$ ($[0.4, 0.45]$) preferred by $R^{2022}_{K^{(*)}}$ ($R^{2021}_{K^{(*)}}$), obtaining the yellow (blue) band. The exclusion bounds from ATLAS are shown in green.

a significant role in Z' production. The production cross section is estimated via the same methodology as for the coloron above. We do not consider any NLO corrections in this case, following the methodology of [363]. In Fig. 4.19b we show that the production via bottoms is larger than the production via valence quarks for a light Z', however the production via valence quarks is larger for $M_{Z'} \gtrsim 2\,\text{TeV}$, and shall not be neglected as it commonly happens in the literature (see e.g. [363]).

We estimate the branching fraction to muons and taus, and we compute the total decay width via the narrow width approximation. We confront our results with the limits from the dilepton resonance searches by ATLAS [338] for muons and Fig. 7 (c) of [340] for taus. We display the results in Figs. 4.21a and 4.21b. In Fig. 4.20b we see that these processes, along with coloron dijet searches, mildly constrain the region of large x^{ψ}_{25}. Ditau searches are more competitive than dimuon searches or coloron dijet searches despite the lesser integrated luminosity, due to the branching fractions to muons and light quarks being suppressed by smaller mixing angles $s^{Q,L}_{25} \sim \mathcal{O}(0.1)$. In contrast, the ditau channel is enhanced by maximal 3-4 mixing, and sets bounds of roughly $M_{Z'} > 1.5\,\text{TeV}$, see Fig. 4.21b.

U_1 signals

Leptoquark pair-production cross sections at the LHC are dominated by QCD dynamics, and thus are largely independent of the leptoquark couplings to fermions. Therefore, we are able to safely compare with the analyses of Refs. [263, 363]. A certain model dependence is present in the form of non-minimal couplings to gluons, however these couplings are absent in models where U_1 has a gauge origin. According to Fig. 3.3 of [263], current bounds over direct production exclude $M_{U_1} < 1.7\,\text{TeV}$, and the future bound is expected to exclude $M_{U_1} < 2.1\,\text{TeV}$ if no NP signal is found during the high-luminosity phase of the LHC.

An important constraint over U_1 arises from modifications of the high-p_T tail in the dilepton invariance mass distribution of the Drell-Yan process $pp \to \tau^+\tau^- + X$, induced by t-channel U_1 exchange [184, 263, 345, 363]. This channel is well motivated by the U_1 explanation of $R_{D^{(*)}}$, which unavoidably predicts a large $b\tau U_1$ coupling. The scenario $\beta^R_{b\tau} = 0$ considered in the study of [263, 363] fits well the twin Pati-Salam framework, up to a re-scaling of the U_1 coupling strength as $g_U \to g_U \beta^L_{b\tau}$, in order to account for the fact that our $\beta^L_{b\tau}$ coupling is not maximal but $\beta^L_{b\tau} \approx c_{\theta_{LQ}} \approx 0.67$ in our benchmark scenario, obtaining $g_U \approx 2.3$. According to the left panel of Fig. 3.3 in [263], the 3 TeV leptoquark of our benchmark easily satisfies the current bounds, but is within projected limits for the high luminosity phase of LHC. Finding U_1 much below 3 TeV is in tension with $pp \to g' \to t\bar{t}$ as explained before, due to the approximate relation $M_{g'} \approx \sqrt{2} M_{U_1}$ that entangles the masses of U_1 and the coloron (although the $pp \to g' \to t\bar{t}$ bound is probably overestimated for our dominantly left-handed model).

The twin Pati-Salam model could provide a good U_1 candidate for the 3σ excess at CMS [367] pointing to a 2 TeV U_1 leptoquark in the well motivated channel $pp \to U_1 \to \tau\tau$, once the extra decay channels to vector-like fermions are considered, assuming that the bound from $pp \to g' \to t\bar{t}$ is indeed overestimated for our model.

Vector-like fermions

The presence of vector-like fermions is of fundamental importance to discriminate between the different implementations of the 4321 model addressing the B-anomalies. A common constraint arises from $\Delta F = 2$ transitions at low energies, which require that the vector-like charged lepton that mixes with muons is light (see Fig. 4.8a). The natural mass of the quark partner of L_5 should not lie far away due to the approximate Pati-Salam universality, the small breaking effects given by the VEV $\langle \Omega_{15} \rangle$. In particular, in our benchmark scenario we obtained $M_5^L \approx 0.8\,\text{TeV}$ and $M_5^Q \approx 1.2\,\text{TeV}$. The flavour structure of the model naturally predicts that both Q_5 and L_5 have sizable couplings to the third generation of SM fermions.

The twin Pati-Salam model features also L_4 and Q_4 as a relevant pair of vector-like fermions, which mix maximally with the third generation in order to obtain the large couplings required for $R_{D^{(*)}}$, and also to explain the top mass without perturbativity issues. This implies that their bare mass terms in the original Lagrangian are small, therefore their physical masses are dominated by $x^{\psi}_{34} \langle \phi_{3,1} \rangle$, see Eqs. (4.87) and (4.93). In the motivated scenario $\langle \phi_3 \rangle \gg \langle \phi_1 \rangle$ which slightly suppresses the production of the coloron, we found L_4 to be very light, roughly 600 GeV in our benchmark. Instead, Q_4 can lie above 1 TeV, being roughly 1.2 TeV in our benchmark. The couplings of L_4 to SM fermions are smaller than those of L_5, but it is dominantly coupled to third family fermions.

Interestingly, CMS recently performed a search for the vector-like leptons of the 4321 model [368], finding a 2.8σ preference for a vector-like lepton with a 600 GeV mass, however the analysis assumes electroweak production only and maximal couplings to the

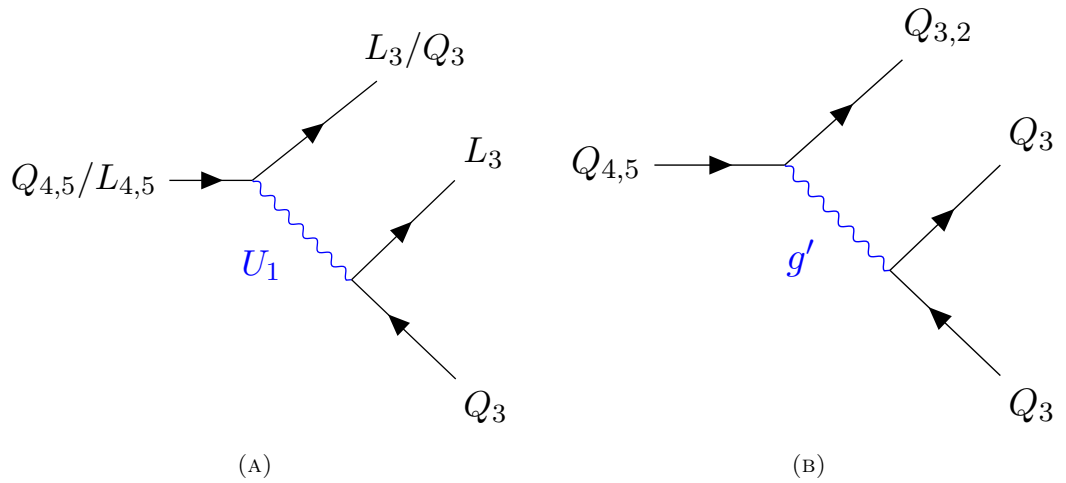

(A) (B)

FIGURE 4.22: Examples of main decay channels for vector-like fermions.

third family. If Z'-assisted production is included, L_5 with 800 GeV mass could be a good candidate for the anomaly. Furthermore, L_4 at 600 GeV could also provide a good fit once non-maximal couplings are considered, however this requires verification in a dedicated analysis. Non-fermiophobic 4321 models, such as [262, 263], predict a heavier vector-like lepton, while [268] also predicts L_5 at around 800 GeV but a heavier L_4. Regarding the sixth vector-like fermions L_6 and Q_6, we expect them to have similar masses as L_5 and Q_5 in order to preserve the GIM-like protection from 1-2 FCNCs, they are feebly coupled to first family fermions but not to the second nor third families.

Current bounds on vector-like quark masses lie around 1 TeV, however the strongest bounds are usually model dependent. Our vector-like quarks are pair produced through gluon fusion and through the decay of the coloron, which is very likely to be kinematically allowed. Their decays leave a large number of third generation fermions in the final state, following a similar pattern as the one discussed in [268], see the example diagrams in Fig. 4.22. The twin Pati-Salam model naturally predicts light vector-like quarks with masses around 1 TeV, which is a feature not present in all other 4321 models and may motivate specific searches.

4.7 Comparison with alternative models

Table 4.7 includes a simplified set of observables that allows to disentangle the twin Pati-Salam model from the ones that are already in the market. A further discussion can be found in the two following subsections.

4.7.1 Non-fermiophobic 4321 models

The twin Pati-Salam model is built as a fermiophobic framework, where all chiral fermions are singlets under the TeV scale $SU(4)$. This is a crucial difference between our model and the non-fermiophobic 4321 models [262, 263, 356, 360, 361] and their UV

	twin PS	fermiophobic 4321	PS^3	non-fermiophobic 4321
Refs.	this thesis	[267, 268]	[115, 170]	[262–264, 356]
Theory of flavour	Yes	No	Yes	No
$R_{D^{(*)}}$	$\Delta R_D = \Delta R_{D^*}$	$\Delta R_D = \Delta R_{D^*}$	$\Delta R_D > \Delta R_{D^*}$	$\Delta R_D > \Delta R_{D^*}$
$\mathcal{B}(\tau \to 3\mu)$	10^{-8}	$\lesssim 10^{-11}$	10^{-9}	-
$\mathcal{B}(\tau \to \mu\gamma)$	10^{-9}	$\lesssim 10^{-11}$	10^{-8}	10^{-8}
$\mathcal{B}(\tau \to \mu\phi)$	10^{-9}	10^{-11}	10^{-10}	10^{-10}
$\mathcal{B}(B_s \to \tau\mu)$	10^{-6}	10^{-7}	10^{-5}	10^{-5}
$\mathcal{B}(B_s \to \tau\tau)$	10^{-5}	-	10^{-3}	10^{-3}
$\mathcal{B}(B \to K\tau\tau)$	10^{-5}	-	10^{-4}	10^{-4}
$\delta\mathcal{B}(B \to K^{(*)}\nu\bar{\nu})$ (2.54)	0.3	-	0.2	0.2
vector-like fermion families	3	3	1	1
High-p_T constraints	Mild	Mild	Tight	Tight

TABLE 4.7: Main observables to distinguish the twin Pati-Salam model from other proposals. The numbers are only indicative, as these predictions may vary along the parameter space of the different models. The dash (-) indicates that the observable was not considered or numbers were not given in the corresponding references. In the high-p_T row we broadly refer to how constrained is the model by high-p_T searches [269].

completions (including the PS^3 model [115]), where the third family of chiral fermions transforms under the TeV scale $SU(4)$. This implies large left- and right-handed third family couplings to $SU(4)$ gauge bosons. By contrast, in our theory of flavour, the right-handed couplings of SM fermions to U_1 (and also to Z' and g') arise via small mixing angles connected to the origin of second family fermion masses, hence the twin Pati-Salam model predicts dominantly left-handed U_1 couplings. The low-energy phenomenology between both approaches is radically different.

In terms of the charged current anomalies $R_{D^{(*)}}$, the twin Pati-Salam model only predicts the effective operator $(\bar{c}_L\gamma_\mu b_L)(\bar{\tau}_L\gamma^\mu\nu_{\tau L})$, and hence both R_D and R_{D^*} are corrected in the same direction and with the same size. In contrast, non-fermiophobic 4321 models also predict the scalar operator $(\bar{c}_L b_R)(\bar{\tau}_R\nu_{\tau L})$. Due to the presence of this operator, the NP effect on ΔR_D is larger than on ΔR_{D^*} (about 5/2 larger for the PS^3 model, see Eq. (27) in [115]).

Another key observable is $B \to K\nu\nu$, for which the twin Pati-Salam model predicts a larger branching fraction that will be fully tested by Belle II. Instead, non-fermiophobic 4321 models predict a smaller branching fraction, see Fig. 4.4 of [263] and compare their purple region with our Fig. 4.15. Moreover, in our analysis of $B \to K\nu\nu$ we have highlighted correlations with $B_s - \bar{B}_s$ mixing due to the loops being dominated by the same vector-like charged lepton, a feature which is missing in the analysis of [263].

Regarding the rest of the observables, broadly speaking the twin PS model predicts larger branching fractions for LFV processes. The exception is $\tau \to \mu\gamma$, which is enhanced in non-fermiophobic models via a chirality flip with the bottom quark running in the loop. The rare decays $B_s \to \tau\tau$ and $B \to K\tau\tau$ are chirally enhanced in non-fermiophobic models due to the presence of scalar operators connected to the third

family right-handed couplings. The LHCb and Belle II collaborations will test significant regions of the parameter space to disentangle the different 4321 approaches.
The lifetime ratio τ_{B_s}/τ_{B_d} introduced in Section 2.3.6 can potentially discriminate as well between the twin PS model and non-fermiophobic 4321 models [4], see Fig. 2.5.

High-p_T searches also offer a window to disentangle both approaches, since most of the constraints afflicting non-fermiophobic 4321 scenarios are relaxed in the dominantly left-handed scenario of the twin PS model. Particularly relevant are also the different implementations of vector-like fermions.

4.7.2 Fermiophobic 4321 models

To our knowledge, the only fermiophobic 4321 model proposed in the literature is that of Ref. [267], whose phenomenology was studied in detail in [268]. This model presents a simplified fermiophobic scenario with a rather ad-hoc flavour structure motivated by the phenomenology, including an ad-hoc alignment of SM-like Yukawas and VL-chiral fermion mixing. Furthermore, [267] does not address the question of quark and lepton masses (is not a theory of flavour), unlike the model proposed here. It lacks quark-lepton unification of SM fermions and leads to a less predictive framework than the twin Pati-Salam model.

The twin Pati-Salam model leads to an effective fermiophobic 4321 model at the TeV scale. However, the underlying twin PS symmetry implies correlations of key parameters, leading to extra constraints and correlations between observables, which are not present in the analyses of [267, 268]. For example, $R_{D^{(*)}}$ and $R_{K^{(*)}}$ are correlated here due to the universality of x_{25}^{ψ} and x_{34}^{ψ}, leading to quasi-universal mixing angles $s_{25}^{Q,L}$ and $s_{34}^{Q,L}$. By contrast, such mixing angles are free parameters in [267, 268] and one can explain $R_{D^{(*)}}$ without giving any contribution to $R_{K^{(*)}}$. As a consequence, a dedicated analysis was required to show that $R_{D^{(*)}}$ can be explained in the twin PS model while being compatible with the recent data on $R_{K^{(*)}}$, as we did in this chapter.

Since the twin Pati-Salam model is a theory of flavour, while [267, 268] is not, new signals are predicted in LFV processes connected to the origin of fermion masses and mixings. The twin PS model predicts non-vanishing $\mu\tau$ mixing, leading to striking signals in $\tau \to 3\mu$ and $\tau \to \mu\gamma$ close to current experimental bounds, as summarised in Figs. 4.9a and 4.9b. The large contributions to the branching fractions of $\tau \to 3\mu$ and $\tau \to \mu\gamma$ are mediated by the Z' boson, see the purple region in Figs. 4.9a and 4.9b. In contrast, in simplified fermiophobic 4321 models [267, 268] only a much smaller 1-loop U_1-mediated signal is predicted. This signal was not computed in Refs. [267, 268] as it is very small compared to the experimental bounds, but we have computed it here for the sake of comparison, and it is depicted as the blue region in Figs. 4.9a and 4.9b. In a similar way, we obtain $\mathcal{B}(\tau \to \mu\phi)$ two orders of magnitude larger than in [267, 268] due to the $\tau\mu$ mixing predicted by the twin Pati-Salam model.

Finally, the fermion mixing predicted by the twin Pati-Salam model avoids current constraints coming from CKM unitarity, $\Delta F = 2$ and electroweak precision observables

as presented in [369]. The reasons are the absence of SM-like Yukawa couplings for chiral fermions in the original basis (as they will be generated indeed via this mixing), along with the fact that vector-like quark $SU(2)_L$ doublets and SM quark $SU(2)_L$ singlets do not mix, hence the vector-like quark doublet remains unsplit. Remarkably, this is different from [267, 268], where mixing between the chiral quark singlets and the vector-like (right-handed) quark doublet was induced due to the presence of the SM-like Yukawa couplings for chiral fermions, leading to possible splitting of the vector-like quark doublet, which constrains the mixing angles for third family quarks according to the analysis in [369].

4.8 Conclusions

We have proposed the twin Pati-Salam model as a multi-scale theory of flavour able to explain the origin of the flavour structure of the SM, connecting the origin of the SM Yukawa couplings with the origin of the couplings to fermions of a TeV scale vector leptoquark U_1 that explains the anomalies in B-physics. The basic idea of this model is that all three families of SM chiral fermions transform under one PS group, while families of vector-like fermions transform under the other one. Vector leptoquark couplings and SM Yukawa couplings emerge together after mixing of the chiral fermions with the vector-like fermions, thereby providing a direct link between B-physics and fermion masses and mixings. In this manner, the twin Pati-Salam model features a fermiophobic framework in complete analogy with the fermiophobic Z' models of Chapter 3, such that both the B-anomalies and the flavour hierarchies are explained via the mechanism of messenger dominance [171]. Remarkably, the need to explain the low-energy B-anomalies fixes the NP scales of flavour $\langle\phi\rangle$ and M (which *a priori* could be anywhere *from the Planck scale to the electroweak scale*) to live close to the TeV scale, at least those involving the origin of second and third family fermion masses.

Firstly, we presented a simplified version of the model where second and third family fermion masses originate from mixing with a "fourth" vector-like family of fermions charged under $SU(4)^I_{PS}$, broken at the TeV scale. $SU(2)_L$ doublet vector-like fermions with masses around the TeV scale are assumed to have a large mixing with left-handed third family fermions, in order to provide their effective Yukawa couplings. In the spirit of messenger dominance [171], hierarchically heavier $SU(2)_L$ vector-like fermion singlets mix with second and third family right-handed fermions, in order to provide second family fermion masses and the small V_{cb} CKM element. The origin of first family fermion masses and their mixing is connected to vector-like fermions charged under the second PS group, broken around the much heavier PeV scale, completing the multi-scale picture for the origin of flavour.

However, with only a single vector-like family charged under $SU(4)^I_{PS}$, the model is unable to explain the B-anomalies in a natural way, as it does not achieve the required flavour structure to avoid constraints by $B_s - \bar{B}_s$ meson mixing mediated by the

heavy neutral vectors of the model. We then extended the simplified model to include three vector-like families, together with a $\mathbb{Z}_4$ discrete symmetry to control the flavour structure. This version of the model allows for larger flavour-violating and dominantly left-handed U_1 couplings as required to address $R_{D^{(*)}}$, thanks to mixing between a fourth and fifth vector-like families which also mix with the second and third generations of SM fermions. A sixth vector-like family is included to mix with the first SM family, for the sake of suppressing any FCNCs involving first and second family fermions. The mechanism resembles the GIM suppression of FCNCs in the SM, featuring a similar Cabbibo-like matrix which is present in leptoquark currents, but not in neutral currents mediated by the coloron and Z'.

This version of the model can explain the $R_{D^{(*)}}$ anomalies at 1σ while being compatible with all data, however we expect small deviations from the SM on the $R_{K^{(*)}}$ ratios, to be tested in the future via more precise tests of LFU by the LHCb collaboration. In contrast to the alternative models, our model predicts dominantly left-handed U_1 couplings to fermions, leading to $\Delta R_D = \Delta R_{D^*}$. The contribution to $R_{D^{(*)}}$ is correlated as well with an universal contribution to the operator $\mathcal{O}_9$, that further improves the overall fit of the model to $b \to s\mu\mu$ data.

Non-negligible $\mu\tau$ mixing is predicted by the theory of flavour, leading to interesting signals in $\tau \to 3\mu$ and $\tau \to \mu\gamma$, mostly due to Z' exchange, which are close to present experimental bounds in some region of the parameter space. Signals in LFV semileptonic processes mediated by U_1 at tree-level are found to lie well below current experimental limits, with the exception of $K_L \to e\mu$ which constrains a small region of the parameter space. However, this tension can be alleviated if the first family U_1 coupling is diluted via mixing with vector-like fermions. Tests of LFU in tau decays set important bounds over the mass of U_1 depending on its coupling to third family fermions. Contributions of U_1 to the rare decays $B_s \to \tau\tau$ and $B \to K\tau\tau$ are broadly below current and projected experimental sensitivity. Instead, the rare decay $B \to K^{(*)}\nu\bar{\nu}$ offers the opportunity to fully test the model in the near future, since Belle II is expected to cover all the parameter space compatible with the B-anomalies. Remarkably, the model can be easily disentangled from all other proposals via the previous set of observables, as discussed in Section 4.7.

Apart from the aforementioned low-energy predictions at LHCb and Belle II, the model is also testable via high-p_T searches at the LHC. The study of the 1-loop contribution of vector leptoquark U_1 exchange to $B_s - \bar{B}_s$ mixing revealed that the fifth vector-like lepton has to be light, around 1-2 TeV, to be compatible with the stringent bound from ΔM_s. This is easily achieved in the twin Pati-Salam model, where light vector-like fermions are well motivated in order to naturally obtain the large mixing needed to fit the $R_{D^{(*)}}$ anomaly, and also to fit the heavy top mass without perturbativity issues. In particular, the fourth and fifth charged leptons are suggested as good candidates to explain the CMS excess [368], but further study is required in this direction. Vector-like quarks are found to lie not far above 1 TeV in the suggested benchmark,

hence motivating specific searches at LHC to be performed. Regarding the heavy vectors, dijet searches and dilepton searches set mild bounds over the mass of the coloron and Z', respectively. The more stringent bound over the scale of the model arises from the ditop searches in [263,363], which push the mass of the coloron to lie above 3.5 TeV, however those bounds could be slightly overestimated for our model as they are obtained for different 4321 scenarios. Finally, the mass range for U_1 is compatible with current bounds, and mostly lie within the projected sensitivity of the high luminosity phase of LHC. A good fit for the 3σ CMS excess in U_1 searches [367] could be provided if the extra decay channels to vector-like fermions are considered, assuming that the bound from ditop searches is indeed overestimated.

As we have shown, the twin Pati-Salam model predicts the NP scenario preferred by the global fits [82] in order to explain B-physics data, and connects explicitly the effective U_1 leptoquark couplings with the origin of Yukawa couplings in the SM. The model exhibits a rich flavour phenomenology with key observables that will allow to disentangle it from all other proposals, along with a TeV-scale phenomenology that can be probed in the near future by high-p_T experiments at the LHC.

Chapter 5

Tri-hypercharge: a path to the origin of flavour

> "You're telling me that people at CERN dug out millions of tons of earth just to smash tiny particles?" Kohler shrugged. "Sometimes to find truth, one must move mountains."
>
> – Dan Brown, *Angels & Demons*

In this chapter, based on Ref. [3], we introduce a theory of flavour based on assigning a separate gauged weak hypercharge to each family of chiral fermions. Assuming that the Higgs doublet only carries third family hypercharge, then only third family fermions get renormalisable Yukawa couplings, explaining their heaviness. Light charged fermion masses and CKM mixing may arise from non-renormalisable operators, connected to the new scalar fields that break the three hypercharge groups down to SM hypercharge. We shall conclude that neutrino masses and mixing may be explained via the addition of vector-like singlet neutrinos that carry cancelling family hypercharges. Finally, we will see that this model has a rich phenomenology if the new physics scales are low, including flavour-violating observables, LHC physics and electroweak precision observables.

5.1 Introduction

Theories of flavour may involve new symmetries (global, local, continuous, discrete, abelian, non-abelian...) beyond the SM group, possibly broken at some high scale down to the SM. Traditionally, new gauge structures beyond the SM have been considered to be flavour universal, as grand unified theories (GUTs) which usually embed all three families in an identical way, or even extended GUTs which embed all three families in a single representation (usually along with extra exotic fermions). Alternatively, there exists the well-motivated case of family symmetries which commute with the SM gauge group, and are then spontaneously broken, leading to family structure. However, there are other

less explored ways in which the SM gauge group could be embedded into a larger gauge structure in a flavour non-universal way. In particular, the *family decomposition* of the SM gauge group (including a hierarchical symmetry breaking pattern down to the SM) was first proposed during the 80s and 90s, with the purpose of motivating lepton non-universality [370–373] or assisting technicolor model building [374–376]. However, the natural origin of flavour hierarchies in such a framework was not explored until more recently in [113, 114, 118]. Here it was proposed that the flavour non-universality of Yukawa couplings in the SM might well find its origin in a flavour non-universal gauge sector, broken in a hierarchical way down to the SM. Interestingly, model building in this direction has received particular attention in recent years [115–117, 119–121]. With the exception of Ref. [121], the remaining recent attempts have been motivated by the need to obtain a TeV scale vector leptoquark from Pati-Salam unification in order to address the B-anomalies[1]. Therefore, all these setups share a similar feature: a low scale $SU(4)$ gauge group under which only the third family of SM fermions transforms in a non-trivial way. In contrast, in this work we want to explore the capabilities of flavour non-universality to address the flavour puzzle in a more minimal, simple and bottom-up approach.

We propose that the SM symmetry originates from a larger gauge group in the UV that contains three separate weak hypercharge gauge factors,

$$SU(3)_c \times SU(2)_L \times U(1)_{Y_1} \times U(1)_{Y_2} \times U(1)_{Y_3}\,, \tag{5.1}$$

which we will denote as the *tri-hypercharge* (TH) $U(1)_Y^3$ gauge group. We will associate each of the three hypercharge gauge groups with a separate SM family, such that each fermion family i only carries hypercharge under the corresponding $U(1)_{Y_i}$ factor. This ensures that each family transforms differently under the gauge group $U(1)_Y^3$, which avoids the family repetition of the SM, and provides the starting point for a theory of flavour. For example, assuming that a single Higgs doublet only carries third family hypercharge, then only the third family Yukawa couplings are allowed at renormalisable level. With two Higgs doublets carrying third family hypercharge, we show that the naturalness of the scheme increases. This simple and economical framework naturally explains the heaviness of the third family, the smallness of V_{cb} and V_{ub}, and delivers Yukawa couplings that preserve an accidental and global $U(2)^5$ flavour symmetry acting on the light families, which is known to provide a good first order description of the SM spectrum plus an efficient suppression of flavour-violating effects for new physics [110].

[1] Remarkably, flavour non-universality is not the only way to connect the TeV-scale Pati-Salam vector leptoquark addressing the B-anomalies with the origin of flavour hierarchies, see the twin Pati-Salam theory of flavour discussed in Chapter 4 of this thesis, which considers the mechanism of messenger dominance [171]

Remarkably, this appears to be the simplest way to provide the $U(2)^5$ flavour symmetry[2]. The masses of first and second family fermions, along with the CKM mixing, then appear as small breaking sources of $U(2)^5$ that arise after the cascade spontaneous symmetry breaking of $U(1)^3_Y$ down to SM hypercharge, which can be parameterised in a model-independent way in terms of spurions. In a realistic model, the spurions will be realised by a choice of "hyperon" scalars which transform under the different family hypercharge groups, breaking the tri-hypercharge symmetry. We will motivate a specific symmetry breaking chain where dynamics at a low scale, which could be as low as the TeV, explain the flavour hierarchies m_2/m_3, while dynamics at a heavier scale explain m_1/m_2. This symmetry breaking pattern will sequentially recover the approximate flavour symmetry of the SM, and provide a natural suppression of FCNCs for TeV new physics, while the rest of flavour-violating effects are suppressed by a naturally heavier scale. In this manner, the tri-hypercharge gauge group is an example of a multi-scale origin of flavour as introduced in Section 1.10. Moreover, later in Chapter 6 we shall see that the tri-hypercharge gauge group, among other gauge non-universal theories, may arise from a gauge unified framework.

The chapter is organised as follows. In Section 5.2 we introduce the TH gauge group, along with the fermion and Higgs doublet content of the model. We discuss the implications for third family fermion masses along with the mass hierarchy between the top and bottom/tau fermions. In Section 5.3 we study the origin of charged fermion masses and mixing in the TH model, firstly via a spurion formalism which reveals model-independent considerations, and secondly by introducing example models with hyperons. In Section 5.4 we study the origin of neutrino masses and mixing in the TH model. In particular, we discuss the impact of the $U(2)^5$ flavour symmetry over the dimension-5 Weinberg operator, and afterwards we provide an example type I seesaw model where neutrino masses and mixing can be accommodated. In Section 5.6 we perform a preliminary exploration of the phenomenological implications and discovery prospects of the $U(1)^3_Y$ theory of flavour. Finally, Section 5.7 outlines our main conclusions.

5.2 Tri-hypercharge gauge theory

The tri-hypercharge gauge group is based on assigning a separate gauged weak hypercharge to each fermion family,

$$SU(3)_c \times SU(2)_L \times U(1)_{Y_1} \times U(1)_{Y_2} \times U(1)_{Y_3}\,, \tag{5.2}$$

[2]An alternative way to deliver $U(2)^5$ consists in decomposing $SU(2)_L$ only and taking advantage of the fact that right-handed rotations remain unphysical in order to remove the remaining $U(2)^5$-breaking entries of the Yukawa matrices (see the complete review of Ref. [122]). Another example [300] considered an extension of the SM by a $U(1)_{Y_3}$ gauge group under which only third family fermions (and the Higgs) are hypercharge-like charged, where $U(1)_{Y_3}$ commutes with SM hypercharge, leading to an accidental $U(2)^5$.

Field	$SU(3)_c$	$SU(2)_L$	$U(1)_{Y_1}$	$U(1)_{Y_2}$	$U(1)_{Y_3}$
Q_1	$\mathbf{3}$	$\mathbf{2}$	$1/6$	0	0
u_1^c	$\overline{\mathbf{3}}$	$\mathbf{1}$	$-2/3$	0	0
d_1^c	$\overline{\mathbf{3}}$	$\mathbf{1}$	$1/3$	0	0
L_1	$\mathbf{1}$	$\mathbf{2}$	$-1/2$	0	0
e_1^c	$\mathbf{1}$	$\mathbf{1}$	1	0	0
Q_2	$\mathbf{3}$	$\mathbf{2}$	0	$1/6$	0
u_2^c	$\overline{\mathbf{3}}$	$\mathbf{1}$	0	$-2/3$	0
d_2^c	$\overline{\mathbf{3}}$	$\mathbf{1}$	0	$1/3$	0
L_2	$\mathbf{1}$	$\mathbf{2}$	0	$-1/2$	0
e_2^c	$\mathbf{1}$	$\mathbf{1}$	0	1	0
Q_3	$\mathbf{3}$	$\mathbf{2}$	0	0	$1/6$
u_3^c	$\overline{\mathbf{3}}$	$\mathbf{1}$	0	0	$-2/3$
d_3^c	$\overline{\mathbf{3}}$	$\mathbf{1}$	0	0	$1/3$
L_3	$\mathbf{1}$	$\mathbf{2}$	0	0	$-1/2$
e_3^c	$\mathbf{1}$	$\mathbf{1}$	0	0	1

TABLE 5.1: Charge assignments of the SM fermions under the TH gauge group. Q_i and L_i (where $i = 1, 2, 3$) are left-handed $SU(2)_L$ doublets of chiral quarks and leptons, while u_i^c, d_i^c and e_i^c are the CP-conjugate right-handed quarks and leptons (so that they become left-handed[3]).

in such a way that the ith fermion family only carries Y_i hypercharge, with the other hypercharges set equal to zero (see Table 5.1), where $Y = Y_1+Y_2+Y_3$ is equal to SM weak hypercharge. Anomalies cancel separately for each family, as in the SM, but without family replication. The TH gauge group is broken down to the SM via appropriate SM singlet scalars, which however carry family hypercharges. We denote these fields linking the family hypercharges as *hyperons*. The TH group could be broken down to the SM in different ways, however we motivate the following symmetry breaking pattern,

$$\begin{aligned} & SU(3)_c \times SU(2)_L \times U(1)_{Y_1} \times U(1)_{Y_2} \times U(1)_{Y_3} \\ \overset{v_{12}}{\to} & \; SU(3)_c \times SU(2)_L \times U(1)_{Y_1+Y_2} \times U(1)_{Y_3} \\ \overset{v_{23}}{\to} & \; SU(3)_c \times SU(2)_L \times U(1)_{Y_1+Y_2+Y_3} \, . \end{aligned} \tag{5.3}$$

This choice is well supported by symmetry arguments that will have phenomenological consequences: At high energies, the TH group discriminates between the three SM fermion families, explicitly breaking the approximate $U(3)^5$ flavour symmetry of the SM. At a heavy scale v_{12}, the first and second hypercharges are broken down to their diagonal subgroup, and the associated Z' boson potentially mediates dangerous 1-2 FCNCs. Nevertheless, the gauge group below the scale v_{12} preserves an accidental $U(2)^5$ flavour symmetry. The groups $U(1)_{Y_1+Y_2} \times U(1)_{Y_3}$ are broken down to their diagonal subgroup (SM hypercharge) at a scale v_{23}, and the associated Z' boson is protected from mediating the most dangerous FCNCs thanks to the $U(2)^5$ symmetry. In this manner, the most dangerous FCNCs are suppressed by the heavier scale v_{12}, while the scale

[3]The reader who is not familiar with this notation based on left-handed 2-component Weyl spinors can find the connection with the traditional 4-component, left-right notation in Appendix A.

v_{23} can be very low with interesting phenomenological implications. We will see that dynamics connected to the scale v_{12} will play a role in the origin of the family hierarchy m_1/m_2, while dynamics connected to the scale v_{23} will play a role in the origin of m_2/m_3. The distribution of the various scales in the model reproduces what we would expect in a multi-scale theory of flavour based on $U(2)^5$, as anticipated in Section 1.9.3 and in Fig. 1.6. Despite the apparently complex gauge sector of the tri-hypercharge setup, consisting of five arbitrary gauge couplings, in Chapter 6 we shall see that such a theory may arise from a gauge unified framework.

Provided that the SM Higgs only carries third family hypercharge, $H(\mathbf{1},\mathbf{2})_{(0,0,-\frac{1}{2})}$, then only third family Yukawa couplings are allowed at renormalisable level and an accidental $U(2)^5$ flavour symmetry acting on the light families emerges in the Yukawa sector,

$$\mathcal{L} = y_t Q_3 \tilde{H} u_3^c + y_b Q_3 H d_3^c + y_\tau L_3 H e_3^c + \text{h.c.} \tag{5.4}$$

where $\tilde{H}$ is the CP-conjugate of H. This setup already provides an explanation for the smallness of light fermion masses with respect to the third family, along with the smallness of quark mixing, as they all must arise from non-renormalisable operators which minimally break the $U(2)^5$ symmetry. Although this is a good first order description of the SM spectrum, the question of why the bottom and tau fermions are much lighter than the top remains unanswered, and assuming only a single Higgs doublet, a tuning of order 2% for the bottom coupling and of 1% for the tau coupling would be required. Given that $m_{s,\mu} \propto \lambda^5 m_t$ while $m_c \propto \lambda^3 m_t$, this setup also requires to generate a stronger fermion hierarchy in the down and charged lepton sectors with respect to the up sector, unless the tuning in the bottom and tau couplings is extended to the second family. As we shall see shortly, the $U(1)_Y^3$ model (and very likely a more general set of theories of flavour based on the family decomposition of the SM group) predicts a similar mass hierarchy for all charged sectors.

Due to the above considerations, it seems natural to consider a type II two Higgs doublet model (2HDM), where both Higgs doublets only carry third family hypercharge,

$$H_u(\mathbf{1},\mathbf{2})_{(0,0,\frac{1}{2})}, \qquad H_d(\mathbf{1},\mathbf{2})_{(0,0,-\frac{1}{2})}\,, \tag{5.5}$$

where as usual for a type II 2HDM, FCNCs can be forbidden by e.g. a softly broken $\mathbb{Z}_2$ discrete symmetry or by Supersymmetry (not necessarily low scale), which we however do not specify in order to preserve the bottom-up spirit of this work. In any case, $\tan\beta = v_u/v_d \sim \lambda^{-2} \approx 20$, which is compatible with current data (see e.g. [377, 378]), will provide the hierarchy between the top and bottom/tau masses with all dimensionless couplings being $\mathcal{O}(1)$. Such an overall hierarchy between the down and charged lepton sectors with respect to the up sector is extended to all families, providing a better description of second family charged fermion masses as we shall see.

5.3 Charged fermion masses and mixing

5.3.1 Lessons from the spurion formalism

In all generality, we introduce $U(2)^5$-breaking *spurions* Φ in the Yukawa matrices of charged fermions

$$\begin{aligned}\mathcal{L} = &(Q_1 \quad Q_2 \quad Q_3)\begin{pmatrix}\Phi(\frac{1}{2},0,-\frac{1}{2}) & \Phi(-\frac{1}{6},\frac{2}{3},-\frac{1}{2}) & \Phi(-\frac{1}{6},0,\frac{1}{6})\\ \Phi(\frac{2}{3},-\frac{1}{6},-\frac{1}{2}) & \Phi(0,\frac{1}{2},-\frac{1}{2}) & \Phi(0,-\frac{1}{6},\frac{1}{6})\\ \Phi(\frac{2}{3},0,-\frac{2}{3}) & \Phi(0,\frac{2}{3},-\frac{2}{3}) & 1\end{pmatrix}\begin{pmatrix}u_1^c\\u_2^c\\u_3^c\end{pmatrix}H_u\\ &+(Q_1 \quad Q_2 \quad Q_3)\begin{pmatrix}\Phi(-\frac{1}{2},0,\frac{1}{2}) & \Phi(-\frac{1}{6},-\frac{1}{3},\frac{1}{2}) & \Phi(-\frac{1}{6},0,\frac{1}{6})\\ \Phi(-\frac{1}{3},-\frac{1}{6},\frac{1}{2}) & \Phi(0,-\frac{1}{2},\frac{1}{2}) & \Phi(0,-\frac{1}{6},\frac{1}{6})\\ \Phi(-\frac{1}{3},0,\frac{1}{3}) & \Phi(0,-\frac{1}{3},\frac{1}{3}) & 1\end{pmatrix}\begin{pmatrix}d_1^c\\d_2^c\\d_3^c\end{pmatrix}H_d \qquad (5.6)\\ &+(L_1 \quad L_2 \quad L_3)\begin{pmatrix}\Phi(-\frac{1}{2},0,\frac{1}{2}) & \Phi(\frac{1}{2},-1,\frac{1}{2}) & \Phi(\frac{1}{2},0,-\frac{1}{2})\\ \Phi(-1,\frac{1}{2},\frac{1}{2}) & \Phi(0,-\frac{1}{2},\frac{1}{2}) & \Phi(0,\frac{1}{2},-\frac{1}{2})\\ \Phi(-1,0,1) & \Phi(0,-1,1) & 1\end{pmatrix}\begin{pmatrix}e_1^c\\e_2^c\\e_3^c\end{pmatrix}H_d + \text{h.c.}\,,\end{aligned}$$

where each spurion carries non-trivial charge assignments under $U(1)_Y^3$. In an EFT approach, each spurion above can be matched to specific ratios of hyperons ϕ_i over EFT cut-off scales Λ_i, i.e.

$$\Phi = \frac{\phi_1 ... \phi_n}{\Lambda_1 ... \Lambda_n}\,, \qquad (5.7)$$

where we have suppressed dimensionless couplings. The choice of hyperons and Λ_i above carries all the model dependence.

Assuming that the cut-off scales Λ_i of the EFT are universal, i.e. that all Λ_i are common to all charged sectors, then the spurion formalism reveals some general considerations about the origin of charged fermion masses and mixing:

- The same spurions (up to conjugation) appear in the diagonal entries of all matrices. Therefore, unless texture zeros are introduced in specific models, this means that the masses of second family fermions are likely to be degenerate up to dimensionless couplings, and the same discussion applies to first family fermions. This motivates again the addition of the second Higgs doublet or an alternative mechanism in order to generate the hierarchy between the charm mass and the lighter strange and muon masses.

- The same spurions appear in the (2,3) entries of the up and down Yukawa matrices. Therefore, the 2-3 mixing in both the up and down sectors is expected to be of a similar size, giving no predictions about the alignment of the CKM element V_{cb}. The similar argument applies to 1-3 mixing and V_{ub}.

- The spurions in the (1,2) entry of the up and down matrices are different. Therefore, specific models have the potential to give predictions about the alignment of the CKM element V_{us}.

- The same spurion (up to conjugation) that enters in all (2,2) entries also populates the (2,3) entry of the charged lepton Yukawa matrix. Similarly, the same spurion

(up to conjugation) that enters in all (1,1) entries also populates the (1,3) entry of the charged lepton Yukawa matrix. In general, this predicts left-handed $\mu - \tau$ ($e - \tau$) mixing of $\mathcal{O}(m_2/m_3)$ ($\mathcal{O}(m_1/m_3)$), unless texture zeros are introduced in specific models (see Section 5.3.2). This leads to a sizable enhancement of LFV $\tau \to \mu$ and $\tau \to e$ transitions above the SM predictions, mediated by heavy Z' bosons in the model (see Section 5.6).

- The spurions in the lower off-diagonal entries of the Yukawa matrices all carry independent charge assignments, so right-handed fermion mixing is model-dependent and can be different in all charged sectors.

In the following, we go beyond the spurion formalism and introduce different sets of hyperons. As we shall wee, the hyperons will provide small $U(2)^5$-breaking effects via non-renormalisable operators, leading to the masses of first and second family charged fermions, along with CKM mixing. In the next few subsections, we will describe example scenarios which provide a good description of charged fermion masses and mixing.

5.3.2 From spurions to hyperons

The physical origin of the spurions of the previous subsection will correspond to new Higgs scalar fields that break the $U(1)_Y^3$ symmetry, which we call *hyperons*. The hyperons induce small $U(2)^5$-breaking effects at the non-renormalisable level that will lead to the masses and mixings of charged fermions. As the most straightforward scenario, we could promote the spurions in the diagonal entries of the matrices in Eq. (5.6) to hyperons, along with the off-diagonal spurions in the upper half of the down matrix[4]. In an EFT approach, the set of hyperons that we have assumed generates the following Yukawa matrices,

$$\mathcal{L}^{d\leq 5} = (Q_1 \quad Q_2 \quad Q_3) \begin{pmatrix} \phi_{\ell 13}^{(\frac{1}{2},0,-\frac{1}{2})}/\Lambda & 0 & \phi_{q13}^{(-\frac{1}{6},0,\frac{1}{6})}/\Lambda \\ 0 & \phi_{\ell 23}^{(0,\frac{1}{2},-\frac{1}{2})}/\Lambda & \phi_{q23}^{(0,-\frac{1}{6},\frac{1}{6})}/\Lambda \\ 0 & 0 & 1 \end{pmatrix} \begin{pmatrix} u_1^c \\ u_2^c \\ u_3^c \end{pmatrix} H_u \tag{5.8}$$

$$+ (Q_1 \quad Q_2 \quad Q_3) \begin{pmatrix} \tilde{\phi}_{\ell 13}^{(-\frac{1}{2},0,\frac{1}{2})}/\Lambda & \phi_{d12}^{(-\frac{1}{6},-\frac{1}{3},\frac{1}{2})}/\Lambda & \phi_{q13}^{(-\frac{1}{6},0,\frac{1}{6})}/\Lambda \\ 0 & \tilde{\phi}_{\ell 23}^{(0,-\frac{1}{2},\frac{1}{2})}/\Lambda & \phi_{q23}^{(0,-\frac{1}{6},\frac{1}{6})}/\Lambda \\ 0 & 0 & 1 \end{pmatrix} \begin{pmatrix} d_1^c \\ d_2^c \\ d_3^c \end{pmatrix} H_d \tag{5.9}$$

$$+ (L_1 \quad L_2 \quad L_3) \begin{pmatrix} \tilde{\phi}_{\ell 13}^{(-\frac{1}{2},0,\frac{1}{2})}/\Lambda & 0 & \phi_{\ell 13}^{(\frac{1}{2},0,-\frac{1}{2})}/\Lambda \\ 0 & \tilde{\phi}_{\ell 23}^{(0,-\frac{1}{2},\frac{1}{2})}/\Lambda & \phi_{\ell 23}^{(0,\frac{1}{2},-\frac{1}{2})}/\Lambda \\ 0 & 0 & 1 \end{pmatrix} \begin{pmatrix} e_1^c \\ e_2^c \\ e_3^c \end{pmatrix} H_d + \text{h.c.}\,, \tag{5.10}$$

where the universal scale Λ is the high cut-off scale of the EFT, and we ignore the $\mathcal{O}(1)$ dimensionless couplings of each entry. Although we have chosen only the specific set

[4]Notice that the same spurions enter in both the (1,3) and (2,3) entries of the up and down matrices in Eq. (5.6).

of hyperons shown, leaving some zeros in the matrices, these zeros may be filled in by higher order operators with dimension larger than 5, which so far we are ignoring.

When the hyperons develop VEVs, assumed to be smaller than the cut-off scale Λ, then each entry of the matrix will receive a suppressed numerical effective coupling given by ratios of the form $\langle\phi\rangle/\Lambda$, whose values can be assumed arbitrarily. Having the freedom to choose arbitrary VEVs for each hyperon, the Yukawa matrices above could provide a good first order description of charged fermion masses and CKM mixing. We choose to fix various $\langle\phi\rangle/\Lambda$ ratios in terms of powers of the Wolfenstein parameter $\lambda \simeq 0.225$, obtaining

$$\mathcal{L} = (u_1 \quad u_2 \quad u_3) \begin{pmatrix} \lambda^6 & 0 & \lambda^3 \\ 0 & \lambda^3 & \lambda^2 \\ 0 & 0 & 1 \end{pmatrix} \begin{pmatrix} u_1^c \\ u_2^c \\ u_3^c \end{pmatrix} \frac{v_{\rm SM}}{\sqrt{2}} \tag{5.11}$$

$$+ (d_1 \quad d_2 \quad d_3) \begin{pmatrix} \lambda^6 & \lambda^4 & \lambda^3 \\ 0 & \lambda^3 & \lambda^2 \\ 0 & 0 & 1 \end{pmatrix} \begin{pmatrix} d_1^c \\ d_2^c \\ d_3^c \end{pmatrix} \lambda^2 \frac{v_{\rm SM}}{\sqrt{2}} \tag{5.12}$$

$$+ (e_1 \quad e_2 \quad e_3) \begin{pmatrix} \lambda^6 & 0 & \lambda^6 \\ 0 & \lambda^3 & \lambda^3 \\ 0 & 0 & 1 \end{pmatrix} \begin{pmatrix} e_1^c \\ e_2^c \\ e_3^c \end{pmatrix} \lambda^2 \frac{v_{\rm SM}}{\sqrt{2}} + \text{h.c.} \tag{5.13}$$

As anticipated from the spurion formalism, the alignment of V_{cb} and V_{ub} is not predicted by the model. In contrast, the model predicts a relevant left-handed $\mu-\tau$ ($e-\tau$) mixing connected to the same hyperon that provides the second family (first family) effective Yukawa couplings. Thanks to the addition of the second Higgs doublet, the model successfully explains third and second family fermion masses with $\mathcal{O}(1)$ dimensionless couplings. The down-quark and electron masses are also reasonably explained, although the up-quark mass is naively a factor $\mathcal{O}(\lambda^{-1.5})$ larger than current data. Notice that so far we are only assuming one universal cut-off scale Λ, while in realistic models several cut-off scales Λ may be associated to different messengers in the UV theory, which could provide a larger suppression for the up-quark effective coupling. Therefore, within the limitations of our EFT approach, the description of charged fermion masses given by the set of Eqs. (5.11-5.13) is very successful.

As an alternative example, one could also consider a model where the (1,1) spurion in Eq. (5.6) is not promoted to hyperon, but instead all the spurions in the (1,2) and (2,1) entries are promoted, so that the Yukawa matrices show an exact texture zero in the (1,1) entry,

$$\mathcal{L}^{d\leq 5} = (Q_1 \quad Q_2 \quad Q_3) \begin{pmatrix} 0 & \phi_{u12}^{(-\frac{1}{6},\frac{2}{3},-\frac{1}{2})} & \phi_{q13}^{(-\frac{1}{6},0,\frac{1}{6})} \\ \phi_{u21}^{(\frac{2}{3},-\frac{1}{6},-\frac{1}{2})} & \phi_{\ell 23}^{(0,\frac{1}{2},-\frac{1}{2})} & \phi_{q23}^{(0,-\frac{1}{6},\frac{1}{6})} \\ 0 & 0 & 1 \end{pmatrix} \begin{pmatrix} u_1^c \\ u_2^c \\ u_3^c \end{pmatrix} H_u \tag{5.14}$$

$$+ (Q_1 \quad Q_2 \quad Q_3) \begin{pmatrix} 0 & \phi_{d12}^{(-\frac{1}{6},-\frac{1}{3},\frac{1}{2})} & \phi_{q13}^{(-\frac{1}{6},0,\frac{1}{6})} \\ \phi_{d21}^{(-\frac{1}{3},-\frac{1}{6},\frac{1}{2})} & \tilde{\phi}_{\ell 23}^{(0,-\frac{1}{2},\frac{1}{2})} & \phi_{q23}^{(0,-\frac{1}{6},\frac{1}{6})} \\ 0 & 0 & 1 \end{pmatrix} \begin{pmatrix} d_1^c \\ d_2^c \\ d_3^c \end{pmatrix} H_d \tag{5.15}$$

$$+ (L_1 \quad L_2 \quad L_3) \begin{pmatrix} 0 & \phi_{e12}^{(\frac{1}{2},-1,\frac{1}{2})} & 0 \\ \phi_{e21}^{(-1,\frac{1}{2},\frac{1}{2})} & \tilde{\phi}_{\ell 23}^{(0,-\frac{1}{2},\frac{1}{2})} & \phi_{\ell 23}^{(0,\frac{1}{2},-\frac{1}{2})} \\ 0 & 0 & 1 \end{pmatrix} \begin{pmatrix} e_1^c \\ e_2^c \\ e_3^c \end{pmatrix} H_d + \text{h.c.}\,, \tag{5.16}$$

where we have omitted the high cut-off Λ suppressing each dimension-5 operator above. The VEV over Λ ratios of the new hyperons can be fixed by the requirement of addressing first family fermion masses, obtaining Yukawa matrices with texture zeros in the (1,1) entry as

$$\mathcal{L} = (u_1 \quad u_2 \quad u_3) \begin{pmatrix} 0 & \lambda^5 & \lambda^3 \\ \lambda^{5.5} & \lambda^3 & \lambda^2 \\ 0 & 0 & 1 \end{pmatrix} \begin{pmatrix} u_1^c \\ u_2^c \\ u_3^c \end{pmatrix} \frac{v_{\text{SM}}}{\sqrt{2}} \tag{5.17}$$

$$+ (d_1 \quad d_2 \quad d_3) \begin{pmatrix} 0 & \lambda^4 & \lambda^3 \\ \lambda^4 & \lambda^3 & \lambda^2 \\ 0 & 0 & 1 \end{pmatrix} \begin{pmatrix} d_1^c \\ d_2^c \\ d_3^c \end{pmatrix} \lambda^2 \frac{v_{\text{SM}}}{\sqrt{2}} \tag{5.18}$$

$$+ (e_1 \quad e_2 \quad e_3) \begin{pmatrix} 0 & \lambda^5 & 0 \\ \lambda^{4.4} & \lambda^3 & \lambda^3 \\ 0 & 0 & 1 \end{pmatrix} \begin{pmatrix} e_1^c \\ e_2^c \\ e_3^c \end{pmatrix} \lambda^2 \frac{v_{\text{SM}}}{\sqrt{2}} + \text{h.c.}\,, \tag{5.19}$$

which provide an even better description of first family fermion masses than the original simplified model. Notice that in this scenario, a sizable left-handed $e - \tau$ mixing is no longer predicted.

We conclude that the most straightforward choices of hyperons, motivated by the spurion formalism, already provide a good description of charged fermion masses and mixings. However, these simplified models leave some questions unanswered. Given that we are assuming the symmetry breaking highlighted in Eq. (5.3), we notice that there are no hyperons breaking the first and second hypercharges down to their diagonal subgroup, and we would expect those to play a role in the origin of fermion hierarchies and mixing. Moreover, in the simplified models introduced so far, several hyperons display unexplained large hierarchies of VEVs whose values are assumed *a posteriori* to fit the fermion masses. Given that all these hyperons participate in the 23-breaking step of Eq. (5.3), we would expect all of them to develop VEVs at a similar scale, rather than the hierarchical scales assumed. This motivates further model building. In the following subsections we discuss a couple of example models which address these issues.

5.3.3 Model 1: Minimal case with three hyperons

We introduce here the following set of three hyperons,

$$\phi_{\ell 23}^{(0,\frac{1}{2},-\frac{1}{2})}\,, \qquad \phi_{q23}^{(0,-\frac{1}{6},\frac{1}{6})}\,, \qquad \phi_{q12}^{(-\frac{1}{6},\frac{1}{6},0)}\,. \tag{5.20}$$

Following the EFT approach of the previous subsection, we now analyse the effective Yukawa matrices obtained by combining the SM charged fermions, the Higgs doublets and the hyperons, in a tower of non-renormalisable operators preserving the $U(1)_Y^3$ gauge

symmetry,

$$\mathcal{L} = (Q_1 \quad Q_2 \quad Q_3) \begin{pmatrix} \tilde{\phi}^3_{q12}\phi_{\ell 23} & \phi_{q12}\phi_{\ell 23} & \phi_{q12}\phi_{q23} \\ \tilde{\phi}^4_{q12}\phi_{\ell 23} & \phi_{\ell 23} & \phi_{q23} \\ \tilde{\phi}^4_{q12}\phi_{\ell 23}\tilde{\phi}_{q23} & \phi_{\ell 23}\tilde{\phi}_{q23} & 1 \end{pmatrix} \begin{pmatrix} u^c_1 \\ u^c_2 \\ u^c_3 \end{pmatrix} H_u \tag{5.21}$$

$$+ (Q_1 \quad Q_2 \quad Q_3) \begin{pmatrix} \phi^3_{q12}\tilde{\phi}_{\ell 23} & \phi_{q12}\tilde{\phi}_{\ell 23} & \phi_{q12}\phi_{q23} \\ \phi^2_{q12}\tilde{\phi}_{\ell 23} & \tilde{\phi}_{\ell 23} & \phi_{q23} \\ \phi^2_{q12}\phi^2_{q23} & \phi^2_{q23} & 1 \end{pmatrix} \begin{pmatrix} d^c_1 \\ d^c_2 \\ d^c_3 \end{pmatrix} H_d \tag{5.22}$$

$$+ (L_1 \quad L_2 \quad L_3) \begin{pmatrix} \phi^3_{q12}\tilde{\phi}_{\ell 23} & \tilde{\phi}^3_{q12}\tilde{\phi}_{\ell 23} & \tilde{\phi}^3_{q12}\phi_{\ell 23} \\ \phi^6_{q12}\tilde{\phi}_{\ell 23} & \tilde{\phi}_{\ell 23} & \phi_{\ell 23} \\ \phi^6_{q12}\tilde{\phi}^2_{\ell 23} & \tilde{\phi}^2_{\ell 23} & 1 \end{pmatrix} \begin{pmatrix} e^c_1 \\ e^c_2 \\ e^c_3 \end{pmatrix} H_d + \text{h.c.}\,, \tag{5.23}$$

where the powers of Λ in the denominator and the dimensionless couplings of each entry are not shown. Once the hyperons above develop VEVs, we obtain very economical and efficient Yukawa textures for modeling the observed pattern of SM Yukawa couplings. In particular, the masses of second family fermions arise at dimension 5 in the EFT, while first family masses have an extra suppression as they arise from dimension-8 operators. Regarding CKM mixing, 2-3 quark mixing leading to V_{cb} arises from dimension-5 operators, while V_{ub} has an extra mild suppression as it arises from dimension-6 operators. In all cases, right-handed fermion mixing is suppressed with respect to left-handed mixing. This is a highly desirable feature, given the strong phenomenological constraints on right-handed flavour-changing currents [238, 239] (see Section 2.3.4), which may be mediated by heavy Z' bosons arising from the symmetry breaking of $U(1)^3_Y$.

In good approximation, quark mixing leading to V_{us} arises as the ratio of the (1,2) and (2,2) entries of the quark matrices above, therefore we expect

$$\frac{\langle \phi_{q12} \rangle}{\Lambda} \sim V_{us} \simeq \lambda\,, \tag{5.24}$$

where $\lambda = \sin\theta_C \simeq 0.225$. In a similar manner, we can fix the ratio $\langle \phi_{q23} \rangle / \Lambda$ by reproducing the observed V_{cb}

$$\frac{\langle \phi_{q23} \rangle}{\Lambda} \sim V_{cb} \simeq \lambda^2\,. \tag{5.25}$$

Given that both $\langle \phi_{q23} \rangle$ and $\langle \phi_{\ell 23} \rangle$ play a role in the last step of the symmetry breaking cascade (see Eq. (5.3)), it is expected that both VEVs live at a similar scale, although they are not expected to be degenerate but differ by an $\mathcal{O}(1)$ factor. This way, we are free to choose

$$\frac{\langle \phi_{\ell 23} \rangle}{\Lambda} \sim \frac{m_c}{m_t} \sim \lambda^3\,, \tag{5.26}$$

which, given that $\langle H_d \rangle$ provides an extra suppression of $\mathcal{O}(\lambda^2)$ for down-quarks and charged lepton Yukawas, allows to predict all second family masses with $\mathcal{O}(1)$ dimensionless couplings. In contrast with the simplified models of Section 5.3.2, this model provides all the 23-breaking VEVs at the same scale, plus a larger 12-breaking VEV, following a mild hierarchy given by $v_{23}/v_{12} \sim \lambda$. This way, the symmetry breaking of

the $U(1)_Y^3$ gauge group proceeds just like in Eq. (5.3), as desired.

Having fixed all the hyperon VEVs with respect to Λ, now we are able to write the full mass matrices for each sector in terms of the Wolfenstein parameter λ,

$$\mathcal{L} = (u_1 \quad u_2 \quad u_3) \begin{pmatrix} \lambda^6 & \lambda^4 & \lambda^3 \\ \lambda^7 & \lambda^3 & \lambda^2 \\ \lambda^9 & \lambda^5 & 1 \end{pmatrix} \begin{pmatrix} u_1^c \\ u_2^c \\ u_3^c \end{pmatrix} \frac{v_{\rm SM}}{\sqrt{2}} \tag{5.27}$$

$$+ (d_1 \quad d_2 \quad d_3) \begin{pmatrix} \lambda^6 & \lambda^4 & \lambda^3 \\ \lambda^5 & \lambda^3 & \lambda^2 \\ \lambda^6 & \lambda^4 & 1 \end{pmatrix} \begin{pmatrix} d_1^c \\ d_2^c \\ d_3^c \end{pmatrix} \lambda^2 \frac{v_{\rm SM}}{\sqrt{2}} \tag{5.28}$$

$$+ (e_1 \quad e_2 \quad e_3) \begin{pmatrix} \lambda^6 & \lambda^6 & \lambda^6 \\ \lambda^9 & \lambda^3 & \lambda^3 \\ \lambda^{12} & \lambda^6 & 1 \end{pmatrix} \begin{pmatrix} e_1^c \\ e_2^c \\ e_3^c \end{pmatrix} \lambda^2 \frac{v_{\rm SM}}{\sqrt{2}} + \text{h.c.} \tag{5.29}$$

We can see that this setup provides a reasonable description of charged fermion masses and mixing. Although the up and down-quark masses are slightly off by $\mathcal{O}(\lambda)$ factors, we remember that we are only assuming one universal cut-off scale Λ, while in realistic models several scales Λ may be associated to different messengers in the UV theory, further improving the fit of first family quark masses, as discussed in Section 5.3.2. All things considered, the description of fermion masses seems very efficient, considering the limitations of our EFT framework.

However, the model does not predict the alignment of V_{us}. Moreover, we also notice that right-handed $s-d$ mixing is just mildly suppressed as $s_{12}^{d_R} \simeq \mathcal{O}(\lambda^2)$ in this model. Given the stringent bounds over left-right scalar operators contributing to $K-\bar{K}$ meson mixing [238,239] (which might arise in this kind of models as we shall see in Section 5.6), the scale v_{12} can be pushed far above the TeV if V_{us} originates from the down sector. From a phenomenological point of view, it would be interesting to find models which give clear predictions about the alignment of V_{us}, and ideally provide a more efficient suppression of right-handed quark mixing. We shall see in the next subsection that this can be achieved by minimally extending the set of hyperons of this model.

5.3.4 Model 2: Five hyperons for a more predictive setup

Model 1 proposed in the previous subsection, despite its simplicity and minimality, does not give clear predictions about the alignment of the CKM matrix. Heavy Z' bosons arising from the symmetry breaking of $U(1)_Y^3$ have the potential to mediate contributions to $K-\bar{K}$ meson mixing, which could set a lower bound over the scale of $U(1)_Y^3$-breaking, but such contributions depend on the alignment of V_{us}. Moreover, the largest contributions to $K-\bar{K}$ mixing depend both on the alignment of V_{us} and on right-handed $s-d$ mixing, which is just mildly suppressed in Model 1. Therefore, we propose here a similar model with slightly extended hyperon content that can account for a clear prediction about the alignment of V_{us}, plus a more efficient suppression of

right-handed fermion mixing. We consider here the hyperons

$$\phi_{\ell 23}^{(0,\frac{1}{2},-\frac{1}{2})}, \qquad \phi_{q23}^{(0,-\frac{1}{6},\frac{1}{6})}, \qquad \phi_{q13}^{(-\frac{1}{6},0,\frac{1}{6})}, \qquad \phi_{d12}^{(-\frac{1}{6},-\frac{1}{3},\frac{1}{2})}, \qquad \phi_{e12}^{(\frac{1}{4},-\frac{1}{4},0)}. \tag{5.30}$$

With this set of hyperons, the effective Yukawa couplings in the EFT are (suppressing as usual powers of Λ and dimensionless couplings)

$$\mathcal{L} = (Q_1 \quad Q_2 \quad Q_3) \begin{pmatrix} \phi_{e12}^2 \tilde{\phi}_{\ell 23} & \phi_{q13}\tilde{\phi}_{q23}\phi_{\ell 23} & \phi_{q13} \\ \phi_{e12}^2 \tilde{\phi}_{q13}\phi_{q23}\phi_{\ell 23} & \phi_{\ell 23} & \phi_{q23} \\ \phi_{e12}^2 \tilde{\phi}_{q13}\phi_{\ell 23} & \phi_{\ell 23}\tilde{\phi}_{q23} & 1 \end{pmatrix} \begin{pmatrix} u_1^c \\ u_2^c \\ u_3^c \end{pmatrix} H_u \tag{5.31}$$

$$+ (Q_1 \quad Q_2 \quad Q_3) \begin{pmatrix} \phi_{e12}^2 \tilde{\phi}_{\ell 23} & \phi_{d12} & \phi_{q13} \\ \phi_{q13}^2 \phi_{q23} & \tilde{\phi}_{\ell 23} & \phi_{q23} \\ \phi_{q13}^2 & \phi_{q23}^2 & 1 \end{pmatrix} \begin{pmatrix} d_1^c \\ d_2^c \\ d_3^c \end{pmatrix} H_d \tag{5.32}$$

$$+ (L_1 \quad L_2 \quad L_3) \begin{pmatrix} \tilde{\phi}_{e12}^2 \tilde{\phi}_{\ell 23} & \phi_{e12}^2 \tilde{\phi}_{\ell 23} & \phi_{e12}^2 \phi_{\ell 23} \\ \tilde{\phi}_{e12}^4 \tilde{\phi}_{\ell 23} & \tilde{\phi}_{\ell 23} & \phi_{\ell 23} \\ \tilde{\phi}_{e12}^4 \tilde{\phi}_{\ell 23}^2 & \tilde{\phi}_{\ell 23}^2 & 1 \end{pmatrix} \begin{pmatrix} e_1^c \\ e_2^c \\ e_3^c \end{pmatrix} H_d + \text{h.c.} \tag{5.33}$$

Following the same approach as with Model 1, we assign the following powers of λ to the VEV over Λ ratios in order to reproduce fermion masses and CKM mixing,

$$\frac{\langle \phi_{\ell 23} \rangle}{\Lambda} = \frac{\langle \phi_{q13} \rangle}{\Lambda} \simeq \lambda^3 , \quad \frac{\langle \phi_{q23} \rangle}{\Lambda} \simeq \lambda^2 , \quad \frac{\langle \phi_{d12} \rangle}{\Lambda} \simeq \lambda^4 , \quad \frac{\langle \phi_{e12} \rangle}{\Lambda} \simeq \lambda . \tag{5.34}$$

Although it would seem that in this scenario there exists a mild hierarchy between 23-breaking VEVs of $\mathcal{O}(\lambda^2)$, since ϕ_{d12} only appears in the 12 entry of the down matrix, it would be very reasonable that the dimensionless coupling in that entry provides a factor λ suppression, such that all 23-breaking VEVs live at the same scale. The largest VEV is still the 12-breaking one, which is now associated to the hyperon ϕ_{e12}, and the mild hierarchy between scales remains as $v_{12}/v_{23} \simeq \lambda$. With these assignments of VEVs over Λ ratios, the Yukawa textures are given by

$$\mathcal{L} = (u_1 \quad u_2 \quad u_3) \begin{pmatrix} \lambda^5 & \lambda^8 & \lambda^3 \\ \lambda^{10} & \lambda^3 & \lambda^2 \\ \lambda^7 & \lambda^5 & 1 \end{pmatrix} \begin{pmatrix} u_1^c \\ u_2^c \\ u_3^c \end{pmatrix} \frac{v_{\text{SM}}}{\sqrt{2}} \tag{5.35}$$

$$+ (d_1 \quad d_2 \quad d_3) \begin{pmatrix} \lambda^5 & \lambda^4 & \lambda^3 \\ \lambda^8 & \lambda^3 & \lambda^2 \\ \lambda^6 & \lambda^4 & 1 \end{pmatrix} \begin{pmatrix} d_1^c \\ d_2^c \\ d_3^c \end{pmatrix} \lambda^2 \frac{v_{\text{SM}}}{\sqrt{2}} \tag{5.36}$$

$$+ (e_1 \quad e_2 \quad e_3) \begin{pmatrix} \lambda^5 & \lambda^5 & \lambda^5 \\ \lambda^7 & \lambda^3 & \lambda^3 \\ \lambda^{10} & \lambda^6 & 1 \end{pmatrix} \begin{pmatrix} e_1^c \\ e_2^c \\ e_3^c \end{pmatrix} \lambda^2 \frac{v_{\text{SM}}}{\sqrt{2}} + \text{h.c.} \tag{5.37}$$

Just like in Model 1, this model provides a compelling description of all charged fermion masses and mixing. Notice that this scenario provides a very efficient suppression of right-handed fermion mixing. Moreover, it is clear that here V_{us} mixing originates from the down sector, providing a more predictive setup than Model 1, which will be useful for phenomenological purposes as discussed in Section 5.6.

Finally we comment that the Higgs doublets and hyperons can mediate FCNCs such as $K-\bar{K}$ mixing. In the present model, this may arise from tree-level exchange of ϕ_{d12} hyperons which can mediate down-strange transitions. Such a coupling originates from $Q_1\phi_{d12}d_2^c H_d/\Lambda$ which will lead to a suppressed down-strange coupling of order $\lambda^2 v_{\rm SM}/\Lambda \approx 10^{-5}$ (taking $\Lambda \approx 100$ TeV as expected if $v_{23} \approx \mathcal{O}(\text{TeV})$). Assuming the mass of the hyperons to be at the scale v_{23}, then we expect these FCNCs to be under control. Since we assume a type II 2HDM, tree-level Higgs doublets exchange contributions are forbidden, and FCNCs mediated by the Higgs doublets can only proceed via their mixing with hyperons, carrying therefore an extra suppression via the mixing angle, along with the suppression of hyperon couplings already discussed. In more general models of this kind, such contributions to $K-\bar{K}$ mixing could be even further suppressed depending on the order of the operator and the alignment of V_{us}, and in all generality we expect all hyperon couplings to be suppressed by at least a factor $v_{\rm SM}/\Lambda \approx 10^{-3}$. A more detailed study of the phenomenology of the scalar sector in this general class of models is beyond the scope of this chapter.

5.4 Neutrino masses and mixing

5.4.1 General considerations and spurion formalism

The origin of neutrino masses and mixing requires a dedicated analysis due to their particular properties. We start by introducing $U(2)^5$-breaking spurions (carrying inverse of mass dimension) for the Weinberg operator

$$\mathcal{L}_{\rm Weinberg} = (L_1 \quad L_2 \quad L_3) \begin{pmatrix} \Phi(1,0,-1) & \Phi(\frac{1}{2},\frac{1}{2},-1) & \Phi(\frac{1}{2},0,-\frac{1}{2}) \\ \Phi(\frac{1}{2},\frac{1}{2},-1) & \Phi(0,1,-1) & \Phi(0,\frac{1}{2},-\frac{1}{2}) \\ \Phi(\frac{1}{2},0,-\frac{1}{2}) & \Phi(0,\frac{1}{2},-\frac{1}{2}) & 1 \end{pmatrix} \begin{pmatrix} L_1 \\ L_2 \\ L_3 \end{pmatrix} H_u H_u \,, \tag{5.38}$$

which reveals that, as expected, the $U(2)^5$ approximate symmetry is naively present in the neutrino sector as well. As a consequence, one generally expects one neutrino to be much heavier than the others, displaying tiny mixing with the other neutrino flavours. In the spirit of the type I seesaw mechanism, one could think of adding a $U(1)_Y^3$ singlet neutrino as $N(0,0,0)$. Such a singlet neutrino can only couple to the third family active neutrino at renormalisable level, i.e. $\mathcal{L}_N \supset L_3 H_u N + m_N NN$, where all fermion fields are written in a left-handed 2-component convention. This way, the coupling $L_2 H_u N$, which is required for large atmospheric neutrino mixing, can only arise at the non-renormalisable level. Therefore, it is expected to be suppressed with respect to $L_3 H_u N$. This seems to be inconsistent with large atmospheric neutrino mixing, at least within the validity of our EFT framework. As anticipated before, this is a consequence of the accidental $U(2)^5$ flavour symmetry delivered by the TH model.

Given such general considerations, we conclude that in order to obtain neutrino masses and mixing from the type I seesaw mechanism, it is required to add SM singlet neutrinos that carry tri-hypercharges (but whose hypercharges add up to zero).

These neutrinos will allow to introduce $U(2)^5$-breaking operators similar for all neutrino flavours, providing a mechanism to obtain the adequate neutrino mixing in a natural way. In order to cancel gauge anomalies, the most simple option is that these singlet neutrinos are vector-like. In the following subsection we include an example of successful type I seesaw mechanism based on this idea.

5.4.2 Example of successful neutrino mixing from the seesaw mechanism

In the following, we provide an example scenario which reproduces the observed pattern of neutrino mixing, as a proof of principle. According to the discussion in the previous subsection, in order to implement a type I seesaw mechanism that delivers large neutrino mixing, we need to add vector-like neutrinos that carry tri-hypercharges (but whose hypercharges add up to zero). We also need to introduce hyperons that will provide small Dirac mass terms for the active neutrinos in the form of non-renormalisable operators. Under these considerations, we start by adding the following vector-like neutrino[5] and hyperon

$$N_{\rm atm}^{(0,\frac{1}{4},-\frac{1}{4})}\,, \qquad \overline{N}_{\rm atm}^{(0,-\frac{1}{4},\frac{1}{4})}\,, \qquad \phi_{\rm atm}^{(0,\frac{1}{4},-\frac{1}{4})}\,, \tag{5.39}$$

where the charge assignments are chosen to provide large *atmospheric neutrino mixing*. This way, we can write the following non-renormalisable operators along with the Majorana and vector-like masses of $N_{\rm atm}$,

$$\begin{aligned}\mathcal{L}_{N_{\rm atm}} \supset & \frac{1}{\Lambda_{\rm atm}}(\phi_{\rm atm}L_2+\tilde{\phi}_{\rm atm}L_3)H_u N_{\rm atm}+\frac{\phi_{\rm atm}}{\Lambda_{\rm atm}}L_3H_u\overline{N}_{\rm atm} \\ & +\phi_{\ell 23}N_{\rm atm}N_{\rm atm}+\tilde{\phi}_{\ell 23}\overline{N}_{\rm atm}\overline{N}_{\rm atm}+M_{N_{\rm atm}}\overline{N}_{\rm atm}N_{\rm atm}\,,\end{aligned} \tag{5.40}$$

where we have ignored the $\mathcal{O}(1)$ dimensionless couplings, and the hyperon $\phi_{\ell 23}^{(0,\frac{1}{2},-\frac{1}{2})}$ is already present in both Model 1 and Model 2 for the charged fermion sector. Notice that $N_{\rm atm}$ provides the couplings $\mathcal{L}_{N_{\rm atm}} \supset L_3H_uN_{\rm atm}+L_2H_uN_{\rm atm}$, as required to explain atmospheric mixing. Notice also that the conjugate neutrino $\overline{N}_{\rm atm}$ unavoidably couples to L_3 as $\phi_{\rm atm}L_3H_u\overline{N}_{\rm atm}$, but not to L_2 because we have not included any hyperon providing this dimension-5 operator.

In a similar spirit, we introduce another vector-like neutrino and other hyperons in order to obtain large *solar neutrino mixing*

$$N_{\rm sol}^{(\frac{1}{4},\frac{1}{4},-\frac{1}{2})}\,, \qquad \overline{N}_{\rm sol}^{(-\frac{1}{4},-\frac{1}{4},\frac{1}{2})}\,, \qquad \phi_{\rm sol}^{(-\frac{1}{2},-\frac{1}{2},1)}, \qquad \phi_{\nu 13}^{(-\frac{1}{4},-\frac{1}{4},\frac{1}{2})}\,, \tag{5.41}$$

which provide the following non-renormalisable operators and mass terms,

$$\mathcal{L}_{N_{\rm sol}} \supset \frac{1}{\Lambda_{\rm sol}}(\phi_{e12}L_1+\tilde{\phi}_{e12}L_2+\phi_{\nu 13}L_3)H_uN_{\rm sol}+\frac{\phi_{\nu 13}}{\Lambda_{\rm sol}}L_3H_u\overline{N}_{\rm sol} \tag{5.42}$$

[5] We remind the reader that in our convention, all fermion fields including $N_{\rm atm}$ and $\overline{N}_{\rm atm}$ are left-handed, see Appendix A.

$$+\,\phi_{\rm sol}N_{\rm sol}N_{\rm sol}+\tilde{\phi}_{\rm sol}\overline{N}_{\rm sol}\overline{N}_{\rm sol}+M_{N_{\rm sol}}\overline{N}_{\rm sol}N_{\rm sol}\,,$$

where we have ignored again the $\mathcal{O}(1)$ dimensionless couplings, and the hyperon $\phi_{e12}^{(\frac{1}{2},-\frac{1}{2},0)}$ is already present in Model 2 for the charged fermion sector. The hyperon $\phi_{\nu 13}$ (which will eventually populate the (1,3) entry of the effective neutrino mass matrix) is not required to obtain non-zero reactor mixing, which would already arise from the other operators, but it is required in order to have enough free parameters to fit all observed neutrino mixing angles and mass splittings. We could have included the $U(1)_Y^3$ singlet neutrino $N(0,0,0)$, but as discussed in the previous subsection, its contributions to the Weinberg operator may be suppressed by its large Majorana mass m_N, resulting in possibly negligible contributions to the seesaw mechanism. We are therefore free to assume that such a neutrino $N(0,0,0)$, if exists, is in any case decoupled from the seesaw, while the atmospheric and solar SM singlet neutrinos $N_{\rm atm}$ and $N_{\rm sol}$ could yield dominant and subdominant contributions, resulting in a natural normal neutrino mass hierarchy as in sequential dominance [354, 355, 379].

Notice that the vector-like neutrinos $N_{\rm atm}$ and $N_{\rm sol}$ get contributions to their masses from the VEVs of the hyperons $\phi_{\ell 23}$ and $\phi_{\rm sol}$, respectively, which we denote generically as v_{23} since they both take part in the 23-breaking step of Eq. (5.3). In addition, $N_{\rm atm}$ and $N_{\rm sol}$ get contributions to their masses from the unspecified vector-like mass terms, that we generically denote as $M_{\rm VL}$. Now we arrange all the couplings of the neutrino sector into Dirac-type mass matrices and Majorana-type mass matrices, i.e.

$$m_{D_L}=\begin{pmatrix} & \overline{N}_{\rm sol} & \overline{N}_{\rm atm} \\ L_1| & 0 & 0 \\ L_2| & 0 & 0 \\ L_3| & \frac{\tilde{\phi}_{\nu 13}}{\Lambda_{\rm sol}} & \frac{\phi_{\rm atm}}{\Lambda_{\rm atm}} \end{pmatrix} H_u\,, \qquad m_{D_R}=\begin{pmatrix} & N_{\rm sol} & N_{\rm atm} \\ L_1| & \frac{\phi_{e12}}{\Lambda_{\rm sol}} & 0 \\ L_2| & \frac{\tilde{\phi}_{e12}}{\Lambda_{\rm sol}} & \frac{\phi_{\rm atm}}{\Lambda_{\rm atm}} \\ L_3| & \frac{\phi_{\nu 13}}{\Lambda_{\rm sol}} & \frac{\tilde{\phi}_{\rm atm}}{\Lambda_{\rm atm}} \end{pmatrix} H_u\,, \tag{5.43}$$

$$M_L=\begin{pmatrix} & \overline{N}_{\rm sol} & \overline{N}_{\rm atm} \\ \overline{N}_{\rm sol}| & \tilde{\phi}_{\rm sol} & 0 \\ \overline{N}_{\rm atm}| & 0 & \tilde{\phi}_{\ell 23} \end{pmatrix} \approx v_{23}\mathbb{I}_{2\times 2}\,, \quad M_R\approx \begin{pmatrix} & N_{\rm sol} & N_{\rm atm} \\ N_{\rm sol}| & \phi_{\rm sol} & 0 \\ N_{\rm atm}| & 0 & \phi_{\ell 23} \end{pmatrix} \approx v_{23}\mathbb{I}_{2\times 2}\,, \tag{5.44}$$

$$M_{LR}=\begin{pmatrix} & N_{\rm sol} & N_{\rm atm} \\ \overline{N}_{\rm sol}| & M_{N_{\rm sol}} & 0 \\ \overline{N}_{\rm atm}| & 0 & M_{N_{\rm atm}} \end{pmatrix} \approx M_{\rm VL}\mathbb{I}_{2\times 2}\,, \tag{5.45}$$

where $\mathbb{I}_{2\times 2}$ is the 2×2 identity matrix and we have ignored $\mathcal{O}(1)$ dimensionless couplings. In Eqs. (5.44) and (5.45) above, we have considered the following approximations and assumptions:

- We have neglected $\mathcal{O}(1)$ dimensionless couplings generally present for each non-zero entry of Eq. (5.44). With this consideration, we find $M_L = M_R$ after the

hyperons develop their VEVs. Furthermore, since the two hyperons appearing in M_L and M_R participate in the 23-breaking step of Eq. (5.3), we have assumed that they both develop a similar VEV $\langle\phi_{\ell 23}\rangle \approx \langle\phi_{\rm sol}\rangle \approx \mathcal{O}(v_{23})$. For simplicity we take them to be equal, although the same conclusions hold as long as they just differ by $\mathcal{O}(1)$ factors, as naturally expected.

- For simplicity, we have assumed a similar vector-like mass for both neutrinos in Eq. (5.45), i.e. $M_{N_{\rm sol}} \approx M_{N_{\rm atm}} \equiv M_{\rm VL}$.

With these definitions, the full mass matrix of the neutrino sector M_ν can be written in a compact form as

$$M_\nu = \begin{pmatrix} & \nu & \overline{N} & N \\ \hline \nu\big| & 0 & m_{D_L} & m_{D_R} \\ \overline{N}\big| & m_{D_L}^{\rm T} & M_L & M_{LR} \\ N\big| & m_{D_R}^{\rm T} & M_{LR}^{\rm T} & M_R \end{pmatrix} \equiv \begin{pmatrix} 0 & m_D \\ m_D^{\rm T} & M_N \end{pmatrix}, \tag{5.46}$$

where we have defined ν as a 3-component vector containing the weak eigenstates of active neutrinos, while N and $\overline{N}$ are 2-component vectors containing the SM singlet neutrinos $N_{\rm atm}$, $N_{\rm sol}$ and conjugate neutrinos $\overline{N}_{\rm atm}$,$\overline{N}_{\rm sol}$, respectively. Dirac-type masses in $m_{D_{L,R}}$ may be orders of magnitude samller than the electroweak scale, because they arise from non-renormalisable operators proportional to the SM VEV. In contrast, the eigenvalues of M_N are not smaller than $\mathcal{O}(v_{23})$, which is at least TeV. Therefore, the condition $m_D \ll M_N$ is fulfilled in Eq. (5.46) and we can safely apply the seesaw formula as

$$\begin{aligned} m_\nu &= m_D M_N^{-1} m_D^{\rm T} \\ &= \begin{pmatrix} m_{D_L} & m_{D_R} \end{pmatrix} \begin{pmatrix} v_{23} & -M_{\rm VL} \\ -M_{\rm VL} & v_{23} \end{pmatrix} \begin{pmatrix} m_{D_L}^{\rm T} \\ m_{D_R}^{\rm T} \end{pmatrix} \frac{1}{v_{23}^2 - M_{\rm VL}^2} \\ &= \left[m_{D_L} m_{D_L}^{\rm T} v_{23} - m_{D_L} m_{D_R}^{\rm T} M_{\rm VL} - m_{D_R} m_{D_L}^{\rm T} M_{\rm VL} + m_{D_R} m_{D_R}^{\rm T} v_{23} \right] \frac{1}{v_{23}^2 - M_{\rm VL}^2} \,. \end{aligned} \tag{5.47}$$

Given the structure of m_{D_L} and m_{D_R} in Eq. (5.43), the products above involving m_{D_L} lead to a hierarchical m_ν matrix where only the entries in the third row and column are populated and the others are zero. In contrast, the product $m_{D_R} m_{D_R}^{\rm T}$ provides a matrix m_ν where all entries are populated. Therefore, if $M_{\rm VL} \gg v_{23}$, then the effective neutrino matrix becomes hierarchical, rendering impossible to explain the observed pattern of neutrino mixing and mass splittings with $\mathcal{O}(1)$ parameters. Instead, if $M_{\rm VL}$ is of the same order or smaller than v_{23}, i.e. $M_{\rm VL} \lesssim v_{23}$, then the resulting matrix is in any case a matrix where all entries are populated, which has the potential to explain the observed patterns of neutrino mixing.

This argument holds as long as m_{D_L} is populated by zeros in at least some of the entries involving L_1 and L_2, like in our example model. Instead, in the very particular case where both m_{D_L} and m_{D_R} are similarly populated matrices and of the same order,

then the terms proportional to $M_{\rm VL}$ in Eq. (5.47) can provide an effective neutrino mass matrix where all entries are populated. In this case, $M_{\rm VL} > v_{23}$ is possible. Nevertheless, even in this scenario we expect $M_{\rm VL}$ not to be very large, since the smallness of m_{D_L} and m_{D_R} (that arise from non-renormalisable operators) may potentially provides most of the suppression for the small neutrino masses. Furthermore, this scenario involves the addition of several extra hyperons with very particular charges, making the model more complicated, so we do not consider it.

Given the above considerations, we proceed the calculation by expanding the term $m_{D_R} m_{D_R}^{\rm T} v_{23}$ in Eq. (5.47)

$$\begin{aligned} m_\nu &\simeq m_{D_R} m_{D_R}^{\rm T} v_{23} \\ &= \begin{pmatrix} \frac{\phi_{e12}^2}{\Lambda_{\rm sol}^2} & \frac{\phi_{e12}\tilde{\phi}_{e12}}{\Lambda_{\rm sol}^2} & \frac{\phi_{e12}\phi_{\nu 13}}{\Lambda_{\rm sol}^2} \\ \frac{\phi_{e12}\tilde{\phi}_{e12}}{\Lambda_{\rm sol}^2} & \frac{\phi_{\rm atm}^2}{\Lambda_{\rm atm}^2} + \frac{\tilde{\phi}_{e12}^2}{\Lambda_{\rm sol}^2} & \frac{\phi_{\rm atm}\tilde{\phi}_{\rm atm}}{\Lambda_{\rm atm}^2} + \frac{\tilde{\phi}_{e12}\phi_{\nu 13}}{\Lambda_{\rm sol}^2} \\ \frac{\phi_{e12}\phi_{\nu 13}}{\Lambda_{\rm sol}^2} & \frac{\phi_{\rm atm}\tilde{\phi}_{\rm atm}}{\Lambda_{\rm atm}^2} + \frac{\tilde{\phi}_{e12}\phi_{\nu 13}}{\Lambda_{\rm sol}^2} & \frac{\phi_{\rm atm}^2}{\Lambda_{\rm atm}^2} + \frac{\phi_{\nu 13}^2}{\Lambda_{\rm sol}^2} \end{pmatrix} \frac{H_u H_u}{v_{23}} \,. \end{aligned} \tag{5.48}$$

Given the symmetry breaking pattern of the model shown in Eq. (5.3), we take $\langle \phi_{e12} \rangle \simeq \mathcal{O}(v_{12})$ and $\langle \phi_{\nu 13} \rangle \approx \langle \phi_{\ell 23} \rangle \approx \langle \phi_{\rm atm} \rangle \approx \langle \phi_{\rm sol} \rangle \approx \mathcal{O}(v_{23})$[6]. Motivated by our discussion of the charged fermion sector (see Section 5.3), we consider the relation $v_{23}/v_{12} \simeq \lambda$. By inserting such VEVs, we obtain

$$m_\nu \simeq \begin{pmatrix} 0 & 0 & 0 \\ 0 & 1 & 1 \\ 0 & 1 & 1 \end{pmatrix} v_{23} \frac{H_u H_u}{\Lambda_{\rm atm}^2} + \begin{pmatrix} 1 & 1 & \lambda \\ 1 & 1 & \lambda \\ \lambda & \lambda & \lambda^2 \end{pmatrix} v_{23} \frac{H_u H_u}{\lambda^2 \Lambda_{\rm sol}^2} \,. \tag{5.49}$$

If $\Lambda_{\rm sol} = \Lambda_{\rm atm}$, we observe that there exists a mild hierarchy of order λ^2 between the 12 and 23 sectors in the matrix above. Considering the dimensionless coefficients that we have ignored so far, the numerical diagonalisation of m_ν would require some parameters of $\mathcal{O}(0.01)$ in order to explain the observed neutrino mixing angles and mass splittings [62, 65]. The situation can be improved if we assume a mild hierarchy between cut-off scales $\Lambda_{\rm atm}/\Lambda_{\rm sol} \simeq \lambda$, obtaining to leading order for each entry (ignoring dimensionless coefficients),

$$m_\nu \simeq \begin{pmatrix} 1 & 1 & \lambda \\ 1 & 1 & 1 \\ \lambda & 1 & 1 \end{pmatrix} v_{23} \frac{v_{\rm SM}^2}{\Lambda_{\rm atm}^2} \,, \tag{5.50}$$

where we have introduced the SM VEV as $\langle H_u \rangle = v_{\rm SM}$ (ignoring the factor $1/\sqrt{2}$). Considering now the dimensionless coefficients in the matrix above, we find that numerical diagonalisation can accommodate all the observed neutrino mixing angles and mass splittings [62, 65] with $\mathcal{O}(1)$ parameters, and we are able to reproduce both normal and inverted ordered scenarios.

[6] In the calculations that follow, we assume for simplicity that these VEVs are equal. However, the same conclusions hold as long as the VEVs vary by $\mathcal{O}(1)$ factors, which is the natural expectation.

Notice that we have been driven to a scenario where the vector-like neutrinos get Majorana masses from the VEVs of hyperons in the model. Furthermore, the vector-like masses necessarily have to be of the same or smaller order than the VEVs of the hyperons in order to explain the observed pattern of neutrino mixing. Therefore, in the particular example included in this section, the vector-like neutrinos get a mass at the scale v_{23} of the 23-breaking step in Eq. (5.3), which could happen at a relatively low scale as we shall see in Section 5.6. As a consequence, the vector-like neutrinos involved in the seesaw mechanism are expected to be relatively light, and the high energy cut-offs of the EFT $\Lambda_{\rm atm}$ and $\Lambda_{\rm sol}$ are expected to provide most the suppression of light neutrino masses. We conclude that, due to the $U(2)^5$ flavour symmetry provided by the TH model, we have been driven to a low scale seesaw in order to predict the observed pattern of neutrino mixing.

5.5 Symmetry breaking and gauge mixing

We are assuming that the symmetry breaking of the tri-hypercharge gauge group down to the SM follows the following pattern

$$\begin{aligned} & SU(3)_c \times SU(2)_L \times U(1)_{Y_1} \times U(1)_{Y_2} \times U(1)_{Y_3} \\ & \overset{v_{12}}{\to} SU(3)_c \times SU(2)_L \times U(1)_{Y_1+Y_2} \times U(1)_{Y_3} \qquad (5.51) \\ & \overset{v_{23}}{\to} SU(3)_c \times SU(2)_L \times U(1)_{Y_1+Y_2+Y_3} \\ & \overset{v_{\rm SM}}{\to} SU(3)_c \times U(1)_Q \,. \qquad (5.52) \end{aligned}$$

Therefore, first and second hypercharges are broken at a high scale down to the diagonal subgroup, and then the remaining factors $U(1)_{Y_1+Y_2} \times U(1)_{Y_3}$ are broken down to SM hypercharge. In this process, heavy Z' bosons arise, with their masses connected to the different scales of symmetry breaking. Given that the tri-hypercharge gauge group is based on a family decomposition of SM hypercharge, the heavy Z' bosons can potentially mix with the SM Z boson, even if kinetic mixing is absent. This mixing breaks custodial symmetry, having significant phenomenological implications if the NP scales are not very heavy. Therefore, in the next subsections we study the several steps of symmetry breaking, including electroweak symmetry breaking, and extract the masses of the massive neutral gauge bosons that arise in this process.

5.5.1 High scale symmetry breaking

Assuming that the 12-breaking scale is far above the electroweak scale, at very high energies we consider only the factors $U(1)_{Y_1} \times U(1)_{Y_2}$ with renormalisable Lagrangian

(neglecting fermion content and any kinetic mixing[7] for simplicity),

$$\mathcal{L} = -\frac{1}{4}F^{(1)}_{\mu\nu}F^{\mu\nu(1)} - \frac{1}{4}F^{(2)}_{\mu\nu}F^{\mu\nu(2)} + (D_\mu\phi_{12})^* D^\mu\phi_{12} - V(\phi_{12})\,, \tag{5.53}$$

where for simplicity we assume only one hyperon $\phi_{12}(q,-q)$, which develops a VEV $\langle\phi_{12}\rangle = v_{12}/\sqrt{2}$ spontaneously breaking $U(1)_{Y_1}\times U(1)_{Y_2}$ down to its diagonal subgroup. The covariant derivative reads

$$D_\mu = \partial_\mu - ig_1Y_1B_{1\mu} - ig_2Y_2B_{2\mu}\,. \tag{5.54}$$

Expanding the kinetic term of ϕ_{12}, we obtain mass terms for the gauge bosons as

$$\mathcal{M}^2 = \frac{q^2v_{12}^2}{2}\begin{pmatrix} & B_1^\mu & B_2^\mu \\ B_{1\mu}| & g_1^2 & -g_1g_2 \\ B_{2\mu}| & -g_1g_2 & g_2^2 \end{pmatrix}. \tag{5.55}$$

The diagonalisation of the matrix above reveals

$$\hat{\mathcal{M}}^2 = \frac{q^2v_{12}^2}{2}\begin{pmatrix} & Y_{12}^\mu & Z'^\mu_{12} \\ Y_{12\mu}| & 0 & 0 \\ Z'_{12\mu}| & 0 & g_1^2+g_2^2 \end{pmatrix}, \tag{5.56}$$

in the basis of mass eigenstates given by

$$\begin{pmatrix} Y_{12\mu} \\ Z'_{12\mu} \end{pmatrix} = \begin{pmatrix} \cos\theta_{12} & \sin\theta_{12} \\ -\sin\theta_{12} & \cos\theta_{12} \end{pmatrix}\begin{pmatrix} B_{1\mu} \\ B_{2\mu} \end{pmatrix}, \qquad \sin\theta_{12} = \frac{g_1}{\sqrt{g_1^2+g_2^2}}\,. \tag{5.57}$$

Therefore, we obtain a massive gauge boson $Z'_{12\mu}$ at the scale v_{12}, while Y_1+Y_2 associated to the gauge boson $Y_{12\mu}$ remains unbroken. These results are trivially generalised for the case of more hyperons. The covariant derivative in the new basis is given by

$$\begin{aligned} D_\mu &= \partial_\mu - i\frac{g_1g_2}{\sqrt{g_1^2+g_2^2}}(Y_1+Y_2)Y_{12\mu} - i\left(-\frac{g_1^2}{\sqrt{g_1^2+g_2^2}}Y_1 + \frac{g_2^2}{\sqrt{g_1^2+g^2}}Y_2\right)Z'_{12\mu} \\ &= \partial_\mu - ig_{12}(Y_1+Y_2)Y_{12\mu} - i\left(-g_1\sin\theta_{12}Y_1 + g_2\cos\theta_{12}Y_2\right)Z'_{12\mu}\,. \end{aligned} \tag{5.58}$$

The fermion couplings in Eq. (5.86) are readily extracted by expanding the fermion kinetic terms applying Eq. (5.58).

5.5.2 Low scale symmetry breaking

The renormalisable Lagrangian of a theory $SU(2)_L\times U(1)_{Y_1+Y_2}\times U(1)_{Y_3}$ with $H(\mathbf{2})_{(0,\frac{1}{2})}$ and $\phi_{23}(\mathbf{1})_{(q,-q)}$ reads (neglecting fermion content and kinetic mixing, although we will

[7] Considering kinetic mixing in the Lagrangian of Eq. (5.53) only leads to a redefinition of either the g_1 or g_2 couplings in the canonical basis (where the kinetic terms are diagonal).

consider the effect of kinetic mixing at the end of the section),

$$\begin{aligned}\mathcal{L}_{\text{ren}} = &-\frac{1}{4}F^{(12)}_{\mu\nu}F^{\mu\nu(12)} - \frac{1}{4}F^{(3)}_{\mu\nu}F^{\mu\nu(3)} - \frac{1}{4}W^a_{\mu\nu}W^{\mu\nu}_a \\ &+ (D_\mu H)^\dagger D^\mu H + (D_\mu \phi_{23})^* D^\mu \phi_{23} \\ &- V(H, \phi_{23})\,,\end{aligned} \tag{5.59}$$

where the covariant derivatives read

$$D_\mu H = (\partial_\mu - i g_L \frac{\sigma^a}{2} W^a_\mu - i\frac{g_3}{2} B_{3\mu}) H\,, \tag{5.60}$$

$$D_\mu \phi_{23} = (\partial_\mu - i g_{12} q B_{12\mu} + i g_3 q B_{3\mu})\phi_{23}\,, \tag{5.61}$$

and σ^a with $a = 1, 2, 3$ are the Pauli matrices. The Higgs doublet develops the usual electroweak symmetry breaking VEV as

$$\langle H \rangle = \frac{1}{\sqrt{2}} \begin{pmatrix} 0 \\ v_{\text{SM}} \end{pmatrix}\,, \tag{5.62}$$

while the hyperon develops a higher scale VEV as

$$\langle \phi_{23} \rangle = \frac{v_{23}}{\sqrt{2}}\,, \tag{5.63}$$

which spontaneously breaks the group $U(1)_{Y_1+Y_2} \times U(1)_{Y_3}$ down to its diagonal subgroup.

Expanding the following kinetic terms with the expressions of the covariant derivatives of Eqs. (5.60) and (5.61), we obtain

$$\begin{aligned}&(D_\mu H)^\dagger D^\mu H + (D_\mu \phi_{23})^* D^\mu \phi_{23} \\ &= \frac{v^2_{\text{SM}} g^2_L}{4} W_\mu W^{\mu\dagger} + \frac{q^2 v^2_{23}}{2} \left(\begin{array}{c|ccc} & W^\mu_3 & B^\mu_{12} & B^\mu_3 \\ \hline W_{3\mu}| & g^2_L r^2 & 0 & -g_L g_3 r^2 \\ B_{12\mu}| & 0 & g^2_{12} & -g_{12} g_3 \\ B_{3\mu}| & -g_L g_3 r^2 & -g_{12} g_3 & g^2_3 + g^2_3 r^2 \end{array}\right),\end{aligned} \tag{5.64}$$

where $r = \frac{v_{\text{SM}}}{2 q v_{23}} \ll 1$, we have defined $W_\mu = (W^1_\mu + i W^2_\mu)/\sqrt{2}$, and we denote M^2_{gauge} as the off-diagonal matrix above. Given the two different scales in the mass matrix above, we first apply the following transformation

$$\begin{pmatrix} W^\mu_3 \\ Y^\mu \\ X^\mu \end{pmatrix} = \begin{pmatrix} 1 & 0 & 0 \\ 0 & \cos\theta_{23} & \sin\theta_{23} \\ 0 & -\sin\theta_{23} & \cos\theta_{23} \end{pmatrix} \begin{pmatrix} W^\mu_3 \\ B^\mu_{12} \\ B^\mu_3 \end{pmatrix} = \begin{pmatrix} W^\mu_3 \\ \cos\theta_{23} B^\mu_{12} + \sin\theta_{23} B^\mu_3 \\ -\sin\theta_{23} B^\mu_{12} + \cos\theta_{23} B^\mu_3 \end{pmatrix}, \tag{5.65}$$

where

$$\sin\theta_{23} = \frac{g_{12}}{\sqrt{g^2_{12} + g^2_3}}\,, \tag{5.66}$$

and we denote the rotation in Eq. (5.65) as $V_{\theta_{23}}$, obtaining

$$V_{\theta_{23}} M^2_{\text{gauge}} V^\dagger_{\theta_{23}} = \frac{q^2 v_{23}^2}{2} \begin{pmatrix} & W_3^\mu & Y^\mu & X^\mu \\ W_{3\mu}| & g_L^2 r^2 & -g_L g_Y r^2 & -g_L g_X r^2 \\ Y_\mu| & -g_L g_Y r^2 & g_Y^2 r^2 & g_Y g_X r^2 \\ X_\mu| & -g_L g_X r^2 & g_Y g_X r^2 & g_F^2 + g_X^2 r^2 \end{pmatrix}, \tag{5.67}$$

where Y^μ is the SM hypercharge gauge boson with gauge coupling

$$g_Y = \frac{g_{12} g_3}{\sqrt{g_{12}^2 + g_3^2}} \simeq 0.36\,, \tag{5.68}$$

where the numeric value depicted is evaluated at the electroweak scale, and X^μ can be interpreted as an effective gauge boson with effective couplings

$$g_X = \frac{g_3^2}{\sqrt{g_{12}^2 + g_3^2}}\,, \qquad\qquad g_F = \sqrt{g_{12}^2 + g_3^2}\,, \tag{5.69}$$

to the Higgs boson and to ϕ_{23}, respectively. In this basis, the covariant derivatives read

$$D_\mu H = (\partial_\mu - i g_L \frac{\sigma^a}{2} W_\mu^a - i \frac{g_Y}{2} Y_\mu - i \frac{g_X}{2} X_\mu) H\,, \tag{5.70}$$

$$D_\mu \phi_{23} = (\partial_\mu - i q g_F X_\mu) \phi_{23}\,. \tag{5.71}$$

The mass matrix in this basis can be block-diagonalised by applying the following transformation

$$\begin{pmatrix} A^\mu \\ (Z^0)^\mu \\ X^\mu \end{pmatrix} = \begin{pmatrix} \sin\theta_W & \cos\theta_W & 0 \\ \cos\theta_W & -\sin\theta_W & 0 \\ 0 & 0 & 1 \end{pmatrix} \begin{pmatrix} W_3^\mu \\ Y^\mu \\ X^\mu \end{pmatrix} = \begin{pmatrix} \cos\theta_W Y^\mu + \sin\theta_W W_3^\mu \\ -\sin\theta_W Y^\mu + \cos\theta_W W_3^\mu \\ X^\mu \end{pmatrix}, \tag{5.72}$$

where the mixing angle is identified with the usual weak mixing angle as

$$\sin\theta_W = \frac{g_Y}{\sqrt{g_Y^2 + g_L^2}}\,, \tag{5.73}$$

and we denote the rotation in Eq. (5.72) as V_{θ_W}[8], obtaining

$$\begin{aligned} &V_{\theta_W} V_{\theta_{23}} M^2_{\text{gauge}} (V_{\theta_W} V_{\theta_{23}})^\dagger \\ &= \frac{q^2 v_{23}^2}{2} \begin{pmatrix} & A^\mu & (Z^0)^\mu & X^\mu \\ A_\mu| & 0 & 0 & 0 \\ (Z^0)_\mu| & 0 & (g_L^2 + g_Y^2) r^2 & -g_X \sqrt{g_Y^2 + g_L^2}\, r^2 \\ X_\mu| & 0 & -g_X \sqrt{g_Y^2 + g_L^2}\, r^2 & g_F^2 + g_X^2 r^2 \end{pmatrix}, \end{aligned} \tag{5.74}$$

[8]Notice that this is not the usual SM convention, because we have ordered W_μ^3 and Y_μ differently.

where we have already identified the massless photon. Now we diagonalise the remaining 2×2 sub-block in the limit of small r^2. We obtain

$$Z_\mu = \cos\theta_{Z-Z'_{23}} \left(-\sin\theta_W Y_\mu + \cos\theta_W W_{3\mu}\right) + \sin\theta_{Z-Z'_{23}} X_\mu \,, \tag{5.75}$$

$$Z'_{23\mu} = -\sin\theta_{Z-Z'_{23}} \left(-\sin\theta_W Y_\mu + \cos\theta_W W_{3\mu}\right) + \cos\theta_{Z-Z'_{23}} X_\mu \,, \tag{5.76}$$

where to leading order in r^2

$$\sin\theta_{Z-Z'_{23}} \approx \frac{\sqrt{g_Y^2+g_L^2}\, g_X}{g_F^2} r^2 = \frac{g_3 \cos\theta_{23}}{\sqrt{g_Y^2+g_L^2}} \left(\frac{M_Z^0}{M_{Z'_{23}}^0}\right)^2 . \tag{5.77}$$

We can see that the SM Z boson carries a small admixture of the X_μ boson, which provides a small shift to its mass as

$$M_Z^2 \approx q^2 v_{23}^2 \left(g_Y^2+g_L^2\right)\left(r^2 - \frac{g_X^2}{g_F^2} r^4\right) = (M_Z^0)^2 \left[1 - \frac{g_3^2 \cos^2\theta_{23}}{(g_Y^2+g_L^2)} \left(\frac{M_Z^0}{M_{Z'_{23}}^0}\right)^2\right] \tag{5.78}$$

$$M_{Z'_{23}}^2 \approx q^2 v_{23}^2 g_F^2 \left(1 + \frac{g_X^2}{g_F^2} r^2\right) = (M_{Z'_{23}}^0)^2 \left[1 + \frac{g_3^2 \cos^2\theta_{23}}{(g_Y^2+g_L^2)} \left(\frac{M_Z^0}{M_{Z'_{23}}^0}\right)^2\right] \tag{5.79}$$

where

$$M_Z^0 = \frac{v_{\rm SM}}{2}\sqrt{g_Y^2+g_L^2}\,, \qquad\qquad M_{Z'_{23}}^0 = q v_{23}\sqrt{g_{12}^2+g_3^2}\,, \tag{5.80}$$

are the masses of the Z boson in the SM and the mass of the Z'_{23} boson in absence of $Z - Z'_{23}$ mixing, respectively. All these results can be generalised for the case of more hyperons or more Higgs doublets.

As expected, the SM Z boson mass arises at order r^2, with a leading correction from $Z - Z'_{23}$ mixing arising at order r^4. Instead, the Z'_{23} boson arises at leading order in the power expansion, with the leading correction from $Z - Z'_{23}$ mixing arising at order r^2. Remarkably, the presence of $Z - Z'_{23}$ mixing always shifts the mass of the Z boson to smaller values with respect to the SM prediction.

The equations obtained match general results in the literature [300,380,381], which consider scenarios where the starting point is a matrix such as Eq. (5.67) with $g_F = g_X$. Our equations match those of these papers when $g_F = g_X$ (and taking into account that we need to perform an extra rotation θ_{23} to arrive to Eq. (5.67)).

In the case that a kinetic mixing term $\sin\chi F_{\mu\nu}^{(12)} F_{\mu\nu}^{(3)}/2$ is included in Eq. (5.59), then one can repeat the calculations of this section to finally obtain

$$\sin\theta_{Z-Z'_{23}} = \frac{g_3 \cos\theta_{23}}{\sqrt{g_Y^2+g_L^2}} (1-\sin\chi) \left(\frac{M_Z^0}{M_{Z'_{23}}^0}\right)^2 , \tag{5.81}$$

where now

$$\cos\theta_{23} = \frac{g_3 \sec^2\chi}{\sqrt{g_{12}^2 + g_3^2\left(\sec\chi - \tan\chi\right)^2}}\,, \qquad g_Y = \frac{g_{12} g_3 \sec^2\chi}{\sqrt{g_{12}^2 + g_3^2\left(\sec\chi - \tan\chi\right)^2}}\,, \tag{5.82}$$

$$M^0_{Z'_{23}} = q v_{23}\sqrt{g_{12}^2 + g_3^2\left(\frac{1-\sin\chi}{1+\sin\chi}\right)}\,. \tag{5.83}$$

Assuming that the kinetic mixing parameter $\sin\chi$ is small compared to unity (e.g. loop generated, as it happens when the tri-hypercharge model emerges from a semi-simple embedding such as the $SU(5)^3$ tri-unification theory of Chapter 6), then the dominant effect is always the original gauge mixing and kinetic mixing can be neglected. As an example, the hyperon $\phi_{23}(\mathbf{1})_{(q,-q)}$ charged under both $U(1)$ groups generates kinetic mixing at 1-loop as $d\sin\chi/d\log\mu = -g_{12}g_3q^2/(16\pi^2)$, which leads to $\sin\chi(\mu) = g_{12}g_3q^2\log(m^2_{\phi_{23}}/\mu^2)/(16\pi^2)$. For the natural benchmark $g_{12}\approx\sqrt{3/2}g_Y$ and $g_3\approx\sqrt{3}g_Y$ motivated in Section 5.6.1, along with typical values $q = 1/2$ and $m_{\phi_{23}} = 1\,\text{TeV}$, we obtain $\sin\chi(M_Z)\simeq 0.002$.

Neglecting the small $Z - Z'_{23}$ mixing, the fermion couplings of the Z'_{23} gauge boson given in Eq. (5.87) are obtained by expanding the fermion kinetic terms in the usual way, using the covariant derivative (where T_3 is the third-component $SU(2)_L$ isospin, and we do not include the terms associated to charge currents nor QCD interactions)

$$\begin{aligned} D_\mu = \partial_\mu - i\Big[&eQA_\mu + \left(T_3 g_L\cos\theta_W - g_Y\sin\theta_W(Y_1+Y_2+Y_3)\right)Z^0_\mu \\ &+\left(-g_{12}\sin\theta_{23}(Y_1+Y_2) + g_3\cos\theta_{23}Y_3\right)Z'_{23\mu}\Big]\,, \end{aligned} \tag{5.84}$$

which is an excellent approximation for all practical purposes other than precision Z boson phenomenology. In that case, one has to consider that the couplings of the Z boson to fermions are shifted due to $Z - Z'_{23}$ mixing as

$$g_Z^{f_L f_L} = \left(g_Z^{f_L f_L}\right)^0 + \sin\theta_{Z-Z'_{23}} g_{Z'_{23}}^{f_L f_L}\,, \tag{5.85}$$

where $g_{Z'_{23}}^{f_L f_L}$ are the fermion couplings of Z'_{23} in the absence of $Z - Z'_{23}$ mixing, as given in Eq. (5.87), and similarly for right-handed fermions by just replacing L by R everywhere. We can see that in any case, the shift in the Z boson couplings is suppressed by the small ratio $(M^0_Z/M^0_{Z'_{23}})^2$.

5.6 Phenomenology

5.6.1 Couplings of the heavy Z' bosons to fermions

In Sections 5.3 and 5.4 we have discussed examples of $U(1)^3_Y$ models which provide a compelling description of all fermion masses and mixings, and we have highlighted model-independent features which are intrinsic to the $U(1)^3_Y$ framework. We have assumed that the symmetry breaking pattern of the $U(1)^3_Y$ group down to the SM is

described by Eq. (5.3), in such a way that at a high scale v_{12}, the group $U(1)_{Y_1} \times U(1)_{Y_2}$ is broken down to its diagonal subgroup. The remaining group $U(1)_{Y_1+Y_2} \times U(1)_{Y_3}$ is broken down to SM hypercharge at a lower scale v_{23}. The hierarchy between the scales v_{12} and v_{23} generally plays a role on the origin of flavour hierarchies in the SM, although in specific models we have found that a mild hierarchy $v_{23}/v_{12} \simeq \lambda$ is enough.

A massive gauge boson Z'_{12} is predicted to live at the higher scale v_{12}, displaying *intrinsically* flavour non-universal couplings to the first two families of SM fermions. Similarly, another massive boson Z'_{23} lives at the lower scale v_{23}, displaying family universal couplings to first and second family fermions, while the couplings to the third family are intrinsically different. In the following, we show the coupling matrices in family space (obtained from Eqs. (5.58) and (5.84)), ignoring fermion mass mixing,

$$\mathcal{L}_{Z'_{12}} \supset Y_{\psi_{L,R}} \overline{\psi}_{L,R} \gamma^\mu \begin{pmatrix} -g_1 \sin\theta_{12} & 0 & 0 \\ 0 & g_2 \cos\theta_{12} & 0 \\ 0 & 0 & 0 \end{pmatrix} \psi_{L,R} Z'_{12\mu} \,, \tag{5.86}$$

$$\sin\theta_{12} = \frac{g_1}{\sqrt{g_1^2+g_2^2}} \,, \qquad \cos\theta_{12} = \frac{g_2}{\sqrt{g_1^2+g_2^2}} \,,$$

$$\mathcal{L}_{Z'_{23}} \supset Y_{\psi_{L,R}} \overline{\psi}_{L,R} \gamma^\mu \begin{pmatrix} -g_{12} \sin\theta_{23} & 0 & 0 \\ 0 & -g_{12} \sin\theta_{23} & 0 \\ 0 & 0 & g_3 \cos\theta_{23} \end{pmatrix} \psi_{L,R} Z'_{23\mu} \,, \tag{5.87}$$

$$\sin\theta_{23} = \frac{g_{12}}{\sqrt{g_{12}^2+g_3^2}} \,, \qquad \cos\theta_{23} = \frac{g_3}{\sqrt{g_{12}^2+g_3^2}} \,,$$

where $Y_{\psi_{L,R}}$ is the SM hypercharge of $\psi_{L,R}$[9], where ψ is a 3-component column vector containing the three families. Explicitly, $\psi_L = Q_L^i, L_L^i$, with $Y_{\psi_L} = 1/6, -1/2$, and $\psi_R = u_R^i, d_R^i, e_R^i$ with $Y_{\psi_R} = 2/3, -1/3, -1$, respectively, ignoring couplings to the SM singlet neutrinos[10] discussed in the Section 5.4. In order to include fermion mass mixing we need to define the $SU(2)_L$ doublets and singlets accordingly, see Eqs. (5.91-5.93).

Notice that the couplings to *right-handed* fermions are larger since their hypercharges are larger in magnitude than those of left-handed fermions. The SM hypercharge gauge coupling $g_Y(M_Z) \simeq 0.36$ is entangled to the g_i couplings via the relations

$$g_Y = \frac{g_{12} g_3}{\sqrt{g_{12}^2+g_3^2}} \,, \qquad\qquad g_{12} = \frac{g_1 g_2}{\sqrt{g_1^2+g_2^2}} \,. \tag{5.88}$$

The expressions above reveal a lower bound on the gauge couplings $g_i \gtrsim g_Y$. Throughout this work we have considered a bottom-up approach where the $U(1)_Y^3$ model is just the next step in our understanding of Nature, which reveals information about the origin of flavour, but nevertheless is an EFT remnant of a more fundamental UV-complete theory. In this spirit, we have studied the RGE evolution of the gauge couplings g_i,

[9] Note that we have departed from our 2-component and purely left-handed notation, used in the rest of the chapter, to use instead a 4-component left-right notation, which is more familiar in phenomenological studies. The connection between both conventions can be found in Appendix A.

[10] Note that such low scale SM singlet neutrinos may be observable at colliders via their gauge couplings to Z'_{23}, which can be obtained from the covariant derivative in Eq. (5.84).

$(\overline{R}R)(\overline{R}R)$		$(\overline{L}L)(\overline{R}R)$	
Q_α	C_α	Q_α	C_α
$[Q_{uu}]_{ijkl}$	$C_{12}\kappa^u_{ij}\kappa^u_{kl}+C_{23}\xi^u_{ij}\xi^u_{kl}$	$\left[Q^{(1)}_{qu}\right]_{ijkl}$	$2C_{12}\kappa^q_{ij}\kappa^u_{kl}+2C_{23}\xi^q_{ij}\xi^u_{kl}$
$[Q_{dd}]_{ijkl}$	$C_{12}\kappa^d_{ij}\kappa^d_{kl}+C_{23}\xi^d_{ij}\xi^d_{kl}$	$\left[Q^{(1)}_{qd}\right]_{ijkl}$	$2C_{12}\kappa^q_{ij}\kappa^d_{kl}+2C_{23}\xi^q_{ij}\xi^d_{kl}$
$\left[Q^{(1)}_{ud}\right]_{ijkl}$	$2C_{12}\kappa^u_{ij}\kappa^d_{kl}+2C_{23}\xi^u_{ij}\xi^d_{kl}$	$[Q_{qe}]_{ijkl}$	$2C_{12}\kappa^q_{ij}\kappa^e_{kl}+2C_{23}\xi^q_{ij}\xi^e_{kl}$
$[Q_{eu}]_{ijkl}$	$2C_{12}\kappa^e_{ij}\kappa^u_{kl}+2C_{23}\xi^e_{ij}\xi^u_{kl}$	$[Q_{\ell u}]_{ijkl}$	$2C_{12}\kappa^\ell_{ij}\kappa^u_{kl}+2C_{23}\xi^\ell_{ij}\xi^u_{kl}$
$[Q_{ed}]_{ijkl}$	$2C_{12}\kappa^e_{ij}\kappa^d_{kl}+2C_{23}\xi^e_{ij}\xi^d_{kl}$	$[Q_{\ell d}]_{ijkl}$	$2C_{12}\kappa^\ell_{ij}\kappa^d_{kl}+2C_{23}\xi^\ell_{ij}\xi^d_{kl}$
$[Q_{ee}]_{ijkl}$	$C_{12}\kappa^e_{ij}\kappa^e_{kl}+C_{23}\xi^e_{ij}\xi^e_{kl}$	$[Q_{\ell e}]_{ijkl}$	$2C_{12}\kappa^\ell_{ij}\kappa^e_{kl}+2C_{23}\xi^\ell_{ij}\xi^e_{kl}$

$(\overline{L}L)(\overline{L}L)$	
Q_α	C_α
$\left[Q^{(1)}_{qq}\right]_{ijkl}$	$C_{12}\kappa^q_{ij}\kappa^q_{kl}+C_{23}\xi^q_{ij}\xi^q_{kl}$
$\left[Q^{(1)}_{\ell q}\right]_{ijkl}$	$2C_{12}\kappa^\ell_{ij}\kappa^q_{kl}+2C_{23}\xi^\ell_{ij}\xi^q_{kl}$
$[Q_{\ell\ell}]_{ijkl}$	$C_{12}\kappa^\ell_{ij}\kappa^\ell_{kl}+C_{23}\xi^\ell_{ij}\xi^\ell_{kl}$

TABLE 5.2: Tree-level SMEFT matching for 4-fermion operators in the $U(1)^3_Y$ model.

obtaining that for $g_i(\text{TeV}) \simeq 1$ the model can be extrapolated to the Planck scale (and beyond). Instead, for $g_i(\text{TeV}) \simeq 2$, a Landau pole is found at a scale $\mathcal{O}(10^4\,\text{TeV})$, which anyway seems like a reasonable scale for an UV embedding, given that we expect the cut-off scale of the effective Yukawa operators (see Section 5.3) to be around $\mathcal{O}(10^2\,\text{TeV})$ in order to provide the required suppression for charged fermion masses. Therefore, in order to protect the perturbativity of the model, we avoid considering $g_i > 2$ in the phenomenological analysis. Nevertheless, we highlight a natural scenario where the three gauge couplings have a similar size $g_1 \simeq g_2 \simeq g_3 \simeq \sqrt{3}g_Y$, which could be connected to a possible *gauge unification*, as we shall see in Chapter 6. This benchmark is depicted as a dashed horizontal line in Figs. 5.1 and 5.2.

5.6.2 Tree-level SMEFT matching for 4-fermion operators

In order to write the tree-level SMEFT matching for 4-fermion operators in our model, we write the Z' couplings of Eqs. (5.86) and (5.87) in a more compact form as

$$\mathcal{L}_{\text{int}} = \sum_{f=q,\ell,u,d,e} \sum_{i,j} (\kappa^f_{ij}\overline{f}_i\gamma^\mu f_j Z'_{12\mu} + \xi^f_{ij}\overline{f}_i\gamma^\mu f_j Z'_{23\mu})\,. \tag{5.89}$$

The Wilson coefficients of SMEFT operators Q_α (see Appendix D.1) are then given in Table 5.2 as a function of the couplings κ^f_{ij}, ξ^f_{ij} and the auxiliary variables

$$C_{12} = -\frac{1}{2M^2_{Z'_{12}}}\,, \qquad C_{23} = -\frac{1}{2M^2_{Z'_{23}}}\,. \tag{5.90}$$

In general, the TH model predicts non-trivial fermion mixing in all charged sectors, and we shall take this into account by defining the $SU(2)_L$ doublets and singlets in the SMEFT accordingly, i.e.

$$q_L^i = \begin{pmatrix} V_{u_L}^{ij} u_L^i & V_{d_L}^{ij} d_L^j \end{pmatrix}^{\mathrm{T}}, \qquad \ell_L^i = \begin{pmatrix} V_{\nu_L}^{ij} \nu_L^j & V_{e_L}^{ij} e_L^i \end{pmatrix}^{\mathrm{T}}, \tag{5.91}$$

$$\hat{u}_R^i = V_{u_R}^{ij} u_R^i, \qquad \hat{d}_R^i = V_{d_R}^{ij} d_R^i, \tag{5.92}$$

$$\hat{e}_R^i = V_{e_R}^{ij} e_R^i. \tag{5.93}$$

Notice as well that different implementations of the TH model may lead to different fermion mixing (see Section 5.3), therefore only the different mixing matrices above need to be exchanged when studying the different implementations of the model.

With the above considerations, the model can then be matched to the LEFT as shown in Appendix D.3, and the contributions to low-energy observables can be computed via the EFT formalism introduced in Chapter 2.

Finally, we note that beyond 4-fermion operators, Higgs-bifermion and purely bosonic SMEFT operators are also induced via $Z - Z'_{23}$ mixing. We do not include them in this section because we discuss electroweak symmetry breaking and $Z - Z'_{23}$ mixing separately in Section 5.5.2.

5.6.3 The high scale boson Z'_{12}

In any implementation of the $U(1)_Y^3$ model, Z'_{12} is expected to mediate sizable tree-level transitions between first and second generation left-handed quarks, either in the up or down sectors depending on the alignment of the CKM matrix predicted by the specific model. Furthermore, our analysis in Section 5.3 reveals that $U(1)_Y^3$ models generally predict non-vanishing charged lepton mixing and mixing among right-handed quarks. This way, contributions to $K - \bar{K}$ and $D - \bar{D}$ meson mixing (Section 2.3.4), along with CLFV processes such as $\mu \to e\gamma$ (Section 2.3.8), have the potential to push the scale v_{12} far above the TeV.

Being more specific, for Model 1 described in Section 5.3.3 we find the stringent bounds over v_{12} to come from the scalar and coloured operator $(\bar{s}_L^\alpha d_R^\beta)(\bar{s}_R^\beta d_L^\alpha)$ obtained after integrating out Z'_{12} at tree-level (and applying a Fierz rearrangement), which contributes to $K - \bar{K}$ mixing. Model 1 predicts the up and down left-handed mixings to be similar up to dimensionless couplings, which must therefore play some role in the alignment of the CKM matrix. In either case, mildly suppressed right-handed $s - d$ mixing $s_{12}^{d_R} \simeq \mathcal{O}(\lambda^2)$ is predicted. If V_{us} originates mostly from the down sector, then $K - \bar{K}$ mixing imposes the stringent bound $M_{Z'_{12}} > 170$ TeV for gauge couplings of $\mathcal{O}(0.5)$. Instead, if the dimensionless coupling provides a mild suppression of $\mathcal{O}(0.1)$ in left-handed $s - d$ mixing, such that V_{us} originates mostly from the up sector, then the bound is relaxed to $M_{Z'_{12}} > 55$ TeV. We find bounds from $D - \bar{D}$ mixing to be always weaker, even if V_{us} originates from the up sector, since right-handed up mixing is strongly suppressed in Model 1.

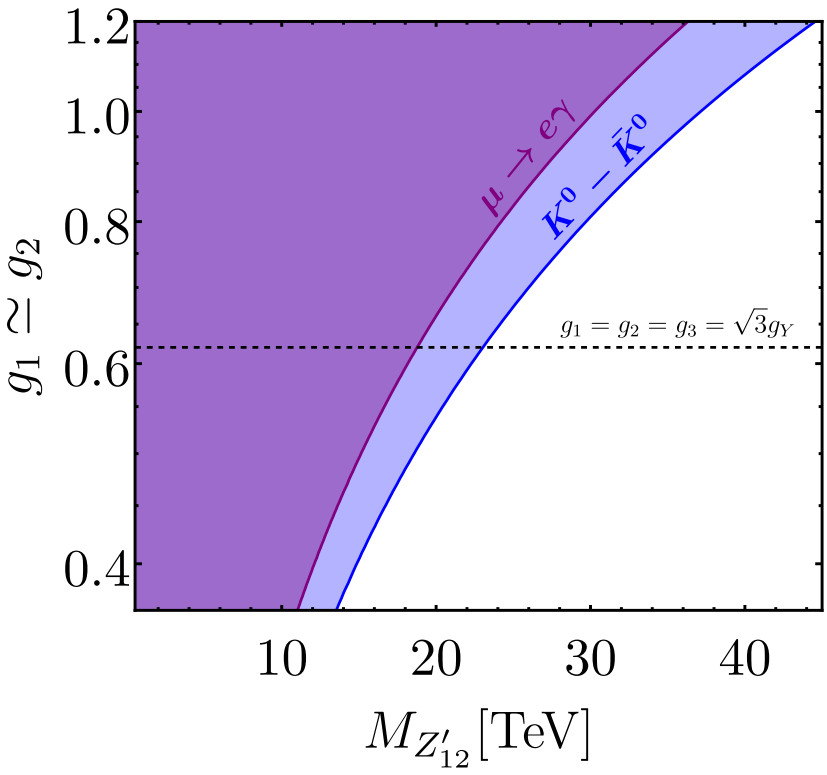

FIGURE 5.1: Parameter space of the high scale breaking, where $M_{Z'_{12}}$ is the mass of the heavy Z'_{12} gauge boson and g_1, g_2 are the gauge couplings of the $U(1)_{Y_1}$ and $U(1)_{Y_2}$ groups, respectively. For simplicity, we assume g_1 and g_2 to be similar, and the non-generic fermion mixing predicted by Model 2 in Section 5.3.4. Shaded regions in the plot depict 95% CL exclusions over the parameter space. The dashed line represents the natural benchmark $g_1 \simeq g_2 \simeq g_3 \simeq \sqrt{3} g_Y$ motivated in the main text.

In contrast with Model 1, Model 2 described in Section 5.3.4 provides a more predictive scenario where V_{us} originates unambiguously from the down sector. Here right-handed quark mixing is more suppressed, obtaining $s_{12}^{d_R} \simeq \mathcal{O}(\lambda^5)$. Nevertheless, $K - \bar{K}$ mixing still imposes the strongest bounds over the parameter case, as can be seen in Fig. 5.1. In this case, the lower bound over the mass of Z'_{12} can be as low as 10-50 TeV, depending on the values of the gauge couplings. We find the CLFV process $\mu \to e\gamma$ to provide a slightly weaker bound over the parameter space, because charged lepton mixing is generally suppressed with respect to quark mixing in Model 2. We find the bound from $\mu \to 3e$ to be very similar to the bound from $\mu \to e\gamma$.

5.6.4 The low scale boson Z'_{23}

Given that the high scale symmetry breaking can be as low as 10-20 TeV for specific models, and considering the hierarchy of scales $v_{23}/v_{12} \simeq \lambda$ suggested by these specific models in Section 5.3, it is possible to find the low scale breaking v_{23} near the TeV. Since Z'_{23} features flavour universal couplings to the first and second families, the stringent bounds from $K - \bar{K}$ mixing and $\mu \to e\gamma$ are avoided, in the spirit of the *GIM mechanism*. This way, Z'_{23} can live at the TeV scale, within the reach of the LHC and future colliders.

Any implementation of the $U(1)_Y^3$ model predicts small *mixing* between Z'_{23} and the SM Z boson given by the mixing angle (see Section 5.5.2)[11]

$$\sin\theta_{Z-Z'_{23}} = \frac{g_3 \cos\theta_{23}}{\sqrt{g_Y^2 + g_L^2}} \left(\frac{M_Z^0}{M_{Z'_{23}}^0} \right)^2 , \tag{5.94}$$

where M_Z^0 and $M_{Z'_{23}}^0$ are the masses of the Z and Z'_{23} bosons in the absence of mixing, respectively, and g_L is the gauge coupling of $SU(2)_L$. This mixing leads to a *small shift* on the mass of the Z boson, which has an impact over the electroweak ρ parameter introduced in Section 1.3,

$$\rho = \frac{M_W^2}{M_Z^2 \cos^2\theta_W} = \frac{1}{1 - g_3^2 \cos^2\theta_{23} \left(\frac{v_{\rm SM}}{2M_{Z'_{23}}^0} \right)^2} , \tag{5.95}$$

which is predicted as $\rho = 1$ at tree-level in the SM. This is a consequence of custodial symmetry in the Higgs potential, introduced as well in Section 1.3, which is explicitly broken in our model via $Z - Z'_{23}$ mixing leading to deviations in ρ. The fact that in our model M_Z is always shifted to smaller values leads to $\rho > 1$ at tree-level. Given that M_Z is commonly an input experimental parameter of the SM used in the determination of g_Y and g_L, the downward shift of M_Z with respect to the SM prediction would be seen from the experimental point of view as an upward shift of M_W with respect to the SM prediction. Nevertheless, the experimental picture of M_W is puzzling after the recent measurement by CDF [83]. This measurement points towards M_W being larger than the SM prediction with high significance, but it is in tension with the combination of measurements by LHC, LEP and Tevatron D0 [21]. Neglecting the recent CDF measurement for the moment, current data[12] provides $\rho = 1.0003 \pm 0.0005$ [21] (assuming that both the oblique parameters T and S are non-zero, as we expect in our model). We obtain the approximate bound $g_3/M_{Z'} < 3.1\,\text{TeV}$ at 95% CL, which translates to an approximate bound over the mixing angle of $\sin\theta_{Z-Z'_{23}} < 0.001$.

$Z - Z'_{23}$ mixing also shifts the couplings of the Z boson to fermions, leading to an important impact over Z-pole EWPOs if Z'_{23} lives at the TeV scale. We find bounds coming from tests of Z boson lepton universality and flavour-violating Z decays not to be competitive with the bound from ρ. The electron asymmetry parameter A_e, which already deviates from the SM by almost 2σ [89], is expected to deviate further in our model. Nevertheless, we expect our model to improve the fit of $A_b^{\rm FB}$, which is in tension with the SM prediction by more than 2σ [89]. In conclusion, the global effect of our model over EWPOs can only by captured by performing a global fit, which we leave

[11] In this section we only discuss the impact of $Z - Z'_{23}$ gauge mixing, while kinetic mixing is found to be negligible as long as the kinetic mixing parameter is smaller than $\mathcal{O}(1)$ (see Section 5.5.2).

[12] The current world average (without the latest CDF measurement) of M_W does not consider the very recent M_W update by ATLAS [382]. Given that the central value and the uncertainty of this measurement are just slightly reduced with respect to the 2017 measurement [383], we do not expect a big impact over the world average.

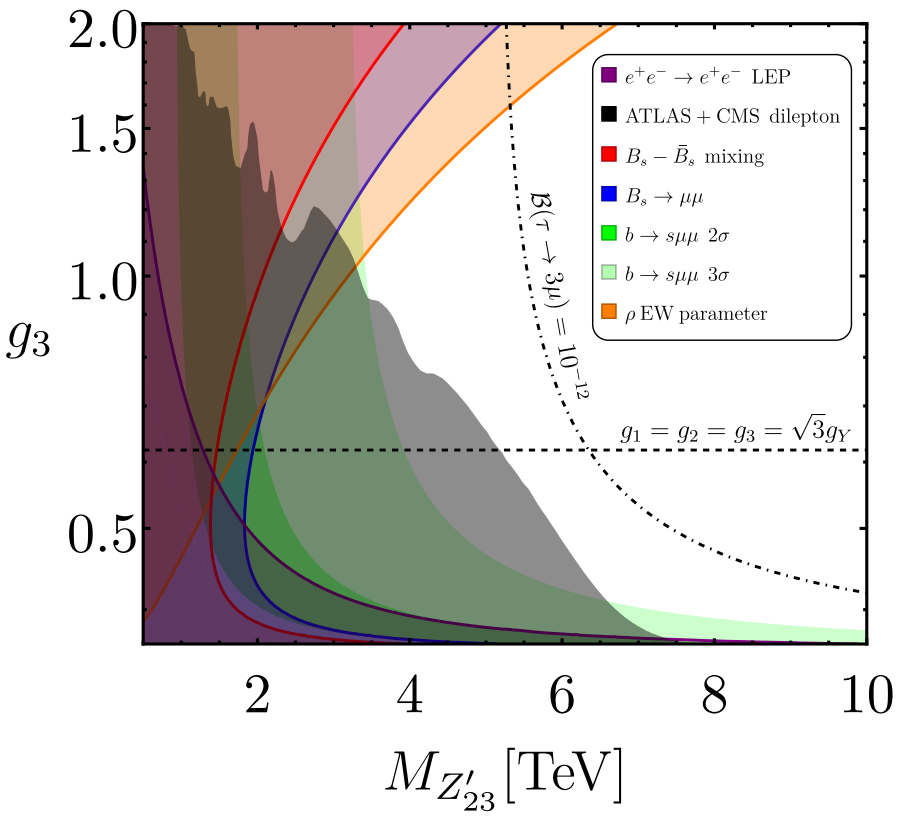

FIGURE 5.2: Parameter space of the low scale breaking, where $M_{Z'_{23}}$ is the mass of the heavy Z'_{23} gauge boson and g_3 is the gauge coupling of the $U(1)_{Y_3}$ group. The gauge coupling g_{12} is fixed in terms of g_3 and g_Y via Eq. (5.88), and we consider the non-generic fermion mixing predicted by Model 2 in Section 5.3.4. Shaded regions in the plot depict 95% CL exclusions over the parameter space, with the exception of the green (light green) region which is preferred by a global fit to $b \to s\mu\mu$ data at 2σ (3σ) [82]. The dashed line represents the natural benchmark $g_1 \simeq g_2 \simeq g_3 \simeq \sqrt{3} g_Y$ motivated in the main text. The dashed-dotted line represents the contour where $\mathcal{B}(\tau \to 3\mu) = 10^{-12}$.

for future work. Global fits of EWPOs in the context of other Z' models have been performed in the literature, see e.g. [384–386], which obtain 95% CL maximum values of $\sin\theta_{Z-Z'}$ ranging from 0.002 to 0.0006 depending on the model. We expect our model to lie on the more restrictive side of that range. We do not expect our model to explain the anomalous CDF M_W measurement, because predicting such a large M_W via large $Z - Z'_{23}$ mixing would lead to intolerably large contributions to other EWPOs, worsening the global fit.

The massive Z'_{23} boson has sizable couplings to light quarks and light charged leptons unless g_3 is very large, which we do not expect based on naturalness arguments and also to protect the extrapolation of the model in the UV, as discussed in Section 5.6.1. Consequently, on general grounds we expect a significant production of a TeV-scale Z'_{23} at the LHC, plus a sizable branching fraction to electrons and muons. We have prepared the UFO model of Z'_{23} using `FeynRules` [336], and then we have computed the Z'_{23} production cross section for 13 TeV pp collisions using `Madgraph5` [337] with the

Z'_{23} decay mode	$\mathcal{B}$
$\bar{t}t$	~ 0.28
$\bar{u}u + \bar{c}c$	~ 0.14
$\bar{t}c + \bar{c}t$	$\sim 10^{-4}$
$\bar{b}b$	~ 0.08
$\bar{d}d + \bar{s}s$	~ 0.04
$\bar{b}s + \bar{s}b$	$\sim 10^{-4}$
$\tau^+\tau^-$	~ 0.25
$e^+e^- + \mu^+\mu^-$	~ 0.12
$\tau^+\mu^- + \tau^-\mu^+$	$\sim 10^{-5}$
$\bar{\nu}\nu$	~ 0.08

TABLE 5.3: Main decay modes of Z'_{23} for the natural benchmark $g_1 \simeq g_2 \simeq g_3 \simeq \sqrt{3}g_Y$. We assume that decays into SM singlet neutrinos are kinematically forbidden or suppressed.

default PDF `NNPDF23LO`. We estimated analytically the branching fraction to electrons and muons, and we computed the total decay width via the narrow width approximation. We confront our results with the limits from the most recent dilepton resonance searches by ATLAS [338] and CMS [339] in order to obtain 95% CL exclusion bounds. The bounds from ditau [340] and ditop [341] searches turn out not to be competitive even for the region of large g_3, where the bound from the ρ EW parameter is stronger. Our results are depicted as the black-shaded region in Fig. 5.2. As expected, the bounds become weaker in the region $g_3 > 1$ where the couplings to light fermions become mildly suppressed. In the region of small g_3 we find the opposite behavior, such that LHC limits can exclude Z'_{23} as heavy as 6-7 TeV. After combining the LHC exclusion with the bounds coming from the ρ EW parameter, we conclude that we can find Z'_{23} as light as 3.5 TeV for $g_3 = 1$, while for the benchmark $g_i \simeq \sqrt{3}g_Y$ we obtain $M_{Z'_{23}} \gtrsim 5$ TeV.

Given that Z'_{23} has sizable couplings to electrons, we have studied the bounds over contact interactions obtained at LEP [387]. For our model, the most competitive bounds arise from contact interactions involving only electrons. Assuming vector-like interactions, the bounds by LEP are only sensitive to regions with very small g_3, where the couplings of Z'_{23} to electrons (and muons) are larger, but can exclude Z'_{23} masses beyond 10 TeV. However, we expect this bound to be slightly overestimated for our model, since the interactions of Z'_{23} are not exactly vector-like due to the different hypercharge of e_L and e_R, as depicted in Eq. (5.87). Nevertheless, the bounds over chiral operators are much weaker than the bound over the vector-like operator, and a dedicated reanalysis of the data would be required in order to obtain the proper bound for our model, which is beyond the scope of this work. Therefore, we prefer to be conservative and depict the largest bound of the vector-like operator as the purple region in Fig. 5.2.

We have also considered implications for B-physics. The heavy boson Z'_{23} has a sizable left-handed $b_L s_L$ coupling and an approximately vector-like and universal coupling to electron and muon pairs. Given these features, a Z'_{23} with a mass of 2 TeV mediates a meaningful contribution to the effective operator $\mathcal{O}_9^{\ell\ell}$ (with $\ell = e, \mu$), where sizable

NP contributions are preferred according to the most recent global fits [82], without contributing to the SM-like $R_{K^{(*)}}$ ratios [185]. However, as depicted in Fig. 5.2, the region where the model could address the anomalies in $b \to s\mu\mu$ data are in tension with the bounds obtained by dilepton searches, as expected for a Z' which has sizable couplings to light quarks. Nevertheless, we can see that a relevant $C_9^{\ell\ell} \sim 0.1$ can be obtained for a heavier Z'_{23} in the region where $g_3 < 0.5$, as in this region couplings to light fermions are enhanced.

$\mathcal{B}(B_s \to \mu\mu)$ is also enhanced above the SM prediction due to both Z'_{23} and Z exchange diagrams. In the region of small g_3 the Z'_{23} exchange dominates, while for large g_3 the Z exchange dominates. As anticipated before, the couplings of the Z'_{23} boson to muons are approximately, but not completely, vector-like. Therefore, a small contribution to the operator $\mathcal{O}_{10}^{\mu\mu}$ is generated in the region of small g_3, where Z'_{23} couplings to muons are larger, leading to Z'_{23} exchange being dominant. However, in the region of large g_3, the flavour-violating coupling $\bar{s}_L b_L Z'_{23}$ mixes into $\bar{s}_L b_L Z$ via $Z - Z'_{23}$ mixing. This provides an effective contribution to $\mathcal{O}_{10}^{\mu\mu}$ mediated by the Z boson that enhances $\mathcal{B}(B_s \to \mu\mu)$ above the SM prediction. Overall, the region excluded at 95% CL by the current HFLAV average [80] (including the latest measurement by CMS [186]) is depicted as blue-shaded in Fig. 5.2. It is clear that the resulting bound is not currently competitive with that from the ρ EW parameter which constrains the size of $Z - Z'_{23}$ mixing.

The flavour-violating structure of Z'_{23} fermion couplings leads to sizable contributions to $B_s - \bar{B}_s$ meson mixing [242] and CLFV processes involving $\tau \to \mu$ transitions and $\tau \to e$ transitions, although well below existing experimental limits. $\tau \to \mu(e)$ transitions arise from mixing angles connected to the flavour hierarchy $\mathcal{O}(m_2/m_3)$ ($\mathcal{O}(m_1/m_3)$), see Section 5.3.1. As an example, in Fig. 5.2 we depict the contour for $\mathcal{B}(\tau \to 3\mu) = 10^{-12}$. We find $\tau \to \mu\gamma$ to be more competitive than $\tau \to 3\mu$ only in the region $g_3 > 1$.

Beyond indirect detection, in the near future Z'_{23} could be directly produced at the LHC, HL-LHC and future colliders such as FCC or a high energy muon collider. The particular pattern of Z'_{23} fermion couplings will allow to disentangle our model from all other proposals. For the natural benchmark $g_1 \simeq g_2 \simeq g_3 \simeq \sqrt{3} g_Y$, Z'_{23} preferentially decays to top pairs and ditaus, as can be seen in Table 5.3. Furthermore, Z'_{23} preferentially couples and decays to *right-handed* charged fermions, given their larger hypercharge with respect to left-handed charged fermions, and this prediction may be tested via suitable asymmetry observables. Similarly, decays to down-type quarks are generally suppressed with respect to (right-handed) up-type quarks and charged leptons, given the smaller hypercharge of the former. Due to the modification of EWPOs, our model can also be tested in an electroweak precision machine such as FCC-*ee*. An alternative way of discovery would be the detection of the hyperon scalars breaking the $U(1)_Y^3$ group down to SM hypercharge, since the hyperons participating in the 23-breaking may be as light as the TeV, however we leave a study about the related phenomenology for future work. In the same spirit, the model naturally predicts SM

singlet neutrinos which could be as light as the TeV scale (see Section 5.4.2), with phenomenological implications yet to be explored in a future work.

5.7 Conclusions

In this chapter we have proposed a tri-hypercharge (TH) embedding of the SM, based on assigning a separate gauged weak hypercharge to each family. The idea is that each fermion family i only carries hypercharge under a corresponding $U(1)_{Y_i}$ factor. This ensures that each family transforms differently under the TH gauge group $U(1)_Y^3$, which avoids the family repetition of the SM and provides the starting point for a theory of flavour.

The three family specific hypercharge groups are spontaneously broken in a cascade symmetry breaking down to SM hypercharge. We have motivated a particular symmetry breaking pattern, where in a first step $U(1)_{Y_1} \times U(1)_{Y_2}$ is broken down to its diagonal subgroup at a high scale v_{12}. The remaining group $U(1)_{Y_1+Y_2} \times U(1)_{Y_3}$ is broken down to SM hypercharge at a scale v_{23}. This symmetry breaking pattern sequentially recovers the accidental flavour symmetry of the SM, providing protection versus FCNCs that allows the NP scales to be relatively low. Dynamics connected to the scale v_{12} play a role in the origin of the family hierarchy m_1/m_2, while dynamics connected to the scale v_{23} play a role in the origin of m_2/m_3. The hierarchy of scales v_{23}/v_{12} generally plays a role on the origin of flavour hierarchies as well, although we have found that a mild hierarchy $v_{23}/v_{12} \simeq \lambda$ is enough for specific implementations of the model, where $\lambda \simeq 0.225$ is the Wolfenstein parameter.

Assuming that the SM Higgs only carries third family hypercharge, then only the third family Yukawa couplings are allowed at renormalisable level. This explains the heaviness of the third family, the smallness of V_{cb} and V_{ub} quark mixing, and delivers an accidental $U(2)^5$ flavour symmetry in the Yukawa sector acting on the light families, which provides a reasonable first order description of the SM spectrum. However, $U(2)^5$ does not explain the hierarchical heaviness of the top quark with respect to the bottom and tau fermions. Furthermore, we have proven that the model generates a similar mass hierarchy for all charged sectors, being unable to explain the heaviness of the charm quark with respect to the strange and muon without small couplings. We have motivated the addition of a second Higgs doublet as a natural and elegant solution, which allows a more natural description of the hierarchies between the different charged fermion sectors.

We have explored the capabilities of the $U(1)_Y^3$ model to explain the observed hierarchies in the charged fermion sector, via the addition of non-renormalisable operators containing $U(1)_Y^3$-breaking scalars which act as small breaking effects of $U(2)^5$. After extracting model-independent considerations from the spurion formalism, we have presented example models where all charged fermion masses and mixings are addressed. Following a similar methodology, we have studied the origin of neutrino masses and

mixing in the TH model. We have shown that due to the $U(1)_Y^3$ gauge symmetry, the implementation of a type I seesaw mechanism naturally leads to a low scale seesaw, where the SM singlet neutrinos in the model may be as light as the TeV scale. We have provided an example model compatible with the observed pattern of neutrino mixing.

As usual for theories of flavour, the NP scales $\langle\phi\rangle$ and Λ that explain the origin of flavour hierarchies in the SM may be anywhere *from the Planck scale to the electroweak scale*, provided that the ratios $\langle\phi\rangle/\Lambda$ are held fixed (see Section 1.10). Intriguingly, a preliminary phenomenological analysis shows that current data allows relatively low NP scales. The heavy gauge boson Z'_{12} arising from the 12-breaking displays completely flavour non-universal couplings to fermions, and generally contributes to $\Delta F = 2$ and CLFV processes. The size of the most dangerous contributions are however model-dependent. In selected specific models provided in this chapter, we have found that the most dangerous contributions to $K - \bar{K}$ mixing and $\mu \to e\gamma$ are strongly suppressed, allowing for Z'_{12} to be as light as 10-50 TeV. Therefore, the lightest gauge boson Z'_{23} arising from the 23-breaking can live at the TeV scale, within the reach of LHC and future colliders, since Z'_{23} avoids bounds from $K - \bar{K}$ mixing and $\mu \to e\gamma$ thanks to an accidental GIM mechanism for light fermions.

We find the gauge boson Z'_{23} to have a rich low-energy phenomenology: mixing with the SM Z boson leads to implications for the W boson mass and EWPOs, plus we expect contributions to flavour-violating processes involving the third family, such as $\tau \to 3\mu(e)$ and $B_s - \bar{B}_s$ meson mixing. After our preliminary analysis, we find that current data allows Z'_{23} to be as light as 3-4 TeV in some regions of the parameter space, the strongest bounds coming from dilepton searches at LHC along with the contribution to the ρ EW parameter. In the case of discovery, the particular pattern of Z'_{23} couplings and decays to fermions will allow to disentangle our model from all other proposals. However, most of the phenomenological consequences are yet to be explored in detail: a global fit to EWPOs and flavour observables will allow to properly confront our model versus current data. An alternative way of discovery would be the detection of the Higgs scalars (hyperons) breaking the $U(1)_Y^3$ down to SM hypercharge, however we leave a discussion about the related phenomenology for future work. In the same spirit, the model naturally predicts SM singlet neutrinos which could be as light as the TeV, with phenomenological implications yet to be explored. The tri-hypercharge gauge group may be the first step towards understanding the origin of three fermion families in Nature, the hierarchical charged fermion masses and CKM mixing, revealing the existence of a flavour non-universal gauge structure encoded in Nature at energies above the electroweak scale.

Despite the apparent complexity of the gauge sector of the tri-hypercharge gauge group, consisting of five arbitrary gauge couplings, in Chapter 6 we shall see that such a theory may arise from a gauge unified framework.

Chapter 6

Tri-unification: the origin of gauge non-universal theories of flavour

> "As a child, I considered such unknowns sinister.
> Now, though, I understand they bear no ill will.
> The Universe is, and we are."
>
> – Solanum in *Outer Wilds*

In this chapter, based on Ref. [5], we propose a grand unified framework consisting on assigning a separate $SU(5)$ to each fermion family. The three $SU(5)$ groups are related by a cyclic permutation symmetry $\mathbb{Z}_3$, such that the model is described by a single gauge coupling in the UV, despite $SU(5)^3$ being a non-simple gauge group. We motivate that such a tri-unification framework may embed gauge non-universal theories, such as the tri-hypercharge model proposed in the previous chapter to address the origin of flavour. In this manner, we discuss a minimal tri-hypercharge example which can account for all the quark and lepton (including neutrino) masses and mixing parameters, with the many gauge couplings of the tri-hypercharge group unifying at the GUT scale into a single gauge coupling associated to the cyclic $SU(5)^3$ group.

6.1 Introduction

Flavour non-universal gauge embeddings of the SM gauge group were first proposed during the 80s and 90s. Back then, it was already highlighted that these frameworks may have many applications, such as motivating lepton non-universality [370–373] or assisting technicolor model building [374, 375]. Other applications include addressing tensions with the SM in electroweak precision data [376], or explaining the baryon asymmetry of the Universe due to the presence of non-universal $SU(2)$ factors embedding the usual $SU(2)_L$ [172]. More recently, such non-universal gauge structures had been shown to

explain the flavour structure of the SM if spontaneously broken in a desired way. Most notable examples include the $SU(2)_L^3$ model [124–126], the $SU(3)_c^3$ model (which is only able to explain the smallness of quark mixing) [388] and the tri-hypercharge model $U(1)_Y^3$ [3] discussed in Chapter 5.

However, these theories explain the flavour structure of the SM at the price of complicating the gauge sector with the introduction of extra, arbitrary gauge couplings. The existing UV completions are all based on variations of the Pati-Salam gauge group [115–117, 119–122], leaving up to nine arbitrary gauge couplings in the UV. In contrast, here we shall attempt to construct a gauge unified framework from which gauge non-universal theories may emerge at relatively low-energies, opening the possibility to build consistent non-universal descriptions of Nature that are valid all the way up to the scale of grand unification. For this we propose a non-supersymmetric $SU(5)^3$ framework,

$$SU(5)_1 \times SU(5)_2 \times SU(5)_3 \,, \tag{6.1}$$

together with a cyclic symmetry $\mathbb{Z}_3$ that relates the three $SU(5)$ factors. This is a generalisation of $SU(5)$ grand unification [93] in which we assign a separate $SU(5)$ group to each fermion family. The cyclic symmetry that relates the three $SU(5)$ factors ensures that at the GUT scale the three gauge couplings are equal, such that the gauge sector is fundamentally described by one gauge coupling. Therefore, although $SU(5)^3$ is not a simple group, it may be regarded as a unified gauge theory. Gauge unified theories including different gauge factors for each fermion family were first sketched in the early days of the GUT program [389–391], and were later considered in supersymmetric scenarios[1] during the 90s and 2000s, where the main motivations were achieving GUT symmetry breaking without adjoint fields [392, 394], solving the doublet-triplet splitting problem [395], or unifying all chiral fermions into the same representation [393].

In contrast with the previous work, here we propose our non-supersymmetric $SU(5)^3$ tri-unification framework as a realistic origin for gauge non-universal physics at lower scales, that had been shown to have many applications for model building purposes as described before. As a proof of concept, in this chapter we will discuss $SU(5)^3$ as an embedding of the tri-hypercharge model [3], showing that it is possible to unify the various gauge couplings of tri-hypercharge into a single gauge coupling associated with the cyclic $SU(5)^3$ gauge group. We also study proton decay in this example, and present the predictions of the proton lifetime in the dominant $e^+\pi^0$ channel.

The layout of the remainder of the chapter is as follows. In Section 6.2 we discuss a general $SU(5)^3$ tri-unification framework for model building. In rather lengthy Section 6.3 we analyse an example $SU(5)^3$ unification model breaking to tri-hypercharge, including the charged fermion mass hierarchies and quark mixing, neutrino masses and mixing, gauge coupling unification and proton decay. Section 6.4 concludes the chapter.

[1] However it is worth mentioning that supersymmetric $SU(5)^3$ scenarios suffer from rapid proton decay via dimension-5 operators generated by coloured triplet Higgs exchange [392, 393], which have large couplings (of order unity) to first generation fermions as a consequence of the discrete symmetry (e.g. cyclic symmetry) that enforces a single gauge coupling at the GUT scale.

Field	$SU(5)_1$	$SU(5)_2$	$SU(5)_3$
F_1	$\bar{\mathbf{5}}$	$\mathbf{1}$	$\mathbf{1}$
F_2	$\mathbf{1}$	$\bar{\mathbf{5}}$	$\mathbf{1}$
F_3	$\mathbf{1}$	$\mathbf{1}$	$\bar{\mathbf{5}}$
T_1	$\mathbf{10}$	$\mathbf{1}$	$\mathbf{1}$
T_2	$\mathbf{1}$	$\mathbf{10}$	$\mathbf{1}$
T_3	$\mathbf{1}$	$\mathbf{1}$	$\mathbf{10}$
Ω_1	$\mathbf{24}$	$\mathbf{1}$	$\mathbf{1}$
Ω_2	$\mathbf{1}$	$\mathbf{24}$	$\mathbf{1}$
Ω_3	$\mathbf{1}$	$\mathbf{1}$	$\mathbf{24}$
H_1	$\mathbf{5}$	$\mathbf{1}$	$\mathbf{1}$
H_2	$\mathbf{1}$	$\mathbf{5}$	$\mathbf{1}$
H_3	$\mathbf{1}$	$\mathbf{1}$	$\mathbf{5}$

TABLE 6.1: Minimal content for the general $SU(5)^3$ tri-unification framework. Due to the cyclic symmetry, there are only four independent representations, one for each of the fermions F_i, T_i and one for each of the scalars Ω_i, H_i.

6.2 General $SU(5)^3$ framework for model building

The basic idea of tri-unification is to embed the SM gauge group into a semi-simple gauge group containing three $SU(5)$ factors,

$$SU(5)_1 \times SU(5)_2 \times SU(5)_3 \,, \tag{6.2}$$

where each $SU(5)$ factor is associated to one family of chiral fermions $i = 1, 2, 3$. Moreover, we incorporate a cyclic permutation symmetry $\mathbb{Z}_3$ that relates the three $SU(5)$ factors, in the spirit of the trinification model [396]. This implies that at the high energy GUT scale where $SU(5)^3$ is broken (typically in excess of 10^{16} GeV) the gauge couplings of the three $SU(5)$ factors are equal by cyclic symmetry, such that the gauge sector is fundamentally described by one gauge coupling. Therefore, although $SU(5)^3$ is not a simple group, it may be regarded as a unified gauge theory. Moreover, the cyclic symmetry also ensures that all SM fermions belong to a single irreducible representation of the complete symmetry group.

The motivation for considering such an $SU(5)^3$ with cyclic symmetry is that it allows gauge non-universal theories of flavour to emerge at low energies[2] from a gauge universal theory, depending on the symmetry breaking chain. In the first step, $SU(5)^3$ may be[3] broken to three copies of the SM gauge group SM^3. Then at lower energies, SM^3 is broken to some universal piece $G_{\text{universal}}$ consisting of some diagonal subgroups, together with some remaining family groups $G_1 \times G_2 \times G_3$. If the light Higgs doublet(s) transform non-trivially under the third family group G_3, but not under the first nor second, then third family fermions get natural masses at the electroweak scale, while first and second family fermions are massless in first approximation. Their small masses naturally arise from

[2] $SU(5)^3$ tri-unification may provide a unified origin for many gauge non-universal theories proposed in the literature to address different questions beyond the flavour puzzle, see e.g. [172, 376].

[3] This first step of symmetry breaking is optional, but may be convenient to control the scale of gauge unification as discussed in Section 6.3.4.

the breaking of the non-universal gauge group down to the SM, which is the diagonal subgroup, and an approximate $U(2)^5$ flavour symmetry emerges, which is known to provide an efficient suppression of the most dangerous flavour-violating effects for new physics [110, 397].

At still lower energies, the non-diagonal group factors $G_1 \times G_2 \times G_3$ are broken down to their diagonal subgroup, eventually leading to a flavour universal SM gauge group factor. This may happen in stages. In particular, the symmetry breaking pattern

$$G_1 \times G_2 \times G_3 \to G_{1+2} \times G_3 \to \mathrm{G}_{1+2+3} \tag{6.3}$$

may naturally explain the origin of fermion mass hierarchies and the smallness of quark mixing, while anarchic neutrino mixing may be incorporated via variations of the type I seesaw mechanism [3, 117].

Minimal examples of this class of theories include the tri-hypercharge model [3], already discussed in Chapter 5, where the universal (diagonal) group consists of the non-Abelian SM gauge group factors $G_{\text{universal}} = SU(3)_c \times SU(2)_L$ while the remaining groups are the three gauge weak hypercharge factors $G_1 \times G_2 \times G_3 = U(1)_{Y_1} \times U(1)_{Y_2} \times U(1)_{Y_3}$. Another example is the $SU(2)_L^3$ model [116, 124–126, 370–373, 375], where $G_{\text{universal}} = SU(3)_c \times U(1)_Y$ and $G_1 \times G_2 \times G_3 = SU(2)_{L1} \times SU(2)_{L2} \times SU(2)_{L3}$. There also exists the $SU(3)_c^3$ model [388] (which is only able to explain the smallness of quark mixing), where $G_{\text{universal}} = SU(2)_L \times U(1)_Y$ and $G_1 \times G_2 \times G_3 = SU(3)_{c1} \times SU(3)_{c2} \times SU(3)_{c3}$. Variations of these theories have been proposed in recent years, several of them assuming a possible embedding into (variations of) a Pati-Salam setup [115, 117, 119–122].

All these theories share a common feature: they explain the origin of the flavour structure of the SM at the price of complicating the gauge sector, which may now contain up to nine arbitrary gauge couplings. We will motivate that $SU(5)^3$ as the embedding of general theories $G_{\text{universal}} \times G_1 \times G_2 \times G_3$ resolves this issue, by unifying the complicated gauge sector of these theories into a single gauge coupling. The main ingredients of our general setup are as follows:

- The presence of the $\mathbb{Z}_3$ symmetry, which is of fundamental importance to achieve gauge unification, imposes that the matter content of the model shall be invariant under cyclic permutations of the three $SU(5)$ factors. This enforces that each $SU(5)$ factor contains the same representations of fermions and scalars, i.e. if the representation $(\mathbf{A}, \mathbf{B}, \mathbf{C})$ is included, then $(\mathbf{C}, \mathbf{A}, \mathbf{B})$ and $(\mathbf{B}, \mathbf{C}, \mathbf{A})$ must be included too.

- Each family of chiral fermions i is embedded in the usual way into $\overline{\mathbf{5}}$ and $\mathbf{10}$ representations of their corresponding $SU(5)_i$ factor, that we denote as $F_i = (d_i^c, \ell_i) \sim \overline{\mathbf{5}}_i$ and $T_i = (q_i, u_i^c, e_i^c) \sim \mathbf{10}_i$ as shown in Table 6.1. This choice is naturally consistent with the $\mathbb{Z}_3$ symmetry.

- In a similar manner, three Higgs doublets H_1, H_2 and H_3 are embedded into **5** representations, one for each $SU(5)_i$ factor. Notice that in non-universal theories of flavour it is commonly assumed the existence of only one Higgs doublet H_3, which transforms only under the third site in order to explain the heaviness of the third family. This way, the $SU(5)^3$ framework involves the restriction of having three Higgses rather than only one, but we will argue that if the $\mathbb{Z}_3$ symmetry is broken below the GUT scale, then only the third family Higgs H_3 may be light and perform electroweak symmetry breaking, while H_1 and H_2 are heavier and may play the role of heavy messengers for the effective Yukawa couplings of the light families.

- Higgs scalars in bi-representations connecting the different sites may be needed to generate the SM flavour structure at the level of the $G_{\text{universal}} \times G_1 \times G_2 \times G_3$ theory, e.g. $(\mathbf{2}, \overline{\mathbf{2}})$ scalars in $SU(2)^3_L$ or $(Y, -Y)$ scalars in tri-hypercharge (the so-called hyperons). These can be embedded in the associated bi-representations of $SU(5)^3$, e.g. $(\mathbf{5}, \overline{\mathbf{5}})$ scalars, $(\mathbf{10}, \overline{\mathbf{10}})$ scalars and so on. In Appendix C we tabulate all such scalars from $SU(5)^3$ representations with dimension up to **45**, along with the hyperons that they generate at low energies.

- Finally, three scalar fields in the adjoint representation of each $SU(5)$, $\Omega_i \sim \mathbf{24}_i$, spontaneously break each $SU(5)_i$. We argue that the three Ω_i are enough to perform *both* horizontal and vertical breaking of the $SU(5)$ groups, thanks to the $\mathbb{Z}_3$ symmetry. Indeed, thanks to the $\mathbb{Z}_3$ symmetry, the three adjoint scalars can get naturally degenerate VEVs, in such a way that the three $SU(5)$ groups can be simultaneously broken at the GUT scale down to the non-universal gauge group $G_{\text{universal}} \times G_1 \times G_2 \times G_3$ of choice that later explains the flavour structure of the SM (e.g. tri-hypercharge or $SU(2)^3_L$). Another possibility that we will explore is breaking $SU(5)^3$ first to three copies of the SM (one for each family) and then to $G_{\text{universal}} \times G_1 \times G_2 \times G_3$ in a second step.

To summarise, the general pattern of symmetry breaking we assume is as follows[4],

$$SU(5)^3 \to \text{SM}_1 \times \text{SM}_2 \times \text{SM}_3 \tag{6.4}$$

$$\to G_{\text{universal}} \times G_1 \times G_2 \times G_3 \tag{6.5}$$

$$\to G_{\text{universal}} \times G_{1+2} \times G_3 \tag{6.6}$$

$$\to \text{SM}_{1+2+3}\,, \tag{6.7}$$

where the SM^3 step is optional but may be convenient to achieve unification. In particular, the first step of symmetry breaking makes use of the three SM singlets contained in $\Omega_i \sim \mathbf{24}_i$, while the second step may be performed via the remaining degrees of freedom

[4]One should note that none of the individual groups, $SU(3)$, $SU(2)$ or $U(1)$, in each SM_i group correspond to the SM's $SU(3)_c$, $SU(2)_L$ or $U(1)_Y$. The latter emerge after symmetry breaking from the diagonal sub-groups of the former. Nevertheless, we will denote each $(SU(3) \times SU(2) \times U(1))_i$ as SM_i and the total $(SU(3) \times SU(2) \times U(1))^3$ group as SM^3 for the sake of brevity.

in the Ω_i[5], depending on the details of the low energy gauge theory that survives. The two final breaking steps are performed by Higgs scalars connecting the different sites that need to be specified for each particular model.

Beyond the general considerations listed in this section, when building a specific model one needs to choose the symmetry group $G_{\text{universal}} \times G_1 \times G_2 \times G_3$, and add explicit scalars and/or fermion messengers that mediate the effective Yukawa couplings of light fermions.

Finally, one needs to study the Renormalization Group Equations (RGEs) of the various gauge couplings at the different steps all the way up to the $SU(5)^3$ scale where all gauge couplings need to unify. This is not a simple task, but we shall see that the relatively light messengers required to generate the effective Yukawa couplings, along with the presence of the approximate $\mathbb{Z}_3$ symmetry at low energies, may naturally help to achieve unification. In the following, we shall illustrate this by describing a working example of the $SU(5)^3$ framework based on tri-hypercharge (see Chapter 5), where the various gauge couplings of the tri-hypercharge model unify at the GUT scale into a single gauge coupling.

6.3 An example $SU(5)^3$ unification model breaking to tri-hypercharge

In the following we discuss an example of the tri-hypercharge model, i.e. $G_{\text{universal}} = SU(3)_c \times SU(2)_L$ and $G_1 \times G_2 \times G_3 = U(1)_{Y_1} \times U(1)_{Y_2} \times U(1)_{Y_3}$ (see Chapter 5), originating from the $SU(5)^3$ tri-unification framework. In this example, the basic idea is that $SU(5)^3$ breaks, via a sequence of scales, to the low energy (well below the GUT scale) tri-hypercharge gauge group with a separate gauged weak hypercharge for each fermion family,

$$SU(5)^3 \to \cdots \to SU(3)_c \times SU(2)_L \times U(1)_{Y_1} \times U(1)_{Y_2} \times U(1)_{Y_3}\,. \tag{6.8}$$

In Chapter 5 it was shown that the low energy tri-hypercharge model can naturally generate the flavour structure of the SM if spontaneously broken to SM hypercharge in a convenient way. The minimal setup involves the vacuum expectation values (VEVs) of the new Higgs "hyperons"

$$\phi_{q12} \sim (\mathbf{1},\mathbf{1})_{(-1/6,1/6,0)}, \qquad \phi_{q23} \sim (\mathbf{1},\mathbf{1})_{(0,-1/6,1/6)}, \qquad \phi_{\ell 23} \sim (\mathbf{1},\mathbf{1})_{(0,1/2,-1/2)}\,. \tag{6.9}$$

At the GUT scale, the hyperons are embedded into bi-$\overline{\mathbf{5}}$ and bi-$\mathbf{10}$ representations of $SU(5)^3$ expressed as $\Phi_{ij}^{T,F}$, which must preserve the cyclic symmetry, as shown in Table 6.2. Although this involves the appearance of many hyperons (and other scalars)

[5] As we shall see later, the SM^3 breaking cannot happen much below the GUT scale in order to ensure both gauge coupling unification and enough lifetime for the proton, hence the Ω_i related by $\mathbb{Z}_3$ can always perform this second breaking step as well.

Field	$SU(5)_1$	$SU(5)_2$	$SU(5)_3$
F_1	$\bar{\mathbf{5}}$	$\mathbf{1}$	$\mathbf{1}$
F_2	$\mathbf{1}$	$\bar{\mathbf{5}}$	$\mathbf{1}$
F_3	$\mathbf{1}$	$\mathbf{1}$	$\bar{\mathbf{5}}$
T_1	$\mathbf{10}$	$\mathbf{1}$	$\mathbf{1}$
T_2	$\mathbf{1}$	$\mathbf{10}$	$\mathbf{1}$
T_3	$\mathbf{1}$	$\mathbf{1}$	$\mathbf{10}$
χ_1	$\mathbf{10}$	$\mathbf{1}$	$\mathbf{1}$
χ_2	$\mathbf{1}$	$\mathbf{10}$	$\mathbf{1}$
χ_3	$\mathbf{1}$	$\mathbf{1}$	$\mathbf{10}$
Ξ_0	$\mathbf{1}$	$\mathbf{1}$	$\mathbf{1}$
Ξ_{12}	$\mathbf{5}$	$\bar{\mathbf{5}}$	$\mathbf{1}$
Ξ_{13}	$\bar{\mathbf{5}}$	$\mathbf{1}$	$\mathbf{5}$
Ξ_{23}	$\mathbf{1}$	$\mathbf{5}$	$\bar{\mathbf{5}}$
Σ_{atm}	$\mathbf{1}$	$\mathbf{10}$	$\overline{\mathbf{10}}$
Σ_{sol}	$\mathbf{10}$	$\mathbf{1}$	$\overline{\mathbf{10}}$
Σ_{cyclic}	$\mathbf{10}$	$\overline{\mathbf{10}}$	$\mathbf{1}$
Ω_1	$\mathbf{24}$	$\mathbf{1}$	$\mathbf{1}$
Ω_2	$\mathbf{1}$	$\mathbf{24}$	$\mathbf{1}$
Ω_3	$\mathbf{1}$	$\mathbf{1}$	$\mathbf{24}$
H_1^u	$\mathbf{5}$	$\mathbf{1}$	$\mathbf{1}$
H_2^u	$\mathbf{1}$	$\mathbf{5}$	$\mathbf{1}$
H_3^u	$\mathbf{1}$	$\mathbf{1}$	$\mathbf{5}$
$H_1^{\bar{\mathbf{5}}}$	$\bar{\mathbf{5}}$	$\mathbf{1}$	$\mathbf{1}$
$H_2^{\bar{\mathbf{5}}}$	$\mathbf{1}$	$\bar{\mathbf{5}}$	$\mathbf{1}$
$H_3^{\bar{\mathbf{5}}}$	$\mathbf{1}$	$\mathbf{1}$	$\bar{\mathbf{5}}$
$H_1^{\mathbf{45}}$	$\mathbf{45}$	$\mathbf{1}$	$\mathbf{1}$
$H_2^{\mathbf{45}}$	$\mathbf{1}$	$\mathbf{45}$	$\mathbf{1}$
$H_3^{\mathbf{45}}$	$\mathbf{1}$	$\mathbf{1}$	$\mathbf{45}$
Φ_{12}^F	$\mathbf{5}$	$\bar{\mathbf{5}}$	$\mathbf{1}$
Φ_{13}^F	$\bar{\mathbf{5}}$	$\mathbf{1}$	$\mathbf{5}$
Φ_{23}^F	$\mathbf{1}$	$\mathbf{5}$	$\bar{\mathbf{5}}$
Φ_{12}^T	$\overline{\mathbf{10}}$	$\mathbf{10}$	$\mathbf{1}$
Φ_{13}^T	$\mathbf{10}$	$\mathbf{1}$	$\overline{\mathbf{10}}$
Φ_{23}^T	$\mathbf{1}$	$\overline{\mathbf{10}}$	$\mathbf{10}$
$\Phi_{12}^{\mathbf{45}}$	$\mathbf{1}$	$\overline{\mathbf{45}}$	$\mathbf{45}$
$\Phi_{13}^{\mathbf{45}}$	$\overline{\mathbf{45}}$	$\mathbf{1}$	$\mathbf{45}$
$\Phi_{12}^{\mathbf{45}}$	$\overline{\mathbf{45}}$	$\mathbf{45}$	$\mathbf{1}$
Φ^{TFT}	$\mathbf{10}$	$\mathbf{5}$	$\mathbf{10}$
Φ^{FTT}	$\mathbf{5}$	$\mathbf{10}$	$\mathbf{10}$
Φ^{TTF}	$\mathbf{10}$	$\mathbf{10}$	$\mathbf{5}$

TABLE 6.2: Fermion and scalar particle content and representations under $SU(5)^3$. F_i and T_i include the chiral fermions of the SM in the usual way, while χ_i, ξ's and Ξ's (highlighted in yellow) are vector-like fermions, thus the conjugate partners must be considered. Ω's, H's and Φ's are scalars.

beyond the minimal set of hyperons that we need, we shall assume that only the desired hyperons get a VEV (and the rest of scalars may remain very heavy). Moreover, the $SU(5)^3$ framework also poses constraints on the possible family hypercharges of the hyperons, as collected in Appendix C. For the $SU(5)^3$ setup, it is convenient to add

$$\phi_{q13} \sim (\mathbf{1},\mathbf{1})_{(-1/6,0,1/6)}\,, \qquad \phi_{\ell 13} \sim (\mathbf{1},\mathbf{1})_{(1/2,0,-1/2)}\,, \tag{6.10}$$

which are anyway required by the cyclic symmetry, to the set of hyperons which get a VEV.

The hyperons allow to write a set of non-renormalisable operators that provide effective Yukawa couplings for light fermions, as described in Chapter 5 by working in an EFT framework. However, in our unified model, we need to introduce heavy messengers that mediate such effective operators in order to obtain a UV complete setup. For this, we add one set of vector-like fermions transforming in the **10** representation for each $SU(5)$ factor, i.e. $\chi_i \sim \mathbf{10}_i$ and $\overline{\chi}_i \sim \overline{\mathbf{10}}_i$. We shall assume that only the quark doublets $Q_i \sim (\mathbf{3},\mathbf{2})_{1/6_i}$ and $\overline{Q}_i \sim (\overline{\mathbf{3}},\mathbf{2})_{-1/6_i}$ are relatively light and play a role in the effective Yukawa couplings, while the remaining degrees of freedom in χ_i and $\overline{\chi}_i$ remain very heavy,

$$\chi_i \sim \mathbf{10}_i \to Q_i \sim (\mathbf{3},\mathbf{2})_{1/6_i}\,, \qquad \overline{\chi}_i \sim \overline{\mathbf{10}}_i \to \overline{Q}_i \sim (\overline{\mathbf{3}},\mathbf{2})_{-1/6_i}\,. \tag{6.11}$$

We shall see that Q_i and $\overline{Q}_i$ also contribute to the RGEs in the desired way to achieve gauge unification. The full field content of this model also includes extra vector-like fermions Σ and Ξ as shown in Table 6.2. These play a role in the origin of neutrino masses as discussed in Section 6.3.2.

Finally, beyond the minimal set of Higgs doublets introduced in Section 6.2, we shall introduce here three pairs of **5**, $\overline{\mathbf{5}}$ and **45** Higgs representations preserving the cyclic symmetry. The doublets in the $\overline{\mathbf{5}}$ and **45** mix, leaving light linear combinations that couple differently to down-quarks and charged leptons in the usual way [94], which we denote as H_i^d.

Therefore, below the GUT scale we effectively have three pairs of Higgs doublets $H_1^{u,d}$, $H_2^{u,d}$ and $H_3^{u,d}$, such that the u- and d- labeled Higgs only couple to up-quarks (and neutrinos) and to down-quarks and charged leptons, respectively, in the spirit of the type II 2HDM. This choice is motivated to explain the mass hierarchies between the different charged sectors, as originally identified in Chapter 5, and could be enforced e.g. by a $\mathbb{Z}_2$ discrete symmetry. We assume that the third family Higgs $H_3^{u,d}$ are the lightest, they perform electroweak symmetry breaking and provide Yukawa couplings for the third family with $\mathcal{O}(1)$ coefficients if $\tan\beta \approx 20$. In contrast, we assume that the Higgs $H_1^{u,d}$, $H_2^{u,d}$ have masses above the TeV (but much below the GUT scale) and act as messengers of the effective Yukawa couplings for the light families.

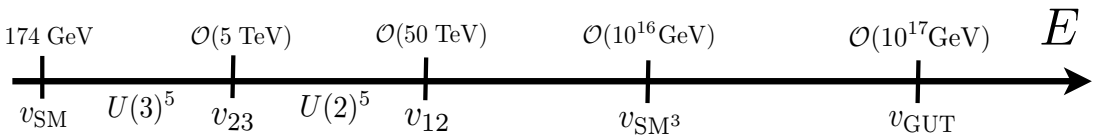

FIGURE 6.1: Diagram showing the different scales of spontaneous symmetry breaking in our example model (see also Eqs.(6.12-6.15)), along with the accidental, approximate flavour symmetries ($U(3)^5$ and $U(2)^5$) that arise at low energies.

In detail, we assume that the $SU(5)^3$ group is broken down to the SM through the following symmetry breaking chain

$$SU(5)^3 \xrightarrow{v_{\rm GUT}} {\rm SM}_1 \times {\rm SM}_2 \times {\rm SM}_3 \tag{6.12}$$

$$\xrightarrow{v_{\rm SM^3}} SU(3)_{1+2+3} \times SU(2)_{1+2+3} \times U(1)_1 \times U(1)_2 \times U(1)_3 \tag{6.13}$$

$$\xrightarrow{v_{12}} SU(3)_{1+2+3} \times SU(2)_{1+2+3} \times U(1)_{1+2} \times U(1)_3 \tag{6.14}$$

$$\xrightarrow{v_{23}} SU(3)_{1+2+3} \times SU(2)_{1+2+3} \times U(1)_{1+2+3}\,. \tag{6.15}$$

The $SU(5)^3$ breaking happens at the GUT scale, while the tri-hypercharge breaking may happen as low as the TeV scale, as allowed by current data (see Section 5.6), while the SM^3 breaking step is optional but may be convenient to achieve unification, and may be regarded as free parameter. This second breaking step is performed by the $SU(3)_i$ octets and $SU(2)_i$ triplets contained in $\Omega_i \sim \mathbf{24}_i$. See also Fig. 6.1 for an illustrative diagram.

We shall show that within this setup, achieving gauge unification just requires further assuming that the three colour octets that live in $\Omega_i \sim \mathbf{24}_i$ are light, while the remaining degrees of freedom of the adjoints remain very heavy. Before that, we shall study in detail how our model explains the origin of the flavour structure of the SM.

6.3.1 Charged fermion mass hierarchies and quark mixing

In this section we shall discuss the origin of charged fermion mass hierarchies and quark mixing at the tri-hypercharge layer. In contrast with Chapter 3, here we shall specify the UV origin of the effective Yukawa couplings as we intend to build a UV-complete GUT model. In this manner, we will show a much more complete framework for the generation of the SM flavour structure than in Chapter 5, where an EFT framework with a common cut-off scale for all effective Yukawa couplings was considered.

The Higgs doublets in the cyclic $\overline{\mathbf{5}}$ and $\mathbf{45}$ split the couplings of down-quarks and charged leptons in the usual way [94]. We denote as H_i^d the linear combinations that remain light, with their effective couplings to down-quarks and charged leptons given by

$$\widetilde{y}_i^d H_i^d T_i F_i \to y_i^d H_i^d q_i d_i^c + y_i^e H_i^d \ell_i e_i^c, \tag{6.16}$$

where

$$y_i^d = y_i^{\overline{\mathbf{5}}} + y_i^{\overline{\mathbf{45}}}\,, \qquad y_i^e = y_i^{\overline{\mathbf{5}}} - 3y_i^{\overline{\mathbf{45}}}\,. \tag{6.17}$$

We focus now on the following set of couplings involving the hyperons, the vector-like fermions χ_i and the light linear combinations of Higgs doublets,

$$\begin{aligned}\mathcal{L} \supset\; & x_{ij}\,\Phi_{ij}^T T_i \overline{\chi}_j + z_i^u\, H_i^u \chi_i T_i + z_i^d\, H_i^d \chi_i F_i \\ & + y_i^u\, H_i^u T_i T_i + \widetilde{y}_i^d\, H_i^d T_i F_i + f_{ij}^u\, H_i^u \widetilde{H}_j^u \widetilde{\Phi}_{ij}^F + f_{ij}^d\, H_i^d \widetilde{H}_j^d \Phi_{ij}^F\,,\end{aligned} \tag{6.18}$$

where $i,j=1,2,3$, $f_{ij}^{u,d}$ have mass dimension and the rest of the couplings are dimensionless. After integrating out the heavy vector-like fermions χ_i, $\overline{\chi}_i$ and Higgs doublets $H_{1,2}^{u,d}$, we obtain the following set of effective Yukawa couplings,

$$\mathcal{L} = (q_1 \quad q_2 \quad q_3) \begin{pmatrix} c_{11}^u \dfrac{\phi_{\ell 13}}{M_{H_1^u}} & c_{12}^u \dfrac{\phi_{\ell 23}}{M_{H_2^u}} \dfrac{\phi_{q12}}{M_{Q_2}} & c_{13}^u \dfrac{\phi_{q13}}{M_{Q_3}} \\ c_{21}^u \dfrac{\phi_{\ell 13}}{M_{H_1^u}} \dfrac{\phi_{q12}}{M_{Q_1}} & c_{22}^u \dfrac{\phi_{\ell 23}}{M_{H_2^u}} & c_{23}^u \dfrac{\phi_{q23}}{M_{Q_3}} \\ c_{31}^u \dfrac{\phi_{\ell 13}}{M_{H_1^u}} \dfrac{\widetilde{\phi}_{q13}}{M_{Q_1}} & c_{32}^u \dfrac{\phi_{\ell 23}}{M_{H_2^u}} \dfrac{\widetilde{\phi}_{q23}}{M_{Q_2}} & c_{33}^u \end{pmatrix} \begin{pmatrix} u_1^c \\ u_2^c \\ u_3^c \end{pmatrix} H_3^u \tag{6.19}$$

$$+ (q_1 \quad q_2 \quad q_3) \begin{pmatrix} c_{11}^d \dfrac{\widetilde{\phi}_{\ell 13}}{M_{H_1^d}} & c_{12}^d \dfrac{\widetilde{\phi}_{\ell 23}}{M_{H_2^d}} \dfrac{\phi_{q12}}{M_{Q_2}} & c_{13}^d \dfrac{\phi_{q13}}{M_{Q_3}} \\ c_{21}^d \dfrac{\phi_{\ell 13}}{M_{H_1^d}} \dfrac{\phi_{q12}}{M_{Q_1}} & c_{22}^d \dfrac{\widetilde{\phi}_{\ell 23}}{M_{H_2^d}} & c_{23}^d \dfrac{\phi_{q23}}{M_{Q_3}} \\ c_{31}^d \dfrac{\phi_{\ell 13}}{M_{H_1^d}} \dfrac{\widetilde{\phi}_{q13}}{M_{Q_1}} & c_{32}^d \dfrac{\phi_{\ell 23}}{M_{H_2^d}} \dfrac{\widetilde{\phi}_{q23}}{M_{Q_2}} & c_{33}^d \end{pmatrix} \begin{pmatrix} d_1^c \\ d_2^c \\ d_3^c \end{pmatrix} H_3^d \tag{6.20}$$

$$+ (\ell_1 \quad \ell_2 \quad \ell_3) \begin{pmatrix} c_{11}^e \dfrac{\widetilde{\phi}_{\ell 13}}{M_{H_1^d}} & 0 & 0 \\ 0 & c_{22}^e \dfrac{\widetilde{\phi}_{\ell 23}}{M_{H_2^d}} & 0 \\ 0 & 0 & c_{33}^e \end{pmatrix} \begin{pmatrix} e_1^c \\ e_2^c \\ e_3^c \end{pmatrix} H_3^d + \text{h.c.}\,, \tag{6.21}$$

where the dimensionless coefficients $c_{ij}^{u,d,e}$ are given by

$$c_{ij}^u = \begin{pmatrix} y_1^u \dfrac{f_{13}^u}{M_{H_1}^u} & x_{12} y_2^u \dfrac{f_{23}^u}{M_{H_2}^u} & x_{13} z_3^u \\ x_{21} y_1^u \dfrac{f_{13}^u}{M_{H_1}^u} & y_2^u \dfrac{f_{23}^u}{M_{H_2}^u} & x_{23} z_3^u \\ x_{31} y_1^u \dfrac{f_{13}^u}{M_{H_1}^u} & x_{32} y_2^u \dfrac{f_{23}^u}{M_{H_2}^u} & y_3^u \end{pmatrix}, \tag{6.22}$$

$$c_{ij}^{d} = \begin{pmatrix} y_1^d \dfrac{f_{13}^d}{M_{H_1}^d} & x_{12} y_2^d \dfrac{f_{23}^d}{M_{H_2}^d} & x_{13} z_3^d \\ x_{21} y_1^d \dfrac{f_{13}^d}{M_{H_1}^d} & y_2^d \dfrac{f_{23}^d}{M_{H_2}^d} & x_{23} z_3^d \\ x_{31} y_1^d \dfrac{f_{13}^d}{M_{H_1}^d} & x_{32} y_2^d \dfrac{f_{23}^d}{M_{H_2}^d} & y_3^d \end{pmatrix} , \tag{6.23}$$

$$c_{ij}^{e} = \text{diag}\left(y_1^e \frac{f_{13}^d}{M_{H_1}^d}, y_2^e \frac{f_{23}^d}{M_{H_2}^d}, y_3^e \right) . \tag{6.24}$$

It is clear that third family charged fermions get their masses from $\mathcal{O}(1)$ Yukawa couplings to the Higgs doublets $H_3^{u,d}$, where the mass hierarchies $m_{b,\tau}/m_t$ are explained via $\tan\beta \approx \lambda^{-2}$, where $\lambda \simeq 0.224$ is the Wolfenstein parameter. In contrast, quark mixing and the masses of first and second family charged fermions arise from effective Yukawa couplings involving the heavy messengers of the model, once the hyperons develop their VEVs. The heavy Higgs doublets $H_1^{u,d}$ and $H_2^{u,d}$ play a role in the origin of the family mass hierarchies, while the origin of quark mixing involves both the heavy Higgs and the vector-like quarks Q_i and $\overline{Q}_i$, as shown in Fig. 6.2. We fix the various $\langle\phi\rangle/M$ ratios in terms of the Wolfenstein parameter $\lambda \simeq 0.224$

$$\frac{\langle\phi_{q23}\rangle}{M_{Q_i}} \approx \lambda^2 , \qquad \frac{\langle\phi_{q13}\rangle}{M_{Q_i}} \approx \lambda^3 , \qquad \frac{\langle\phi_{\ell 23}\rangle}{M_{H_2^{u,d}}} \approx \lambda^3 , \qquad \frac{\langle\phi_{q12}\rangle}{M_{Q_i}} \approx \lambda , \qquad \frac{\langle\phi_{\ell 23}\rangle}{M_{H_1^{u,d}}} \approx \lambda^6 . \tag{6.25}$$

We notice that the tiny masses of the first family are explained via the hierarchies of Higgs messengers

$$M_{H_3^{u,d}} \ll M_{H_2^{u,d}} \ll M_{H_1^{u,d}} , \tag{6.26}$$

in the spirit of messenger dominance [171]. In other words, the heavy Higgs doublets $H_1^{u,d}$ and $H_2^{u,d}$ can be thought of gaining small effective VEVs from mixing with $H_3^{u,d}$, which are light and perform electroweak symmetry breaking, and these effective VEVs provide naturally small masses for light charged fermions. This is in contrast with the original spirit of tri-hypercharge, where the m_1/m_2 mass hierarchies find their natural origin due to the higher dimension of the effective Yukawa couplings involving the first family (see e.g. Section 5.3.3). However, we note that in the $SU(5)^3$ framework, the three pairs of Higgs doublets $H_i^{u,d}$ are required by the $\mathbb{Z}_3$ symmetry, hence it seems natural that they play a role on the origin of fermion masses. Moreover, the introduction of these Higgs provides a very minimal framework to UV-complete the effective Yukawa couplings of tri-hypercharge, which otherwise would require a much larger set of heavy messengers that are not desired, as they may enhance too much the RGE of the gauge couplings, eventually leading to a non-perturbative gauge coupling at the GUT scale.

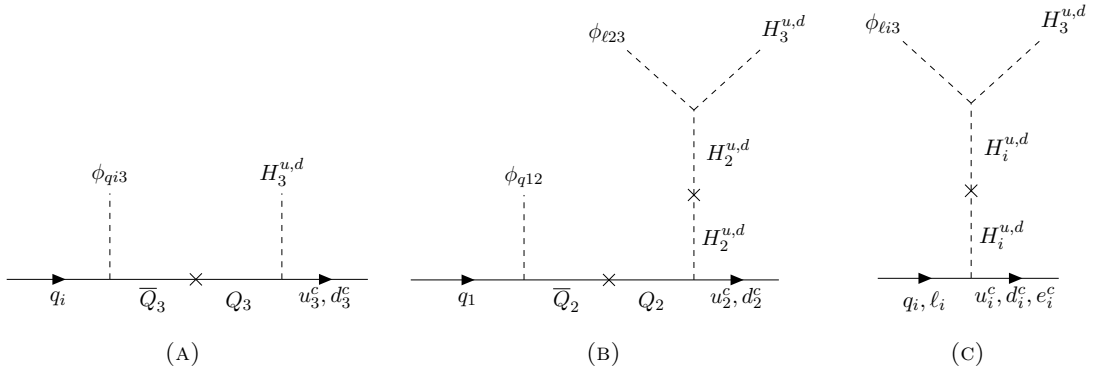

FIGURE 6.2: Diagrams in the model which lead to the origin of light charged fermion masses and quark mixing, where $i = 1, 2$.

The numerical values for the ratios in Eq. (6.25) provide the following Yukawa textures (ignoring dimensionless coefficients)

$$\mathcal{L} = (q_1 \quad q_2 \quad q_3) \begin{pmatrix} \lambda^6 & \lambda^4 & \lambda^3 \\ \lambda^7 & \lambda^3 & \lambda^2 \\ \lambda^9 & \lambda^5 & 1 \end{pmatrix} \begin{pmatrix} u_1^c \\ u_2^c \\ u_3^c \end{pmatrix} v_{\rm SM} \tag{6.27}$$

$$+ (q_1 \quad q_2 \quad q_3) \begin{pmatrix} \lambda^6 & \lambda^4 & \lambda^3 \\ \lambda^7 & \lambda^3 & \lambda^2 \\ \lambda^9 & \lambda^5 & 1 \end{pmatrix} \begin{pmatrix} d_1^c \\ d_2^c \\ d_3^c \end{pmatrix} \lambda^2 \, v_{\rm SM} \tag{6.28}$$

$$+ (\ell_1 \quad \ell_2 \quad \ell_3) \begin{pmatrix} \lambda^6 & 0 & 0 \\ 0 & \lambda^3 & 0 \\ 0 & 0 & 1 \end{pmatrix} \begin{pmatrix} e_1^c \\ e_2^c \\ e_3^c \end{pmatrix} \lambda^2 \, v_{\rm SM} + \text{h.c.}\,, \tag{6.29}$$

where $v_{\rm SM}$ is the usual SM electroweak VEV and the fit of the up-quark mass may be improved by assuming a mild difference between $M_{H_1^u}$ and $M_{H_1^d}$. In general, the alignment of the CKM matrix is not predicted but depends on the choice of dimensionless coefficients and on the difference between $M_{H_2^u}$ and $M_{H_2^d}$. Any charged lepton mixing is suppressed by the very heavy masses of the required messengers contained in χ_i and $\overline{\chi}_i$, leading to the off-diagonal zeros in Eq. (6.29), in such a way that the PMNS matrix must dominantly arise from the neutrino sector, as we shall see. We notice that a mild hierarchy of dimensionless couplings $y_1^e/y_1^d \approx \lambda^{1.4}$ may be needed to account for the mass hierarchy between the down-quark and the electron.

The larger suppression of the (2,1), (3,1) and (3,2) entries in the quark Yukawa textures ensures a significant suppression of right-handed quark mixing. This is a very desirable feature, given the strong phenomenological constraints on right-handed flavour-changing currents [238,239]. This way, we expect the model to reproduce the low energy phenomenology of Model 2 in Chapter 5, where the VEVs of the 23 and 13 hyperons may be as low as the TeV scale, while the VEVs of the 12 hyperons may be as low as 50 TeV or so. In this manner, we provide the following benchmark values for the mass

scales involved in the flavour sector[6]

$$\langle \phi_{q23} \rangle \approx \langle \phi_{q13} \rangle \approx \langle \phi_{\ell 23} \rangle \approx \langle \phi_{\ell 13} \rangle \sim \mathcal{O}(5\,\text{TeV})\,, \tag{6.30}$$

$$\langle \phi_{q12} \rangle \sim \mathcal{O}(50\,\text{TeV})\,, \tag{6.31}$$

$$M_{Q_i} \sim \mathcal{O}(100\,\text{TeV})\,, \tag{6.32}$$

$$M_{H_2^{u,d}} \sim \mathcal{O}(100\,\text{TeV})\,, \tag{6.33}$$

$$M_{H_1^{u,d}} \sim \mathcal{O}(10^4\,\text{TeV})\,. \tag{6.34}$$

6.3.2 Neutrino masses and mixing

Explaining the observed pattern of neutrino mixing and mass splittings in gauge non-universal theories of flavour is usually difficult, due to the accidental $U(2)^5$ flavour symmetry predicted by these models, which is naively present in the neutrino sector as well. However, exotic variations of the type I seesaw mechanism have been shown to be successful in accommodating neutrino observations within non-universal theories of flavour, see Refs. [3, 117]. Here we will incorporate the mechanism of [3] (also described in Section 5.4 of this thesis), which consists of adding SM singlet neutrinos which carry family hypercharges (although their sum must of course vanish). These neutrinos can be seen as the fermionic counterpart of hyperons, as they will connect the different hypercharge sites, therefore breaking the $U(2)^5$ flavour symmetry in the neutrino sector. In this manner, these neutrinos allow to write effective operators which may provide a successful pattern for neutrino mixing. However, the particular model presented in Section 5.4 incorporates SM singlet neutrinos with 1/4 family hypercharge factors, which cannot be obtained from $SU(5)^3$, at least not from representations with dimension smaller than **45**[7] according to a search with `GroupMath` [398].

Following the recipe of Section 5.4, we start by introducing two right-handed neutrinos: $N_{\text{atm}} \sim (\mathbf{1},\mathbf{1})_{(0,2/3,-2/3)}$ and $N_{\text{sol}} \sim (\mathbf{1},\mathbf{1})_{(2/3,0,-2/3)}$, which will be responsible for atmospheric and solar neutrino mixing, respectively. These neutrinos are embedded in $\Sigma_{23} \sim (\mathbf{1},\mathbf{10},\overline{\mathbf{10}})$ and $\Sigma_{13} \sim (\mathbf{10},\mathbf{1},\overline{\mathbf{10}})$ representations of $SU(5)^3$, respectively. We also need to add the cyclic permutation N_{cyclic} embedded in $\Sigma_{12} \sim (\mathbf{10},\overline{\mathbf{10}},\mathbf{1})$ to preserve the cyclic symmetry of $SU(5)^3$. However, we find that if the "cyclic" neutrino contained in Σ_{12} is much heavier than the other neutrinos, then we can ignore it as it decouples from the seesaw, and we recover the minimal framework of Section 5.4. Finally, in order to cancel gauge anomalies, we choose to make these neutrinos vector-like by introducing the three corresponding conjugate neutrinos.

[6] We note that all VEVs and masses listed here may vary by $\mathcal{O}(1)$ factors, as naturally expected, without affecting our final conclusions.

[7] Since these singlet neutrinos can be seen as the fermionic counterpart of hyperons, the search for $SU(5)^3$ hyperon embeddings shown in Appendix C shows that no neutrinos with 1/4 family hypercharge factors are found from $SU(5)^3$ representations with dimension up to **45**.

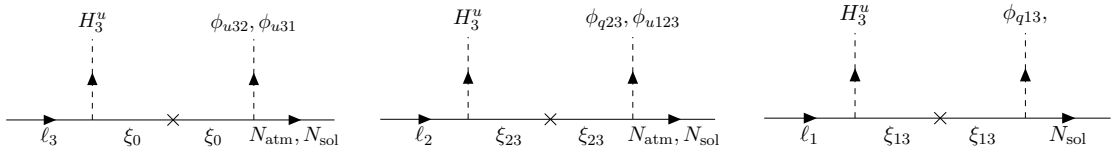

FIGURE 6.3: Diagrams leading to effective Yukawa couplings in the neutrino sector.

The next step is adding hyperons that provide effective Yukawa couplings and Majorana masses for the singlet neutrinos. These are summarised in the Dirac and Majorana mass matrices that follow (ignoring the $\mathcal{O}(1)$ dimensionless couplings and the much heavier cyclic neutrinos)

$$m_{D_L} = \begin{pmatrix} & \overline{N}_{\rm sol} & \overline{N}_{\rm atm} \\ L_1 & 0 & 0 \\ L_2 & 0 & 0 \\ L_3 & \widetilde{\phi}_{u31}^{(-\frac{2}{3},0,\frac{2}{3})} & \widetilde{\phi}_{u32}^{(0,-\frac{2}{3},\frac{2}{3})} \end{pmatrix} \frac{H_u}{M_\xi}, \quad m_{D_R} = \begin{pmatrix} & N_{\rm sol} & N_{\rm atm} \\ L_1 & \phi_{q13}^{(-\frac{1}{6},0,\frac{1}{6})} & 0 \\ L_2 & \phi_{u123}^{(-\frac{2}{3},\frac{1}{2},\frac{1}{6})} & \phi_{q23}^{(0,-\frac{1}{6},\frac{1}{6})} \\ L_3 & \phi_{u31}^{(-\frac{2}{3},0,\frac{2}{3})} & \phi_{u32}^{(0,-\frac{2}{3},\frac{2}{3})} \end{pmatrix} \frac{H_u}{M_\xi}, \tag{6.35}$$

$$M_L = \begin{pmatrix} & \overline{N}_{\rm sol} & \overline{N}_{\rm atm} \\ \overline{N}_{\rm sol} & \widetilde{\phi}_{\rm sol}^{(-\frac{4}{3},0,\frac{4}{3})} & 0 \\ \overline{N}_{\rm atm} & 0 & \widetilde{\phi}_{\rm atm}^{(0,-\frac{4}{3},\frac{4}{3})} \end{pmatrix}, \qquad M_R = \begin{pmatrix} & N_{\rm sol} & N_{\rm atm} \\ N_{\rm sol} & \phi_{\rm sol}^{(-\frac{4}{3},0,\frac{4}{3})} & 0 \\ N_{\rm atm} & 0 & \phi_{\rm atm}^{(0,-\frac{4}{3},\frac{4}{3})} \end{pmatrix}, \tag{6.36}$$

$$M_{LR} = \begin{pmatrix} & N_{\rm sol} & N_{\rm atm} \\ \overline{N}_{\rm sol} & M_{N_{\rm sol}} & 0 \\ \overline{N}_{\rm atm} & 0 & M_{N_{\rm atm}} \end{pmatrix}, \tag{6.37}$$

where the heavy scale M_ξ is associated to the mass of the heavy vector-like fermions $\xi_0 \sim (\mathbf{1},\mathbf{1})_{(0,0,0)}$, $\xi_{23} \sim (\mathbf{1},\mathbf{1})_{(0,1/2,-1/2)}$ (plus cyclic permutations), which are embedded in the representations $\Xi_0 \sim (\mathbf{1},\mathbf{1},\mathbf{1})$ and $\Xi_{23} \sim (\mathbf{1},\mathbf{5},\overline{\mathbf{5}})$ (plus conjugate, plus cyclic permutations) of $SU(5)^3$. Example diagrams are shown in Fig 6.3. We now construct the full neutrino mass matrix as

$$M_\nu = \begin{pmatrix} & \nu & \overline{N} & N \\ \nu & 0 & m_{D_L} & m_{D_R} \\ \overline{N} & m_{D_L}^{\rm T} & M_L & M_{LR} \\ N & m_{D_R}^{\rm T} & M_{LR}^{\rm T} & M_R \end{pmatrix} \equiv \begin{pmatrix} 0 & m_D \\ m_D^{\rm T} & M_N \end{pmatrix}, \tag{6.38}$$

where we have defined ν as a 3-component vector containing the weak eigenstates of active neutrinos, while N and $\overline{N}$ are 2-component vectors containing the SM singlets N and conjugate neutrinos $\overline{N}$, respectively. Now we assume that all the hyperons

in Eqs. (6.36-6.37) get VEVs at the scale v_{23} of 23 hypercharge breaking according to Eq. (6.14), and we have into account that $\langle\phi_{q13}\rangle / \langle\phi_{q23}\rangle \approx \lambda$ as obtained from the discussion of the charged fermion sector in Section 6.3.1. It is also required to assume $M_{N_{\rm atm}}$, $M_{N_{\rm atm}} \lesssim v_{23}$ in order to obtain the observed neutrino mixing with the textures of Eqs. (6.36-6.37).

Dirac-type masses in $m_{D_{L,R}}$ may be orders of magnitude smaller than the electroweak scale, because they arise from non-renormalisable operators proportional to the SM VEV. In contrast, the eigenvalues of M_N are not smaller than $\mathcal{O}(v_{23})$, which is at least TeV. Therefore, the condition $m_D \ll M_N$ is fulfilled in Eq. (6.38) and we can safely apply the seesaw formula to obtain, up to $\mathcal{O}(1)$ factors,

$$m_\nu \simeq m_D M_N^{-1} m_D^{\rm T} \approx \begin{pmatrix} 1 & 1 & \lambda \\ 1 & 1 & 1 \\ \lambda & 1 & 1 \end{pmatrix} v_{23} \frac{v_{\rm SM}^2}{M_\xi^2} \,. \tag{6.39}$$

This is the same texture that was obtained in Section 5.4, which is able to accommodate all the observed neutrino mixing angles and mass splittings [62,65] with $\mathcal{O}(1)$ parameters once the dimensionless coefficients implicit in Eq. (6.39) are considered. Remarkably, the singlet neutrinos $N_{\rm atm}$ and $N_{\rm sol}$ get masses around the TeV scale (v_{23}) and contribute to the RGE, while the cyclic neutrino is assumed to get a very heavy vector-like mass and decouples, as mentioned before.

6.3.3 Energy regimes, symmetries and particle content

Having discussed how the flavour structure of the SM is dynamically generated by the tri-hypercharge layer, now we discuss in detail the symmetries and particle content of our model at each energy regime between the GUT and electroweak scales.

Regime 1: $SU(5)^3$ breaking scale $\rightarrow$ $(SU(3) \times SU(2) \times U(1))^3$ breaking scale

As a result of $SU(5)^3$ breaking, each of the fermion representations F_i and T_i becomes charged under an $SU(3) \times SU(2) \times U(1)$ factor. Regarding the rest of the fields, most get masses at the $M_{\rm GUT} \sim v_{\rm GUT}$ unification scale and decouple. We will assume that only those explicitly required at low energies remain light. For instance, out of all the components of the Ω_i scalars, only the Θ_i and Δ_i states, belonging to the adjoint representations of $SU(3)_i$ and $SU(2)_i$, respectively, remain in the particle spectrum. Similarly, only some SM singlets in the Φ_i scalar fields are assumed to be present at this energy scale. For instance, this is the case of $\Phi_{\ell 23}$, contained in $\Phi_{23}^{(5)}$, a $(\mathbf{1},\mathbf{5},\bar{\mathbf{5}})$ representation of $SU(5)^3$, as shown in Table C.1. These representations eventually become the tri-hypercharge hyperons at lower energies. Similarly, the Q_i vector-like quarks in the χ_i and $\overline{\chi}_i$ multiplets are also assumed to be present at this energy scale. The full fermion and scalar particle content of the model in this energy regime is shown in Table 6.3.

Field	$SU(3)_1$	$SU(2)_1$	$U(1)_1$	$SU(3)_2$	$SU(2)_2$	$U(1)_2$	$SU(3)_3$	$SU(2)_3$	$U(1)_3$
q_1	**3**	**2**	$\frac{1}{6}$	**1**	**1**	0	**1**	**1**	0
u_1^c	$\bar{\mathbf{3}}$	**1**	$-\frac{2}{3}$	**1**	**1**	0	**1**	**1**	0
d_1^c	$\bar{\mathbf{3}}$	**1**	$\frac{1}{3}$	**1**	**1**	0	**1**	**1**	0
ℓ_1	**1**	**2**	$-\frac{1}{2}$	**1**	**1**	0	**1**	**1**	0
e_1^c	**1**	**1**	1	**1**	**1**	0	**1**	**1**	0
q_2	**1**	**1**	0	**3**	**2**	$\frac{1}{6}$	**1**	**1**	0
u_2^c	**1**	**1**	0	$\bar{\mathbf{3}}$	**1**	$-\frac{2}{3}$	**1**	**1**	0
d_2^c	**1**	**1**	0	$\bar{\mathbf{3}}$	**1**	$\frac{1}{3}$	**1**	**1**	0
ℓ_2	**1**	**1**	0	**1**	**2**	$-\frac{1}{2}$	**1**	**1**	0
e_2^c	**1**	**1**	0	**1**	**1**	1	**1**	**1**	0
q_3	**1**	**1**	0	**1**	**1**	0	**3**	**2**	$\frac{1}{6}$
u_3^c	**1**	**1**	0	**1**	**1**	0	$\bar{\mathbf{3}}$	**1**	$-\frac{2}{3}$
d_3^c	**1**	**1**	0	**1**	**1**	0	$\bar{\mathbf{3}}$	**1**	$\frac{1}{3}$
ℓ_3	**1**	**1**	0	**1**	**1**	0	**1**	**2**	$-\frac{1}{2}$
e_3^c	**1**	**1**	0	**1**	**1**	0	**1**	**1**	1
ξ_0	**1**	**1**	0	**1**	**1**	0	**1**	**1**	0
ξ_{12}	**1**	**1**	$\frac{1}{2}$	**1**	**1**	$-\frac{1}{2}$	**1**	**1**	0
ξ_{13}	**1**	**1**	$\frac{1}{2}$	**1**	**1**	0	**1**	**1**	$-\frac{1}{2}$
ξ_{23}	**1**	**1**	0	**1**	**1**	$\frac{1}{2}$	**1**	**1**	$-\frac{1}{2}$
Q_1	**3**	**2**	$\frac{1}{6}$	**1**	**1**	0	**1**	**1**	0
Q_2	**1**	**1**	0	**3**	**2**	$\frac{1}{6}$	**1**	**1**	0
Q_3	**1**	**1**	0	**1**	**1**	0	**3**	**2**	$\frac{1}{6}$
N_{atm}	**1**	**1**	0	**1**	**1**	$\frac{2}{3}$	**1**	**1**	$-\frac{2}{3}$
N_{sol}	**1**	**1**	$\frac{2}{3}$	**1**	**1**	0	**1**	**1**	$-\frac{2}{3}$
N_{cyclic}	**1**	**1**	$\frac{2}{3}$	**1**	**1**	$-\frac{2}{3}$	**1**	**1**	0
Θ_1	**8**	**1**	0	**1**	**1**	0	**1**	**1**	0
Θ_2	**1**	**1**	0	**8**	**1**	0	**1**	**1**	0
Θ_3	**1**	**1**	0	**1**	**1**	0	**8**	**1**	0
Δ_1	**1**	**3**	0	**1**	**1**	0	**1**	**1**	0
Δ_2	**1**	**1**	0	**1**	**3**	0	**1**	**1**	0
Δ_3	**1**	**1**	0	**1**	**1**	0	**1**	**3**	0
H_1^u	**1**	**2**	$\frac{1}{2}$	**1**	**1**	0	**1**	**1**	0
H_1^d	**1**	**2**	$-\frac{1}{2}$	**1**	**1**	0	**1**	**1**	0
H_2^u	**1**	**1**	0	**1**	**2**	$\frac{1}{2}$	**1**	**1**	0
H_2^d	**1**	**1**	0	**1**	**2**	$-\frac{1}{2}$	**1**	**1**	0
H_3^u	**1**	**1**	0	**1**	**1**	0	**1**	**2**	$\frac{1}{2}$
H_3^d	**1**	**1**	0	**1**	**1**	0	**1**	**2**	$-\frac{1}{2}$
$\Phi_{\ell 12}$	**1**	**1**	$\frac{1}{2}$	**1**	**1**	$-\frac{1}{2}$	**1**	**1**	0
$\Phi_{\ell 13}$	**1**	**1**	$\frac{1}{2}$	**1**	**1**	0	**1**	**1**	$-\frac{1}{2}$
$\Phi_{\ell 23}$	**1**	**1**	0	**1**	**1**	$\frac{1}{2}$	**1**	**1**	$-\frac{1}{2}$
Φ_{q12}	**1**	**1**	$-\frac{1}{6}$	**1**	**1**	$\frac{1}{6}$	**1**	**1**	0
Φ_{q13}	**1**	**1**	$-\frac{1}{6}$	**1**	**1**	0	**1**	**1**	$\frac{1}{6}$
Φ_{q23}	**1**	**1**	0	**1**	**1**	$-\frac{1}{6}$	**1**	**1**	$\frac{1}{6}$
Φ_{u12}	**1**	**1**	$-\frac{2}{3}$	**1**	**1**	$\frac{2}{3}$	**1**	**1**	0
Φ_{u13}	**1**	**1**	$-\frac{2}{3}$	**1**	**1**	0	**1**	**1**	$\frac{2}{3}$
Φ_{u23}	**1**	**1**	0	**1**	**1**	$-\frac{2}{3}$	**1**	**1**	$\frac{2}{3}$

TABLE 6.3: Fermion and scalar representations under $(SU(3) \times SU(2) \times U(1))^3$ in energy regime 1. Fermions highlighted in yellow belong to a vector-like pair and thus have a conjugate representation not shown in this table.

Regime 2: $(SU(3) \times SU(2) \times U(1))^3$ breaking scale $\rightarrow \xi$ scale

The $(SU(3) \times SU(2) \times U(1))^3$ gauge symmetry gets broken by the non-zero VEVs of the Θ_i and Δ_i scalars. The Θ_i octets break $SU(3)_1 \times SU(3)_2 \times SU(3)_3 \rightarrow SU(3)_{1+2+3} \equiv SU(3)_c$, while the Δ_i triplets play an analogous role for the $SU(2)$ factors. We assume these two breakings to take place simultaneously at $v_{\text{SM}^3} = \langle \Theta_i \rangle = \langle \Delta_i \rangle$, slightly below

Field	$SU(3)_c$	$SU(2)_L$	$U(1)_{Y_1}$	$U(1)_{Y_2}$	$U(1)_{Y_3}$
q_1	**3**	**2**	$\frac{1}{6}$	0	0
u_1^c	$\bar{\mathbf{3}}$	**1**	$-\frac{2}{3}$	0	0
d_1^c	$\bar{\mathbf{3}}$	**1**	$\frac{1}{3}$	0	0
ℓ_1	**1**	**2**	$-\frac{1}{2}$	0	0
e_1^c	**1**	**1**	1	0	0
q_2	**3**	**2**	0	$\frac{1}{6}$	0
u_2^c	$\bar{\mathbf{3}}$	**1**	0	$-\frac{2}{3}$	0
d_2^c	$\bar{\mathbf{3}}$	**1**	0	$\frac{1}{3}$	0
ℓ_2	**1**	**2**	0	$-\frac{1}{2}$	0
e_2^c	**1**	**1**	0	1	0
q_3	**3**	**2**	0	0	$\frac{1}{6}$
u_3^c	$\bar{\mathbf{3}}$	**1**	0	0	$-\frac{2}{3}$
d_3^c	$\bar{\mathbf{3}}$	**1**	0	0	$\frac{1}{3}$
ℓ_3	**1**	**2**	0	0	$-\frac{1}{2}$
e_3^c	**1**	**1**	0	0	1
ξ_0	**1**	**1**	0	0	0
ξ_{12}	**1**	**1**	$\frac{1}{2}$	$-\frac{1}{2}$	0
ξ_{13}	**1**	**1**	$\frac{1}{2}$	0	$-\frac{1}{2}$
ξ_{23}	**1**	**1**	0	$\frac{1}{2}$	$-\frac{1}{2}$
Q_1	**3**	**2**	$\frac{1}{6}$	0	0
Q_2	**3**	**2**	0	$\frac{1}{6}$	0
Q_3	**3**	**2**	0	0	$\frac{1}{6}$
N_{atm}	**1**	**1**	0	$\frac{2}{3}$	$-\frac{2}{3}$
N_{sol}	**1**	**1**	$\frac{2}{3}$	0	$-\frac{2}{3}$
Θ_1	**8**	**1**	0	0	0
Θ_2	**8**	**1**	0	0	0
Θ_3	**8**	**1**	0	0	0
H_1^u	**1**	**2**	$\frac{1}{2}$	0	0
H_1^d	**1**	**2**	$-\frac{1}{2}$	0	0
H_2^u	**1**	**2**	0	$\frac{1}{2}$	0
H_2^d	**1**	**2**	0	$-\frac{1}{2}$	0
H_3^u	**1**	**2**	0	0	$\frac{1}{2}$
H_3^d	**1**	**2**	0	0	$-\frac{1}{2}$
$\phi_{\ell 12}$	**1**	**1**	$\frac{1}{2}$	$-\frac{1}{2}$	0
$\phi_{\ell 13}$	**1**	**1**	$\frac{1}{2}$	0	$-\frac{1}{2}$
$\phi_{\ell 23}$	**1**	**1**	0	$\frac{1}{2}$	$-\frac{1}{2}$
ϕ_{q12}	**1**	**1**	$-\frac{1}{6}$	$\frac{1}{6}$	0
ϕ_{q13}	**1**	**1**	$-\frac{1}{6}$	0	$\frac{1}{6}$
ϕ_{q23}	**1**	**1**	0	$-\frac{1}{6}$	$\frac{1}{6}$
ϕ_{u12}	**1**	**1**	$-\frac{2}{3}$	$\frac{2}{3}$	0
ϕ_{u13}	**1**	**1**	$-\frac{2}{3}$	0	$\frac{2}{3}$
ϕ_{u23}	**1**	**1**	0	$-\frac{2}{3}$	$\frac{2}{3}$

TABLE 6.4: Fermion and scalar representations under $SU(3)_c \times SU(2)_L \times U(1)_{Y_1} \times U(1)_{Y_2} \times U(1)_{Y_3}$ in energy regimes 2, 3, 4, 5 and 6. Some states in this table get decoupled at intermediate scales and are not present at all energy regimes, see text for details. Fermions highlighted in yellow belong to a vector-like pair and thus have a conjugate representation not shown in this table.

the GUT scale, where we expect $\mathbb{Z}_3$ to remain exact in order to ensure the degenerate VEVs of Θ_i and Δ_i. As a result of this, the remnant symmetry is the tri-hypercharge

group (see Chapter 5), $SU(3)_c \times SU(2)_L \times U(1)_{Y_1} \times U(1)_{Y_2} \times U(1)_{Y_3}$:

$$(SU(3) \times SU(2) \times U(1))^3 \xrightarrow{\langle\Theta_i\rangle,\langle\Delta_i\rangle} SU(3)_c \times SU(2)_L \times U(1)_{Y_1} \times U(1)_{Y_2} \times U(1)_{Y_3} \tag{6.40}$$

The gauge couplings above (g_{s_i} and g_{L_i}, with $i = 1, 2, 3$) and below (g_s and g_L) the breaking scale verify the matching relations

$$\frac{g_{s_1}\, g_{s_2}\, g_{s_3}}{\sqrt{g_{s_1}^2 g_{s_2}^2 + g_{s_1}^2 g_{s_3}^2 + g_{s_2}^2 g_{s_3}^2}} = g_s \,, \tag{6.41}$$

$$\frac{g_{L_1}\, g_{L_2}\, g_{L_3}}{\sqrt{g_{L_1}^2 g_{L_2}^2 + g_{L_1}^2 g_{L_3}^2 + g_{L_2}^2 g_{L_3}^2}} = g_L \,, \tag{6.42}$$

which are equivalent to

$$\alpha_{s_1}^{-1} + \alpha_{s_2}^{-1} + \alpha_{s_3}^{-1} = \alpha_s^{-1} \,, \tag{6.43}$$

$$\alpha_{L_1}^{-1} + \alpha_{L_2}^{-1} + \alpha_{L_3}^{-1} = \alpha_L^{-1} \,, \tag{6.44}$$

with $\alpha_i^{-1} = 4\pi/g_i^2$.

The main difference with respect to the original tri-hypercharge model proposed in Chapter 5 is that a complete ultraviolet completion for the generation of the flavour structure is provided in our setup. As already explained in the previous two Sections, we achieve this with the hyperons and vector-like fermions present in the particle spectrum, which originate from $SU(5)^3$ representations. We assume N_{cyclic} as well as the conjugate representation $\overline{N}_{\text{cyclic}}$ to be decoupled at this energy scale. Similarly, the Δ_i triplets are also assumed to get masses of the order of the SM^3 breaking scale and decouple. The resulting fermion and scalar particle content of the model is shown in Table 6.4.

Regime 3: ξ scale $\rightarrow$ H_1 scale

The next energy threshold is given by the ξ singlets, responsible for the flavour structure of the neutrino sector, with masses $M_\xi \sim 10^{10}$ GeV. At this scale, the ξ_0 as well as the ξ_{12}, ξ_{13}, ξ_{23} and their conjugate representations are integrated out and no longer contribute to the running of the gauge couplings. The gauge symmetry does not change and stays the same as in the previous energy regime. The resulting particle spectrum is that of Table 6.4 removing the ξ singlet fermions.

Regime 4: H_1 scale $\rightarrow$ H_2 scale

At energies of the order of $M_{H_1^{u,d}} \sim 10^4$ TeV, the $H_1^{u,d}$ scalar doublets decouple from the particle spectrum of the model. Again, the gauge symmetry does not change. The particle spectrum at this stage is that shown on Table 6.4 removing the ξ singlet fermions and the $H_1^{u,d}$ scalar doublets.

Field	$SU(3)_c$	$SU(2)_L$	$U(1)_{Y_{12}}$	$U(1)_{Y_3}$
q_1	**3**	**2**	$\frac{1}{6}$	0
u_1^c	$\bar{\mathbf{3}}$	**1**	$-\frac{2}{3}$	0
d_1^c	$\bar{\mathbf{3}}$	**1**	$\frac{1}{3}$	0
ℓ_1	**1**	**2**	$-\frac{1}{2}$	0
e_1^c	**1**	**1**	1	0
q_2	**3**	**2**	$\frac{1}{6}$	0
u_2^c	$\bar{\mathbf{3}}$	**1**	$-\frac{2}{3}$	0
d_2^c	$\bar{\mathbf{3}}$	**1**	$\frac{1}{3}$	0
ℓ_2	**1**	**2**	$-\frac{1}{2}$	0
e_2^c	**1**	**1**	1	0
q_3	**3**	**2**	0	$\frac{1}{6}$
u_3^c	$\bar{\mathbf{3}}$	**1**	0	$-\frac{2}{3}$
d_3^c	$\bar{\mathbf{3}}$	**1**	0	$\frac{1}{3}$
ℓ_3	**1**	**2**	0	$-\frac{1}{2}$
e_3^c	**1**	**1**	0	1
N_{atm}	**1**	**1**	$\frac{2}{3}$	$-\frac{2}{3}$
N_{sol}	**1**	**1**	$\frac{2}{3}$	$-\frac{2}{3}$
H_3^u	**1**	**2**	0	$\frac{1}{2}$
H_3^d	**1**	**2**	0	$-\frac{1}{2}$
$\phi_{\ell 13}$	**1**	**1**	$\frac{1}{2}$	$-\frac{1}{2}$
$\phi_{\ell 23}$	**1**	**1**	$\frac{1}{2}$	$-\frac{1}{2}$
ϕ_{q13}	**1**	**1**	$-\frac{1}{6}$	$\frac{1}{6}$
ϕ_{q23}	**1**	**1**	$-\frac{1}{6}$	$\frac{1}{6}$
ϕ_{u13}	**1**	**1**	$-\frac{2}{3}$	$\frac{2}{3}$
ϕ_{u23}	**1**	**1**	$-\frac{2}{3}$	$\frac{2}{3}$

TABLE 6.5: Fermion and scalar representations under $SU(3)_c \times SU(2)_L \times U(1)_{Y_{12}} \times U(1)_{Y_3}$ in energy regime 7. Fermions highlighted in yellow belong to a vector-like pair and thus have a conjugate representation not shown in this table.

Regime 5: H_2 scale $\rightarrow$ Q, Θ scale

At energies of the order of $M_{H_2^{u,d}} \sim 100$ TeV, the $H_2^{u,d}$ scalar doublets decouple from the particle spectrum of the model. As in the previous two energy thresholds, the gauge symmetry remains the same. The particle spectrum at this stage is that shown on Table 6.4 removing the ξ singlet fermions and the $H_{1,2}^{u,d}$ scalar doublets.

Regime 6: Q, Θ scale $\rightarrow$ $SU(3)_c \times SU(2)_L \times U(1)_{Y_1} \times U(1)_{Y_2} \times U(1)_{Y_3}$ breaking scale

At $M_Q \lesssim M_{H_2^{u,d}}$, the Q_i vector-like quarks and the Θ_i colour octets decouple from the particle spectrum of the model. As in the previous two energy thresholds, the gauge symmetry is not altered. The particle spectrum at this stage is that shown on Table 6.4 removing the ξ singlet fermions, the $H_{1,2}^{u,d}$ scalar doublets, the Q_i vector-like quarks and the Θ_i colour octets.

Hyperons are responsible for the breaking of the tri-hypercharge symmetry. In a first hypercharge breaking step, $U(1)_{Y_1} \times U(1)_{Y_2} \times U(1)_{Y_3}$ gets broken to $U(1)_{Y_{12}} \times U(1)_{Y_3}$,

where $Y_{12} = Y_1 + Y_2$, by the non-zero VEV of the ϕ_{q12} hyperon, $v_{12} = \langle\phi_{q12}\rangle \sim 50$ TeV:

$$SU(3)_c \times SU(2)_L \times U(1)_{Y_1} \times U(1)_{Y_2} \times U(1)_{Y_3} \xrightarrow{\langle\phi_{q12}\rangle} SU(3)_c \times SU(2)_L \times U(1)_{Y_{12}} \times U(1)_{Y_3} \tag{6.45}$$

The gauge couplings above (g_{Y_1} and g_{Y_2}) and below ($g_{Y_{12}}$) the breaking scale verify the matching relation

$$\frac{g_{Y_1}\, g_{Y_2}}{\sqrt{g_{Y_1}^2 + g_{Y_2}^2}} = g_{Y_{12}}\,, \tag{6.46}$$

which is equivalent to

$$\alpha_{Y_1}^{-1} + \alpha_{Y_2}^{-1} = \alpha_{Y_{12}}^{-1}\,. \tag{6.47}$$

The "12 hyperons" $\phi_{\ell 12}$, ϕ_{q12} and ϕ_{u12} get masses of the order of $\langle\phi_{q12}\rangle$ and decouple at this stage. We also assume the Θ_i colour octets get a mass $M_\Theta \sim M_Q$ and are integrated out at this scale scale as well. The resulting fermion and scalar particle content is shown in Table 6.5.

Regime 7: $SU(3)_c \times SU(2)_L \times U(1)_{Y_1} \times U(1)_{Y_2} \times U(1)_{Y_3}$ breaking scale $\to SU(3)_c \times SU(2)_L \times U(1)_{Y_{12}} \times U(1)_{Y_3}$ breaking scale

The $SU(3)_c \times SU(2)_L \times U(1)_{Y_{12}} \times U(1)_{Y_3}$ gauge symmetry also gets broken by hyperon VEVs, leaving as a remnant the conventional SM gauge symmetry with $Y = Y_{12} + Y_3 = Y_1 + Y_2 + Y_3$. In this case, the hyperons responsible for the breaking are $\phi_{\ell 13}$, $\phi_{\ell 23}$, ϕ_{q13} and ϕ_{q23}, which get VEVs of the order of $v_{23} \sim 5$ TeV:

$$SU(3)_c \times SU(2)_L \times U(1)_{Y_{12}} \times U(1)_{Y_3} \xrightarrow{\langle\phi_{\ell 13,23}\rangle, \langle\phi_{q13,23}\rangle} SU(3)_c \times SU(2)_L \times U(1)_Y \tag{6.48}$$

The gauge couplings above ($g_{Y_{12}}$ and g_{Y_3}) and below (g_Y) the breaking scale verify the matching relation

$$\frac{g_{Y_{12}}\, g_{Y_3}}{\sqrt{g_{Y_{12}}^2 + g_{Y_3}^2}} = g_Y\,, \tag{6.49}$$

which is equivalent to

$$\alpha_{Y_{12}}^{-1} + \alpha_{Y_3}^{-1} = \alpha_Y^{-1}\,. \tag{6.50}$$

All the remaining hyperons as well as the neutrino mass messengers $N_{\rm atm}$ and $N_{\rm sol}$ (as well as their conjugate representations) decouple at this stage. The resulting particle spectrum is that of a two Higgs doublet model, with universal charges for all fermions.

Regime 8: $SU(3)_c \times SU(2)_L \times U(1)_{Y_{12}} \times U(1)_{Y_3}$ breaking scale $\to SU(3)_c \times SU(2)_L \times U(1)_Y$ breaking scale

Finally, at the scale $v_{\rm SM}$, the electroweak symmetry gets broken in the usual way, by the VEVs of the $H_3^{u,d}$ scalar doublets:

$$SU(3)_c \times SU(2)_L \times U(1)_Y \quad \xrightarrow{\langle H_3^{u,d}\rangle} \quad SU(3)_c \times U(1)_{\rm em} \tag{6.51}$$

Regime	**Gauge group**	b_i **coefficients**
1	SM^3	$\left(-\frac{22}{3}, -3, \frac{46}{15}, -\frac{22}{3}, -3, \frac{46}{15}, -\frac{22}{3}, -3, \frac{46}{15}\right)$
2	$SU(3)_c \times SU(2)_L \times U(1)_{Y_1} \times U(1)_{Y_2} \times U(1)_{Y_3}$	$\left(0, \frac{11}{3}, \frac{122}{45}, \frac{122}{45}, \frac{46}{15}\right)$
3	$SU(3)_c \times SU(2)_L \times U(1)_{Y_1} \times U(1)_{Y_2} \times U(1)_{Y_3}$	$\left(0, \frac{11}{3}, \frac{104}{45}, \frac{104}{45}, \frac{8}{3}\right)$
4	$SU(3)_c \times SU(2)_L \times U(1)_{Y_1} \times U(1)_{Y_2} \times U(1)_{Y_3}$	$\left(0, \frac{10}{3}, \frac{19}{9}, \frac{104}{45}, \frac{8}{3}\right)$
5	$SU(3)_c \times SU(2)_L \times U(1)_{Y_1} \times U(1)_{Y_2} \times U(1)_{Y_3}$	$\left(0, 3, \frac{19}{9}, \frac{19}{9}, \frac{8}{3}\right)$
6	$SU(3)_c \times SU(2)_L \times U(1)_{Y_1} \times U(1)_{Y_2} \times U(1)_{Y_3}$	$\left(-4, -3, \frac{89}{45}, \frac{89}{45}, \frac{38}{15}\right)$
7	$SU(3)_c \times SU(2)_L \times U(1)_{Y_{12}} \times U(1)_{Y_3}$	$\left(-7, -3, \frac{11}{3}, \frac{38}{15}\right)$
8	$SU(3)_c \times SU(2)_L \times U(1)_Y$	$\left(-7, -3, \frac{21}{5}\right)$

TABLE 6.6: b_i coefficients of our model. See Section 6.3.3 for details on the gauge symmetries and particle content at each energy regime.

6.3.4 Gauge coupling unification

In order to ensure that the gauge couplings of our model do indeed unify into a single value at some high energy scale, we must solve their one-loop RGEs, which take the generic form [399]

$$\frac{dg_i}{d\ln\mu} = \frac{g_i^3}{16\,\pi^2}\, b_i\,. \tag{6.52}$$

The b_i coefficients depend on the specific group G_i, with gauge coupling g_i, and the representations in the model. They are given by

$$b_i = -\frac{11}{3}\, C_2(G_i) + \frac{4}{3}\,\kappa\, S_2(F_i) + \frac{1}{6}\,\eta\, S_2(S_i)\,. \tag{6.53}$$

Here μ is the renormalization scale, $C_2(G_i)$ is the quadratic Casimir of the adjoint representation of G_i and $S_2(F_i)$ and $S_2(S_i)$ are the sums of the Dynkin indices of all fermion and scalar non-trivial representations under G_i. Finally, $\kappa = 1\,(1/2)$ for Dirac (Weyl) fermions and $\eta = 2\,(1)$ for complex (real) scalars.

We computed the b_i coefficients of our model, taking into account not only the gauge group for each energy regime, but also the particle content, since a particle decouples and does not contribute to the running at energies below its mass. The gauge symmetries and particle content at each energy regime are described in detail in the previous section, whereas our results for the b_i coefficients of the model are given in Table 6.6. Finally, we display results for the running of the gauge couplings in Fig. 6.4. This figure has been obtained by fixing the intermediate energy scales to

$$\begin{aligned}
&v_{23} = 5\ \text{TeV}\,, && v_{12} = 50\,\text{TeV}\,, && M_Q = 100\ \text{TeV}\,,\\
&M_\Theta = 100\ \text{TeV}\,, && M_{H_2^{u,d}} = 400\,\text{TeV}, && M_{H_1^{u,d}} = 4\cdot 10^4\ \text{TeV}\,,\\
&M_\xi = 10^{10}\ \text{GeV}\,, && v_{\mathrm{SM}^3} = 6\cdot 10^{16}\ \text{GeV}\,.
\end{aligned} \tag{6.54}$$

The nine gauge couplings of the SM^3 group unify at a very high unification scale $M_{\mathrm{GUT}} \approx 10^{17}$ GeV, slightly above the SM^3 breaking scale, with a unified gauge coupling $g_{\mathrm{GUT}} \approx 1.44$. We note the important role played by the three Θ_i colour octets embedded into

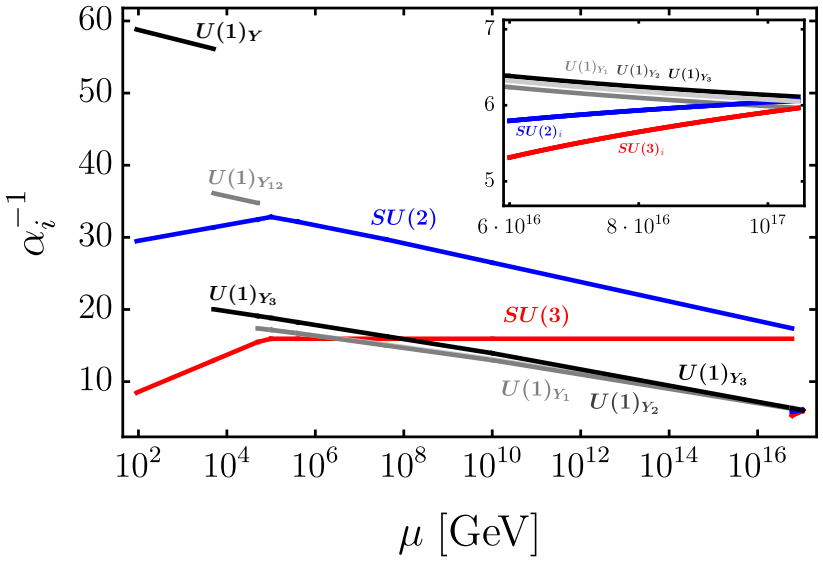

FIGURE 6.4: Running of the gauge couplings. The red lines correspond to the $SU(3)$ gauge couplings, the blue ones to the $SU(2)$ gauge couplings and the black/grey ones to the $U(1)$ gauge couplings. A zoom-in with the high-energy region close to the unification scale is also shown. These results have been obtained with $v_{23} = 5$ TeV, $v_{12} = 50$ TeV, $M_Q = 100$ TeV, $M_{H_2^{u,d}} = 400$ TeV, $M_{H_1^{u,d}} = 4 \cdot 10^4$ TeV, $M_\xi = 10^{10}$ GeV and $v_{\text{SM}^3} = 6 \cdot 10^{16}$ GeV.

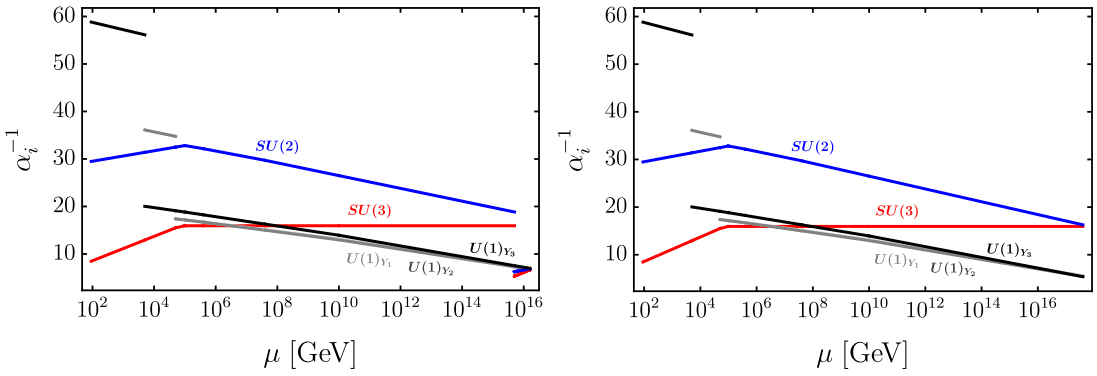

FIGURE 6.5: Running of the gauge couplings. Colour code as in Fig. 6.4. These results have been obtained with $v_{\text{SM}^3} = 5 \cdot 10^{15}$ GeV (left) and $v_{\text{SM}^3} = 4 \cdot 10^{17}$ GeV (right). The rest of the intermediate scales have been chosen as in Eq. (6.54).

$\Omega_i \sim \mathbf{24}_i$, and by the Q_i vector-like quarks which also act as heavy messengers of the flavour theory, which are crucial to modify the running of the $SU(3)$ and $SU(2)$ gauge couplings in order to achieve unification. We also highlight that the discontinuities in Figs. 6.4 and 6.5 are due to the gauge coupling matching conditions that apply at the steps in which the $U(1)_Y$ group is decomposed into two (first discontinuity) and three hypercharges (second discontinuity) and in which the $SU(3)$ and $SU(2)$ groups are decomposed into one for each family (third discontinuity).

Even though the $\mathbb{Z}_3$ symmetry gets broken at the SM^3 breaking scale, it stays approximately conserved at low energies, down to the tri-hypercharge breaking scale, and only the running of $U(1)_{Y_3}$ is slightly different from that of the other two hypercharge

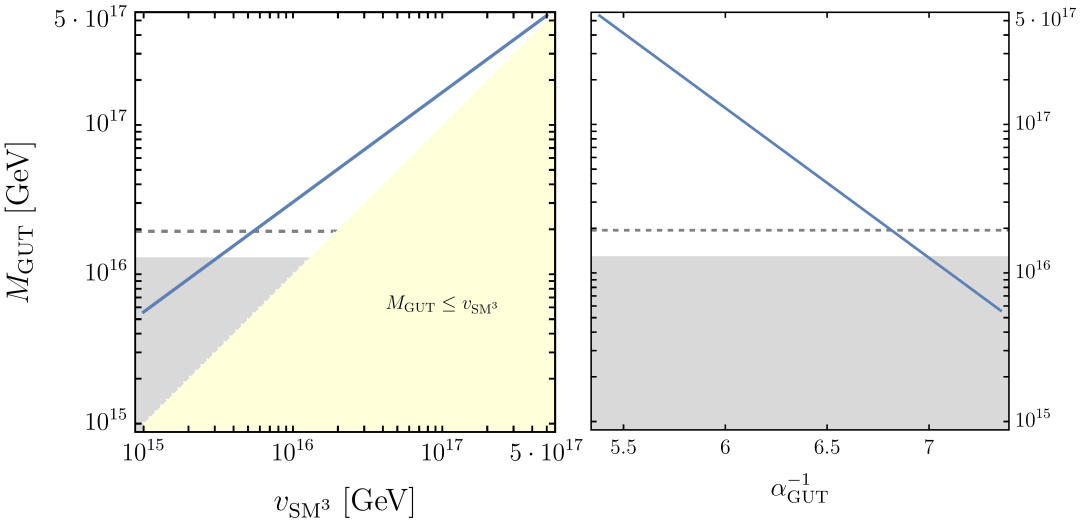

FIGURE 6.6: $M_{\rm GUT}$ as a function of $v_{\rm SM^3}$ (left) and $\alpha_{\rm GUT}^{-1}$ (right). The SM^3 breaking scale $v_{\rm SM^3}$ varies in these plots, while the rest of the intermediate scales have been fixed to the values in Eq. (6.54). The shaded grey region is excluded by the existing Super-Kamiokande 90% C.L. limit on the $p \to e^+\pi^0$ lifetime, $\tau(p \to e^+\pi^0) > 2.4 \cdot 10^{34}$ years [400], whereas the horizontal dashed line corresponds to the projected Hyper-Kamiokande sensitivity at 90% C.L. after 20 years of runtime, $\tau(p \to e^+\pi^0) > 1.2 \cdot 10^{35}$ years, obtained in [401]. See Section 6.3.5 for details on the proton decay calculation. Finally, the shaded yellow region on the left-hand plot is excluded due to $M_{\rm GUT} \leq v_{\rm SM^3}$.

groups. In fact, the gauge couplings of the $U(1)_{Y_1}$ and $U(1)_{Y_2}$ groups almost overlap and cannot be distinguished in Fig. 6.4. This can be easily understood by inspecting the b_i coefficients on Table 6.6. Then, the matching conditions at $v_{12} = 50$ TeV split the low energy $g_{Y_{12}}$ and g_{Y_3} couplings, which become clearly different: $g_{Y_{12}}(v_{12}) \approx 0.59$ and $g_{Y_3}(v_{12}) \approx 0.79$. Finally, at $v_{23} = 5$ TeV one recovers the standard $SU(3)_c \times SU(2)_L \times U(1)_Y$ gauge group, which remains unbroken down to the electroweak scale.

In order to study how unification changes with the scale of SM^3 breaking, $v_{\rm SM^3}$, we consider the values $v_{\rm SM^3} = 5 \cdot 10^{15}$ GeV and $v_{\rm SM^3} = 4 \cdot 10^{17}$ GeV and fix the rest of the intermediate scales as in Eq. (6.54). Results for the running of the gauge couplings in these two scenarios are shown in Fig. 6.5. On the left-hand side we show the case $v_{\rm SM^3} = 5 \cdot 10^{15}$ GeV whereas on the right-hand side we display our results for $v_{\rm SM^3} = 4 \cdot 10^{17}$ GeV. In the first case, our choice of SM^3 breaking scale leads to unification of the gauge couplings at a relatively low scale, $M_{\rm GUT} \approx 1.8 \cdot 10^{16}$ GeV. This is potentially troublesome, as it may lead to too fast proton decay, as explained below. In contrast, when the SM^3 breaking scale is chosen to be very high, as in the second scenario, unification also gets delayed to much higher energies. In fact, we note that with our choice $v_{\rm SM^3} = 4 \cdot 10^{17}$ GeV, gauge coupling unification already takes place at the SM^3 breaking scale, $M_{\rm GUT} \approx v_{\rm SM^3}$. In this case, $SU(5)^3$ breaks directly to the tri-hypercharge group $SU(3)_c \times SU(2)_L \times U(1)_{Y_1} \times U(1)_{Y_2} \times U(1)_{Y_3}$ and there is no intermediate SM^3 scale. Finally, the impact of $v_{\rm SM^3}$ is further illustrated in Fig. 6.6.

Gauge group	γ_{iL} coefficients	γ_{iR} coefficients
SM^3	$\left(2, \frac{9}{4}, \frac{23}{20}, 0, 0, 0, 0, 0, 0\right)$	$\left(2, \frac{9}{4}, \frac{11}{20}, 0, 0, 0, 0, 0, 0\right)$
$SU(3)_c \times SU(2)_L \times U(1)_{Y_1} \times U(1)_{Y_2} \times U(1)_{Y_3}$	$\left(2, \frac{9}{4}, \frac{23}{20}, 0, 0\right)$	$\left(2, \frac{9}{4}, \frac{11}{20}, 0, 0\right)$
$SU(3)_c \times SU(2)_L \times U(1)_{Y_{12}} \times U(1)_{Y_3}$	$\left(2, \frac{9}{4}, \frac{23}{20}, 0\right)$	$\left(2, \frac{9}{4}, \frac{11}{20}, 0\right)$
$SU(3)_c \times SU(2)_L \times U(1)_Y$	$\left(2, \frac{9}{4}, \frac{23}{20}\right)$	$\left(2, \frac{9}{4}, \frac{11}{20}\right)$

TABLE 6.7: Anomalous dimension coefficients $\gamma_{iL,R}$ for proton decay operators in our model. These are computed as 1-loop quantum corrections (vertex corrections and self-energy corrections via the various gauge bosons at each intermediate scale) to the proton decay operators $\mathcal{O}_L^{d=6}$ and $\mathcal{O}_R^{d=6}$ defined in Eqs. (2.107) and (2.108). We compute them by following the algorithm of Appendix A in Ref. [287].

Here we show the relation between M_{GUT}, v_{SM^3} and $\alpha_{\mathrm{GUT}}^{-1} = 4\pi/g_{\mathrm{GUT}}^2$. These two plots have been made by varying v_{SM^3} and all the other intermediate scales fixed as in Eq. (6.54). The left-hand side of this figure confirms that larger v_{SM^3} values lead to higher unification scales and smaller gaps between these two energy scales. The right-hand side of the figure shows the relation between the unified gauge coupling and the GUT scale. Again, the larger M_{GUT} (or, equivalently, larger v_{SM^3}) is, the larger g_{GUT} (and smaller $\alpha_{\mathrm{GUT}}^{-1}$) becomes. In particular, in this plot g_{GUT} ranges from ~ 1.30 to ~ 1.53.

6.3.5 Proton decay

As in any GUT, proton decay is a major prediction in our setup. In standard, non-supersymmetric $SU(5)$ the most relevant proton decay mode is usually $p \to e^+\pi^0$. This process is induced by the tree-level exchange of the $X \sim (\mathbf{3}, \mathbf{2})_{-5/6}$ (and complex conjugate $X^* \sim (\overline{\mathbf{3}}, \overline{\mathbf{2}})_{5/6}$) gauge bosons contained in the **24** (adjoint) representation. Integrating out these heavy vector leptoquarks leads to effective dimension-6 operators that violate both baryon and lepton number, as described in Section 2.3.11. The resulting proton life time can be roughly estimated as

$$\tau_p \approx \frac{m_X^4}{\alpha_{\mathrm{GUT}}^2 m_p^5}\,, \tag{6.55}$$

where m_X is the mass of the heavy leptoquark, $m_p \approx 0.938$ GeV is the proton mass and $\alpha_{\mathrm{GUT}} = g_{\mathrm{GUT}}^2/(4\pi)$ is the value of the fine structure constant at the unification scale. One can easily estimate that for $m_X = 10^{17}$ GeV and $g_{\mathrm{GUT}} \sim 1.5$, the proton life time is $\tau_p \sim 10^{38}$ years, well above the current experimental limit, $\tau(p \to e^+\pi^0) > 2.4 \cdot 10^{34}$ years at 90% C.L. [400]. Therefore, a large unification scale suffices to guarantee that our model respects the current limits on the proton lifetime. In fact, such a long life time is beyond the reach of near future experiments, which will increase the current limit by about one order of magnitude [401].

A more precise determination of the $p \to e^+\pi^0$ decay width is obtained by following the formalism of Section 2.3.11 and applying Eq. (2.111). One needs to know the β-function coeficients (b_i) given for our model in Table 6.6, along with the anomalous dimensions ($\gamma_{iL(R)}$) of the proton decay operators, given for each intermediate scale of our model in Table 6.7.

Given that in our model we have three $SU(5)$ groups, we actually have three generations of the usual $SU(5)$ leptoquarks, coupling only to their corresponding family of chiral fermions. However, since the three $SU(5)_i$ groups are all broken down to their SM_i subgroups at the same scale, in practice the model reproduces the phenomenology of a flavour universal leptoquark as in conventional $SU(5)$, albeit with the specific fermion mixing predicted by our flavour model as shown in Section 6.3.1. The effect of fermion mixing is encoded via the coefficients C_L and C_R defined in Eqs. (2.109) and (2.110) in all generality. In our especific model, their expression is obtained by just setting $\Lambda_2 = 0$[8], i.e.

$$C_L = (V_{u^c}^\dagger V_u)^{11}(V_{e^c}^\dagger V_d)^{11} + (V_{u^c}^\dagger V_u V_{\mathrm{CKM}})^{11}(V_{e^c}^\dagger V_d V_{\mathrm{CKM}}^\dagger)^{11}\,, \tag{6.56}$$

$$C_R = (V_{u^c}^\dagger V_u)^{11}(V_{d^c}^\dagger V_e)^{11}\,, \tag{6.57}$$

where $V_{\mathrm{CKM}} = V_u^\dagger V_d$. Notice that even though our flavour model predicts non-generic fermion mixing, the alignment of the CKM matrix is not univocally predicted but relies on the choice of dimensionless coefficients. Assuming the CKM mixing to originate mostly from the down sector we find $C_L \simeq 1.946$ and $C_R \simeq 0.999$, while if the CKM mixing originates mostly from the up sector we find $C_L \simeq 1.946$ and $C_R \simeq 0.974$. Both cases lead to very similar low-energy phenomenology regarding proton decay.

We show our numerical results for the $p \to e^+\pi^0$ lifetime in Fig. 6.7. Again, v_{SM^3} varies in the left panel of this figure, while the rest of intermediate scales have been chosen as in Eq. (6.54). The right panel shows an equivalent plot with the $p \to e^+\pi^0$ lifetime as a function of M_{GUT}. This figure provides complementary information to that already shown in Fig. 6.6. In both cases we have used the precise determination of the lifetime in Eq. (2.111), but we note that the estimate in Eq. (6.55) actually provides a very good approximation, with $\tau_p/\tau_p^{\mathrm{app}} \in [0.5, 1.2]$ in the parameter region covered in Fig. 6.7. The current Super-Kamiokande 90% C.L. limit on the $p \to e^+\pi^0$ lifetime, $\tau(p \to e^+\pi^0) > 2.4 \cdot 10^{34}$ years [400], excludes values of the GUT scale below $M_{\mathrm{GUT}} \sim 1.3 \cdot 10^{16}$ GeV, while the projected Hyper-Kamiokande sensitivity at 90% C.L. after 20 years of runtime, $\tau(p \to e^+\pi^0) > 1.2 \cdot 10^{35}$ years [401], would push this limit on the unification scale in our model to $M_{\mathrm{GUT}} \sim 2 \cdot 10^{16}$ GeV. Therefore, our model will be probed in the next round of proton decay searches, although large regions of the parameter space predict a long proton lifetime, well beyond any foreseen experiment.

[8] This is due to the fact that Λ_2 is associated to the $X' \sim (\mathbf{3}, \mathbf{2})_{-1/6}$ gauge bosons which are not present in $SU(5)$ frameworks, as discussed in Section 2.3.11.

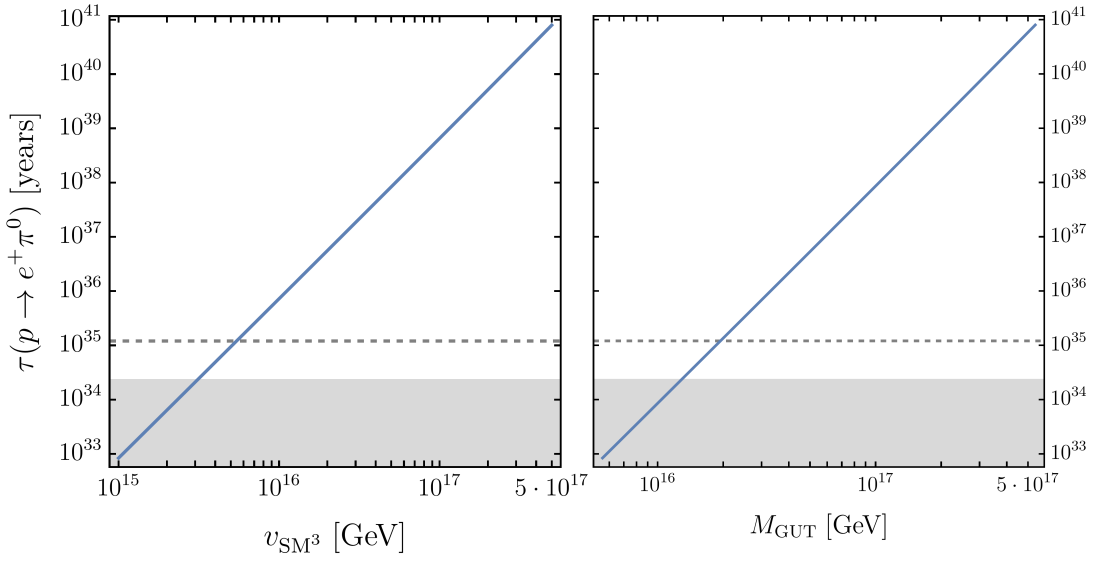

FIGURE 6.7: $\tau(p \to e^+\pi^0)$ as a function of v_{SM^3} (left) and M_{GUT} (right). The SM^3 breaking scale v_{SM^3} varies in these plots, while the rest of the intermediate scales have been fixed to the values in Eq. (6.54). The shaded grey region is excluded by the existing Super-Kamiokande 90% C.L. limit on the $p \to e^+\pi^0$ lifetime, $\tau(p \to e^+\pi^0) > 2.4 \cdot 10^{34}$ years [400], whereas the horizontal dashed line corresponds to the projected Hyper-Kamiokande sensitivity at 90% C.L. after 20 years of runtime, $\tau(p \to e^+\pi^0) > 1.2 \cdot 10^{35}$ years, obtained in [401].

6.4 Conclusions

In this chapter we have discussed $SU(5)^3$ with cyclic symmetry ("tri-unification") as the possible gauge unified origin of many gauge non-universal theories at low energies. The $SU(5)^3$ with cyclic symmetry setup consists of a single gauge coupling and unifies all SM fermions into a single irreducible representation. When spontaneously broken, such framework may lead to gauge non-universal theories and family structure. These theories are known to have many applications for model building purposes, and more recently have been proposed as a possible explanation for the flavour structure of the SM.

As a proof of concept, we have developed an $SU(5)^3$ tri-unification example that is spontaneously broken to the tri-hypercharge gauge group discussed in Chapter 5, which dynamically generates the flavour structure of the SM (including the neutrino sector). We have shown how the five gauge couplings of tri-hypercharge unify into the single gauge coupling of the cyclic $SU(5)^3$ group, by assuming minimal multiplet splitting, together with a set of relatively light colour octet scalars that also play a role in spontaneous symmetry breaking. The approximate conservation of the cyclic symmetry at low energies is also crucial to achieve gauge unification, plus the heavy messengers required to generate the flavour structure also modify the RGE in the desired way, highlighting the minimality of the framework.

We have also studied proton decay in this example, and presented the predictions of the proton lifetime in the dominant $e^+\pi^0$ channel. If $SU(5)^3$ breaks to tri-hypercharge

in one step, then we have shown that gauge unification happens at a very high scale $M_{\rm GUT} \sim 10^{17}\,{\rm GeV}$, predicting a long proton lifetime well beyond any foreseen experiment. In contrast, if we assume that $SU(5)^3$ first breaks to three SM groups (which then break to tri-hypercharge), then the scale of $\rm SM^3$ breaking becomes essentially a free parameter that allows to lower $M_{\rm GUT}$, predicting a proton lifetime to be possibly observable at Hyper-Kamiokande. In this manner, the signals on proton decay may allow to test the model at high scales, while low energy signals associated with tri-hypercharge enable the model to be tested by collider and flavour experiments.

More generally, as a take home message, we conclude that $SU(5)^3$ tri-unification reconciles the idea of gauge non-universality with the idea of gauge coupling unification, opening up the possibility to build consistent non-universal descriptions of Nature that are valid all the way up to the scale of grand unification. This is remarkable given that gauge non-universal theories are known to predict a rather complicated gauge sector consisting of many arbitrary gauge couplings. Our work opens the possibility to take these theories seriously all the way to the GUT scale, providing a consistent framework were new phenomenology such as cosmological imprints of the spontaneous symmetry breaking may be studied, being complementary to the low energy signals predicted by the gauge non-universal layer of physics.

Chapter 7

Final thoughts and the future ahead

-"After decades of flavour model building, we understood nothing about the origin of flavour."
-"Maybe it is you that understood nothing!"

– Graham G. Ross, to a comment from Álvaro de Rújula in a physics conference[1]

If you are reading this, and you went through the whole thesis before reaching these lines, thanks! Despite all the sacrifices, I had my best time while writing this and I hope I could somehow transmit you my personal view of physics throughout all those lengthy chapters. You may be wondering now what are the final conclusions, maybe you are wondering if I learnt something about Nature after writing all those pages. The honest truth is that I do not have many definite conclusions, though. Nature is not giving much hints right now about her unsolved mysteries, and the flavour puzzle is no exception. As I tried to introduce in Chapter 1, the new dynamics connected to the origin of flavour might be hidden *anywhere* from the Planck scale to the electroweak scale, giving its name to this thesis.

Unlike other solutions to open puzzles in Nature, such as TeV-scale SUSY and the QCD axion, the flavour puzzle does not point to any particularly accessible energy scale or region in the parameter space, with most solutions being decoupling theories where everything can always be very heavy, recovering the low-energy phenomenology of the Standard Model. Some even think that there is no puzzle to solve at all, claiming that all flavour parameters are "technically natural" (in the sense that they are stable under radiative corrections [68]), or that we may never understand what is Nature hiding behind the flavour puzzle, at least not in humanity's lifetime. In this thesis, however, I hope I managed to convince you that this is *not* my view of particle physics. I believe that sooner or later we will find that an existing (or yet to be written) well-motivated

[1] Michele Frigerio, private communication.

theory is realised in Nature, just as it has happened several times in the past when it was thought as well that (particle) physics was over. Even if nothing is found, we will still have learnt more about our Universe, just by failing once more. My work on this thesis was motivated by this spirit.

In Chapter 1 I did a somewhat lengthy introduction to the SM, focusing on its open questions and on the particular role of flavour. Surprisingly, while doing this I learnt about fermion unification in GUTs, about custodial symmetry, about the open problems in cosmology, about the Froggatt-Nielsen mechanism and many more things. Then in Chapter 2 I discussed key flavour observables which show experimental anomalies or which are correlated in well-motivated BSM scenarios to the anomalous observables, hence being important for discovery prospects. I included the EFT description of these observables in terms of the LEFT, which can then be easily matched to the SMEFT, both being very useful EFTs for phenomenological studies. During this writing, I learnt not only about these observables but also about the aforementioned EFTs, and most notably I learnt how difficult it can be to keep updated the experimental data of several (flavour) observables during the few-months period of writing a PhD thesis. I will always remember this when I have the urge to ask experimentalists about timelines in their data analyses.

In Chapter 3 I studied a class of local $U(1)'$ extensions of the SM, where chiral fermions are uncharged under the $U(1)'$ but an exotic family of vector-like fermions is charged, providing effective Z' couplings for chiral fermions via mixing. This feature gives the name *fermiophobic* to this class of models. Despite the many theoretical puzzles behind the $(g-2)_\mu$ anomaly, I decided to study its BSM interpretation and I provided a very simple $U(1)'$ fermiophobic scenario where the solution to $(g-2)_\mu$ is correlated to a suppression of the decay of the Higgs boson to two photons, which can test the validity of this scenario with the sufficient experimental precision. The basic idea is the chiral enhancement provided by vector-like leptons that couple to the SM Higgs doublet. Afterwards, I considered a theory of flavour with fermiophobic Z' that can explain the origin of the SM flavour structure. In this model, both the effective Yukawa couplings of second and third family chiral fermions along with their effective Z' couplings arise via mixing with the heavy vector-like fermions, hence connecting the origin of Yukawa couplings in the SM with the low-energy phenomenology of the model. First family masses are then implemented via a heavy Higgs doublet that gets a small effective VEV via mixing with the Higgs doublets that break the electroweak symmetry. The mechanism of messenger dominance [171] points to several NP scales in the UV, hinting to a multi-scale origin of flavour. If the $U(1)'$ factor is broken at a relatively low scale, then there could be some signals in low energy observables that could test the model. A connection with the $(g-2)_\mu$ anomaly requires a minimal extension of the model in order to obtain an effective coupling of the vector-like leptons to the SM Higgs, however we find that ultimately it is not possible to address the anomaly in the flavour model due to a correlated chiral enhancement of $\mathcal{B}(\tau \to \mu\gamma)$. Nevertheless, by dropping

the extra content required for $(g-2)_\mu$, we have found that current data allows for the Z' boson to be as light as 1 TeV, with the leading constraint being $B_s - \bar{B}_s$ mixing. By exploring this model I learnt about messenger dominance, and I learnt how heavy Higgs doublets can be an alternative to vector-like fermions in order to play the role of heavy messengers that UV-complete the effective Yukawa operators of a theory of flavour. I also learnt about Higgs diphoton decay and its future projections at HL-LHC, and of course I learnt about chiral enhancement and its crucial relation with $(g-2)_\mu$. This work was motivated by a previous work made in 2021 where we connected both the $R_{K^{(*)}}$ and $(g-2)_\mu$ anomalies in a fermiophobic Z' framework [1].

In Chapter 4 I studied a twin Pati-Salam theory of flavour which contains a TeV-scale vector leptoquark $U_1 \sim (\mathbf{3},\mathbf{1},2/3)$ [2]. This twin Pati-Salam symmetry is broken down to the SM in a two-step process, such that in an intermediate step at the TeV scale the model is described by a 4321 gauge group [267]. This two-step pattern of symmetry breaking hints to a multi-scale origin of flavour. The model features a fermiophobic framework as well, where both the effective Yukawa couplings for chiral fermions and their effective U_1 couplings originate again from mixing with heavy vector-like fermions. The mechanism of messenger dominance plays a fundamental role here in order to simultaneously explain the fermion mass hierarchies and deliver the flavour structure required to explain the so-called B-anomalies. I discovered that one vector-like fermion family is not enough to achieve such flavour structure, but indeed three vector-like fermion families are required. In this case, the model predicts a plethora of low-energy signals in flavour observables, several of them fundamentally related to the origin of fermion mass hierarchies and mixing. The model can also be tested via direct searches of the new heavy degrees of freedom at the LHC, including the vector-like fermions, the U_1 leptoquark, and a coloron $g' \sim (\mathbf{8},\mathbf{1},0)$ and Z' gauge bosons. While doing this work I learnt much about low-energy flavour observables and their description in an EFT framework, via performing a lengthy phenomenological analysis involving each low-energy process correlated to the explanation of the B-anomalies. I also learnt more about very useful tools for phenomenological studies, including `DsixTools` [174], `Madgraph5` [337], `FeynRules` [336] and `package-X` [402].

In Chapter 5 I studied the possibility that the SM originates from a non-universal gauge theory in the UV. We argue that one of the most simple ways to achieve this is by assigning a separate gauge hypercharge to each fermion family at high energies [3], broken down to the usual weak hypercharge which is the diagonal subgroup. This simple framework avoids the family replication of the SM, and could be the first step towards a deep non-universal gauge structure in the UV. If the Higgs doublet(s) only carry third family hypercharge, then only third family renormalisable Yukawa couplings are allowed by the gauge symmetry, explaining their heaviness. The light fermions are massless in first approximation, delivering an accidental $U(2)^5$ flavour symmetry in the Yukawa couplings. The small masses and mixing of the light charged fermions are then introduced via non-renormalisable operators, as a minimal breaking of the $U(2)^5$

symmetry. These non-renormalisable operators depend explicitly on the scalars linking the different hypercharge groups (hyperons), which get VEVs in order to break the "tri-hypercharge" symmetry down to SM hypercharge. In minimal models with simple sets of hyperons, we found that a mildly hierarchical breaking of tri-hypercharge naturally explains the mass hierarchies between first and second family charged fermions, which naturally arise via several mass insertions of the hyperons. In this manner, the tri-hypercharge gauge model also hints to a multi-scale origin of flavour. We also found that in order to explain neutrino mixing, it is useful to introduce right-handed neutrinos which carry non-zero hypercharges (although their sum must vanish), which then turn out to get Majorana masses at the lowest scale of symmetry breaking, that could be as low as a few TeV. Indeed, the model has a rich phenomenology if the NP scales are low: from flavour violating observables to LHC physics and electroweak precision observables. We observe that the Z' boson contributing to the most dangerous FCNCs is naturally heavier, while a second Z' boson may be as light as a few TeV because it is protected by the $U(2)^5$ symmetry. The most promising discovery channels for this Z' boson are dilepton searches at the LHC and electroweak precision observables, which are altered via an unavoidable $Z - Z'$ gauge mixing. During this project, I learnt much about model building, including the different implementations of the type I seesaw mechanism and the different textures for neutrino mass matrices. I also learnt about the very interesting physics of electroweak precision observables and about gauge mixing and/or kinetic mixing.

Finally, in Chapter 6 I proposed a gauge unified origin for gauge non-universal frameworks such as the aforementioned tri-hypercharge theory. In this manner, such theories may be taken seriously all the way up to the GUT scale. The model consists on assigning a separate $SU(5)$ group to each fermion family. However, assuming that the three $SU(5)$ groups are related by a cyclic permutation symmetry $\mathbb{Z}_3$, then the model is described by a single gauge coupling in the UV, despite $SU(5)^3$ being a non-simple group. Moreover, the cyclic symmetry in such a framework also ensures that all SM fermions belong to a single representation of the complete group. First, I discussed a general $SU(5)^3$ "tri-unification" framework for model building, where gauge non-universal theories of flavour may be embedded. Secondly, I constructed an explicit, minimal tri-hypercharge example model originating from $SU(5)^3$ tri-unification, which can account for all the quark and lepton (including neutrino) masses and mixing parameters. I achieved the successful unification of the five gauge couplings of the tri-hypercharge group into a single gauge coupling associated to the cyclic $SU(5)^3$ group, and I also studied the implications for the stability of the proton in such a setup. During this project, I learnt much about model building, about the group theory of $SU(5)$ and about proton decay. I also learnt much about UV-completing the effective Yukawa couplings of a theory of flavour via different sets of various vector-like fermions and/or scalar fields. I also increased my knowledge in the very interesting physics of gauge unification and RGE, along with the model building helpful to achieve the successful unification of gauge couplings.

So this is all, isn't it? During my PhD I have studied a bunch of theories of flavour and explored the discovery prospects if (some of) the new physics scales are low. A significant part of my thesis work was originally motivated by the $R_{K^{(*)}}$ anomalies, that turned out to disappear when I was just starting my final year of PhD. The flavour anomalies that remain are mostly under question, either in the theory side such as $(g-2)_\mu$ and $b \to s\mu\mu$, or in the experimental side such as $R_{D^{(*)}}$, where an upcoming measurement by the BaBar collaboration might lead to a decrease in the overall significance [403]. Nevertheless, more data keeps coming from the various particle physics experiments, and new anomalies in well-motivated channels such as the recent measurement of $\mathcal{B}(B^+ \to K^+\nu\bar{\nu})$ by Belle II [81] may eventually establish as solid evidence for physics beyond the Standard Model. The origin of flavour may still be around the corner, waiting to be discovered in particle physics experiments that test the origin of flavour *from the bottom-up*.

Additionally, in recent years cosmological observations, especially the detection of gravitational waves, have been suggested as a possible way to test BSM scenarios that are inaccessible to current particle physics experiments. For example, in the tri-hypercharge model discussed in Chapters 5 and 6, the hierarchical breaking of $U(1)$ gauge factors in the early Universe may produce (metastable) cosmic strings if the symmetry breaking happens at very high scales, with the associated emission of a characteristic signal of gravitational waves. In the same spirit, if the breaking of the $U(1)$ factors is associated to first order phase transitions in the early Universe, a characteristic multi-peaked signal of gravitational waves may be within the reach of current and upcoming gravitational waves observatories. This opens the possibility of testing multi-scale theories such as those proposed in this thesis, among others, which may explain some of the most fundamental open questions of the Standard Model. These cosmological probes may be complementary to the existing searches at particle physics experiments, such that the origin of flavour could be tested *from the top-down and from the bottom-up*. The future ahead of us is exciting, with the possibility of testing theories that were thought inaccessible, such as the type I seesaw mechanism and Grand Unified Theories. I am strongly convinced that only by learning and studying the many faces and aspects of Nature we will obtain a better understanding of our Universe, and I hope that in the near future I can study the many open questions in fundamental physics, propose new theories that address these problems and test such new theories up to whatever new physics scales are possible, all the way *from the Planck scale to the electroweak scale*.

Appendix A

Four-component and two-component spinor notation

In this appendix, we introduce the two-component notation taking all fermions as left-handed Weyl spinors, which is common in the literature for model building studies. We show the connection with the four-component, left-right notation, showing explicit examples.

A.1 Two-component spinors

In the chiral spinor representation, a (4-component) Dirac spinor Ψ consists of two independent (2-component) Weyl spinors ψ_L and ψ_R with well-defined chirality,

$$\Psi = \begin{pmatrix} \psi_L \\ \psi_R \end{pmatrix} . \tag{A.1}$$

The spinor fields ψ_L and ψ_R transform under the Lorentz group $SO^+(1,3) \cong SU(2)_L \times SU(2)_R$ as $(\mathbf{2},\mathbf{1})$ and $(\mathbf{1},\mathbf{2})$, respectively, and by convention we denote ψ_L as the *left-handed* Weyl spinor and ψ_R as the *right-handed* Weyl spinor. Notice that if ψ_L is a left-handed spinor, then the hermitian conjugate $\psi_L^\dagger$ is a right-handed spinor. In a similar way, if $\psi_R^\dagger$ is a right-handed spinor, then $\psi_R^\dagger$ is a left-handed spinor. Therefore, any particular fermionic degrees of freedom can be described equally well using a left-handed Weyl spinor or a right-handed one. Given this relation, it is tempting to get rid of chiral subscripts and write our quantum field theory in terms of Weyl spinors with the same chirality. Let us redefine the Weyl spinors as

$$\left.\begin{matrix} \psi_L \equiv \psi \\ \psi_R \equiv \psi^{c\dagger} \end{matrix}\right\} \Rightarrow \Psi = \begin{pmatrix} \psi \\ \psi^{c\dagger} \end{pmatrix} . \tag{A.2}$$

In this notation, ψ is a left-handed spinor and ψ^c is a left-handed spinor as well. ψ^c is usually referred as the CP-conjugate of the original right-handed spinor ψ_R, because the CP transformation maps Weyl spinors to their *own* hermitian conjugate, and this is the reason behind the c superscript in the notation. However, notice that in general ψ and ψ^c

are fundamentally independent degrees of freedom, not related by any c transformation despite what the notation may suggest. Majorana fermions are a remarkable exception, for which the two spinors are related through hermitian conjugation, i.e. $\psi^c = \psi$.

In our quest to describe our chiral fermions via left-handed Weyl spinors (rather than with 4-component, left-right Dirac spinors), it is convenient to introduce the adjoint Dirac spinor $\overline{\Psi}$ and the gamma matrices in the 2-component formalism,

$$\overline{\Psi} \equiv \Psi^\dagger \gamma^0 = \begin{pmatrix} \psi^c & \psi^\dagger \end{pmatrix} , \qquad \gamma^\mu = \begin{pmatrix} 0 & \sigma^\mu \\ \bar{\sigma}^\mu & 0 \end{pmatrix} , \tag{A.3}$$

with

$$\sigma^\mu = (1, \vec{\sigma}) , \qquad \bar{\sigma}^\mu = (1, -\vec{\sigma}) , \tag{A.4}$$

where $\vec{\sigma} = (\sigma_1, \sigma_2, \sigma_3)$ contains the Pauli matrices. In the chiral representation, left-handed and right-handed Dirac spinors in 4-component notation are given by

$$\Psi_L \equiv P_L \Psi = \begin{pmatrix} \psi \\ 0 \end{pmatrix} , \qquad \Psi_R \equiv P_R \Psi = \begin{pmatrix} 0 \\ \psi^{c\dagger} \end{pmatrix} , \tag{A.5}$$

where $P_{L,R} = (1 \mp \gamma_5)/2$ are the usual chiral projectors.

In terms of SM fermions (and right-handed neutrinos), this formalism allows to relate the 4-component, left-right spinors with the 2-component left-handed spinors as

$$(Q_i, L_i) \equiv (Q_{Li}, L_{Li}) , \quad (u_i^c, d_i^c, \nu_i^c, e_i^c) \overset{CP}{\to} (u_{Ri}, d_{Ri}, \nu_{Ri}, e_{Ri}) , \tag{A.6}$$

where $i = 1, 2, 3$ is a flavour index. Notice that the SM quantum numbers of ψ^c are flipped with respect to those of ψ_R. In theories with vector-like fermions, the relations above can be generalised to

$$(Q_a, L_a) \equiv (Q_{La}, L_{La}) , \qquad \left(\overline{Q}_a, \overline{L}_a\right) \overset{CP}{\to} \left(\widetilde{Q}_{Ra}, \widetilde{L}_{Ra}\right) , \tag{A.7}$$

$$(u_a^c, d_a^c, \nu_a^c, e_a^c) \overset{CP}{\to} (u_{Ra}, d_{Ra}, \nu_{Ra}, e_{Ra}) , \qquad \left(\overline{u_a^c}, \overline{d_a^c}, \overline{\nu_a^c}, \overline{e_a^c}\right) \equiv \left(\widetilde{u}_{La}, \widetilde{d}_{La}, \widetilde{\nu}_{La}, \widetilde{e}_{La}\right) . \tag{A.8}$$

where a is a flavour index that runs for the given vector-like fermion generations of the specific model. We note that in 2-component notation, the bar for vector-like fermions has nothing to do with any transformation, but just denotes the conjugate fermion partner, which carries the opposite quantum numbers.

We highlight that the 4-component Dirac notation with explicit chiral indices is common for phenomenological studies, while the 2-component notation in which all spinors are left-handed is common for model building. The reason is that the 2-component notation is useful to describe extended gauge groups or grand unified theories like $SU(5)$, where left-handed fermions ψ unify with conjugate right-handed fermions ψ^c in the same representations. It is also useful for supersymmetric theories [72]. For extended reviews of 2-component notation, we recommend [404, 405].

As an example of these relations between 4-component and 2-component notations, in the following we transform fermion kinetic terms, Yukawa couplings and the Weinberg operator from 4-component to 2-component notation.

A.2 Kinetic terms and gauge interactions

In 4-component notation, the fermion kinetic terms in the Lagrangian are generically given by

$$\mathcal{L}_{\text{kin}} \supset i\overline{\Psi}_L \gamma^\mu D_\mu \Psi_L + i\overline{\Psi}_R \gamma^\mu D_\mu \Psi_R \,. \tag{A.9}$$

Let us now obtain the kinetic terms in 2-component notation by using Eq. (A.5),

$$i\overline{\Psi}_L \gamma^\mu D_\mu \Psi_L = i \begin{pmatrix} 0 & \psi^\dagger \end{pmatrix} \gamma^\mu D_\mu \begin{pmatrix} \psi \\ 0 \end{pmatrix} \tag{A.10}$$

$$= i \begin{pmatrix} 0 & \psi^\dagger \bar{\sigma}^\mu \end{pmatrix} D_\mu \begin{pmatrix} \psi \\ 0 \end{pmatrix} = i\psi^\dagger \bar{\sigma}^\mu D_\mu \psi \,, \tag{A.11}$$

$$i\overline{\Psi}_R \gamma^\mu D_\mu \Psi_R = i \begin{pmatrix} \psi^c & 0 \end{pmatrix} \gamma^\mu D_\mu \begin{pmatrix} 0 \\ \psi^{c\dagger} \end{pmatrix} \tag{A.12}$$

$$= i \begin{pmatrix} \psi^c \sigma^\mu & 0 \end{pmatrix} D_\mu \begin{pmatrix} 0 \\ \psi^{c\dagger} \end{pmatrix} = i\psi^c \sigma^\mu D_\mu \psi^{c\dagger} \,. \tag{A.13}$$

As an example, the couplings of the generic quarks Q_i and d_i^c to the Z_μ boson would be given as

$$\mathcal{L}_{Z_\mu} \supset \left(g_Q Q_i^\dagger \bar{\sigma}^\mu Q_i + g_{d^c} d_i^c \sigma^\mu d_i^{c\dagger} \right) Z_\mu \,. \tag{A.14}$$

However, in the literature it is common to heavily abuse the notation and write $\sigma^\mu, \bar{\sigma}^\mu \to \gamma^\mu$, i.e.

$$\mathcal{L}_{Z_\mu} \supset \left(g_Q Q_i^\dagger \gamma^\mu Q_i + g_{d^c} d_i^c \gamma^\mu d_i^{c\dagger} \right) Z_\mu \,. \tag{A.15}$$

We advise the reader to remember that in 2-component notation the gamma (also called Dirac) matrices must be formally exchanged by σ^μ and $\bar{\sigma}^\mu$.

A.3 Yukawa interactions

In 4-component notation, the SM Yukawa interactions for a generic fermion family are given by

$$\mathcal{L}_{\text{Yukawa}} = y_{ij} \overline{\Psi}_{Li} H \Psi_{Rj} + \text{h.c.} \,, \tag{A.16}$$

where remember that $H \sim (\mathbf{1}, \mathbf{2}, 1/2)$. In 2-component notation

$$\mathcal{L}_{\text{Yukawa}} = y_{ij} \begin{pmatrix} 0 & \psi_i^\dagger \end{pmatrix} H \begin{pmatrix} 0 \\ \psi_j^{c\dagger} \end{pmatrix} + \text{h.c.} = y_{ij} \psi_i^\dagger H \psi_j^{c\dagger} + y_{ji}^* \psi_i H^\dagger \psi_j^c \,. \tag{A.17}$$

Then in 2-component notation it is convenient to redefine the Higgs doublet as $H(\mathbf{1},\mathbf{2},1/2) \to H(\mathbf{1},\mathbf{2},-1/2)$[1] (and exchange the Yukawa matrix by its hermitian conjugate), such that the Yukawa couplings are

$$\mathcal{L}_{\text{Yukawa}} = y_{ij}\psi_i H \psi_j^c + \text{h.c.} \tag{A.18}$$

In this manner, the SM Yukawa couplings for each fermion family are given by

$$\mathcal{L}_{\text{Yukawa}} = y^u_{ij} Q_i \widetilde{H} u^c_j + y^d_{ij} Q_i H d^c_j + y^e_{ij} L_i H e^c_j + \text{h.c.}\,, \tag{A.19}$$

where $\tilde{H} = i\sigma_2 H^\dagger$ is the CP-conjugate of H.

A.4 Weinberg operator

In 4-component notation, the Weinberg operator (see Eq. (1.84)) is given by[2]

$$\mathcal{L}^{d=5}_{\text{Weinberg}} = c_{ij}\left(\bar{L}^C_{Li}\widetilde{H}\right)\left(L_{Lj}\widetilde{H}\right) + \text{h.c.}\,, \tag{A.20}$$

where we have absorbed the cut-off scale in the dimensionful coefficients c_{ij}. We need to apply charge conjugation C to the 4-component Dirac spinor,

$$\Psi^C = C\overline{\Psi}^{\text{T}} = \begin{pmatrix} \psi^c \\ \psi^\dagger \end{pmatrix}, \tag{A.21}$$

in order to obtain

$$\begin{aligned} \mathcal{L}^{d=5}_{\text{Weinberg}} =& c_{ij}\left(\bar{L}^C_{Li}\widetilde{H}\right)\left(L_{Lj}\widetilde{H}\right) + \text{h.c.} = c_{ij}\left[\begin{pmatrix} L_i & 0 \end{pmatrix}\widetilde{H}\right]\left[\widetilde{H}\begin{pmatrix} L_j \\ 0 \end{pmatrix}\right] + \text{h.c.} \\ =& c_{ij}\left(L_i\widetilde{H}\right)\left(L_j\widetilde{H}\right) + \text{h.c.} \end{aligned} \tag{A.22}$$

[1] Notice that in doing this one has to be careful with the implicit $SU(2)_L$ indices of the Yukawa operator.

[2] Remember that we now define the Higgs doublet as $H \sim (\mathbf{1},\mathbf{2},-1/2)$ which is more convenient for the 2-component notation.

Appendix B

Large mixing angle formalism and mass insertion approximation

In this thesis, we study several models where heavy vector-like fermions mix with the chiral fermions of the SM. For illustration purposes, let us assume the following generic terms in the mass Lagrangian,

$$\mathcal{L}_{\text{mass}} \supset x_{34}^{\psi} \phi \psi_3 \overline{\psi}_4 + M_4^{\psi} \psi_4 \overline{\psi}_4 + \text{h.c.}\,, \tag{B.1}$$

where we work in a 2-component notation with left-handed Weyl fermions, as discussed in Appendix A. The heavy vector-like "fourth" family fermion obtains mass from the arbitrary vector-like mass term M_4^{ψ}. Besides, in the example above, a scalar SM singlet couples the heavy vector-like fermion to a third family chiral fermion. Once the scalar singlet develops a VEV, $\langle\phi\rangle$, the first term in Eq. (B.1) provides mixing between the third and fourth family (left-handed) fermions. In all generality, we obtain (see [168] for further details)

$$x_{34}^{\psi} \langle\phi\rangle \psi_3 \overline{\psi}_4 + M_4^{\psi} \psi_4 \overline{\psi}_4 = \left(x_{34}^{\psi} \langle\phi\rangle \psi_3 + M_4^{\psi} \psi_4 \right) \overline{\psi}_4 = \hat{M}_4^{\psi} \frac{x_{34}^{\psi} \langle\phi\rangle \psi_3 + M_4^{\psi} \psi_4}{\sqrt{\left(x_{34}^{\psi} \langle\phi\rangle \right)^2 + \left(M_4^{\psi} \right)^2}} \overline{\psi}_4\,, \tag{B.2}$$

where in the last step we have normalised the vector in order to obtain

$$\hat{M}_4^{\psi} = \sqrt{\left(x_{34}^{\psi} \langle\phi\rangle \right)^2 + \left(M_4^{\psi} \right)^2} \tag{B.3}$$

as the physical mass of the vector-like fermion. We can identify the mixing angles as

$$s_{34}^{\psi} = \frac{x_{34}^{\psi} \langle\phi\rangle}{\sqrt{\left(x_{34}^{\psi} \langle\phi\rangle \right)^2 + \left(M_4^{\psi} \right)^2}}\,, \qquad c_{34}^{\psi} = \frac{M_4^{\psi}}{\sqrt{\left(x_{34}^{\psi} \langle\phi\rangle \right)^2 + \left(M_4^{\psi} \right)^2}}\,. \tag{B.4}$$

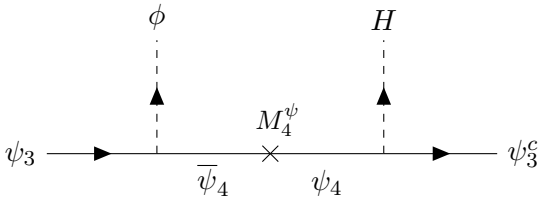

FIGURE B.1: Example of effective Yukawa coupling in the mass insertion approximation.

This way, the mass eigenstates are given by

$$\hat{\psi}_4 = c_{34}^\psi \psi_4 + s_{34}^\psi \psi_3 \,, \qquad \hat{\psi}_3 = c_{34}^\psi \psi_3 - s_{34}^\psi \psi_4 \,. \tag{B.5}$$

In this manner, we have obtained an accurate description of fermion mixing valid in all regimes: this is called the *large mixing angle formalism*.

Notice that if the vector-like mass is much larger than the VEV of the scalar singlet, i.e. $\langle\phi\rangle \ll M_4^\psi$, we may approximate the mass eigenstates of physical fermions as

$$\hat{\psi}_4 \approx \psi_4 + s_{34}^\psi \psi_3 \,, \qquad \hat{\psi}_3 \approx \psi_3 - s_{34}^\psi \psi_3 \,, \tag{B.6}$$

where

$$s_{34}^\psi \approx x_{34}^\psi \frac{\langle\phi\rangle}{M_4^\psi} \ll 1 \,, \tag{B.7}$$

such that in good approximation $\hat{\psi}_4 \approx \psi_4$ and $\hat{\psi}_3 \approx \psi_3$, and the physical mass of the vector-like fermion is given in good approximation by M_4^ψ. This is denoted as the *mass insertion approximation*.

More generally, along with the mass terms of the Lagrangian in Eq. (B.1), in the models studied in this thesis we shall also find couplings that connect chiral and vector-like fermions via Higgs doublets,

$$\mathcal{L}_{\text{mass}} \supset y_{43}^\psi H \psi_4 \psi_3^c + x_{34}^\psi \phi \psi_3 \overline{\psi}_4 + M_4^\psi \psi_4 \overline{\psi}_4 + \text{h.c.} \tag{B.8}$$

In the regime $\langle H\rangle \ll \langle\phi\rangle \,, M_4^\psi$, which is accurate to describe models with heavy NP much above the electroweak scale, the first term in Eq. (B.8) provides an effective Higgs Yukawa coupling for the third family fermion via the mixing mediated by ϕ, i.e.

$$y_{43}^\psi H \psi_4 \psi_3^c \approx y_{43}^\psi H (c_{34}^\psi \hat{\psi}_4 + s_{34}^\psi \hat{\psi}_3) \psi_3^c \to y_{43}^\psi s_{34}^\psi H \hat{\psi}_3 \psi_3^c \,. \tag{B.9}$$

Therefore, the effective Yukawa coupling is given by

$$y_3 = y_{43}^\psi s_{34}^\psi = y_{43}^\psi \frac{x_{34}^\psi \langle\phi\rangle}{\sqrt{\left(x_{34}^\psi \langle\phi\rangle\right)^2 + \left(M_4^\psi\right)^2}} \,, \tag{B.10}$$

where s_{34}^ψ is given in the large mixing angle formalism by Eq. (B.4). By taking the

limit $\langle\phi\rangle \ll M_4^\psi$ above, one can find the effective Yukawa coupling in the mass insertion approximation as

$$y_3 \approx y_{43}^\psi x_{34}^\psi \frac{\langle\phi\rangle}{M_4^\psi} \,. \tag{B.11}$$

This Yukawa coupling can also be extracted from the mass insertion diagrams in Fig. B.1. This process can be easily generalised to vector-like fermions which mix with CP-conjugate right-handed fermions ψ^c. Notice that with the set of couplings introduced so far, the conjugate fermions $\overline{\psi}_4$ and $\overline{\psi_4^c}$ do not mix with chiral fermions (only the fermions ψ_4 and ψ_4^c do mix with chiral fermions). They would mix if Yukawa couplings of the form $y_4^\psi H \psi_4 \psi_4^c$ are introduced in the Lagrangian, as discussed in Chapter 3, although such mixing is usually negligible in the regime $\langle H\rangle \ll \langle\phi\rangle \,, M_4^\psi$.

Appendix C

Hyperons from $SU(5)^3$

Gauge non-universal theories of flavour are usually spontaneously broken down to the SM via the VEVs of scalar fields in bi-representations of the different sites. In the case of the tri-hypercharge model (see Chapter 5) such fields carry family hypercharges that add up to zero, and we call them hyperons. The embedding of hyperons into the $SU(5)^3$ tri-unification framework proposed in Chapter 6 constrains their possible family hypercharge assignments. Tables C.1 and C.2 list all possible hyperon embeddings in $SU(5)^3$ representations with dimension up to **45**. These tables have been obtained with the help of `GroupMath` [398].

Hyperon			$\boldsymbol{SU(5)^3}$ **representations**
0	$-\frac{1}{3}$	$\frac{1}{3}$	$(\mathbf{1},\mathbf{5},\overline{\mathbf{5}}),(\mathbf{1},\mathbf{5},\overline{\mathbf{45}}),(\mathbf{1},\mathbf{45},\overline{\mathbf{5}}),(\mathbf{1},\mathbf{45},\overline{\mathbf{45}}),(\mathbf{24},\mathbf{5},\overline{\mathbf{5}}),(\mathbf{24},\mathbf{5},\overline{\mathbf{45}}),(\mathbf{24},\mathbf{45},\overline{\mathbf{5}}),(\mathbf{24},\mathbf{45},\overline{\mathbf{45}})$
0	$\frac{1}{2}$	$-\frac{1}{2}$	$(\mathbf{1},\mathbf{5},\overline{\mathbf{5}}),(\mathbf{1},\mathbf{5},\overline{\mathbf{45}}),(\mathbf{1},\mathbf{45},\overline{\mathbf{5}}),(\mathbf{1},\mathbf{45},\overline{\mathbf{45}}),(\mathbf{24},\mathbf{5},\overline{\mathbf{5}}),(\mathbf{24},\mathbf{5},\overline{\mathbf{45}}),(\mathbf{24},\mathbf{45},\overline{\mathbf{5}}),(\mathbf{24},\mathbf{45},\overline{\mathbf{45}})$
0	$-\frac{2}{3}$	$\frac{2}{3}$	$(\mathbf{1},\mathbf{10},\overline{\mathbf{10}}),(\mathbf{1},\mathbf{10},\overline{\mathbf{40}}),(\mathbf{1},\mathbf{15},\overline{\mathbf{15}}),(\mathbf{1},\mathbf{35},\overline{\mathbf{35}}),(\mathbf{1},\mathbf{35},\overline{\mathbf{40}}),(\mathbf{1},\mathbf{40},\overline{\mathbf{10}}),(\mathbf{1},\mathbf{40},\overline{\mathbf{35}}),(\mathbf{1},\mathbf{40},\overline{\mathbf{40}}),$ $(\mathbf{24},\mathbf{10},\overline{\mathbf{10}}),(\mathbf{24},\mathbf{10},\overline{\mathbf{15}}),(\mathbf{24},\mathbf{10},\overline{\mathbf{35}}),(\mathbf{24},\mathbf{10},\overline{\mathbf{40}}),(\mathbf{24},\mathbf{15},\overline{\mathbf{10}}),(\mathbf{24},\mathbf{15},\overline{\mathbf{15}}),(\mathbf{24},\mathbf{15},\overline{\mathbf{40}}),$ $(\mathbf{24},\mathbf{35},\overline{\mathbf{10}}),(\mathbf{24},\mathbf{35},\overline{\mathbf{35}}),(\mathbf{24},\mathbf{35},\overline{\mathbf{40}}),(\mathbf{24},\mathbf{40},\overline{\mathbf{10}}),(\mathbf{24},\mathbf{40},\overline{\mathbf{15}}),(\mathbf{24},\mathbf{40},\overline{\mathbf{35}}),(\mathbf{24},\mathbf{40},\overline{\mathbf{40}})$
0	$\frac{1}{6}$	$-\frac{1}{6}$	$(\mathbf{1},\mathbf{10},\overline{\mathbf{10}}),(\mathbf{1},\mathbf{10},\overline{\mathbf{15}}),(\mathbf{1},\mathbf{10},\overline{\mathbf{40}}),(\mathbf{1},\mathbf{15},\overline{\mathbf{10}}),(\mathbf{1},\mathbf{15},\overline{\mathbf{15}}),(\mathbf{1},\mathbf{15},\overline{\mathbf{40}}),(\mathbf{1},\mathbf{35},\overline{\mathbf{35}}),$ $(\mathbf{1},\mathbf{35},\overline{\mathbf{40}}),(\mathbf{1},\mathbf{40},\overline{\mathbf{10}}),(\mathbf{1},\mathbf{40},\overline{\mathbf{15}}),(\mathbf{1},\mathbf{40},\overline{\mathbf{35}}),(\mathbf{1},\mathbf{40},\overline{\mathbf{40}}),(\mathbf{24},\mathbf{10},\overline{\mathbf{10}}),(\mathbf{24},\mathbf{10},\overline{\mathbf{15}}),$ $(\mathbf{24},\mathbf{10},\overline{\mathbf{35}}),(\mathbf{24},\mathbf{10},\overline{\mathbf{40}}),(\mathbf{24},\mathbf{15},\overline{\mathbf{10}}),(\mathbf{24},\mathbf{15},\overline{\mathbf{15}}),(\mathbf{24},\mathbf{15},\overline{\mathbf{35}}),(\mathbf{24},\mathbf{15},\overline{\mathbf{40}}),(\mathbf{24},\mathbf{35},\overline{\mathbf{10}}),$ $(\mathbf{24},\mathbf{35},\overline{\mathbf{15}}),(\mathbf{24},\mathbf{35},\overline{\mathbf{35}}),(\mathbf{24},\mathbf{35},\overline{\mathbf{40}}),(\mathbf{24},\mathbf{40},\overline{\mathbf{10}}),(\mathbf{24},\mathbf{40},\overline{\mathbf{15}}),(\mathbf{24},\mathbf{40},\overline{\mathbf{35}}),(\mathbf{24},\mathbf{40},\overline{\mathbf{40}})$
0	1	-1	$(\mathbf{1},\mathbf{10},\overline{\mathbf{10}}),(\mathbf{1},\mathbf{15},\overline{\mathbf{15}}),(\mathbf{1},\mathbf{35},\overline{\mathbf{35}}),(\mathbf{1},\mathbf{40},\overline{\mathbf{40}}),(\mathbf{24},\mathbf{10},\overline{\mathbf{10}}),(\mathbf{24},\mathbf{10},\overline{\mathbf{15}}),(\mathbf{24},\mathbf{10},\overline{\mathbf{40}}),$ $(\mathbf{24},\mathbf{15},\overline{\mathbf{10}}),(\mathbf{24},\mathbf{15},\overline{\mathbf{15}}),(\mathbf{24},\mathbf{35},\overline{\mathbf{35}}),(\mathbf{24},\mathbf{35},\overline{\mathbf{40}}),(\mathbf{24},\mathbf{40},\overline{\mathbf{10}}),(\mathbf{24},\mathbf{40},\overline{\mathbf{35}}),(\mathbf{24},\mathbf{40},\overline{\mathbf{40}})$
0	$\frac{5}{6}$	$-\frac{5}{6}$	$(\mathbf{1},\mathbf{24},\mathbf{24})$, $(\mathbf{24},\mathbf{24},\mathbf{24})$
0	$-\frac{3}{2}$	$\frac{3}{2}$	$(\mathbf{1},\mathbf{35},\overline{\mathbf{35}}),(\mathbf{1},\mathbf{40},\overline{\mathbf{40}}),(\mathbf{24},\mathbf{35},\overline{\mathbf{35}}),(\mathbf{24},\mathbf{35},\overline{\mathbf{40}}),(\mathbf{24},\mathbf{40},\overline{\mathbf{35}}),(\mathbf{24},\mathbf{40},\overline{\mathbf{40}})$
0	$\frac{4}{3}$	$-\frac{4}{3}$	$(\mathbf{1},\mathbf{45},\overline{\mathbf{45}})$, $(\mathbf{24},\mathbf{45},\overline{\mathbf{45}})$
0	$-\frac{7}{6}$	$\frac{7}{6}$	$(\mathbf{1},\mathbf{45},\overline{\mathbf{45}})$, $(\mathbf{24},\mathbf{45},\overline{\mathbf{45}})$

TABLE C.1: Hyperons charged under two individual hypercharge groups and their $SU(5)^3$ origin. All $SU(5)^3$ representations that involve up to **45** and $\overline{\mathbf{45}}$ of $SU(5)$ are included. Other hyperons can be obtained by reordering the hypercharge values or by conjugating the $SU(5)^3$ representations.

Hyperon			$SU(5)^3$ representations
$-\frac{1}{3}$	$-\frac{1}{3}$	$\frac{2}{3}$	(5,5,$\overline{10}$),(5,5,$\overline{15}$),(5,5,$\overline{40}$),(5,45,$\overline{10}$),(5,45,$\overline{15}$),(5,45,$\overline{35}$),(5,45,$\overline{40}$),(45,5,$\overline{10}$), (45,5,$\overline{15}$),(45,5,$\overline{35}$),(45,5,$\overline{40}$),(45,45,$\overline{10}$),(45,45,$\overline{15}$),(45,45,$\overline{35}$),(45,45,$\overline{40}$)
$-\frac{1}{3}$	$\frac{1}{2}$	$-\frac{1}{6}$	(5,5,$\overline{10}$),(5,5,$\overline{15}$),(5,5,$\overline{40}$),(5,45,$\overline{10}$),(5,45,$\overline{15}$),(5,45,$\overline{35}$),(5,45,$\overline{40}$),(45,5,$\overline{10}$), (45,5,$\overline{15}$),(45,5,$\overline{35}$),(45,5,$\overline{40}$),(45,45,$\overline{10}$),(45,45,$\overline{15}$),(45,45,$\overline{35}$),(45,45,$\overline{40}$)
$\frac{1}{2}$	$\frac{1}{2}$	-1	(5,5,$\overline{10}$),(5,5,$\overline{15}$),(5,45,$\overline{10}$),(5,45,$\overline{15}$),(5,45,$\overline{40}$),(45,5,$\overline{10}$), (45,5,$\overline{15}$),(45,5,$\overline{40}$),(45,45,$\overline{10}$),(45,45,$\overline{15}$),(45,45,$\overline{35}$),(45,45,$\overline{40}$)
$-\frac{1}{3}$	$-\frac{1}{2}$	$\frac{5}{6}$	(5,$\bar{5}$,24),(5,$\overline{45}$,24),(45,$\bar{5}$,24),(45,$\overline{45}$,24)
$-\frac{1}{3}$	$-\frac{2}{3}$	1	(5,10,10),(5,10,40),(5,15,35),(5,15,40),(5,35,15),(5,40,10),(5,40,15), (5,40,40),(45,10,10),(45,10,15),(45,10,40),(45,15,10),(45,15,35),(45,15,40), (45,35,10),(45,35,15),(45,35,40),(45,40,10),(45,40,15),(45,40,40)
$-\frac{1}{3}$	$\frac{1}{6}$	$\frac{1}{6}$	(5,10,10),(5,10,15),(5,10,35),(5,10,40),(5,15,10),(5,15,15),(5,15,35), (5,15,40),(5,35,10),(5,35,15),(5,35,40),(5,40,10),(5,40,15),(5,40,35), (5,40,40),(45,10,10),(45,10,15),(45,10,35),(45,10,40),(45,15,10), (45,15,15),(45,15,35),(45,15,40),(45,35,10),(45,35,15),(45,35,35), (45,35,40),(45,40,10),(45,40,15),(45,40,35),(45,40,40)
$\frac{1}{2}$	$-\frac{2}{3}$	$\frac{1}{6}$	(5,10,10),(5,10,15),(5,10,40),(5,15,35),(5,15,40),(5,35,10),(5,35,15), (5,35,40),(5,40,10),(5,40,15),(5,40,40),(45,10,10),(45,10,15),(45,10,35), (45,10,40),(45,15,10),(45,15,15),(45,15,35),(45,15,40),(45,35,10),(45,35,15), (45,35,35),(45,35,40),(45,40,10),(45,40,15),(45,40,35),(45,40,40)
$\frac{1}{2}$	1	$-\frac{3}{2}$	(5,10,40),(5,15,35),(5,15,40),(45,10,40),(45,15,35),(45,15,40),(45,40,40)
$-\frac{1}{3}$	-1	$\frac{4}{3}$	(5,$\overline{10}$,45),(5,$\overline{40}$,45),(45,$\overline{10}$,45),(45,$\overline{15}$,45),(45,$\overline{35}$,45),(45,$\overline{40}$,45)
$\frac{1}{2}$	$\frac{2}{3}$	$-\frac{7}{6}$	(5,$\overline{10}$,45),(5,$\overline{35}$,45),(5,$\overline{40}$,45),(45,$\overline{10}$,45),(45,$\overline{15}$,45),(45,$\overline{35}$,45),(45,$\overline{40}$,45)
$-\frac{1}{3}$	$-\frac{5}{6}$	$\frac{7}{6}$	(5,24,$\overline{45}$),(45,24,$\overline{45}$)
$\frac{1}{2}$	$\frac{5}{6}$	$-\frac{4}{3}$	(5,24,$\overline{45}$),(45,24,$\overline{45}$)
$-\frac{1}{3}$	$\frac{3}{2}$	$-\frac{7}{6}$	(5,$\overline{40}$,45),(45,$\overline{35}$,45),(45,$\overline{40}$,45)
$-\frac{2}{3}$	$-\frac{2}{3}$	$\frac{4}{3}$	(10,10,45),(10,15,45),(10,40,45),(15,10,45),(15,40,45),(35,35,45), (35,40,45),(40,10,45),(40,15,45),(40,35,45),(40,40,45)
$\frac{1}{6}$	1	$-\frac{7}{6}$	(10,10,45),(10,15,45),(10,40,45),(15,10,45),(15,15,45), (15,40,45),(35,40,45),(40,10,45),(40,15,45),(40,40,45)
$-\frac{2}{3}$	$-\frac{1}{6}$	$\frac{5}{6}$	(10,$\overline{10}$,24),(10,$\overline{15}$,24),(10,$\overline{35}$,24),(10,$\overline{40}$,24),(15,$\overline{10}$,24),(15,$\overline{15}$,24),(15,$\overline{40}$,24),(35,$\overline{10}$,24), (35,$\overline{15}$,24),(35,$\overline{35}$,24),(35,$\overline{40}$,24),(40,$\overline{10}$,24),(40,$\overline{15}$,24),(40,$\overline{35}$,24),(40,$\overline{40}$,24)
$\frac{1}{6}$	-1	$\frac{5}{6}$	(10,$\overline{10}$,24),(10,$\overline{15}$,24),(10,$\overline{40}$,24),(15,$\overline{10}$,24),(15,$\overline{15}$,24),(15,$\overline{40}$,24), (35,$\overline{35}$,24),(35,$\overline{40}$,24),(40,$\overline{10}$,24),(40,$\overline{15}$,24),(40,$\overline{35}$,24),(40,$\overline{40}$,24)
$-\frac{2}{3}$	$-\frac{5}{6}$	$\frac{3}{2}$	(10,24,$\overline{40}$),(35,24,$\overline{35}$),(35,24,$\overline{40}$),(40,24,$\overline{35}$),(40,24,$\overline{40}$)
$\frac{1}{6}$	$-\frac{3}{2}$	$\frac{4}{3}$	(10,40,45),(15,40,45),(40,40,45)
$\frac{1}{6}$	$-\frac{4}{3}$	$\frac{7}{6}$	(10,$\overline{45}$,$\overline{45}$),(15,$\overline{45}$,$\overline{45}$),(35,$\overline{45}$,$\overline{45}$),(40,$\overline{45}$,$\overline{45}$)

TABLE C.2: Hyperons charged under the three individual hypercharge groups and their $SU(5)^3$ origin. All $SU(5)^3$ representations that involve up to **45** and $\overline{\mathbf{45}}$ of $SU(5)$ are included. Other hyperons can be obtained by reordering the hypercharge values or by conjugating the $SU(5)^3$ representations.

Appendix D

EFT operators and tree-level matching

In this appendix, we list the SMEFT and LEFT operators in the Warsaw and San Diego basis, respectively, including the tree-level matching conditions between SMEFT and LEFT Wilson coefficients.

D.1 The SMEFT operators

This appendix lists the SMEFT operators up to dimension six in the so-called Warsaw basis. The operators were listed in Ref. [39]. They are reproduced in Tables D.1-D.3 since we make significant use of them in this thesis.

D.2 The LEFT operators

This appendix lists the LEFT operators up to dimension six in the so-called San Diego basis. The operators were listed in Ref. [175]. They are reproduced in Tables D.4 and D.5 since we make significant use of them in this thesis.

D.3 Tree-level matching conditions

This appendix includes the tree-level matching conditions between the Warsaw basis of SMEFT operators and the San Diego basis of LEFT operators. This matching conditions were listed in Ref. [175]. They are reproduced in Tables D.6-D.18 since we make significant use of them in this thesis. In all cases, we use C to denote SMEFT Wilson coefficients.

Note that electroweak symmetry breaking is modified in the SMEFT by the presence of dimension-six operators. The scalar field can be written in the unitary gauge as [175]

$$H = \frac{1}{\sqrt{2}} \begin{pmatrix} 0 \\ [1 + c_{H,\text{kin}}]\, h + v_T \end{pmatrix}, \tag{D.1}$$

where

$$c_{H,\text{kin}} \equiv \left(C_{H\Box} - \frac{1}{4}C_{HD}\right) v_{\text{SM}}^2\,, \qquad v_T \equiv \left(1 + \frac{3C_H v_{\text{SM}}^2}{8\lambda}\right) v_{\text{SM}}\,, \tag{D.2}$$

The rescaling of h in Eq. (D.1) is necessary for h to have a conventionally normalised kinetic energy term, and the VEV v_T in the SMEFT is not the same as v_{SM} in the SM Lagrangian due to the dimension-six contributions to the Higgs interactions Q_H, $Q_{H\Box}$ and Q_{HD}, which contribute to the scalar potential and kinetic energy terms.

One also needs to perform gauge field and gauge coupling redefinitions to yield gauge kinetic terms and mass terms that are properly normalised and diagonal

$$G_\mu^A = \mathcal{G}_\mu^A \left(1 + C_{HG} v_T^2\right), \quad W_\mu^I = \mathcal{W}_\mu^I \left(1 + C_{HW} v_T^2\right), \quad B_\mu = \mathcal{B}_\mu \left(1 + C_{HB} v_T^2\right), \tag{D.3}$$

$$\overline{g}_3 = g_3 \left(1 + C_{HG}\, v_T^2\right), \quad \overline{g}_2 = g_2 \left(1 + C_{HW}\, v_T^2\right), \quad \overline{g}_1 = g_1 \left(1 + C_{HB}\, v_T^2\right), \tag{D.4}$$

and

$$\begin{pmatrix} \mathcal{Z}_\mu \\ \mathcal{A}_\mu \end{pmatrix} = \begin{pmatrix} \bar{c} - \frac{\epsilon}{2}\bar{s} & -\bar{s} + \frac{\epsilon}{2}\bar{c} \\ \bar{s} + \frac{\epsilon}{2}\bar{c} & \bar{c} + \frac{\epsilon}{2}\bar{s} \end{pmatrix} \begin{pmatrix} \mathcal{W}_\mu^3 \\ \mathcal{B}_\mu \end{pmatrix}, \quad \epsilon \equiv C_{HWB} v_T^2\,. \tag{D.5}$$

The neutral gauge boson mass eigenstates $\mathcal{Z}^\mu$ and $\mathcal{A}^\mu$ in the above equation depend on the weak mixing angle $\overline{\theta}$ through

$$\begin{aligned} \cos\overline{\theta} \equiv \bar{c} &= \frac{\overline{g}_2}{\sqrt{\overline{g}_1^2 + \overline{g}_2^2}} \left[1 - \frac{\epsilon}{2}\,\frac{\overline{g}_1}{\overline{g}_2}\left(\frac{\overline{g}_2^2 - \overline{g}_1^2}{\overline{g}_1^2 + \overline{g}_2^2}\right)\right], \\ \sin\overline{\theta} \equiv \bar{s} &= \frac{\overline{g}_1}{\sqrt{\overline{g}_1^2 + \overline{g}_2^2}} \left[1 + \frac{\epsilon}{2}\,\frac{\overline{g}_2}{\overline{g}_1}\left(\frac{\overline{g}_2^2 - \overline{g}_1^2}{\overline{g}_1^2 + \overline{g}_2^2}\right)\right]. \end{aligned} \tag{D.6}$$

The massive gauge bosons of the SM receive NP contributions to their masses as

$$\begin{aligned} M_{\mathcal{W}}^2 &= \frac{1}{4}\overline{g}_2^2 v_T^2, \\ M_{\mathcal{Z}}^2 &= \frac{1}{4}\left(\overline{g}_2^2 + \overline{g}_1^2\right) v_T^2 \left(1 + \frac{1}{2}C_{HD} v_T^2\right) + \frac{\epsilon}{2}\overline{g}_1\overline{g}_2 v_T^2\,. \end{aligned} \tag{D.7}$$

In the above equations, G_μ^A, W_μ^I, and B_μ and g_3, g_2, and g_1 are the gauge fields and coupling constants in the SM (without NP contributions), while $\mathcal{G}_\mu^A$, $\mathcal{W}_\mu^I$, and $\mathcal{B}_\mu$ and $\overline{g}_3$, $\overline{g}_2$, and $\overline{g}_1$ are the gauge fields and coupling constants modified by NP contributions from dimension-six SMEFT operators. Note that products of gauge couplings and gauge fields $g_3 G_\mu^A = \overline{g}_3 \mathcal{G}_\mu^A$, $g_2 W_\mu^I = \overline{g}_2 \mathcal{W}_\mu^I$ and $g_1 B_\mu = \overline{g}_1 \mathcal{B}_\mu$ are unchanged by the above redefinitions. In a similar manner, one can check that the effective couplings $\overline{e}$ and $\overline{g}_Z$ are given by

$$\overline{e} = \overline{g}_2\, \sin\overline{\theta} - \frac{1}{2}\,\cos\overline{\theta}\,\overline{g}_2\, v_T^2\, C_{HWB},$$

$$\overline{g}_Z = \frac{\overline{e}}{\sin\overline{\theta}\cos\overline{\theta}}\left[1 + \frac{\overline{g}_1^2 + \overline{g}_2^2}{2\overline{g}_1\overline{g}_2} v_T^2 C_{HWB}\right]. \tag{D.8}$$

The fermion couplings to the massive gauge bosons $\mathcal{W}_\mu^\pm$ and $\mathcal{Z}_\mu$ in the SMEFT take the usual form

$$\mathcal{L} = -\frac{\overline{g}_2}{\sqrt{2}}\left\{\mathcal{W}_\mu^+ j_{\mathcal{W}}^\mu + \text{h.c.}\right\} - \overline{g}_Z \mathcal{Z}_\mu j_{\mathcal{Z}}^\mu\,. \tag{D.9}$$

However, notice that the couplings of the massive gauge bosons to fermions get modified via dimension-six SMEFT operators,

$$\begin{aligned}
j_{\mathcal{W}}^\mu &= [W_l]_{pr}\overline{\nu}_{Lp}\gamma^\mu e_{Lr} + [W_q]_{pr}\overline{u}_{Lp}\gamma^\mu d_{Lr} + [W_R]_{pr}\overline{u}_{Rp}\gamma^\mu d_{Rr},\\
j_Z^\mu &= [Z_{\nu_L}]_{pr}\overline{\nu}_{Lp}\gamma^\mu \nu_{Lr} + [Z_{e_L}]_{pr}\overline{e}_{Lp}\gamma^\mu e_{Lr} + [Z_{e_R}]_{pr}\overline{e}_{Rp}\gamma^\mu e_{Rr}\\
&\quad + [Z_{u_L}]_{pr}\overline{u}_{Lp}\gamma^\mu u_{Lr} + [Z_{u_R}]_{pr}\overline{u}_{Rp}\gamma^\mu u_{Rr} + [Z_{d_L}]_{pr}\overline{d}_{Lp}\gamma^\mu d_{Lr} + [Z_{d_R}]_{pr}\overline{d}_{Rp}\gamma^\mu d_{Rr},
\end{aligned} \tag{D.10}$$

where

$$\begin{aligned}
[W_l]_{pr} &= \left[\delta_{pr} + v_T^2 C^{(3)}_{\substack{Hl\\pr}}\right], \qquad [W_q]_{pr} = \left[\delta_{pr} + v_T^2 C^{(3)}_{\substack{Hq\\pr}}\right], \qquad [W_R]_{pr} = \left[\frac{1}{2} v_T^2 C_{\substack{Hud\\pr}}\right],\\
[Z_{\nu_L}]_{pr} &= \left[\delta_{pr}\left(\frac{1}{2}\right) - \frac{1}{2} v_T^2 C^{(1)}_{\substack{Hl\\pr}} + \frac{1}{2} v_T^2 C^{(3)}_{\substack{Hl\\pr}}\right],\\
[Z_{e_L}]_{pr} &= \left[\delta_{pr}\left(-\frac{1}{2} + \overline{s}^2\right) - \frac{1}{2} v_T^2 C^{(1)}_{\substack{Hl\\pr}} - \frac{1}{2} v_T^2 C^{(3)}_{\substack{Hl\\pr}}\right], \qquad [Z_{e_R}]_{pr} = \left[\delta_{pr}\left(+\overline{s}^2\right) - \frac{1}{2} v_T^2 C_{\substack{He\\pr}}\right],\\
[Z_{u_L}]_{pr} &= \left[\delta_{pr}\left(\frac{1}{2} - \frac{2}{3}\overline{s}^2\right) - \frac{1}{2} v_T^2 C^{(1)}_{\substack{Hq\\pr}} + \frac{1}{2} v_T^2 C^{(3)}_{\substack{Hq\\pr}}\right], \qquad [Z_{u_R}]_{pr} = \left[\delta_{pr}\left(-\frac{2}{3}\overline{s}^2\right) - \frac{1}{2} v_T^2 C_{\substack{Hu\\pr}}\right],\\
[Z_{d_L}]_{pr} &= \left[\delta_{pr}\left(-\frac{1}{2} + \frac{1}{3}\overline{s}^2\right) - \frac{1}{2} v_T^2 C^{(1)}_{\substack{Hq\\pr}} - \frac{1}{2} v_T^2 C^{(3)}_{\substack{Hq\\pr}}\right], \quad [Z_{d_R}]_{pr} = \left[\delta_{pr}\left(+\frac{1}{3}\overline{s}^2\right) - \frac{1}{2} v_T^2 C_{\substack{Hd\\pr}}\right].
\end{aligned} \tag{D.11}$$

Here $[W_l]_{pr}$, $[W_q]_{pr}$ and $[W_R]_{pr}$ are the couplings of $\mathcal{W}_\mu^+$ to $(\overline{\nu}_{Lp}\gamma^\mu e_{Lr})$, $(\overline{u}_{Lp}\gamma^\mu d_{Lr})$, and $(\overline{u}_{Rp}\gamma^\mu d_{Rr})$, respectively, and $[Z_\psi]_{pr}$ are the couplings of $\mathcal{Z}_\mu$ to $(\overline{\psi}_p\gamma^\mu\psi_r)$ for $\psi = \nu_L, e_L, e_R, u_L, u_R, d_L, d_R$. Note that the couplings in Eq. (D.11) are written in the weak-eigenstate basis, so the SM contribution is proportional to Kronecker-delta symbols. The dimension-six $\psi^2 H^2 D$ operators in the SMEFT give the $1/\Lambda^2$ contributions proportional to coefficients C in Eq. (D.11). Interestingly, in spontaneously broken SMEFT, $\mathcal{W}_\mu^+$ couples to the right-handed charged current $(\overline{u}_{Rp}\gamma^\mu d_{Rr})$ with coupling $[W_R]_{pr}$ due to the dimension-six operator Q_{Hud} . In general, the modified couplings of the massive gauge bosons give NP contributions to LEFT operators, as shown in Tables D.6-D.18 which contain the tree-level matching conditions.

We also note that for the tree-level matching we assume the same normalisation for SMEFT and LEFT operators.

$\boldsymbol{\Delta L = 2}$	$\boldsymbol{(LL)HH + \text{h.c.}}$
Q_5	$\epsilon^{ij}\epsilon^{k\ell}(l_{ip}^T C l_{kr}) H_j H_\ell$

TABLE D.1: Dimension-five $\Delta L = 2$ operator Q_5 in SMEFT (Weinberg operator). There is also the Hermitian conjugate $\Delta L = -2$ operator $Q_5^\dagger$, as indicated by $+\,\text{h.c.}$ in the table heading. Subscripts p and r are weak-eigenstate indices. Table taken from [175].

	$\boldsymbol{\Delta B = \Delta L = 1 + \text{h.c.}}$
Q_{duql}	$\epsilon^{\alpha\beta\gamma}\epsilon^{ij}(d_{\alpha p}^T C u_{\beta r})(q_{\gamma is}^T C l_{jt})$
Q_{qque}	$\epsilon^{\alpha\beta\gamma}\epsilon^{ij}(q_{\alpha ip}^T C q_{\beta jr})(u_{\gamma s}^T C e_t)$
Q_{qqql}	$\epsilon^{\alpha\beta\gamma}\epsilon^{i\ell}\epsilon^{jk}(q_{\alpha ip}^T C q_{\beta jr})(q_{\gamma ks}^T C l_{\ell t})$
Q_{duue}	$\epsilon^{\alpha\beta\gamma}(d_{\alpha p}^T C u_{\beta r})(u_{\gamma s}^T C e_t)$

TABLE D.2: Dimension-six $\Delta B = \Delta L = 1$ operators in SMEFT. There are also Hermitian conjugate $\Delta B = \Delta L = -1$ operators, as indicated by $+\,\text{h.c.}$ in the table heading. Subscripts p, r, s and t are flavour indices. Table taken from [175].

1 : X^3	
Q_G	$f^{ABC}G^{A\nu}_{\mu}G^{B\rho}_{\nu}G^{C\mu}_{\rho}$
$Q_{\widetilde{G}}$	$f^{ABC}\widetilde{G}^{A\nu}_{\mu}G^{B\rho}_{\nu}G^{C\mu}_{\rho}$
Q_W	$\epsilon^{IJK}W^{I\nu}_{\mu}W^{J\rho}_{\nu}W^{K\mu}_{\rho}$
$Q_{\widetilde{W}}$	$\epsilon^{IJK}\widetilde{W}^{I\nu}_{\mu}W^{J\rho}_{\nu}W^{K\mu}_{\rho}$

2 : H^6	
Q_H	$(H^\dagger H)^3$

3 : H^4D^2	
$Q_{H\Box}$	$(H^\dagger H)\Box(H^\dagger H)$
Q_{HD}	$\left(H^\dagger D_\mu H\right)^*\left(H^\dagger D_\mu H\right)$

5 : ψ^2H^3 + h.c.	
Q_{eH}	$(H^\dagger H)(\bar{l}_p e_r H)$
Q_{uH}	$(H^\dagger H)(\bar{q}_p u_r \widetilde{H})$
Q_{dH}	$(H^\dagger H)(\bar{q}_p d_r H)$

4 : X^2H^2	
Q_{HG}	$H^\dagger H\, G^A_{\mu\nu}G^{A\mu\nu}$
$Q_{H\widetilde{G}}$	$H^\dagger H\, \widetilde{G}^A_{\mu\nu}G^{A\mu\nu}$
Q_{HW}	$H^\dagger H\, W^I_{\mu\nu}W^{I\mu\nu}$
$Q_{H\widetilde{W}}$	$H^\dagger H\, \widetilde{W}^I_{\mu\nu}W^{I\mu\nu}$
Q_{HB}	$H^\dagger H\, B_{\mu\nu}B^{\mu\nu}$
$Q_{H\widetilde{B}}$	$H^\dagger H\, \widetilde{B}_{\mu\nu}B^{\mu\nu}$
Q_{HWB}	$H^\dagger\tau^I H\, W^I_{\mu\nu}B^{\mu\nu}$
$Q_{H\widetilde{W}B}$	$H^\dagger\tau^I H\, \widetilde{W}^I_{\mu\nu}B^{\mu\nu}$

6 : ψ^2XH + h.c.	
Q_{eW}	$(\bar{l}_p\sigma^{\mu\nu}e_r)\tau^I H W^I_{\mu\nu}$
Q_{eB}	$(\bar{l}_p\sigma^{\mu\nu}e_r)H B_{\mu\nu}$
Q_{uG}	$(\bar{q}_p\sigma^{\mu\nu}T^A u_r)\widetilde{H}\, G^A_{\mu\nu}$
Q_{uW}	$(\bar{q}_p\sigma^{\mu\nu}u_r)\tau^I\widetilde{H}\, W^I_{\mu\nu}$
Q_{uB}	$(\bar{q}_p\sigma^{\mu\nu}u_r)\widetilde{H}\, B_{\mu\nu}$
Q_{dG}	$(\bar{q}_p\sigma^{\mu\nu}T^A d_r)H\, G^A_{\mu\nu}$
Q_{dW}	$(\bar{q}_p\sigma^{\mu\nu}d_r)\tau^I H\, W^I_{\mu\nu}$
Q_{dB}	$(\bar{q}_p\sigma^{\mu\nu}d_r)H\, B_{\mu\nu}$

7 : ψ^2H^2D	
$Q^{(1)}_{Hl}$	$(H^\dagger i\overleftrightarrow{D}_\mu H)(\bar{l}_p\gamma^\mu l_r)$
$Q^{(3)}_{Hl}$	$(H^\dagger i\overleftrightarrow{D}^I_\mu H)(\bar{l}_p\tau^I\gamma^\mu l_r)$
Q_{He}	$(H^\dagger i\overleftrightarrow{D}_\mu H)(\bar{e}_p\gamma^\mu e_r)$
$Q^{(1)}_{Hq}$	$(H^\dagger i\overleftrightarrow{D}_\mu H)(\bar{q}_p\gamma^\mu q_r)$
$Q^{(3)}_{Hq}$	$(H^\dagger i\overleftrightarrow{D}^I_\mu H)(\bar{q}_p\tau^I\gamma^\mu q_r)$
Q_{Hu}	$(H^\dagger i\overleftrightarrow{D}_\mu H)(\bar{u}_p\gamma^\mu u_r)$
Q_{Hd}	$(H^\dagger i\overleftrightarrow{D}_\mu H)(\bar{d}_p\gamma^\mu d_r)$
Q_{Hud} + h.c.	$i(\widetilde{H}^\dagger D_\mu H)(\bar{u}_p\gamma^\mu d_r)$

8 : $(\bar{L}L)(\bar{L}L)$	
Q_{ll}	$(\bar{l}_p\gamma^\mu l_r)(\bar{l}_s\gamma_\mu l_t)$
$Q^{(1)}_{qq}$	$(\bar{q}_p\gamma^\mu q_r)(\bar{q}_s\gamma_\mu q_t)$
$Q^{(3)}_{qq}$	$(\bar{q}_p\gamma^\mu\tau^I q_r)(\bar{q}_s\gamma_\mu\tau^I q_t)$
$Q^{(1)}_{lq}$	$(\bar{l}_p\gamma^\mu l_r)(\bar{q}_s\gamma_\mu q_t)$
$Q^{(3)}_{lq}$	$(\bar{l}_p\gamma^\mu\tau^I l_r)(\bar{q}_s\gamma_\mu\tau^I q_t)$

8 : $(\bar{R}R)(\bar{R}R)$	
Q_{ee}	$(\bar{e}_p\gamma^\mu e_r)(\bar{e}_s\gamma_\mu e_t)$
Q_{uu}	$(\bar{u}_p\gamma^\mu u_r)(\bar{u}_s\gamma_\mu u_t)$
Q_{dd}	$(\bar{d}_p\gamma^\mu d_r)(\bar{d}_s\gamma_\mu d_t)$
Q_{eu}	$(\bar{e}_p\gamma^\mu e_r)(\bar{u}_s\gamma_\mu u_t)$
Q_{ed}	$(\bar{e}_p\gamma^\mu e_r)(\bar{d}_s\gamma_\mu d_t)$
$Q^{(1)}_{ud}$	$(\bar{u}_p\gamma^\mu u_r)(\bar{d}_s\gamma_\mu d_t)$
$Q^{(8)}_{ud}$	$(\bar{u}_p\gamma^\mu T^A u_r)(\bar{d}_s\gamma_\mu T^A d_t)$

8 : $(\bar{L}L)(\bar{R}R)$	
Q_{le}	$(\bar{l}_p\gamma^\mu l_r)(\bar{e}_s\gamma_\mu e_t)$
Q_{lu}	$(\bar{l}_p\gamma^\mu l_r)(\bar{u}_s\gamma_\mu u_t)$
Q_{ld}	$(\bar{l}_p\gamma^\mu l_r)(\bar{d}_s\gamma_\mu d_t)$
Q_{qe}	$(\bar{q}_p\gamma^\mu q_r)(\bar{e}_s\gamma_\mu e_t)$
$Q^{(1)}_{qu}$	$(\bar{q}_p\gamma^\mu q_r)(\bar{u}_s\gamma_\mu u_t)$
$Q^{(8)}_{qu}$	$(\bar{q}_p\gamma^\mu T^A q_r)(\bar{u}_s\gamma_\mu T^A u_t)$
$Q^{(1)}_{qd}$	$(\bar{q}_p\gamma^\mu q_r)(\bar{d}_s\gamma_\mu d_t)$
$Q^{(8)}_{qd}$	$(\bar{q}_p\gamma^\mu T^A q_r)(\bar{d}_s\gamma_\mu T^A d_t)$

8 : $(\bar{L}R)(\bar{R}L)$ + h.c.	
Q_{ledq}	$(\bar{l}^j_p e_r)(\bar{d}_s q_{tj})$

8 : $(\bar{L}R)(\bar{L}R)$ + h.c.	
$Q^{(1)}_{quqd}$	$(\bar{q}^j_p u_r)\epsilon_{jk}(\bar{q}^k_s d_t)$
$Q^{(8)}_{quqd}$	$(\bar{q}^j_p T^A u_r)\epsilon_{jk}(\bar{q}^k_s T^A d_t)$
$Q^{(1)}_{lequ}$	$(\bar{l}^j_p e_r)\epsilon_{jk}(\bar{q}^k_s u_t)$
$Q^{(3)}_{lequ}$	$(\bar{l}^j_p\sigma_{\mu\nu}e_r)\epsilon_{jk}(\bar{q}^k_s\sigma^{\mu\nu}u_t)$

TABLE D.3: The 76 dimension-six operators that conserve baryon and lepton number in the SMEFT. The operators are divided into eight classes according to their field content. The class-8 four-fermion operators are further divided into subclasses according to their chiral properties. Operators with + h.c. have Hermitian conjugates. The subscripts p, r, s, t are flavour indices indices. Table taken from [175].

$\boldsymbol{\nu\nu}$ + h.c.	
$\%_{\nu}$	$(\nu_{Lp}^T C \nu_{Lr})$

$(\boldsymbol{\nu\nu})\boldsymbol{X}$ + h.c.	
$\%_{\nu\gamma}$	$(\nu_{Lp}^T C \sigma^{\mu\nu} \nu_{Lr}) F_{\mu\nu}$

$(\boldsymbol{\overline{L}R})\boldsymbol{X}$ + h.c.	
$\%_{e\gamma}$	$\bar{e}_{Lp} \sigma^{\mu\nu} e_{Rr} \, F_{\mu\nu}$
$\%_{u\gamma}$	$\bar{u}_{Lp} \sigma^{\mu\nu} u_{Rr} \, F_{\mu\nu}$
$\%_{d\gamma}$	$\bar{d}_{Lp} \sigma^{\mu\nu} d_{Rr} \, F_{\mu\nu}$
$\%_{uG}$	$\bar{u}_{Lp} \sigma^{\mu\nu} T^A u_{Rr} \, G^A_{\mu\nu}$
$\%_{dG}$	$\bar{d}_{Lp} \sigma^{\mu\nu} T^A d_{Rr} \, G^A_{\mu\nu}$

$\boldsymbol{X^3}$	
$\%_{G}$	$f^{ABC} G^{A\nu}_{\mu} G^{B\rho}_{\nu} G^{C\mu}_{\rho}$
$\%_{\widetilde{G}}$	$f^{ABC} \widetilde{G}^{A\nu}_{\mu} G^{B\rho}_{\nu} G^{C\mu}_{\rho}$

$(\boldsymbol{\overline{L}L})(\boldsymbol{\overline{L}L})$	
$\%^{V,LL}_{\nu\nu}$	$(\bar{\nu}_{Lp} \gamma^\mu \nu_{Lr})(\bar{\nu}_{Ls} \gamma_\mu \nu_{Lt})$
$\%^{V,LL}_{ee}$	$(\bar{e}_{Lp} \gamma^\mu e_{Lr})(\bar{e}_{Ls} \gamma_\mu e_{Lt})$
$\%^{V,LL}_{\nu e}$	$(\bar{\nu}_{Lp} \gamma^\mu \nu_{Lr})(\bar{e}_{Ls} \gamma_\mu e_{Lt})$
$\%^{V,LL}_{\nu u}$	$(\bar{\nu}_{Lp} \gamma^\mu \nu_{Lr})(\bar{u}_{Ls} \gamma_\mu u_{Lt})$
$\%^{V,LL}_{\nu d}$	$(\bar{\nu}_{Lp} \gamma^\mu \nu_{Lr})(\bar{d}_{Ls} \gamma_\mu d_{Lt})$
$\%^{V,LL}_{eu}$	$(\bar{e}_{Lp} \gamma^\mu e_{Lr})(\bar{u}_{Ls} \gamma_\mu u_{Lt})$
$\%^{V,LL}_{ed}$	$(\bar{e}_{Lp} \gamma^\mu e_{Lr})(\bar{d}_{Ls} \gamma_\mu d_{Lt})$
$\%^{V,LL}_{\nu edu}$	$(\bar{\nu}_{Lp} \gamma^\mu e_{Lr})(\bar{d}_{Ls} \gamma_\mu u_{Lt})$ + h.c.
$\%^{V,LL}_{uu}$	$(\bar{u}_{Lp} \gamma^\mu u_{Lr})(\bar{u}_{Ls} \gamma_\mu u_{Lt})$
$\%^{V,LL}_{dd}$	$(\bar{d}_{Lp} \gamma^\mu d_{Lr})(\bar{d}_{Ls} \gamma_\mu d_{Lt})$
$\%^{V1,LL}_{ud}$	$(\bar{u}_{Lp} \gamma^\mu u_{Lr})(\bar{d}_{Ls} \gamma_\mu d_{Lt})$
$\%^{V8,LL}_{ud}$	$(\bar{u}_{Lp} \gamma^\mu T^A u_{Lr})(\bar{d}_{Ls} \gamma_\mu T^A d_{Lt})$

$(\boldsymbol{\overline{R}R})(\boldsymbol{\overline{R}R})$	
$\%^{V,RR}_{ee}$	$(\bar{e}_{Rp} \gamma^\mu e_{Rr})(\bar{e}_{Rs} \gamma_\mu e_{Rt})$
$\%^{V,RR}_{eu}$	$(\bar{e}_{Rp} \gamma^\mu e_{Rr})(\bar{u}_{Rs} \gamma_\mu u_{Rt})$
$\%^{V,RR}_{ed}$	$(\bar{e}_{Rp} \gamma^\mu e_{Rr})(\bar{d}_{Rs} \gamma_\mu d_{Rt})$
$\%^{V,RR}_{uu}$	$(\bar{u}_{Rp} \gamma^\mu u_{Rr})(\bar{u}_{Rs} \gamma_\mu u_{Rt})$
$\%^{V,RR}_{dd}$	$(\bar{d}_{Rp} \gamma^\mu d_{Rr})(\bar{d}_{Rs} \gamma_\mu d_{Rt})$
$\%^{V1,RR}_{ud}$	$(\bar{u}_{Rp} \gamma^\mu u_{Rr})(\bar{d}_{Rs} \gamma_\mu d_{Rt})$
$\%^{V8,RR}_{ud}$	$(\bar{u}_{Rp} \gamma^\mu T^A u_{Rr})(\bar{d}_{Rs} \gamma_\mu T^A d_{Rt})$

$(\boldsymbol{\overline{L}L})(\boldsymbol{\overline{R}R})$	
$\%^{V,LR}_{\nu e}$	$(\bar{\nu}_{Lp} \gamma^\mu \nu_{Lr})(\bar{e}_{Rs} \gamma_\mu e_{Rt})$
$\%^{V,LR}_{ee}$	$(\bar{e}_{Lp} \gamma^\mu e_{Lr})(\bar{e}_{Rs} \gamma_\mu e_{Rt})$
$\%^{V,LR}_{\nu u}$	$(\bar{\nu}_{Lp} \gamma^\mu \nu_{Lr})(\bar{u}_{Rs} \gamma_\mu u_{Rt})$
$\%^{V,LR}_{\nu d}$	$(\bar{\nu}_{Lp} \gamma^\mu \nu_{Lr})(\bar{d}_{Rs} \gamma_\mu d_{Rt})$
$\%^{V,LR}_{eu}$	$(\bar{e}_{Lp} \gamma^\mu e_{Lr})(\bar{u}_{Rs} \gamma_\mu u_{Rt})$
$\%^{V,LR}_{ed}$	$(\bar{e}_{Lp} \gamma^\mu e_{Lr})(\bar{d}_{Rs} \gamma_\mu d_{Rt})$
$\%^{V,LR}_{ue}$	$(\bar{u}_{Lp} \gamma^\mu u_{Lr})(\bar{e}_{Rs} \gamma_\mu e_{Rt})$
$\%^{V,LR}_{de}$	$(\bar{d}_{Lp} \gamma^\mu d_{Lr})(\bar{e}_{Rs} \gamma_\mu e_{Rt})$
$\%^{V,LR}_{\nu edu}$	$(\bar{\nu}_{Lp} \gamma^\mu e_{Lr})(\bar{d}_{Rs} \gamma_\mu u_{Rt})$ + h.c.
$\%^{V1,LR}_{uu}$	$(\bar{u}_{Lp} \gamma^\mu u_{Lr})(\bar{u}_{Rs} \gamma_\mu u_{Rt})$
$\%^{V8,LR}_{uu}$	$(\bar{u}_{Lp} \gamma^\mu T^A u_{Lr})(\bar{u}_{Rs} \gamma_\mu T^A u_{Rt})$
$\%^{V1,LR}_{ud}$	$(\bar{u}_{Lp} \gamma^\mu u_{Lr})(\bar{d}_{Rs} \gamma_\mu d_{Rt})$
$\%^{V8,LR}_{ud}$	$(\bar{u}_{Lp} \gamma^\mu T^A u_{Lr})(\bar{d}_{Rs} \gamma_\mu T^A d_{Rt})$
$\%^{V1,LR}_{du}$	$(\bar{d}_{Lp} \gamma^\mu d_{Lr})(\bar{u}_{Rs} \gamma_\mu u_{Rt})$
$\%^{V8,LR}_{du}$	$(\bar{d}_{Lp} \gamma^\mu T^A d_{Lr})(\bar{u}_{Rs} \gamma_\mu T^A u_{Rt})$
$\%^{V1,LR}_{dd}$	$(\bar{d}_{Lp} \gamma^\mu d_{Lr})(\bar{d}_{Rs} \gamma_\mu d_{Rt})$
$\%^{V8,LR}_{dd}$	$(\bar{d}_{Lp} \gamma^\mu T^A d_{Lr})(\bar{d}_{Rs} \gamma_\mu T^A d_{Rt})$
$\%^{V1,LR}_{uddu}$	$(\bar{u}_{Lp} \gamma^\mu d_{Lr})(\bar{d}_{Rs} \gamma_\mu u_{Rt})$ + h.c.
$\%^{V8,LR}_{uddu}$	$(\bar{u}_{Lp} \gamma^\mu T^A d_{Lr})(\bar{d}_{Rs} \gamma_\mu T^A u_{Rt})$ + h.c.

$(\boldsymbol{\overline{L}L})(\boldsymbol{\overline{R}R})$ + h.c.	
$\%^{S,RR}_{ee}$	$(\bar{e}_{Lp} e_{Rr})(\bar{e}_{Ls} e_{Rt})$
$\%^{S,RR}_{eu}$	$(\bar{e}_{Lp} e_{Rr})(\bar{u}_{Ls} u_{Rt})$
$\%^{T,RR}_{eu}$	$(\bar{e}_{Lp} \sigma^{\mu\nu} e_{Rr})(\bar{u}_{Ls} \sigma_{\mu\nu} u_{Rt})$
$\%^{S,RR}_{ed}$	$(\bar{e}_{Lp} e_{Rr})(\bar{d}_{Ls} d_{Rt})$
$\%^{T,RR}_{ed}$	$(\bar{e}_{Lp} \sigma^{\mu\nu} e_{Rr})(\bar{d}_{Ls} \sigma_{\mu\nu} d_{Rt})$
$\%^{S,RR}_{\nu edu}$	$(\bar{\nu}_{Lp} e_{Rr})(\bar{d}_{Ls} u_{Rt})$
$\%^{T,RR}_{\nu edu}$	$(\bar{\nu}_{Lp} \sigma^{\mu\nu} e_{Rr})(\bar{d}_{Ls} \sigma_{\mu\nu} u_{Rt})$
$\%^{S1,RR}_{uu}$	$(\bar{u}_{Lp} u_{Rr})(\bar{u}_{Ls} u_{Rt})$
$\%^{S8,RR}_{uu}$	$(\bar{u}_{Lp} T^A u_{Rr})(\bar{u}_{Ls} T^A u_{Rt})$
$\%^{S1,RR}_{ud}$	$(\bar{u}_{Lp} u_{Rr})(\bar{d}_{Ls} d_{Rt})$
$\%^{S8,RR}_{ud}$	$(\bar{u}_{Lp} T^A u_{Rr})(\bar{d}_{Ls} T^A d_{Rt})$
$\%^{S1,RR}_{dd}$	$(\bar{d}_{Lp} d_{Rr})(\bar{d}_{Ls} d_{Rt})$
$\%^{S8,RR}_{dd}$	$(\bar{d}_{Lp} T^A d_{Rr})(\bar{d}_{Ls} T^A d_{Rt})$
$\%^{S1,RR}_{uddu}$	$(\bar{u}_{Lp} d_{Rr})(\bar{d}_{Ls} u_{Rt})$
$\%^{S8,RR}_{uddu}$	$(\bar{u}_{Lp} T^A d_{Rr})(\bar{d}_{Ls} T^A u_{Rt})$

$(\boldsymbol{\overline{L}R})(\boldsymbol{\overline{R}L})$ + h.c.	
$\%^{S,RL}_{eu}$	$(\bar{e}_{Lp} e_{Rr})(\bar{u}_{Rs} u_{Lt})$
$\%^{S,RL}_{ed}$	$(\bar{e}_{Lp} e_{Rr})(\bar{d}_{Rs} d_{Lt})$
$\%^{S,RL}_{\nu edu}$	$(\bar{\nu}_{Lp} e_{Rr})(\bar{d}_{Rs} u_{Lt})$

TABLE D.4: The operators for LEFT of dimension three, five, and six that conserve baryon and lepton number, and the dimension-three and dimension-five $\Delta L = \pm 2$ operators. The dimension-three $\Delta L = 2$ operator $\mathcal{O}_\nu$ is the Majorana-neutrino mass operator, while the dimension-five $\Delta L = 2$ operator $\mathcal{O}_{\nu\gamma}$ is the Majorana-neutrino dipole operator. There are 5 additional dimension-five dipole operators $(\bar{L}R)X$. The 80 dimension-six operators consist of 2 pure gauge operators X^3 and 78 four-fermion operators ψ^4, which are further divided by their chiral structure. The ψ^4 operator superscripts V, S, T refer to products of vector, scalar, and tensor fermion bilinears, and the additional two labels L or R refer to the chiral projectors in the bilinears. Operators with + h.c. have Hermitian conjugates. The subscripts p, r, s, t are flavour indices. Table taken from [175].

$\Delta L = 4 + \text{h.c.}$

$\%_{\nu\nu}^{S,LL}$	$(\nu_{Lp}^T C \nu_{Lr})(\nu_{Ls}^T C \nu_{Lt})$

$\Delta L = 2 + \text{h.c.}$

$\%_{\nu e}^{S,LL}$	$(\nu_{Lp}^T C \nu_{Lr})(\bar{e}_{Rs} e_{Lt})$
$\%_{\nu e}^{T,LL}$	$(\nu_{Lp}^T C \sigma^{\mu\nu} \nu_{Lr})(\bar{e}_{Rs} \sigma_{\mu\nu} e_{Lt})$
$\%_{\nu e}^{S,LR}$	$(\nu_{Lp}^T C \nu_{Lr})(\bar{e}_{Ls} e_{Rt})$
$\%_{\nu u}^{S,LL}$	$(\nu_{Lp}^T C \nu_{Lr})(\bar{u}_{Rs} u_{Lt})$
$\%_{\nu u}^{T,LL}$	$(\nu_{Lp}^T C \sigma^{\mu\nu} \nu_{Lr})(\bar{u}_{Rs} \sigma_{\mu\nu} u_{Lt})$
$\%_{\nu u}^{S,LR}$	$(\nu_{Lp}^T C \nu_{Lr})(\bar{u}_{Ls} u_{Rt})$
$\%_{\nu d}^{S,LL}$	$(\nu_{Lp}^T C \nu_{Lr})(\bar{d}_{Rs} d_{Lt})$
$\%_{\nu d}^{T,LL}$	$(\nu_{Lp}^T C \sigma^{\mu\nu} \nu_{Lr})(\bar{d}_{Rs} \sigma_{\mu\nu} d_{Lt})$
$\%_{\nu d}^{S,LR}$	$(\nu_{Lp}^T C \nu_{Lr})(\bar{d}_{Ls} d_{Rt})$
$\%_{\nu edu}^{S,LL}$	$(\nu_{Lp}^T C e_{Lr})(\bar{d}_{Rs} u_{Lt})$
$\%_{\nu edu}^{T,LL}$	$(\nu_{Lp}^T C \sigma^{\mu\nu} e_{Lr})(\bar{d}_{Rs} \sigma_{\mu\nu} u_{Lt})$
$\%_{\nu edu}^{S,LR}$	$(\nu_{Lp}^T C e_{Lr})(\bar{d}_{Ls} u_{Rt})$
$\%_{\nu edu}^{V,RL}$	$(\nu_{Lp}^T C \gamma^{\mu} e_{Rr})(\bar{d}_{Ls} \gamma_{\mu} u_{Lt})$
$\%_{\nu edu}^{V,RR}$	$(\nu_{Lp}^T C \gamma^{\mu} e_{Rr})(\bar{d}_{Rs} \gamma_{\mu} u_{Rt})$

$\Delta B = \Delta L = 1 + \text{h.c.}$

$\%_{udd}^{S,LL}$	$\epsilon_{\alpha\beta\gamma}(u_{Lp}^{\alpha T} C d_{Lr}^{\beta})(d_{Ls}^{\gamma T} C \nu_{Lt})$
$\%_{duu}^{S,LL}$	$\epsilon_{\alpha\beta\gamma}(d_{Lp}^{\alpha T} C u_{Lr}^{\beta})(u_{Ls}^{\gamma T} C e_{Lt})$
$\%_{uud}^{S,LR}$	$\epsilon_{\alpha\beta\gamma}(u_{Lp}^{\alpha T} C u_{Lr}^{\beta})(d_{Rs}^{\gamma T} C e_{Rt})$
$\%_{duu}^{S,LR}$	$\epsilon_{\alpha\beta\gamma}(d_{Lp}^{\alpha T} C u_{Lr}^{\beta})(u_{Rs}^{\gamma T} C e_{Rt})$
$\%_{uud}^{S,RL}$	$\epsilon_{\alpha\beta\gamma}(u_{Rp}^{\alpha T} C u_{Rr}^{\beta})(d_{Ls}^{\gamma T} C e_{Lt})$
$\%_{duu}^{S,RL}$	$\epsilon_{\alpha\beta\gamma}(d_{Rp}^{\alpha T} C u_{Rr}^{\beta})(u_{Ls}^{\gamma T} C e_{Lt})$
$\%_{dud}^{S,RL}$	$\epsilon_{\alpha\beta\gamma}(d_{Rp}^{\alpha T} C u_{Rr}^{\beta})(d_{Ls}^{\gamma T} C \nu_{Lt})$
$\%_{ddu}^{S,RL}$	$\epsilon_{\alpha\beta\gamma}(d_{Rp}^{\alpha T} C d_{Rr}^{\beta})(u_{Ls}^{\gamma T} C \nu_{Lt})$
$\%_{duu}^{S,RR}$	$\epsilon_{\alpha\beta\gamma}(d_{Rp}^{\alpha T} C u_{Rr}^{\beta})(u_{Rs}^{\gamma T} C e_{Rt})$

$\Delta B = -\Delta L = 1 + \text{h.c.}$

$\%_{ddd}^{S,LL}$	$\epsilon_{\alpha\beta\gamma}(d_{Lp}^{\alpha T} C d_{Lr}^{\beta})(\bar{e}_{Rs} d_{Lt}^{\gamma})$
$\%_{udd}^{S,LR}$	$\epsilon_{\alpha\beta\gamma}(u_{Lp}^{\alpha T} C d_{Lr}^{\beta})(\bar{\nu}_{Ls} d_{Rt}^{\gamma})$
$\%_{ddu}^{S,LR}$	$\epsilon_{\alpha\beta\gamma}(d_{Lp}^{\alpha T} C d_{Lr}^{\beta})(\bar{\nu}_{Ls} u_{Rt}^{\gamma})$
$\%_{ddd}^{S,LR}$	$\epsilon_{\alpha\beta\gamma}(d_{Lp}^{\alpha T} C d_{Lr}^{\beta})(\bar{e}_{Ls} d_{Rt}^{\gamma})$
$\%_{ddd}^{S,RL}$	$\epsilon_{\alpha\beta\gamma}(d_{Rp}^{\alpha T} C d_{Rr}^{\beta})(\bar{e}_{Rs} d_{Lt}^{\gamma})$
$\%_{udd}^{S,RR}$	$\epsilon_{\alpha\beta\gamma}(u_{Rp}^{\alpha T} C d_{Rr}^{\beta})(\bar{\nu}_{Ls} d_{Rt}^{\gamma})$
$\%_{ddd}^{S,RR}$	$\epsilon_{\alpha\beta\gamma}(d_{Rp}^{\alpha T} C d_{Rr}^{\beta})(\bar{e}_{Ls} d_{Rt}^{\gamma})$

TABLE D.5: The LEFT dimension-six four-fermion operators that violate baryon and/or lepton number. All operators have Hermitian conjugates. The operator superscripts V, S, T refer to products of vector, scalar, and tensor fermion bilinears, and the additional two labels L or R refer to the chiral projectors in the bilinears. The subscripts p, r, s, t are flavour indices. Table taken from [175]

$\Delta L = 2$ $\quad \nu\nu + \text{h.c.}$

	Number	SM	Matching
$\%_{\nu}$	$\frac{1}{2} n_\nu (n_\nu + 1)$	6	$\frac{1}{2} C^{\ 5}_{pr}\, v_T^2$

TABLE D.6: Dimension-three $\Delta L = 2$ Majorana neutrino mass operators in LEFT. There are also Hermitian conjugate $\Delta L = -2$ operators $\mathcal{O}_\nu^\dagger$, as indicated in the table heading. The second column is the number of operators for an arbitrary number of neutrino flavours n_ν, and the third column is the number in the SM LEFT with $n_\nu = 3$. The last column is the tree-level matching coefficient in SMEFT. Table taken from [175].

$\Delta L = 2$ $\quad (\nu\nu)X + \text{h.c.}$

	Number	SM	Matching
$\%_{\nu\gamma}$	$\frac{1}{2} n_\nu (n_\nu - 1)$	3	0

TABLE D.7: Dimension-five $\Delta L = 2$ Majorana neutrino dipole operators in LEFT. There are also Hermitian conjugate $\Delta L = -2$ operators $\mathcal{O}_{\nu\gamma}^\dagger$, as indicated in the table heading. The second column is the number of operators for an arbitrary number of neutrino flavours n_ν, and the third column is number in the SM LEFT with $n_\nu = 3$. The last column is the tree-level matching coefficient in SMEFT, which vanishes. Table taken from [175].

$(\bar{L}R)X + \text{h.c.}$

	Number	SM	Matching
		Leptonic	
$\%_{e\gamma}$	n_e^2	9	$\frac{1}{\sqrt{2}}\left(-C_{\substack{eW\\pr}}\bar{s} + C_{\substack{eB\\pr}}\bar{c}\right)v_T$
		Nonleptonic	
$\%_{u\gamma}$	n_u^2	4	$\frac{1}{\sqrt{2}}\left(C_{\substack{uW\\pr}}\bar{s} + C_{\substack{uB\\pr}}\bar{c}\right)v_T$
$\%_{d\gamma}$	n_d^2	9	$\frac{1}{\sqrt{2}}\left(-C_{\substack{dW\\pr}}\bar{s} + C_{\substack{dB\\pr}}\bar{c}\right)v_T$
$\%_{uG}$	n_u^2	4	$\frac{1}{\sqrt{2}}C_{\substack{uG\\pr}}v_T$
$\%_{dG}$	n_d^2	9	$\frac{1}{\sqrt{2}}C_{\substack{dG\\pr}}v_T$
Total	$2n_u^2 + 2n_d^2$	26	

TABLE D.8: Dimension-five $(\bar{L}R)X$ dipole operators in LEFT. There are also Hermitian conjugate dipole operators $(\bar{R}L)X$, as indicated in the table heading. The operators are divided into the leptonic and nonleptonic operators. The second column is the number of operators for an arbitrary number of charged lepton flavours n_e, u-type quark flavours n_u, and d-type quark flavours n_d, and the third column is the number in the SM LEFT with $n_e = 3$, $n_u = 2$ and $n_d = 3$. The last column is the tree-level matching coefficient in SMEFT. $\bar{s}$ and $\bar{c}$ are defined in Eq. (D.6). Table taken from [175].

X^3

	Number	SM	Matching
$\%_{G}$	1	1	C_G
$\%_{\widetilde{G}}$	1	1	$C_{\widetilde{G}}$
Total	2	2	

TABLE D.9: Dimension-six triple-gauge-boson operators in LEFT. The tree-level matching coefficient of each operator is equal to the coefficient of the corresponding operator in SMEFT. Table taken from [175].

$(\bar{L}L)(\bar{L}L)$

	Number	SM	Matching
		Leptonic	
$\%_{\nu\nu}^{V,LL}$	$\frac{1}{4}n_\nu^2(n_\nu+1)^2$	36	$C_{\substack{ll\\prst}} - \frac{\bar{g}_Z^2}{4M_Z^2}[Z_\nu]_{pr}[Z_\nu]_{st} - \frac{\bar{g}_Z^2}{4M_Z^2}[Z_\nu]_{pt}[Z_\nu]_{sr}$
$\%_{ee}^{V,LL}$	$\frac{1}{4}n_e^2(n_e+1)^2$	36	$C_{\substack{ll\\prst}} - \frac{\bar{g}_Z^2}{4M_Z^2}[Z_{e_L}]_{pr}[Z_{e_L}]_{st} - \frac{\bar{g}_Z^2}{4M_Z^2}[Z_{e_L}]_{pt}[Z_{e_L}]_{sr}$
$\%_{\nu e}^{V,LL}$	$n_e^2 n_\nu^2$	81	$C_{\substack{ll\\prst}} + C_{\substack{ll\\stpr}} - \frac{\bar{g}_2^2}{2M_W^2}[W_l]_{pt}[W_l]_{rs}^* - \frac{\bar{g}_Z^2}{M_Z^2}[Z_\nu]_{pr}[Z_{e_L}]_{st}$
Total	$n_e^2n_\nu^2 + \frac{1}{4}n_e^2(n_e+1)^2$ $+ \frac{1}{4}n_\nu^2(n_\nu+1)^2$	153	
		Semileptonic	
$\%_{\nu u}^{V,LL}$	$n_\nu^2 n_u^2$	36	$C^{(1)}_{\substack{lq\\prst}} + C^{(3)}_{\substack{lq\\prst}} - \frac{\bar{g}_Z^2}{M_Z^2}[Z_\nu]_{pr}[Z_{u_L}]_{st}$
$\%_{\nu d}^{V,LL}$	$n_\nu^2 n_d^2$	81	$C^{(1)}_{\substack{lq\\prst}} - C^{(3)}_{\substack{lq\\prst}} - \frac{\bar{g}_Z^2}{M_Z^2}[Z_\nu]_{pr}[Z_{d_L}]_{st}$
$\%_{eu}^{V,LL}$	$n_e^2 n_u^2$	36	$C^{(1)}_{\substack{lq\\prst}} - C^{(3)}_{\substack{lq\\prst}} - \frac{\bar{g}_Z^2}{M_Z^2}[Z_{e_L}]_{pr}[Z_{u_L}]_{st}$
$\%_{ed}^{V,LL}$	$n_e^2 n_d^2$	81	$C^{(1)}_{\substack{lq\\prst}} + C^{(3)}_{\substack{lq\\prst}} - \frac{\bar{g}_Z^2}{M_Z^2}[Z_{e_L}]_{pr}[Z_{d_L}]_{st}$
$\%_{\nu edu}^{V,LL}$ + h.c.	$2 \times n_e n_\nu n_u n_d$	2×54	$2C^{(3)}_{\substack{lq\\prst}} - \frac{\bar{g}_2^2}{2M_W^2}[W_l]_{pr}[W_q]_{ts}^*$
Total	$(n_e^2+n_\nu^2)(n_u^2+n_d^2)$ $+ 2n_e n_\nu n_u n_d$	342	
		Nonleptonic	
$\%_{uu}^{V,LL}$	$\frac{1}{2}n_u^2(n_u^2+1)$	10	$C^{(1)}_{\substack{qq\\prst}} + C^{(3)}_{\substack{qq\\prst}} - \frac{\bar{g}_Z^2}{2M_Z^2}[Z_{u_L}]_{pr}[Z_{u_L}]_{st}$
$\%_{dd}^{V,LL}$	$\frac{1}{2}n_d^2(n_d^2+1)$	45	$C^{(1)}_{\substack{qq\\prst}} + C^{(3)}_{\substack{qq\\prst}} - \frac{\bar{g}_Z^2}{2M_Z^2}[Z_{d_L}]_{pr}[Z_{d_L}]_{st}$
$\%_{ud}^{V1,LL}$	$n_u^2 n_d^2$	36	$C^{(1)}_{\substack{qq\\prst}} + C^{(1)}_{\substack{qq\\stpr}} - C^{(3)}_{\substack{qq\\prst}} - C^{(3)}_{\substack{qq\\stpr}} + \frac{2}{N_c}C^{(3)}_{\substack{qq\\ptsr}} + \frac{2}{N_c}C^{(3)}_{\substack{qq\\srpt}}$ $-\frac{\bar{g}_2^2}{2M_W^2}[W_q]_{pt}[W_q]_{rs}^*\frac{1}{N_c} - \frac{\bar{g}_Z^2}{M_Z^2}[Z_{u_L}]_{pr}[Z_{d_L}]_{st}$
$\%_{ud}^{V8,LL}$	$n_u^2 n_d^2$	36	$4C^{(3)}_{\substack{qq\\ptsr}} + 4C^{(3)}_{\substack{qq\\srpt}} - \frac{\bar{g}_2^2}{M_W^2}[W_q]_{pt}[W_q]_{rs}^*$
Total	$2n_u^2n_d^2 + \frac{1}{2}n_u^2(n_u^2+1)$ $+ \frac{1}{2}n_d^2(n_d^2+1)$	127	

TABLE D.10: Dimension-six four-fermion operators: two left-handed currents in LEFT. The $(\bar{L}L)(\bar{L}L)$ operators are divided into leptonic, semileptonic, and nonleptonic operators. The semileptonic operator $\%_{\nu edu}^{V,LL}$ and its Hermitian conjugate $\%_{\nu edu}^{V,LL\dagger}$ are both present. All other operators are Hermitian. The second column is the number of operators for an arbitrary number of neutrino flavours n_ν, charged lepton flavours n_e, u-type quark flavours n_u, and d-type quark flavours n_d, and the third column is the number in the SM LEFT with $n_\nu = 3$, $n_e = 3$, $n_u = 2$, and $n_d = 3$. The last column is the tree-level matching coefficient in SMEFT. Table taken from [175].

$(\bar{R}R)(\bar{R}R)$

	Number	SM	Matching
		Leptonic	
$\%_{ee}^{V,RR}$	$\frac{1}{4}n_e^2(n_e+1)^2$	36	$C_{\substack{ee\\prst}} - \frac{\bar{g}_Z^2}{4M_Z^2}[Z_{e_R}]_{pr}[Z_{e_R}]_{st} - \frac{\bar{g}_Z^2}{4M_Z^2}[Z_{e_R}]_{pt}[Z_{e_R}]_{sr}$
		Semileptonic	
$\%_{eu}^{V,RR}$	$n_e^2 n_u^2$	36	$C_{\substack{eu\\prst}} - \frac{\bar{g}_Z^2}{M_Z^2}[Z_{e_R}]_{pr}[Z_{u_R}]_{st}$
$\%_{ed}^{V,RR}$	$n_e^2 n_d^2$	81	$C_{\substack{ed\\prst}} - \frac{\bar{g}_Z^2}{M_Z^2}[Z_{e_R}]_{pr}[Z_{d_R}]_{st}$
Total	$n_e^2(n_u^2+n_d^2)$	117	
		Nonleptonic	
$\%_{uu}^{V,RR}$	$\frac{1}{2}n_u^2(n_u^2+1)$	10	$C_{\substack{uu\\prst}} - \frac{\bar{g}_Z^2}{2M_Z^2}[Z_{u_R}]_{pr}[Z_{u_R}]_{st}$
$\%_{dd}^{V,RR}$	$\frac{1}{2}n_d^2(n_d^2+1)$	45	$C_{\substack{dd\\prst}} - \frac{\bar{g}_Z^2}{2M_Z^2}[Z_{d_R}]_{pr}[Z_{d_R}]_{st}$
$\%_{ud}^{V1,RR}$	$n_u^2 n_d^2$	36	$C^{(1)}_{\substack{ud\\prst}} - \frac{\bar{g}_2^2}{2M_W^2}[W_R]_{pt}[W_R]^*_{rs}\frac{1}{N_c} - \frac{\bar{g}_Z^2}{M_Z^2}[Z_{u_R}]_{pr}[Z_{d_R}]_{st}$
$\%_{ud}^{V8,RR}$	$n_u^2 n_d^2$	36	$C^{(8)}_{\substack{ud\\prst}} - \frac{\bar{g}_2^2}{M_W^2}[W_R]_{pt}[W_R]^*_{rs}$
Total	$2n_u^2n_d^2 + \frac{1}{2}n_u^2(n_u^2+1)$ $+ \frac{1}{2}n_d^2(n_d^2+1)$	127	

TABLE D.11: Dimension-six four-fermion operators: two right-handed currents in LEFT. The $(\bar{R}R)(\bar{R}R)$ operators are divided into leptonic, semileptonic, and nonleptonic operators. The second column is the number of operators for an arbitrary number of charged lepton flavours n_e, u-type quark flavours n_u, and d-type quark flavours n_d, and the third column is the number in the SM LEFT with $n_e = 3$, $n_u = 2$, and $n_d = 3$. The last column is the tree-level matching coefficient in SMEFT. Table taken from [175].

$(\bar{L}L)(\bar{R}R)$

	Number	SM	Matching
		Leptonic	
$\%_{\nu e}^{V,LR}$	$n_e^2 n_\nu^2$	81	$C_{prst}^{le} - \frac{\bar{g}_Z^2}{M_Z^2}[Z_\nu]_{pr}[Z_{e_R}]_{st}$
$\%_{ee}^{V,LR}$	n_e^4	81	$C_{prst}^{le} - \frac{\bar{g}_Z^2}{M_Z^2}[Z_{e_L}]_{pr}[Z_{e_R}]_{st}$
Total	$n_e^2(n_e^2+n_\nu^2)$	162	
		Semileptonic	
$\%_{\nu u}^{V,LR}$	$n_\nu^2 n_u^2$	36	$C_{prst}^{lu} - \frac{\bar{g}_Z^2}{M_Z^2}[Z_\nu]_{pr}[Z_{u_R}]_{st}$
$\%_{\nu d}^{V,LR}$	$n_\nu^2 n_d^2$	81	$C_{prst}^{ld} - \frac{\bar{g}_Z^2}{M_Z^2}[Z_\nu]_{pr}[Z_{d_R}]_{st}$
$\%_{eu}^{V,LR}$	$n_e^2 n_u^2$	36	$C_{prst}^{lu} - \frac{\bar{g}_Z^2}{M_Z^2}[Z_{e_L}]_{pr}[Z_{u_R}]_{st}$
$\%_{ed}^{V,LR}$	$n_e^2 n_d^2$	81	$C_{prst}^{ld} - \frac{\bar{g}_Z^2}{M_Z^2}[Z_{e_L}]_{pr}[Z_{d_R}]_{st}$
$\%_{ue}^{V,LR}$	$n_e^2 n_u^2$	36	$C_{prst}^{qe} - \frac{\bar{g}_Z^2}{M_Z^2}[Z_{u_L}]_{pr}[Z_{e_R}]_{st}$
$\%_{de}^{V,LR}$	$n_e^2 n_d^2$	81	$C_{prst}^{qe} - \frac{\bar{g}_Z^2}{M_Z^2}[Z_{d_L}]_{pr}[Z_{e_R}]_{st}$
$\%_{\nu edu}^{V,LR}$ + h.c.	$2 \times n_e n_\nu n_u n_d$	2×54	$-\frac{\bar{g}_2^2}{2M_W^2}[W_l]_{pr}[W_R]_{ts}^*$
Total	$(2n_e^2+n_\nu^2)(n_u^2+n_d^2)$ $+ 2n_e n_\nu n_u n_d$	459	
		Nonleptonic	
$\%_{uu}^{V1,LR}$	n_u^4	16	$C_{qu\,prst}^{(1)} - \frac{\bar{g}_Z^2}{M_Z^2}[Z_{u_L}]_{pr}[Z_{u_R}]_{st}$
$\%_{uu}^{V8,LR}$	n_u^4	16	$C_{qu\,prst}^{(8)}$
$\%_{ud}^{V1,LR}$	$n_u^2 n_d^2$	36	$C_{qd\,prst}^{(1)} - \frac{\bar{g}_Z^2}{M_Z^2}[Z_{u_L}]_{pr}[Z_{d_R}]_{st}$
$\%_{ud}^{V8,LR}$	$n_u^2 n_d^2$	36	$C_{qd\,prst}^{(8)}$
$\%_{du}^{V1,LR}$	$n_u^2 n_d^2$	36	$C_{qu\,prst}^{(1)} - \frac{\bar{g}_Z^2}{M_Z^2}[Z_{d_L}]_{pr}[Z_{u_R}]_{st}$
$\%_{du}^{V8,LR}$	$n_u^2 n_d^2$	36	$C_{qu\,prst}^{(8)}$
$\%_{dd}^{V1,LR}$	n_d^4	81	$C_{qd\,prst}^{(1)} - \frac{\bar{g}_Z^2}{M_Z^2}[Z_{d_L}]_{pr}[Z_{d_R}]_{st}$
$\%_{dd}^{V8,LR}$	n_d^4	81	$C_{qd\,prst}^{(8)}$
$\%_{uddu}^{V1,LR}$ + h.c.	$2 \times n_u^2 n_d^2$	2×36	$-\frac{\bar{g}_2^2}{2M_W^2}[W_q]_{pr}[W_R]_{ts}^*$
$\%_{uddu}^{V8,LR}$ + h.c.	$2 \times n_u^2 n_d^2$	2×36	0
Total	$2(n_u^4+n_d^4+4n_u^2n_d^2)$	482	

TABLE D.12: Dimension-six four-fermion operators: left-handed times right-handed currents in LEFT. The $(\bar{L}L)(\bar{R}R)$ operators are divided into leptonic, semileptonic, and nonleptonic operators. Semileptonic operators $\%_{\nu edu}^{V,LR}$ and nonleptonic operators $\%_{uddu}^{V1,LR}$ and $\%_{uddu}^{V8,LR}$ all come with additional Hermitian conjugate operators. All other operators are Hermitian. The second column is the number of operators for an arbitrary number of neutrino flavours n_ν, charged lepton flavours n_e, u-type quark flavours n_u, and d-type quark flavours n_d, and the third column is the number in the SM LEFT with $n_\nu = 3$, $n_e = 3$, $n_u = 2$, and $n_d = 3$. The last column is the tree-level matching coefficient in SMEFT. Table taken from [175].

$(\bar{L}R)(\bar{R}L)$ + h.c.

	Number	SM	Matching
	Semileptonic		
$\%_{eu}^{S,RL}$	$n_e^2 n_u^2$	36	0
$\%_{ed}^{S,RL}$	$n_e^2 n_d^2$	81	$C_{\substack{ledq \\ prst}}$
$\%_{\nu edu}^{S,RL}$	$n_e n_\nu n_u n_d$	54	$C_{\substack{ledq \\ prst}}$
Total	$n_e^2(n_u^2 + n_d^2) + n_e n_\nu n_u n_d$	171	

TABLE D.13: Dimension-six four-fermion operators: $(\bar{L}R)(\bar{R}L)$ scalar bilinears in LEFT. There are also Hermitian conjugate operators, as indicated in the table heading. All of the operators are semileptonic operators. The second column is the number of operators for an arbitrary number of neutrino flavours n_ν, charged lepton flavours n_e, u-type quark flavours n_u, and d-type quark flavours n_d, and the third column is the number in the SM LEFT with $n_\nu = 3$, $n_e = 3$, $n_u = 2$, and $n_d = 3$. The last column is the tree-level matching coefficient in SMEFT. Table taken from [175].

$(\bar{L}R)(\bar{L}R)$ + h.c.

	Number	SM	Matching
	Leptonic		
$\%_{ee}^{S,RR}$	$\frac{1}{2}n_e^2(n_e^2+1)$	45	0
	Semileptonic		
$\%_{eu}^{S,RR}$	$n_e^2 n_u^2$	36	$-C^{(1)}_{lequ\ prst}$
$\%_{eu}^{T,RR}$	$n_e^2 n_u^2$	36	$-C^{(3)}_{lequ\ prst}$
$\%_{ed}^{S,RR}$	$n_e^2 n_d^2$	81	0
$\%_{ed}^{T,RR}$	$n_e^2 n_d^2$	81	0
$\%_{\nu edu}^{S,RR}$	$n_e n_\nu n_u n_d$	54	$C^{(1)}_{lequ\ prst}$
$\%_{\nu edu}^{T,RR}$	$n_e n_\nu n_u n_d$	54	$C^{(3)}_{lequ\ prst}$
Total	$2n_e^2(n_u^2+n_d^2)+2n_e n_\nu n_u n_d$	342	
	Nonleptonic		
$\%_{uu}^{S1,RR}$	$\frac{1}{2}n_u^2(n_u^2+1)$	10	0
$\%_{uu}^{S8,RR}$	$\frac{1}{2}n_u^2(n_u^2+1)$	10	0
$\%_{ud}^{S1,RR}$	$n_u^2 n_d^2$	36	$C^{(1)}_{quqd\ prst}$
$\%_{ud}^{S8,RR}$	$n_u^2 n_d^2$	36	$C^{(8)}_{quqd\ prst}$
$\%_{dd}^{S1,RR}$	$\frac{1}{2}n_d^2(n_d^2+1)$	45	0
$\%_{dd}^{S8,RR}$	$\frac{1}{2}n_d^2(n_d^2+1)$	45	0
$\%_{uddu}^{S1,RR}$	$n_u^2 n_d^2$	36	$-C^{(1)}_{quqd\ stpr}$
$\%_{uddu}^{S8,RR}$	$n_u^2 n_d^2$	36	$-C^{(8)}_{quqd\ stpr}$
Total	$4n_u^2 n_d^2 + n_u^2(n_u^2+1)$ $+ n_d^2(n_d^2+1)$	254	

TABLE D.14: Dimension-six four-fermion operators: $(\bar{L}R)(\bar{L}R)$ scalar and tensor bilinears in LEFT. There are also Hermitian conjugate operators, as indicated in the table heading. The operators are divided into leptonic, semileptonic, and nonleptonic operators. The second column is the number of operators for an arbitrary number of neutrino flavours n_ν, charged lepton flavours n_e, u-type quark flavours n_u, and d-type quark flavours n_d, and the third column is the number in the SM LEFT with $n_\nu = 3$, $n_e = 3$, $n_u = 2$, and $n_d = 3$. The last column is the tree-level matching coefficient in SMEFT. Table taken from [175].

$\Delta L = 4 + \text{h.c.}$			
	Number	SM	Matching
$\%_{\nu\nu}^{S,LL}$	$\frac{1}{12}n_\nu^2(n_\nu^2-1)$	6	0

TABLE D.15: Dimension-six $\Delta L = 4$ operators in LEFT. There are also Hermitian conjugate operators, as indicated in the table heading. The second column is the number of operators for an arbitrary number of neutrino flavours n_ν, and the third column is the number in the SM LEFT with $n_\nu = 3$. The last column is the tree-level matching coefficient in SMEFT. Table taken from [175].

$\Delta L = 2 + \text{h.c.}$			
	Number	SM	Matching
	Leptonic		
$\%_{\nu e}^{S,LL}$	$\frac{1}{2}n_\nu(n_\nu+1)n_e^2$	54	0
$\%_{\nu e}^{T,LL}$	$\frac{1}{2}n_\nu(n_\nu-1)n_e^2$	27	0
$\%_{\nu e}^{S,LR}$	$\frac{1}{2}n_\nu(n_\nu+1)n_e^2$	54	0
Total	$\frac{1}{2}n_\nu(3n_\nu+1)n_e^2$	135	
	Semileptonic		
$\%_{\nu u}^{S,LL}$	$\frac{1}{2}n_\nu(n_\nu+1)n_u^2$	24	0
$\%_{\nu u}^{T,LL}$	$\frac{1}{2}n_\nu(n_\nu-1)n_u^2$	12	0
$\%_{\nu u}^{S,LR}$	$\frac{1}{2}n_\nu(n_\nu+1)n_u^2$	24	0
$\%_{\nu d}^{S,LL}$	$\frac{1}{2}n_\nu(n_\nu+1)n_d^2$	54	0
$\%_{\nu d}^{T,LL}$	$\frac{1}{2}n_\nu(n_\nu-1)n_d^2$	27	0
$\%_{\nu d}^{S,LR}$	$\frac{1}{2}n_\nu(n_\nu+1)n_d^2$	54	0
$\%_{\nu edu}^{S,LL}$	$n_e n_\nu n_u n_d$	54	0
$\%_{\nu edu}^{T,LL}$	$n_e n_\nu n_u n_d$	54	0
$\%_{\nu edu}^{S,LR}$	$n_e n_\nu n_u n_d$	54	0
$\%_{\nu edu}^{V,RL}$	$n_e n_\nu n_u n_d$	54	0
$\%_{\nu edu}^{V,RR}$	$n_e n_\nu n_u n_d$	54	0
Total	$\frac{1}{2}n_\nu(3n_\nu+1)(n_u^2+n_d^2)+5n_e n_\nu n_u n_d$	465	

TABLE D.16: Dimension-six $\Delta L = 2$ operators in LEFT. There are also Hermitian conjugate operators, as indicated in the table heading. The operators are divided into leptonic and semileptonic operators. The second column is the number of operators for an arbitrary number of neutrino flavours n_ν, charged lepton flavours n_e, u-type quark flavours n_u, and d-type quark flavours n_d, and the third column is the number in the SM LEFT with $n_\nu = 3$, $n_e = 3$, $n_u = 2$, and $n_d = 3$. The last column is the tree-level matching coefficient in SMEFT. Table taken from [175].

$\Delta B = \Delta L = 1 + \text{h.c.}$

	Number	SM	Matching
$\%^{S,LL}_{udd}$	$n_\nu n_u n_d^2$	54	$-C_{qqql}_{prst} - C_{qqql}_{rpst}$
$\%^{S,LL}_{duu}$	$n_e n_d n_u^2$	36	$-C_{qqql}_{prst} - C_{qqql}_{rpst}$
$\%^{S,LR}_{uud}$	$\frac{1}{2} n_d n_u (n_u - 1) n_e$	9	0
$\%^{S,LR}_{duu}$	$n_e n_u^2 n_d$	36	$-C_{qque}_{prst} - C_{qque}_{rpst}$
$\%^{S,RL}_{uud}$	$\frac{1}{2} n_d n_u (n_u - 1) n_e$	9	0
$\%^{S,RL}_{duu}$	$n_e n_u^2 n_d$	36	C_{duql}_{prst}
$\%^{S,RL}_{dud}$	$n_\nu n_u n_d^2$	54	$-C_{duql}_{prst}$
$\%^{S,RL}_{ddu}$	$\frac{1}{2} n_d (n_d - 1) n_u n_\nu$	18	0
$\%^{S,RR}_{duu}$	$n_e n_d n_u^2$	36	C_{duue}_{prst}
Total	$\frac{5}{2} n_d^2 n_\nu n_u + 5 n_d n_e n_u^2 - n_d n_e n_u - \frac{1}{2} n_d n_\nu n_u$	288	

TABLE D.17: Dimension-six $\Delta B = \Delta L = 1$ operators in LEFT. There are also Hermitian conjugate $\Delta B = \Delta L = -1$ operators, as indicated in the table heading. The second column is the number of operators for an arbitrary number of neutrino flavours n_ν, charged lepton flavours n_e, u-type quark flavours n_u, and d-type quark flavours n_d, and the third column is the number in the SM LEFT with $n_\nu = 3$, $n_e = 3$, $n_u = 2$, and $n_d = 3$. The last column is the tree-level matching coefficient in SMEFT. Table taken from [175].

$\Delta B = -\Delta L = 1 + \text{h.c.}$

	Number	SM	Matching
$\%^{S,LL}_{ddd}$	$\frac{1}{3} n_d (n_d^2 - 1) n_e$	24	0
$\%^{S,LR}_{udd}$	$n_\nu n_u n_d^2$	54	0
$\%^{S,LR}_{ddu}$	$\frac{1}{2} n_d (n_d - 1) n_u n_\nu$	18	0
$\%^{S,LR}_{ddd}$	$\frac{1}{2} n_d^2 (n_d - 1) n_e$	27	0
$\%^{S,RL}_{ddd}$	$\frac{1}{2} n_d^2 (n_d - 1) n_e$	27	0
$\%^{S,RR}_{udd}$	$n_\nu n_u n_d^2$	54	0
$\%^{S,RR}_{ddd}$	$\frac{1}{3} n_d (n_d^2 - 1) n_e$	24	0
Total	$\frac{5}{3} n_d^3 n_e + \frac{5}{2} n_\nu n_d^2 n_u - n_d^2 n_e - \frac{1}{2} n_d n_\nu n_u - \frac{2}{3} n_d n_e$	228	

TABLE D.18: Dimension-six $\Delta B = -\Delta L = 1$ operators in LEFT. There are also Hermitian conjugate $\Delta B = -\Delta L = -1$ operators, as indicated in the table heading. The second column is the number of operators for an arbitrary number of neutrino flavours n_ν, charged lepton flavours n_e, u-type quark flavours n_u, and d-type quark flavours n_d, and the third column is the number in the SM LEFT with $n_\nu = 3$, $n_e = 3$, $n_u = 2$, and $n_d = 3$. The last column is the tree-level matching coefficient in SMEFT. Table taken from [175].

References

[1] M. Fernández Navarro and S.F. King, *Fermiophobic Z' model for simultaneously explaining the muon anomalies $R_{K^{(*)}}$ and $(g-2)_\mu$*, *Phys. Rev. D* **105** (2022) 035015 [2109.08729]. [Cited on pages xv, 51, 56, 64, 87, 88, 118, and 249.]

[2] M. Fernández Navarro and S.F. King, *B-anomalies in a twin Pati-Salam theory of flavour including the 2022 LHCb $R_{K^{(*)}}$ analysis*, *JHEP* **02** (2023) 188 [2209.00276]. [Cited on pages xv, 51, 56, 58, 70, 72, 83, 121, 123, and 249.]

[3] M. Fernández Navarro and S.F. King, *Tri-hypercharge: a separate gauged weak hypercharge for each fermion family as the origin of flavour*, *JHEP* **08** (2023) 020 [2305.07690]. [Cited on pages xv, 45, 51, 74, 134, 185, 220, 222, 231, and 249.]

[4] M. Bordone and M. Fernández Navarro, *τ_{B_s}/τ_{B_d} and $\Delta\Gamma_s$ confront new physics in $b \to s\tau\tau$*, *Eur. Phys. J. C* **83** (2023) 842 [2307.07013]. [Cited on pages xv, 68, 72, 168, and 180.]

[5] M. Fernández Navarro, S.F. King and A. Vicente, *Tri-unification: a separate $SU(5)$ for each fermion family*, 2311.05683. [Cited on pages xv, 45, 51, and 219.]

[6] M. Fernández Navarro, *Flavour hierarchies and B-anomalies in a twin Pati-Salam theory of flavour*, in *8th Symposium on Prospects in the Physics of Discrete Symmetries*, 2, 2023 [2302.10829]. [Cited on pages xv, 121, and 123.]

[7] M. Fernández Navarro, *Twin Pati-Salam theory of flavour for a new picture of B-anomalies*, in *57th Rencontres de Moriond on Electroweak Interactions and Unified Theories*, 5, 2023 [2305.19356]. [Cited on pages xv, 121, and 123.]

[8] S. Weinberg, *The Cosmological Constant Problem*, *Rev. Mod. Phys.* **61** (1989) 1. [Cited on pages 1, 17, and 32.]

[9] P. Langacker, *The Standard Model and Beyond*, Series in High Energy Physics, Cosmology and Gravitation, CRC Press (2009). [Cited on page 5.]

[10] A. Vicente, *The Standard Model of particle physics and beyond*, ISAPP 2016 "Physics and astrophysics of cosmic rays in space". [Cited on page 5.]

[11] J.I. Illana and A. Jimenez Cano, *Quantum field theory and the structure of the Standard Model*, *PoS* **CORFU2021** (2022) 314 [2211.14636]. [Cited on page 5.]

[12] A. Pich, *The Standard Model of Electroweak Interactions*, in *2010 European School of High Energy Physics*, 1, 2012 [1201.0537]. [Cited on page 5.]

[13] D.J. Gross and F. Wilczek, *Ultraviolet Behavior of Nonabelian Gauge Theories*, *Phys. Rev. Lett.* **30** (1973) 1343. [Cited on pages 10 and 46.]

[14] H.D. Politzer, *Reliable Perturbative Results for Strong Interactions?*, *Phys. Rev. Lett.* **30** (1973) 1346. [Cited on page 10.]

[15] S.R. Coleman and D.J. Gross, *Price of asymptotic freedom*, *Phys. Rev. Lett.* **31** (1973) 851. [Cited on page 10.]

[16] H. Fritzsch, M. Gell-Mann and H. Leutwyler, *Advantages of the Color Octet Gluon Picture*, *Phys. Lett. B* **47** (1973) 365. [Cited on page 10.]

[17] H.D. Politzer, *Asymptotic Freedom: An Approach to Strong Interactions*, *Phys. Rept.* **14** (1974) 129. [Cited on page 10.]

[18] G. Altarelli and J. Wells, *Qcd: The theory of strong interactions*, in *Collider Physics within the Standard Model: A Primer*, (Cham), pp. 27–96, Springer International Publishing (2017), DOI. [Cited on page 10.]

[19] L.D. Faddeev and V.N. Popov, *Feynman Diagrams for the Yang-Mills Field*, *Phys. Lett. B* **25** (1967) 29. [Cited on page 10.]

[20] M. Peskin and D. Schroeder, *An Introduction To Quantum Field Theory*, Frontiers in Physics, Avalon Publishing (1995). [Cited on page 11.]

[21] Particle Data Group collaboration, *Review of Particle Physics*, *PTEP* **2022** (2022) 083C01. [Cited on pages 11, 16, 17, 21, 22, 23, 24, 25, 26, 35, 46, 74, 75, 76, 78, 94, 132, and 212.]

[22] P.W. Higgs, *Broken Symmetries and the Masses of Gauge Bosons*, *Phys. Rev. Lett.* **13** (1964) 508. [Cited on page 11.]

[23] F. Englert and R. Brout, *Broken Symmetry and the Mass of Gauge Vector Mesons*, *Phys. Rev. Lett.* **13** (1964) 321. [Cited on page 11.]

[24] A. Salam and J.C. Ward, *Electromagnetic and weak interactions*, *Phys. Lett.* **13** (1964) 168. [Cited on page 11.]

[25] S. Weinberg, *A Model of Leptons*, *Phys. Rev. Lett.* **19** (1967) 1264. [Cited on page 11.]

[26] A. Salam, *Weak and Electromagnetic Interactions*, *Conf. Proc. C* **680519** (1968) 367. [Cited on page 11.]

[27] S.L. Glashow, *Partial Symmetries of Weak Interactions*, *Nucl. Phys.* **22** (1961) 579. [Cited on pages 11 and 15.]

[28] J. Ellis, M.K. Gaillard and D.V. Nanopoulos, *A Historical Profile of the Higgs Boson*, in *The standard theory of particle physics: Essays to celebrate CERN's 60th anniversary*, L. Maiani and L. Rolandi, eds., pp. 255–274 (2016), DOI [1504.07217]. [Cited on page 13.]

[29] J. Goldstone, *Field Theories with Superconductor Solutions*, *Nuovo Cim.* **19** (1961) 154. [Cited on page 16.]

[30] ATLAS collaboration, *Observation of a new particle in the search for the Standard Model Higgs boson with the ATLAS detector at the LHC*, *Phys. Lett. B* **716** (2012) 1 [1207.7214]. [Cited on page 17.]

[31] CMS collaboration, *Observation of a New Boson at a Mass of 125 GeV with the CMS Experiment at the LHC*, *Phys. Lett. B* **716** (2012) 30 [1207.7235]. [Cited on page 17.]

[32] ATLAS, CMS collaboration, *Higgs Physics at HL-LHC*, in *30th International Workshop on Deep-Inelastic Scattering and Related Subjects*, 7, 2023 [2307.07772]. [Cited on page 17.]

[33] G. Durieux, G. Durieux, M. McCullough, M. McCullough, E. Salvioni and E. Salvioni, *Charting the Higgs self-coupling boundaries*, *JHEP* **12** (2022) 148 [2209.00666]. [Cited on page 17.]

[34] R.J. Adler, B. Casey and O.C. Jacob, *Vacuum catastrophe: An Elementary exposition of the cosmological constant problem*, *Am. J. Phys.* **63** (1995) 620. [Cited on pages 17 and 32.]

[35] J. Sola, *Cosmological constant and vacuum energy: old and new ideas*, *J. Phys. Conf. Ser.* **453** (2013) 012015 [1306.1527]. [Cited on pages 17 and 32.]

[36] D. Haidt, *The Discovery of Weak Neutral Currents*, *Adv. Ser. Direct. High Energy Phys.* **23** (2015) 165. [Cited on page 20.]

[37] N. Cabibbo, *Unitary Symmetry and Leptonic Decays*, *Phys. Rev. Lett.* **10** (1963) 531. [Cited on pages 21 and 24.]

[38] M. Kobayashi and T. Maskawa, *CP Violation in the Renormalizable Theory of Weak Interaction*, *Prog. Theor. Phys.* **49** (1973) 652. [Cited on pages 21 and 46.]

[39] B. Grzadkowski, M. Iskrzynski, M. Misiak and J. Rosiek, *Dimension-Six Terms in the Standard Model Lagrangian*, *JHEP* **10** (2010) 085 [1008.4884]. [Cited on pages 21, 54, and 263.]

[40] L.-L. Chau and W.-Y. Keung, *Comments on the Parametrization of the Kobayashi-Maskawa Matrix*, *Phys. Rev. Lett.* **53** (1984) 1802. [Cited on page 23.]

[41] J.H. Christenson, J.W. Cronin, V.L. Fitch and R. Turlay, *Evidence for the* 2π *Decay of the* K_2^0 *Meson*, *Phys. Rev. Lett.* **13** (1964) 138. [Cited on page 24.]

[42] BaBar collaboration, *Observation of CP violation in the* B^0 *meson system*, *Phys. Rev. Lett.* **87** (2001) 091801 [hep-ex/0107013]. [Cited on page 24.]

[43] LHCb collaboration, *Observation of CP Violation in Charm Decays*, *Phys. Rev. Lett.* **122** (2019) 211803 [1903.08726]. [Cited on page 24.]

[44] C. Jarlskog, *Commutator of the Quark Mass Matrices in the Standard Electroweak Model and a Measure of Maximal CP Nonconservation*, *Phys. Rev. Lett.* **55** (1985) 1039. [Cited on page 24.]

[45] A.J. Buras, *Standard Model predictions for rare K and B decays without new physics infection*, *Eur. Phys. J. C* **83** (2023) 66 [2209.03968]. [Cited on page 25.]

[46] L. Del Debbio and A. Ramos, *Lattice determinations of the strong coupling*, 2101.04762. [Cited on page 25.]

[47] D. Buttazzo, G. Degrassi, P.P. Giardino, G.F. Giudice, F. Sala, A. Salvio et al., *Investigating the near-criticality of the Higgs boson*, *JHEP* **12** (2013) 089 [1307.3536]. [Cited on page 25.]

[48] P. Fileviez Perez, *Fermion mixings versus* $d = 6$ *proton decay*, *Phys. Lett. B* **595** (2004) 476 [hep-ph/0403286]. [Cited on pages 25 and 81.]

[49] M. Shifman and A. Vainshtein, *(In)dependence of* Θ *in the Higgs regime without axions*, *Mod. Phys. Lett. A* **32** (2017) 1750084 [1701.00467]. [Cited on pages 25 and 26.]

[50] P. Fileviez Perez and H.H. Patel, *The Electroweak Vacuum Angle*, *Phys. Lett. B* **732** (2014) 241 [1402.6340]. [Cited on page 26.]

[51] J. Dragos, T. Luu, A. Shindler, J. de Vries and A. Yousif, *Confirming the Existence of the strong CP Problem in Lattice QCD with the Gradient Flow*, *Phys. Rev. C* **103** (2021) 015202 [1902.03254]. [Cited on pages 26 and 33.]

[52] Super-Kamiokande collaboration, *Evidence for oscillation of atmospheric neutrinos*, *Phys. Rev. Lett.* **81** (1998) 1562 [hep-ex/9807003]. [Cited on page 26.]

[53] Super-Kamiokande, Kamiokande collaboration, *Atmospheric neutrino results from Super-Kamiokande and Kamiokande: Evidence for neutrino(mu) oscillations*, *Nucl. Phys. B Proc. Suppl.* **77** (1999) 123 [hep-ex/9810001]. [Cited on page 26.]

[54] T. Kajita, *Discovery of neutrino oscillations*, *Rept. Prog. Phys.* **69** (2006) 1607. [Cited on page 26.]

[55] SNO collaboration, *Direct evidence for neutrino flavor transformation from neutral current interactions in the Sudbury Neutrino Observatory*, *Phys. Rev. Lett.* **89** (2002) 011301 [nucl-ex/0204008]. [Cited on page 26.]

[56] B.J.P. Jones, *The Physics of Neutrinoless Double Beta Decay: A Primer*, in *Theoretical Advanced Study Institute in Elementary Particle Physics: The Obscure Universe: Neutrinos and Other Dark Matters*, 8, 2021 [2108.09364]. [Cited on page 28.]

[57] P. Minkowski, $\mu \to e\gamma$ *at a Rate of One Out of* 10^9 *Muon Decays?*, *Phys. Lett. B* **67** (1977) 421. [Cited on page 28.]

[58] R.N. Mohapatra and J.W.F. Valle, *Neutrino Mass and Baryon Number Nonconservation in Superstring Models*, *Phys. Rev. D* **34** (1986) 1642. [Cited on page 28.]

[59] J. Schechter and J.W.F. Valle, *Neutrino Masses in SU(2) x U(1) Theories*, *Phys. Rev. D* **22** (1980) 2227. [Cited on page 28.]

[60] R. Foot, H. Lew, X.G. He and G.C. Joshi, *Seesaw Neutrino Masses Induced by a Triplet of Leptons*, *Z. Phys. C* **44** (1989) 441. [Cited on page 28.]

[61] S. Weinberg, *Baryon and Lepton Nonconserving Processes*, *Phys. Rev. Lett.* **43** (1979) 1566. [Cited on page 28.]

[62] M.C. Gonzalez-Garcia, M. Maltoni and T. Schwetz, *NuFIT: Three-Flavour Global Analyses of Neutrino Oscillation Experiments*, *Universe* **7** (2021) 459 [2111.03086]. [Cited on pages 30, 100, 201, and 233.]

[63] E.K. Akhmedov, *Do charged leptons oscillate?*, *JHEP* **09** (2007) 116 [0706.1216]. [Cited on page 29.]

[64] E. Akhmedov, *Quantum mechanics aspects and subtleties of neutrino oscillations*, in *International Conference on History of the Neutrino: 1930-2018*, 1, 2019 [1901.05232]. [Cited on page 30.]

[65] P.F. de Salas, D.V. Forero, S. Gariazzo, P. Martínez-Miravé, O. Mena, C.A. Ternes et al., *2020 global reassessment of the neutrino oscillation picture*, *JHEP* **02** (2021) 071 [2006.11237]. [Cited on pages 30, 100, 201, and 233.]

[66] Planck collaboration, *Planck 2018 results. VI. Cosmological parameters*, *Astron. Astrophys.* **641** (2020) A6 [1807.06209]. [Cited on page 32.]

[67] D.V. Nanopoulos and S. Weinberg, *Mechanisms for Cosmological Baryon Production*, *Phys. Rev. D* **20** (1979) 2484. [Cited on page 32.]

[68] G. 't Hooft, *Naturalness, chiral symmetry, and spontaneous chiral symmetry breaking*, *NATO Sci. Ser. B* **59** (1980) 135. [Cited on pages 33 and 247.]

[69] S. Klett, M. Lindner and A. Trautner, *Generating the electro-weak scale by vector-like quark condensation*, *SciPost Phys.* **14** (2023) 076 [2205.15323]. [Cited on page 33.]

[70] F. Vissani, *Do experiments suggest a hierarchy problem?*, *Phys. Rev. D* **57** (1998) 7027 [hep-ph/9709409]. [Cited on page 33.]

[71] J.D. Clarke, R. Foot and R.R. Volkas, *Electroweak naturalness in the three-flavor type I seesaw model and implications for leptogenesis*, *Phys. Rev. D* **91** (2015) 073009 [1502.01352]. [Cited on page 33.]

[72] S.P. Martin, *A Supersymmetry primer*, *Adv. Ser. Direct. High Energy Phys.* **18** (1998) 1 [hep-ph/9709356]. [Cited on pages 33, 36, and 254.]

[73] H.E. Haber and L. Stephenson Haskins, *Supersymmetric Theory and Models*, in *Proceedings TASI 2016: Boulder, CO, USA, June 6-July 1, 2016*, pp. 355–499, WSP, 2018, DOI [1712.05926]. [Cited on page 33.]

[74] C. Csáki, S. Lombardo and O. Telem, *TASI Lectures on Non-supersymmetric BSM Models*, in *Proceedings TASI 2016: Boulder, CO, USA, June 6-July 1, 2016*, pp. 501–570, WSP (2018), DOI [1811.04279]. [Cited on page 33.]

[75] L. Di Luzio, M. Giannotti, E. Nardi and L. Visinelli, *The landscape of QCD axion models*, *Phys. Rept.* **870** (2020) 1 [2003.01100]. [Cited on page 34.]

[76] C.B. Adams et al., *Axion Dark Matter*, in *Snowmass 2021*, 3, 2022 [2203.14923]. [Cited on page 34.]

[77] A. Crivellin, *Anomalies in Particle Physics*, in *8th Symposium on Prospects in the Physics of Discrete Symmetries*, 4, 2023 [2304.01694]. [Cited on page 34.]

[78] Muon g-2 collaboration, *Measurement of the Positive Muon Anomalous Magnetic Moment to 0.46 ppm*, *Phys. Rev. Lett.* **126** (2021) 141801 [2104.03281]. [Cited on pages 35, 51, 62, and 85.]

[79] Muon g-2 collaboration, *Measurement of the Positive Muon Anomalous Magnetic Moment to 0.20 ppm*, 2308.06230. [Cited on pages 35, 51, 62, and 94.]

[80] Heavy Flavor Averaging Group, HFLAV collaboration, *Averages of b-hadron, c-hadron, and τ-lepton properties as of 2021*, *Phys. Rev. D* **107** (2023) 052008 [2206.07501]. [Cited on pages 35, 59, 60, 65, 69, 80, 155, 167, and 215.]

[81] Belle II collaboration, "Recent Belle II results on radiative and electroweak penguin decays." EPS-HEP 2023 conference. [Cited on pages 35, 73, 112, 155, 170, and 251.]

[82] M. Algueró, A. Biswas, B. Capdevila, S. Descotes-Genon, J. Matias and M. Novoa-Brunet, *To (b)e or not to (b)e: no electrons at LHCb*, *Eur. Phys. J. C* **83** (2023) 648 [2304.07330]. [Cited on pages 35, 59, 82, 83, 123, 159, 183, 213, and 215.]

[83] CDF collaboration, *High-precision measurement of the W boson mass with the CDF II detector*, *Science* **376** (2022) 170. [Cited on pages 35 and 212.]

[84] V. Cirigliano, A. Crivellin, M. Hoferichter and M. Moulson, *Scrutinizing CKM unitarity with a new measurement of the Kμ3/Kμ2 branching fraction*, *Phys. Lett. B* **838** (2023) 137748 [2208.11707]. [Cited on page 35.]

[85] CMS collaboration, *Search for a standard model-like Higgs boson in the mass range between 70 and 110* GeV *in the diphoton final state in proton-proton collisions at* $\sqrt{s} = 13$ TeV, . [Cited on page 35.]

[86] ATLAS collaboration, *Search for diphoton resonances in the 66 to 110 GeV mass range using 140* fb^{-1} *of 13 TeV pp collisions collected with the ATLAS detector*, . [Cited on page 35.]

[87] ATLAS collaboration, *Search for dark matter in events with missing transverse momentum and a Higgs boson decaying into two photons in pp collisions at* $\sqrt{s}$ *= 13 TeV with the ATLAS detector*, *JHEP* **10** (2021) 013 [2104.13240]. [Cited on page 35.]

[88] ATLAS collaboration, *Search for resonances decaying into photon pairs in 139* fb^{-1} *of pp collisions at* $\sqrt{s}$*=13 TeV with the ATLAS detector*, *Phys. Lett. B* **822** (2021) 136651 [2102.13405]. [Cited on page 35.]

[89] ALEPH, DELPHI, L3, OPAL, SLD, LEP Electroweak Working Group, SLD Electroweak Group, SLD Heavy Flavour Group collaboration, *Precision electroweak measurements on the Z resonance*, *Phys. Rept.* **427** (2006) 257 [hep-ex/0509008]. [Cited on pages 35, 97, and 212.]

[90] D.H. Weinberg, M.J. Mortonson, D.J. Eisenstein, C. Hirata, A.G. Riess and E. Rozo, *Observational Probes of Cosmic Acceleration*, *Phys. Rept.* **530** (2013) 87 [1201.2434]. [Cited on page 35.]

[91] E. Di Valentino, O. Mena, S. Pan, L. Visinelli, W. Yang, A. Melchiorri et al., *In the realm of the Hubble tension—a review of solutions*, *Class. Quant. Grav.* **38** (2021) 153001 [2103.01183]. [Cited on page 35.]

[92] U. Amaldi, W. de Boer and H. Furstenau, *Comparison of grand unified theories with electroweak and strong coupling constants measured at LEP*, *Phys. Lett. B* **260** (1991) 447. [Cited on page 36.]

[93] H. Georgi and S.L. Glashow, *Unity of All Elementary Particle Forces*, *Phys. Rev. Lett.* **32** (1974) 438. [Cited on pages 36 and 220.]

[94] H. Georgi and C. Jarlskog, *A New Lepton - Quark Mass Relation in a Unified Theory*, *Phys. Lett. B* **86** (1979) 297. [Cited on pages 38, 226, and 227.]

[95] Super-Kamiokande collaboration, *Search for proton decay via $p \to e^+\pi^0$ and $p \to \mu^+\pi^0$ in 0.31 megaton · years exposure of the Super-Kamiokande water Cherenkov detector*, *Phys. Rev. D* **95** (2017) 012004 [1610.03597]. [Cited on pages 38 and 40.]

[96] H. Fritzsch and P. Minkowski, *Unified Interactions of Leptons and Hadrons*, *Annals Phys.* **93** (1975) 193. [Cited on page 38.]

[97] H. Georgi, *The State of the Art—Gauge Theories*, *AIP Conf. Proc.* **23** (1975) 575. [Cited on page 38.]

[98] R.M. Fonseca, *On the chirality of the SM and the fermion content of GUTs*, *Nucl. Phys. B* **897** (2015) 757 [1504.03695]. [Cited on page 38.]

[99] B.C. Allanach, B. Gripaios and J. Tooby-Smith, *Semisimple extensions of the Standard Model gauge algebra*, *Phys. Rev. D* **104** (2021) 035035 [2104.14555]. [Cited on page 38.]

[100] J.C. Pati and A. Salam, *Lepton Number as the Fourth Color*, *Phys. Rev. D* **10** (1974) 275. [Cited on pages 38, 70, 78, 121, and 124.]

[101] N.S. Manton, *Topology in the Weinberg-Salam Theory*, *Phys. Rev. D* **28** (1983) 2019. [Cited on page 40.]

[102] R. Foot, *New Physics From Electric Charge Quantization?*, *Mod. Phys. Lett. A* **6** (1991) 527. [Cited on page 41.]

[103] T. Araki, J. Heeck and J. Kubo, *Vanishing Minors in the Neutrino Mass Matrix from Abelian Gauge Symmetries*, *JHEP* **07** (2012) 083 [1203.4951]. [Cited on page 41.]

[104] S.L. Glashow, J. Iliopoulos and L. Maiani, *Weak Interactions with Lepton-Hadron Symmetry*, *Phys. Rev. D* **2** (1970) 1285. [Cited on page 41.]

[105] G. D'Ambrosio, G.F. Giudice, G. Isidori and A. Strumia, *Minimal flavor violation: An Effective field theory approach*, *Nucl. Phys. B* **645** (2002) 155 [hep-ph/0207036]. [Cited on page 42.]

[106] R.K. Ellis et al., *Physics Briefing Book: Input for the European Strategy for Particle Physics Update 2020*, 1910.11775. [Cited on page 42.]

[107] V. Cirigliano, B. Grinstein, G. Isidori and M.B. Wise, *Minimal flavor violation in the lepton sector*, *Nucl. Phys. B* **728** (2005) 121 [hep-ph/0507001]. [Cited on page 43.]

[108] CMS collaboration, CMS EXO Summary Plots. [Cited on page 44.]

[109] K. Agashe, M. Papucci, G. Perez and D. Pirjol, *Next to minimal flavor violation*, hep-ph/0509117. [Cited on page 44.]

[110] R. Barbieri, G. Isidori, J. Jones-Perez, P. Lodone and D.M. Straub, *$U(2)$ and Minimal Flavour Violation in Supersymmetry*, *Eur. Phys. J. C* **71** (2011) 1725 [1105.2296]. [Cited on pages 44, 186, and 222.]

[111] G. Isidori and D.M. Straub, *Minimal Flavour Violation and Beyond*, *Eur. Phys. J. C* **72** (2012) 2103 [1202.0464]. [Cited on page 44.]

[112] R. Barbieri, D. Buttazzo, F. Sala and D.M. Straub, *Flavour physics from an approximate $U(2)^3$ symmetry*, *JHEP* **07** (2012) 181 [1203.4218]. [Cited on page 44.]

[113] N. Craig, D. Green and A. Katz, *(De)Constructing a Natural and Flavorful Supersymmetric Standard Model*, *JHEP* **07** (2011) 045 [1103.3708]. [Cited on pages 45, 51, and 186.]

[114] G. Panico and A. Pomarol, *Flavor hierarchies from dynamical scales*, *JHEP* **07** (2016) 097 [1603.06609]. [Cited on pages 45, 51, 134, and 186.]

[115] M. Bordone, C. Cornella, J. Fuentes-Martin and G. Isidori, *A three-site gauge model for flavor hierarchies and flavor anomalies*, *Phys. Lett. B* **779** (2018) 317 [1712.01368]. [Cited on pages 45, 51, 70, 72, 122, 123, 127, 134, 138, 152, 155, 157, 167, 170, 179, 186, 220, and 222.]

[116] L. Allwicher, G. Isidori and A.E. Thomsen, *Stability of the Higgs Sector in a Flavor-Inspired Multi-Scale Model*, *JHEP* **01** (2021) 191 [2011.01946]. [Cited on pages 45, 51, 70, 72, 123, 134, 138, 152, 186, 220, and 222.]

[117] J. Fuentes-Martin, G. Isidori, J. Pagès and B.A. Stefanek, *Flavor non-universal Pati-Salam unification and neutrino masses*, *Phys. Lett. B* **820** (2021) 136484 [2012.10492]. [Cited on pages 45, 51, 70, 72, 122, 123, 134, 138, 152, 186, 220, 222, and 231.]

[118] R. Barbieri, *A View of Flavour Physics in 2021*, *Acta Phys. Polon. B* **52** (2021) 789 [2103.15635]. [Cited on pages 45, 51, 134, and 186.]

[119] J. Fuentes-Martin, G. Isidori, J.M. Lizana, N. Selimovic and B.A. Stefanek, *Flavor hierarchies, flavor anomalies, and Higgs mass from a warped extra dimension*, *Phys. Lett. B* **834** (2022) 137382 [2203.01952]. [Cited on pages 45, 51, 70, 72, 122, 123, 134, 138, 152, 186, 220, and 222.]

[120] J. Davighi, G. Isidori and M. Pesut, *Electroweak-flavour and quark-lepton unification: a family non-universal path*, *JHEP* **04** (2023) 030 [2212.06163]. [Cited on pages 45, 51, 70, 72, 122, 123, 134, 138, 152, 186, 220, and 222.]

[121] J. Davighi and J. Tooby-Smith, *Electroweak flavour unification*, *JHEP* **09** (2022) 193 [2201.07245]. [Cited on pages 45, 51, 134, 186, 220, and 222.]

[122] J. Davighi and G. Isidori, *Non-universal gauge interactions addressing the inescapable link between Higgs and flavour*, *JHEP* **07** (2023) 147 [2303.01520]. [Cited on pages 45, 51, 187, 220, and 222.]

[123] J. Davighi and B.A. Stefanek, *Deconstructed Hypercharge: A Natural Model of Flavour*, 2305.16280. [Cited on pages 45 and 51.]

[124] C.-W. Chiang, N.G. Deshpande, X.-G. He and J. Jiang, *The Family $SU(2)_l$ x $SU(2)_h$ x $U(1)$ Model*, *Phys. Rev. D* **81** (2010) 015006 [0911.1480]. [Cited on pages 45, 51, 220, and 222.]

[125] J. Davighi, A. Gosnay, D.J. Miller and S. Renner, *Phenomenology of a Deconstructed Electroweak Force*, 2312.13346. [Cited on pages 45, 51, 220, and 222.]

[126] B. Capdevila, A. Crivellin, J.M. Lizana and S. Pokorski, *$SU(2)_L$ deconstruction and flavour (non)-universality*, 2401.00848. [Cited on pages 45, 51, 220, and 222.]

[127] J. Fuentes-Martín and J.M. Lizana, *Deconstructing flavor anomalously*, 2402.09507. [Cited on pages 45 and 51.]

[128] N. Arkani-Hamed and M. Schmaltz, *Hierarchies without symmetries from extra dimensions*, *Phys. Rev. D* **61** (2000) 033005 [hep-ph/9903417]. [Cited on page 48.]

[129] G.R. Dvali and M.A. Shifman, *Families as neighbors in extra dimension*, *Phys. Lett. B* **475** (2000) 295 [hep-ph/0001072]. [Cited on page 48.]

[130] F. Feruglio, *Pieces of the Flavour Puzzle*, *Eur. Phys. J. C* **75** (2015) 373 [1503.04071]. [Cited on page 48.]

[131] M. Leurer, Y. Nir and N. Seiberg, *Mass matrix models*, *Nucl. Phys. B* **398** (1993) 319 [hep-ph/9212278]. [Cited on page 48.]

[132] M. Leurer, Y. Nir and N. Seiberg, *Mass matrix models: The Sequel*, *Nucl. Phys. B* **420** (1994) 468 [hep-ph/9310320]. [Cited on page 48.]

[133] C.D. Froggatt and H.B. Nielsen, *Hierarchy of Quark Masses, Cabibbo Angles and CP Violation*, *Nucl. Phys. B* **147** (1979) 277. [Cited on page 48.]

[134] M. Gupta and G. Ahuja, *Flavor mixings and textures of the fermion mass matrices*, *Int. J. Mod. Phys. A* **27** (2012) 1230033 [1302.4823]. [Cited on page 50.]

[135] P.O. Ludl and W. Grimus, *A complete survey of texture zeros in the lepton mass matrices*, *JHEP* **07** (2014) 090 [1406.3546]. [Cited on page 50.]

[136] M. Gupta, P. Fakay, S. Sharma and G. Ahuja, *Fermion mass matrices, textures and beyond*, *Mod. Phys. Lett. A* **30** (2015) 1530024 [1604.03335]. [Cited on page 50.]

[137] W. Altmannshofer and J. Zupan, *Snowmass White Paper: Flavor Model Building*, in *Snowmass 2021*, 3, 2022 [2203.07726]. [Cited on page 50.]

[138] C. Cornella, D. Curtin, E.T. Neil and J.O. Thompson, *Mapping and Probing Froggatt-Nielsen Solutions to the Quark Flavor Puzzle*, 2306.08026. [Cited on page 50.]

[139] R. Barbieri, L.J. Hall, S. Raby and A. Romanino, *Unified theories with U(2) flavor symmetry*, *Nucl. Phys. B* **493** (1997) 3 [hep-ph/9610449]. [Cited on page 50.]

[140] S.F. King and G.G. Ross, *Fermion masses and mixing angles from SU (3) family symmetry and unification*, *Phys. Lett. B* **574** (2003) 239 [hep-ph/0307190]. [Cited on page 50.]

[141] S.F. King, *Predicting neutrino parameters from SO(3) family symmetry and quark-lepton unification*, *JHEP* **08** (2005) 105 [hep-ph/0506297]. [Cited on page 50.]

[142] M. Dimou, S.F. King and C. Luhn, *Approaching Minimal Flavour Violation from an $SU(5) \times S_4 \times U(1)$ SUSY GUT*, *JHEP* **02** (2016) 118 [1511.07886]. [Cited on page 50.]

[143] A.S. Belyaev, S.F. King and P.B. Schaefers, *Muon g-2 and dark matter suggest nonuniversal gaugino masses: $\mathbf{SU(5)} \times \mathbf{A_4}$ case study at the LHC*, *Phys. Rev. D* **97** (2018) 115002 [1801.00514]. [Cited on page 50.]

[144] J. Bernigaud, B. Herrmann, S.F. King and S.J. Rowley, *Non-minimal flavour violation in $A_4\times$ SU(5) SUSY GUTs with smuon assisted dark matter*, *JHEP* **03** (2019) 067 [1812.07463]. [Cited on page 50.]

[145] A. Ekstedt, R.M. Fonseca and M. Malinský, *Flavorgenesis in an SU(19) model*, *Phys. Lett. B* **816** (2021) 136212 [2009.03909]. [Cited on page 50.]

[146] R.M. Fonseca, *Explaining the SM flavor structure with grand unified theories*, *PoS* **ICHEP2020** (2021) 241 [2012.08410]. [Cited on page 50.]

[147] B. Fu, S.F. King, L. Marsili, S. Pascoli, J. Turner and Y.-L. Zhou, *A predictive and testable unified theory of fermion masses, mixing and leptogenesis*, *JHEP* **11** (2022) 072 [2209.00021]. [Cited on page 50.]

[148] G. Altarelli and F. Feruglio, *Tri-bimaximal neutrino mixing, A(4) and the modular symmetry*, *Nucl. Phys. B* **741** (2006) 215 [hep-ph/0512103]. [Cited on page 51.]

[149] R. de Adelhart Toorop, F. Feruglio and C. Hagedorn, *Finite Modular Groups and Lepton Mixing*, *Nucl. Phys. B* **858** (2012) 437 [1112.1340]. [Cited on page 51.]

[150] F. Feruglio, *Are neutrino masses modular forms?*, 1706.08749. [Cited on page 51.]

[151] I. de Medeiros Varzielas, S.F. King and Y.-L. Zhou, *Multiple modular symmetries as the origin of flavor*, *Phys. Rev. D* **101** (2020) 055033 [1906.02208]. [Cited on page 51.]

[152] S.J.D. King and S.F. King, *Fermion mass hierarchies from modular symmetry*, *JHEP* **09** (2020) 043 [2002.00969]. [Cited on page 51.]

[153] T. Kobayashi and M. Tanimoto, *Modular flavor symmetric models*, 2307.03384. [Cited on page 51.]

[154] F.J. de Anda, S.F. King and E. Perdomo, *$SU(5)$ grand unified theory with A_4 modular symmetry*, *Phys. Rev. D* **101** (2020) 015028 [1812.05620]. [Cited on page 51.]

[155] G.-J. Ding, S.F. King and C.-Y. Yao, *Modular $S_4 \times SU(5)$ GUT*, 2103.16311. [Cited on page 51.]

[156] S.F. King and Y.-L. Zhou, *Twin modular S_4 with SU(5) GUT*, *JHEP* **04** (2021) 291 [2103.02633]. [Cited on page 51.]

[157] P. Chen, G.-J. Ding and S.F. King, *SU(5) GUTs with A_4 modular symmetry*, *JHEP* **04** (2021) 239 [2101.12724]. [Cited on page 51.]

[158] G.-J. Ding, S.F. King and J.-N. Lu, *SO(10) models with A_4 modular symmetry*, *JHEP* **11** (2021) 007 [2108.09655]. [Cited on page 51.]

[159] BaBar collaboration, *Evidence for an excess of $\bar{B} \to D^{(*)}\tau^-\bar{\nu}_\tau$ decays*, *Phys. Rev. Lett.* **109** (2012) 101802 [1205.5442]. [Cited on pages 51 and 60.]

[160] I. de Medeiros Varzielas and G. Hiller, *Clues for flavor from rare lepton and quark decays*, *JHEP* **06** (2015) 072 [1503.01084]. [Cited on page 51.]

[161] G. Hiller and I. Nisandzic, *R_K and R_{K^*} beyond the standard model*, *Phys. Rev. D* **96** (2017) 035003 [1704.05444]. [Cited on page 51.]

[162] S.F. King, *Flavourful Z' models for $R_{K^{(*)}}$*, *JHEP* **08** (2017) 019 [1706.06100]. [Cited on pages 51, 64, and 86.]

[163] S.F. King, *$R_{K^{(*)}}$ and the origin of Yukawa couplings*, *JHEP* **09** (2018) 069 [1806.06780]. [Cited on pages 51, 56, 64, 87, and 111.]

[164] I. de Medeiros Varzielas and S.F. King, *$R_{K^{(*)}}$ with leptoquarks and the origin of Yukawa couplings*, *JHEP* **11** (2018) 100 [1807.06023]. [Cited on pages 51, 87, and 121.]

[165] B. Grinstein, S. Pokorski and G.G. Ross, *Lepton non-universality in B decays and fermion mass structure*, *JHEP* **12** (2018) 079 [1809.01766]. [Cited on page 51.]

[166] I. de Medeiros Varzielas and J. Talbert, *Simplified Models of Flavourful Leptoquarks*, *Eur. Phys. J. C* **79** (2019) 536 [1901.10484]. [Cited on page 51.]

[167] I. De Medeiros Varzielas and S.F. King, *Origin of Yukawa couplings for Higgs bosons and leptoquarks*, *Phys. Rev. D* **99** (2019) 095029 [1902.09266]. [Cited on pages 51 and 87.]

[168] S.J.D. King, S.F. King, S. Moretti and S.J. Rowley, *Discovering the origin of Yukawa couplings at the LHC with a singlet Higgs and vector-like quarks*, *JHEP* **21** (2020) 144 [2102.06091]. [Cited on pages 51 and 257.]

[169] S.F. King, *Twin Pati-Salam theory of flavour with a TeV scale vector leptoquark*, *JHEP* **11** (2021) 161 [2106.03876]. [Cited on pages 51, 56, 70, 72, 122, 123, 124, 127, 136, and 137.]

[170] M. Bordone, C. Cornella, J. Fuentes-Martín and G. Isidori, *Low-energy signatures of the* PS^3 *model: from B-physics anomalies to LFV*, *JHEP* **10** (2018) 148 [1805.09328]. [Cited on pages 51, 70, 155, 167, and 179.]

[171] L. Ferretti, S.F. King and A. Romanino, *Flavour from accidental symmetries*, *JHEP* **11** (2006) 078 [hep-ph/0609047]. [Cited on pages 51, 87, 102, 119, 123, 134, 181, 186, 229, and 248.]

[172] J. Shu, T.M.P. Tait and C.E.M. Wagner, *Baryogenesis from an Earlier Phase Transition*, *Phys. Rev. D* **75** (2007) 063510 [hep-ph/0610375]. [Cited on pages 51, 219, and 221.]

[173] A. Greljo, T. Opferkuch and B.A. Stefanek, *Gravitational Imprints of Flavor Hierarchies*, *Phys. Rev. Lett.* **124** (2020) 171802 [1910.02014]. [Cited on page 51.]

[174] J. Fuentes-Martin, P. Ruiz-Femenia, A. Vicente and J. Virto, *DsixTools 2.0: The Effective Field Theory Toolkit*, *Eur. Phys. J. C* **81** (2021) 167 [2010.16341]. [Cited on pages 54, 71, 157, 163, 168, and 249.]

[175] E.E. Jenkins, A.V. Manohar and P. Stoffer, *Low-Energy Effective Field Theory below the Electroweak Scale: Operators and Matching*, *JHEP* **03** (2018) 016 [1709.04486]. [Cited on pages 55, 57, 263, 266, 267, 268, 269, 270, 271, 272, 273, 274, 275, 276, and 277.]

[176] M. Bordone, G. Isidori and A. Pattori, *On the Standard Model predictions for* R_K *and* R_{K^*}, *Eur. Phys. J. C* **76** (2016) 440 [1605.07633]. [Cited on page 55.]

[177] LHCb collaboration, *Test of lepton universality in beauty-quark decays*, *Nature Phys.* **18** (2022) 277 [2103.11769]. [Cited on pages 56 and 85.]

[178] LHCb collaboration, *Test of lepton universality with* $B^0 \to K^{*0}\ell^+\ell^-$ *decays*, *JHEP* **08** (2017) 055 [1705.05802]. [Cited on page 56.]

[179] N. Gubernari, M. Reboud, D. van Dyk and J. Virto, *Improved theory predictions and global analysis of exclusive* $b \to s\mu^+\mu^-$ *processes*, *JHEP* **09** (2022) 133 [2206.03797]. [Cited on pages 56 and 59.]

[180] LHCb collaboration, *Analysis of Neutral B-Meson Decays into Two Muons*, *Phys. Rev. Lett.* **128** (2022) 041801 [2108.09284]. [Cited on page 56.]

[181] L.-S. Geng, B. Grinstein, S. Jäger, S.-Y. Li, J. Martin Camalich and R.-X. Shi, *Implications of new evidence for lepton-universality violation in* $b \to s\ell+\ell-$ *decays*, *Phys. Rev. D* **104** (2021) 035029 [2103.12738]. [Cited on pages 56 and 155.]

[182] C. Bobeth, M. Gorbahn, T. Hermann, M. Misiak, E. Stamou and M. Steinhauser, *$B_{s,d} \to l^+ l^-$ in the Standard Model with Reduced Theoretical Uncertainty*, *Phys. Rev. Lett.* **112** (2014) 101801 [1311.0903]. [Cited on pages 56 and 67.]

[183] S. Bruggisser, R. Schäfer, D. van Dyk and S. Westhoff, *The Flavor of UV Physics*, *JHEP* **05** (2021) 257 [2101.07273]. [Cited on page 57.]

[184] A. Angelescu, D. Bečirević, D.A. Faroughy, F. Jaffredo and O. Sumensari, *Single leptoquark solutions to the B-physics anomalies*, *Phys. Rev. D* **104** (2021) 055017 [2103.12504]. [Cited on pages 58, 73, 121, 155, and 177.]

[185] LHCb collaboration, *Test of lepton universality in $b \to s\ell^+\ell^-$ decays*, *Phys. Rev. Lett.* **131** (2023) 051803 [2212.09152]. [Cited on pages 57, 111, and 215.]

[186] CMS collaboration, *Measurement of the $B_S^0 \to \mu^+\mu^-$ decay properties and search for the $B^0 \to \mu^+\mu^-$ decay in proton-proton collisions at $\sqrt{s}$ = 13 TeV*, *Phys. Lett. B* **842** (2023) 137955 [2212.10311]. [Cited on pages 57 and 215.]

[187] B. Allanach and J. Davighi, *The Rumble in the Meson: a leptoquark versus a Z' to fit $b \to s\mu^+\mu^-$ anomalies including 2022 LHCb $R_{K^{(*)}}$ measurements*, *JHEP* **04** (2023) 033 [2211.11766]. [Cited on pages 57 and 85.]

[188] A. Greljo, J. Salko, A. Smolkovič and P. Stangl, *Rare b decays meet high-mass Drell-Yan*, *JHEP* **05** (2023) 087 [2212.10497]. [Cited on pages 57 and 159.]

[189] D. Bečirević, O. Sumensari and R. Zukanovich Funchal, *Lepton flavor violation in exclusive $b \to s$ decays*, *Eur. Phys. J. C* **76** (2016) 134 [1602.00881]. [Cited on pages 58, 67, 76, and 77.]

[190] Fermilab Lattice, MILC, Fermilab Lattice, MILC collaboration, *Semileptonic form factors for $B \to D^*\ell\nu$ at nonzero recoil from 2 + 1-flavor lattice QCD: Fermilab Lattice and MILC Collaborations*, *Eur. Phys. J. C* **82** (2022) 1141 [2105.14019]. [Cited on page 60.]

[191] J. Harrison and C.T.H. Davies, *$B \to D^*$ vector, axial-vector and tensor form factors for the full q^2 range from lattice QCD*, 2304.03137. [Cited on page 60.]

[192] JLQCD collaboration, *$B \to D^*\ell\nu_\ell$ semileptonic form factors from lattice QCD with Möbius domain-wall quarks*, 2306.05657. [Cited on page 60.]

[193] BaBar collaboration, *Measurement of an Excess of $\bar{B} \to D^{(*)}\tau^-\bar{\nu}_\tau$ Decays and Implications for Charged Higgs Bosons*, *Phys. Rev. D* **88** (2013) 072012 [1303.0571]. [Cited on page 60.]

[194] Belle collaboration, *Measurement of the branching ratio of $\bar{B} \to D^{(*)}\tau^-\bar{\nu}_\tau$ relative to $\bar{B} \to D^{(*)}\ell^-\bar{\nu}_\ell$ decays with hadronic tagging at Belle*, *Phys. Rev. D* **92** (2015) 072014 [1507.03233]. [Cited on page 60.]

[195] Belle collaboration, *Measurement of the τ lepton polarization and $R(D^*)$ in the decay $\bar{B} \to D^* \tau^- \bar{\nu}_\tau$*, *Phys. Rev. Lett.* **118** (2017) 211801 [1612.00529]. [Cited on page 60.]

[196] Belle collaboration, *Measurement of the τ lepton polarization and $R(D^*)$ in the decay $\bar{B} \to D^* \tau^- \bar{\nu}_\tau$ with one-prong hadronic τ decays at Belle*, *Phys. Rev. D* **97** (2018) 012004 [1709.00129]. [Cited on page 60.]

[197] Belle collaboration, *Measurement of $\mathcal{R}(D)$ and $\mathcal{R}(D^*)$ with a semileptonic tagging method*, *Phys. Rev. Lett.* **124** (2020) 161803 [1910.05864]. [Cited on page 60.]

[198] LHCb collaboration, *Test of lepton flavour universality using $B^0 \to D^{*-} \tau^+ \nu_\tau$ decays with hadronic τ channels*, 2305.01463. [Cited on page 60.]

[199] LHCb collaboration, *Measurement of the ratios of branching fractions $\mathcal{R}(D^*)$ and $\mathcal{R}(D^0)$*, 2302.02886. [Cited on page 60.]

[200] LHCb collaboration, *Measurement of the ratio of branching fractions $\mathcal{B}(B_c^+ \to J/\psi \tau^+ \nu_\tau)/\mathcal{B}(B_c^+ \to J/\psi \mu^+ \nu_\mu)$*, *Phys. Rev. Lett.* **120** (2018) 121801 [1711.05623]. [Cited on page 61.]

[201] LHCb collaboration, *Observation of the decay $\Lambda_b^0 \to \Lambda_c^+ \tau^- \bar{\nu}_\tau$*, *Phys. Rev. Lett.* **128** (2022) 191803 [2201.03497]. [Cited on page 61.]

[202] C. Murgui, A. Peñuelas, M. Jung and A. Pich, *Global fit to $b \to c\tau\nu$ transitions*, *JHEP* **09** (2019) 103 [1904.09311]. [Cited on page 61.]

[203] R. Mandal, C. Murgui, A. Peñuelas and A. Pich, *The role of right-handed neutrinos in $b \to c\tau\bar{\nu}$ anomalies*, *JHEP* **08** (2020) 022 [2004.06726]. [Cited on page 61.]

[204] S. Iguro, T. Kitahara and R. Watanabe, *Global fit to $b \to c\tau\nu$ anomalies 2022 mid-autumn*, 2210.10751. [Cited on page 61.]

[205] Muon g-2 collaboration, *Final Report of the Muon E821 Anomalous Magnetic Moment Measurement at BNL*, *Phys. Rev. D* **73** (2006) 072003 [hep-ex/0602035]. [Cited on page 62.]

[206] T. Aoyama et al., *The anomalous magnetic moment of the muon in the Standard Model*, *Phys. Rept.* **887** (2020) 1 [2006.04822]. [Cited on pages 62 and 94.]

[207] G. Colangelo, M. Hoferichter and P. Stoffer, *Two-pion contribution to hadronic vacuum polarization*, *JHEP* **02** (2019) 006 [1810.00007]. [Cited on page 62.]

[208] M. Davier, A. Hoecker, B. Malaescu and Z. Zhang, *A new evaluation of the hadronic vacuum polarisation contributions to the muon anomalous magnetic moment and to $\boldsymbol{\alpha}(\mathbf{m_Z^2})$*, *Eur. Phys. J. C* **80** (2020) 241 [1908.00921]. [Cited on page 62.]

[209] A. Keshavarzi, D. Nomura and T. Teubner, $g-2$ *of charged leptons,* $\alpha(M_Z^2)$ *, and the hyperfine splitting of muonium*, *Phys. Rev. D* **101** (2020) 014029 [1911.00367]. [Cited on page 62.]

[210] S. Borsanyi et al., *Leading hadronic contribution to the muon magnetic moment from lattice QCD*, *Nature* **593** (2021) 51 [2002.12347]. [Cited on page 62.]

[211] M. Cè et al., *Window observable for the hadronic vacuum polarization contribution to the muon g-2 from lattice QCD*, *Phys. Rev. D* **106** (2022) 114502 [2206.06582]. [Cited on page 62.]

[212] Extended Twisted Mass collaboration, *Lattice calculation of the short and intermediate time-distance hadronic vacuum polarization contributions to the muon magnetic moment using twisted-mass fermions*, *Phys. Rev. D* **107** (2023) 074506 [2206.15084]. [Cited on page 62.]

[213] T. Blum et al., *An update of Euclidean windows of the hadronic vacuum polarization*, 2301.08696. [Cited on page 62.]

[214] RBC, UKQCD collaboration, *Calculation of the hadronic vacuum polarization contribution to the muon anomalous magnetic moment*, *Phys. Rev. Lett.* **121** (2018) 022003 [1801.07224]. [Cited on page 62.]

[215] A. Crivellin, M. Hoferichter, C.A. Manzari and M. Montull, *Hadronic Vacuum Polarization:* $(g-2)_\mu$ *versus Global Electroweak Fits*, *Phys. Rev. Lett.* **125** (2020) 091801 [2003.04886]. [Cited on page 63.]

[216] CMD-3 collaboration, *Measurement of the* $e^+e^- \to \pi^+\pi^-$ *cross section from threshold to 1.2 GeV with the CMD-3 detector*, 2302.08834. [Cited on page 63.]

[217] M. Pospelov, *Secluded U(1) below the weak scale*, *Phys. Rev. D* **80** (2009) 095002 [0811.1030]. [Cited on pages 63 and 86.]

[218] P. Athron, C. Balázs, D.H.J. Jacob, W. Kotlarski, D. Stöckinger and H. Stöckinger-Kim, *New physics explanations of* a_μ *in light of the FNAL muon* $g-2$ *measurement*, *JHEP* **09** (2021) 080 [2104.03691]. [Cited on page 63.]

[219] L.L. Everett, G.L. Kane, S. Rigolin and L.-T. Wang, *Implications of muon g-2 for supersymmetry and for discovering superpartners directly*, *Phys. Rev. Lett.* **86** (2001) 3484 [hep-ph/0102145]. [Cited on page 64.]

[220] A. Czarnecki and W.J. Marciano, *The Muon anomalous magnetic moment: A Harbinger for 'new physics'*, *Phys. Rev. D* **64** (2001) 013014 [hep-ph/0102122]. [Cited on page 64.]

[221] K. Kannike, M. Raidal, D.M. Straub and A. Strumia, *Anthropic solution to the magnetic muon anomaly: the charged see-saw*, *JHEP* **02** (2012) 106 [1111.2551]. [Cited on page 64.]

[222] K. Kowalska and E.M. Sessolo, *Expectations for the muon g-2 in simplified models with dark matter*, *JHEP* **09** (2017) 112 [1707.00753]. [Cited on page 64.]

[223] A. Crivellin, M. Hoferichter and P. Schmidt-Wellenburg, *Combined explanations of $(g-2)_{\mu,e}$ and implications for a large muon EDM*, *Phys. Rev. D* **98** (2018) 113002 [1807.11484]. [Cited on pages 64 and 86.]

[224] A. Crivellin and M. Hoferichter, *Consequences of chirally enhanced explanations of $(g-2)_\mu$ for $h \to \mu\mu$ and $Z \to \mu\mu$*, *JHEP* **07** (2021) 135 [2104.03202]. [Cited on pages 64 and 86.]

[225] A.E.C. Hernández, S.F. King and H. Lee, *Fermion mass hierarchies from vectorlike families with an extended 2HDM and a possible explanation for the electron and muon anomalous magnetic moments*, *Phys. Rev. D* **103** (2021) 115024 [2101.05819]. [Cited on pages 64 and 86.]

[226] A. Djouadi, T. Kohler, M. Spira and J. Tutas, *(e b), (e t) TYPE LEPTOQUARKS AT e p COLLIDERS*, *Z. Phys. C* **46** (1990) 679. [Cited on page 64.]

[227] K.-m. Cheung, *Muon anomalous magnetic moment and leptoquark solutions*, *Phys. Rev. D* **64** (2001) 033001 [hep-ph/0102238]. [Cited on page 64.]

[228] M. Bauer and M. Neubert, *Minimal Leptoquark Explanation for the $R_{D^{(*)}}$, R_K , and $(g-2)_\mu$ Anomalies*, *Phys. Rev. Lett.* **116** (2016) 141802 [1511.01900]. [Cited on page 64.]

[229] E. Coluccio Leskow, G. D'Ambrosio, A. Crivellin and D. Müller, *$(g-2)\mu$, lepton flavor violation, and Z decays with leptoquarks: Correlations and future prospects*, *Phys. Rev. D* **95** (2017) 055018 [1612.06858]. [Cited on page 64.]

[230] A. Crivellin, D. Mueller and F. Saturnino, *Correlating $h \to \mu^+\mu^-$ to the Anomalous Magnetic Moment of the Muon via Leptoquarks*, *Phys. Rev. Lett.* **127** (2021) 021801 [2008.02643]. [Cited on page 64.]

[231] S. Raby and A. Trautner, *Vectorlike chiral fourth family to explain muon anomalies*, *Phys. Rev. D* **97** (2018) 095006 [1712.09360]. [Cited on pages 64 and 86.]

[232] G. Bélanger, C. Delaunay and S. Westhoff, *A Dark Matter Relic From Muon Anomalies*, *Phys. Rev. D* **92** (2015) 055021 [1507.06660]. [Cited on pages 64 and 86.]

[233] A. Falkowski, S.F. King, E. Perdomo and M. Pierre, *Flavourful Z' portal for vector-like neutrino Dark Matter and $R_{K^{(*)}}$*, *JHEP* **08** (2018) 061 [1803.04430]. [Cited on pages 64, 86, and 96.]

[234] A.E. Cárcamo Hernández, S.F. King, H. Lee and S.J. Rowley, *Is it possible to explain the muon and electron $g-2$ in a Z' model?*, *Phys. Rev. D* **101** (2020) 115016 [1910.10734]. [Cited on pages 64, 86, and 163.]

[235] J. Kawamura, S. Raby and A. Trautner, *Complete vectorlike fourth family and new U(1)' for muon anomalies*, *Phys. Rev. D* **100** (2019) 055030 [1906.11297]. [Cited on pages 64 and 86.]

[236] J. Kawamura, S. Raby and A. Trautner, *Complete vectorlike fourth family with U(1)' : A global analysis*, *Phys. Rev. D* **101** (2020) 035026 [1911.11075]. [Cited on pages 64 and 86.]

[237] R.H. Good, R.P. Matsen, F. Muller, O. Piccioni, W.M. Powell, H.S. White et al., *Regeneration of Neutral K Mesons and Their Mass Difference*, *Phys. Rev.* **124** (1961) 1223. [Cited on page 64.]

[238] UTfit collaboration, *Model-independent constraints on $\Delta F = 2$ operators and the scale of new physics*, *JHEP* **03** (2008) 049 [0707.0636]. [Cited on pages 65, 194, 195, and 230.]

[239] G. Isidori and F. Teubert, *Status of indirect searches for New Physics with heavy flavour decays after the initial LHC run*, *Eur. Phys. J. Plus* **129** (2014) 40 [1402.2844]. [Cited on pages 65, 194, 195, and 230.]

[240] UTfit collaboration, *Unitarity Triangle analysis beyond the Standard Model from UTfit*, *PoS* **ICHEP2016** (2016) 149. [Cited on page 65.]

[241] LHCb collaboration, *Precise determination of the B^0_s–$\overline{B}^0_s$ oscillation frequency*, *Nature Phys.* **18** (2022) 1 [2104.04421]. [Cited on page 65.]

[242] L. Di Luzio, M. Kirk, A. Lenz and T. Rauh, *ΔM_s theory precision confronts flavour anomalies*, *JHEP* **12** (2019) 009 [1909.11087]. [Cited on pages 65, 66, 67, 155, and 215.]

[243] Flavour Lattice Averaging Group collaboration, *FLAG Review 2019: Flavour Lattice Averaging Group (FLAG)*, *Eur. Phys. J. C* **80** (2020) 113 [1902.08191]. [Cited on pages 65 and 66.]

[244] Fermilab Lattice, MILC collaboration, *$B^0_{(s)}$-mixing matrix elements from lattice QCD for the Standard Model and beyond*, *Phys. Rev. D* **93** (2016) 113016 [1602.03560]. [Cited on page 65.]

[245] RBC/UKQCD collaboration, *SU(3)-breaking ratios for $D_{(s)}$ and $B_{(s)}$ mesons*, 1812.08791. [Cited on page 65.]

[246] R.J. Dowdall, C.T.H. Davies, R.R. Horgan, G.P. Lepage, C.J. Monahan, J. Shigemitsu et al., *Neutral B-meson mixing from full lattice QCD at the physical point*, *Phys. Rev. D* **100** (2019) 094508 [1907.01025]. [Cited on page 65.]

[247] M. Kirk, A. Lenz and T. Rauh, *Dimension-six matrix elements for meson mixing and lifetimes from sum rules*, *JHEP* **12** (2017) 068 [1711.02100]. [Cited on page 66.]

[248] A.G. Grozin, R. Klein, T. Mannel and A.A. Pivovarov, $B^0 - \bar{B}^0$ *mixing at next-to-leading order*, *Phys. Rev. D* **94** (2016) 034024 [1606.06054]. [Cited on page 66.]

[249] D. King, A. Lenz and T. Rauh, B_s *mixing observables and* $|V_{td}/V_{ts}|$ *from sum rules*, *JHEP* **05** (2019) 034 [1904.00940]. [Cited on page 66.]

[250] G. Buchalla, A.J. Buras and M.E. Lautenbacher, *Weak decays beyond leading logarithms*, *Rev. Mod. Phys.* **68** (1996) 1125 [hep-ph/9512380]. [Cited on page 66.]

[251] HPQCD collaboration, *Standard Model Predictions for* $B \to K\ell^+\ell^-$ *with Form Factors from Lattice QCD*, *Phys. Rev. Lett.* **111** (2013) 162002 [1306.0434]. [Cited on page 67.]

[252] LHCb collaboration, *Search for the decays* $B_s^0 \to \tau^+\tau^-$ *and* $B^0 \to \tau^+\tau^-$, *Phys. Rev. Lett.* **118** (2017) 251802 [1703.02508]. [Cited on pages 68, 69, 155, and 167.]

[253] LHCb collaboration, *Physics case for an LHCb Upgrade II - Opportunities in flavour physics, and beyond, in the HL-LHC era*, 1808.08865. [Cited on pages 68, 70, 77, and 167.]

[254] BaBar collaboration, *Search for* $B^+ \to K^+\tau^+\tau^-$ *at the BaBar experiment*, *Phys. Rev. Lett.* **118** (2017) 031802 [1605.09637]. [Cited on pages 68, 155, and 167.]

[255] Belle II collaboration, *The Belle II Physics Book*, *PTEP* **2019** (2019) 123C01 [1808.10567]. [Cited on pages 68, 73, 75, 78, 162, 163, 164, 167, and 170.]

[256] A. Lenz, M.L. Piscopo and A.V. Rusov, *Disintegration of beauty: a precision study*, *JHEP* **01** (2023) 004 [2208.02643]. [Cited on page 69.]

[257] M. Bordone, B. Capdevila and P. Gambino, *Three loop calculations and inclusive Vcb*, *Phys. Lett. B* **822** (2021) 136679 [2107.00604]. [Cited on page 69.]

[258] M. Bordone and P. Gambino, *The semileptonic* B_s *and* Λ_b *widths*, *PoS* **CKM2021** (2023) 055 [2203.13107]. [Cited on page 69.]

[259] P. Gambino, A. Melis and S. Simula, *Extraction of heavy-quark-expansion parameters from unquenched lattice data on pseudoscalar and vector heavy-light meson masses*, *Phys. Rev. D* **96** (2017) 014511 [1704.06105]. [Cited on page 69.]

[260] P. Gambino, A. Melis and S. Simula, *HQE parameters from unquenched lattice data on pseudoscalar and vector heavy-light meson masses*, *EPJ Web Conf.* **175** (2018) 13028 [1710.10168]. [Cited on page 69.]

[261] F. Bernlochner, M. Fael, K. Olschewsky, E. Persson, R. van Tonder, K.K. Vos et al., *First extraction of inclusive* V_{cb} *from* q^2 *moments*, *JHEP* **10** (2022) 068 [2205.10274]. [Cited on page 69.]

[262] C. Cornella, J. Fuentes-Martin and G. Isidori, *Revisiting the vector leptoquark explanation of the B-physics anomalies*, *JHEP* **07** (2019) 168 [1903.11517]. [Cited on pages 70, 72, 122, 155, 162, 164, 167, 170, 178, and 179.]

[263] C. Cornella, D.A. Faroughy, J. Fuentes-Martin, G. Isidori and M. Neubert, *Reading the footprints of the B-meson flavor anomalies*, *JHEP* **08** (2021) 050 [2103.16558]. [Cited on pages 70, 72, 122, 155, 159, 162, 163, 164, 167, 168, 169, 170, 173, 174, 176, 177, 178, 179, and 183.]

[264] A. Greljo and B.A. Stefanek, *Third family quark–lepton unification at the TeV scale*, *Phys. Lett. B* **782** (2018) 131 [1802.04274]. [Cited on pages 70, 72, and 179.]

[265] L. Calibbi, A. Crivellin and T. Li, *Model of vector leptoquarks in view of the B-physics anomalies*, *Phys. Rev. D* **98** (2018) 115002 [1709.00692]. [Cited on page 70.]

[266] M. Blanke and A. Crivellin, *B Meson Anomalies in a Pati-Salam Model within the Randall-Sundrum Background*, *Phys. Rev. Lett.* **121** (2018) 011801 [1801.07256]. [Cited on page 70.]

[267] L. Di Luzio, A. Greljo and M. Nardecchia, *Gauge leptoquark as the origin of B-physics anomalies*, *Phys. Rev. D* **96** (2017) 115011 [1708.08450]. [Cited on pages 70, 72, 121, 122, 138, 157, 162, 163, 167, 179, 180, 181, and 249.]

[268] L. Di Luzio, J. Fuentes-Martin, A. Greljo, M. Nardecchia and S. Renner, *Maximal Flavour Violation: a Cabibbo mechanism for leptoquarks*, *JHEP* **11** (2018) 081 [1808.00942]. [Cited on pages 70, 72, 122, 144, 151, 153, 157, 159, 162, 163, 167, 171, 173, 178, 179, 180, and 181.]

[269] J. Aebischer, G. Isidori, M. Pesut, B.A. Stefanek and F. Wilsch, *Confronting the vector leptoquark hypothesis with new low- and high-energy data*, *Eur. Phys. J. C* **83** (2023) 153 [2210.13422]. [Cited on pages 70, 123, 157, and 179.]

[270] G. Buchalla and A.J. Buras, *The rare decays $K \to \pi\nu\bar{\nu}$, $B \to X\nu\bar{\nu}$ and $B \to l^+l^-$: An Update*, *Nucl. Phys. B* **548** (1999) 309 [hep-ph/9901288]. [Cited on page 72.]

[271] BaBar collaboration, *Search for $B \to K^{(*)}\nu\bar{\nu}$ and invisible quarkonium decays*, *Phys. Rev. D* **87** (2013) 112005 [1303.7465]. [Cited on pages 73 and 155.]

[272] Belle collaboration, *Search for $\boldsymbol{B \to h\nu\bar{\nu}}$ decays with semileptonic tagging at Belle*, *Phys. Rev. D* **96** (2017) 091101 [1702.03224]. [Cited on pages 73 and 155.]

[273] Y. Kuno and Y. Okada, *Muon decay and physics beyond the standard model*, *Rev. Mod. Phys.* **73** (2001) 151 [hep-ph/9909265]. [Cited on pages 74 and 75.]

[274] MEG II collaboration, *The design of the MEG II experiment*, *Eur. Phys. J. C* **78** (2018) 380 [1801.04688]. [Cited on page 75.]

[275] A. Blondel et al., *Research Proposal for an Experiment to Search for the Decay $\mu \to eee$*, 1301.6113. [Cited on page 75.]

[276] Flavour Lattice Averaging Group (FLAG) collaboration, *FLAG Review 2021*, *Eur. Phys. J. C* **82** (2022) 869 [2111.09849]. [Cited on page 76.]

[277] LHCb collaboration, *Search for the lepton-flavour-violating decays $B_s^0 \to \tau^\pm\mu^\mp$ and $B^0 \to \tau^\pm\mu^\mp$*, *Phys. Rev. Lett.* **123** (2019) 211801 [1905.06614]. [Cited on pages 77, 155, and 164.]

[278] BaBar collaboration, *A search for the decay modes $B^{+-} \to h^{+-}\tau^{+-}l$*, *Phys. Rev. D* **86** (2012) 012004 [1204.2852]. [Cited on pages 77, 155, and 164.]

[279] A. Pich, *Precision Tau Physics*, *Prog. Part. Nucl. Phys.* **75** (2014) 41 [1310.7922]. [Cited on pages 78 and 79.]

[280] Belle collaboration, *Search for Lepton-Flavor-Violating tau Decays into a Lepton and a Vector Meson*, *Phys. Lett. B* **699** (2011) 251 [1101.0755]. [Cited on pages 78 and 155.]

[281] A. Crivellin, G. D'Ambrosio, M. Hoferichter and L.C. Tunstall, *Violation of lepton flavor and lepton flavor universality in rare kaon decays*, *Phys. Rev. D* **93** (2016) 074038 [1601.00970]. [Cited on page 78.]

[282] BNL collaboration, *New limit on muon and electron lepton number violation from K0(L) —> mu+- e-+ decay*, *Phys. Rev. Lett.* **81** (1998) 5734 [hep-ex/9811038]. [Cited on pages 78, 125, and 155.]

[283] G. Valencia and S. Willenbrock, *Quark - lepton unification and rare meson decays*, *Phys. Rev. D* **50** (1994) 6843 [hep-ph/9409201]. [Cited on pages 78 and 125.]

[284] A. De Rujula, H. Georgi and S.L. Glashow, *FLAVOR GONIOMETRY BY PROTON DECAY*, *Phys. Rev. Lett.* **45** (1980) 413. [Cited on page 81.]

[285] S.M. Barr, *A New Symmetry Breaking Pattern for SO(10) and Proton Decay*, *Phys. Lett. B* **112** (1982) 219. [Cited on page 81.]

[286] P. Nath and P. Fileviez Perez, *Proton stability in grand unified theories, in strings and in branes*, *Phys. Rept.* **441** (2007) 191 [hep-ph/0601023]. [Cited on page 81.]

[287] J. Chakrabortty, R. Maji and S.F. King, *Unification, Proton Decay and Topological Defects in non-SUSY GUTs with Thresholds*, *Phys. Rev. D* **99** (2019) 095008 [1901.05867]. [Cited on pages 81 and 242.]

[288] Y. Aoki, T. Izubuchi, E. Shintani and A. Soni, *Improved lattice computation of proton decay matrix elements*, *Phys. Rev. D* **96** (2017) 014506 [1705.01338]. [Cited on page 81.]

[289] B. Capdevila, A. Crivellin, S. Descotes-Genon, L. Hofer and J. Matias, *Searching for New Physics with $b \to s\tau^+\tau^-$ processes*, *Phys. Rev. Lett.* **120** (2018) 181802 [1712.01919]. [Cited on page 82.]

[290] M. Algueró, J. Matias, B. Capdevila and A. Crivellin, *Disentangling lepton flavor universal and lepton flavor universality violating effects in $b \to s\ell+\ell-$ transitions*, *Phys. Rev. D* **105** (2022) 113007 [2205.15212]. [Cited on page 82.]

[291] A. Crivellin, C. Greub, D. Müller and F. Saturnino, *Importance of Loop Effects in Explaining the Accumulated Evidence for New Physics in B Decays with a Vector Leptoquark*, *Phys. Rev. Lett.* **122** (2019) 011805 [1807.02068]. [Cited on pages 82 and 158.]

[292] A. Crivellin, B. Fuks and L. Schnell, *Explaining the hints for lepton flavour universality violation with three S_2 leptoquark generations*, *JHEP* **06** (2022) 169 [2203.10111]. [Cited on pages 82 and 121.]

[293] A. Crivellin, D. Müller and T. Ota, *Simultaneous explanation of $R(D^{(*)})$ and $b \to s\mu^+\ \mu^-$: the last scalar leptoquarks standing*, *JHEP* **09** (2017) 040 [1703.09226]. [Cited on pages 82 and 121.]

[294] D. Buttazzo, A. Greljo, G. Isidori and D. Marzocca, *B-physics anomalies: a guide to combined explanations*, *JHEP* **11** (2017) 044 [1706.07808]. [Cited on pages 82 and 121.]

[295] J. Davighi, *Anomalous Z' bosons for anomalous B decays*, *JHEP* **08** (2021) 101 [2105.06918]. [Cited on page 86.]

[296] C. Bonilla, T. Modak, R. Srivastava and J.W.F. Valle, *$U(1)_{B_3-3L_\mu}$ gauge symmetry as a simple description of $b \to s$ anomalies*, *Phys. Rev. D* **98** (2018) 095002 [1705.00915]. [Cited on page 86.]

[297] R. Alonso, P. Cox, C. Han and T.T. Yanagida, *Flavoured $B-L$ local symmetry and anomalous rare B decays*, *Phys. Lett. B* **774** (2017) 643 [1705.03858]. [Cited on page 86.]

[298] E.J. Chun, A. Das, J. Kim and J. Kim, *Searching for flavored gauge bosons*, *JHEP* **02** (2019) 093 [1811.04320]. [Cited on page 86.]

[299] B.C. Allanach, *$U(1)_{B_3-L_2}$ explanation of the neutral current $B-$anomalies*, *Eur. Phys. J. C* **81** (2021) 56 [2009.02197]. [Cited on page 86.]

[300] B.C. Allanach and J. Davighi, *Third family hypercharge model for $R_{K^{(*)}}$ and aspects of the fermion mass problem*, *JHEP* **12** (2018) 075 [1809.01158]. [Cited on pages 86, 187, and 206.]

[301] B.C. Allanach and J. Davighi, *Naturalising the third family hypercharge model for neutral current B-anomalies*, *Eur. Phys. J. C* **79** (2019) 908 [1905.10327]. [Cited on page 86.]

[302] B.C. Allanach, J. Davighi and S. Melville, *An Anomaly-free Atlas: charting the space of flavour-dependent gauged $U(1)$ extensions of the Standard Model*, *JHEP* **02** (2019) 082 [1812.04602]. [Cited on page 86.]

[303] B.C. Allanach, B. Gripaios and J. Tooby-Smith, *Anomaly cancellation with an extra gauge boson*, *Phys. Rev. Lett.* **125** (2020) 161601 [2006.03588]. [Cited on page 86.]

[304] P. Arnan, A. Crivellin, M. Fedele and F. Mescia, *Generic Loop Effects of New Scalars and Fermions in $b \to s\ell^+\ell^-$, $(g-2)_\mu$ and a Vector-like 4^{th} Generation*, *JHEP* **06** (2019) 118 [1904.05890]. [Cited on page 86.]

[305] E. Ma, D.P. Roy and S. Roy, *Gauged L(mu) - L(tau) with large muon anomalous magnetic moment and the bimaximal mixing of neutrinos*, *Phys. Lett. B* **525** (2002) 101 [hep-ph/0110146]. [Cited on page 86.]

[306] A.E. Cárcamo Hernández, S. Kovalenko, R. Pasechnik and I. Schmidt, *Phenomenology of an extended IDM with loop-generated fermion mass hierarchies*, *Eur. Phys. J. C* **79** (2019) 610 [1901.09552]. [Cited on page 86.]

[307] B. Allanach, F.S. Queiroz, A. Strumia and S. Sun, *Z' models for the LHCb and $g-2$ muon anomalies*, *Phys. Rev. D* **93** (2016) 055045 [1511.07447]. [Cited on page 86.]

[308] J. Kawamura and S. Raby, *Signal of four muons or more from a vector-like lepton decaying to a muon-philic Z' boson at the LHC*, *Phys. Rev. D* **104** (2021) 035007 [2104.04461]. [Cited on page 86.]

[309] R. Dermisek, J.P. Hall, E. Lunghi and S. Shin, *Limits on Vectorlike Leptons from Searches for Anomalous Production of Multi-Lepton Events*, *JHEP* **12** (2014) 013 [1408.3123]. [Cited on page 89.]

[310] J.F. Gunion, H.E. Haber, G.L. Kane and S. Dawson, *The Higgs Hunter's Guide*, vol. 80 (2000). [Cited on page 92.]

[311] A. Joglekar, P. Schwaller and C.E.M. Wagner, *Dark Matter and Enhanced Higgs to Di-photon Rate from Vector-like Leptons*, *JHEP* **12** (2012) 064 [1207.4235]. [Cited on page 93.]

[312] J. Kearney, A. Pierce and N. Weiner, *Vectorlike Fermions and Higgs Couplings*, *Phys. Rev. D* **86** (2012) 113005 [1207.7062]. [Cited on page 93.]

[313] N. Bizot and M. Frigerio, *Fermionic extensions of the Standard Model in light of the Higgs couplings*, *JHEP* **01** (2016) 036 [1508.01645]. [Cited on page 93.]

[314] CMS collaboration, *Sensitivity projections for Higgs boson properties measurements at the HL-LHC*, CMS-PAS-FTR-18-011. [Cited on pages 94, 97, and 98.]

[315] ATLAS collaboration, *Projections for measurements of Higgs boson cross sections, branching ratios, coupling parameters and mass with the ATLAS detector at the HL-LHC*, ATL-PHYS-PUB-2018-054. [Cited on pages 94, 97, and 98.]

[316] CMS, ATLAS collaboration, *Evidence for the Higgs boson decay to a Z boson and a photon at the LHC*, *Phys. Rev. Lett.* **132** (2024) 021803 [2309.03501]. [Cited on page 94.]

[317] M. Carena, I. Low and C.E.M. Wagner, *Implications of a Modified Higgs to Diphoton Decay Width*, *JHEP* **08** (2012) 060 [1206.1082]. [Cited on page 94.]

[318] W. Altmannshofer, M. Bauer and M. Carena, *Exotic Leptons: Higgs, Flavor and Collider Phenomenology*, *JHEP* **01** (2014) 060 [1308.1987]. [Cited on page 94.]

[319] F. Jegerlehner and A. Nyffeler, *The Muon g-2*, *Phys. Rept.* **477** (2009) 1 [0902.3360]. [Cited on page 95.]

[320] R. Dermisek and A. Raval, *Explanation of the Muon g-2 Anomaly with Vectorlike Leptons and its Implications for Higgs Decays*, *Phys. Rev. D* **88** (2013) 013017 [1305.3522]. [Cited on page 95.]

[321] CHARM-II collaboration, *First observation of neutrino trident production*, *Phys. Lett. B* **245** (1990) 271. [Cited on page 96.]

[322] CCFR collaboration, *Neutrino tridents and W Z interference*, *Phys. Rev. Lett.* **66** (1991) 3117. [Cited on page 96.]

[323] NuTeV collaboration, *Neutrino trident production from NuTeV*, in *29th International Conference on High-Energy Physics*, pp. 631–634, 7, 1998 [hep-ex/9811012]. [Cited on page 96.]

[324] W. Altmannshofer, S. Gori, M. Pospelov and I. Yavin, *Neutrino Trident Production: A Powerful Probe of New Physics with Neutrino Beams*, *Phys. Rev. Lett.* **113** (2014) 091801 [1406.2332]. [Cited on page 96.]

[325] CMS collaboration, *Observation of Z Decays to Four Leptons with the CMS Detector at the LHC*, *JHEP* **12** (2012) 034 [1210.3844]. [Cited on page 96.]

[326] ATLAS collaboration, *Measurements of Four-Lepton Production at the Z Resonance in pp Collisions at $\sqrt{s} = 7$ and 8 TeV with ATLAS*, *Phys. Rev. Lett.* **112** (2014) 231806 [1403.5657]. [Cited on page 96.]

[327] W. Altmannshofer, S. Gori, M. Pospelov and I. Yavin, *Quark flavor transitions in $L_\mu - L_\tau$ models*, *Phys. Rev. D* **89** (2014) 095033 [1403.1269]. [Cited on page 96.]

[328] W. Altmannshofer, S. Gori, S. Profumo and F.S. Queiroz, *Explaining dark matter and B decay anomalies with an $L_\mu - L_\tau$ model*, *JHEP* **12** (2016) 106 [1609.04026]. [Cited on page 96.]

[329] U. Haisch and S. Westhoff, *Massive Color-Octet Bosons: Bounds on Effects in Top-Quark Pair Production*, *JHEP* **08** (2011) 088 [1106.0529]. [Cited on page 96.]

[330] A. Hook, E. Izaguirre and J.G. Wacker, *Model Independent Bounds on Kinetic Mixing*, *Adv. High Energy Phys.* **2011** (2011) 859762 [1006.0973]. [Cited on page 97.]

[331] J. Hernandez-Garcia and S.F. King, *New Weinberg operator for neutrino mass and its seesaw origin*, *JHEP* **05** (2019) 169 [1903.01474]. [Cited on pages 101 and 119.]

[332] S.F. King, *B anomalies linked to the problem of the origin of Yukawa couplings.*, *PoS* **CORFU2019** (2020) 016. [Cited on page 111.]

[333] P. Athron, R. Martinez and C. Sierra, *B meson anomalies and large $B^+ \to K^+ \nu\bar{\nu}$ in non-universal $U(1)'$ models*, 2308.13426. [Cited on page 112.]

[334] ATLAS collaboration, *Search for heavy resonances decaying into a W or Z boson and a Higgs boson in final states with leptons and b-jets in 36 fb^{-1} of $\sqrt{s} = 13$ TeV pp collisions with the ATLAS detector*, *JHEP* **03** (2018) 174 [1712.06518]. [Cited on page 112.]

[335] CMS collaboration, *Search for heavy resonances decaying into a vector boson and a Higgs boson in final states with charged leptons, neutrinos and b quarks at $\sqrt{s} = 13$ TeV*, *JHEP* **11** (2018) 172 [1807.02826]. [Cited on page 112.]

[336] A. Alloul, N.D. Christensen, C. Degrande, C. Duhr and B. Fuks, *FeynRules 2.0 - A complete toolbox for tree-level phenomenology*, *Comput. Phys. Commun.* **185** (2014) 2250 [1310.1921]. [Cited on pages 112, 174, 213, and 249.]

[337] J. Alwall, R. Frederix, S. Frixione, V. Hirschi, F. Maltoni, O. Mattelaer et al., *The automated computation of tree-level and next-to-leading order differential cross sections, and their matching to parton shower simulations*, *JHEP* **07** (2014) 079 [1405.0301]. [Cited on pages 112, 174, 213, and 249.]

[338] ATLAS collaboration, *Search for high-mass dilepton resonances using 139 fb^{-1} of pp collision data collected at $\sqrt{s}$ =13 TeV with the ATLAS detector*, *Phys. Lett. B* **796** (2019) 68 [1903.06248]. [Cited on pages 113, 176, and 214.]

[339] CMS collaboration, *Search for resonant and nonresonant new phenomena in high-mass dilepton final states at $\sqrt{s}$ = 13 TeV*, *JHEP* **07** (2021) 208 [2103.02708]. [Cited on pages 113 and 214.]

[340] ATLAS collaboration, *Search for additional heavy neutral Higgs and gauge bosons in the ditau final state produced in 36 fb^{-1} of pp collisions at $\sqrt{s} = 13$*

TeV with the ATLAS detector, *JHEP* **01** (2018) 055 [1709.07242]. [Cited on pages 113, 176, and 214.]

[341] ATLAS collaboration, *Search for $t\bar{t}$ resonances in fully hadronic final states in pp collisions at $\sqrt{s}$ = 13 TeV with the ATLAS detector*, *JHEP* **10** (2020) 061 [2005.05138]. [Cited on pages 113 and 214.]

[342] CMS collaboration, *Search for pair production of vectorlike quarks in the fully hadronic final state*, *Phys. Rev. D* **100** (2019) 072001 [1906.11903]. [Cited on page 113.]

[343] D. Bečirević and O. Sumensari, *A leptoquark model to accommodate $R_K^{\rm exp} < R_K^{\rm SM}$ and $R_{K^*}^{\rm exp} < R_{K^*}^{\rm SM}$*, *JHEP* **08** (2017) 104 [1704.05835]. [Cited on page 121.]

[344] D. Bečirević, I. Doršner, S. Fajfer, D.A. Faroughy, F. Jaffredo, N. Košnik et al., *Model with two scalar leptoquarks: R2 and S3*, *Phys. Rev. D* **106** (2022) 075023 [2206.09717]. [Cited on page 121.]

[345] B. Diaz, M. Schmaltz and Y.-M. Zhong, *The leptoquark Hunter's guide: Pair production*, *JHEP* **10** (2017) 097 [1706.05033]. [Cited on pages 121, 138, and 177.]

[346] H. Georgi and Y. Nakai, *Diphoton resonance from a new strong force*, *Phys. Rev. D* **94** (2016) 075005 [1606.05865]. [Cited on page 121.]

[347] T. Fukuyama, *SO(10) GUT in Four and Five Dimensions: A Review*, *Int. J. Mod. Phys. A* **28** (2013) 1330008 [1212.3407]. [Cited on page 127.]

[348] R.A. Porto and A. Zee, *The Private Higgs*, *Phys. Lett. B* **666** (2008) 491 [0712.0448]. [Cited on page 134.]

[349] R.A. Porto and A. Zee, *Neutrino Mixing and the Private Higgs*, *Phys. Rev. D* **79** (2009) 013003 [0807.0612]. [Cited on page 134.]

[350] Y. BenTov and A. Zee, *Private Higgs at the LHC*, *Int. J. Mod. Phys. A* **28** (2013) 1350149 [1207.0467]. [Cited on page 134.]

[351] W. Rodejohann and U. Saldaña Salazar, *Multi-Higgs-Doublet Models and Singular Alignment*, *JHEP* **07** (2019) 036 [1903.00983]. [Cited on page 134.]

[352] R. Gatto, G. Sartori and M. Tonin, *Weak Selfmasses, Cabibbo Angle, and Broken SU(2) x SU(2)*, *Phys. Lett. B* **28** (1968) 128. [Cited on page 135.]

[353] S.F. King, *SU(4) x SU(2)-L x SU(2)-R as a surrogate SUSY GUT*, *Phys. Lett. B* **325** (1994) 129. [Cited on page 136.]

[354] S.F. King, *Atmospheric and solar neutrinos with a heavy singlet*, *Phys. Lett. B* **439** (1998) 350 [hep-ph/9806440]. [Cited on pages 137 and 199.]

[355] S.F. King, *Large mixing angle MSW and atmospheric neutrinos from single right-handed neutrino dominance and U(1) family symmetry*, *Nucl. Phys. B* **576** (2000) 85 [hep-ph/9912492]. [Cited on pages 137 and 199.]

[356] R. Barbieri, C. Cornella and G. Isidori, *Simplified models of vector $SU(4)$ leptoquarks at the TeV*, 2207.14248. [Cited on pages 155, 164, 167, 170, 178, and 179.]

[357] K. Hayasaka et al., *Search for Lepton Flavor Violating Tau Decays into Three Leptons with 719 Million Produced Tau+Tau- Pairs*, *Phys. Lett. B* **687** (2010) 139 [1001.3221]. [Cited on page 155.]

[358] HFLAV collaboration, *Averages of b-hadron, c-hadron, and τ-lepton properties as of 2018*, *Eur. Phys. J. C* **81** (2021) 226 [1909.12524]. [Cited on page 155.]

[359] M. Algueró, B. Capdevila, S. Descotes-Genon, J. Matias and M. Novoa-Brunet, *$b \to s\ell^+\ell^-$ global fits after R_{K_S} and $R_{K^{*+}}$*, *Eur. Phys. J. C* **82** (2022) 326 [2104.08921]. [Cited on pages 158 and 159.]

[360] J. Fuentes-Martín, G. Isidori, M. König and N. Selimović, *Vector Leptoquarks Beyond Tree Level III: Vector-like Fermions and Flavor-Changing Transitions*, *Phys. Rev. D* **102** (2020) 115015 [2009.11296]. [Cited on pages 159, 163, 164, 168, 169, and 178.]

[361] J. Fuentes-Martín and P. Stangl, *Third-family quark-lepton unification with a fundamental composite Higgs*, *Phys. Lett. B* **811** (2020) 135953 [2004.11376]. [Cited on pages 164 and 178.]

[362] F. Goertz, J.F. Kamenik, A. Katz and M. Nardecchia, *Indirect Constraints on the Scalar Di-Photon Resonance at the LHC*, *JHEP* **05** (2016) 187 [1512.08500]. [Cited on page 170.]

[363] M.J. Baker, J. Fuentes-Martín, G. Isidori and M. König, *High- p_T signatures in vector–leptoquark models*, *Eur. Phys. J. C* **79** (2019) 334 [1901.10480]. [Cited on pages 173, 176, 177, and 183.]

[364] J. Fuentes-Martín, G. Isidori, M. König and N. Selimović, *Vector Leptoquarks Beyond Tree Level*, *Phys. Rev. D* **101** (2020) 035024 [1910.13474]. [Cited on page 174.]

[365] J. Fuentes-Martín, G. Isidori, M. König and N. Selimović, *Vector leptoquarks beyond tree level. II. $\mathcal{O}(\alpha_s)$ corrections and radial modes*, *Phys. Rev. D* **102** (2020) 035021 [2006.16250]. [Cited on page 174.]

[366] CMS collaboration, *Search for high mass dijet resonances with a new background prediction method in proton-proton collisions at $\sqrt{s} = 13$ TeV*, *JHEP* **05** (2020) 033 [1911.03947]. [Cited on page 174.]

[367] CMS collaboration, *Search for a third-generation leptoquark coupled to a τ lepton and a b quark through single, pair, and nonresonant production in proton-proton collisions at $\sqrt{s} = 13$ TeV*, 2308.07826. [Cited on pages 177 and 183.]

[368] CMS collaboration, *Search for pair-produced vector-like leptons in final states with third-generation leptons and at least three b quark jets in proton-proton collisions at s=13TeV*, *Phys. Lett. B* **846** (2023) 137713 [2208.09700]. [Cited on pages 177 and 182.]

[369] S. Fajfer, A. Greljo, J.F. Kamenik and I. Mustac, *Light Higgs and Vector-like Quarks without Prejudice*, *JHEP* **07** (2013) 155 [1304.4219]. [Cited on page 181.]

[370] X. Li and E. Ma, *Gauge Model of Generation Nonuniversality*, *Phys. Rev. Lett.* **47** (1981) 1788. [Cited on pages 186, 219, and 222.]

[371] E. Ma, X. Li and S.F. Tuan, *Gauge Model of Generation Nonuniversality Revisited*, *Phys. Rev. Lett.* **60** (1988) 495. [Cited on pages 186, 219, and 222.]

[372] E. Ma and D. Ng, *Gauge and Higgs Bosons in a Model of Generation Nonuniversality*, *Phys. Rev. D* **38** (1988) 304. [Cited on pages 186, 219, and 222.]

[373] X.-y. Li and E. Ma, *Gauge model of generation nonuniversality reexamined*, *J. Phys. G* **19** (1993) 1265 [hep-ph/9208210]. [Cited on pages 186, 219, and 222.]

[374] C.T. Hill, *Topcolor assisted technicolor*, *Phys. Lett. B* **345** (1995) 483 [hep-ph/9411426]. [Cited on pages 186 and 219.]

[375] D.J. Muller and S. Nandi, *Top flavor: A Separate SU(2) for the third family*, *Phys. Lett. B* **383** (1996) 345 [hep-ph/9602390]. [Cited on pages 186, 219, and 222.]

[376] E. Malkawi, T.M.P. Tait and C.P. Yuan, *A Model of strong flavor dynamics for the top quark*, *Phys. Lett. B* **385** (1996) 304 [hep-ph/9603349]. [Cited on pages 186, 219, and 221.]

[377] A. Beniwal, F. Rajec, M.T. Prim, P. Scott, W. Su, M. White et al., *Global fit of 2HDM with future collider results*, in *Snowmass 2021*, 3, 2022 [2203.07883]. [Cited on page 189.]

[378] A. de Giorgi, F. Koutroulis, L. Merlo and S. Pokorski, *Flavour and Higgs physics in Z_2-symmetric 2HD models near the decoupling limit*, 2304.10560. [Cited on page 189.]

[379] S.F. King, *Constructing the large mixing angle MNS matrix in seesaw models with right-handed neutrino dominance*, *JHEP* **09** (2002) 011 [hep-ph/0204360]. [Cited on page 199.]

[380] P. Langacker, *The Physics of Heavy Z' Gauge Bosons*, *Rev. Mod. Phys.* **81** (2009) 1199 [0801.1345]. [Cited on page 206.]

[381] T. Bandyopadhyay, G. Bhattacharyya, D. Das and A. Raychaudhuri, *Reappraisal of constraints on Z' models from unitarity and direct searches at the LHC*, *Phys. Rev. D* **98** (2018) 035027 [1803.07989]. [Cited on page 206.]

[382] ATLAS collaboration, *Improved W boson Mass Measurement using 7 TeV Proton-Proton Collisions with the ATLAS Detector*, (Geneva) (2023), http://cds.cern.ch/record/2853290. [Cited on page 212.]

[383] ATLAS collaboration, *Measurement of the W-boson mass in pp collisions at $\sqrt{s} = 7$ TeV with the ATLAS detector*, *Eur. Phys. J. C* **78** (2018) 110 [1701.07240]. [Cited on page 212.]

[384] J. Erler, P. Langacker, S. Munir and E. Rojas, *Constraints on the mass and mixing of Z-prime bosons*, *AIP Conf. Proc.* **1200** (2010) 790 [0910.0269]. [Cited on page 213.]

[385] B.C. Allanach, J.E. Camargo-Molina and J. Davighi, *Global fits of third family hypercharge models to neutral current B-anomalies and electroweak precision observables*, *Eur. Phys. J. C* **81** (2021) 721 [2103.12056]. [Cited on page 213.]

[386] B. Allanach and J. Davighi, *M_W helps select Z' models for $b \to s\ell\ell$ anomalies*, *Eur. Phys. J. C* **82** (2022) 745 [2205.12252]. [Cited on page 213.]

[387] LEP, ALEPH, DELPHI, L3, OPAL, LEP Electroweak Working Group, SLD Electroweak Group, SLD Heavy Flavor Group collaboration, *A Combination of preliminary electroweak measurements and constraints on the standard model*, hep-ex/0312023. [Cited on page 214.]

[388] C.D. Carone and H. Murayama, *Third family flavor physics in an $SU(3)^3$ x SU(2) -L x U(1) -Y model*, *Phys. Rev. D* **52** (1995) 4159 [hep-ph/9504393]. [Cited on pages 220 and 222.]

[389] A. Salam, *A gauge appreciation of developments in particle physics*, in *Proceedings of the European Physical Society International Conference on High Energy Physics*, (CERN, Geneva, 1979), footnote 41 therein. [Cited on page 220.]

[390] S. Rajpoot, *Some Consequences of Extending the SU(5) Gauge Symmetry to the Generation Symmetry SU(5) e X SU(5) μ X SU(5) τ*, *Phys. Rev. D* **24** (1981) 1890. [Cited on page 220.]

[391] H. Georgi, *Composite/Fundamental Higgs Mesons II: Model Building*, *Nucl. Phys. B* **202** (1982) 397. [Cited on page 220.]

[392] R. Barbieri, G.R. Dvali and A. Strumia, *Fermion masses and mixings in a flavor symmetric GUT*, *Nucl. Phys. B* **435** (1995) 102 [hep-ph/9407239]. [Cited on page 220.]

[393] K.S. Babu, S.M. Barr and I. Gogoladze, *Family Unification with SO(10)*, *Phys. Lett. B* **661** (2008) 124 [0709.3491]. [Cited on page 220.]

[394] C.-L. Chou, *Fermion mass hierarchy without flavor symmetry*, *Phys. Rev. D* **58** (1998) 093018 [hep-ph/9804325]. [Cited on page 220.]

[395] T. Asaka and Y. Takanishi, *Masses and mixing of quarks and leptons in product-group unification*, hep-ph/0409147. [Cited on page 220.]

[396] S.L. Glashow, *Trinification of All Elementary Particle Forces*, in *Fifth Workshop on Grand Unification*, 7, 1984. [Cited on page 221.]

[397] L. Allwicher, C. Cornella, G. Isidori and B.A. Stefanek, *New Physics in the Third Generation: A Comprehensive SMEFT Analysis and Future Prospects*, 2311.00020. [Cited on page 222.]

[398] R.M. Fonseca, *GroupMath: A Mathematica package for group theory calculations*, *Comput. Phys. Commun.* **267** (2021) 108085 [2011.01764]. [Cited on pages 231 and 261.]

[399] M.E. Machacek and M.T. Vaughn, *Two Loop Renormalization Group Equations in a General Quantum Field Theory. 1. Wave Function Renormalization*, *Nucl. Phys. B* **222** (1983) 83. [Cited on page 239.]

[400] Super-Kamiokande collaboration, *Search for proton decay via $p \to e^+\pi^0$ and $p \to \mu^+\pi^0$ with an enlarged fiducial volume in Super-Kamiokande I-IV*, *Phys. Rev. D* **102** (2020) 112011 [2010.16098]. [Cited on pages 241, 242, 243, and 244.]

[401] P.N. Bhattiprolu, S.P. Martin and J.D. Wells, *Statistical significances and projections for proton decay experiments*, *Phys. Rev. D* **107** (2023) 055016 [2210.07735]. [Cited on pages 241, 242, 243, and 244.]

[402] H.H. Patel, *Package-X 2.0: A Mathematica package for the analytic calculation of one-loop integrals*, *Comput. Phys. Commun.* **218** (2017) 66 [1612.00009]. [Cited on page 249.]

[403] B. Allanach, *Fits to measurements of rare heavy flavour decays*, in *31st International Symposium on Lepton Photon Interactions at High Energies* , 7, 2023 [2307.07532]. [Cited on page 251.]

[404] H.K. Dreiner, H.E. Haber and S.P. Martin, *Two-component spinor techniques and Feynman rules for quantum field theory and supersymmetry*, *Phys. Rept.* **494** (2010) 1 [0812.1594]. [Cited on page 254.]

[405] S.P. Martin, *TASI 2011 lectures notes: two-component fermion notation and supersymmetry*, in *Theoretical Advanced Study Institute in Elementary Particle Physics: The Dark Secrets of the Terascale*, pp. 199–258 (2013), DOI [1205.4076]. [Cited on page 254.]